NTIS # PB2015-

SSC-470

FINITE ELEMENT MODELING METHODS: VIBRATION ANALYSIS FOR SHIPS

SHIP STRUCTURE COMMITTEE

2015

Ship Structure Committee

Member Agencies:

American Bureau of Shipping
Defence Research and Development Canada
Maritime Administration
Military Sealift Command
Naval Sea Systems Command
Office of Naval Research
Society of Naval Architects & Marine Engineers
Transport Canada
United States Coast Guard

Ship
Structure
Committee

Address Correspondence to:

COMMANDANT (CG-ENG-2/SSC)
ATTN (EXECUTIVE DIRECTOR/SHIP
STRUCTURE COMMITTEE)
US COAST GUARD
2703 MARTIN LUTHER KING JR. AVE SE
WASHINGTON DC 20593-7509
Website: http://www.shipstructure.org

SSC – 470
SR – 1472

March 25, 2015

FINITE ELEMENT MODELING METHODS VIBRATION ANALYSIS FOR SHIPS

The objective of this project was to identify acceptable methods of creating and analyzing finite element models to predict vibration amplitudes of local vessel structures in response to forced input from both hard and resiliently mounted machinery. The recommended modeling methods are intended to provide a degree of model simplification that will minimize loss of accuracy while improving the speed with which models can be created and analyzed.

This report combines two phases of modeling and testing results, and includes discussions of model sensitivity analyses, test results, and comparisons of test data to measurements. In Phase I, a finite element model of a small catamaran was created with the purpose of performing sensitivity studies to various modeling parameters, which is presented in Part I of this report. In Phase II, vibration measurements were performed on a large, steel hulled vessel and compared against predictions made with finite element models. A general outline for finite element modeling and analysis methods has been developed along with identification of prediction accuracy in Part III.

We thank the authors and Project Technical Committee for their dedication and research toward completing the objectives and tasks detailed throughout this paper and continuing the Ship Structure Committee's mission to enhance the safety of life at sea.

Paul F. Thomas
PAUL F. THOMAS
Rear Admiral, U.S. Coast Guard
Co-Chairman, Ship Structure Committee

L.B. Fuller
L. BRYANT FULLER
Rear Admiral, U.S. Navy
Co-Chairman, Ship Structure Committee

1. Report No. SSC - 470	2. Government Accession No.	3. Recipient's Catalog No.
4. Title and Subtitle FINITE ELEMENT MODELING METHODS Vibration Analysis for Ships		5. Report Date 3/25/2015 6. Performing Organization Code
7. Author(s) Spence, J. H.; Favini, E. A.; Page, C. A.		8. Performing Organization Report No. RPT13-007
9. Performing Organization Name and Address Noise Control Engineering, Inc. 799 Middlesex Tpke. Billerica, MA 01821		10. Work Unit No. (TRAIS) 11. Contract or Grant No. W7707-135623/HAL-2-69212
12. Sponsoring Agency Name and Address Ship Structure Committee U. S. Coast Guard (CG-ENG-2/SSC) 2703 Martin Luther King Jr. Ave. SE Washington, D.C. 20593-7509		13. Type of Report and Period Covered Final Report 14. Sponsoring Agency Code CG-5P
15. Supplementary Notes Sponsored by the Ship Structure Committee and its member agencies. Reviewed by designated Project Technical Committee.		

16. Abstract

Accurate accounting of the vibration induced by machinery is important for the design of vessels that have a low adverse impact on the crew, the ocean environment, and the vessel's structural integrity. The objective of this project is to identify acceptable methods of creating and analyzing finite element models using commercially available software in order to predict vibration amplitudes of local vessel structures in response to forced input from both hard and resiliently mounted machinery. This includes identification of the baseline requirements for finite element models of ship structures, such as minimum element density, model extents, boundary conditions, damping loss factors, and other ship specific features. The degree of accuracy that can be expected by using these baseline procedures has been identified. The recommended modeling methods are intended to provide a degree of model simplification that will minimize loss of accuracy while improving the speed with which models can be created and analyzed.

This report combines two phases of modeling and testing results, and includes discussions of model sensitivity analyses, test results, and comparisons of test data to measurements. Parts I and II discuss the detailed results from Phases I and II, respectively. A summary of modeling recommendations is provided in Part III.

17. Key Words		18. Distribution Statement	
Finite Element Analysis, Vibration, Ship Structure, Structural Analysis (Engineering), Response, Mesh, Damping, Resonance Frequency Stiffener, Excitation		Distribution unlimited, available from: National Technical Information Service Springfield, VA 22161 (703) 487-4650	
19. Security Classif. (of this report) Unclassified	20. Security Classif. (of this page) Unclassified	21. No. of Pages 318	22. Price

CONVERSION FACTORS
(Approximate conversions to metric measures)

To convert from	to	Function	Value
LENGTH			
inches	meters	divide	39.3701
inches	millimeters	multiply by	25.4000
feet	meters	divide by	3.2808
VOLUME			
cubic feet	cubic meters	divide by	35.3149
cubic inches	cubic meters	divide by	61,024
SECTION MODULUS			
inches^2 feet	centimeters^2 meters	multiply by	1.9665
inches^2 feet	centimeters^3	multiply by	196.6448
inches^3	centimeters^3	multiply by	16.3871
MOMENT OF INERTIA			
inches^2 feet^2	centimeters^2 meters^2	divide by	1.6684
inches^2 feet^2	centimeters^4	multiply by	5993.73
inches^4	centimeters^4	multiply by	41.623
FORCE OR MASS			
long tons	tonne	multiply by	1.0160
long tons	kilograms	multiply by	1016.047
pounds	tonnes	divide by	2204.62
pounds	kilograms	divide by	2.2046
pounds	Newtons	multiply by	4.4482
PRESSURE OR STRESS			
pounds/inch^2	Newtons/meter^2 (Pascals)	multiply by	6894.757
kilo pounds/inch^2	mega Newtons/meter^2 (mega Pascals)	multiply by	6.8947
BENDING OR TORQUE			
foot tons	meter tons	divide by	3.2291
foot pounds	kilogram meters	divide by	7.23285
foot pounds	Newton meters	multiply by	1.35582
ENERGY			
foot pounds	Joules	multiply by	1.355826
STRESS INTENSITY			
kilo pound/inch^2 inch^{½}(ksi$\sqrt{\text{in}}$)	mega Newton MNm$^{3/2}$	multiply by	1.0998
J-INTEGRAL			
kilo pound/inch	Joules/mm^2	multiply by	0.1753
kilo pound/inch	kilo Joules/m^2	multiply by	175.3

TABLE OF CONTENTS

LIST OF ILLUSTRATIONS

LIST OF TABLES

LIST OF ABBREVIATIONS

ABL – Above Baseline
FEA – Finite Element Analysis
FRF – Frequency Response Function
KVI – Kvichak Marine Industries
MMA – Maine Maritime Academy
NCE – Noise Control Engineering, Inc.
ODS – Operational Deflection Shape

LIST OF SYMBOLS

[C] – Damping Matrix
[D] – Dynamic stiffness matrix
[H] – FRF (Frequency Response Function) Matrix
[K] – Stiffness Matrix
C_w – Warping Constant
E – Modulus of Elasticity
F – Force
G – Shear Modulus
J – Beam warping constant
L – Length of beam
[M] – Mass Matrix
T – Applied torque
X – Displacement
j – $\sqrt{-1}$
p_k – *k*-th pole
q_k – Complex scaling quantity for the *k*-th mode
{x} – Displacement vector
ω – Angular frequency (rad/s)
ω_n – Natural frequency
ζ – Damping ratio
φ_k – *k*-th mode shape or 'eigenvector'
η – Damping loss factor
ϕ – Angle of twist

INTRODUCTION TO REPORT

Finite Element Analysis (FEA) is a powerful tool used for analysis of ship vibrations to assess 'habitability' vibration response (i.e. vibrations that would affect crew/passenger comfort) as well as vibration-induced fatigue. Vibration analyses using finite element methods have become standard practice during various stages of vessel design since potential issues can be identified and remedied before construction begins. This is an invaluable tool which can be used to avoid serious vibration problems and save on costly remediation that might be needed on completed vessels.

However, creating finite element models is time consuming. In many cases, weeks to multiple person-months are required to create models, depending on the required model size. As a result of these time requirements such analyses are often pushed to later design stages. This can impact the available options for mitigation strategies when a vibration problem is detected. If problems are found late in the design, structural modification may not be practical and other factors such as weight and cost impacts may be onerous.

The accuracy of any finite element analysis will be subject to the modeling and analysis methodology that is used as well as the quality of the inputs. Selection of element types, mesh size, model extents, and how vibration sources are defined, among other factors will influence the model results. In many cases it is difficult to validate FEA models of vessels because measured data are limited, the measurement conditions do not line up with the modeling conditions, source forces or vibration levels are not known, budgetary considerations, and other influences.

The objective of this project is to identify effective and efficient methods of creating finite element models using commercially available software allowing for assessments of vibrations of local vessel structures due to excitation from shipboard machinery. The desire is to identify methods of creating and analyzing FEA models that are relatively quick and efficient, which have been shown through validation tests to have a reasonable degree of accuracy.

This effort has been performed in two phases. In Phase I, a finite element model of a small catamaran was created with the purpose of performing sensitivity studies to various modeling parameters. These parameters include:

- Mesh density
- Element types
- Model extents
- Boundary conditions
- Effects of vessel outfitting
- Effects of localized masses and structural simplifications
- Damping

Many models were created and analyzed with multiple excitation and response points to determine the model's vibration sensitivity to these factors. The results of these analyses are presented in Part I of this report. Measurements of this vessel were originally intended, though due to logistical and timing issues, no measurements were performed.

In Phase II, vibration measurements were performed on a large, steel hulled vessel and compared against predictions made with finite element models. This was done to further refine modeling recommendations from Phase I and define the accuracy that is possible with different modeling and analysis approaches. Measurements were also performed to assess appropriate damping values for use in finite element modeling, and to determine methods for modeling machinery sources. The results of this study are discussed in Part II of this report.

Using the results of both Phase I and Phase II analyses, a general outline for finite element modeling and analysis methods has been developed along with identification of prediction accuracy. This is provided in Part III of this report.

PART I – FEA Sensitivity Studies

1.0 BACKGROUND

The sections within Part I of this report discuss the efforts performed under Phase I of this effort, which includes sensitivity studies to various modeling parameters and defining a general analysis approach.

1.1 Vessel Details

The vessel that was investigated in this phase is a 57' 8" aluminum catamaran built by Kvichak Marine Industries (KVI); all vessel information was provided by KVI. Table 1 summarizes the general design characteristics of the vessel. Figure 1 provides the outboard profile of the vessel. Additional drawings are provided in Appendix A.

Table 1: General Parameters of the KVI Catamaran

Parameter	Value
Length, Overall	57' 8"
Length, On Deck	54' 8"
Length, on Waterline	50' 3"
Beam, molded	20' 7"
Draft, approximate	33"
Weight, LightWeight	50,000 pounds
Weight, Full Load	70,000 pounds
Fuel Tank Capacity	1200 gallons
FreshWater Tank Capacity	150 gallons
WasteWater Tank Capacity	150 gallons

The vessel contains two resiliently mounted propulsion diesels, which are Scania DI12 69M, rated at 691BHP at 2300 RPM. There are four mounts per engine. There is a single Northern Lights genset which is resiliently mounted in the starboard engine room, rated at 12kW at 1800 RPM. The vessel also has various hard mounted auxiliary machinery items that are used to support the diesels and vessel operations, located throughout the vessel.

Details of the vessel structure were provided by KVI primarily via a 3-D Solidworks model. All plating and stiffener dimensions were extracted from the Solidworks model. A weight report was also provided, which details the weight of the structure, fluids in tanks, equipment weight, and other masses throughout the vessel. Additional details such as window and door arrangements were provided separately.

Figure 1: Vessel Outboard Profile

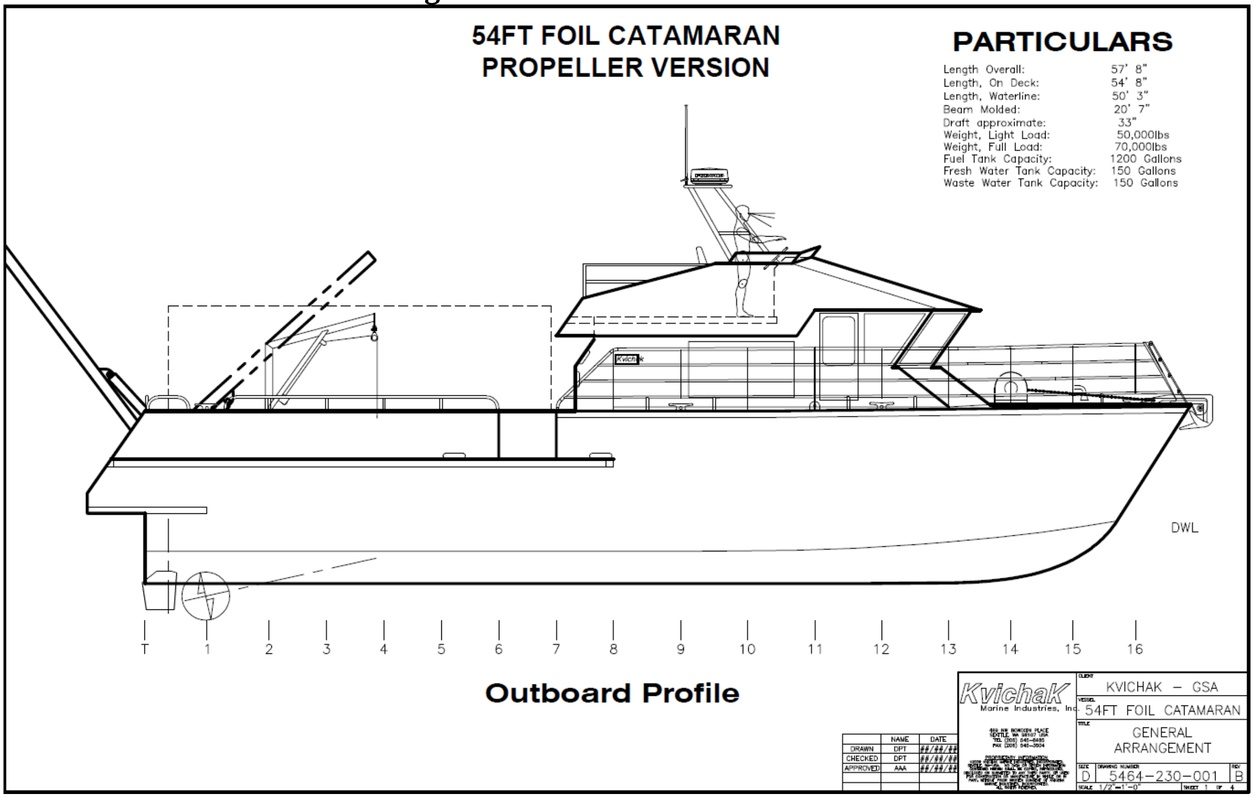

1.2 Notes on General Modeling Approach

When performing dynamic analyses of ship structures, there are a variety of finite element modeling approaches that may be employed. Selection of a particular approach is highly dependent on the nature and frequency range of the desired results and the desired accuracy.

There can be many different finite element analysis approaches to creating a vibration model. These can range from

- A simple "equivalent beam" model, where the equivalent sectional properties at each transverse frame (or other location) are computed and used to generate a beam model of the vessel along its length, as described in Reference [1].
- A full 3-dimensional solid element mesh of everything and anything on the vessel.

This is a wide spectrum of possibilities, and each model on this spectrum will have its advantages and disadvantages. Each will typically provide some sort of tradeoff between accuracy (which may be frequency or source-type dependent) and speed with which the model can be created and analyzed. For example "equivalent beam" models can be used to predict the low frequency (< 10 Hz) modes of the ship where large portions of the vessel are moving together. More detailed models comprised of individual plating and stiffeners would be required when localized modes or response characteristics are required. Solid meshes of large vessel sections are likely not practical or necessary for a majority of ship modeling applications.

While models with greater detail can provide more accurate and higher fidelity results, they can also take longer to create and analyze. For example, finer FEA meshes generally provide better results at a given frequency [3]. However, finer meshes also require more computing power and it is very easy to overwhelm the memory and processing capabilities of commercially available computers with very large ship models. As will be shown in this report, solution times for finite element models will increase non-linearly as the number of model degrees of freedom is increased[1]. Therefore it is desirable to strike a balance between the model size (and complexity) and the required accuracy of the results.

The focus of this effort is to identify methods of modeling and vibrations of local structures, so it is reasonable to expect that local structural details such as plating and stiffeners will need to be modeled. For example, if an estimation of the vibration levels of the deck in a particular compartment are desired, it would be required, as a minimum, to create a model that includes the nuances of the compartment's deck in that compartment so that some degree of vibration contour could be obtained. It then follows that other nearby structures would also have the same or similar model fidelity.

In this project, an approach similar to that described in Reference [2] has been used, where structural plating and stiffeners have been modeled explicitly using 2-noded beam elements and 3- & 4-noded plate elements. Example screenshots of one of the various models used in these analyses are provided in Figure 2 and Figure 3. Figure 2 shows an overview of the model, illustrating the basic approach with respect to element size and degree of detail of the model. Figure 3 shows a cutaway view of a section of the side shell, further illustrating the discretization of plating and stiffeners using separate elements.

Figure 2: Overview of Finite Element Model

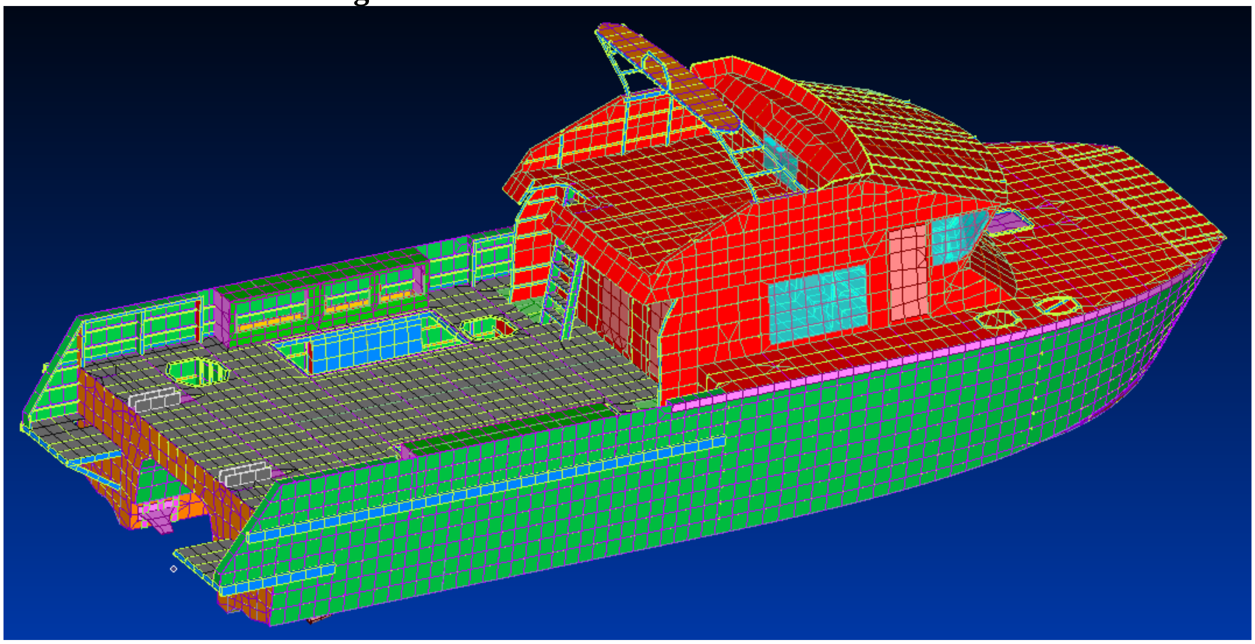

[1] Actual solution time is dependent on the type of solver, computing power, and other factors. Such discussions are not the focus of this effort.

Figure 3: Detail showing Stiffened Plating

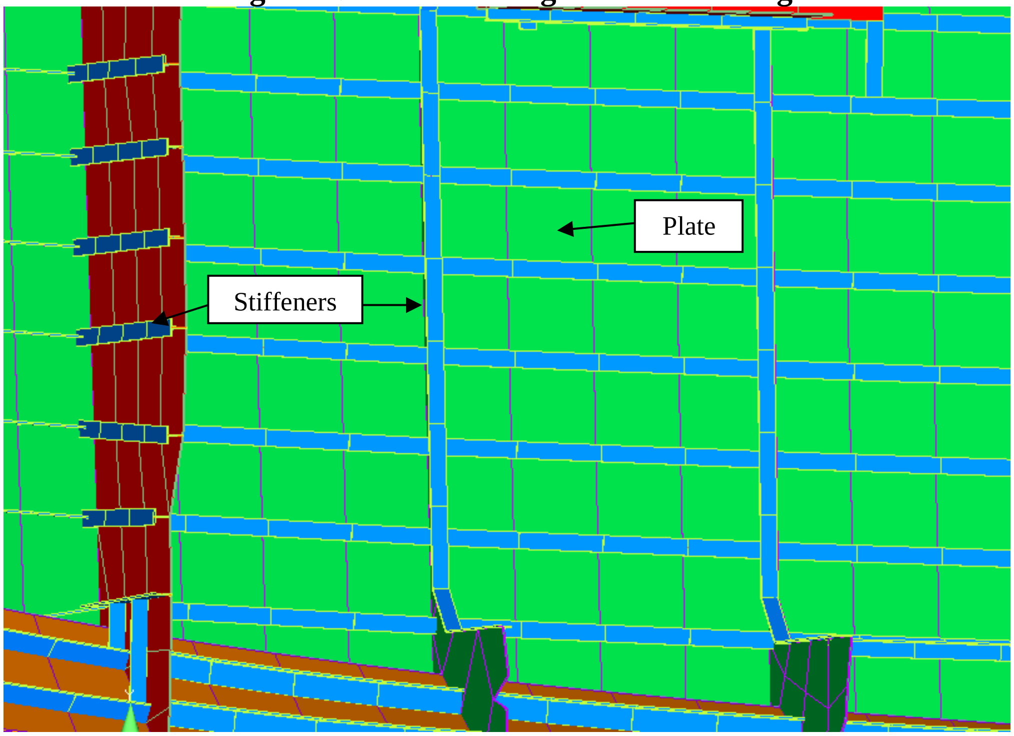

Even within this framework, there are many possible options for developing finite element models. Such options include the degree of mesh refinement, stiffener element type, limiting the extents of the model, damping, and other common finite element modeling factors. Other options specific to modeling vessels may also be important in the tradeoff of model complexity vs. accuracy, such as neglecting certain small machinery masses, doors and hatches, and other components of the vessel. Methods of interpreting the results are also a factor in obtaining accuracy while minimizing analysis time.

The effects of such choices are discussed in this report. The investigations discussed in Part I are limited to sensitivity analyses since measurements on the subject vessel were not performed. In this phase of the effort, 'accuracy' is seen more by convergence of model results than comparisons to measurements. Comparisons of models to measurements have been performed and are discussed in Part II of this report.

2.0 MODELS AND METHODOLOGY

2.1 Overview

The following sections discuss the methodologies used to investigate the sensitivity of the vibration response to various model parameters.

For all analyses, the general analysis approach was to excite the model at a point in a single direction and calculate the vibration response at various near-by and remote locations. All analyses were run in the frequency range of 1-100 Hz, as this is the range of primary interest for many standard requirements for vibration levels affecting the crew as well as for structural fatigue. Examples of such standards include ISO 6954, ANSI S2.25, ANSI S3.18, ABS

HAB/HAB+, DNV Rules for Classification of Ships, and SNAME T&R 2-29A, as well Reference [2].

Multiple forcing and response locations were used throughout this investigation. This was done in an attempt to reduce the likelihood that an anomaly of any particular force/receiver location set would lead to false conclusions about proper modeling methodology.

Excitation points for the various models include the following:

- On the foundation of the propulsion engine
- On the superstructure, upper deck
- On the aft deck
- On the Frame 2 bulkhead

The resulting velocity of ship structures due to these forces was extracted both at specific points (nodes) and as an average over a large area, as deemed appropriate depending on the analysis being performed. Additional details are provided in the following sections.

It is noted that reciprocity relations exist for any force/receiver pair; the response at one location from a force at a second location is the same as the response at the second location as a result of a force applied at the first (assuming the same direction of force and response for both). This aspect is used in various analyses throughout this report.

Damping is an important parameter for any forced response vibration analysis. A specific investigation into the effects of changing damping has been performed as part of this phase, and additional discussion and analysis is provided in Part II. For most models discussed in Part I of this report, a 'baseline' damping loss factor of 0.03 has been applied at all frequencies. This value is in line with the recommended value in Reference [2].

No attempt was made to correct for the effect of water loading on the hull of the vessel for the models created in this phase (Phase I). As discussed in Reference [1], the water will create an added mass effect at the frequencies of interest for this study, thereby lowering natural frequencies of certain modes. Discussion of approximate modeling techniques to account for this phenomenon is provided in Part II of this report.

All analyses have been performed using the commercially available NEiNastran finite element software package[2]. This software is meant for general purpose use and is not specific to ships or vibration analysis. In selected cases, the specifics of this software (such as element formulation) have been noted, particularly when it impacts model results. Because only one software package is being used for this investigation, it is likely unavoidable that some of the results will be specific to the NEiNastran approach. However, in general it is assumed that the results presented

[2] It is noted that NEiNastran uses the Lanczos method for solving modal analyses. Direct frequency response solutions have been used for forced vibration response analyses. NEiNastran uses a direct sparse matrix solver (VSS) for models greater than 50,000 DOF and a parallel sparse iterative solver (PCGLSS) for models less than 50,000 DOF.

here are applicable to other general purpose FEA software. Discussions of such instances are provided when applicable.

One related item to note is the use of NEiNastran's CQUADR and CTRIAR elements. These plate elements have been used exclusively in all analyses discussed in this report. As discussed in the NEiNastran documentation [18], these elements are more accurate than the CQUAD4 and CTRIA4 element formulations since they include the "drill" degree of freedom (i.e. they have 6 DOF per node vs. 5). NEiNastran also uses an increased number of integration points in the CQUADR and CTRIAR element formulation, leading to improved accuracy and tolerance for irregular geometries. CQUADR and CTRIAR elements are required when modeling with both plate and beam elements. It is likely that there are similar considerations to be made when using other commercially available finite element software.

2.2 Mesh Density

A wide range of mesh densities are possible in any finite element model. Three different mesh densities have been considered in Part I of this report. These are summarized in Table 2, and examples from models used as part of this analysis are shown in Figure 4 to Figure 6.

The mesh density shown in Figure 4 has been called the "minimum" mesh density as it is the smallest density (largest element size) that can be created while still explicitly modeling the stiffeners attached to the plates. Two levels of refinement have been investigated, being "2x mesh" and "4x mesh", where the length of each element side is split in two or four, respectively, for all plate and beam elements. This increases the plate element count by 4 and 16, respectively, and has a similar effect on the total number of degrees of freedom in the model.

To investigate the influence of mesh density, forced vibration responses were calculated at specific locations given in Table 3 below. The response to a unit force was compared as a function of frequency for the varying mesh densities for each source/receiver pair.
Single node responses were used in this case to maintain uniformity for differing mesh densities. The response was calculated in all translational directions, though out-of-plane response was typically of primary interest. The input force locations are shown in boldface type in Table 3; the direction of applied force is normal to the structure.

The models used for this analysis were full ship models. No tank loads, doors, windows, or machinery masses were included in the model. The sensitivity of the model to these items was assessed separately (see Section 2.8). It is assumed that the relative results from one mesh density to the next should not be significantly influenced by these factors.

Small stiffeners were modeled using beam elements while larger girders were modeled using a combination of plate and beam elements – additional information on stiffener modeling methods is provided in Section 2.4. Plate elements used to model the girder webs were also refined for the 2x and 4x mesh models.

Table 2: Mesh Density Summary

Mesh Density	The number of elements in a given area. A higher mesh density equates to a higher number of elements in a given area. 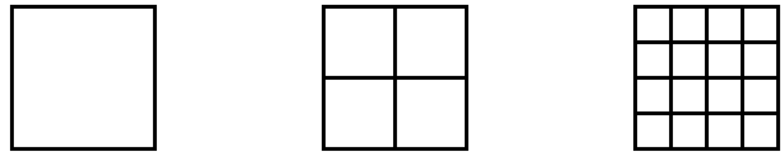 **Minimum Mesh Density** **2x Mesh Density** **4x Mesh Density**
Minimum Mesh Density	The nominal length of each side of an element is equal to the frame spacing of the vessel.
2x Mesh Density	The nominal length of each side of an element is equal to one-half the frame spacing of the vessel. There are generally two equally spaced elements per frame.
4x Mesh Density	The nominal length of each side of an element is equal to one-fourth the frame spacing of the vessel. There are generally four equally spaced elements per frame.

Table 3: Force Input and Response Output Locations

Node ID	Location	Global Coordinates (inches)			Normal Direction
		Long.	Vert.	Trans.	
1214	**Aft Main Deck, Stbd**	**58.5**	**78.0**	**33.5**	**Vertical**
1462	**Frame 2 Bulkhead, Port**	**78.0**	**44.6**	**-78.2**	**Longitudinal**
2226	Outboard Hull, Port	132.0	45.6	-119.9	Transverse
2775	Inboard Hull, Port	168.0	44.7	-44.3	Transverse
2807	**Engine Foundation, Port**	**168.0**	**17.9**	**-101.0**	**Vertical**
3358	Mid Main Deck, Port	204.0	78.0	-22.4	Vertical
5023	Frame 8 Bulkhead above deck, Port	294.0	99.4	-44.7	Longitudinal
5089	Frame 8 Bulkhead below deck, Port	294.0	51.7	-50.0	Longitudinal
5675	Mast, Port	320.5	252.5	-39.0	Vertical
6188	**Top Wheelhouse Deck, Port**	**345.6**	**166.0**	**-44.5**	**Vertical**
6326	Top Wheelhouse Deck, Stbd	355.4	165.1	60.0	Vertical
6565	Pilothouse Bulkhead, Port	367.5	99.3	-89.7	Transverse
7175	Main Deck Pilothouse, Stbd	399.0	78.0	22.4	Vertical
9575	Frame 13 Bulkhead, Port	504.0	68.2	-84.6	Longitudinal
9793	Front Bulkhead Pilothouse, CL	509.2	127.1	0.0	Vertical
10478	Forward Main Deck, Port	562.5	111.1	-60.0	Vertical

Figure 4: Minimum Quad Mesh

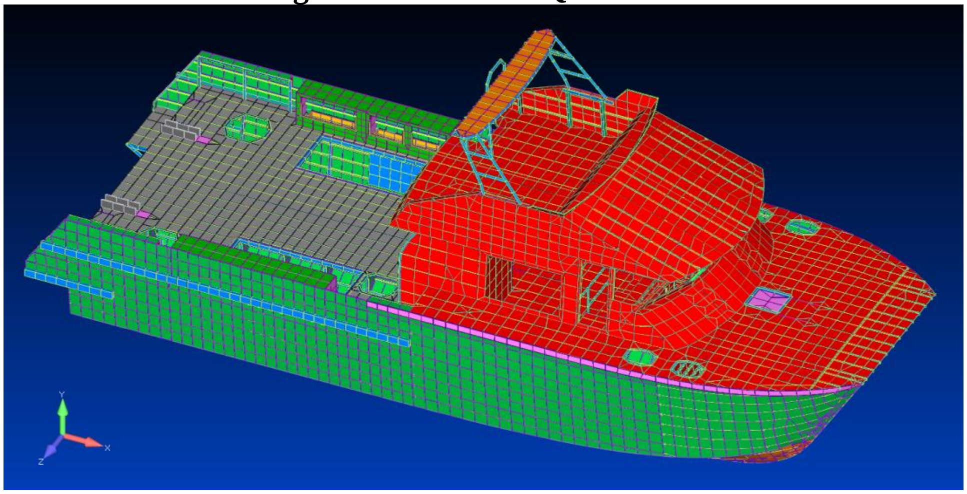

Figure 5: 2x Quad Mesh

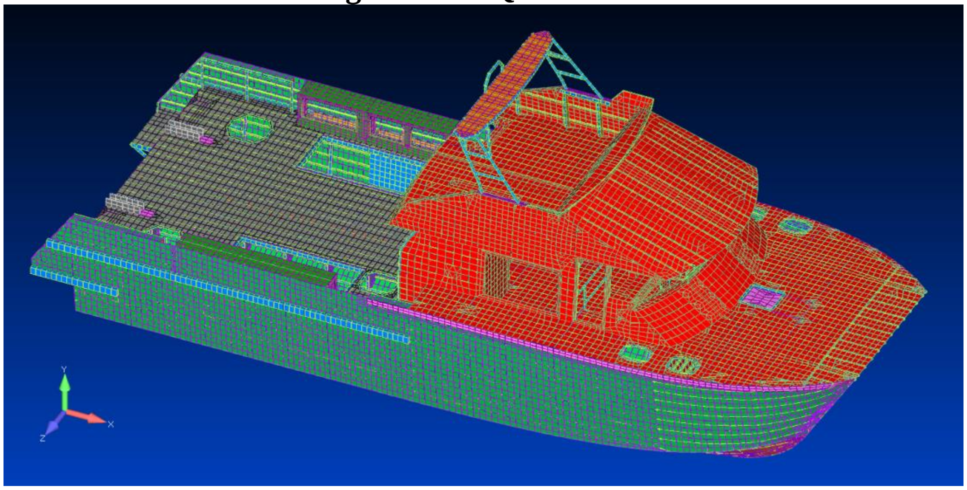

Figure 6: 4x Quad Mesh

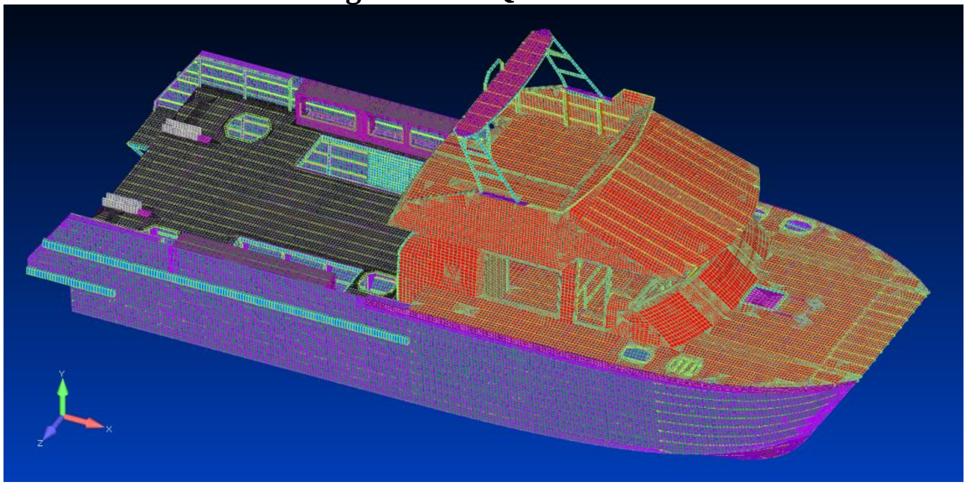

2.3 Plate Element Type – Quad vs. Tri Elements

An analysis was performed where all quad (4-noded) plate elements in the 'minimum mesh density' and 2x mesh density models discussed in Section 2.2 were converted to tri (3-noded) plate elements. Screen captures of the minimum tri mesh density model as well as the 2x refined tri mesh are shown in Figure 7 and Figure 8, respectively.

Figure 7: Minimum Tri Mesh

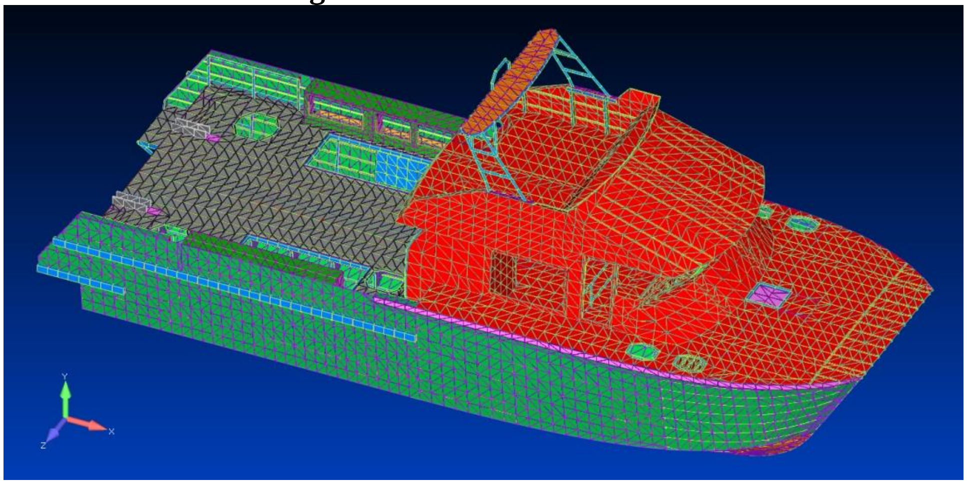

Figure 8: 2x Tri Mesh

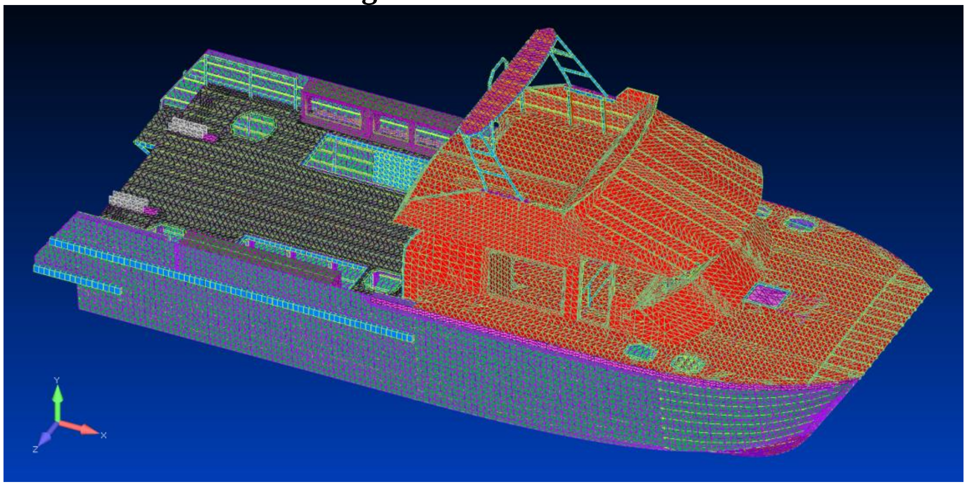

In general, it is assumed that the exclusive use of tri-elements would not be pursued as they are known to exhibit "shear locking[3]" [3], at least for some element formulations. However, the exclusive use of quad-elements is not possible for practical models, and therefore tri-elements must be used in some cases. The extreme use of tri-elements in this investigation is meant to show the maximum deviation that can be expected, with the understanding that this approach would not be used in practice.

---

[3] Shear locking is a finite element phenomenon where triangular elements exhibit excessive stiffness when subjected to in-plane loads.

The forcing and response locations were the same for this model as for the models discussed in Section 2.2. For each source/receiver pair, the response to a unit force was compared as a function of frequency for the varying mesh densities.

2.4 Stiffener Element Types

Stiffeners can be modeled in various ways using beam elements, plate elements, or both. For example, the simplest approach is to use a beam element which would incorporate the web and flange in a single element. An alternative is to use a plate element for the web and a beam element for the flange. A third option is to use plate element for both web and flange.

By using a beam to model the entire stiffener (web and flange), nodes that already exist on plating elements are the only nodes that are used, and no additional nodes are created. Conversely, if a plate is used to model any part of the stiffener then additional nodes are created. These nodes must be connected to adjacent structures. This typically requires mesh refinement, and increases modeling time. Conversely, the connection of the stiffener plate to an adjacent bulkhead provides additional coupling and stiffness which may be necessary in order to obtain accurate results.

Various models have been created to examine the sensitivity of vibration results to these factors. To start, some basic models of cantilevered beams were generated using the three modeling approaches described above (beam only, plate web/flange beam, and plate web/plate flange). An expansion of the cantilever beam models was also generated where a section of plating was attached to multiple beams, making a cantilevered section of stiffened plating. Examples of these models can be seen in Figure 9.

Figure 9: Cantilever Beam and Stiffened Plating Models

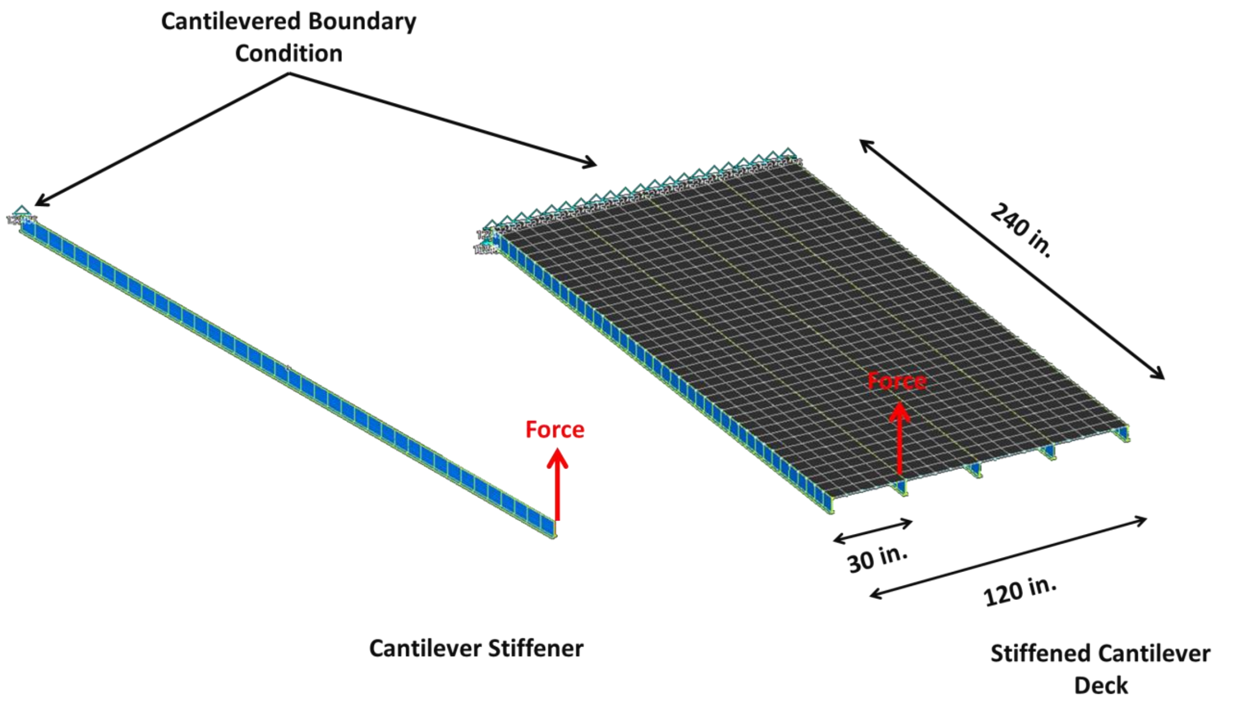

A force was applied at the free end of the cantilever models in the vertical (out of plane) direction and the resulting displacements at the point of force application as a function of frequency was determined. It is noted that the fixed constraint was applied to all available nodes at the fixed end of the models, which is different for the beam stiffener models (1 node) vs. the plate stiffener models (2-4 nodes).

These models were created in an attempt to determine the degree of equivalency between modeling stiffeners with beams vs. plates, without the effects of adjacent structures. Two different stiffener cross-sections were studied, specifically an L and a T shape. Figure 10 provides a sketch of the stiffener cross sections studied. Note that the L cross-section has a shear center that is offset from the web.

Figure 10: Beam Sections for Initial Stiffener Study

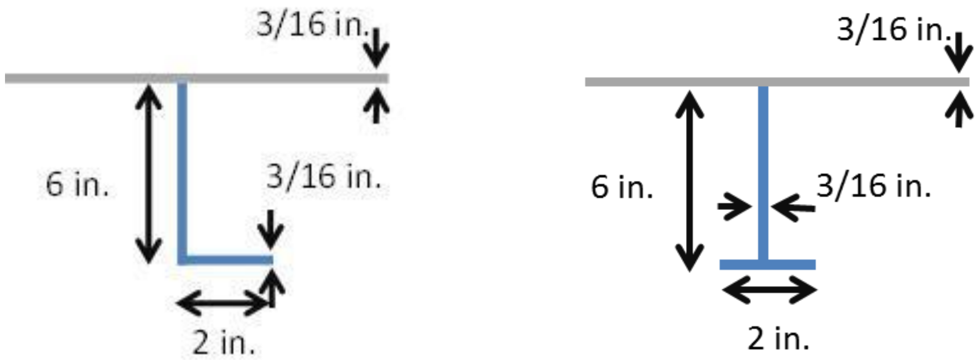

(a) L-Section (b) T-Section

Subsequent to this analysis, different stiffener modeling approaches were applied to the "minimum mesh density" full ship model discussed in Section 2.2. Three scenarios were tested:

- All deck and bulkhead stiffeners modeled as beams
- Only small stiffeners modeled as beams – large girders and frames with web heights on the order of stiffener spacing were modeled with plate webs and beams flanges
- All stiffeners modeled using plate webs and beam flanges

The relative differences in vibration response at selected locations as a result of various forces (similar to those discussed in Section 2.2) were investigated to identify differences between these models and to assist in determining which approach may lead to reasonable accuracy while minimizing model development time.

2.5 Model Extents

To save time in generating finite element models it may be desirable to model only a portion of the ship. This is particularly true for large ships such as tankers, or when the vibration source and response locations are within a small portion of the vessel. However, this simplification is expected to have an impact on the accuracy of the results. This accuracy may be acceptable in some frequency ranges, and unacceptable in others.

The “minimum mesh density” model discussed in Section 2.2 has been used to determine the effects of truncating the model. Various models have been created, ranging from the full ship to the source room only. Descriptions of the various models are provided in Table 4 and Figure 11. A pinned (no translation in any direction) boundary condition was applied at the extents of the sub-models around the perimeter of the section that was cut (i.e. locations where stiffened plating would otherwise continue past the cut). No constraints were applied to the full ship model.

Figure 11: Models Used for Model Extents Analysis

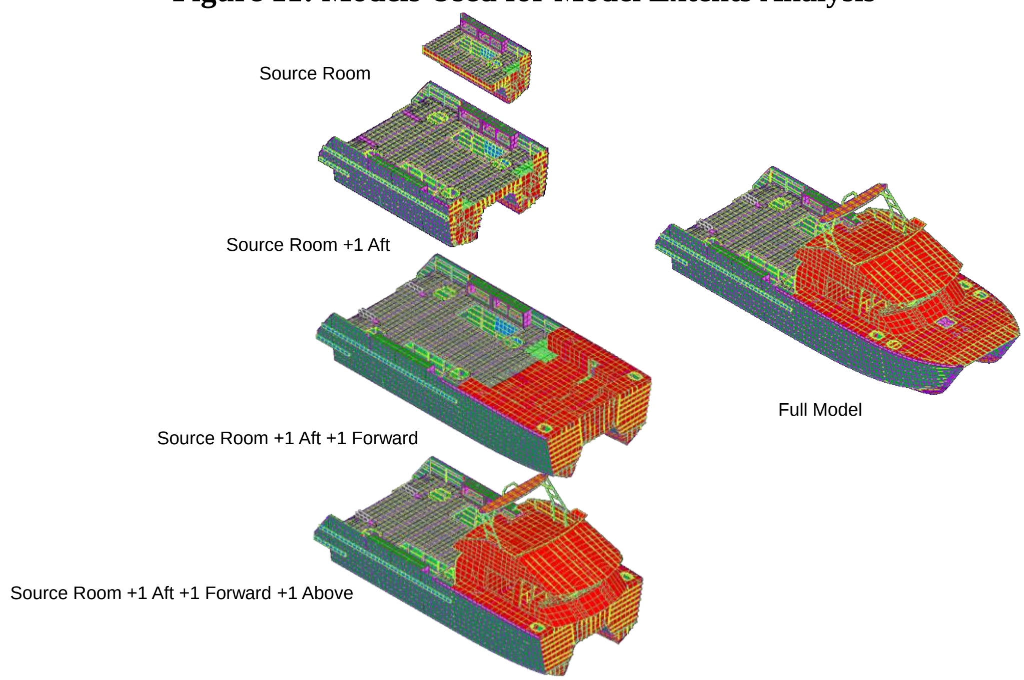

Table 4: Description of Models Used for Model Extents Analysis

Model	Description	Boundary Condition
Full Ship	Standard Quad Mesh	Free Boundary Condition
Source Room	Frame 2 to Frame 8 Portside to Centerline	Stiffeners and plating along perimeter of frames 2 and 8 were pinned
Source Room + 1 Room Aft	Transom to Frame 8 Portside to Starboard	Plating and Stiffeners along Frame 8 perimeter were pinned, Transom was unconstrained
Source Room + 1 Aft and +1 Forward	Transom to Frame 13 Portside to Starboard No Superstructure	Plating and Stiffeners along the perimeter of Frame 13 were pinned, Transom unconstrained
Source Room + 1 Aft and +1 Forward +1 Above	Transom to Frame 13 Portside to Starboard Superstructure up to Frame 13	Plating and Stiffeners along the perimeter of Frame 13 were pinned, Transom unconstrained

These models have all been ‘cut’ at locations where there are major structural divisions (i.e. a major bulkhead or deck). This approach was used in an attempt to minimize the effects of the artificial breaks in the model which would enforce false local structural modes. For example, if the model were transversely cut at a location mid-way between two transverse bulkheads (i.e. the middle of a compartment), the boundary condition would prevent any mode from occurring where there is motion of the deck or bulkheads in the middle of the space, essentially allowing (or simulating) only higher order modes to occur. The accuracy of lower order modes is also compromised in this example. The initial assumption was that by truncating the model at major divisions, such effects would be minimized as the interfaces of bulkheads and decks are expected to have reduced amplitudes, at least for local modes. However, this may not be the case for whole body modes.

All models were excited by a single point force in the vertical direction on the port engine foundation, as shown in Figure 12.

Figure 12: Engine Room Excitation Location

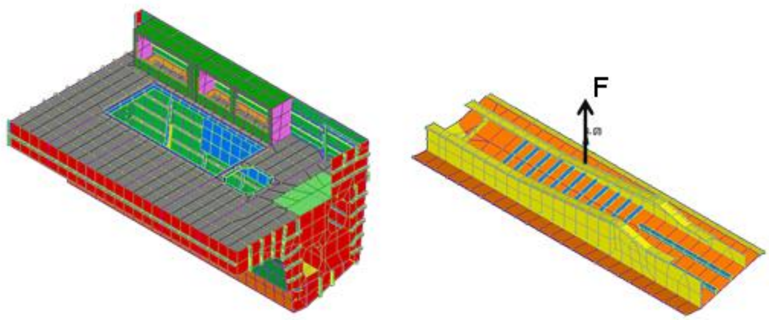

Because of the small size of the vessel, this analysis has been limited to investigations on the impact to the predicted response at locations close to the source excitation when the model is truncated. Several response 'regions' within the Engine Room were chosen for this analysis, including:

- Hull side
- Hull bottom
- Transverse frames/bulkheads
- "Engine Room Plate" (see below)
- Main Deck plating

These regions are shown in more detail in Figure 13. For this analysis, the average response in the vertical, longitudinal and athwartship directions over the nodes that make up these regions was computed.

It is noted that the "Engine Room Plate" receiver location is a small plate that is attached to the outboard hull frames. It does not have its own stiffeners, and the top and bottom edges are unconstrained. Therefore this plate is relatively weak as compared to the other vessel structures included in the analysis. The engine room plate was chosen as a response location in an attempt to investigate how a weakly coupled structure would react to different model extents (the other response locations are more strongly coupled to the ship as a whole). Additional discussion is provided in Section 3.5.

Figure 13: Regions of Interest in Model Extents Study

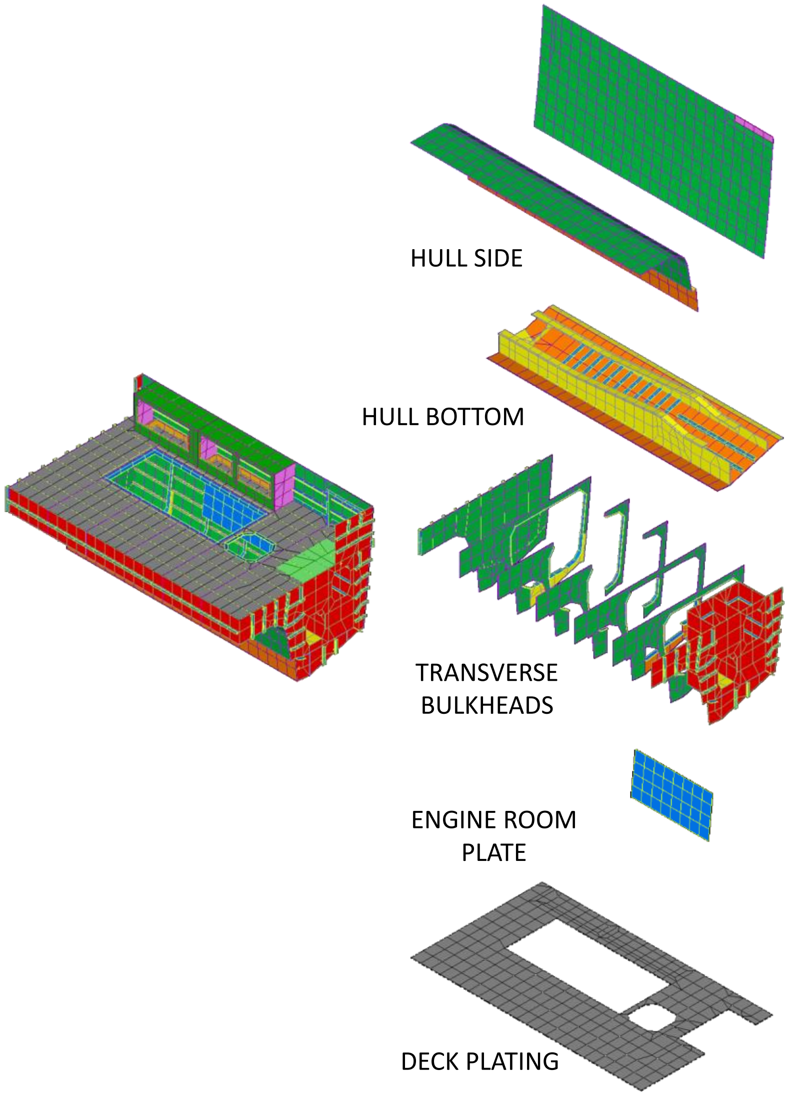

2.6 Boundary Conditions

A related aspect to truncating a model is determining appropriate boundary conditions to apply at the model termination. Conventionally, boundary conditions are limited to 'free' (no constraints on any degree of freedom), pinned (all translations are constrained), and fixed (all degrees of freedom are constrained). These constraints can be applied to multiple nodes, and combinations of these constraints can also be applied to simulate symmetry and other boundary conditions.

Boundary constraints can also be made up of more complex 'impedance' conditions which attempt to apply a more realistic model termination (which may be frequency dependent). For these constraints the edges of a model are not completely free to move nor are they completely constrained; the intention is to mimic a continuation of the structure beyond what is actually modeled.

Investigations performed as part of this analysis have been limited to uniformly applied, conventional free, pinned, and fixed boundary conditions. This is due in large part to the ease with which these conditions can be applied to the model using commercial FEA software, taking into consideration likely approaches that would be used by an analyst during the design phase of a vessel. It is noted that Reference [10] discourages the use of symmetry boundary conditions for vibration analyses. The application of symmetry boundary conditions will neglect asymmetric modes, and at a minimum would require separate analyses with symmetric and asymmetric boundary conditions. Careful combination of such results would need to be performed if an analysis was done in this way.

More sophisticated approaches such as Frequency Based Sub-structuring (FBS), also known as impedance or hybrid modeling, are available in many commercial FEA software packages. Realistic boundary conditions at the edges of a sub-model are complex and frequency dependent. FBS is a structural dynamic modeling technique which can be utilized to replicate the dynamic boundary condition imparted by an un-modeled structure [11 - 13].

FBS has a distinct advantage over other structural dynamic modeling techniques in that it can use measured FRF's to describe component structures and thereby avoid errors in the modal parameter estimation process or errors due to modal truncation. However, when measurements of a component structure cannot be made, as is the case with new ship construction, FRF's must be synthesized from an FE model or some other analytical model. Generally, this would require the user to completely model the removed structure first and then perform operations to compact that model section into an effective boundary condition. Therefore, time savings are not likely to be achieved in the model development phase. This approach can be useful if multiple iterations of a model section are needed to determine appropriate solutions to a vibration problem, if a significant refinement of a certain area in a model is required, or if the model would be too large to otherwise solve. Although these are potentially beneficial applications of FBS, this approach has not been investigated here in favor of investigating methods of reducing the up-front modeling time that is required.

For this analysis, the same models discussed in Section 2.5 and shown in Table 4 and Figure 11 were used, along with the same port engine foundation excitation point. The vibration response as a function of frequency at this location was compared for the various models and boundary conditions.

2.7 Damping

Damping is an important factor in any vibration analysis. The response magnitude is directly related to the degree of damping when excitation occurs at any resonance frequency.

For a simple, single degree of freedom system (spring-mass-damper) where the mass is directly forced, the response of the mass can be characterized using the following equation

$$\frac{Xk}{F_o} = \frac{1}{1 - \left(\frac{\omega}{\omega_n}\right)^2 + i2\zeta\left(\frac{\omega}{\omega_n}\right)} \tag{1}$$

where ω is the angular frequency of the force in radians per second (frequency in Hz times 2π), ω_n is the natural frequency of the system, ζ is the 'damping ratio' or 'damping factor', i is the square root of negative 1 (imaginary constant), k is the spring stiffness, F_o is the force, and X is the displacement. At a resonance, $\omega = \omega_n$ and the first term in the denominator vanishes. This leaves the second term which is completely controlled by the damping.

This equation can be extended to multi-degree of freedom systems, where the response at a given point is the summation of the modal responses at that point from a given input. However, the basic concept remains, where if the excitation frequency matches a particular mode the damping will play a critical role in the response of the structure.

It is noted that the above equation uses a viscous damping model. Other models are also possible. For example, at a resonance the factor 2ζ can be replaced by the "loss factor", η, for a lightly damped system[4]. This would be the approach used for a 'structural damping' model, and is the approach used throughout this report. In the frequency domain these are roughly equivalent, though formally they have different physical meanings. Additional details can be found in Reference [4]. This nuance is mentioned here because different commercial FEA software may require the input of one or the other form of damping, or sometimes both. Care must be used when assigning damping.

It is important to recognize that multiple damping mechanisms may be at work for any given ship structure or for the vessel as a whole. The modeling process requires that these mechanisms be simplified for the purpose of analysis. In this analysis, an 'equivalent' damping is assumed to exist, which may encompass multiple damping phenomena.

Discussions of measured damping values of ship structures are provided in Part II of this report. However, as part of the Phase I effort a preliminary investigation has been performed to illustrate the effects of different damping values. The predicted vibration levels for multiple force and response location sets have been studied for loss factors ranging from 0.003 (light damping) to 0.1 (heavily damped). These results are compared across the entire analysis frequency range. The 'minimum mesh density' model discussed in Section 2.2 has been used for this analysis.

2.8 Masses and Structural Simplifications

Ships are complex structures that often have a multitude of concentrated and distributed masses that are strongly and weakly coupled to the structure. For example, all ships will have varying amounts of auxiliary machinery, stationary masses such as cargo and deck equipment, piping, and outfitting, some or all of which may or may not have an influence on the vibration response at a given location. It is beneficial to know what types of masses are important for the purposes of modeling and obtaining accurate results and which can be ignored for the sake of modeling speed.

For this investigation the 'minimum mesh density' model discussed in Section 2.2 has been used and modified to create additional models with various additional structures and masses. These include:

[4] Formally, the term $2\zeta(\omega/\omega_0)$ in Eq. (1) is replaced by the loss factor, η, in this case.

- Addition of doors and windows to the superstructure
- Addition of removable deck plating from the Main Deck
- Addition of a small mass (ship's anchor)
- Addition of a large mass (A-Frame)
- Addition of fluids in tanks

Details of the discrete masses and tank masses added to the model are provided in Table 5.

Table 5: Details of Additional Masses

Item Description	Weight (lb)	Mass (slugs)	Center of Gravity Relative to Frame 0, baseline (inches)		
			Longitude	Vertical	Transverse
Anchor	304	0.787	542.38	123.92	0
Port Fuel Tank	443	2.295	294.05	46.34	83.5
Stbd Fuel Tank	443	2.295	294.05	46.34	-83.6
A-Frame	2201	5.702	10.00	138.60	0

As is the case with other aspects of finite element modeling, including these items in a model can be done in many different ways, from explicit solid element modeling to the inclusion of simple masses.

Windows, doors, and removable deck plating were implemented by adding plate elements with appropriate material and thickness properties to the model. It is noted that the nodes of these additional structures were merged with the nodes of the base structure, creating a perfect 'weld' of the adjacent items within the model. This is not always the case; for example, rubber gaskets may be implemented at the attachment points of windows. In such cases there may be some frequency where decoupling occurs and the added mass and stiffness of the window would become smaller or negligible. However, it is currently assumed as a worst case that the gaskets would be sufficiently stiff so that the implemented modeling approach would be approximately valid within the analysis frequency range.

Discrete mass items were added using rigid elements with masses located at the approximate center-of-gravity of the modeled items.

Tank fluids were modeled using non-structural masses applied to the plating making up the tank boundaries (i.e. the mass of the fluid was smeared across the plates). The fluid mass in the tanks was equally divided across the full surface area of all tank walls for each tank.

The influence of adding these masses has been investigated. Masses and additional structures were added to the model in sequence from (approximately) lightest to heaviest to assist in the analysis process. After the addition of each item, the vibration levels from various source and receiver locations were calculated and compared to estimate the impact of the modifications.

2.9 Joiner and Deck Coverings

A similar analysis was performed to assess the influence of joiner panels and deck coverings. The 'minimum mesh density' model discussed in Section 2.2 has been used for these analyses. The model was modified by adding non-structural mass to selected areas of the model. Pertinent details of the additional non-structural mass added to the model are provided in Table 6. The area density used for joiner and deck coverings are believed to be typical; note that the modeled deck covering was roughly 1" of a lightweight marine leveling compound.

For comparison, the area density of the joiner and deck coating are provided in addition to the area density of both a bare aluminum and steel 5/32" plate. Clearly, the relative addition of mass for aluminum is greater than for steel. Therefore, it is expected that the addition of joiner panels and deck coatings would have a greater impact when added to an aluminum structure compared to a steel structure due to the difference in material density. Because of this expected effect, comparisons were made for the same base model discussed previously (all aluminum) as well as for the same model but with the added mass changed to reflect the mass ratios for steel shown in Table 6.

Table 6: Details of Additional Non-Structural Mass

	Area Density				**Total Area in Model**	**Total Weight in Model**
	kg/m^2	**slinch/in^2**	**Ratio to Aluminum**	**Ratio to Steel**	**in^2**	**lb**
5/32" Bare Aluminum Plate	*10.8*	*3.97E-05*				
5/32" Bare Steel Plate	*31.1*	*1.15E-04*				
Joiner Panels	15	5.53E-05	1.4	0.5	44,284	945
Decks Coatings	25	9.21E-05	2.3	0.8	49,798	1,771

Deck covering non-structural mass was added to the Main Deck in the Pilothouse and the top wheelhouse deck, shown in Figure 14. Note that the top wheelhouse deck is not a location that is typically coated, but it was included in this study because deck spaces were limited on this particular vessel. Joiner non-structural mass was added to the bulkheads of the superstructure (i.e. Pilothouse), shown in Figure 15.

Figure 14: Decks with Additional Non-Structural Mass
(Pilothouse Deck shown at left, Wheelhouse Deck shown at right)

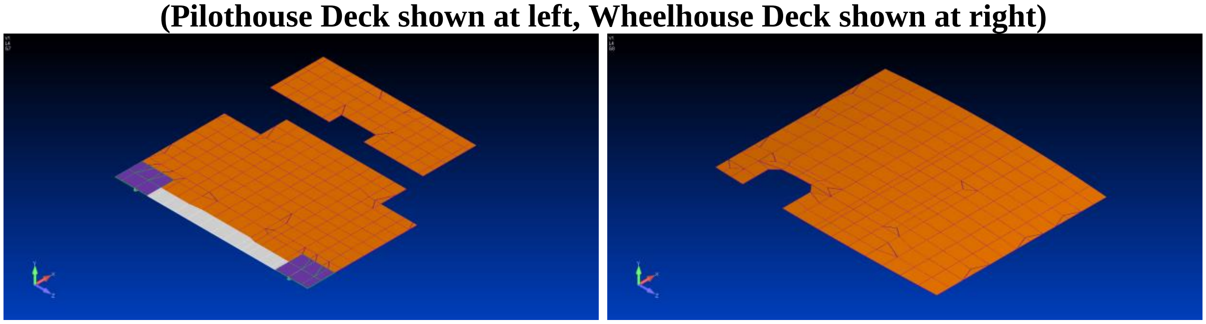

Figure 15: Superstructure Bulkheads with Additional Non-Structural Mass

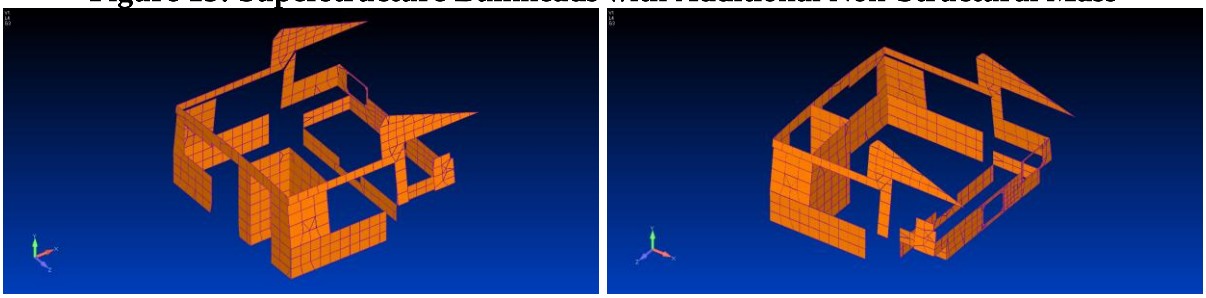

It is should be noted that non-structural mass does not change the stiffness of a given element. Likewise, non-structural mass is a perfectly coupled mass across all frequencies, though in reality joiner panels may not be coupled at higher frequencies. The exact frequency range at which the joiner panel becomes de-coupled from the bulkhead depends on several factors, with a major factor being the spacing between the joiner and the structure. Since this analysis is a sensitivity study, this aspect was neglected during modeling but is discussed further with the analysis results.

2.10 Notes on Analysis

The amount of data generated from these models is quite large. For these analyses, many results have been generated and inspected on a general level, and then specific examples showing seemingly 'typical' and worst case results have been selected for further analysis and presentation in this report.

Comparisons of frequency response between two models can be performed in several different ways. As one example, take the curves shown in Figure 16 which can be assumed to be a comparison of the response predicted from various models at a given point. If the blue curve is taken to be the correct curve, then the difference in vibration amplitude between the blue and black curves *at the frequency of the blue curve peak* is very large. However, if the maximum level across a frequency range that encompasses both the blue and black curves is used, then the error is much smaller. The seemingly large error that occurs if the single frequency comparison is used is simply a result of a shift in predicted peak frequency for the black curve.

Note that the red curve is a better approximation of the blue curve, so if the same 'maximum response' approach is used then the analysis frequency range over which the maximum level is taken could be reduced for the model used to produce the red curve as compared to the black curve.

Figure 16: Example Difference in Spectra

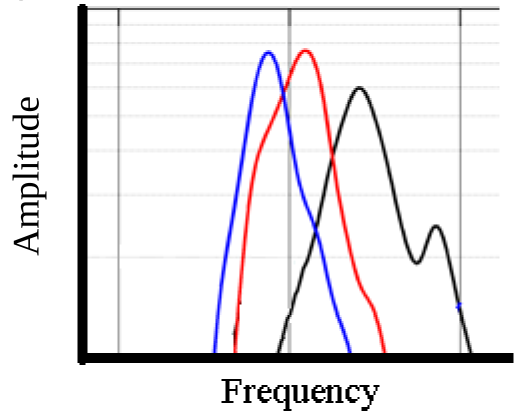

It is not reasonable to expect that any model will be able to achieve 100% accuracy, and frequency (and amplitude) shifts will occur within any model, particularly when simplifications are implemented. Due to the nature of vibration response, large response peaks similar to those seen in Figure 16 are to be expected, and some account must be taken for the phenomenon described above.

In this report, errors in both frequency and response magnitude are discussed. However, reported errors in magnitude are determined by calculating ratios of peak response magnitude either for a frequency range or for modes of similar mode shape.

It is suggested that a formal analysis of ship vibration should also follow a similar procedure. For example, for a source excitation frequency of X, an analysis should be performed over a frequency range encompassing X plus or minus some tolerance. The tolerance to use is part of what this analysis attempts to define. The maximum predicted response level over that analysis frequency range can then be used to determine a worst case response at the excitation frequency. The actual response will depend on exactly how the real excitation frequency lines up with a given mode (or set of modes), but this approach would yield a conservative (i.e. high or worst case) estimate and would identify if remedial action is needed. Additional discussion is provided in Section 4.

3.0 RESULTS

3.1 Overview of Results

3.1.1 General Approach to Reporting Results

The results presented in this section are meant to apply to ship FEA models generally. An attempt has been made whenever possible to remove the details of the model itself and apply findings in more general terms. However, because only one model has been analyzed as part of this effort, some results may turn out to be model specific.

The vessel investigated here is relatively small when compared to other vessels that are commonly investigated for vibration using finite element methods, such as Platform Supply Vessels, ferries, tankers, military craft, and cruise ships, to name a few. This has implications on the frequencies where certain phenomena will occur.

For example, the frequencies where the 'whole body modes' occur in the vessel used for this investigation are higher than for larger ships. Whole body modes are the lowest natural frequencies of a vessel and incorporate bending and twisting motions of the entire vessel, similar to that of a beam. The mode shapes of the lowest six whole body modes for this vessel are shown in Figure 17, and occur at frequencies ranging from approximately 20-45 Hz[5,6]. Typically, larger vessels will have whole body modes in the frequency range below 5 Hz.

Figure 17: Whole Body Mode Shapes

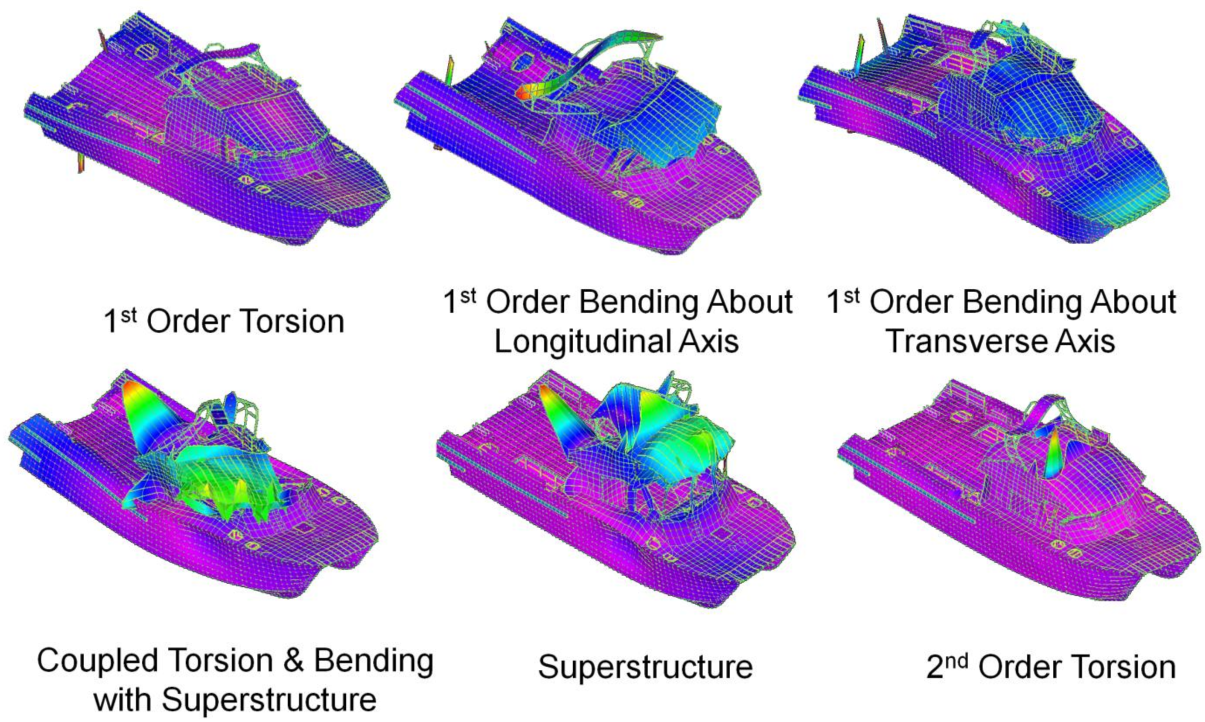

Taking these results into account, it is not desirable to make a direct correlation to frequency for results that pertain to motions of the vessel that are dominated by whole body modes. Instead, the results have been generalized to the 'whole body mode frequency range' which may be different for different vessels.

A similar effect applies to local modes of deck and bulkhead structures. Local modes are modes of vibration in which the dominant motion and vibrational energy is confined to a relatively small area or sub-structure within a larger structure. These motions are typically confined to areas of decks and bulkheads that are between other decks and bulkheads, though it is still common to have multiple areas of the vessel moving simultaneously for any given mode. Examples of local modes are provided in the response plots in subsequent sections.

---

[5] Note that this calculation does not take water loading mass effects into account. Actual whole body mode frequencies will be lower than those predicted, possibly by as much as 60%. However, this fact is not pertinent to the immediate discussion.

[6] There are a few local modes that occur in this model below the whole body modes. These involve the 'mast' structure primarily and are not considered whole body modes. However, their minor influence can be seen in some of the response plots shown in later sections.

Many of the pertinent local modes for this vessel have been calculated to occur at frequencies that may be higher than for other vessels for a given mode shape. As was discussed for whole body modes an attempt has been made to generalize the results for local modes, referring to low order and high order local modes instead of specific frequencies.

3.1.2 Modal Influence

An example is presented here to further illustrate the influence of whole body and local modes on the response of the ship structure. Figure 18 shows the average vibration response taken over the hull side plating in the Engine Room as a result of vertical forcing on the engine foundation in that same space. The model used here is the minimum mesh density, quad element model discussed in Section 2.2. The vibration response is presented in the three translational directions.

Figure 18: Velocity Response on Hull Side in the Source Room from Vertical Engine Foundation Forcing

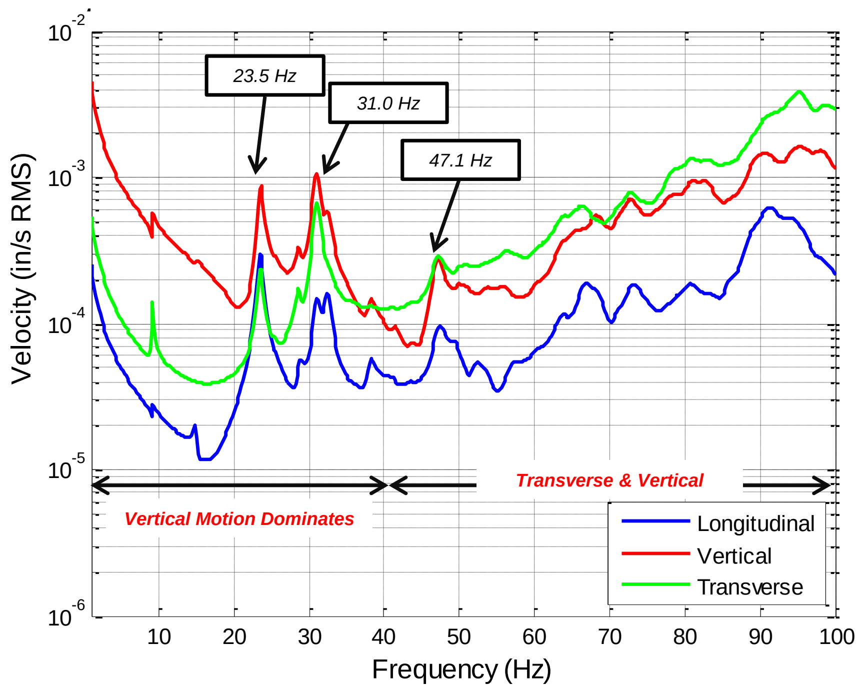

Below 50 Hz the response is dominated by three resonant peaks at 25.3 Hz, 31.0 Hz and 47.1 Hz. A modal analysis shows that these peaks correspond to four of the whole body modes shown in Figure 17: 1st order torsion, 1st order bending about the longitudinal axis, 1st order bending about the transverse axis, and 2nd order torsion. Inspection of the associated mode shapes indicates that strong excitation of these modes is likely for the location and direction of force input and these mode shapes produce significant motion at the response point; more so than, for example, the superstructure mode.

The influence of the individual whole body modes on this force/receiver combination is shown in Figure 19. The spectra of individual mode contributions are superimposed over the summation of the mode contributions and the total predicted vertical response. (See Appendix B for more information on modal summation.) Clearly the vertical response of the hull between 20 and 50 Hz is dominated by these whole body modes. There are additional minor peaks in this frequency range that add to the response at frequencies between those of the whole body modes, though these modes are more local in nature (i.e. do not encompass the entire vessel) and their resulting influence on the velocity spectrum is less prominent.

Figure 19: Modal Components of Vertical Velocity on Hull Response

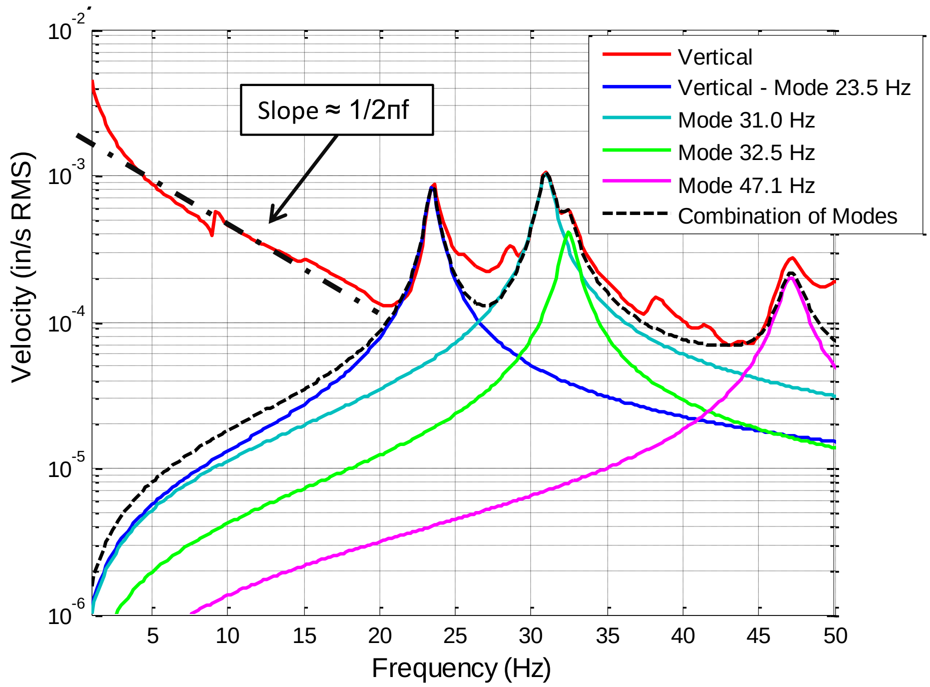

The response on the hull side at frequencies below 20 Hz is controlled by the (predicted) rigid body motion of the entire ship[7]. The prominence of the rigid body modes in the analytical response is an artifact of the analysis. In reality, the ship's buoyancy will provide some constraint and will lower the vibration levels in this band. The use of "buoyancy springs" to modify the low frequency response of the ship could be used, as discussed in Reference [8], though this has not been investigated further here.

Above 50 Hz, the response on the hull side increases with increasing frequency, up to a frequency near 95 Hz. It will be shown in Section 3.5 that the response above 95 Hz is controlled in large part from a local mode that occurs at this frequency and involves motion of the hull side in the Engine Room. However, the vessel as a whole is modally dense in this frequency range, creating the smaller peaks and dips in response above 50 Hz. In general, local modes that affect the vibration response at locations investigated for this study will control the vibration response at frequencies above the global modes identified in Figure 17. This will be shown in more detail in the subsequent sections.

[7] There is a minor response peak and dip seen at approximately 9 Hz which corresponds to a local mode in the superstructure.

3.2 Mesh Density

Results for the mesh density study are separated into two categories: modal analysis and forced response analysis. Details of each analysis are provided below.

3.2.1 Modal Analysis Results

The results of the modal analysis are presented in Table 7, including the frequency and description of the observed global modes up to 50 Hz. This table presents the predicted 'whole body' natural frequencies of the vessel for the different mesh densities. The lower density models are compared to the highest density model since the results converge with increasing mesh density.

Table 7: Modal Analysis Results for Varying Quad Mesh Densities

	Model 03	Model 01		Model 02	
	4x Quad Mesh	Minimum Quad Mesh		2x Quad Mesh	
Mode Description	Freq. (Hz)	Freq. (Hz)	Difference w.r.t Model 03	Freq. (Hz)	Difference w.r.t Model 03
1st order torsion	22.9	23.5	3%	23.1	1%
1st order bending about longitudinal axis	29.6	31.1	5%	30.1	2%
1st order bending about transverse axis	31.7	32.5	2%	32.0	1%
Coupled torsion & bending with superstructure	33.7	35.7	6%	34.3	2%
Superstructure	35.1	38.4	10%	35.8	2%
2nd order torsion	45.0	47.2	5%	45.4	1%

All models predict the natural frequencies of these modes to within 10% of the 4x mesh model, with most frequencies being within 6% or less. As noted above, the predicted natural frequencies are seen to converge with increasing the mesh density. The natural frequencies predicted using the minimum mesh clearly show greater differences with the 4x mesh model as compared to the 2x mesh model, which has frequency variations of only 1-2%.

Increasing the mesh density is seen to uniformly decrease the frequency of the observed modes. Since the mass remains constant when varying the mesh density, this result suggests that increasing the mesh density reduces the model stiffness.

3.2.2 Forced Response Results

The forced response analysis results are presented here as velocity levels at multiple response locations resulting from different input force locations. A selection of force/response combinations from the full list of force/response couples listed in Section 2.2 are presented here for illustration purposes. Locations chosen for presentation here were biased to show the range from 'typical' to the largest differences in response between the mesh densities.

Table 8 presents the differences in frequency and velocity magnitude between the minimum quad mesh and the 4x quad mesh for the selected force/response locations. All differences are relative to the 4x mesh density model. Frequency differences are presented as a percentage and velocity response differences are presented as a ratio (i.e. higher magnitude divided by lower magnitude). The predicted spectra for selected force/response locations for all three mesh densities are presented in Figure 20- Figure 28. These figures highlight the differences in frequency, magnitude, and deflection of particular resonances of the structure at different frequencies.

Table 8: Forced Response Analysis Results for Varying Quad Mesh Densities

		Frequency, Hz			Velocity, in/s		
Force Location	**Response Location**	**Minimum Quad Mesh**	**4x Quad Mesh**	**Diff. Rel. 4x**	**Minimum Quad Mesh**	**4x Quad Mesh**	**Diff. Ratio Rel. 4x**
Aft Main Deck, Stbd	Frame 2 Bulkhead, Port (see Figure 20)	56	53	5%	3.0E-03	2.5E-03	1.2
		74	68	8%	6.0E-03	7.5E-03	1.3
		92	85	8%	1.4E-03	3.0E-03	2.1
	Mid Main Deck, Port (see Figure 21)	56	52	7%	9.0E-04	6.5E-04	1.4
		64	60	6%	1.2E-03	8.0E-04	1.5
	Top Wheelhouse Deck, Port (see Figure 22)	33	32	3%	2.5E-03	3.0E-03	1.2
		55	53	4%	2.2E-03	8.0E-04	2.8
		67	61	9%	2.0E-03	1.0E-03	2.0
		80.4	73	9%	1.2E-03	6.0E-04	2.0
		90	84	7%	5.7E-04	7.0E-04	1.2
Engine Foundation Port	Mid Main Deck, Port (see Figure 23)	31	29.4	5%	1.5E-04	1.3E-04	1.2
		38.6	35	9%	9.5E-05	1.2E-04	1.3
		78	73	6%	1.3E-03	1.8E-03	1.4
		90	85	6%	1.8E-03	2.7E-03	1.5
	Frame 8 Bulkhead Above Deck, Port (see Figure 24)	39	35	10%	2.4E-04	3.2E-04	1.3
		55	52	5%	4.9E-03	4.8E-03	1.0
		73	67	8%	9.0E-03	4.0E-03	2.3
		84	82	2%	5.0E-03	4.5E-03	1.1
	Top Wheelhouse Deck, Stbd (see Figure 25)	64	62	3%	6.0E-04	1.2E-03	2.0
		94	88	6%	2.6E-03	5.0E-03	1.9
	Main Deck Pilothouse, Stbd (see Figure 26)	65	64	2%	1.2E-03	2.0E-03	1.7
		91	85	7%	2.0E-03	3.1E-03	1.6
		97	92	5%	3.0E-03	1.1E-03	2.7
	Forward Main Deck, Port (see Figure 27)	47	45	4%	9.5E-04	8.5E-04	1.1
		56	53	5%	5.0E-04	8.0E-04	1.6
		66	62	6%	8.5E-04	1.2E-03	1.4
		95	88	7%	9.0E-03	5.5E-03	1.6
Frame 2 Bulkhead, Port	Outboard Hull, Port (see Figure 28)	56	53	5%	6.0E-03	7.0E-03	1.2
		78	69	12%	3.1E-02	2.8E-02	1.1
		92	84	9%	1.3E-02	6.0E-03	2.2

Inspection of Table 8 indicates that the predicted resonance frequencies in the 4x quad mesh are lower than those predicted by the minimum density mesh by as much as 12%, though lesser differences are seen in many cases.

The difference in response magnitude between the minimum mesh density model and the 4x mesh density model (taken at the frequency of the peak response for each model and not at the same frequency across all models) shows that within the frequency range of the first several whole body modes (approximately 20-45 Hz for this vessel) there are small differences in the velocity response magnitudes between the different mesh densities, on the order of 1.3x or less. However, at higher frequencies the velocity magnitude can vary quite a bit, and in extreme cases is off by a factor of 2 or more.

Inspection of the predicted spectral responses provides some additional insight into these differences. Again, there is generally good agreement in the lower, whole body mode frequency range. In the frequency range corresponding to the lowest order local modes, such as the mode seen in the upper left graph of Figure 20, there is reasonable agreement in the magnitude of the response. Differences in response magnitude between models are typically less than a factor of 2 in this range, though there are some notable exceptions (see Figure 22, 52-53 Hz). The differences at higher frequencies tend to be larger, and in some cases the response differs by a factor of nearly 3, though there is still good correlation among some modes.

Figure 20: Quad Mesh Comparison, Forced Response at Mid Main Deck Port from Input Force at Aft Main Deck Stbd

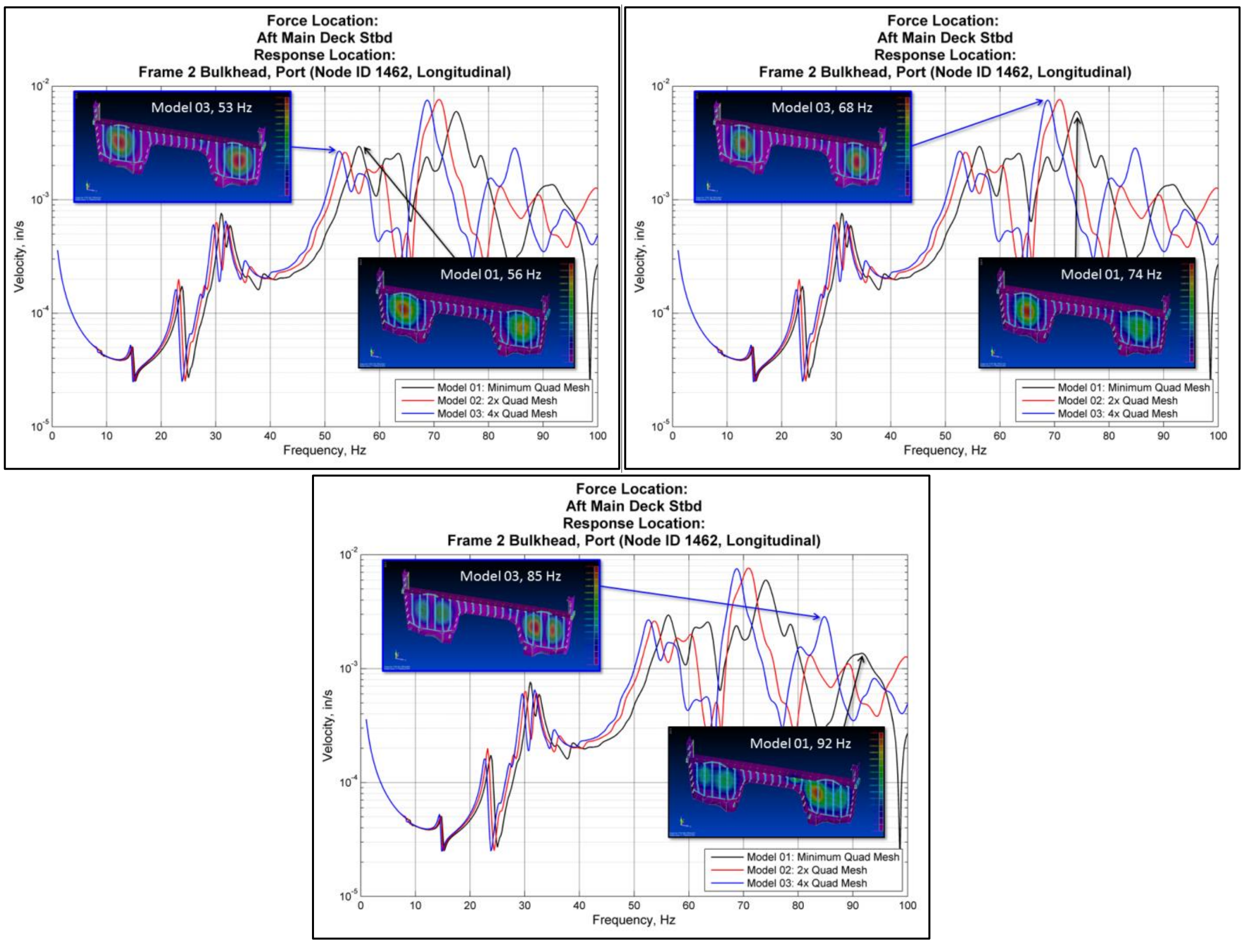

Figure 21: Quad Mesh Comparison, Forced Response at Mid Main Deck Port from Input Force at Aft Main Deck Stbd

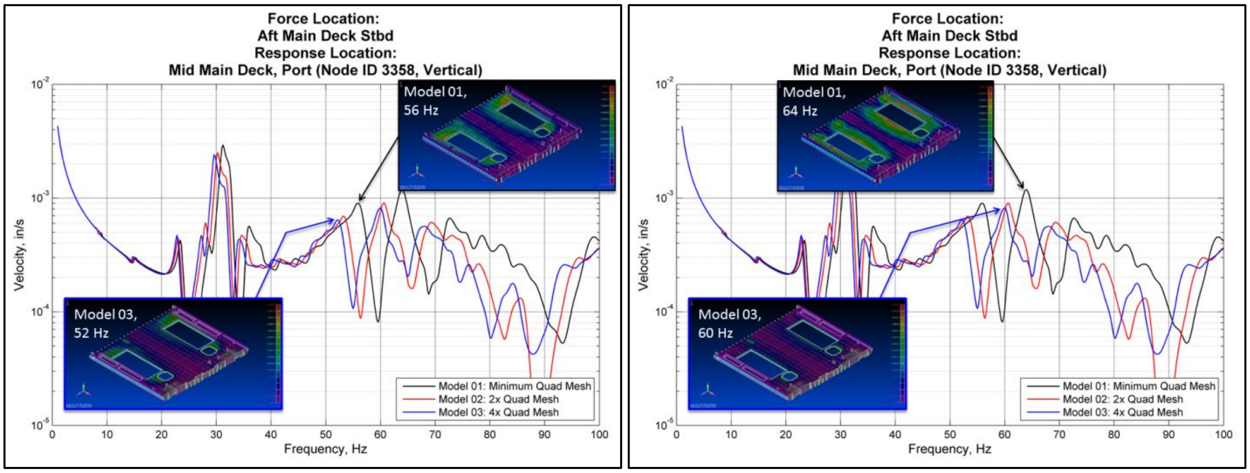

Figure 22: Quad Mesh Comparison, Forced Response at Top Wheelhouse Deck Port from Input Force at Aft Main Deck Stbd

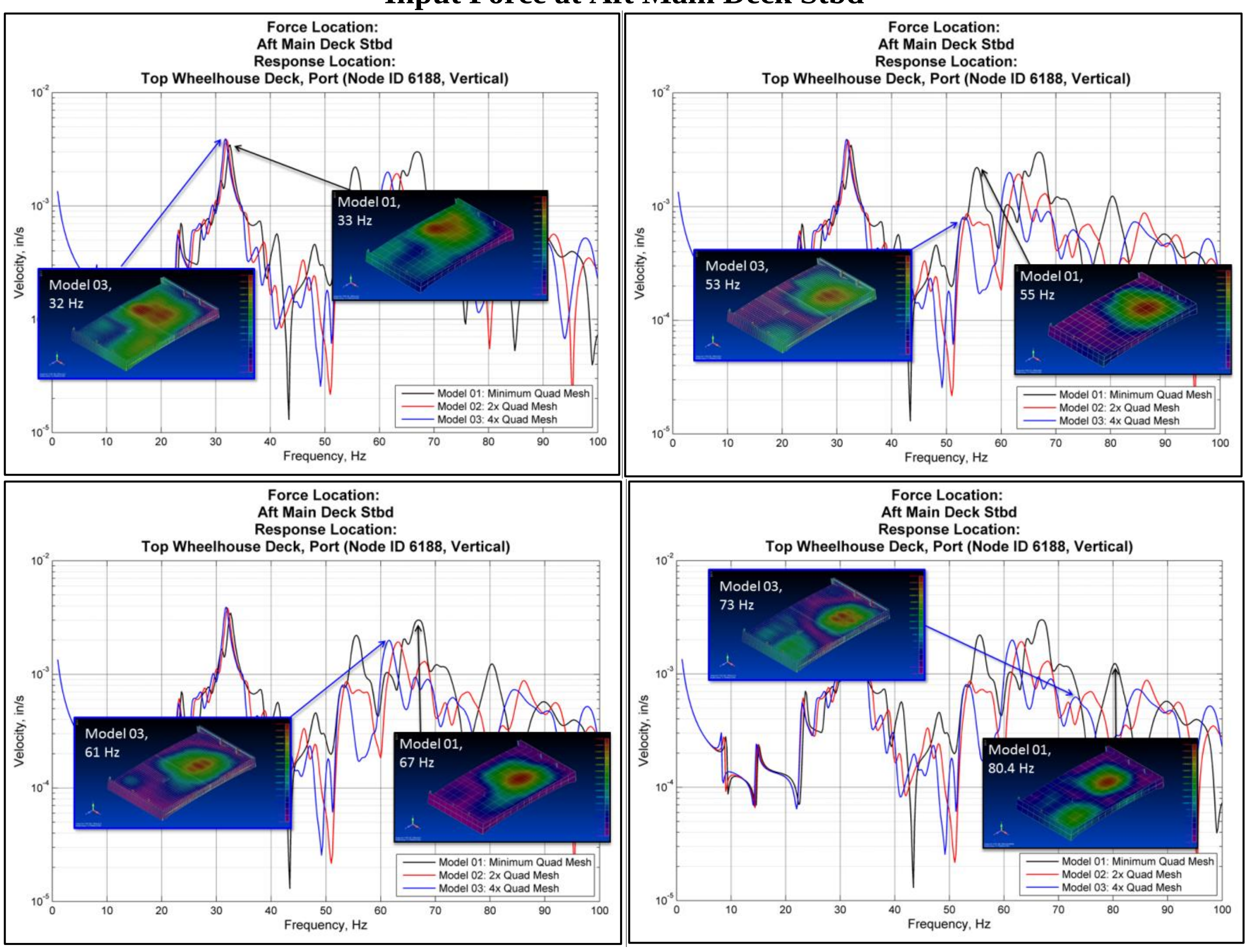

Figure 23: Quad Mesh Comparison, Forced Response at Mid Main Deck Port from Input Force at Engine Foundation Port

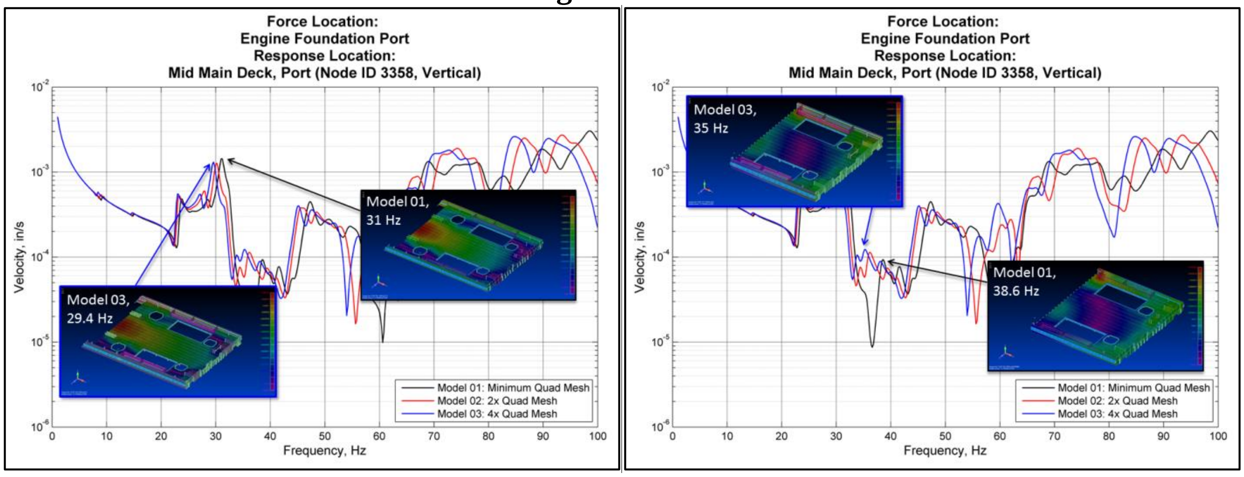

Figure 24: Quad Mesh Comparison, Forced Response at Frame 8 Bulkhead from Input Force at Engine Foundation Port

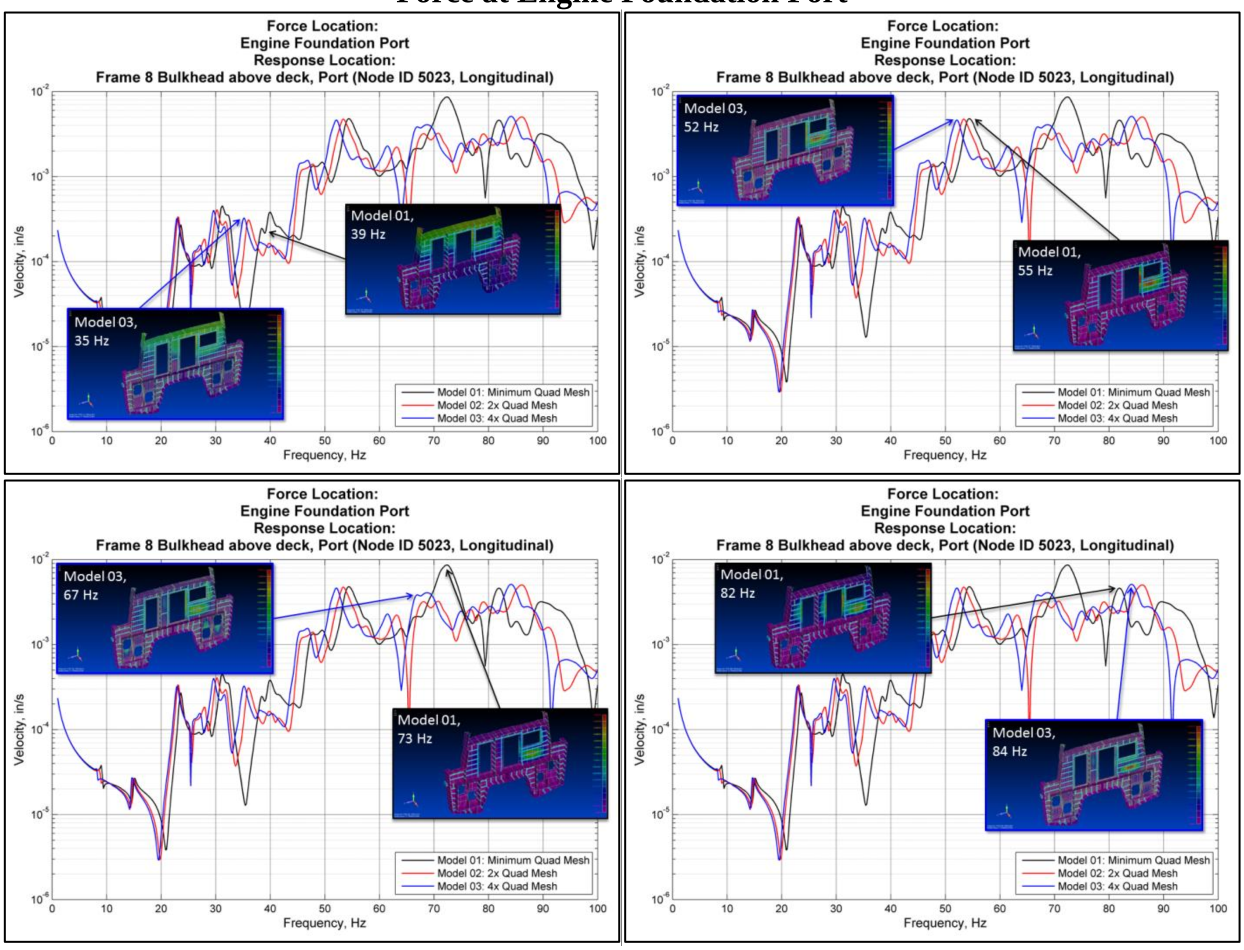

Figure 25: Quad Mesh Comparison, Forced Response at Top Wheelhouse Deck Stbd from Input Force at Engine Foundation Port

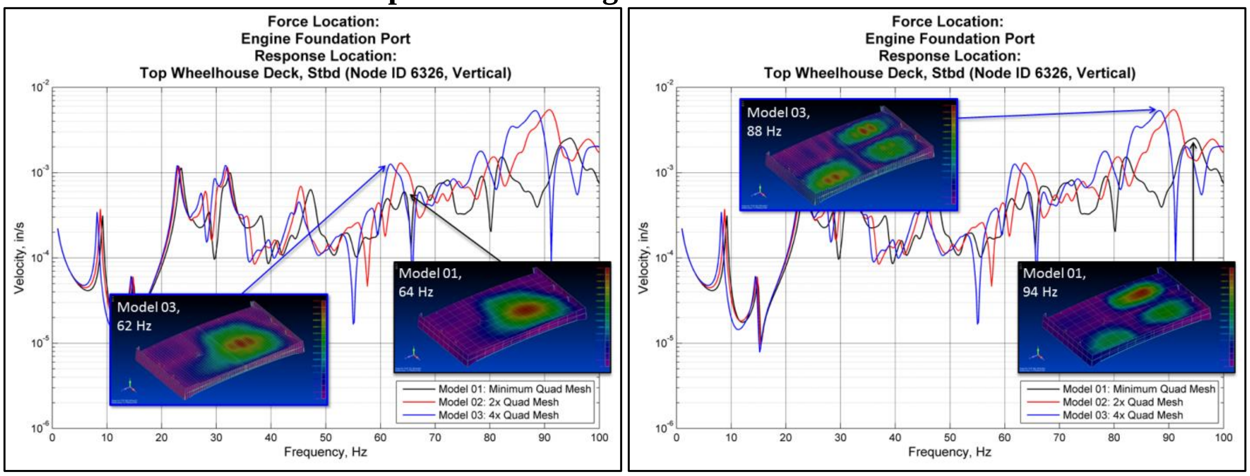

Figure 26: Quad Mesh Comparison, Forced Response at Main Deck Pilothouse Stbd from Input Force at Engine Foundation Port

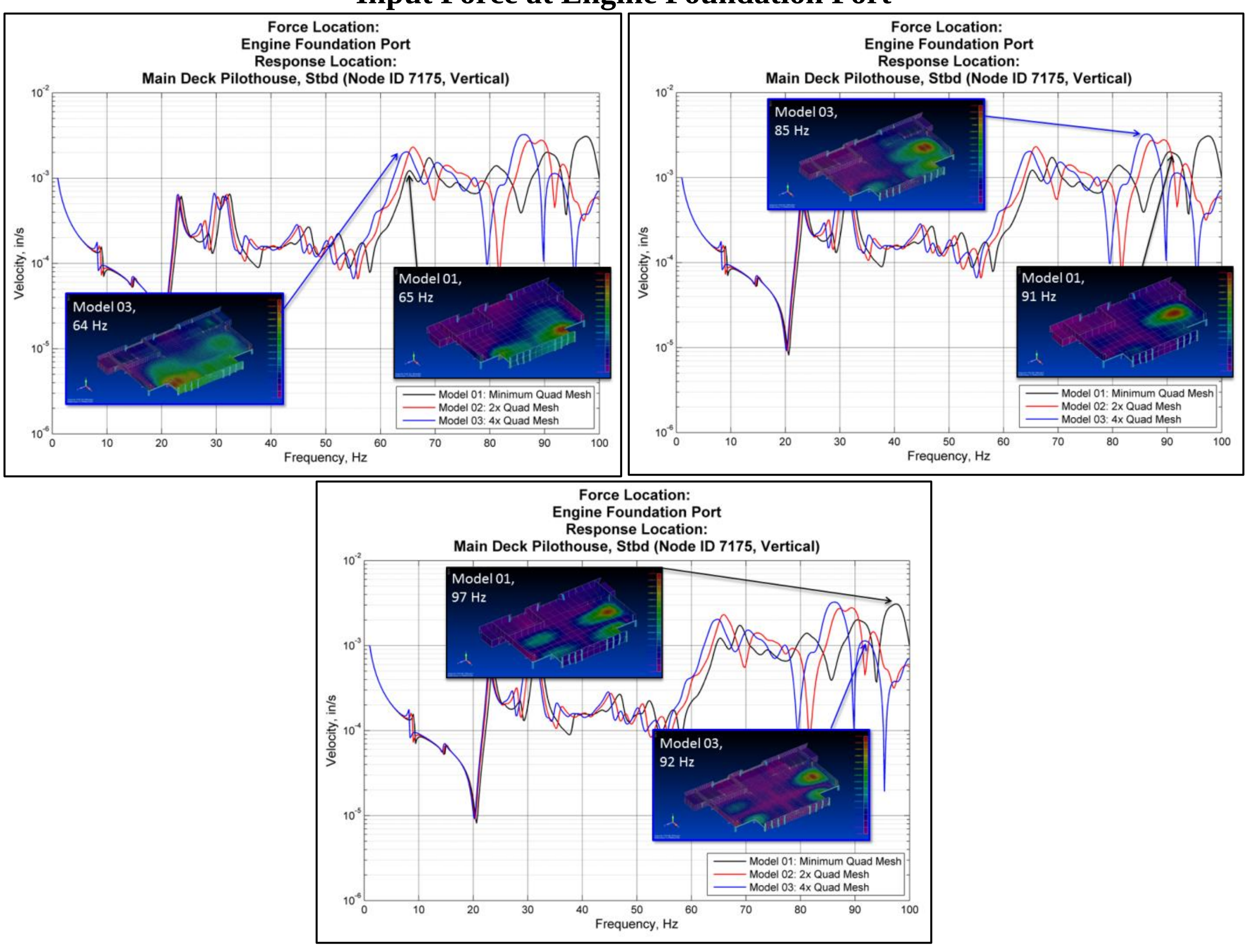

Figure 27: Quad Mesh Comparison, Forced Response at Forward Main Deck Port from Input Force at Engine Foundation Port

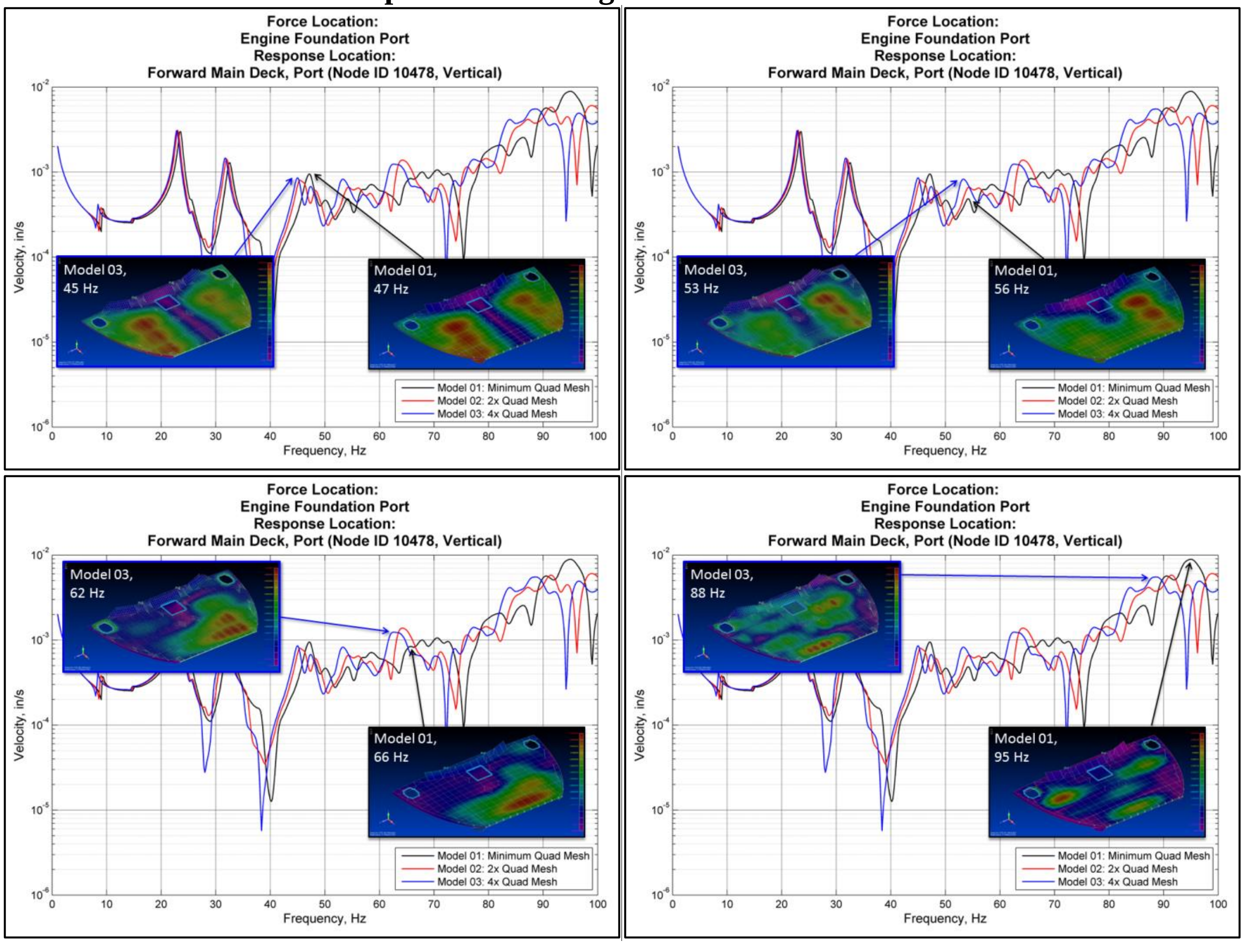

Figure 28: Quad Mesh Comparison, Forced Response at Outboard Hull Port from Input Force at Frame 2 Bulkhead Port

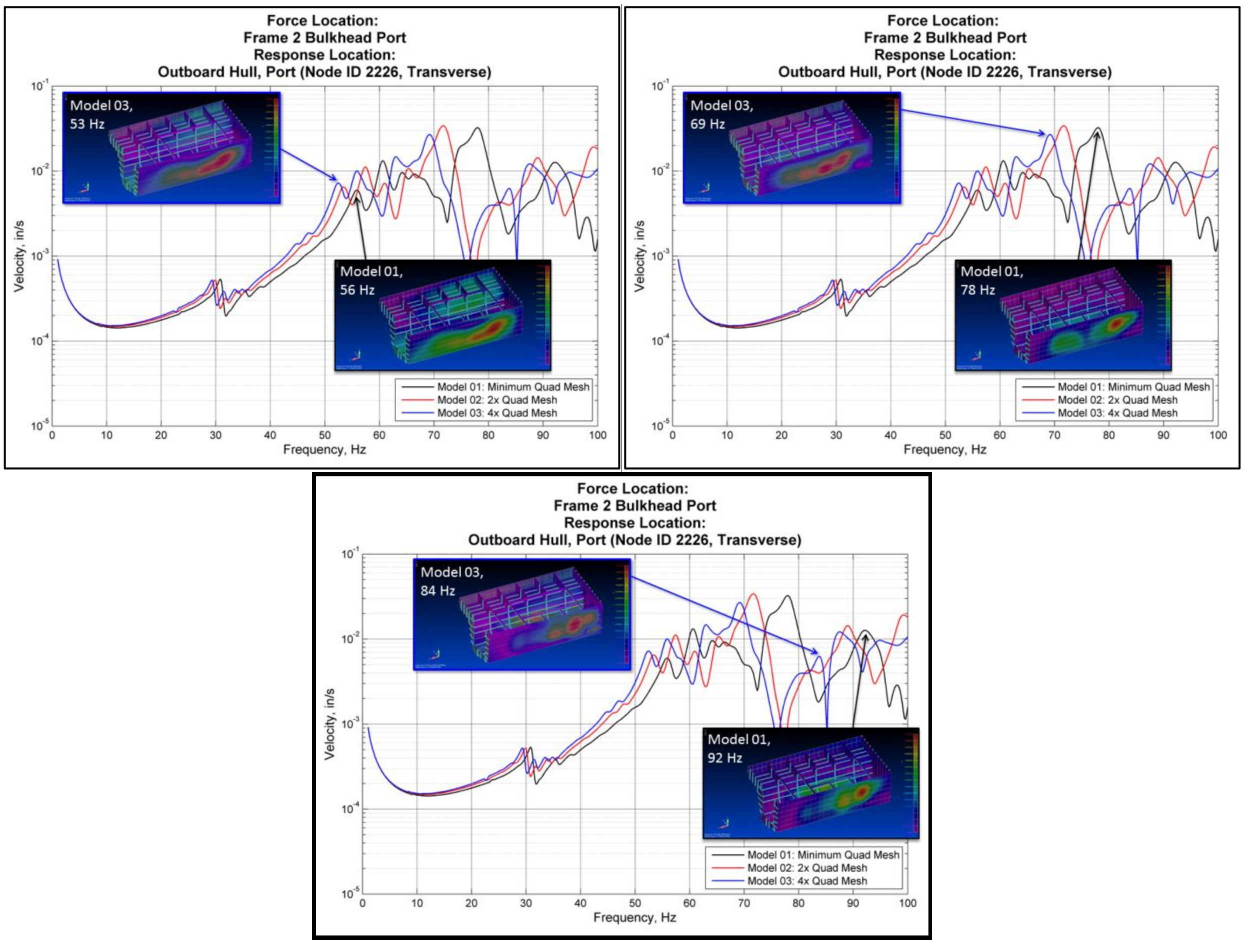

An additional example of how the response differences change with frequency is shown through a detailed inspection of Figure 20. Below 40 Hz where the whole body modes dominate the response, the agreement between models is good. In the frequency range from 50 – 75 Hz, where the response is controlled by low order mode shapes of the bulkhead itself, the response diverges somewhat between models, though the primary features can be seen in each model. Above this frequency, mode shapes can still be correlated between the models but the relative behavior of the responses becomes muddled, and the additional degrees of freedom in the refined models begin to show spectral nuances that are not captured in the reduced mesh density model.

These overall characteristics can also be seen in the other plots of response spectra from other force/receiver location pairs. Clearly, the degree of error in the higher frequency range is dependent on the specific force/receiver pair, but as a general rule this range appears to benefit the most from an increased mesh density.

Note that there does not appear to be an observable pattern as to whether the velocity magnitude increases or decreases when the mesh density is increased. Transverse bulkheads and decks that span multiple frames and are supported by girders are areas of this vessel that were seen to be the most sensitive to changes in mesh density.

The spectral responses show significantly closer agreement between the 2x and 4x meshes than the minimum density mesh and the 4x mesh. In general, the large errors seen in the minimum mesh density model in Figure 22 (55, 67, & 87 Hz), Figure 24 (73 Hz), Figure 25 (64 & 94 Hz), Figure 26 (91 & 97 Hz) and elsewhere are greatly reduced by moving to a 2x mesh density. Note that there is still a frequency shift in these peaks between the 2x and 4x models, but the magnitudes of the peak responses are very close in most cases. Some exceptions do exist though, such as for Figure 20 in the 80-90 Hz range.

3.2.3 Summary of Mesh Density Study

These results indicate that the required mesh density is dependent on the mode type and order that is required for the frequency range of interest.

- For whole body mode predictions, the minimum mesh density model predicts errors in the predicted frequency of upwards of 10% but typically 6% or less.
- Reduced mesh density models appear to only predict frequencies higher than the increased mesh density models. The predicted peak response for the minimum mesh density model is typically within a factor of 1.3 of the 4x mesh density model in the frequency range of whole body modes.
- For predictions that include the lowest order local modes of decks and bulkheads, the minimum mesh density model shows reasonable correlation in many cases, with errors in predicted frequency for specific modes being less than 10% and with errors in predicted response magnitudes typically being on the order of 2x or less when compared to the 4x mesh density model. However, in some cases errors are greater. The 2x mesh density model significantly outperforms the minimum mesh density model in this frequency range, removing nearly all areas of high error and reducing error at essentially all frequencies. Small frequency shifts at peak response frequencies is seen for the 2x model as compared to the 4x model.
- For predictions at frequencies that include higher order local modes, the minimum mesh density model diverges significantly in several cases from the 4x mesh, with errors in vibration response often on the order of a factor of 2-3. The 2x mesh again performs significantly better than the minimum mesh density model, with reduced error magnitudes and only a few cases where errors on the order of a factor of 2-3 exist.

This analysis has assumed that the higher density mesh is more accurate since the results tend to converge as mesh density is increased. This is in line with general FEA practice [3]. It will typically be more desirable to use as high of a mesh density as possible, though limitations in computer speed and memory will prevent high density meshes from being used on full ship models that are larger than the vessel modeled here.

For reference, Table 9 provides the number of degrees of freedom for each of the three mesh density models, along with a normalized analysis time to solve for the response at all frequencies. Also presented is a 'time per DOF'. The absolute time required to solve any model will be dependent on the specific of the computer being used, and is not the subject of this study.

However, it can clearly be seen that as the number of DOFs increases, not only does the total analysis time increase but the rate of solution (time per DOF) increases as well.

Table 9: Comparison of Analysis Times for Mesh Density Models

Model	# DOF	Normalized Analysis Time	Normalized Time per DOF ($x10^{-5}$)
Minimum Mesh Density	67,806	1	1.5
2x Mesh Density	275,604 (4.06x Min. Mesh Density)	4.9	1.8
4x Mesh Density	1,108,878 (16.35x Min. Mesh Density)	28.3	2.6

3.3 Plate Element Type

Before introducing the results of this analysis, it should be clarified that the "quad" mesh models contain some 3-noded tri elements. At the minimum mesh density there are 10966 quad elements and 1273 tri elements (approximately 10% of all plate elements). In practical models tri elements are unavoidable. The 'tri mesh' models are exclusively tri elements (not including beam stiffeners).

3.3.1 Modal Analysis Results

Table 10 presents a comparison of the predicted natural frequencies for whole body modes for the minimum and 2x tri and quad meshes. At the same mesh density, the difference in frequency between an all-quad mesh and an all-tri mesh is no greater than 1%. Clearly, differences between mesh densities are similar if not identical to those discussed in Section 3.2.

Table 10: Modal Analysis Results for Varying Plate Element Type

	Model 01	Model 04		Model 02	Model 05	
	Minimum Quad Mesh	Minimum Tri Mesh		2x Quad Mesh	2x Tri Mesh	
Mode Description	Freq. (Hz)	Freq. (Hz)	Difference w.r.t Model 01	Freq. (Hz)	Freq. (Hz)	Difference w.r.t Model 02
1st order torsion	23.5	23.6	0%	23.1	23.1	0%
1st order bending about longitudinal axis	31.1	31.3	1%	30.1	30.2	0%
1st order bending about transverse axis	32.5	32.4	0%	32.0	32.0	0%
Coupled torsion & bending with superstructure	35.7	35.4	1%	34.3	34.3	0%
Superstructure	38.4	37.9	1%	35.8	35.8	0%
2nd order torsion	47.2	46.9	1%	45.4	45.7	1%

3.3.2 Forced Response Analysis Results

Example forced response results for the minimum tri mesh density model compared to the minimum quad mesh model are provided in Figure 29.

Figure 29: Plate Element Type Comparison at Minimum Mesh Density, Various Forced Response Locations from Input Forces Locations at Engine Foundation and Aft Main Deck

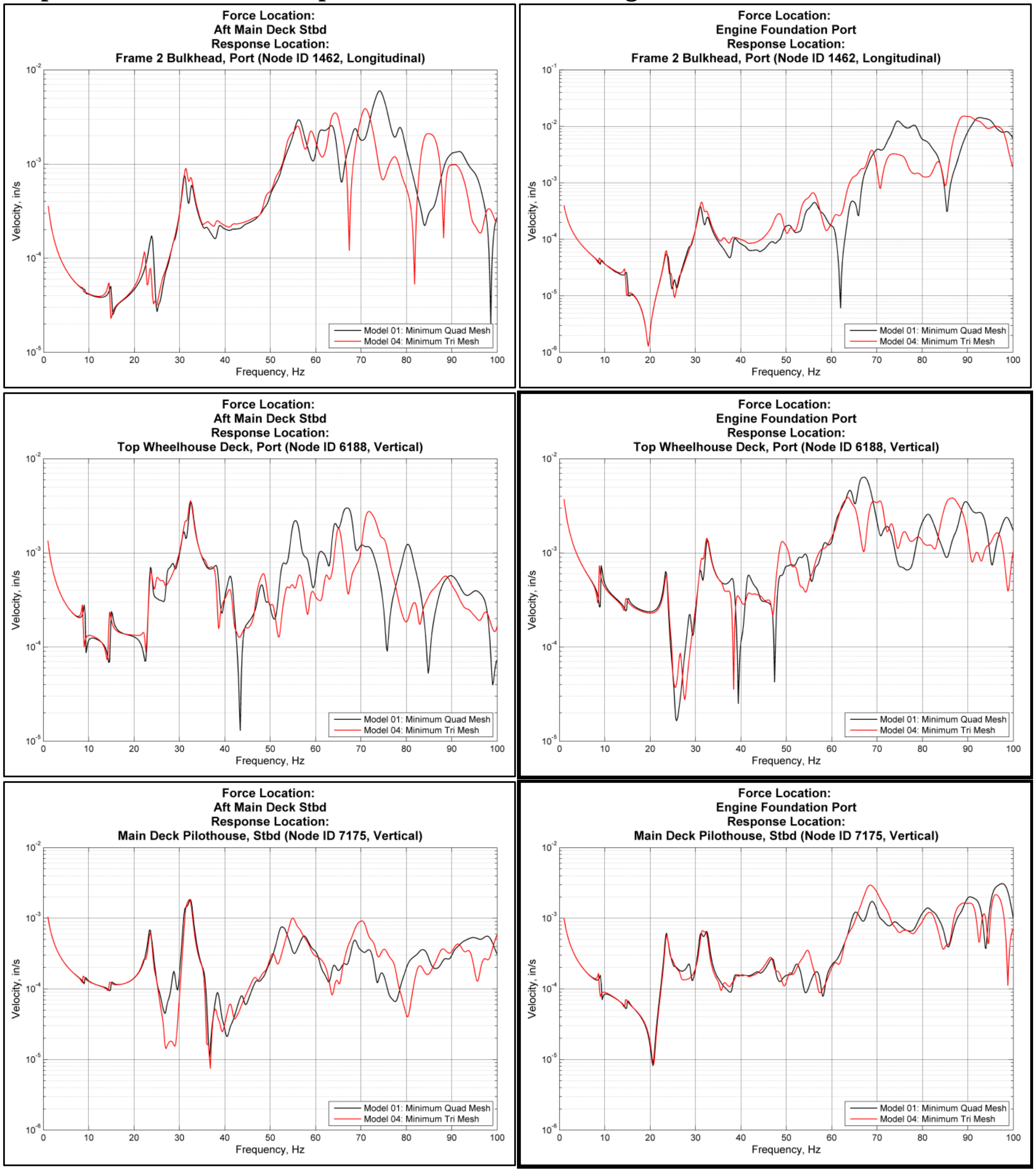

As was found with the quad mesh models, the frequency range encompassing the first several whole body modes of the vessel (i.e. 20-45 Hz) shows good agreement in the response magnitude at peak frequencies. At higher frequencies (in the range of local structural modes) some differences are present. The magnitude of these differences depends on the specific force/response location pair. For example, the bottom two plots of Figure 29 show good correlation at all frequencies, while the middle plots show the largest discrepancies. In general, the lowest order modes show the best correlation (response ratios less than 2) while higher order modes have higher differences (response ratios of 3 or more), depending on location. (Note that the 55 Hz peak in the quad mesh result at the portside Top Wheelhouse Deck from the Aft Main Deck force location can be seen in Section 4.2 to be 'erroneous', in that it does not remain at the higher mesh densities. This response peak is ignored here).

Figure 30 provides a similar comparison for the 2x tri and quad meshes. The differences in response are much less for this mesh density as compared to the minimum mesh density. Response ratios of approximately 2 are still seen for the highest order modes (frequencies above 90 Hz here) at some locations, but in general the 2x mesh is a significant improvement over the minimum mesh density.

Figure 30: Plate Element Type Comparison at 2x Mesh Density, Various Forced Response Locations from Input Forces Locations at Engine Foundation and Aft Main Deck

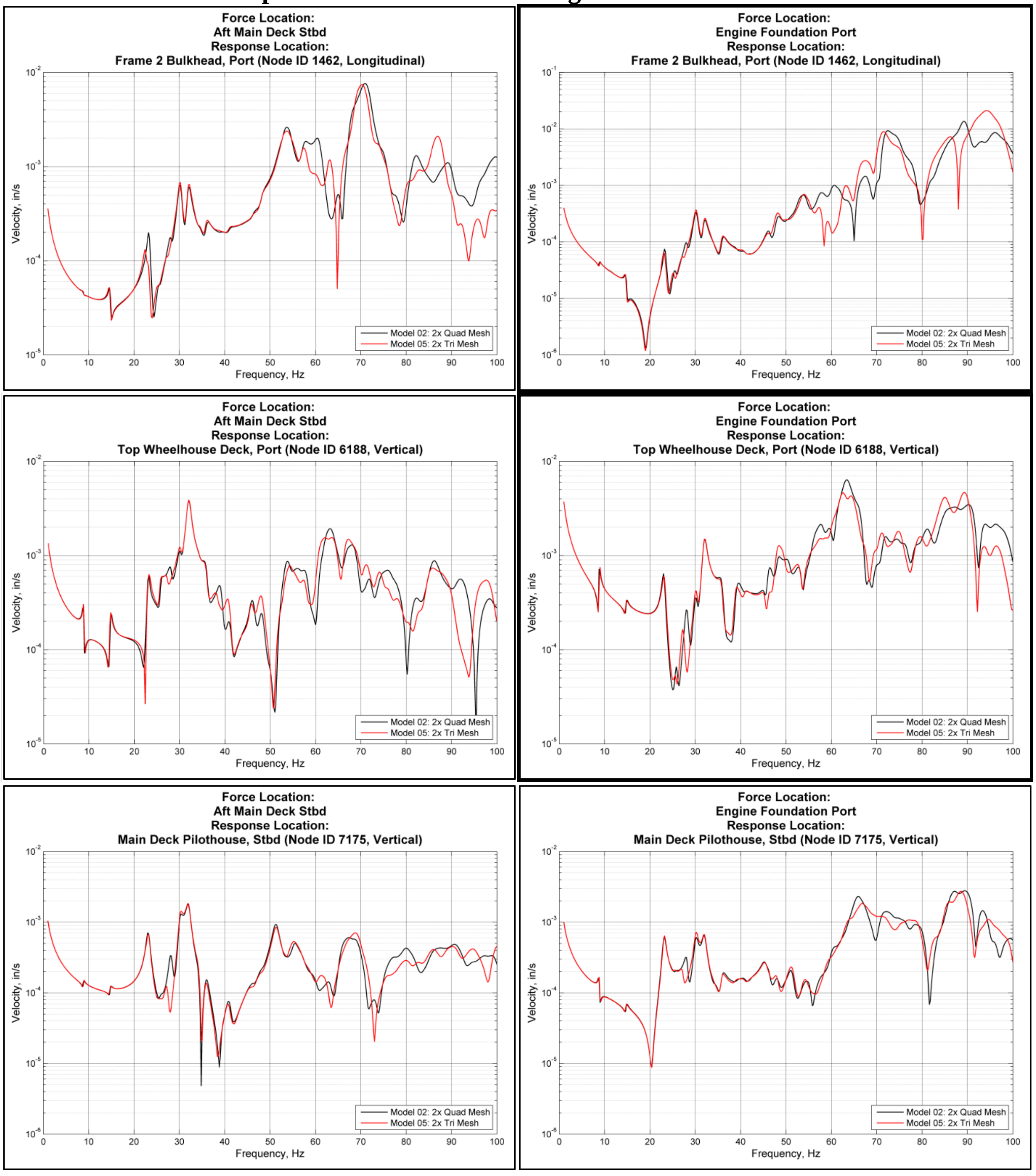

3.3.3 Summary of Plate Type Analysis

The overall similarity of results between the tri and quad mesh models is promising, in that it indicates that the occasional use of tri elements is not detrimental to model accuracy. The convergence of the results for the 2x tri mesh density model to the 2x quad mesh model indicates that when tri elements are used their size should be minimized (i.e. use a greater mesh density).

It is not expected that an entire model would be made of tri elements, and therefore the results presented here are worst case.

3.4 Stiffener Element Type

3.4.1 Cantilever Model Results

Figure 31 presents the vibration response as a function of frequency at the point of force application for the cantilever stiffener-only models described in Section 3.4. For the specific geometry that was chosen, the frequency range of 1-100 Hz covers the first three cantilever bending modes.

Figure 31: Cantilever Stiffener-Only Point Response Comparison

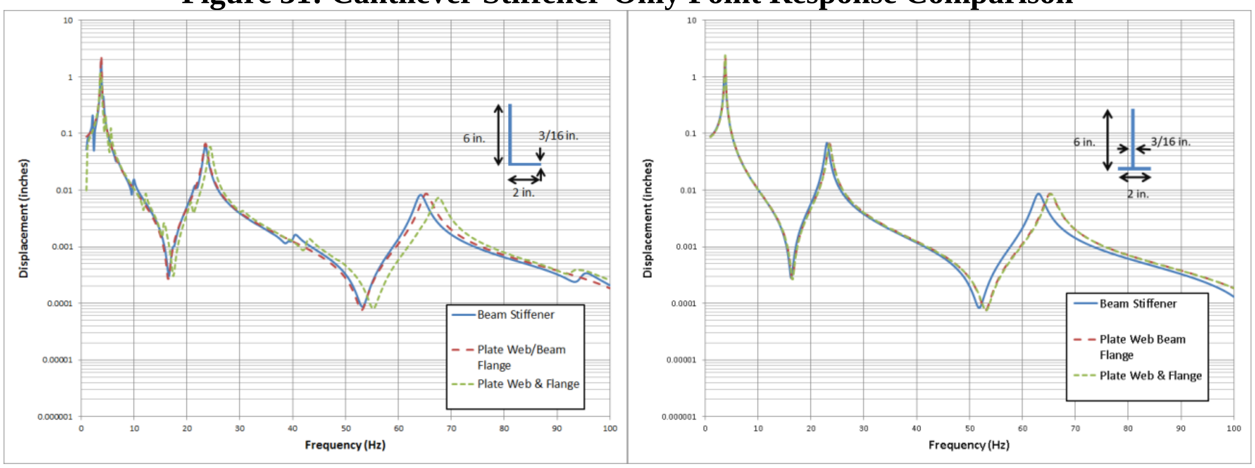

There is generally good agreement between all models with small deviations in resonant frequency, particularly at frequencies below 50 Hz. The frequency predicted for the third cantilever mode diverges by roughly 5% or less among the models, but the response magnitude at the peak remains nearly the same.

This result shows that there is a high degree of equivalency between modeling stiffeners of these types *by themselves* with beams and plates, at least for the direction of applied force. The differences between these models may be due to one or two factors, explained as follows.

First, simply modeling the web separately from the flange allows for additional motion of the stiffener, and more specifically allows for relative motion between the web and flange that is not allowed for the beam-only model. This difference may produce increasing differences as the mode order increases.

Second, beam elements in NEiNastran do not account for restraints on warping (i.e. a rotation of the beam cross section about a vertical axis, in this case). Such restraints would increase the effective stiffness of the beam, and would increase the predicted natural frequency. In the results shown above, the beam model consistently predicts natural frequencies that are lower than the other models. The plate stiffener models, by virtue of having all nodes along the web and flange constrained, also constrain warping, increasing their natural frequency. Additional information on warping constraints is provided in Appendix C. The only caveat is that the L stiffener model shows a lesser frequency shift than the T stiffener model; this would appear to be inconsistent with warping being the cause of these differences.

Figure 32 presents the vibration response as a function of frequency at the point of force application for the cantilevered stiffened plate models described in Section 3.4. It is seen that the analysis frequency range includes more modes than the stiffener-only model. The modes of this structure include shapes that are analogous to the first three cantilever modes seen for the stiffener-only model, though these mode shapes are more complex due to the added plating and stiffeners.

Figure 32: Cantilever Stiffened Plate Point Response Comparison

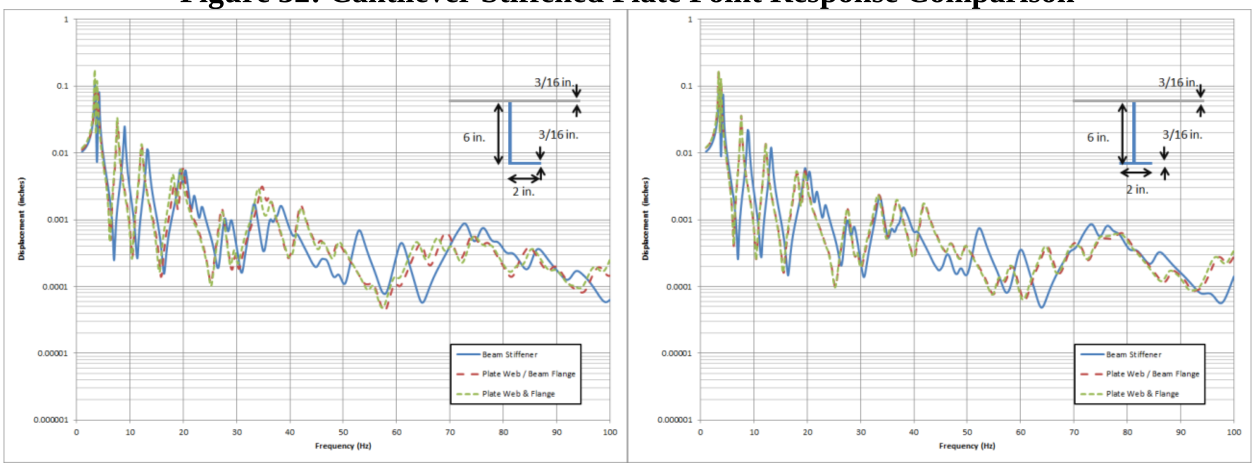

These results show a high degree of equivalency between the two models where the stiffener web is modeled as a plate. However, there are some notable differences between these models and the beam-stiffener model. At frequencies below 20 Hz (corresponding to the first four strongly excited modes of the structure) there is a shift in the predicted natural frequency on the order of 10%.

At higher frequencies there is a lower degree of correlation between specific modes, and comparisons of natural frequency are difficult. The overall spectrum shape is similar to within the same order of magnitude, though errors could result depending on the processing method used. For example, if a maximum level over the frequency range of 50-55 Hz was used, the error between models is roughly a factor of 1.7.

The reasons for these differences are likely related to the fact that a more refined model of the stiffener will provide a different, if not more accurate, representation of the response spectrum as compared to a beam element. Furthermore, although the load in these models has been applied in the vertical direction, the stiffeners do experience some degree of twisting, particularly for the stiffened plate models, and the details of the stiffener at the flange become more important.

For beam elements there is no relative flexibility between the web and flange. When twisting occurs the internal torque between the deck plating and stiffener passes through the interface node (i.e. the shared node between the plate and stiffener elements) and is subsequently transferred from the interface node to the shear center of the beam cross-section. The resulting angle of twist at the interface node is also the angle of twist of the shear center of the beam's cross-section. The internal torque applied to the stiffener webbing is governed by the physics of the entire beam cross section subject to torsion.

When the stiffener is modeled using plate elements, the dynamic internal torque is applied directly to the web only at the interface node. As a result it is the torsional rigidity of the web plate which is most significant. The flange obviously plays a role as well, though its influence occurs through the web plate and not at the interface to the deck plating.

Figure 33 depicts the differences in the internal force balance between a beam stiffener and a stiffener modeled using plate elements. In summary, the response of the stiffener due to a torque applied at the deck node will be different for the beam element, which responds with the stiffness of the full (rigid) cross section, whereas the plate models respond primarily with the web plate stiffness and the (flexible) flange playing a secondary role through the web.

Figure 33: Schematic of Internal Force Balance within Deck Stiffened FE Model

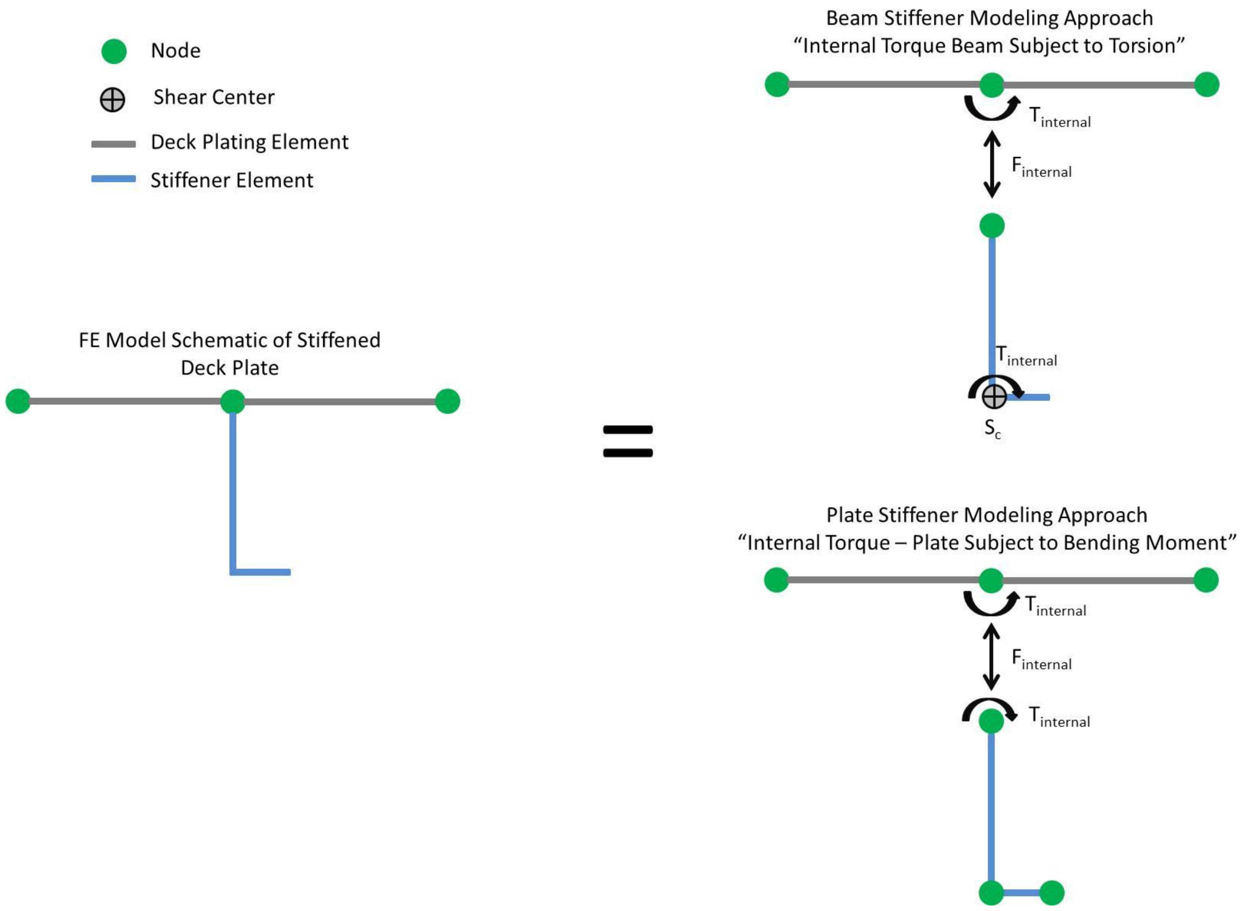

3.4.2 Full Model Results

Three different approaches for modeling stiffeners in the full model were analyzed. Table 11 provides the model names and a description of the stiffener modeling approach used for documentation purposes in this section. Stiffeners with plate webs and flanges were not investigated in this section due to their similarity with stiffeners modeled with plate webs and beam flanges discussed in the previous section.

Table 11: Description of Stiffener Element Modeling Approaches

Stiffener Element Type	Model Description
Model 01 – Plate Girders, Beam Small Stiffeners	Only small stiffeners modeled as beams – large girders and frames with web heights on the order of plate element sizes were modeled with plate webs and flange beams
Model 07 – Beam Girders, Beam Small Stiffeners	All deck and bulkhead stiffeners modeled as beams
Model 08 – Plate Girders, Plate Small Stiffeners	All stiffeners modeled using plate webs and flange beams

Table 12 presents a comparison of the natural frequencies of whole body modes predicted for the different beam models. All results are referenced to Model 01, which was chosen arbitrarily (this is the model used in most other studies discussed in Part I of this report).

Table 12: Modal Analysis Results for Varying Stiffener Element Type

	Model 01	Model 07		Model 08	
	Plate Girders, Beam Small Stiffeners	Beam Girders, Beam Small Stiffeners		Plate Girders, Plate Small Stiffeners	
Mode Description	Freq. (Hz)	Freq. (Hz)	Difference w.r.t Model 01	Freq. (Hz)	Difference w.r.t Model 01
1st order torsion	23.5	23.3	1%	23.5	0%
1st order bending about longitudinal axis	31.1	30.9	1%	31.1	0%
1st order bending about transverse axis	32.5	32.1	1%	32.4	0%
Coupled torsion & bending with superstructure	35.7	34.9	2%	35.4	1%
Superstructure	38.4	36.3	6%	37.9	1%
2nd order torsion	47.2	45.0	5%	46.1	2%

The identified whole body modes of the vessel show 6% or lower variation between the stiffener element types. Greater differences are seen between the all-beam model as compared to the all-plate model.

The results of the forced response analyses are summarized in Table 13. The results are formatted similarly to the results for the mesh density analysis (Section 4.2), such that the frequencies and response magnitudes at observed resonances are compared amongst the three stiffener modeling approaches. As was done previously, frequency differences are shown as a percentage change relative to Model 01, and response magnitude differences are shown as a ratio (i.e. higher magnitude divided by lower magnitude). Spectral response results and comparisons are also provided in Figure 34 – Figure 39.

Table 13: Forced Response Analysis Results for Stiffener Element Types

		Frequency, Hz					Velocity, in/s				
Force Location	**Response**	**Model 01**	**Model 07**	**Diff.**	**Model 08**	**Diff.**	**Model 01**	**Model 07**	**Diff. Ratio**	**Model 08**	**Diff. Ratio**
Aft Main Deck, Stbd	Frame 2 Bulkhead, Port (see Figure 34)	**30.6**	30.6	0%	30.6	0%	**7.5E-04**	5.5E-04	1.4	9.0E-04	1.2
		55	52	-5%	55	0%	**3.0E-03**	3.5E-03	1.2	3.0E-03	1.0
		74	72	-3%	64	-14%	**6.0E-03**	4.0E-03	1.5	9.0E-03	1.5
	Mid Main Deck, Port (see Figure 35)	**29**	29	0%	29	0%	**4.0E-04**	1.5E-03	3.8	3.5E-04	1.1
		56	53	-5%	55	-2%	**9.0E-04**	9.0E-04	1.0	8.0E-04	1.1
		64	60	-6%	64	0%	**1.2E-03**	1.7E-03	1.4	1.1E-03	1.1
	Top Wheelhouse Deck, Port (see Figure 36)	**23.4**	23.4	0%	23.4	0%	**3.0E-04**	5.0E-04	1.7	3.0E-04	1.0
		32	32	0%	32	0%	**3.5E-03**	6.0E-03	1.7	3.8E-03	1.1
		55	54	-2%	55	0%	**2.1E-03**	1.6E-03	1.3	2.6E-03	1.2
		67	n/a	-	71	6%	**3.0E-03**	n/a	-	2.1E-03	1.4
		81	81	0%	81	0%	**1.2E-03**	7.9E-04	1.5	4.1E-04	2.9
Engine Foundation, Port	Inboard Hull, Port (see Figure 37)	**23**	23	0%	23	0%	**1.5E-04**	1.7E-04	1.1	1.4E-04	1.1
		31	31	0%	31	0%	**1.3E-04**	3.0E-04	2.3	9.0E-05	1.4
		47	45	-4%	49	4%	**6.3E-04**	8.0E-04	1.3	4.5E-04	1.4
		66	69	5%	66	0%	**1.1E-03**	5.5E-03	5.0	1.1E-03	1.0
		96	85	-11%	95	-1%	**7.0E-03**	6.2E-03	1.1	5.5E-03	1.3
	Main Deck Pilothouse, Stbd (see Figure 38)	**29**	29	0%	29	0%	**2.2E-04**	5.0E-04	2.3	2.2E-04	1.0
		52	54	4%	54	4%	**2.2E-04**	4.0E-04	1.8	3.4E-04	1.5
		65	66	2%	68	5%	**1.3E-03**	2.2E-03	1.7	2.5E-03	1.9
		91	90	-1%	91	0%	**2.0E-03**	2.0E-03	1.0	2.6E-03	1.3
	Forward Main Deck, Port (see Figure 39)	**47**	45	-4%	49	4%	**9.5E-04**	1.0E-03	1.1	7.0E-04	1.4
		73	65	-11%	71	-3%	**9.0E-04**	2.2E-03	2.4	1.5E-03	1.7
		82	80	-2%	82	0%	**2.0E-03**	1.2E-02	6.0	2.0E-03	1.0

Inspection of Table 13 indicates that variations in frequency at the selected resonances are typically small (6% or less), though in some instances large variations can occur (upwards of 14%). In general, differences between the all-beam stiffener model and Model 01 are greater than for the all plate stiffener model, though exceptions do exist. Note that in the frequency range beyond the first several global modes it is more difficult to compare specific resonances because changing the stiffener element type leads to complex changes to the localized stiffness (this behavior was also seen for the cantilever models discussed in the previous section).

The response spectra comparisons show that there is a general similarity between Model 01 and Model 08 (large girders with plate webs & small stiffeners as beams vs. all stiffeners with plate webs), though the correlation for some force/receiver pairs is less than ideal. The best correlation between these two models is seen in Figure 35, Figure 37, Figure 38, and Figure 39. Small errors (close to a factor of 1) are seen in Figure 36 at frequencies corresponding to whole body modes and low order local resonances, but response magnitude differences on the order of a factor of 3 appear for higher order local resonances.

Figure 34 arguably shows the worst-case correlation between Model 01 and Model 08, where higher order local modes have significant differences in both frequency and response magnitude. It is interesting to note that this section of the vessel only has smaller stiffeners and therefore the modeling approach for larger girders is of reduced importance. However, even for this plot there is good correlation in the whole body mode range and for the first local resonance.

Figure 34: Stiffener Modeling Comparison, Forced Response at Frame 2 Bulkhead Port from Input Force at Aft Main Deck Stbd

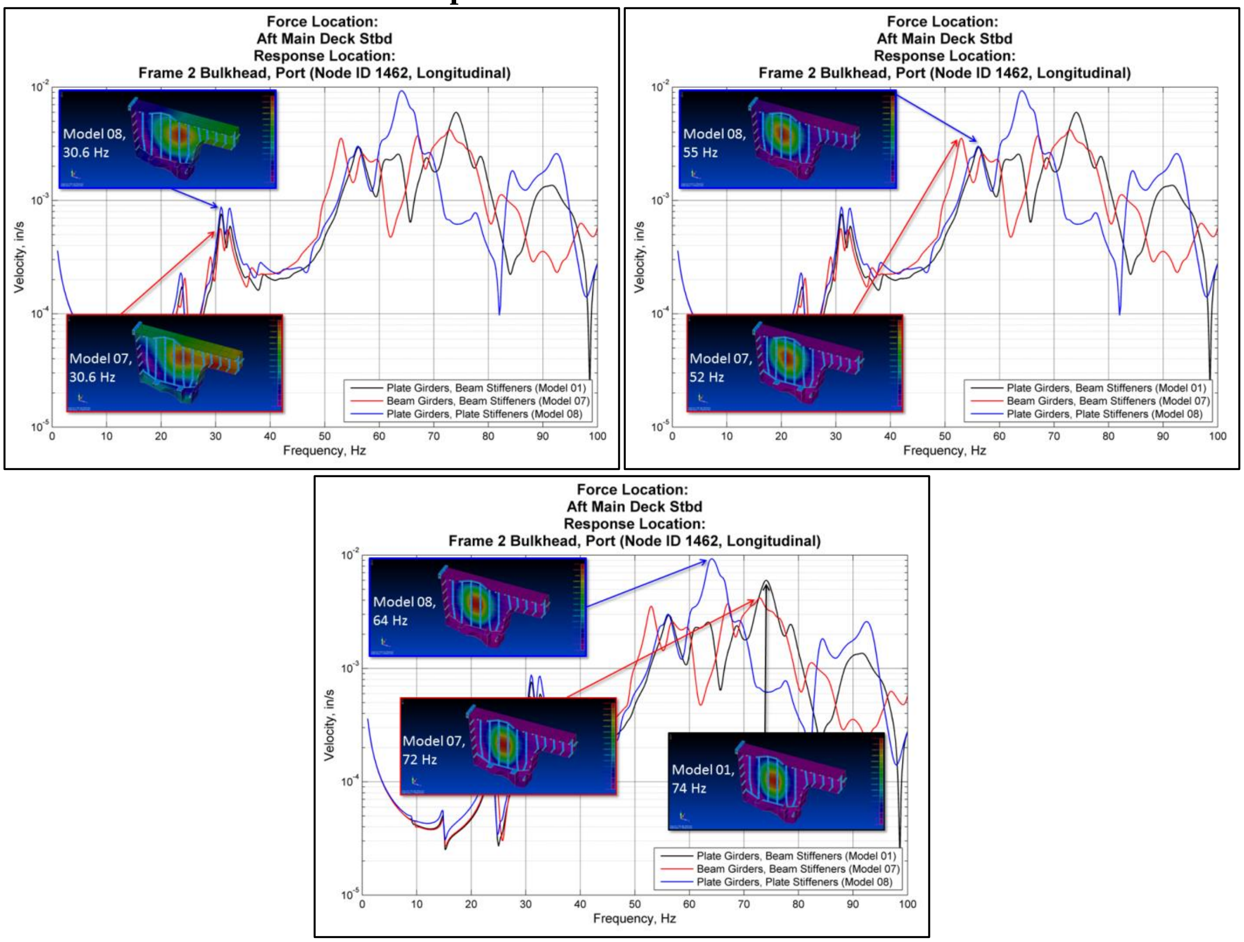

Figure 35: Stiffener Modeling Comparison, Forced Response at Mid Main Deck Port from Input Force at Aft Main Deck Stbd

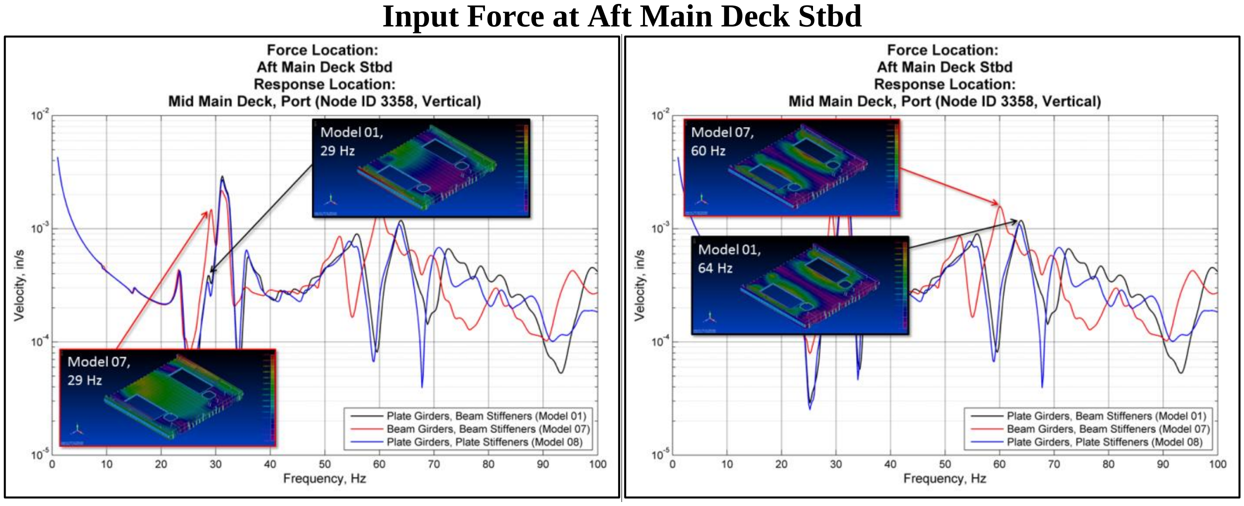

Figure 36: Stiffener Modeling Comparison, Forced Response at Top Wheelhouse Deck Port from Input Force at Aft Main Deck Stbd

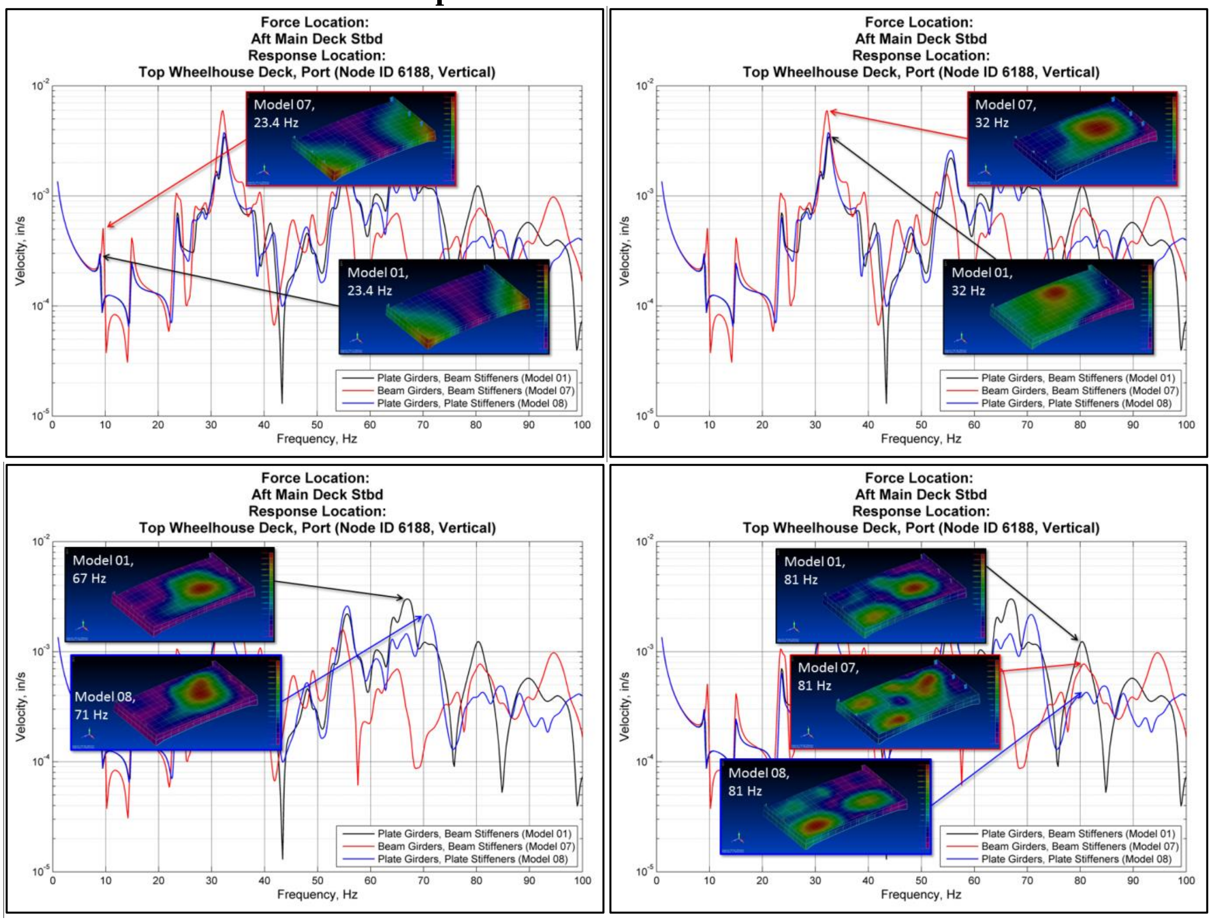

Figure 37: Stiffener Modeling Comparison, Forced Response at Inboard Hull Port from input force at Engine Foundation Port

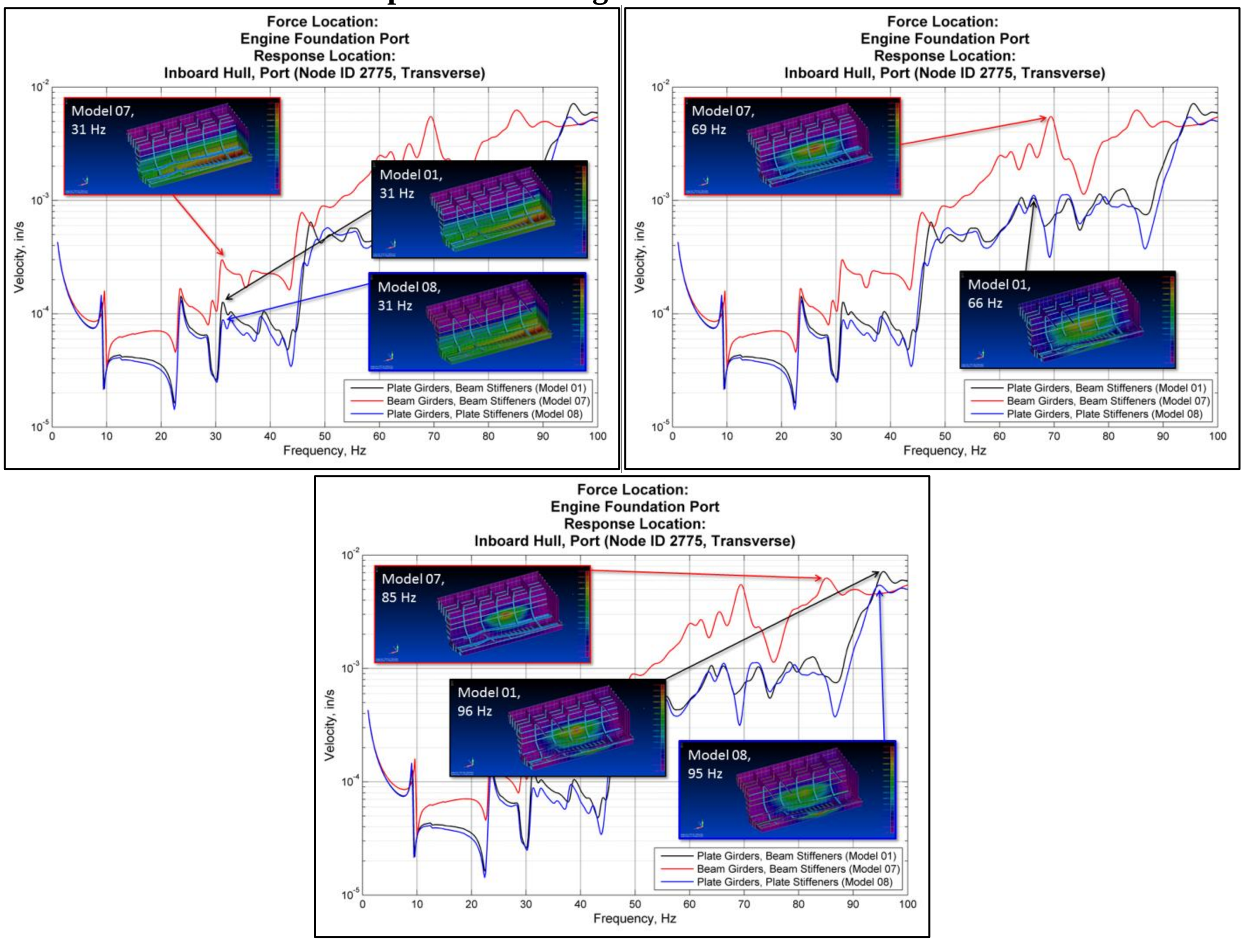

Figure 38: Stiffener Modeling Comparison, Forced Response at Main Deck Pilothouse Stbd from input force at Engine Foundation Port

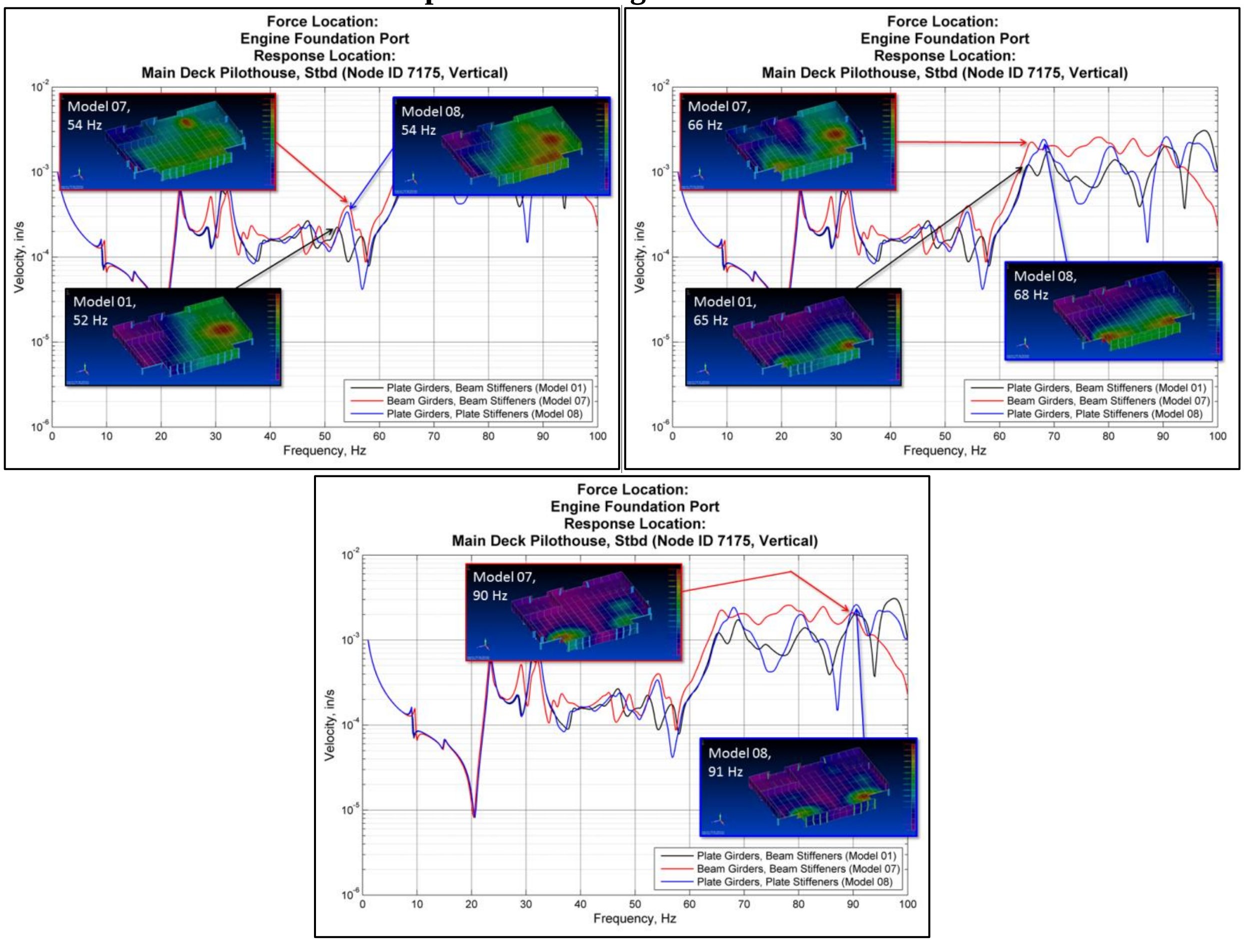

Figure 39: Stiffener Modeling Comparison, Forced Response at Forward Main Deck Port from input force at Engine Foundation Port

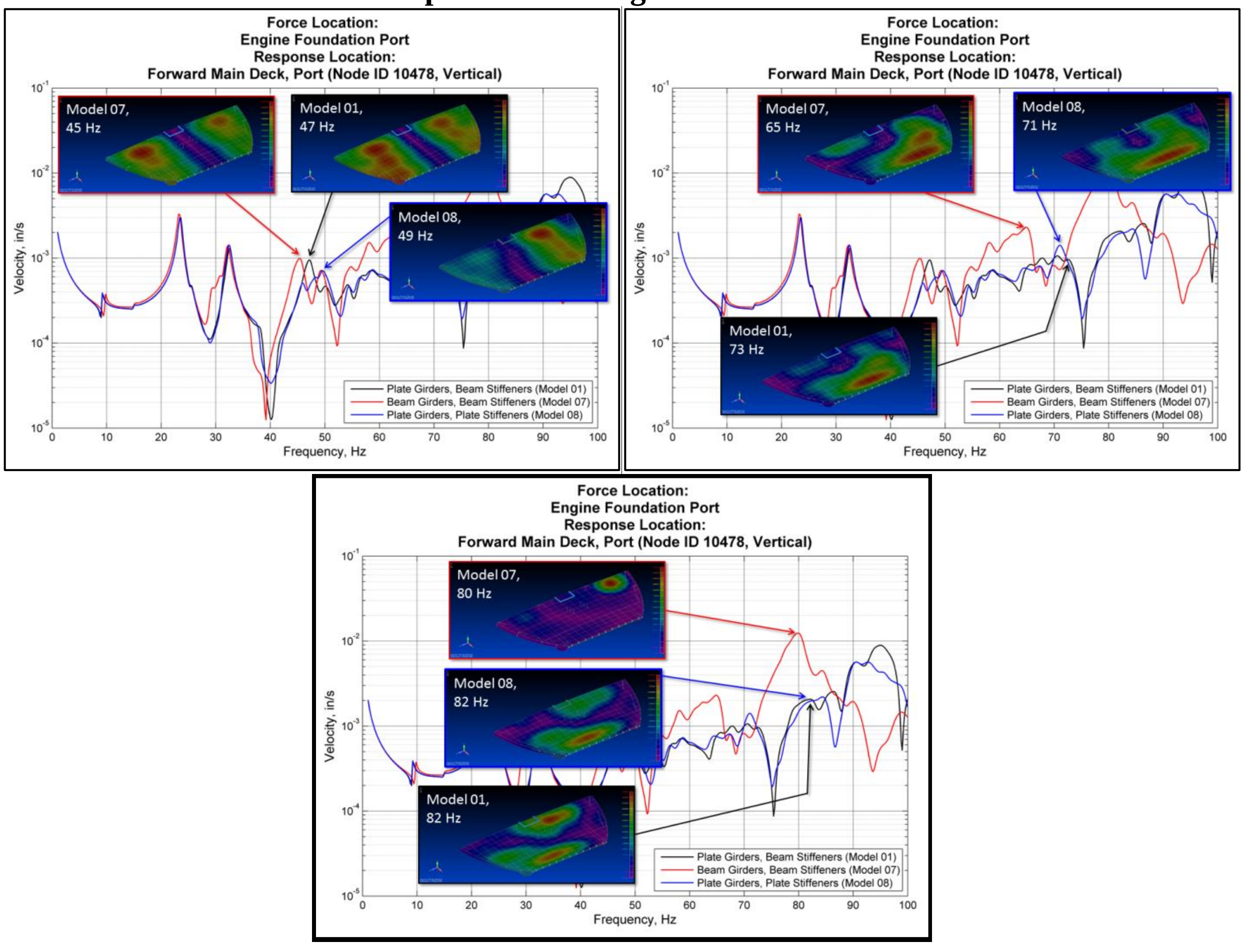

Differences between Model 07 (all stiffeners modeled as beams) and the other models are being as high as a factor of 2 or more different from the Model 01 results at frequencies corresponding to higher order local modes. Furthermore, for some force/response pairs there are response ratios greater than 2 even for low order local modes.

The location that displayed the greatest changes in response for the all-beam stiffener model is the inboard port hull plating response to engine foundation excitation, shown in Figure 37. The relatively large differences in the magnitude of the response suggest the curved hull areas are particularly sensitive to changes in large stiffener element type. The forces transmitted along the web appear to play a significant role for this location, and the plate-girder representation provides a better coupling across pertinent degrees of freedom for curved surfaces such as the hull.

3.4.3 Summary of Results for Stiffener Element Type

Clearly, the approach used to model stiffeners will have an impact on the predicted response spectrum. Similar to the case of mesh density, the impact of stiffener element selection changes with mode shape & frequency.

- For whole body modes, modeling all stiffeners with beams causes shifts in modal frequency of 6% or less.
- For frequency ranges that include local modes, the all-beam models can diverge significantly from the other models. The response magnitude of all-beam models can reach differences of a factor of 2 or higher from the other models, particularly in curved hull sections where large stiffeners (girders) are used and for higher order modes. Significant improvements are seen when using plates to model girder webs.
- Differences between modeling only girders with plates for webs and modeling all stiffeners with plates for webs are small for frequencies including both whole body modes and low order local modes. Higher order modes show good correlation in some cases and poor correlation in others (response ratios greater than 3).
- Based on the results of the cantilever beam models, modeling the flange of a stiffener as a plate does not appear to increase the accuracy of the model. Beams can be used for flanges as a modeling simplification.

3.5 Model Extents

3.5.1 Overview of Results

When attempting to identify appropriate locations to truncate a model, the modes that are accurately predicted by the sub-model will directly indicate the frequency range where the model can be used. As was shown in Section 3.1.2 and elsewhere, the force/response locations chosen for this analysis are generally dominated by whole body modes below 50 Hz, and are controlled by local modes at higher frequencies. Note however that for other vessels, and for some selected locations within this vessel, these frequencies can overlap.

It was shown in Section 3.1.2 that for response locations on the hull sides in the Engine Room the vibration resulting from a vertical force on the engine foundation will be dominated by the whole body modes in the frequency range of 20-50 Hz. Additional investigations of the modes of the model indicate that the first local mode of the Engine Room hull (occurring between Frames 2 and 8 along with other motion between Frames 8 and 13) does not occur until 95.3 Hz. Figure 40 is a plot of the ship mode at 95.3 Hz.

The response of the hull side at frequencies above 50 Hz presented in Figure 18 (see Section 4.1.2) shows an upward sloping response up to a frequency of approximately 95 Hz. This frequency matches the frequency of the mode shown in Figure 40. In the frequency range between 50 and 95 Hz, the vibration at the response location is approximately ‘spring-like’ (i.e. it is proportional to frequency), and a response peak is seen at 95 Hz. This mode, in combination with the whole body modes identified in Section 4.1.2, controls the vibration response of the hull side structure in the engine room that results from a vertical force on the engine foundation.

Therefore, in order for any sub-model to be able to capture the velocity response on the hull side in the Engine Room between 20-100 Hz, it must predict the whole body modes at 23.5, 31.0, 32.5 and 44.1 Hz with reasonable accuracy, as well as the local mode at 95 Hz.

Figure 40: Mode at 95.3 Hz

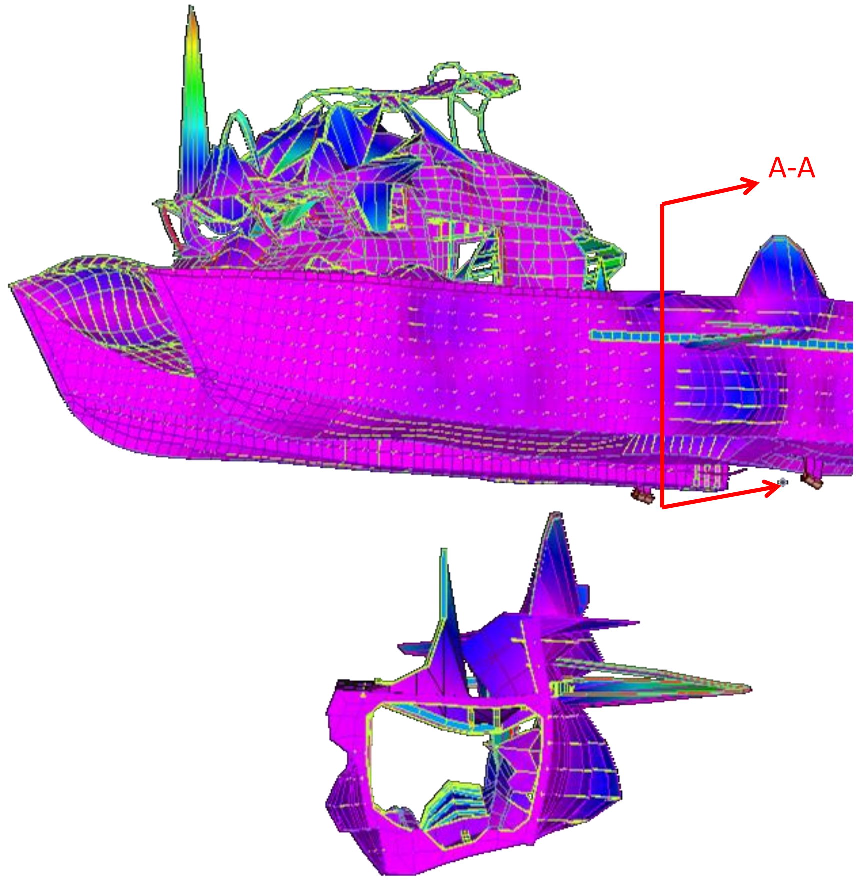

SECTION A-A – FRAME 7 LOOKING AFT

3.5.2 Details of Results

The five models discussed in Section 2.5 have been analyzed first to determine how well they capture these modes. Table 14 shows the predicted frequencies for the five modes identified above as being important for the Engine Room hull side response for each model, along with the percentage change in frequency relative to the full model. Also shown is the Modal Acceptance Criteria (MAC), which is an indication of how well the mode shapes correlate. A value of 1 indicates a high degree of correlation and a value of 0 indicates no correlation. Additional information on MAC can be found in Reference [9] and Appendix B.

Table 14: Mode Shape Pairs of Important Source Room Response Modes

Full Model		Source Room Only			Transom to Frame 8			Transom to Frame 13 (No Superstructure)			Transom to Frame 13		
Shape	**Freq (Hz)**	Freq (Hz)	% Diff	MAC	Freq (Hz)	% Diff	MAC	Freq (Hz)	% Diff	MAC	Freq (Hz)	% Diff	MAC
1st Order Torsion	23.5	91.5	289.4	0.0	29.7	26.4	0.7	16.7	-28.9	0.5	17.1	-27.2	0.5
1st order bending about long. axis	31.0	61.7	99.0	0.0	47.0	51.6	0.8	31.3	1.0	0.8	35.6	14.8	0.8
1st order bending about trans. axis	32.5	95.1	192.6	0.0	20.9	-35.7	0.3	38.7	19.1	0.8	37.2	14.5	0.7
2nd Torsion Mode	47.1	61.8	23.8	0.2	58.8	24.8	0.3	44.5	-5.8	0.8	46.7	-1.0	0.8
1st Local Mode	95.3	96.8	1.6	0.6	96.2	0.9	0.5	95.6	0.3	0.6	95.4	0.1	0.8

The Source Room Only model is seen to have very poor correlation to the whole body modes of the vessel. This is to be expected because the Source Room Only model has too many constraints to effectively replicate the motions of these modes. The Source Room Only model does a little better at predicting the local mode at 95 Hz, though the MAC is still well below 1.

The larger models do better at recreating the whole body modes since they can better mimic the motions of the full ship model, but issues are still present. In all cases, the predicted frequency for the majority of these modes has been shifted anywhere from 15-50% or more. The correlation of the predicted mode shape to the full model does improve with increased model extent, though a MAC of 0.5 is still shown for the first mode in the largest models.

Figure 41 is a plot comparing the hull side velocity response in the vertical direction to the applied force on the engine foundation for the different model extents. These spectra are consistent with the results shown in Table 14. The Source Room Only model is far too rigid and cannot replicate the low frequency response in the whole body mode region. However, this model does do a reasonable job at matching the response near the 95 Hz mode, with a response ratio of roughly 2.

Figure 41 shows the larger models have some large errors in the frequency range of the whole body modes, even though they do a better job at predicting the frequencies of these modes. For example, the resonant peak at approximately 20 Hz in the ‘Transom to Frame 8’ model might suggest that the peak near 20 Hz corresponds to the global torsional resonance at 25.3 Hz in the full ship model. However the peak at 20 Hz in the ‘Transom to Frame 8’ model actually corresponds to the global bending mode at 32.5 Hz in the full ship model, and therefore this seeming coincidence is actually an error. Furthermore, this model shows an extraneous peak near 76 Hz which does not appear in the full ship model. This is due to additional, false modes predicted for this model; false modes are also predicted for the other models, as discussed below.

For the larger models that extend to Frame 13, there is a low frequency mode at approximately 9 Hz which does not correlate to any low frequency modes of the full ship model. This resonant peak is purely artificial and a function of the boundary condition applied to the model (see Section 3.6). A screen capture of this mode is shown in Figure 42, and can be identified as being similar to a cantilever beam. Additional, higher order versions of this mode also appear at higher frequencies, leading to other spikes in the response spectra.

Figure 41: Comparison of Hull Side Vibration in the Vertical Direction for Different Model Extents

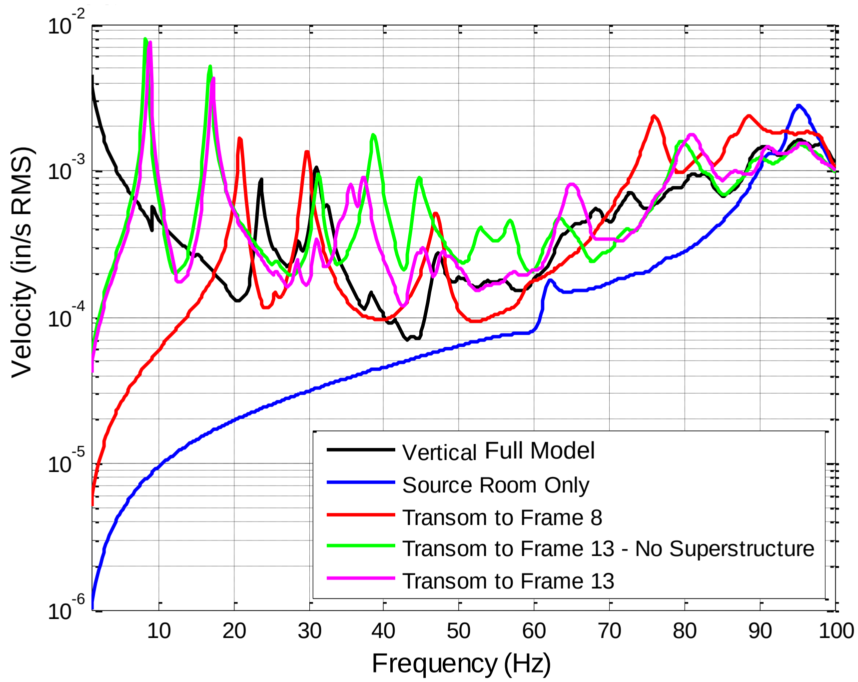

Figure 42: Example of Erroneous Mode in Truncated Model

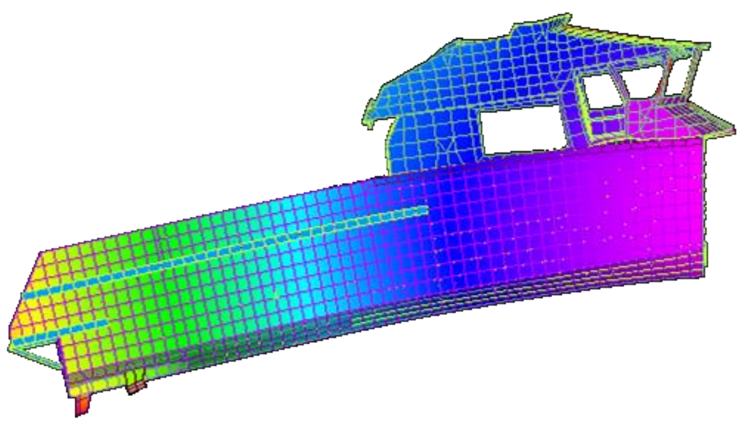

All of the models tend towards convergence to the full model response at frequencies above 50 Hz. This is consistent with the correlation results shown in Table 14, where both the frequency and the MAC are significantly improved relative to the whole body modes. Again, this can be expected because the major motions of the areas of interest (being both the forcing and response locations) are contained within the models. However, the presence of other false modes does lead to errors in the response spectra, even for the largest of models.

Similar results were seen for other response locations (using the same force location and direction). Figure 43 shows the full model velocity response on the hull bottom in the Engine Room. The response in this area is dominated by two whole body modes between 20-40 Hz, being the 1st global torsion mode and the 1st order bending about the longitudinal axis, as well as the local Engine Room mode at 95 Hz. The other whole body modes do not play as much of a role at this location.

Figure 44 compares the predicted vertical vibration on the bottom hull plate for various model extents. Similar to the response on the hull sides, the smaller models are unable to accurately replicate the shape and frequency of the whole body modes. Above 50 Hz the truncated model response more closely matches the full model response, though again extraneous modes appear to exaggerate the response at some frequencies.

Figure 43: Velocity on the Bottom Hull in the Engine Room from a Vertical Force on the Engine Foundation, Full Model

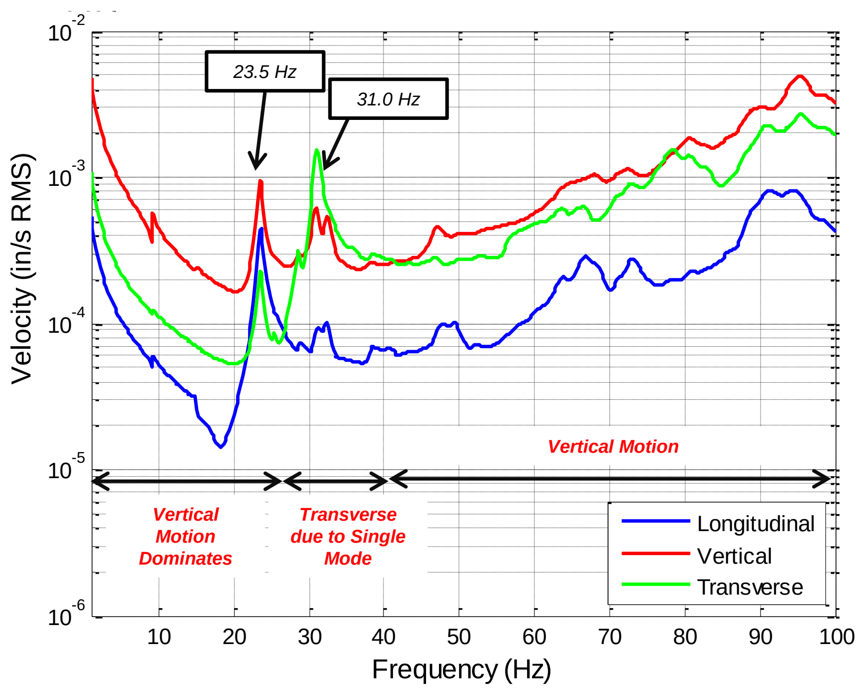

Figure 44: Comparison of Velocity on the Bottom Hull Panel in the Engine Room for Different Model Extents

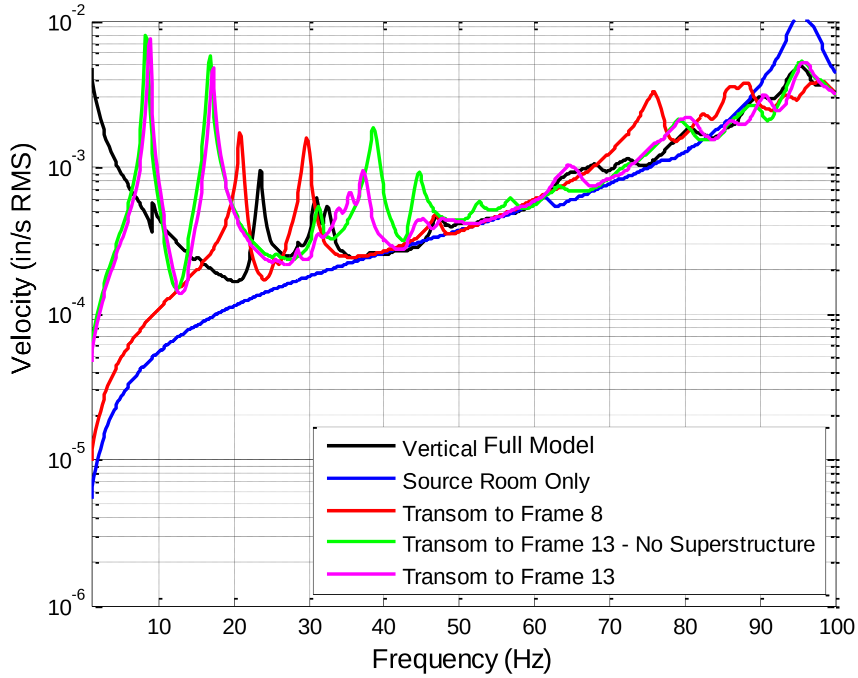

The results at the transverse bulkheads and Main Deck response locations show similar results to those presented above and have been omitted from this report for the sake of brevity.

However, the results for the 'Engine Room Plate,' being a large plate of relatively low stiffness within the Engine Room (See Section 2.5) are worth reviewing here. Figure 45 provides the full model velocity response at this location as a result of a vertical force applied at the engine foundation. Like the other regions of interest, the engine room plate has high levels of response at the whole body modes of the ship. However, the plate also has numerous local modes which dominate its response. These local modes occur at 12.4, 18.8, 37.4, 44.3 and 46.0 Hz, and are interspersed with the whole body modes.

Table 15 lists the local modes of this plate for each model along with the percentage change in frequency and MAC. It can be clearly seen that all models capture these modes both in frequency and shape.

Figure 46 compares the average transverse (out-of-plane) velocity response on the Engine Room Plate for the different models.

Figure 45: Velocity of the Engine Room Plate Located in the Source Room, Full Ship Model

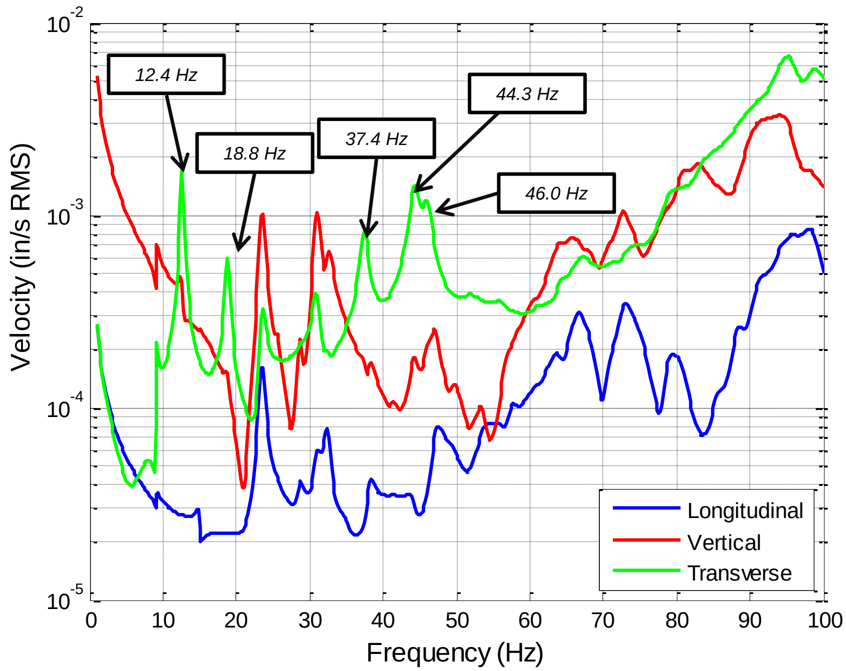

Table 15: Mode Shape Pairs of Important Engine Room Plate Response Modes

Full Model	**Source Room Only**			**Transom to Frame 8**			**Transom to Frame 13 (No Superstructure)**			**Transom to Frame 13**		
Freq (Hz)	Freq (Hz)	% Diff	MAC	Freq (Hz)	% Diff	MAC	Freq (Hz)	% Diff	MAC	Freq (Hz)	% Diff	MAC
12.4	12.4	0	1.0	12.4	0	1.0	12.4	0	1.0	12.4	0	1.0
18.8	18.8	0	1.0	18.8	0	1.0	18.8	0	1.0	18.8	0	1.0
37.4	37.4	0	1.0	37.4	0	1.0	37.4	0	1.0	37.4	0	1.0
44.3	44.3	0	1.0	44.3	0	1.0	44.3	0	1.0	44.3	0	1.0
46.0	46.0	0	1.0	46.0	0	1.0	46.0	0	1.0	46.0	0	1.0

Figure 46: Comparison of Velocity on Engine Room Plate, Transverse Vibration, for Different Model Extents

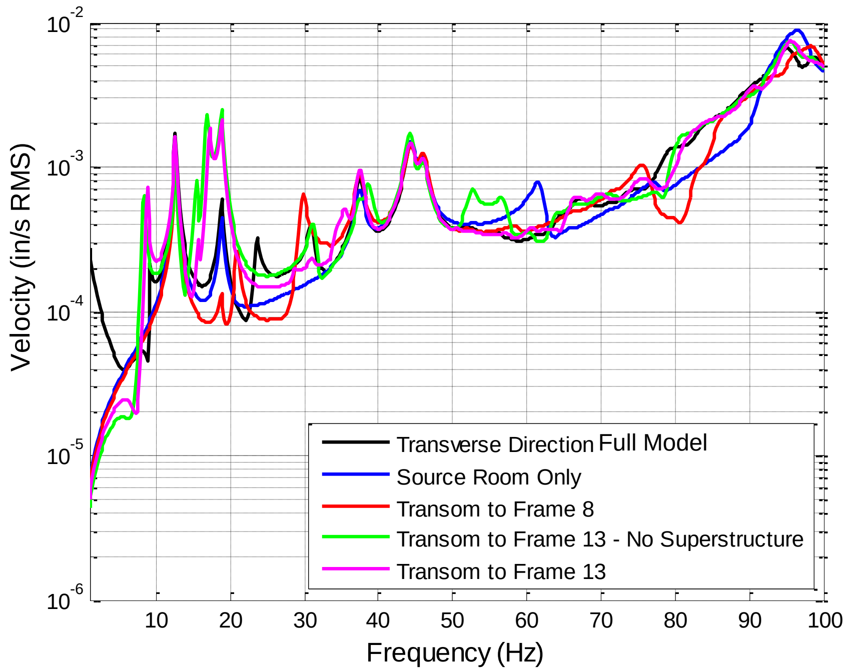

It is seen that all models accurately capture the response around four of the five local modes, being 12.4, 37.4, 44.3 and 46.0 Hz. However, at 18.8 Hz only the Source Room Only model captures the response velocity with a high degree of accuracy – errors for the other models at this frequency are on the order of a factor of 3-4. The reason for this error in the models that extend to Frame 13 is they have artificial ship resonances near this frequency imposed by the boundary condition. For the 'Transom to Frame 8' model, the discrepancy is due to the fact that it does not accurately capture the global ship torsion mode at 23.5 Hz. The absence of the global torsion mode's contribution to the engine room plate's response has the effect of lowering the overall level of response.

Other errors are present in the whole body mode frequency range, though as a whole the correlation for this receiver area is better than those seen elsewhere in the vessel. The response at frequencies above 50 Hz can again be seen to have false peaks in the response relative to the full ship model.

It is noted that the response of all truncated models below the whole body mode frequency range tends towards zero, while the response of the full ship model tends towards infinity. This is a direct result of the pinned boundary condition being applied to the truncated models, limiting motion at low frequencies. Neither model is formally correct in this frequency range, as the buoyancy of the vessel would control the motions at very low frequencies (see the discussion of buoyancy springs in Section 3.1.2).

3.5.3 Summary of Model Extent Analysis

In order to accurately truncate a model of a vessel the predicted modes of the sub-model must accurately capture both the frequency and shape of the modes of the full model in the frequency range of interest. These modes can include both whole body modes as well as local modes, depending again on the goals of the analysis. In some cases these frequency ranges are separate, though additional complications will arise when they overlap.

As was seen here is it possible, if not likely, that the truncated model will predict modes at frequencies that are significantly shifted from the full vessel model unless the model extents are far from the area of interest, which should encompass both the forcing and response locations (and structures in between). Furthermore, the process of model truncation and addition of boundary conditions can generate false modes that are not present in the full model, further complicating analysis and leading to erroneous results. Put simply, it is not possible to truncate a model and achieve good results at all frequencies.

An important fact that must be remembered when analyzing these results is the vessel being modeled here is small relative to some vessel types that commonly require vibration analysis, such as research vessels, tankers, cruise ships, etc. The conclusions noted above will almost certainly hold for those vessels as well, though their implications on the errors in predicted response may be more muted.

The results from the "Engine Room Plate" response location and the results near the local mode at 95 Hz do provide some insight into options for truncating models for larger ships. For the Engine Room Plate location, all models provide a good approximation of the response at the local modes of this structure with the exception of frequencies where whole body modes were seen to interfere with the predicted response. Furthermore, nearly all models show good correlation to the full ship model for the response peak at 95 Hz, regardless of the response location (errors in response magnitude were much less than a factor of 2 for all models except the Source Room Only model).

These results indicate that it may be possible to create an accurate sub model when investigating the response of local structures, provided the frequencies of predicted (false) whole body modes do not coincide with frequencies of local modes, and the model extent is not part of or adjacent to the area of interest. Based on these results, it is estimated that for larger vessels this can occur if the model is truncated at least one if not several major structural divisions (i.e. bulkheads and decks) away from the force and response locations. However, caution must be used whenever interpreting results from a truncated model. For small vessels such as the one modeled here, truncation is not recommended since there may be overlapping frequency bands for whole body and local modes.

3.6 Boundary Conditions

For the sub-models studied as part of the model extents analysis described in Section 3.5, pinned boundary conditions were applied at all model extents (except the transom). Selected models from that analysis have been further analyzed to determine if the results can be improved by changing the boundary conditions applied to the model.

Figure 47 compares the transverse response on the 'Engine Room Plate' located within the Engine Room for different boundary conditions as a result of a vertical force on the engine foundation for the 'Transom to Frame 13' model. Also shown is the transverse response in the full model. As described in Section 3.6, pinned (no translation), fixed (no translations or rotation) and free boundary conditions were applied to the edges of the model on Frame 13.

Figure 47: Comparison of Transverse Response on Engine Room Plate in Transom to Frame 13 Sub-Model under Various Artificial Boundary Conditions

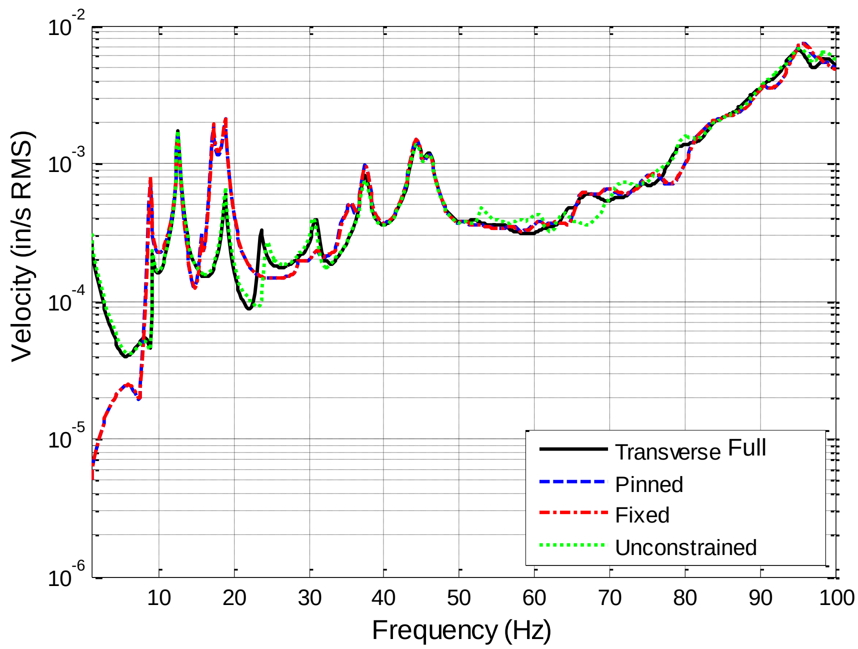

Negligible differences are seen in the vibration response between the pinned and fixed boundary conditions, though both exhibit the errors discussed in Section 4.5 that result from inaccurate prediction of the whole body modes. For this model the unconstrained boundary condition performs considerably better, as the prediction of whole body modes is much closer to those of the full model. Keep in mind that this model is of nearly the same extent as the full ship model, which accounts for the similarity in whole body modes.

Figure 48 presents a similar comparison for the transverse response on the Engine Room Plate for the 'Transom to Frame 8' model. Again there is negligible difference between the pinned and fixed boundary conditions, and both still suffer from the inability to capture the whole body modes. However, the unconstrained boundary condition does not perform as well for this model as it did for the larger model.

Figure 48: Comparison of Transverse Response on Engine Room Plate in Transom to Frame 8 Sub-Model under Various Artificial Boundary Conditions

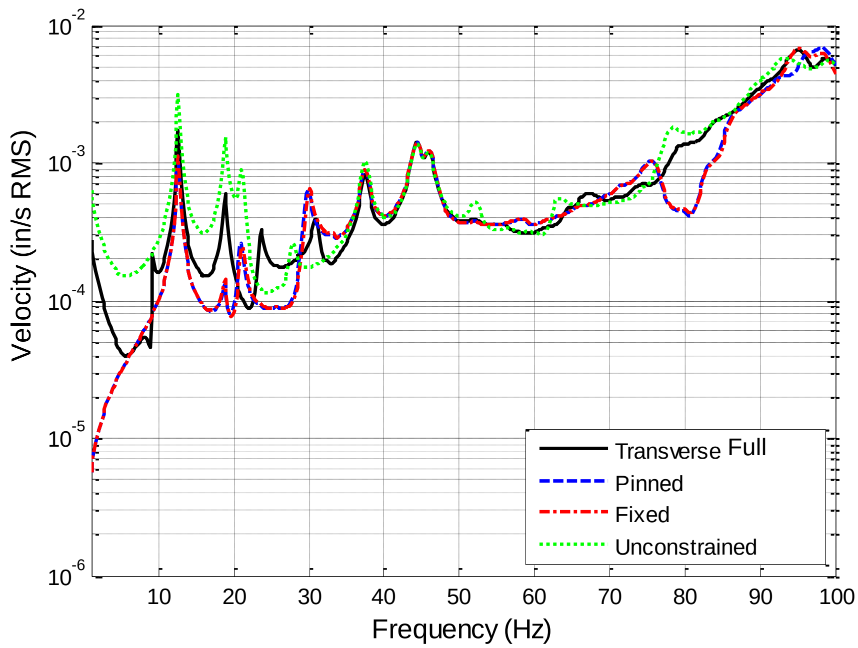

The unconstrained 'Transom to Frame 8' model shows higher levels of response at the majority of resonant peaks below 40 Hz, with differences in response as high as a factor of 2-3. Furthermore, there are shifts in peak response frequencies that are present with this model relative to the full model which were not seen with the larger model. This is because the unconstrained, smaller model still contains false modes as a result of truncation.

At higher frequencies the differences between imposed boundary conditions diminishes. This suggests that as the frequencies of interest move to local modes, where the vessel motion is localized and is also far from the boundaries, the specific boundary condition that is used is of less importance.

Similar results were seen for other response locations, but are not provided here for brevity.

Although these results are limited by the size of the modeled vessel, they do confirm that any truncated model will generate false modes, and the frequency and mode shape of those modes will be dependent on the specific boundary condition used. Unfortunately there is no "good" boundary condition that can be identified as a result of this study. However, this analysis does show that by changing boundary conditions the frequencies of false modes can be identified.

One of the conclusions of the previous section is if a model must be truncated, the location of truncation should be as far as possible from the area where forces are being applied and responses are of interest. Ideally, the influence of false and inaccurate whole body modes from the truncated model will be minimal in the frequency range of interest. If this is the case, then the predicted vibration response should be in large part independent of the specific boundary condition that is used.

3.7 Damping

The damping loss factor applied to the model was investigated using forced response analyses. The 'baseline' damping loss factor used for all previous analyses was 0.03. Additional analyses were investigated for loss factors of 0.003, 0.01, 0.06, and 0.1 for all frequencies.

A summary of the forced response analysis for different loss factors is shown in Figure 49. As expected, increasing the damping loss factor attenuates the 'peak and dip' response at resonances, while decreasing the damping loss factor increases the response.

For models with loss factors of 0.03 and less, the attenuation of response is consistent across all frequencies and all locations. For models with very light damping, the influence of what appear to be otherwise weakly excited modes is seen to drastically increase. For higher values of damping the opposite happens, and only the modes that are strongly excited are seen to have an effect on the predicted spectrum.

For example, for the response at the port inboard hull with a force on the Aft Main Deck Stbd (lower right plot of Figure 49), the response below 25 Hz shows a dramatic change in the peak response as the loss factor is changed. At frequencies above 50 Hz, the models with the highest levels of damping show a very slowly changing response with increasing frequency. In particular, the response around 60 Hz is seen to vary quite slowly for the model with the largest damping, whereas the model with the lowest damping has the same overall characteristic but there are many more sharp peaks and dips in the response. Furthermore, as the damping is increased, the effect of one strongly excited mode that may occur at one frequency has an increasing effect on the total response at frequencies near other strongly excited modes.

Clearly, this analysis cannot be used to determine which damping loss factor is correct; additional information on the range of absolute damping levels that are applicable for ship vibration is presented in Part II. The results presented in this section do show that there is a potential for significant changes in the magnitude of response depending on the actual level of damping in the vessel, which may change with frequency.

It is worth noting that the absolute level of the response magnitude cited in other sections of this report, as well as for results of any model, are obviously dependent on the damping applied to the model. However, the results of peak response ratios (i.e. the maximum response divided by the minimum response) between two models that are presented throughout Part I of this report should remain approximately the same even after updating the damping loss factor. This is because a change in the damping creates a linear change in the response, thereby leaving the ratio of peak responses the same.

Figure 49: Damping Loss Factor Comparison at Minimum Mesh Density, Various Forced Response Locations from Input Forces Locations at Engine Foundation and Aft Main Deck

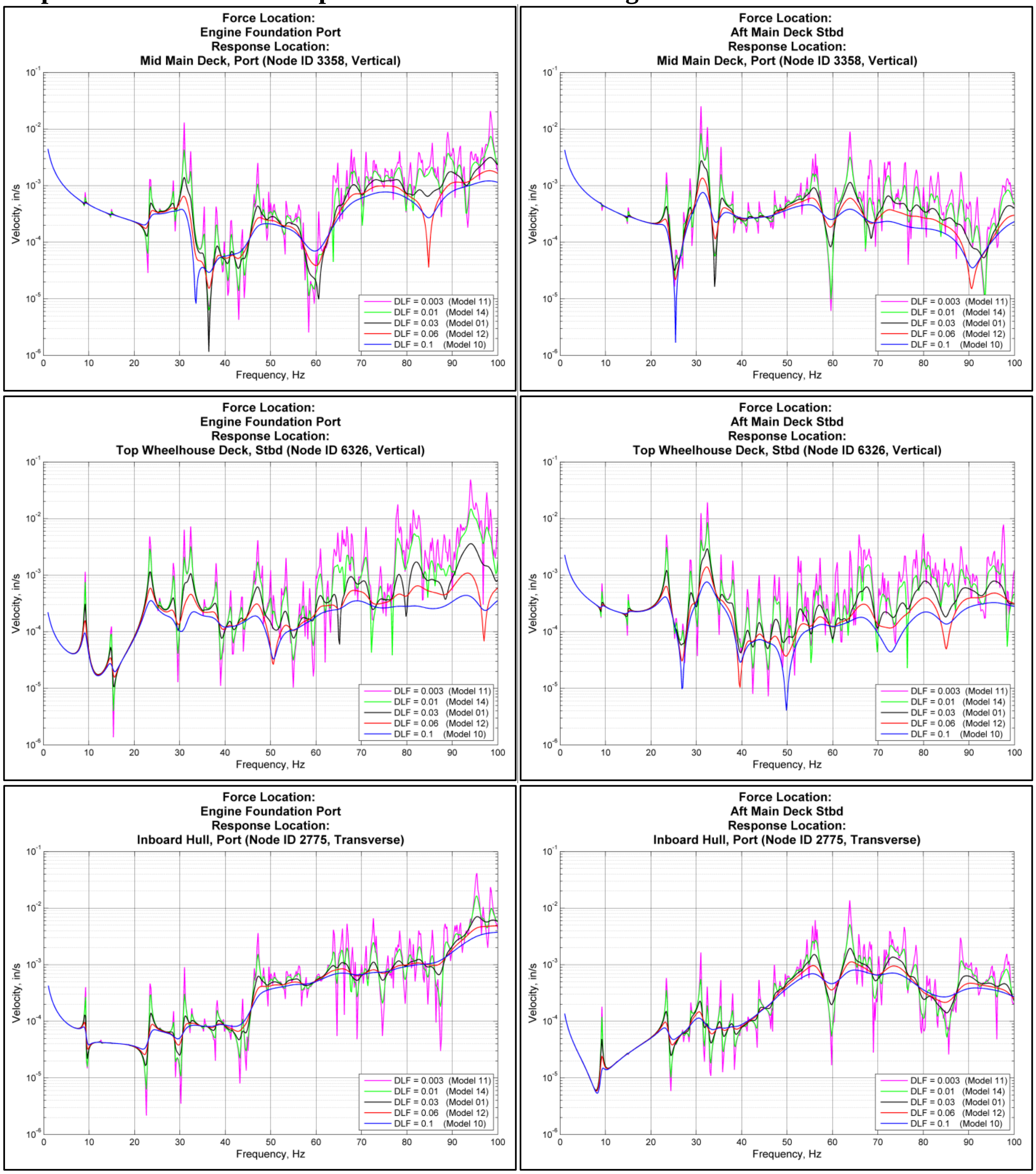

3.8 Masses and Structural Simplifications

3.8.1 Supplementary Structural Elements

To investigate the influence of explicitly modeling specific structural elements, various items were added to the baseline model described in Section 2.2. The models that result are as follows:

- No additional structure – baseline (Model #01)
- Added windows to the Superstructure (Model #20)
- Added doors to the Superstructure (Model #21)
- Added removable deck sections on the Main Deck (Model #22)

These changes were performed sequentially (i.e. Model #21 includes the modifications to Model #20, etc.).

Table 16 presents the predicted frequencies of the whole body modes for each model along with percentage change in frequency. The variation in frequency was generally less than 6% with a few exceptions. Adding windows shifted the frequency of the first mode of the superstructure by 20% (35.7 Hz to 46.1 Hz). Furthermore, adding removable deck sections to the main deck shifted the frequency of the first torsional mode of the vessel by 10% (25.2 to 27.7 Hz).

Table 16: Modal Analysis Results for Supplementary Structural Elements

	Model 01	Model 20		Model 21		Model 22	
	No Additional Structure	Superstructure Windows		Superstructure Doors		Removable Decks	
Mode Description	Freq (Hz)	Freq (Hz)	Diff. w.r.t Model 01	Freq (Hz)	Diff. w.r.t Model 20	Freq (Hz)	Diff. w.r.t Model 21
1st order torsion	23.5	25.0	6%	25.2	1%	27.7	10%
1st order bending about longitudinal axis	31.1	32.4	4%	32.6	1%	32.8	1%
1st order bending about transverse axis	32.5	33.9	4%	34.2	1%	34.6	1%
Superstructure	38.4	46.1	20%	46.7	1%	46.8	0%
2nd order torsion	47.2	48.1	2%	50.2	5%	49.9	1%

The change in the superstructure mode is logical because the superstructure of this vessel contains a significant portion of otherwise open area, and when windows are added there is a substantial increase in structural stiffness. However, these modifications had reduced effects on the other whole body modes. The change in the 1^{st} torsion mode as a result of the addition of the removable decks is the result of a closing of a significant portion of open area on the Main Deck. Similar ratios of open area to structure may not exist on other vessels, particularly large vessels, and therefore the results presented here may be a worst case example of the effects that are possible.

The results of the forced response analysis are provided in Table 17, including differences in frequency and velocity magnitude for selected response peaks between the different models. All differences are relative to the previous model. As was done previously, this table presents frequency differences as a percentage and the velocity response differences a ratio (i.e. higher magnitude divided by lower magnitude). Also presented in Figure 50 – Figure 54 are the predicted spectra for selected force/response locations for all models.

Table 17: Forced Response Analysis Results for Supplementary Structural Elements

		Frequency, Hz						
Force Location	**Response**	**Model 01**	**Model 20**	**Diff. Rel. Model 01**	**Model 21**	**Diff. Rel. Model 20**	**Model 22**	**Diff. Rel. Model 21**
Engine Foundation, Port	Mid Main Deck, Port (see Figure 50)	**24**	26	8%	26.2	1%	28	7%
		31	33.8	9%	34	1%	34.6	2%
		47	48	2%	52	8%	50	4%
		69	69.6	1%	69.6	0%	70.4	1%
		78	79	1%	79	0%	79.6	1%
		90	90	0%	90	0%	89	1%
	Top Wheelhouse Deck, Port (see Figure 51)	**23**	24	4%	25	4%	27	8%
		33	33	0%	33	0%	33	0%
		67	66	1%	66	0%	66	0%
		81	84	4%	83	1%	84	1%
		89	89	0%	89	0%	89	0%
		98	97	1%	97	0%	97	0%
Aft Main Deck, Stbd	Frame 8 Bulkhead above deck, Port (see Figure 52)	**32**	33	3%	33.5	2%	33.5	0%
		54	45	17%	46	2%	46	0%
		73	70	4%	70	0%	72	3%
		79	73	8%	73	0%	72	1%
	Pilothouse Longitudinal Bulkhead, Port (see Figure 53)	**23**	25	9%	26	4%	24	8%
		31	34	10%	34.5	1%	35	1%
		57	57	0%	57	0%	57.5	1%
		64	64	0%	64	0%	64	0%
		71	75	6%	77	3%	76	1%
		89	89	0%	88	1%	87	1%
	Mast, Port (see Figure 54)	**29**	24	17%	26	8%	28	8%
		41	41.5	1%	41.5	0%	41.5	0%
		55	57	4%	57	0%	60	5%
		64	64	0%	64	0%	63	2%
		84	84	0%	83	1%	83	0%

Table 17: Forced Response Analysis Results for Supplementary Structural Elements (continued)

Force Location	Response	Velocity, in/s Model 01	Model 20	Ratio Rel. Model 01	Model 21	Ratio Rel. Model 20	Model 22	Ratio Rel. Model 21
Engine Foundation, Port	Mid Main Deck, Port (see Figure 50)	**4.9E-04**	3.6E-04	1.4	3.0E-04	1.2	2.9E-04	1.0
		1.5E-03	1.0E-03	1.5	1.2E-03	1.2	1.6E-03	1.3
		4.5E-04	5.6E-04	1.2	4.5E-04	1.2	4.0E-04	1.1
		1.3E-03	9.0E-04	1.4	6.8E-04	1.3	5.9E-04	1.2
		1.3E-03	1.7E-03	1.3	1.6E-03	1.1	2.3E-03	1.4
		1.9E-03	2.3E-03	1.2	2.3E-03	1.0	7.1E-04	3.2
	Top Wheelhouse Deck, Port (see Figure 51)	**6.3E-04**	5.9E-04	1.1	4.3E-04	1.4	5.0E-04	1.2
		1.4E-03	2.1E-03	1.5	1.9E-03	1.1	1.8E-03	1.1
		6.2E-03	5.2E-03	1.2	6.0E-03	1.2	5.0E-03	1.2
		2.6E-03	2.5E-03	1.0	4.0E-03	1.6	4.1E-03	1.0
		3.5E-03	4.0E-03	1.1	5.4E-03	1.4	3.9E-03	1.4
		2.3E-03	3.3E-03	1.4	4.0E-03	1.2	3.1E-03	1.3
Aft Main Deck, Stbd	Frame 8 Bulkhead above deck, Port (see Figure 52)	**1.0E-03**	1.6E-03	1.6	1.2E-03	1.3	1.2E-03	1.0
		6.0E-03	1.1E-03	5.5	8.2E-04	1.3	8.0E-04	1.0
		3.0E-03	2.4E-03	1.3	1.4E-03	1.7	1.5E-03	1.1
		2.3E-03	1.8E-03	1.3	8.0E-04	2.3	1.5E-03	1.9
	Pilothouse Longitudinal Bulkhead, Port (see Figure 53)	**7.0E-04**	2.1E-04	3.3	1.7E-04	1.2	1.8E-05	9.4
		1.1E-03	4.5E-04	2.4	5.4E-04	1.2	5.9E-04	1.1
		2.9E-04	5.0E-04	1.7	4.5E-04	1.1	2.7E-04	1.7
		3.6E-04	2.9E-04	1.2	2.9E-04	1.0	1.0E-04	2.9
		3.0E-04	2.9E-04	1.0	2.0E-04	1.5	3.0E-04	1.5
		1.2E-04	1.7E-04	1.4	1.5E-04	1.1	3.1E-04	2.1
	Mast, Port (see Figure 54)	**8.0E-03**	3.0E-03	2.7	3.0E-03	1.0	6.0E-03	2.0
		3.0E-03	2.9E-03	1.0	2.9E-03	1.0	2.7E-03	1.1
		9.0E-04	2.1E-03	2.3	2.1E-03	1.0	9.5E-04	2.2
		6.0E-04	1.5E-03	2.5	8.0E-04	1.9	5.6E-04	1.4
		1.2E-03	8.5E-04	1.4	1.3E-03	1.5	1.7E-03	1.3

Figure 50: Structural Modeling Comparison, Forced Response at Mid Main Deck Port from Input Force at Engine Foundation Port

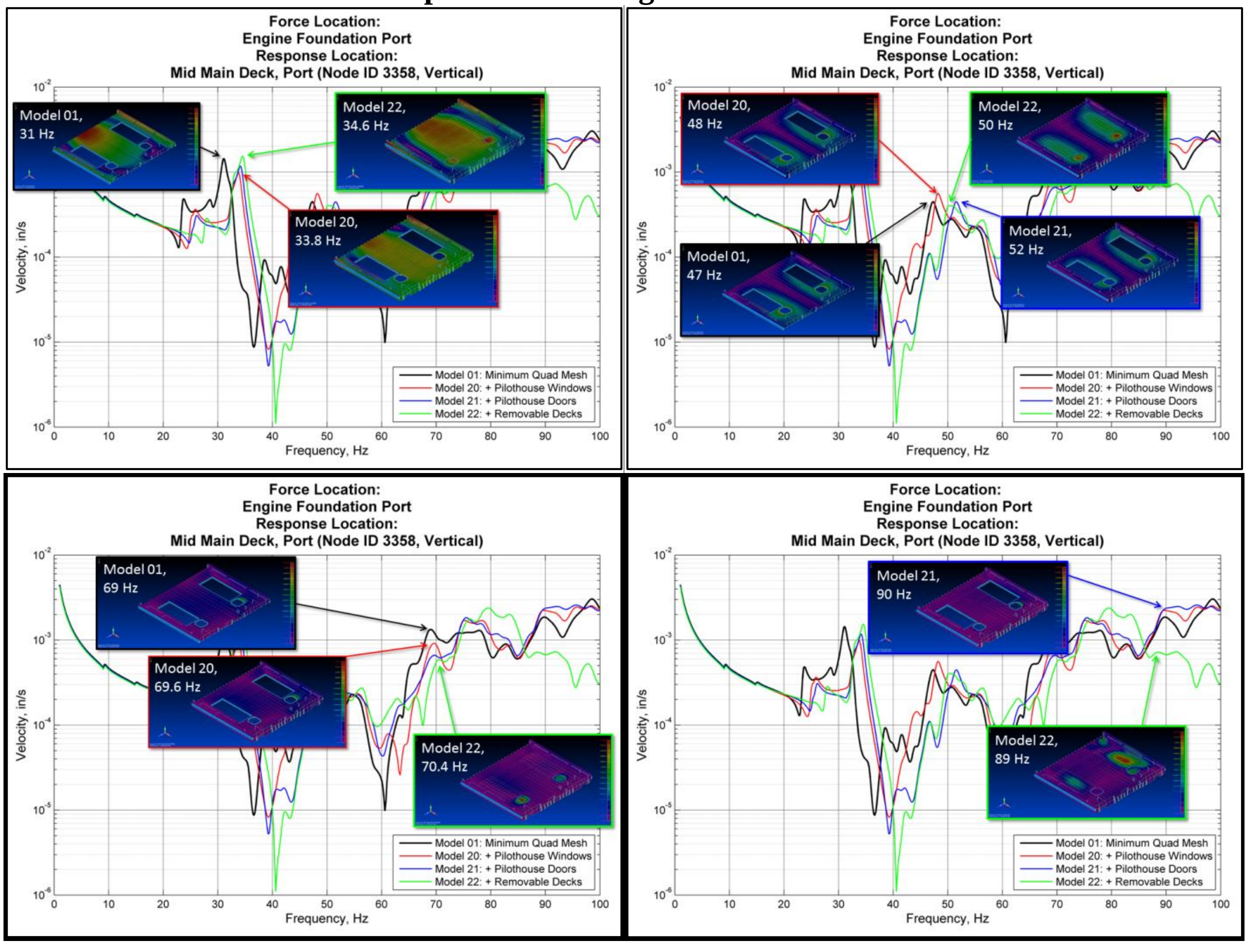

Figure 51: Structural Modeling Comparison, Forced Response at Top Wheelhouse Deck Port from Input Force at Engine Foundation Port

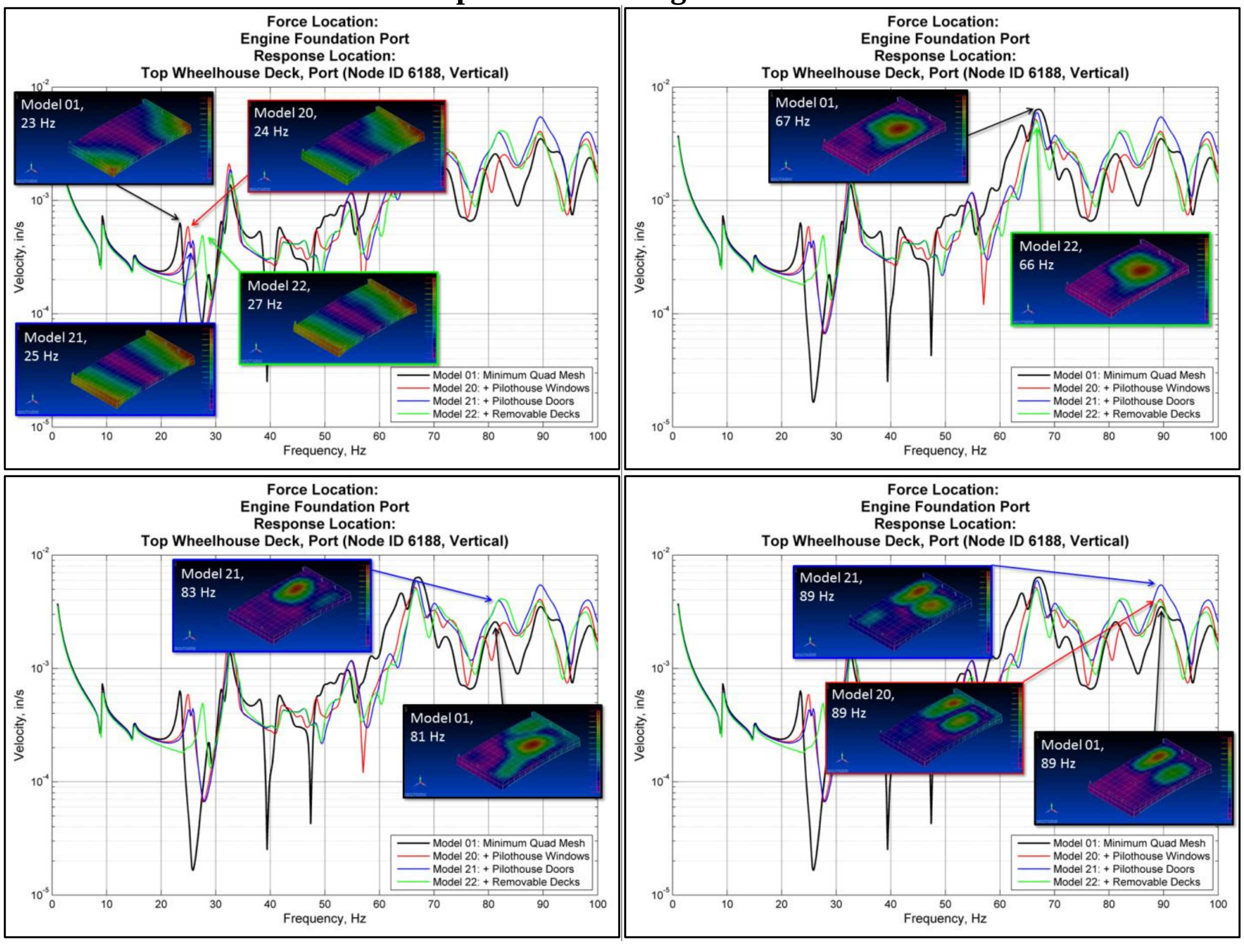

Figure 52: Structural Modeling Comparison, Forced Response at Frame 8 Bulkhead Port from Input Force at Aft Main Deck Port

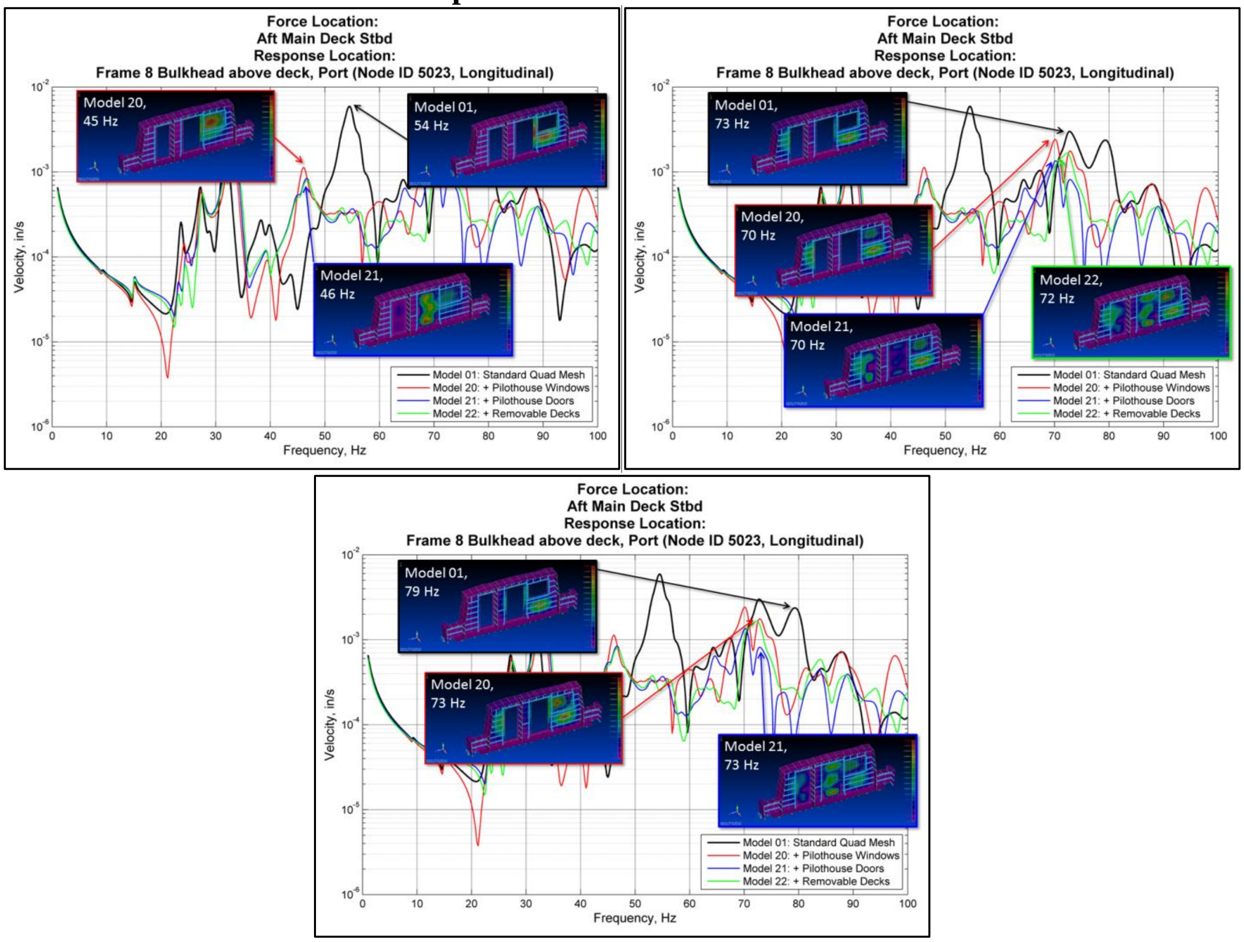

Figure 53: Structural Modeling Comparison, Forced Response at Outboard Port Superstructure Bulkhead from Input Force at Aft Main Deck Port

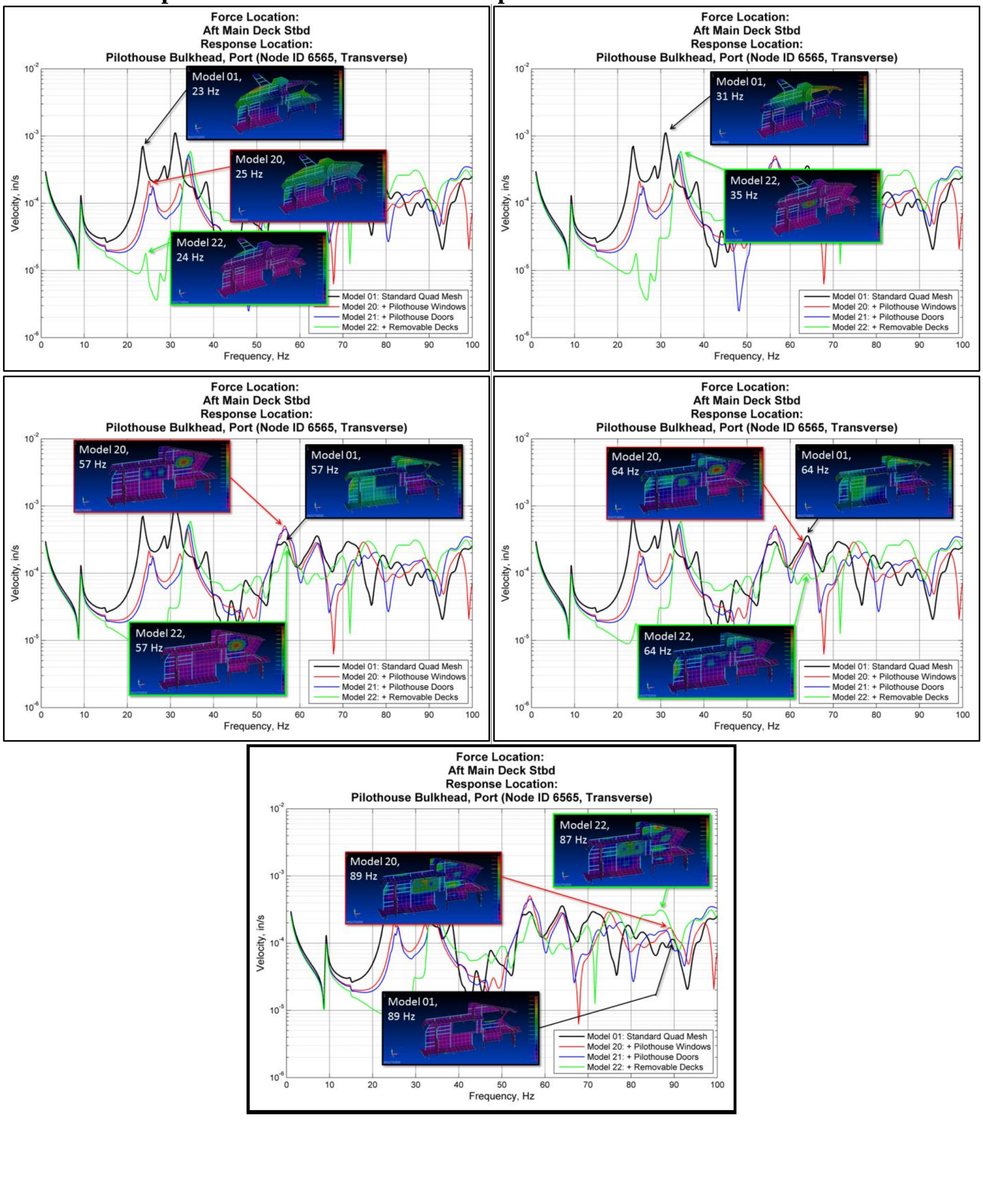

Figure 54: Structural Modeling Comparison, Forced Response at Mast Port from Input Force at Aft Main Deck Port

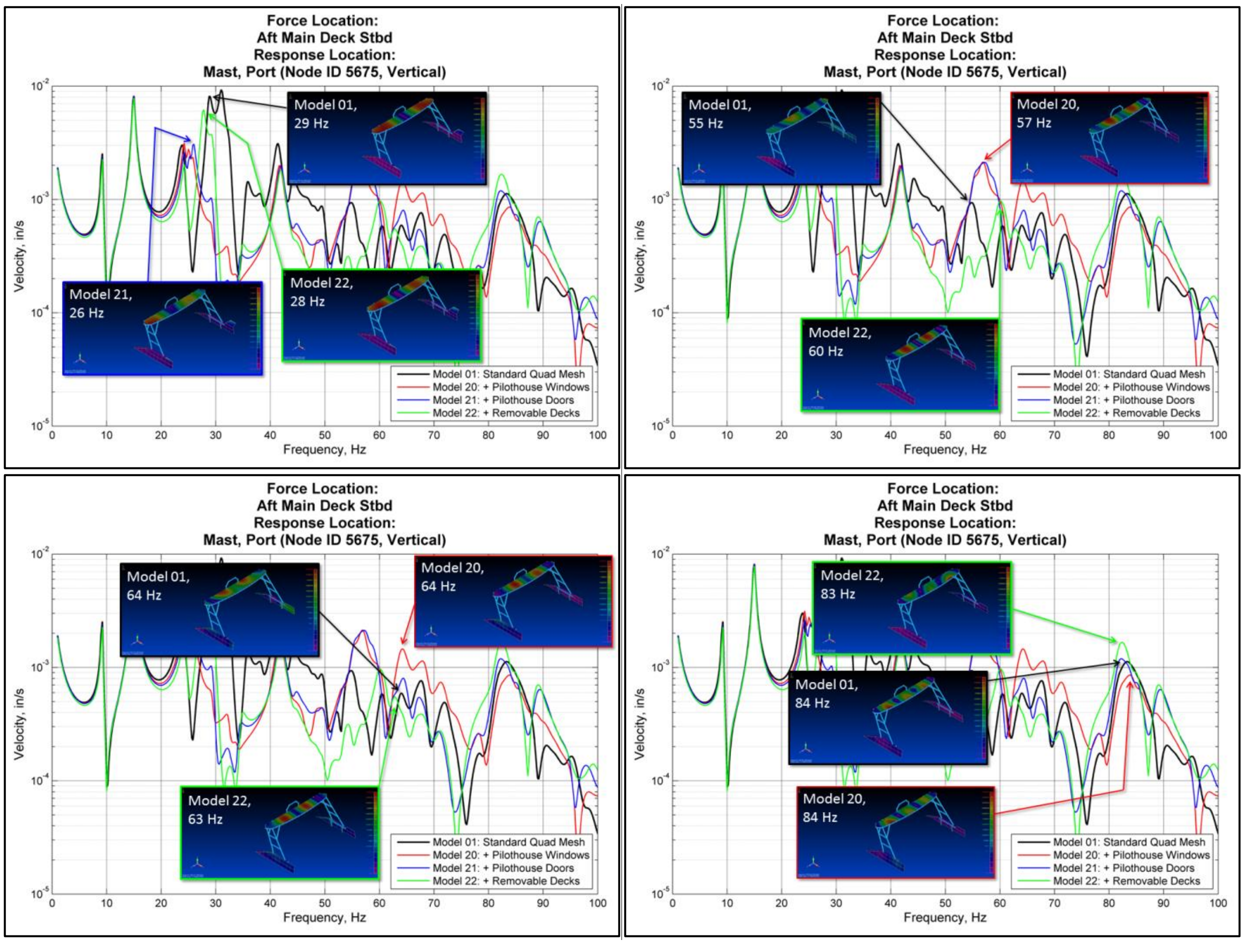

The results of the forced response analysis suggest the most significant variations in response are in the areas of closest proximity to the structural changes. Adding windows and doors to the superstructure had a greater effect on the response throughout the superstructure as compared to elsewhere in the vessel, though the addition of windows presented a greater change to the vessel's overall response.

When the windows were added the shift in frequency peaks were typically between 0-10%, though some frequencies shifted by as much as 17%. Variations in magnitude were less than a factor of 1.5 for response locations not part of the superstructure, but factors upwards of 5.5 were seen for different parts of the superstructure. As noted above, these differences are likely due to the fact that the windows make up a significant percentage of the total superstructure area. The addition of doors to the superstructure has a significantly reduced effect.

The addition of removable deck sections changed the response on the Main Deck as well as the all areas of the vessel when the force was applied to the Main Deck. Variations in frequency were typically low (0-1%) though some peaks have changes upwards of 8%. Variations in response magnitude were less than a factor of 1.5 when neither the force or response locations were on the Main Deck. Response factors were generally less than 2 for other force/response pairs at multiple frequencies. However, a response ratio over 9 was seen for one location when the aft deck was the site of the force location, and other locations have factors near and above 3.

Due to the small size of this vessel, the changes performed here have significant impacts on the vessel response. These impacts appear to affect different locations differently, with changes occurring across the frequency range. For vessels of this size, these changes can impact the strength of the structure, and therefore impact not only local modes but also whole body modes.

For larger vessels, it is likely that similar changes will have a reduced impact. However, changes to the response in areas close to the additional structure can still be expected. This proximity can be thought of as being relative to the pertinent mode shape. As discussed above, the change to the lowest superstructure mode produced effects at many locations in the vessel near the frequency of that mode, both in the superstructure as well as other locations attached to the superstructure. Conversely, the change in response at frequencies of higher order local modes of bulkheads and decks are more localized.

3.8.2 Supplementary Mass Elements

To investigate the influence of discrete and smeared masses, various items were added to Model #22 described in Section 3.8.1. The models that result are as follows:

- No additional mass (Model #22)
- Anchor attached at forward main deck (Model #23)
- Weight of fluid in fuel tanks added to the tank plating (Model #24)
- A-Frame attached to aft main deck (Model #25)

These changes were performed sequentially (i.e. Model #24 includes the modifications to Model #23, etc.).

Table 18 presents the predicted frequencies for whole body mode for the various models. Differences in the predicted frequency as compared to the previous model are presented as a percentage change.

The additional mass of the anchor and the fluid weight in the fuel tanks had a relatively minor effect on the whole body modes of the vessel. The change in whole body mode frequencies was often negligible, and no greater than 2%. Conversely, the addition of the A-frame caused larger changes to some of these modes, and an extra mode was added to the system at a 22 Hz. This mode resembles a 1st order bending shape about the transverse axis. The 1st order torsional mode varied by 13% with the addition of the A-frame, though there was only a 0.1% difference in frequency of the 1st mode of the superstructure and the 2nd order torsional mode.

The results of the forced response analysis are provided in Table 19. A comparison of the response spectra from the forced response analysis for selected locations and forces are presented in Figure 55 – Figure 59.

Table 18: Modal Analysis Results for Additional Mass Details

	Model 22	Model 23		Model 24		Model 25	
	No Additional Mass	Anchor		Tanks		A-Frame	
Mode Description	Freq (Hz)	Freq (Hz)	Diff. w.r.t Model 22	Freq (Hz)	Diff. w.r.t Model 23	Freq (Hz)	Diff. w.r.t Model 24
Additional bending mode about transverse axis	n/a	n/a	-	n/a	-	22.0	-
1st order torsion	27.7	27.6	0%	27.6	0%	24.1	13%
1st order bending about transverse axis	32.8	32.5	1%	32.0	2%	29.7	7%
1st order bending about longitudinal axis	34.6	34.6	0%	34.3	1%	35.5	4%
Superstructure	46.8	46.7	0%	46.6	0%	46.6	0%
2nd order torsion	49.9	50.0	0%	49.6	1%	49.6	0%

Table 19: Forced Response Analysis Results for Supplementary Mass Elements

		Frequency, Hz						
Force Location	**Response**	**Model 22**	**Model 23**	**Diff. Rel. Model 22**	**Model 24**	**Diff. Rel. Model 23**	**Model 25**	**Diff. Rel. Model 24**
Engine Foundation, Port	Top Wheelhouse Deck, Port (see Figure 55)	**27**	27	0%	27	0%	24	11%
		33	33	0%	32	3%	29.8	7%
		67	67	0%	67	0%	67	0%
		83	81	2%	81	0%	81	0%
		89	89	0%	89	0%	90	1%
		98	97	1%	97	0%	98	1%
	Forward Main Deck, Port (see Figure 56)	**33**	33	0%	32	3%	29.8	7%
		49	49	0%	49	0%	49	0%
		57	57	0%	57	0%	57	0%
		89	89	0%	89	0%	89	0%
		98	98	0%	98	0%	98	0%
	Mid Main Deck, Port (see Figure 57)	**28**	28	0%	28	0%	30	7%
		34	34	0%	34	0%	36	6%
		50	50	0%	49	2%	49	0%
		57	57	0%	56	2%	57	2%
		76	76	0%	76	0%	73	4%
		79	79	0%	78	1%	78	0%
		84	84	0%	84	0%	84	0%
Aft Main Deck, Stbd	Frame 2 Bulkhead, Port (see Figure 58)	**24**	24	0%	24	0%	24	0%
		33	33	0%	32	3%	29.6	8%
		35	35	0%	34.5	1%	36	4%
		62	62	0%	62	0%	67	8%
		74	74	0%	74	0%	74	0%
		99	98.6	0%	98.2	0%	99.6	1%
	Main Deck Pilothouse, Stbd (see Figure 59)	**27**	27	0%	27	0%	24	11%
		33	33	0%	32	3%	29.6	8%
		54	54	0%	53	2%	53	0%
		71	70.6	1%	70.6	0%	69	2%
		85	88	4%	88	0%	89	1%

Table 19: Forced Response Analysis Results for Supplementary Mass Elements (continued)

		Velocity, in/s						
Force Location	**Response**	**Model 22**	**Model 23**	**Ratio Rel. Model 22**	**Model 24**	**Ratio Rel. Model 23**	**Model 25**	**Ratio Rel. Model 24**
Engine Foundation, Port	Top Wheelhouse Deck, Port (see Figure 55)	**5.0E-04**	5.0E-04	1.0	5.0E-04	1.0	4.1E-04	1.2
		1.7E-03	1.6E-03	1.1	1.2E-03	1.3	2.1E-03	1.8
		5.0E-03	5.0E-03	1.0	5.0E-03	1.0	9.1E-03	1.8
		4.0E-03	5.0E-03	1.3	5.0E-03	1.0	4.6E-03	1.1
		3.9E-03	1.7E-03	2.3	1.6E-03	1.1	1.5E-03	1.1
		3.1E-03	1.8E-03	1.7	1.7E-03	1.1	1.3E-03	1.3
	Forward Main Deck, Port (see Figure 56)	**1.7E-03**	1.6E-03	1.1	1.2E-03	1.3	1.9E-03	1.6
		9.5E-04	9.0E-04	1.1	9.5E-04	1.1	2.9E-03	3.1
		1.4E-03	1.4E-03	1.0	8.0E-04	1.8	2.9E-03	3.6
		5.8E-03	2.0E-03	2.9	1.8E-03	1.1	1.9E-03	1.1
		5.0E-03	1.2E-02	2.4	1.3E-02	1.1	1.2E-02	1.1
	Mid Main Deck, Port (see Figure 57)	**3.0E-04**	3.0E-04	1.0	3.0E-04	1.0	7.9E-04	2.6
		1.5E-03	1.5E-03	1.0	1.5E-03	1.0	1.3E-03	1.2
		4.0E-04	4.0E-04	1.0	4.0E-04	1.0	6.0E-04	1.5
		2.7E-04	2.7E-04	1.0	2.5E-04	1.1	6.0E-04	2.4
		1.8E-03	1.8E-03	1.0	1.8E-03	1.0	1.9E-03	1.1
		2.4E-03	2.1E-03	1.1	1.9E-03	1.1	1.9E-03	1.0
		1.9E-03	2.0E-03	1.1	2.0E-03	1.0	2.1E-03	1.1
Aft Main Deck, Stbd	Frame 2 Bulkhead, Port (see Figure 58)	**1.4E-04**	1.4E-04	1.0	1.4E-04	1.0	1.9E-04	1.4
		6.9E-04	6.7E-04	1.0	5.0E-04	1.3	7.8E-04	1.6
		6.9E-04	6.9E-04	1.0	6.9E-04	1.0	2.6E-04	2.7
		1.4E-03	1.4E-03	1.0	1.4E-03	1.0	7.9E-04	1.8
		7.0E-03	6.8E-03	1.0	5.3E-03	1.3	3.7E-03	1.4
		1.9E-03	1.8E-03	1.1	1.7E-03	1.1	8.1E-04	2.1
	Main Deck Pilothouse, Stbd (see Figure 59)	**6.4E-04**	6.4E-04	1.0	6.4E-04	1.0	6.1E-04	1.0
		1.8E-03	1.9E-03	1.1	1.6E-03	1.2	1.0E-03	1.6
		4.2E-04	4.1E-04	1.0	4.9E-04	1.2	3.1E-04	1.6
		8.2E-04	6.1E-04	1.3	6.8E-04	1.1	6.0E-04	1.1
		7.0E-04	6.9E-04	1.0	6.8E-04	1.0	6.5E-04	1.0

Figure 55: Mass Modeling Comparison, Forced Response at Top Wheelhouse Deck Port from Input Force at Engine Foundation Port

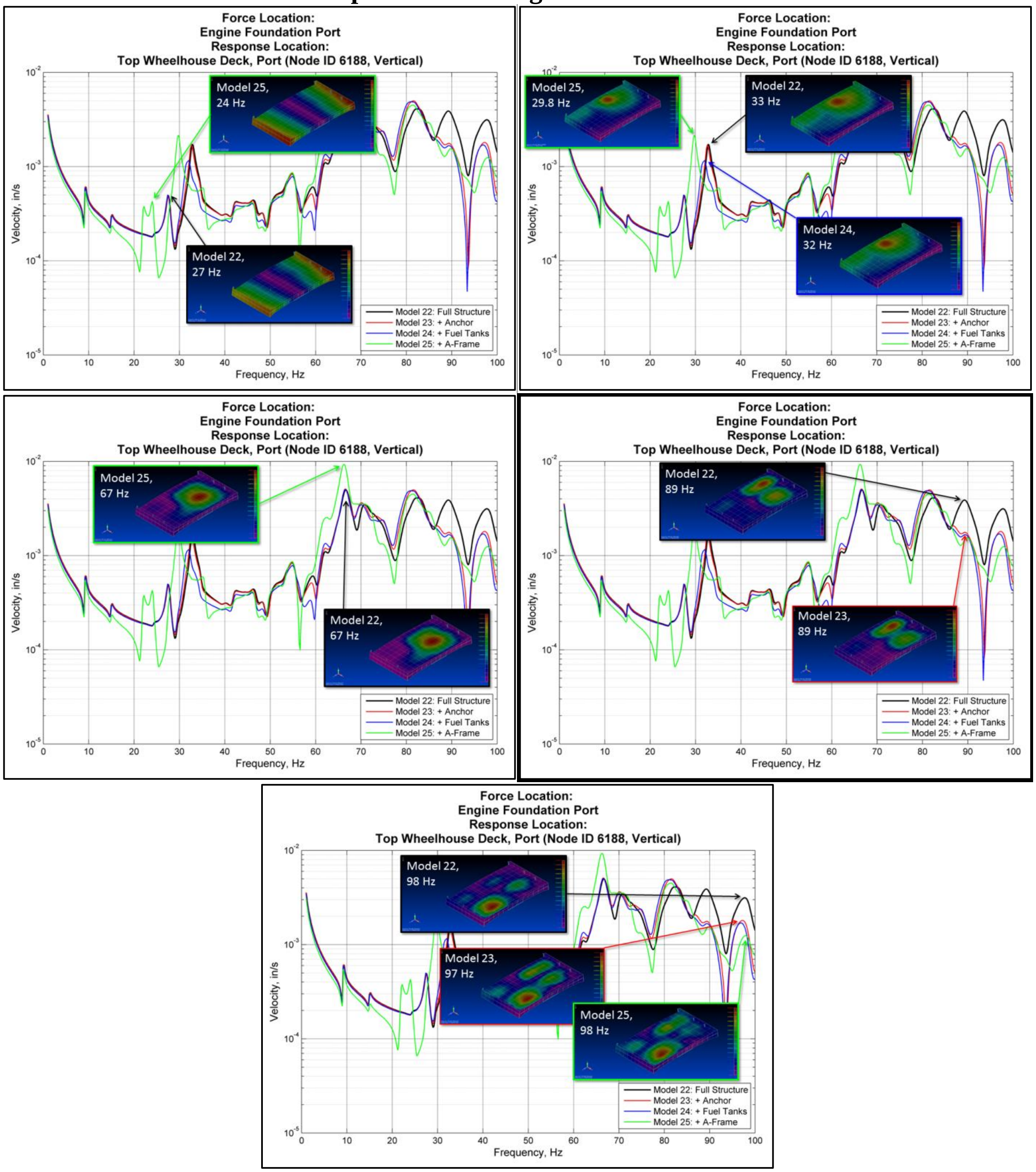

Figure 56: Mass Modeling Comparison, Forced Response at Forward Main Deck Port from Input Force at Engine Foundation Port

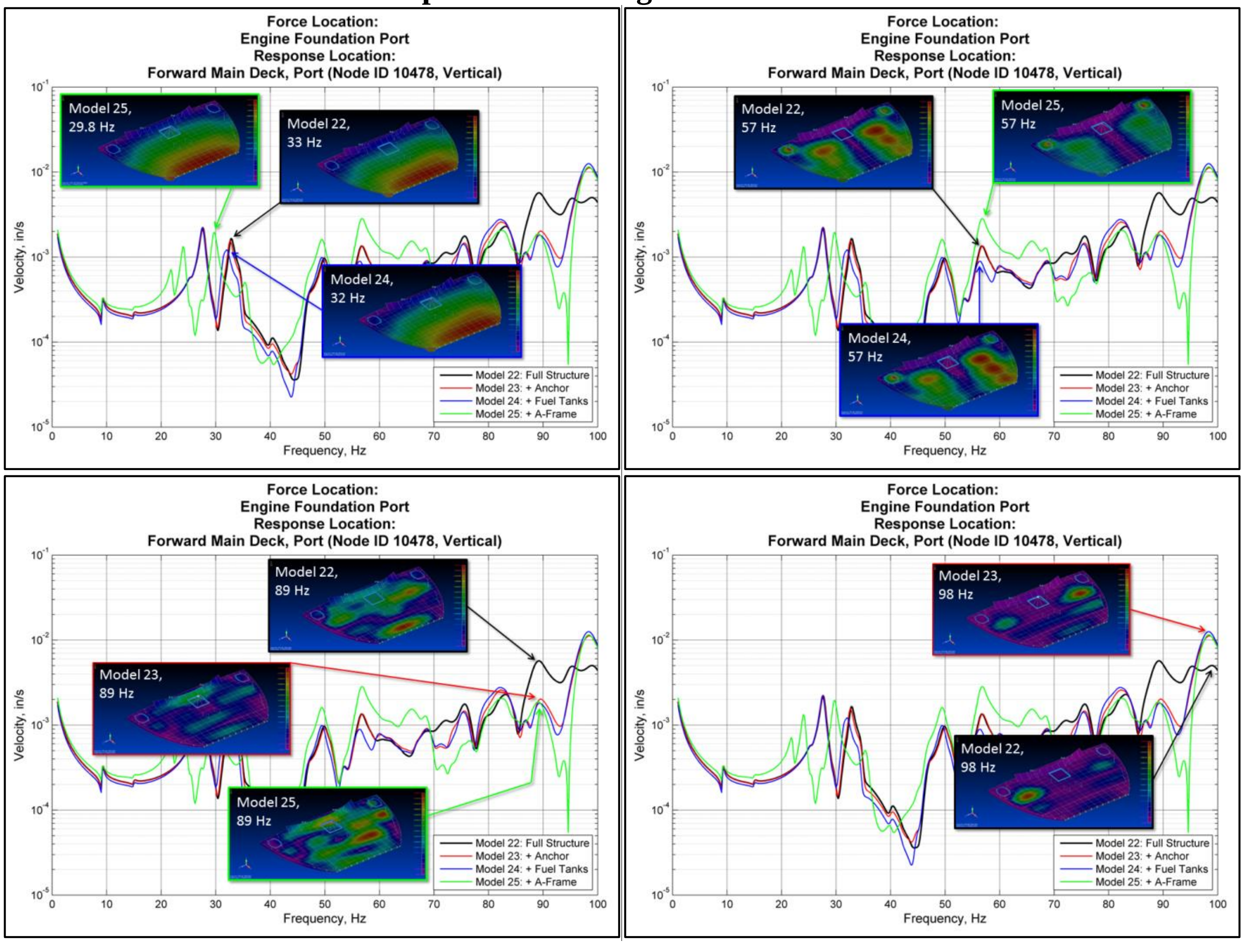

Figure 57: Mass Modeling Comparison, Forced Response at Mid Main Deck Port from Input Force at Engine Foundation Port

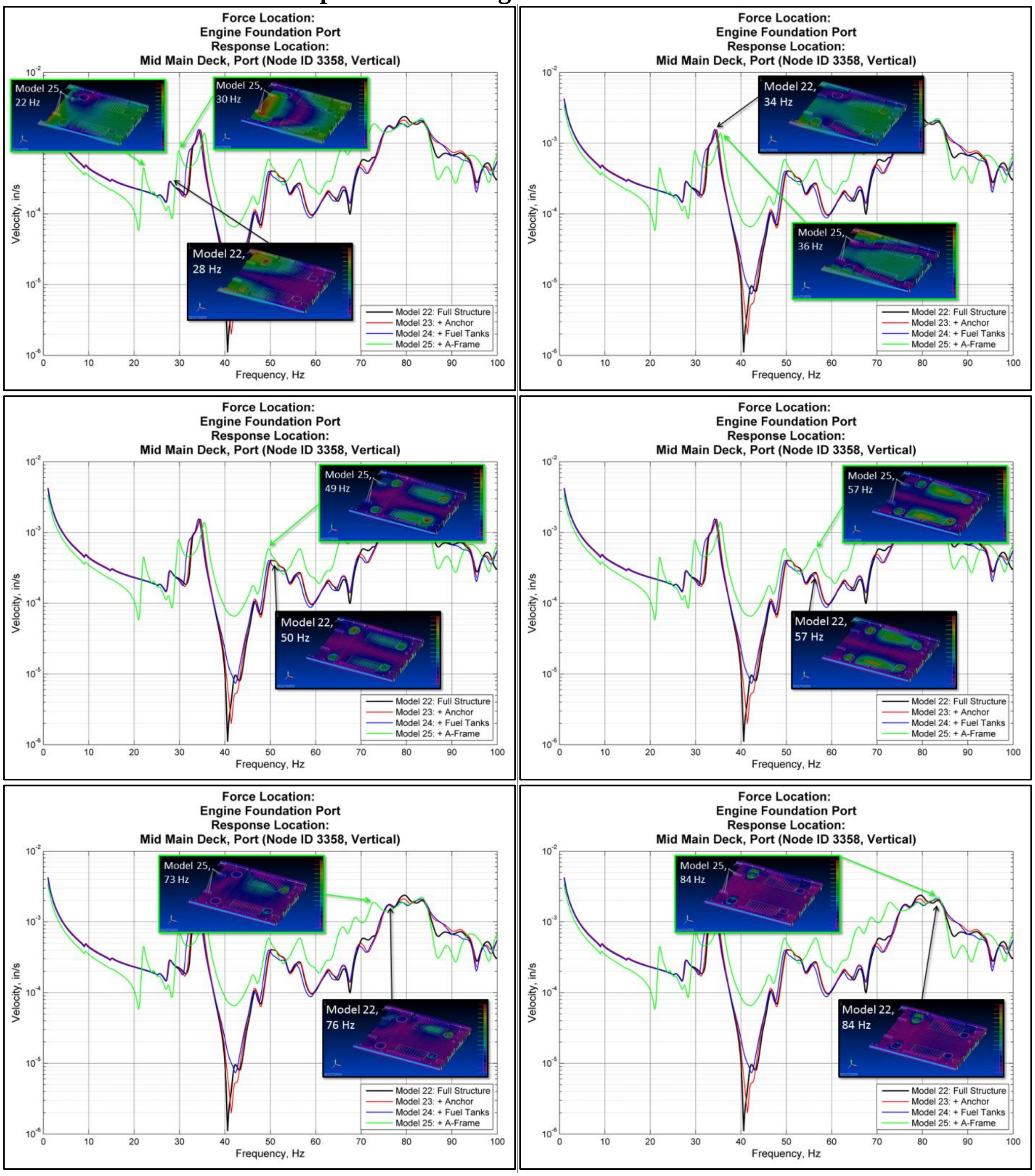

Figure 58: Mass Modeling Comparison, Forced Response at Frame 2 Bulkhead Port from Input Force at Aft Main Deck Stbd

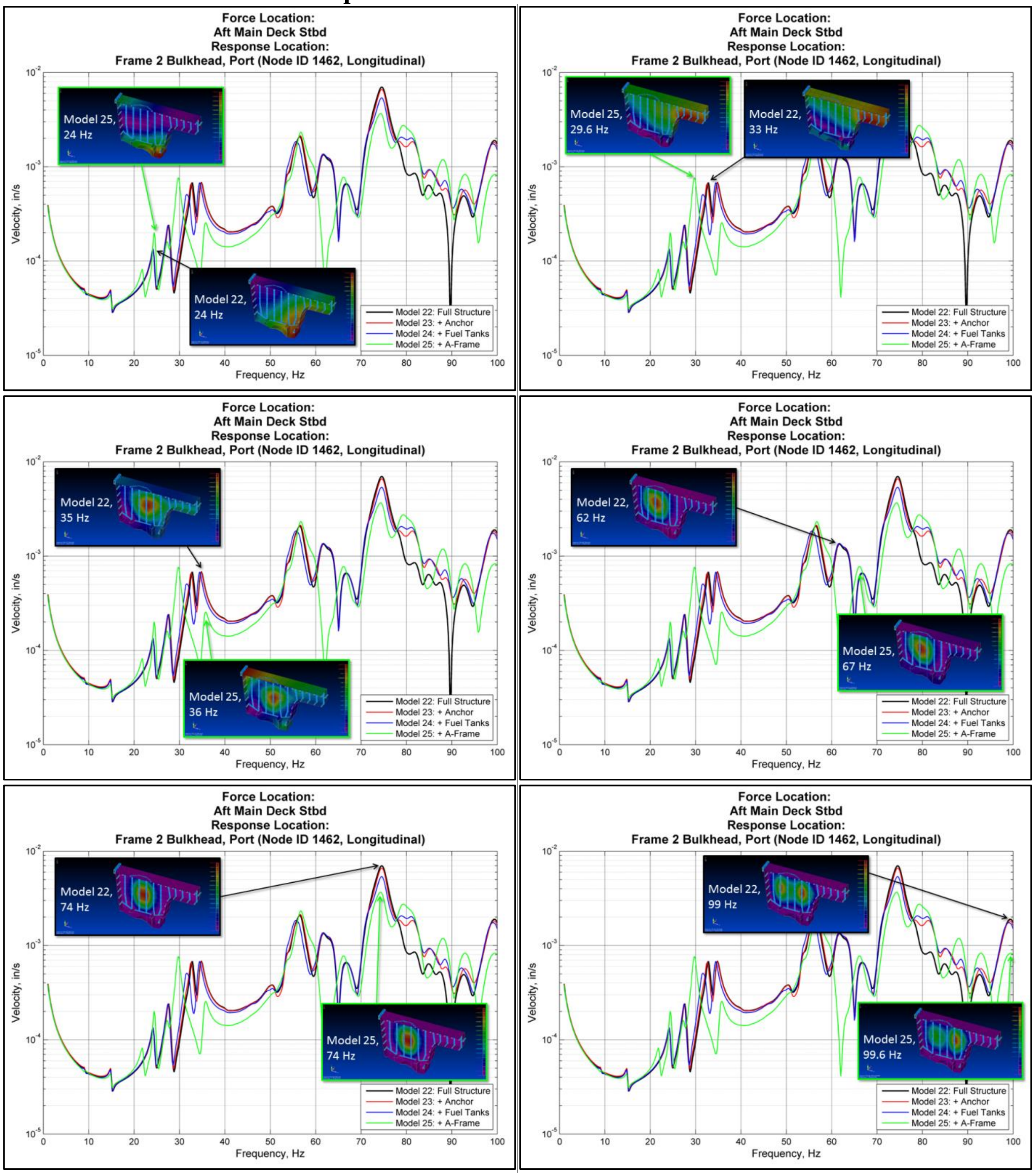

Figure 59: Mass Modeling Comparison, Forced Response at Main Deck Superstructure Stbd from Input Force at Aft Main Deck Stbd

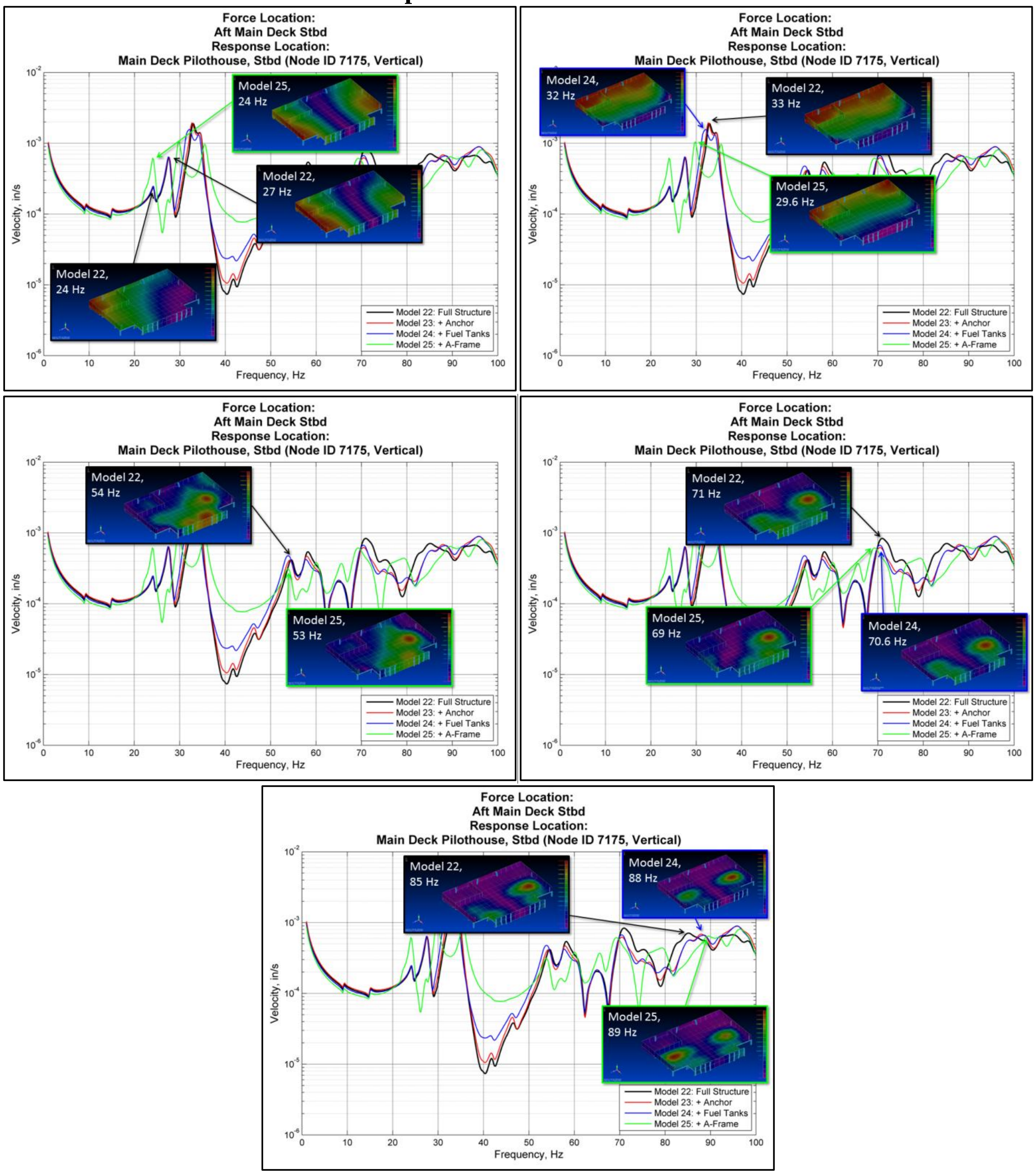

Generally, the additional mass of the anchor and the fluid in the fuel tanks had a relatively minor impact on the forced response results throughout the vessel. The largest differences were observed for response areas in close proximity to the additional mass, such as the forward main deck near the anchor, and at the extremities of the vessel such as the top wheelhouse deck and mast (which is dynamically weaker than a deck or bulkhead).

The response magnitude varied by a factor of less than 2 when the anchor and fluid masses were added, though some specific locations varied by a factor of nearly 3. Differences in resonance frequencies were mostly less than 1% with specific locations varying by as much as 4%. Stiffened areas such as the inboard and outboard hull plating were practically unaffected by adding the anchor mass and the fluid weight in the fuel tanks. Furthermore, the differences in the response were only observable in the frequency range of higher order localized modes (approximately 70-100 Hz for this vessel). The differences were negligible at frequencies in the range of the global modes of the vessel and even some lower order localized modes (below 70 Hz).

The additional mass of the A-frame, as well as the increase in stiffness of the rigid element connections used to model the A-frame, had a significant effect on the forced response in all areas of the vessel. It should be noted that the mass of the A-frame relative to the light-ship weight of the vessel was approximately 9%, which is a relatively large percentage of the total mass. The additional mass and stiffness from the A-frame was significant enough to drastically change the lower-frequency global modes of the vessel.

Large variations in the peak frequency and magnitude of the response were seen at all frequencies after adding the A-frame, starting at the range of the first global mode of the vessel. The magnitude of response varied by a factor near 2 in many locations, and deviations up to a factor of 3.6 were also seen. The most significant effects are arguably in the frequency range of the first several global modes of the vessel (approximately 20-50 Hz), though for some response locations, particularly those near the A-frame, significant differences are seen at higher frequencies corresponding to local modes as well.

These results show that certain types of masses can affect the response of the vessel, though in some cases the effects are negligible. In the case of the anchor and tank loads, the added mass was on the order of 4% or less of the total mass of the model, and only small changes were seen to the response. Any change that was seen was largely focused in the area of the added mass, and at frequencies of high order modes.

The addition of the A-frame caused much greater changes, and is likely due to the fact that not only mass was added but stiffness was also added through rigid elements. The specific approach used here is common for modeling certain structures on vessels such as A-frame, cranes, and similar appendages, though the accuracy of such approaches may be suspect particularly for a structure such as an A-Frame.

As noted above the A-frame makes up a large percentage of the mass of the vessel (9%) and the tank masses added roughly 4% to the total model mass. The location of these masses, as well as their implementation into the model, likely plays a role in the change to the predicted vibration response. Given the size of this model it is difficult to develop strong conclusions as to when certain structures should be added, though a rough guideline of any mass over 5% of the vessel weight could be used until additional data becomes available.

3.9 Joiner and Deck Coverings

3.9.1 Aluminum Base Structure

Multiple models were created to investigate the influence of adding non-structural mass corresponding to joiner and deck coverings. All models started with Model 22 as the reference model, described in Section 3.8.1. The models that result are as follows:

- Baseline (Model #22)
- Both joiner and deck covering non-structural mass (Model #30)
- Baseline model with only joiner mass added (Model #31)
- Baseline model with only deck mass added (Model #32)

A comparison of the predicted whole body modes is provided in Table 20. Also provided in the table is the approximate difference of the total weight between the finite element models. With non-structural mass added to both the bulkheads and decks, there is approximately 11% more mass added to the model. As discussed previously, this increase is relatively high since the base structure is aluminum and the vessel is small.

All models predict the natural frequencies of the 'whole-body' global modes of the vessel to within 6% of the baseline model, with most frequencies being within 2%. The largest differences were observed in the 1st order bending mode about the transverse axis, where the natural frequency shifted by approximately 5% with additional mass on the decks and by 6% with additional mass on both the decks and the bulkheads.

Table 20: Summary of Results for Modal Analysis

	Model 22	Model 30		Model 31		Model 32	
	No Additional Mass	Joiner and Deck Mass		Joiner Mass ONLY		Deck Mass ONLY	
Mode Description	Freq. (Hz)	Freq. (Hz)	Diff. w.r.t Model 22	Freq. (Hz)	Diff. w.r.t Model 22	Freq. (Hz)	Diff. w.r.t Model 22
1st order torsion	27.7	27.3	1%	27.5	1%	27.4	1%
1st order bending about transverse axis	32.8	30.9	6%	32.3	1%	31.3	5%
1st order bending about longitudinal axis	34.6	34.4	1%	34.6	0%	34.4	1%
Superstructure	46.8	45.8	2%	46.1	1%	46.7	0%
2nd order torsion	49.9	49.2	2%	49.7	0%	49.5	1%
Total Weight (lb)	23,129	25,845	11.7%	24,074	4.1%	24,900	7.7%

The results of the forced-response analysis are provided in Table 21. As was done previously, this table presents frequency differences as a percentage and the velocity response differences as a ratio (i.e. higher magnitude divided by lower magnitude). The predicted spectra for selected force/response locations for the models with and without the added non-structural mass are presented in Figure 60 - Figure 65.

The results show that the additional non-structural mass can have a large impact on the response at locations where mass was added. Other response locations throughout the vessel showed small to negligible changes in response. The results presented in Table 21 and the associated figures are focused primarily on locations where the non-structural mass was added to best illustrate the worst-case differences.

Generally, the frequencies of resonance peaks varied by as much as 5%, though at specific locations some resonances varied by as much as 10-15%. The degree of frequency shift appeared to increase with frequency; higher-order modes showed greater variation in frequency than lower-order modes.

The difference in response magnitude between the models with and without non-structural mass shows that in general there are moderate differences in the velocity response magnitudes, on the order of 2 or less. However, there are several locations and frequencies where the velocity magnitude can change my much more than this, and in extreme cases is off by a factor of 10 or more.

Based on the results presented here, the differences in frequency and magnitude of resonances appear to be on the same order as variations with other changes to finite element modeling parameters (i.e. mesh density, plate element type, stiffener element type, etc.). However, upon inspection of the 3-dimensional displacement contours, it is clear the resonance peaks most comparable in frequency and magnitude are not similar in the operational deflection shape (at least at higher order modes above 50 Hz).

For instance in Figure 60, the response on the top wheelhouse deck is quite similar at lower-order local modes (i.e. at 31-32 Hz), but quickly diverges at higher-order local modes (above 50 Hz). At 66-67 Hz, the response of the model without additional mass appears to be a lower-order ‘breathing’ mode of the entire deck, yet the response of the model with additional mass appears to be more akin to a higher-order, more localized mode despite being at the same frequency.

Similar behavior is observed on the Frame 8 bulkhead in Figure 62. Note the deflection contours of the bulkhead without additional mass (at 71.4 Hz) and the bulkhead with additional mass (52.8 Hz and 75.6 Hz). The deflected shape appears to be most similar at frequencies 71.4 Hz (no additional mass) and 52.8 Hz (additional mass). At these resonances, there is a larger difference in frequency, but less of a difference in magnitude. When comparing the resonances at 71.4 Hz (no additional mass) and 75.6 Hz (additional mass), there is little correlation between the deflection shape yet the difference in frequency is much less and the difference in magnitude is greater. Similar results are seen for the other response locations.

It is seen that in general the additional mass can have a large impact on the response magnitude over large frequency ranges. However these changes appear to be limited to the areas where the mass is added. This can be seen directly by comparing the response at a given location (Main Deck Pilothouse, Figure 65, for example) for the baseline model and the addition of the joiner (bulkhead) mass and deck covering mass separately. It is seen that the change in response on the deck is only significant when the mass is added to the deck. The response on the deck as a result of adding joiner mass is nearly the same as the baseline model. Given reciprocity, it can be inferred that a similar effect would also occur for added mass at the location of force excitation.

Table 21: Summary of Results for Forced Response Analysis

		Frequency, Hz			Velocity, in/s		
Force Location	**Response Location**	**Model 22**	**Model 30**	**Diff.**	**Model 22**	**Model 30**	**Diff. Ratio**
Aft Main Deck, Stbd	Top Wheelhouse Deck, Stbd (see Figure 60)	32.8	31	5%	2.4E-03	2.3E-03	1.0
		54.8	54.2	1%	1.7E-04	3.7E-04	2.2
		67.6	66.4	2%	4.9E-04	1.2E-03	2.4
		76.6	82.8	8%	5.8E-04	5.8E-04	1.0
		81.6	82.8	1%	8.0E-04	5.8E-04	1.4
		86.8	87.4	1%	7.9E-04	4.6E-04	1.7
	Pilothouse Longitudinal Bulkhead, Port (see Figure 61)	24.2	24.6	2%	1.8E-05	3.0E-05	1.7
		29.8	27.2	9%	3.1E-05	1.1E-04	3.4
		34.6	34.4	1%	5.9E-04	7.6E-04	1.3
		56.8	56.4	1%	2.6E-04	3.1E-04	1.2
		75.8	76	0%	3.0E-04	3.7E-04	1.2
		86.8	85.4	2%	3.1E-04	9.5E-04	3.1
		98.6	99	0%	3.1E-04	7.1E-04	2.3
Engine Foundation, Port	Frame 8 Bulkhead Above Deck, Port (see Figure 62)	22.8	21.6	5%	1.3E-05	1.5E-04	11.8
		33	31	6%	5.6E-04	8.9E-04	1.6
		46.8	39.8	15%	1.4E-03	2.7E-03	2.0
		46.8	52.8	13%	1.4E-03	1.5E-03	1.1
		71.4	75.6	6%	8.4E-03	8.0E-04	10.5
		81	78.4	3%	2.3E-03	8.5E-04	2.7
		96.2	96.2	0%	2.1E-03	1.1E-03	1.9
	Mast, Port (see Figure 63)	27.6	27.2	1%	5.0E-03	4.2E-03	1.2
		42	43.2	3%	7.5E-04	3.9E-03	5.2
		55.8	55.4	1%	2.3E-04	5.4E-04	2.3
		83.4	85.8	3%	6.6E-03	5.7E-03	1.2
	Top Wheelhouse Deck, Port (see Figure 64)	27.6	27.2	1%	4.9E-04	7.3E-04	1.5
		32.8	31	5%	1.7E-03	1.6E-03	1.1
		42.6	40.6	5%	4.3E-04	3.3E-03	7.9
		54.8	50	9%	8.4E-04	3.4E-04	2.5
		66.6	66.6	0%	5.0E-03	6.5E-04	7.6
		82.4	80	3%	4.1E-03	3.9E-03	1.0
		83.2	89.4	7%	3.5E-03	3.9E-03	1.1
		97.8	96.6	1%	3.1E-03	4.8E-03	1.5
	Main Deck Pilothouse, Stbd (see Figure 65)	33	31	6%	8.8E-04	5.4E-04	1.6
		65.6	63.2	4%	5.4E-04	1.2E-03	2.3
		70	71.2	2%	1.3E-03	4.6E-03	3.6
		80.4	76.6	5%	2.0E-03	7.3E-03	3.6
		96.2	94.8	1%	3.1E-03	4.3E-03	1.4

Figure 60: Forced Response Analysis Results of force at Aft Main Deck and response at Top Wheelhouse Deck

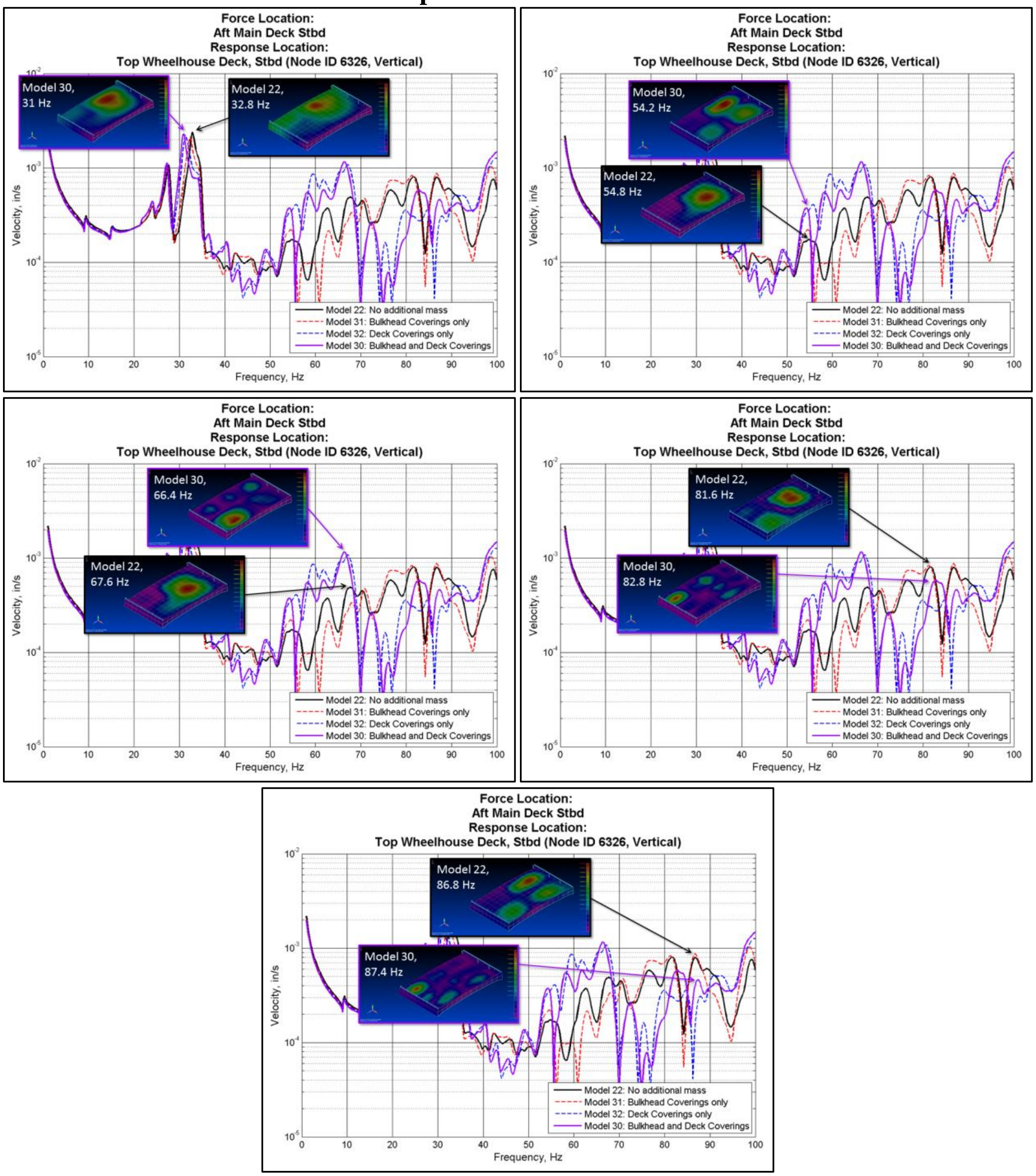

Figure 61: Forced Response Analysis Results of force at Aft Main Deck and response at Port Pilothouse Longitudinal Bulkhead

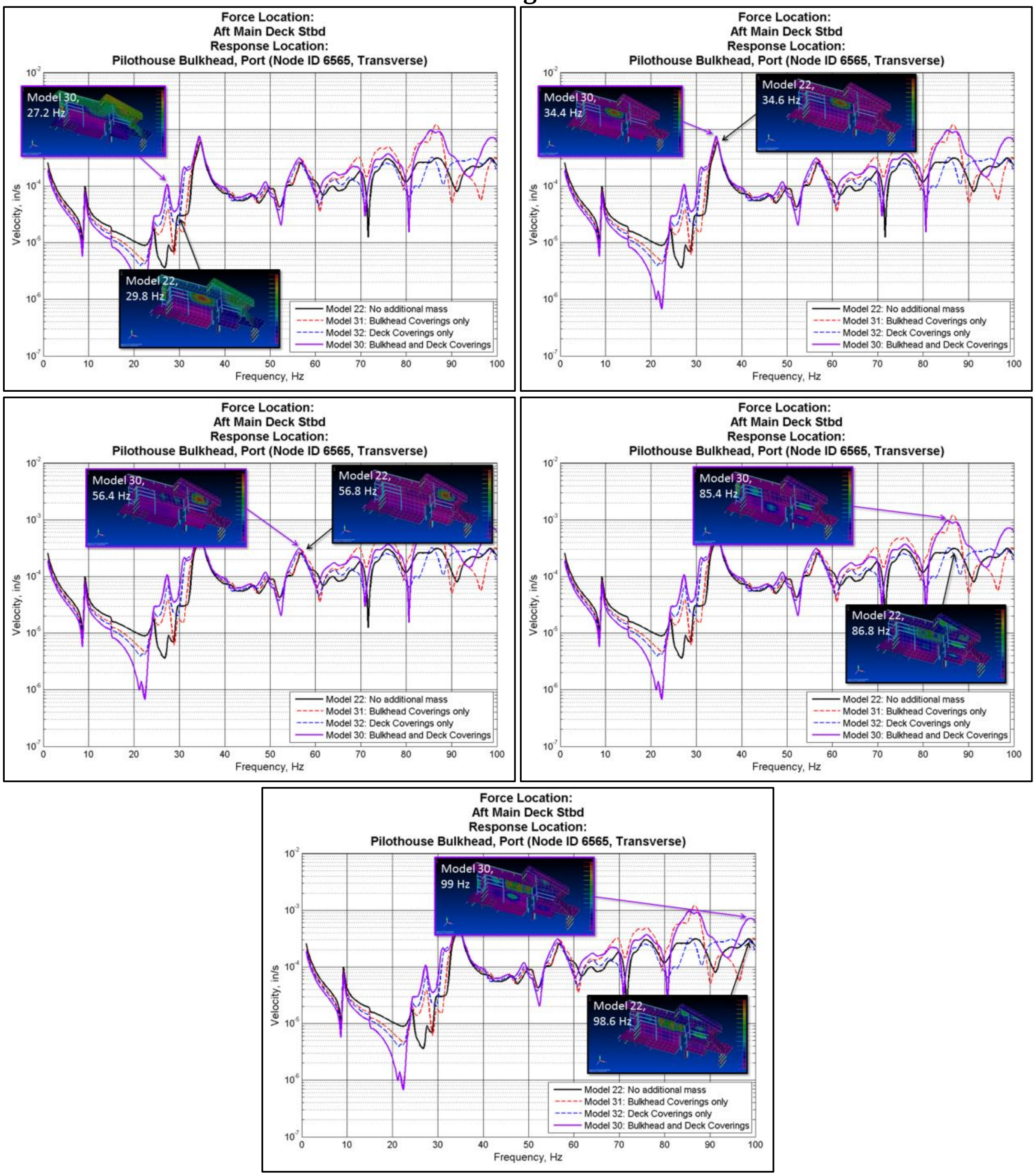

Figure 62: Forced Response Analysis Results of force at Port Engine Foundation and response at Frame 8 Bulkhead Above Deck

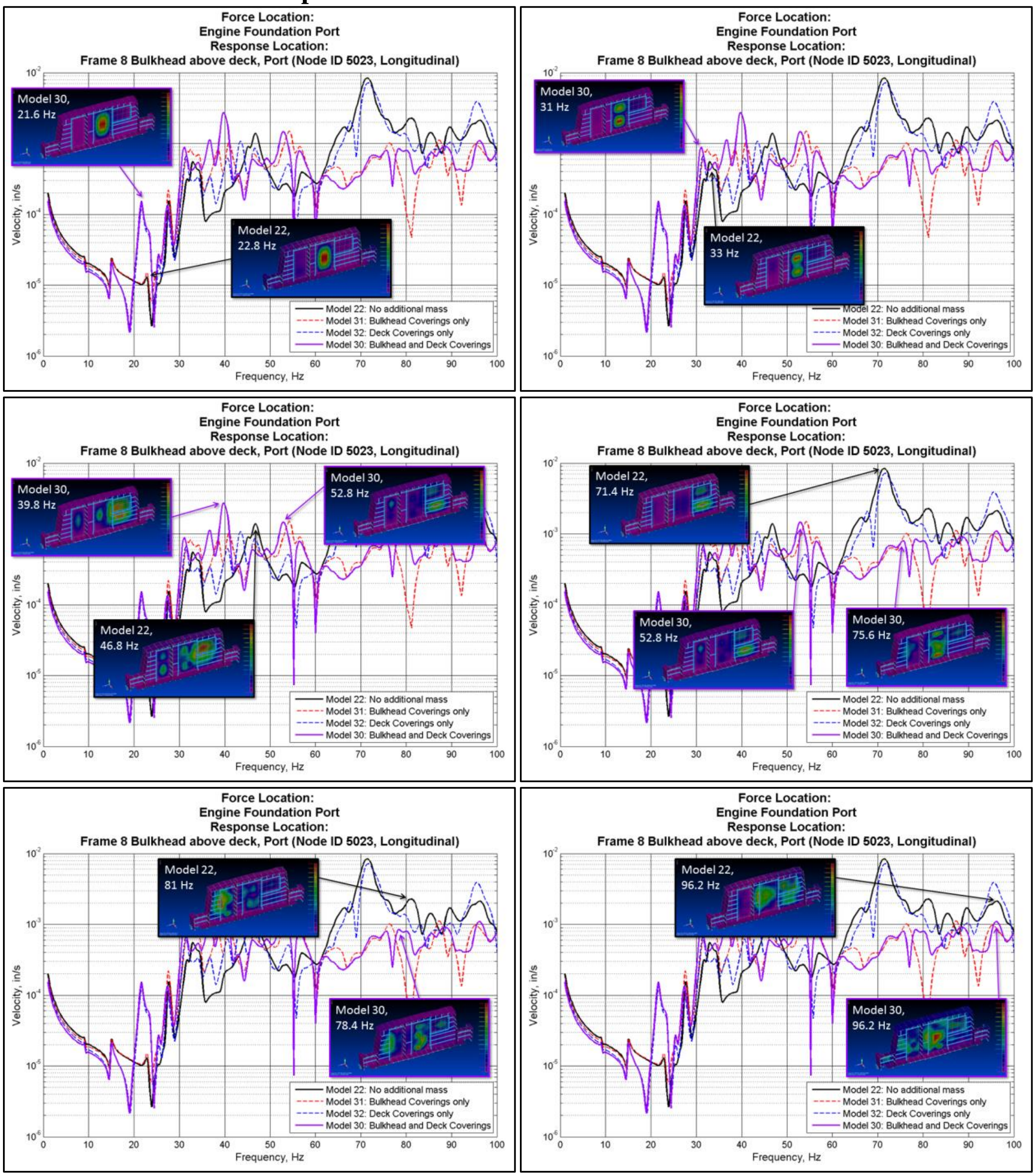

Figure 63: Forced Response Analysis Results of force at Port Engine Foundation and response at the Mast

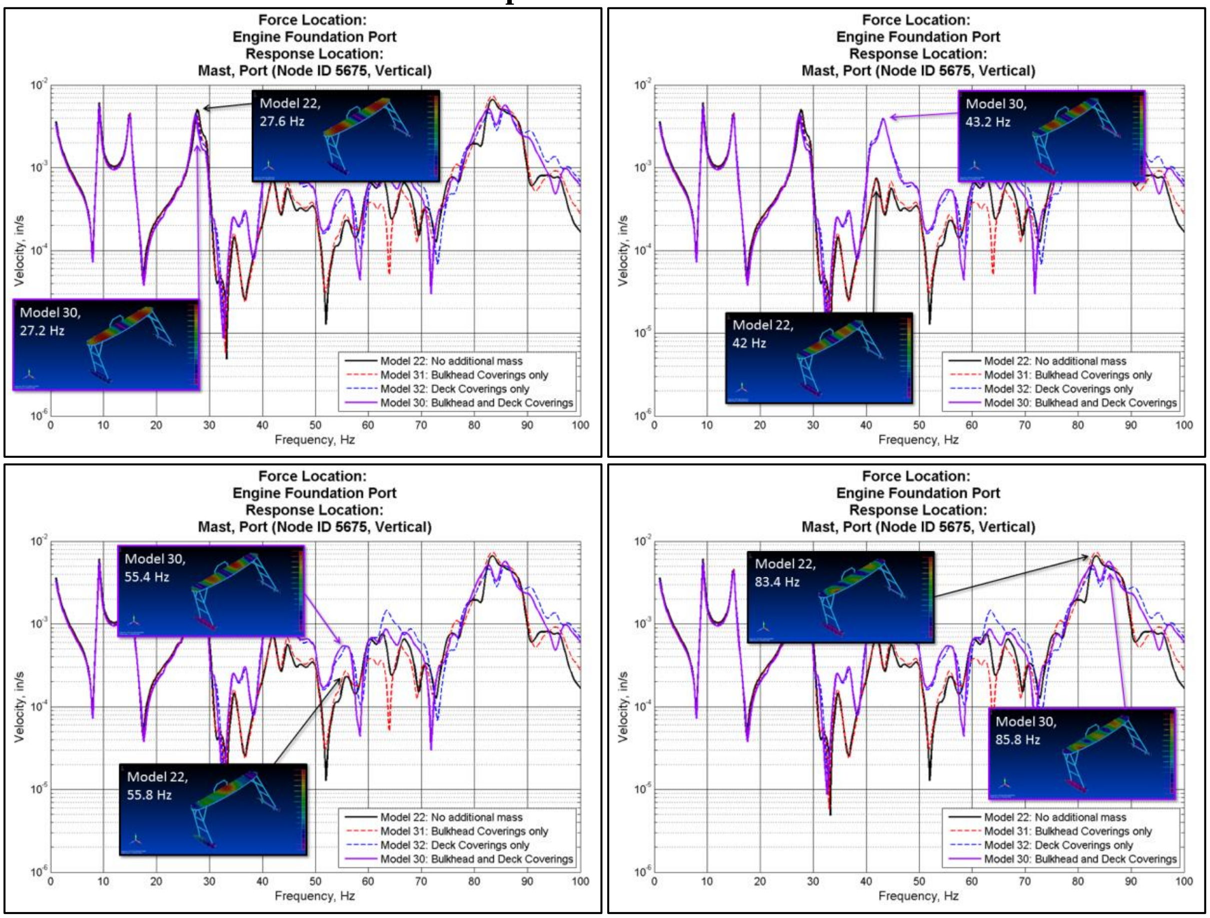

Figure 64: Forced Response Analysis Results of force at Port Engine Foundation and response at Top Wheelhouse Deck

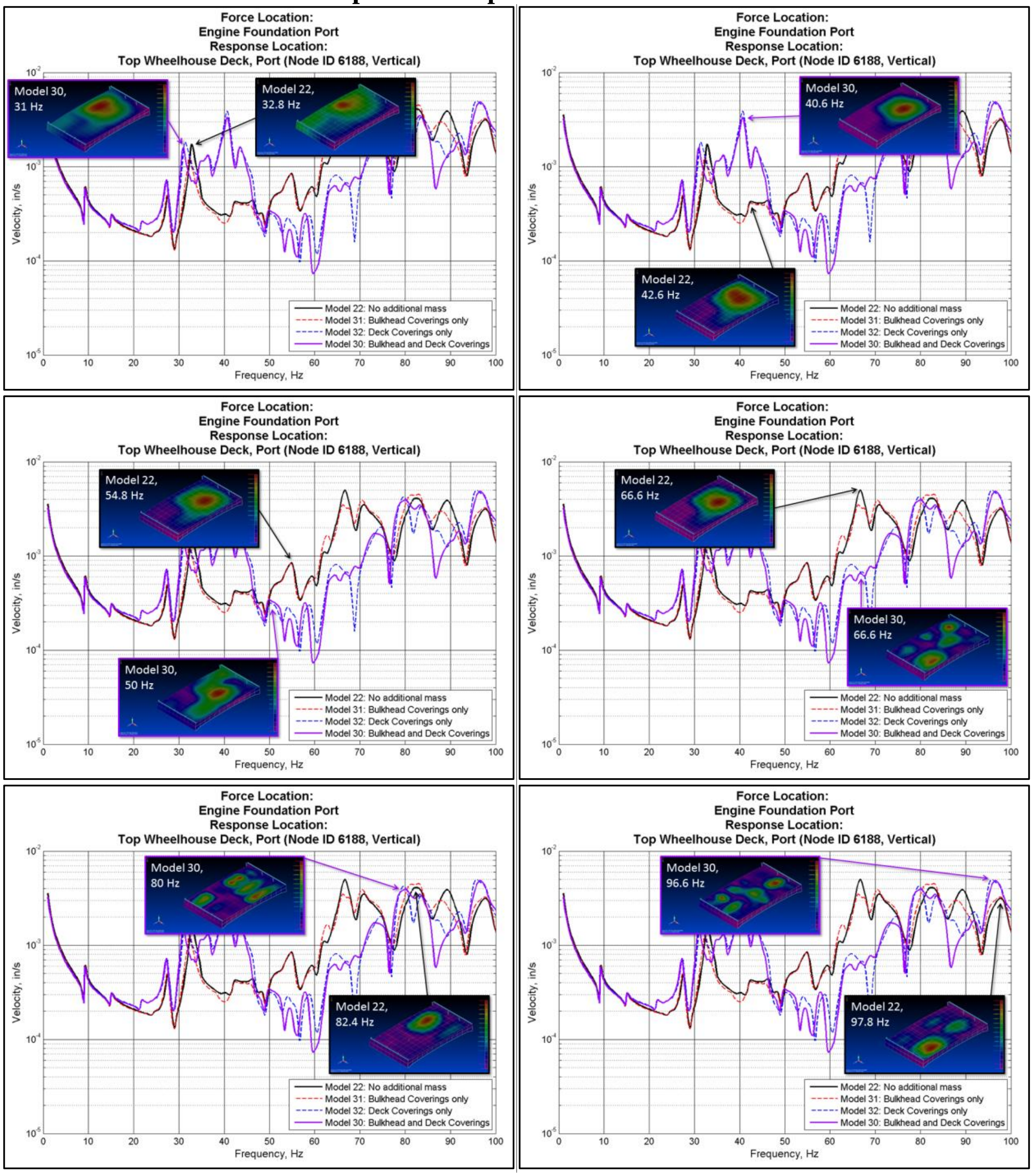

Figure 65: Forced Response Analysis Results of force at Port Engine Foundation and response at Main Deck Pilothouse

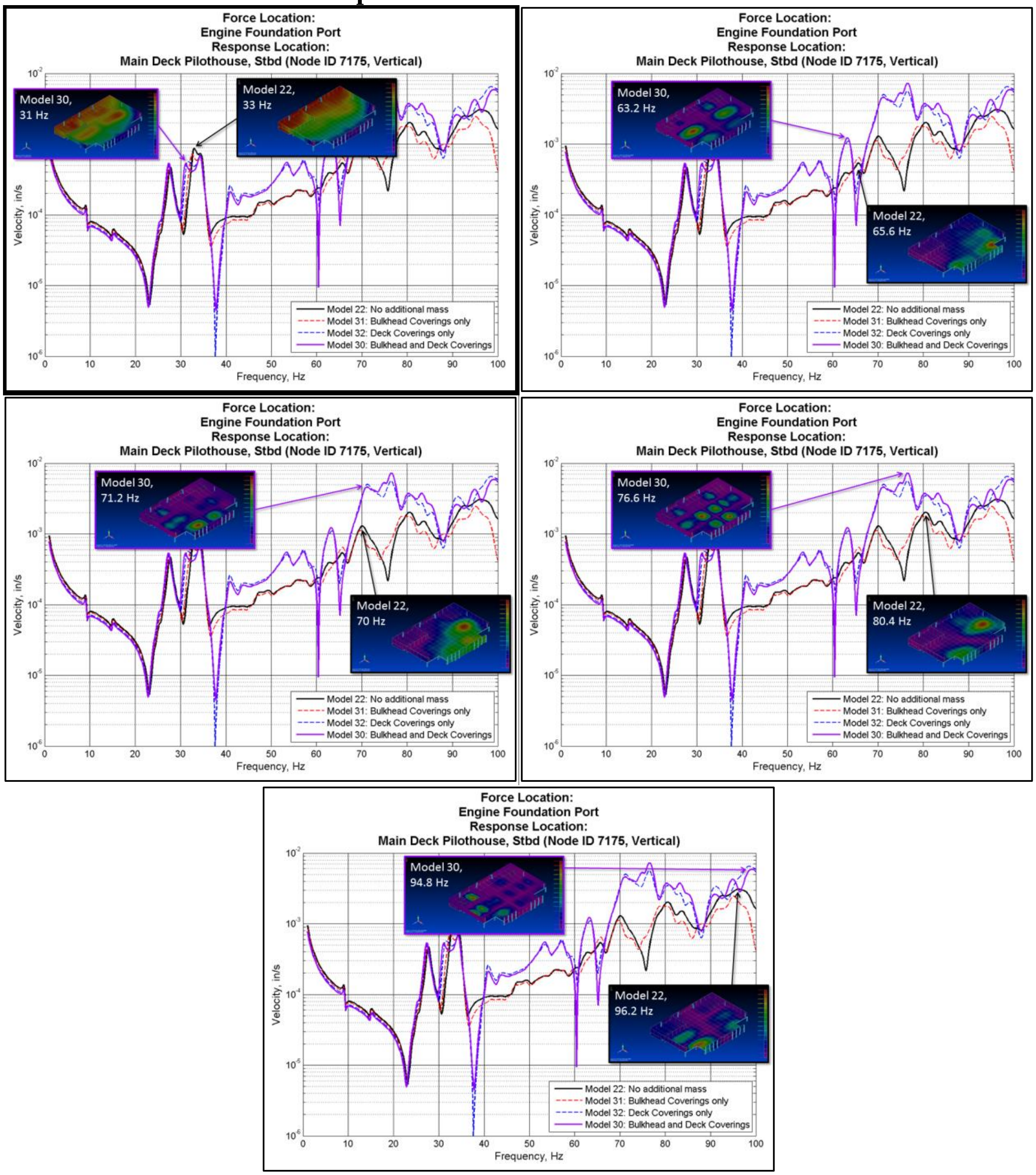

3.9.2 Results for Steel Structure

The results from the previous section shows a high degree of change when joiner and deck coverings are added to the aluminum base structure. It has been hypothesized that this is due to the relatively large change in mass that these items create for a small aluminum vessel, and when applied on a steel structure the relative change would be reduced.

An additional model was created (Model 33) in which the non-structural mass of the joiner panels and deck coverings was changed to represent the same area density ratio for an equivalent steel structure. In this report this is referred to as the "steel" model. The mass was changed in this way to facilitate direct comparison of results between baseline and treated models.

Table 22 provides a summary of the modal analysis for this model as compared to both the baseline model (Model 22) and the previous 'aluminum' model with both joiner and deck covering mass (Model 30). Within the first five 'whole body' low frequency modes of the vessel, there is no more than 2% difference in frequency from the baseline model to the 'steel' model, compared to a maximum 6% difference to the 'aluminum' model.

Table 22: Summary of Results for Modal Analysis

	Model 22	Model 30		Model 33	
	No Additional Mass	Non-structural Mass Proportional to Aluminum		Non-structural Mass Proportional to Steel	
Mode Description	Freq. (Hz)	Freq. (Hz)	Difference w.r.t Model 22	Freq. (Hz)	Difference w.r.t Model 22
1st order torsion	27.7	27.3	1%	27.5	1%
1st order bending about transverse axis	32.8	30.9	6%	32.2	1%
1st order bending about longitudinal axis	34.6	34.4	1%	34.5	0%
Superstructure	46.8	45.8	2%	46.2	1%
2nd order torsion	49.9	49.2	2%	49.7	0%

An attempt was made to match the deflection shape at specific peaks between models in order to identify how much a particular mode was impacted by the addition of mass. A brief comparison of the forced response analysis results are provided in Table 23, which includes one 'worst case' result. The corresponding frequency spectra can be found in Figure 66. For this comparison, the response on the Top Wheelhouse deck was analyzed with the input force at the port engine foundation. The entire deck was evaluated (rather than just a single node) to provide a more comprehensive comparison of the resonance response at any location on the deck.

Table 23: Summary of Results for Forced-Response Analysis

Frequency, Hz					**Velocity, in/s**				
Model 22	**Model 30 (Alu)**	**Diff. Model 22**	**Model 33 (Steel)**	**Diff. Model 22**	**Model 22**	**Model 30 (Alu)**	**Diff. Ratio Model 22**	**Model 33 (Steel)**	**Diff. Ratio Model 22**
66.6	*40.6*	*39%*	*52*	*22%*	*5.9E-03*	*3.9E-03*	*1.5*	*3.1E-03*	*1.9*
83	*53*	*36%*	*69.4*	*16%*	*1.1E-02*	*1.1E-03*	*9.8*	*2.0E-03*	*5.3*

Figure 66: Forced Response Analysis Results for Force at Port Engine Foundation and Response at Top Wheelhouse Deck

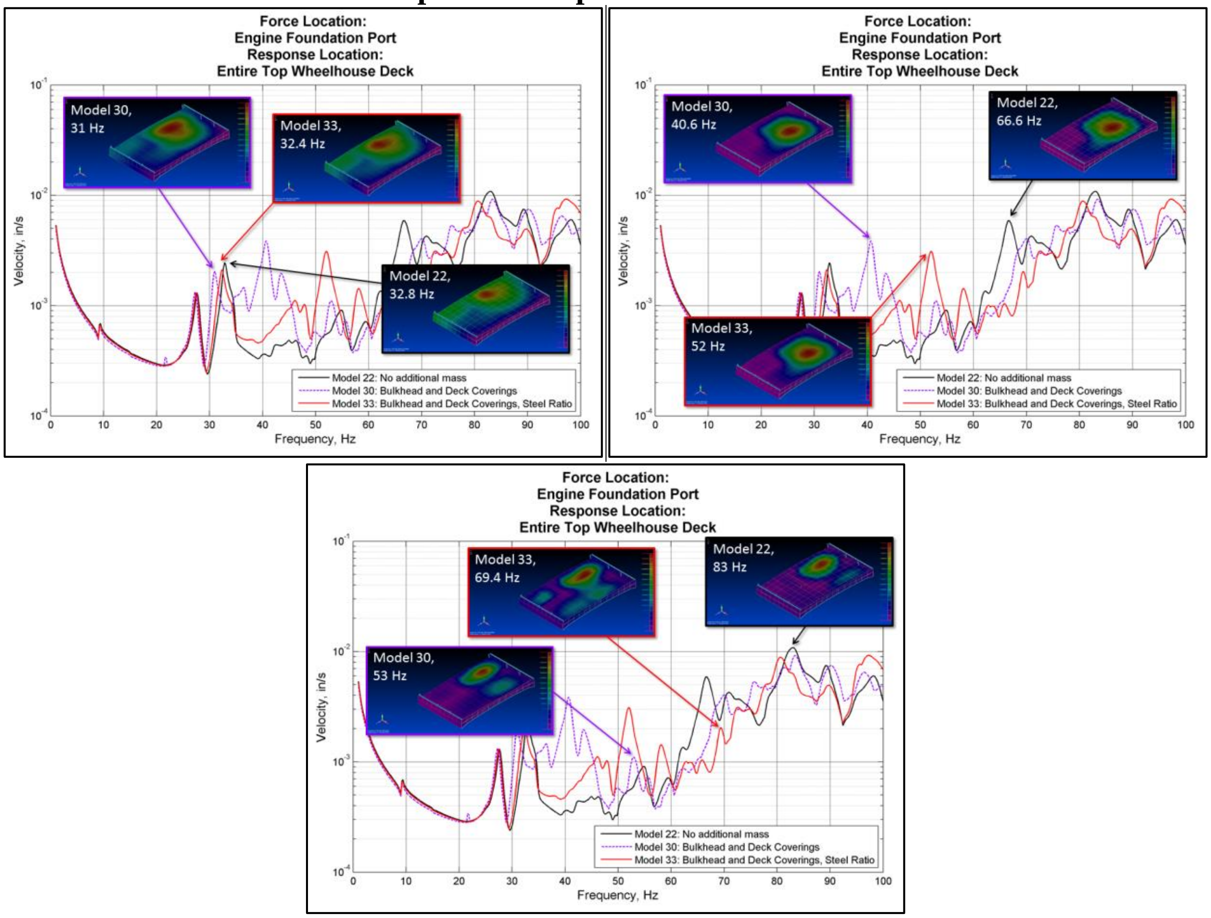

The change in the frequency of response peaks is seen to be greater for the aluminum model as compared to the equivalent steel model, though in both cases the change can be significant. The difference in magnitude of the higher order resonances also appears, on the surface, to be significant; the maximum difference ratio is nearly 10 for the aluminum model. However, given the large change in frequency these differences are believed to be due to summation with other nearby modes. For example, for the baseline aluminum model the 83 Hz peak is likely higher in amplitude due to the presence of other nearby modes which act to increase the overall vibration response in this frequency range; conversely, the same peak in the aluminum model is at 53 Hz which is seen to be a frequency range with lower modal density.

Additional force/response location pairs were analyzed and are presented in Figure 67 and Figure 68. Generally, the resonance response is changed to a lesser degree when the same non-structural mass is added to a steel structure (Model 33) compared to an aluminum structure (Model 30). It is also seen that for many of these combinations the changes in frequency is less significant particularly at the lower order modes of the structure.

Figure 67: Forced Response Analysis Results at Various Response Locations due to Force at Port Engine Foundation

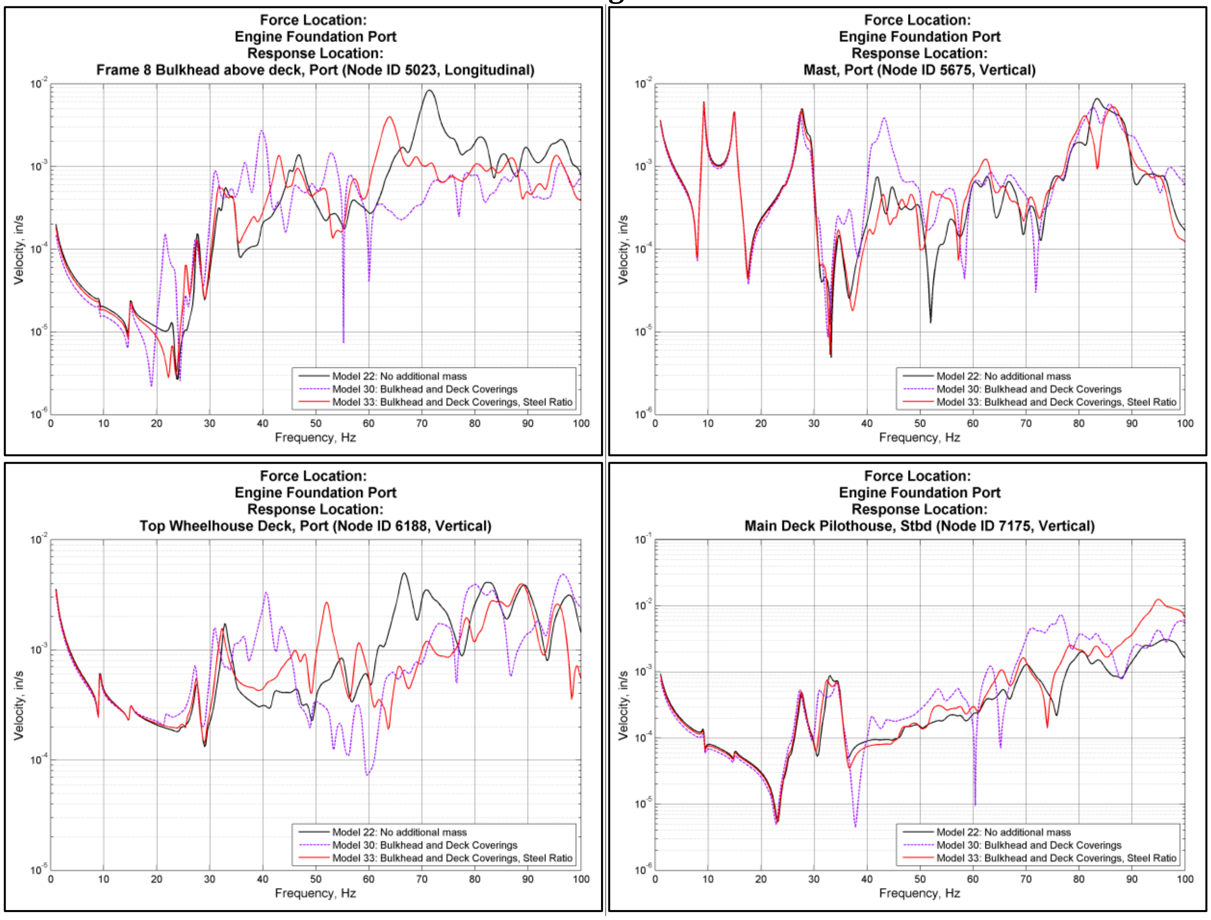

Figure 68: Forced Response Analysis Results at Various Response Locations due to Force at Aft Main Deck

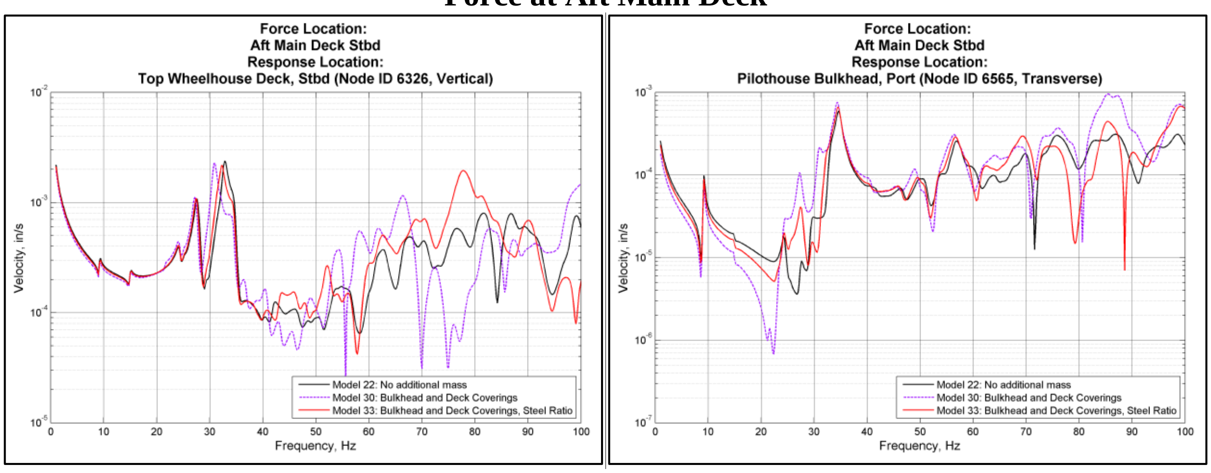

4.0 PHASE I CONCLUSIONS

The results of Phase I must be taken in conjunction with a proposed analysis approach for assessing ship vibration. As discussed in Section 2.10 and shown throughout this report, the predicted peak frequency for any given mode will shift depending on how the model is created. The general analysis approach applied to assessing ship vibration levels must take this shift into account. Although many machinery sources generate forces at specific frequencies (e.g. a genset may generate forces at 15 Hz, 30 Hz, 45 Hz, etc.), assessing the predicted vibration levels at a single frequency is not recommended as large errors can result.

Instead, it is suggested that a 'prediction frequency range' be used for any single excitation frequency, as illustrated in Figure 69. The prediction frequency range would be centered on the actual excitation frequency, but would span a range of frequencies which includes the peak in predicted response. In this case, the maximum response in the prediction frequency range would yield an accurate prediction of the actual response even though the predicted peak response frequency does not exactly match the excitation frequency of the real source. In theory, this approach can yield accurate predictions even with errors in the raw modeling results. The analysis frequency range would be chosen based on the expected error in the predicted frequency of controlling modes.

Figure 69: Example of Proposed Analysis over a Frequency Range

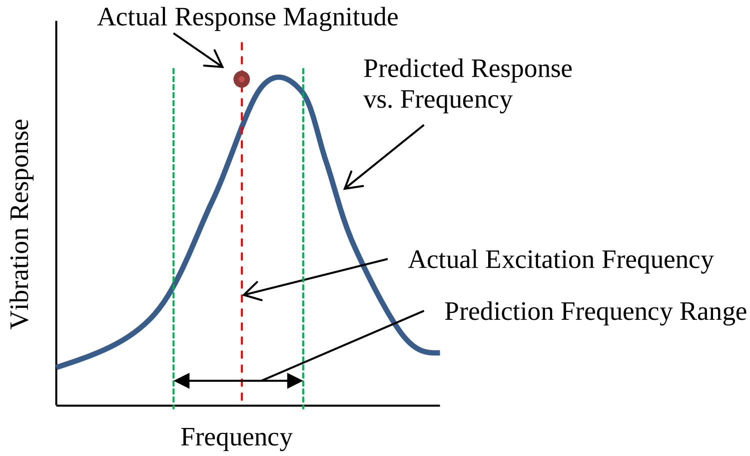

The example provided above is clearly idealized. When taking the maximum level over a frequency range it can be expected that the resulting prediction will tend towards conservative results (i.e. will predict higher levels than what would be found on the vessel). For example, if the excitation frequency from a machinery item does not line up with a response peak in the structure then the actual response magnitude would be low (relatively speaking); if the prediction frequency range includes a peak in response then the predicted level will be greater than the actual response.

Another option for analysis is to use the average response over the prediction frequency range. This approach yields a less conservative result, though may lead to greater accuracy for a frequency range where no strong peaks in response exist. Clearly, this approach would under-predict the response at strong resonances, which are likely to be those conditions leading to vibration excesses.

Ultimately, both methods may be useful in performing predictions of ship vibrations. The 'maximum level' approach can be used to identify potential worst-case situations where machinery vibrations excite structural resonances. The 'average level' approach can be used when there is a low risk of excitation of strong resonances with large peaks in response.

The following recommendations for modeling have been developed using the results from Phase I assuming that these approaches to analysis will be used. Note that these recommendations are further refined as a result of the Phase II study. Final recommendations are provided in Part III of this report.

- ***Mesh Density*** – A minimum mesh density model can be used to predict whole body modes if an error in predicted frequency of up to 10% is tolerable. This would imply the use of an analysis frequency range of +/- 10%. The minimum mesh density model tends to predict frequencies higher than they actually occur (or at least higher than the frequencies where higher mesh densities converge), and therefore a bias towards higher frequencies could be used in the analysis frequency range (e.g. -5% +10%). Use of the minimum mesh density can lead to errors in response magnitude on the order of a factor of 1.3 for whole body modes and 2 for low order local modes.

  Although the minimum mesh density model appears to provide similar accuracy for the first local mode of structures, it will be shown in Part II of this report that significant errors can result for this mesh density for any local mode. In general a 2x mesh size (or finer) is recommended; significant improvements in both the error in frequency and response magnitude can be gained. This analysis shows a reduction in errors of predicted peak frequencies to 5%. The errors in response for whole body modes and low order local modes are also reduced to less than a factor of 2 (significantly less in many cases).

  A mesh size of 2x or finer is strongly recommended if analyses must be performed at frequencies corresponding to higher order local modes.

- ***Quad vs. Tri Elements*** – The use of 3-noded 'tri' elements is unavoidable in practical models. The results presented here indicate that use of tri elements will present additional (potential) errors above those discussed for different mesh densities. These errors are greatest for higher order local modes, and minimal for global modes and low order local modes. It is suggested that the use of tri elements be minimized where possible, though their use would not have an overwhelmingly detrimental effect. When needed, tri elements should be made as small as possible or refined to a 2x mesh level, at a minimum.

- ***Stiffener Modeling*** – When modeling whole body modes, the use of beam elements for all stiffeners (girders and smaller stiffeners) produces errors in frequency prediction on the order of 6%, and errors in response magnitude on the order of a factor of 2 or more. It is presumed that this approach would only be used with a minimum mesh density model, and therefore the prediction frequency range of +/-10% of the forcing frequency suggested for the minimum mesh density model would still apply. However, use of all-beam models will increase the error in magnitude response for these models.

In most cases it is recommended that girders and frames be modeled with plates for the webs and beams for the flanges. This is certainly true if predictions are to be made at frequencies of local resonances, but accuracy improvements can also be seen for whole body modes.

Predictions at frequencies corresponding to higher order local modes may require that small stiffeners be modeled using plates for webs and beams for flanges, as response ratios greater than 3 were noted for some specific locations.

Based on the results of these analyses, stiffener flanges can be modeled using beam elements. The use of plates for flanges does not appear to cause significant changes to the predicted vibration response. This will help to reduce model complexity, creation time, and analysis time.

- ***Model Extents & Boundary Conditions*** – Truncating a finite element model will impose limitations on the frequency range where valid results are possible. The selected sub-model must be capable of capturing (or approximating) the modes that dominate the response in the analysis frequency range. In general, it will not be possible to model whole body modes with a truncated model, and analyses will be limited to local modes.

  In order to achieve reliable results, the frequencies of 'false' whole body modes predicted by the truncated model must not coincide with frequencies of local modes. Although the results of Phase I are limited, it is estimated that the model must extend at least one if not several major structural divisions (i.e. bulkheads and decks) away from the force and response locations, as well as the structures in between.

  Caution must be used whenever interpreting results from a truncated model. Identification of false modes should be performed before performing detailed analyses of local results. False mode identification can be performed by running multiple analyses on the same model with various boundary conditions, or by changing the extent of the model. The predicted (false) whole body modes shift when different boundary conditions are applied (i.e. free vs. pinned), whereas local modes far from the boundary are mostly unaffected by changing boundary conditions. Therefore, any shift in response peaks in the analysis frequency range resulting from a change in boundary conditions is a modeling artifact. Such peaks should be investigated further by inspecting the deflection or mode shape, and it may be possible to ignore them in the analysis.

  For small vessels such as the one modeled here, truncation is not recommended since there may be overlapping frequency bands for whole body and local modes.

- ***Damping*** – The selection of an appropriate damping loss factor is studied in more detail in Part II of this report. Examples of the effects of different damping have been provided herein. Most of the models used in this analysis use a loss factor of 0.03, which is based on the recommendation of Reference [2]. Changing this loss factor will certainly change the absolute magnitude of the predicted response, though the relative differences in peak response between models that have been reported will remain essentially the same even when the damping is changed.

- ***Additional Structure*** – The investigations performed in this phase indicate that the modeling of doors, windows, and removable deck plating can have an effect on the predicted response spectrum. These effects will be most significant in areas 'close' to the additional structure, where distance is measured in relation to the extent of the structures involved in a particular mode shape.

  In the case of the relatively small vessel modeled for Phase I of this project, the predicted whole body modes changed when windows and deck plating were added, and this had impacts to the vessel response as a whole. Changes to the whole body modes occurred because the added structure makes up a significant percentage of the structure's surface area, and therefore added a high degree of stiffness to the model.

  The addition of doors to this model did not change the whole body modes, and the resulting impact to the response was limited to changes at structures in the immediate area of the additions for local modes. Impacts to larger vessels may be even more limited to this local type of impact. Changes in response at frequencies of higher order modes of bulkheads and decks near additional structures can certainly be expected if the additional structure presents a significant change to the local stiffness and/or mass of the vessel.

  Note that these findings are subject to the approach that was used to modeling doors, windows, and removable deck plating. Approximations were used, with the assumption of a perfect 'weld' between materials being implemented. Different approximations may be more appropriate.

- ***Additional Masses*** – Small masses (such as the anchor in this case) which make up a small percentage of the total mass of the vessel (~1%) present negligible changes to the structural response at essentially all locations for whole body modes and low order local modes. Even for the highest order modes, the influence of this mass was very small except for those response positions that were attached to the same deck area as the added mass or directly adjacent to it. The mass of fluids in tanks, which represent a change in total model mass of approximately 4%, produced negligible changes in the response at all force/receiver pairs at nearly all frequencies.

  The addition of the A-frame, which was a 9% addition to the total model mass, produced much greater changes to the vibration response of the vessel. The largest changes were seen in the area of the whole body modes, but local modes were also impacted at areas close to the A-frame. Some of these changes may have been due to the specific method of modeling the A-frame with rigid and mass elements.

  Given these results, it is difficult to assign specific guidelines as to when to include masses of auxiliary equipment and machinery, or even the specific manner in which they should be modeled. A rough guideline would be to include masses on the order of 5% and above of the total vessel mass, though this will likely be dependent on the specific location of the mass and how it is implemented in the model. Additional efforts are needed to better refine this recommendation.

- ***Joiner and Deck Coverings*** – Adding non-structural mass to the model to approximate the effects of joiner and deck coverings results in small changes in response at global mode frequencies, though much larger changes are possible at for local modes, particularly higher order local modes. In all cases the changes are primarily seen on the structure where the joiner or deck coverings are applied. These changes are generally more significant when the added mass is a larger percentage of the base structure's mass – the same joiner and deck coverings would have greater impacts on an aluminum structure as compared to a steel structure.

  Based on the analysis performed in this phase it is recommended that the mass of deck coverings and joiner be taken into account. Additional analysis and discussion is provided in Part II of this report.

PART II – Measured vs. Modeled Vessel Vibration

5.0 BACKGROUND

5.1 Overview

The goal of this phase is to perform vibration measurements on a vessel and compare the measured vibration response of various structures to predicted levels using finite element methods. These comparisons have been used to further refine the modeling and analysis recommendations developed in Phase I, as well as identify appropriate levels of damping and methods for modeling machinery sources. Investigations into the effects of water loading on the wetted hull have also been performed.

Originally, measurements were to be performed on the same vessel modeled in Phase I. Unfortunately the aluminum catamaran modeled in Phase I was not available for testing in the required timeframe for Phase II efforts. Furthermore, given the issues identified in Part I of this report related to modeling and generating generalized conclusions from a small aluminum vessel (which includes interference of global modes with local modes), it was decided that a larger steel hulled vessel should be used for this phase. The 'lessons learned' from Phase I have been applied to Phase II, as applicable, to avoid duplication of efforts.

Noise Control Engineering, Inc. identified a vessel at the beginning of the Phase II effort. The vessel is the *STATE OF MAINE*, a training vessel for the Maine Maritime Academy (MMA). This vessel is cooperatively owned and operated by the MMA and the US Department of Transportation. Both entities granted NCE access to the vessel, support during the measurement phase, and provided all available vessel drawings for modeling purposes (See Section 11).

5.2 Vessel Details

The *STATE OF MAINE* is a steel vessel originally constructed in 1990. It was built as a US military ship (TAGS-19, *USNS TANNER*), and was operated by the Military Sealift Command until 1993. The MMA began use of the vessel in 1996. General parameters of the vessel are provided in Table 24. An outboard profile is provided in Figure 70. Additional drawings are provided in Appendix A.

Table 24: General Parameters of the *STATE OF MAINE*

Parameter	Value
Length, Overall	499' – ½"
Beam, molded	72'
Depth to Main Deck	42'
Draft (max)	28' – ¼"
Light Ship Displacement	9267.29 LT

The vessel contains an MAK Model 6M01 propulsion diesel, rated at 8046 HP, 425 RPM. It also contains a Siemens/Reliance electric propulsion motor rated at 2010 HP, 597 RPM. Both are mounted to a common raft which was initially isolation mounted; the isolation mounts have since been removed and replaced with steel blocks (see Section 6.2.4).

The vessel also contains three gensets, MaK Model 6M332, rated at 1207 HP, 900 RPM. All three are individually isolation mounted on the 23’ Flat deck. The make and model of the isolators are not known, though visually they appear to be solid rubber blocks.

Figure 70: Outboard Profile of the *STATE OF MAINE*

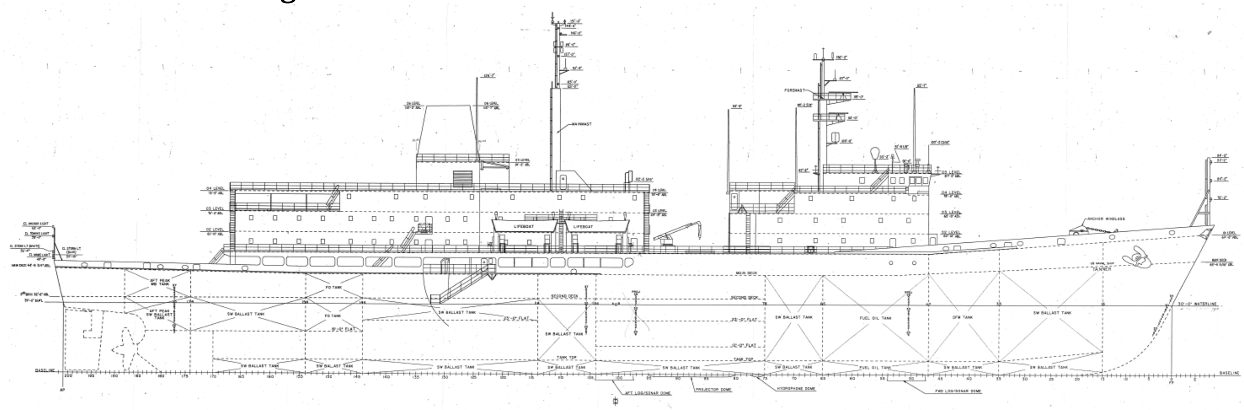

Many structural modifications have been performed to the vessel since its initial construction. Details of these modifications were not available in drawing form, but were identified when on-board. These modifications ranged from changes in stiffener dimensions to removal of bulkheads. Changes that affect the results of this study have been indicated when identifiable.

The waterline during testing was approximately 26 feet above baseline. This is slightly above the 23’ Flat deck.

5.3 General Approach to Phase II

Measurements of vibration levels that are generated from both machinery and artificial sources (an impact hammer) were performed on the *STATE OF MAINE*. Details of testing are provided in Section 6.

Direct comparisons of dynamic mobility[8] measurements to predictions have been made, and provide indications of modeling accuracy over a large frequency range. These comparisons also provide insight into items investigated in Phase I such as proper mesh density, stiffener element types, model extents, and boundary conditions; allowing for refinement of general modeling procedures. Appropriate levels of damping and other real world considerations such as the influence of auxiliary structures (piping, joiner panels, etc.) have also been investigated using the results from these measurements.

Comparisons of measured and modeled vibration levels that result from operation of real, “distributed” (i.e. non-point source) machinery sources have been performed, and allow for the assessment and refinement of the analysis approaches outlined in Phase I (Section 4) that would be applied to the analysis of a new build. The collected data has also been used to determine a methodology for identifying and applying appropriate forces from machinery to finite element models.

[8] Mobility is the ratio of vibration velocity response to the input force. It is the inverse of impedance.

6.0 TESTING

Vibration tests were performed on the *STATE OF MAINE* from September 2-5, 2013. Tests were performed while the vessel was docked at the Maine Maritime Academy in Castine, ME. The vessel was running on shore power for all tests; this allowed for a minimum of additional machinery to be operational in order to isolate vibration from the test sources and minimize background noise. (Some machinery items could not be secured during testing, though in most cases this had a small or negligible impact on the test results.)

The *STATE OF MAINE* is a very large vessel. To help focus modeling efforts most measurements were performed below the Main Deck, from the Main Engine Room to the Steering Gear Room (aft of Frame 114). Additional data was collected on the aft superstructure bulkhead on the 04 Deck. Structural drawings of pertinent vessel sections are provided in Appendix A.

6.1 Impact Testing

An instrumented impact hammer was used to provide a broadband excitation of local structures. (An electro-mechanical shaker was also tested but did not provide data that was appreciably different from the impact hammer.) In general, vibration levels were measured at multiple locations both at the point of impact and elsewhere on the same and adjacent ship structures. This allowed for measurement of point mobilities (response at point A to input at point A) and transfer mobilities (response at point B to input at point A) on various structures. Testing with the impact hammer was convenient as it is portable and allows for measurements in areas that do not otherwise have vibration sources. However, the power output is limited and measurements were confined to locations close to the point of impact.

Impact testing was also performed to help establish the modes of the structure and damping loss factors. Impacts were performed over a 'grid' on several test structures to allow for determination of mode and operational deflection shapes. Additional details of measurements performed on each test structure are provided in the following sub-sections. In all cases where structures other than machinery foundations were being measured (i.e. for bulkheads, decks, side shell) vibration levels were measured in the out-of-plane direction (i.e. normal to the plating).

6.1.1 Steering Gear Room (2-188-0)

Impact measurements were performed in the Steering Gear Room on both the starboard side shell and Transom. These structures were selected since they are relatively clear of obstructions with no insulation or joiner and a minimum of attached appendages. Pictures of these structures are provided in Figure 71 and Figure 72. Drawings are provided in Appendix A. The impact grids used for these structures are provided in Figure 73 and Figure 74. Impact points were only located on stiffeners. Accelerometer locations are noted in Figure 73 by circled numbers.

Figure 71: Starboard Side Shell Test Structure

Figure 72: Transom Test Structure

Figure 73: Measurement Grid for Starboard Side Shell

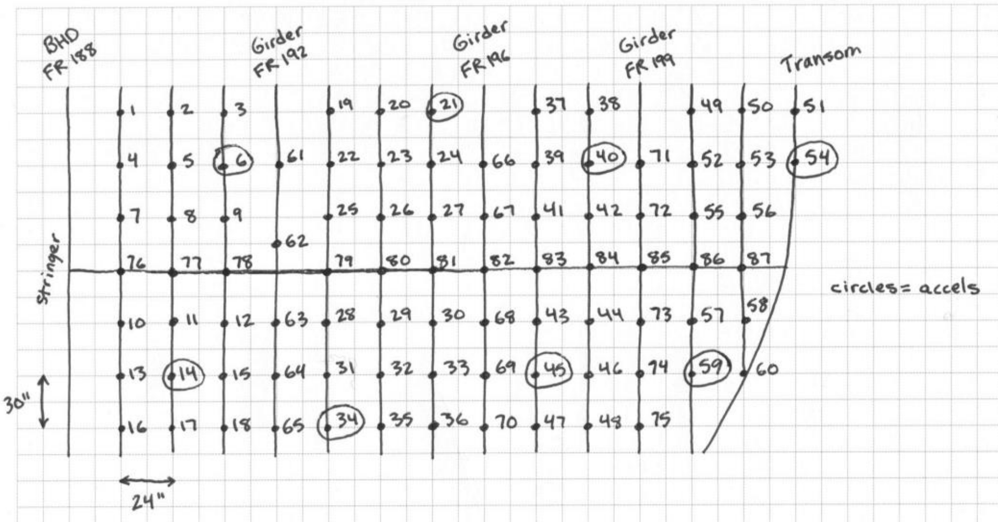

Figure 74: Measurement Grid for Transom (Looking Aft)

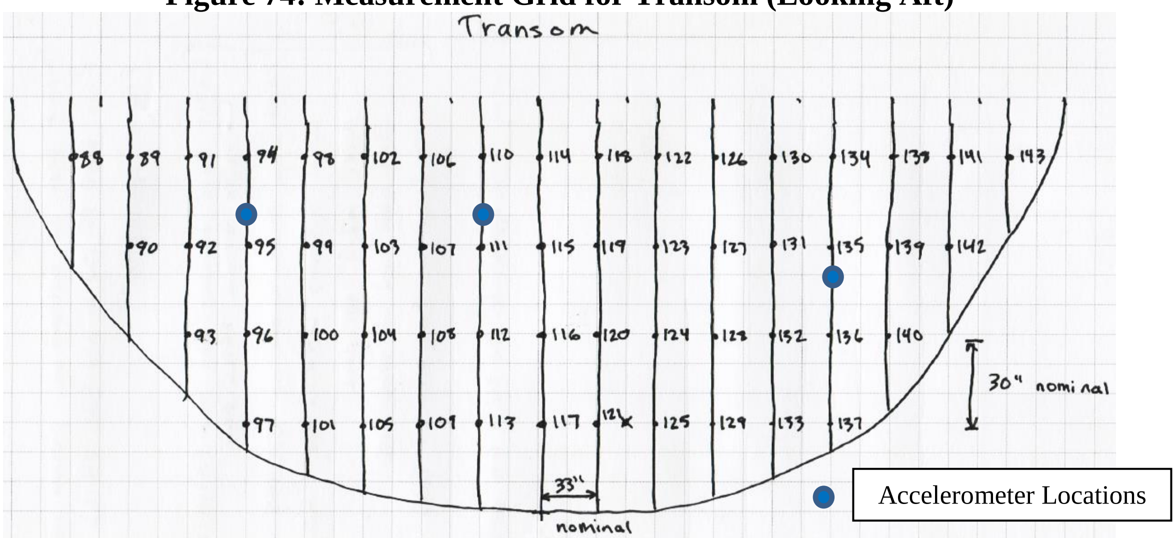

The stiffeners used on the side shell are large relative to the Transom and other internal (non-hull) structures and provide significant stiffness. The dimensions of the stiffeners and plating on the side shell and Transom are provided in Table 25 and Table 26.

Table 25: Stiffener and Plating Dimensions for Steering Gear Room Side Shell

Item	Dimensions	Notes
Plate thickness	7/16"	
Small Stiffeners	7" x 4" x 7/16"	"L" Beam
Large Stiffeners	20" x 7/16" W/ 5" x 1"	"L" Beam
Stringer	18.5" x 5/8" W/ 4-1/8" x 5/8"	"L" Beam

Table 26: Stiffener and Plating Dimensions for Transom

Item	Dimensions	Notes
Plate thickness	9/16"	
Small Inboard Stiffeners	7" x 4" x 7/16"	"L" Beam
Small Outboard Stiffeners	6" x 4" x 7/16"	"L" Beam
Other Small Stiffeners	9" x 4" x 1/2"	"L" Beam, cut from C-Channel 18" x 45.8#

The side shell was mostly free of attachments, though two small pipes were connected at a few locations. The Transom had several items directly attached including additional stiffeners between the primary stiffeners to help support items such as alarm sirens and other small equipment – this can be seen in Figure 72. A transformer and storage locker were also located close to the Transom. The steering gear itself was located in the middle of the compartment on a large foundation, though it was not directly connected to either test structure – a picture of the Steering Gear is provided in Figure 75.

The test structures are several feet above the waterline.

Figure 75: Steering Gear

6.1.2 Engine Lab (2-158-0)

Impact measurements were performed on the starboard, longitudinal bulkhead of the Engine Lab (2nd Deck), seen in Figure 76. This structure was selected since it is relatively "clean"; there were no insulation or joiner treatments and there was a minimum of additional items attached to the bulkhead. This structure does contain a door.

A grid of 67 points was created on the test bulkhead, as shown in Figure 77. Impact points were located approximately 20" apart in the vertical direction, with points located both on the stiffeners and plating between stiffeners. Two reference accelerometers were used at points 30 and 50, as shown in Figure 77.

Figure 76: Engine Lab Test Bulkhead

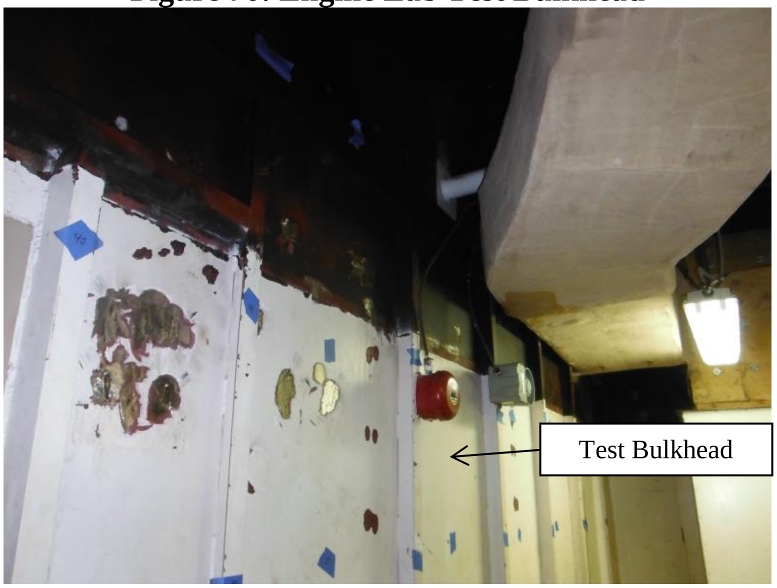

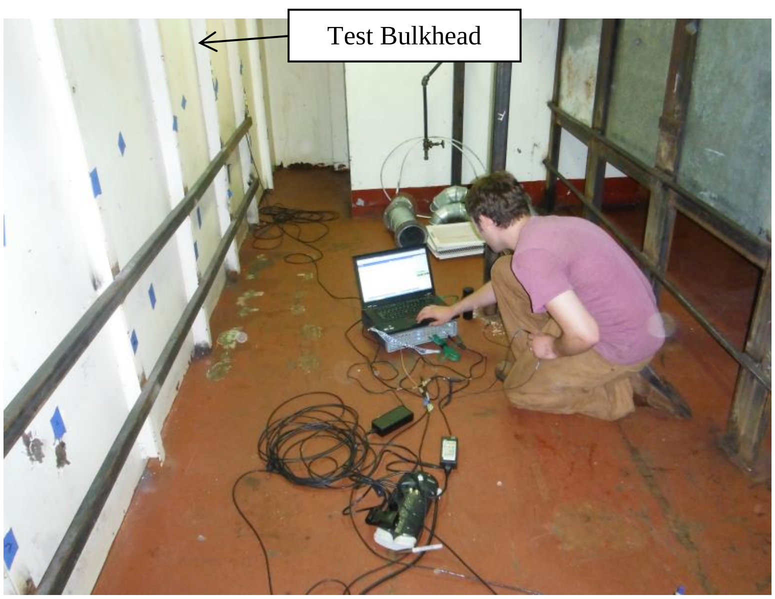

The test structure has several vertical stiffeners, as seen in Figure 76 and the structural drawing in Appendix A; the webs and flanges of most of these stiffeners are sniped so that they do not connect to adjacent structures. There is an HVAC duct that is connected to the upper portion of the bulkhead. On the opposite side of the bulkhead there is also a cableway attached near the deckhead. There is a door at the forward end of the bulkhead, shown in the sketch of Figure 77 and Appendix A. All tests were performed with the door open. In addition, there were two square tubes attached to the stiffeners on the lower portion of the bulkhead.

Figure 77: Test Grid for Engine Lab Bulkhead

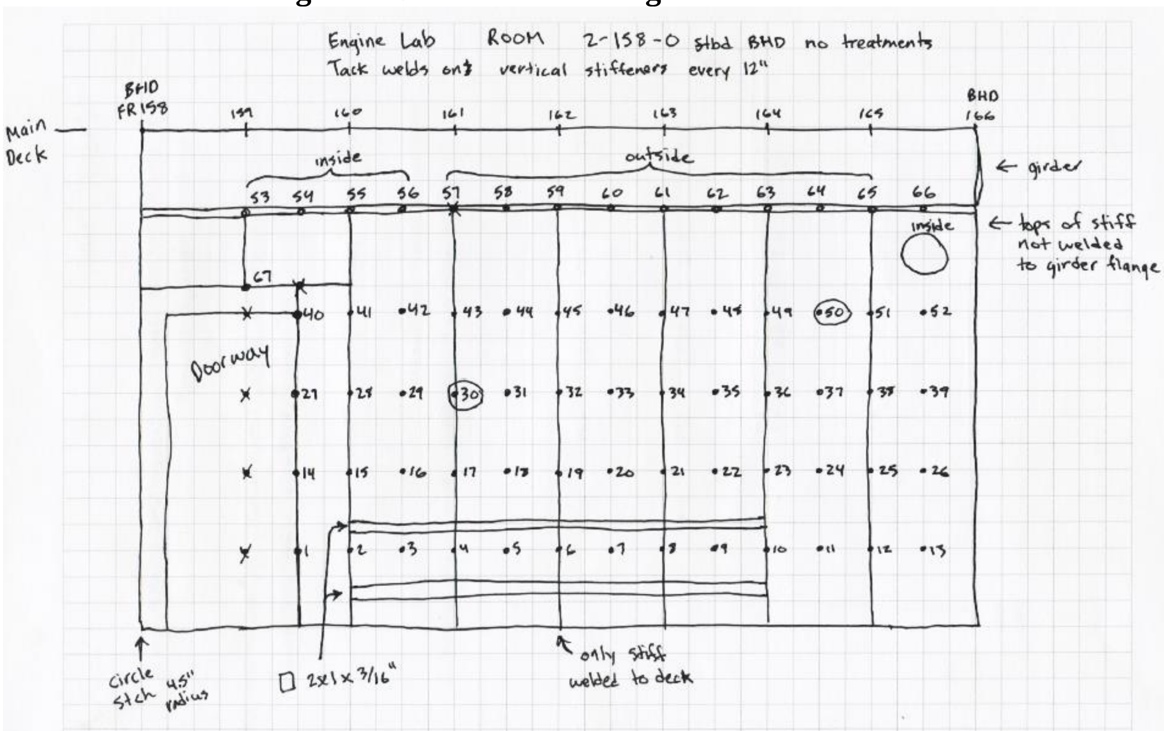

It is important to note that the available drawings of this structure do not indicate the presence of the square tubing attached to the stiffeners. These were clearly added at some point after initial construction. In addition, it was found that the stiffener size shown on the drawing is not correct. The stiffeners are indicated as being 3” x 2” x 3/8” “L” beams, though direct measurements by MMA personnel show them as being 3” x 1-5/8” x 3/8” “L” beams. The thickness of the plating could not be verified but it is currently assumed the drawings are correct.

A summary of the dimensions of the stiffeners and plating on the test structure are provided in Table 27.

Table 27: Stiffener and Plating Dimensions for Engine Lab Bulkhead

Item	Dimensions	Notes
Plate thickness	1/4"	
Vertical Stiffeners	3" x 1-5/8" x 3/8"	"L" Beam
Horizontal Stiffener	2" x 1" x 3/16"	Rectangular Tube Beam

Lastly, while NCE was able to obtain a drawing for this structure, no structural drawing of the areas directly forward of this compartment or directly above this compartment exist. This includes the forward bulkhead of this space. This unfortunate fact was double checked with the Maine Maritime Academy. Estimations were made of these structures during modeling based on physical measurements made while on site as well as information relating to other nearby structures.

6.1.3 Battery Room Bulkhead (04-62-2)

The Battery Room is located on the 04 Deck, aft of the Pilothouse on the port side of the vessel. The port bulkhead was selected for testing since this bulkhead is relatively simple (based on a review of structural drawings) but also contains insulation and metal sheathing inside the compartment. Direct access to the steel structure is available from the outboard (Topside) side of the bulkhead. A picture of the test structure from the exterior and interior are provided in Figure 78 and Figure 79. A detail of the impact grid is provided in Figure 80. Two accelerometers were located on the bulkhead and one additional accelerometer was positioned on the deck.

Figure 78: Battery Room Test Bulkhead, Exterior View

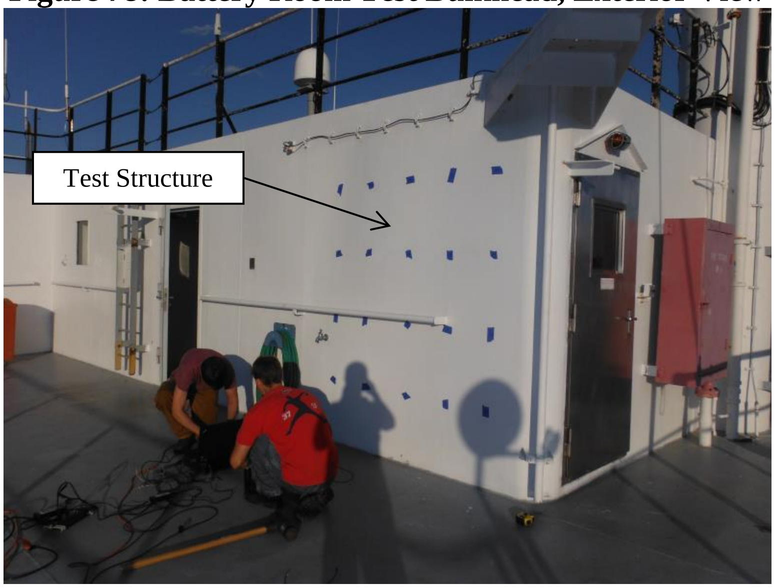

The actual structure making up this bulkhead could not be verified due to the presence of the metal sheathing. It is seen that there are two large batteries directly attached to the base of the bulkhead inside the compartment. There is also an appendage at the upper aft corner of the bulkhead, seen in the exterior view.

Figure 79: Battery Room Test Bulkhead, Interior View (Door Open)

Figure 80: Measurement Grid for Battery Room Bulkhead

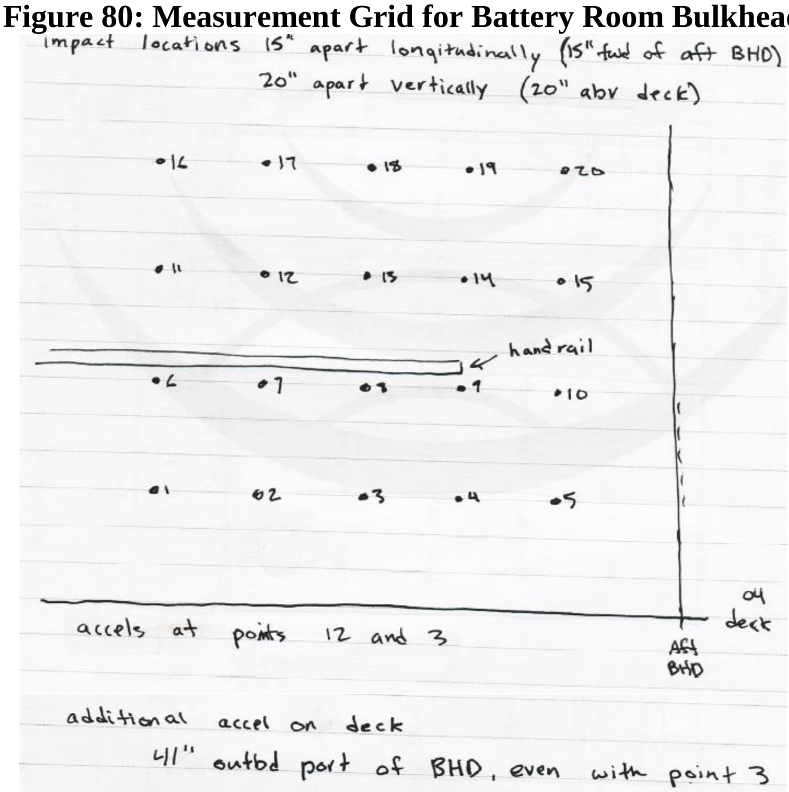

A summary of the stiffener and plating dimensions is provided in Table 28.

Table 28: Stiffener and Plating Dimensions for Battery Room Bulkhead

Item	Dimensions	Notes
Plate thickness	1/4"	
Vertical Stiffeners	3-1/2" x 3" x 1/4"	"L" Beam

An overall insulation and sheathing arrangement was provided in drawing format (see Appendix A). The visual appearance of the sheathing in the Battery Room appeared to match this drawing.

There are a few 'auxiliary structures' attached to this bulkhead. An antenna support is attached to the upper aft corner of the bulkhead; a detail is seen in Figure 81, and structural details are part of the available structural drawings. There is also a handrail attached to the exterior of the bulkhead, seen in Figure 78. Lastly, there are four large batteries on the deck of the Battery room, each resting on a foundation made up of angle stiffeners. These can be seen in Figure 79.

Figure 81: Image of Antenna Support

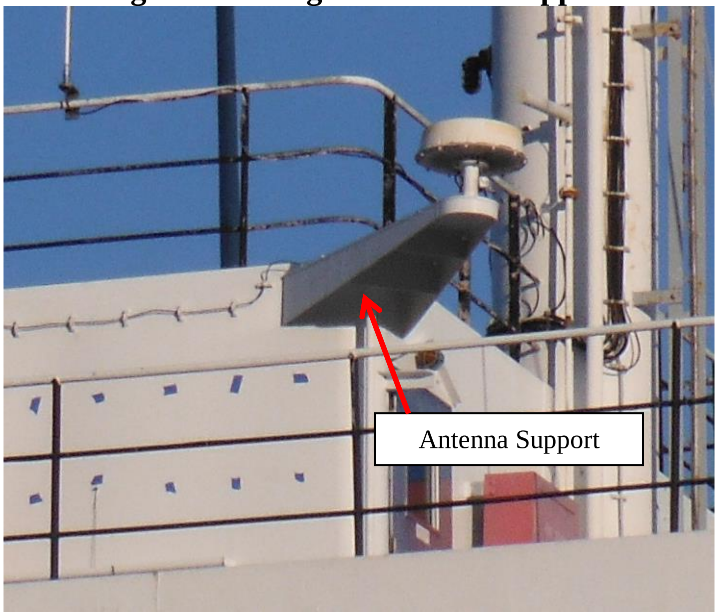

6.1.4 Machinery Room Side Shell (5-114-0)

Impact measurements were performed in the Tanktop level of the Engine Room on a section of the port side shell between Frames 129 and 133. This structure is below the waterline, and was tested to investigate the effects of water loading. This structure was also selected since there is no insulation, allowing for direct access to the steel structure.

Pictures of the test structure are provided in Figure 82. The structure is located behind many different pipes as well as a hard mounted bilge pump. A support beam can also be seen that is directly attached to the bulkhead.

A sketch of the impact grid is provided in Figure 83. Two vibration measurement locations were used within the impact grid; one additional position was used below the stringer at 162” ABL.

Figure 82: Machinery Room Side Shell Test Structure

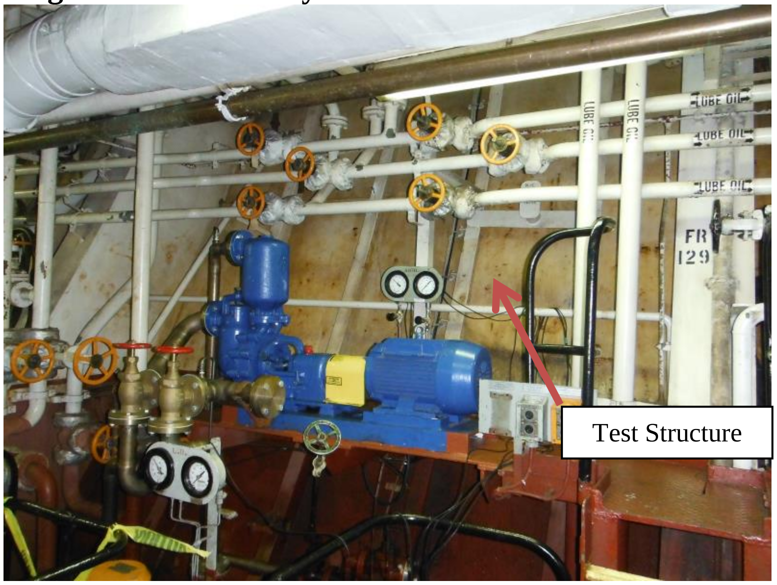

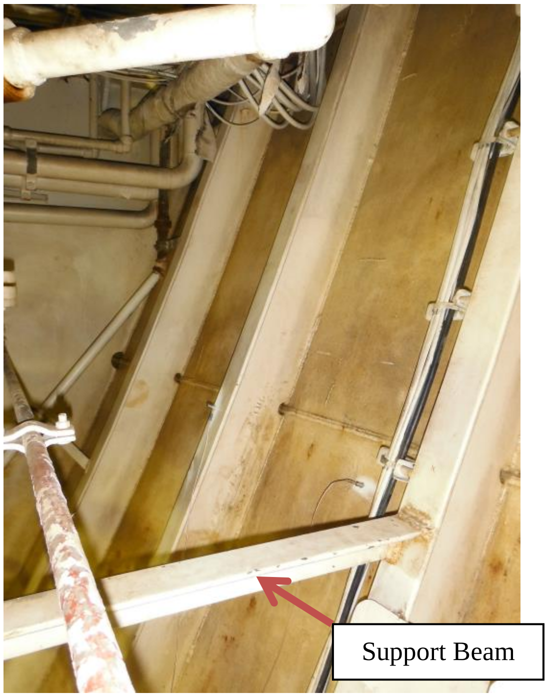

Figure 83: Measurement Grid for Machinery Room Side Shell

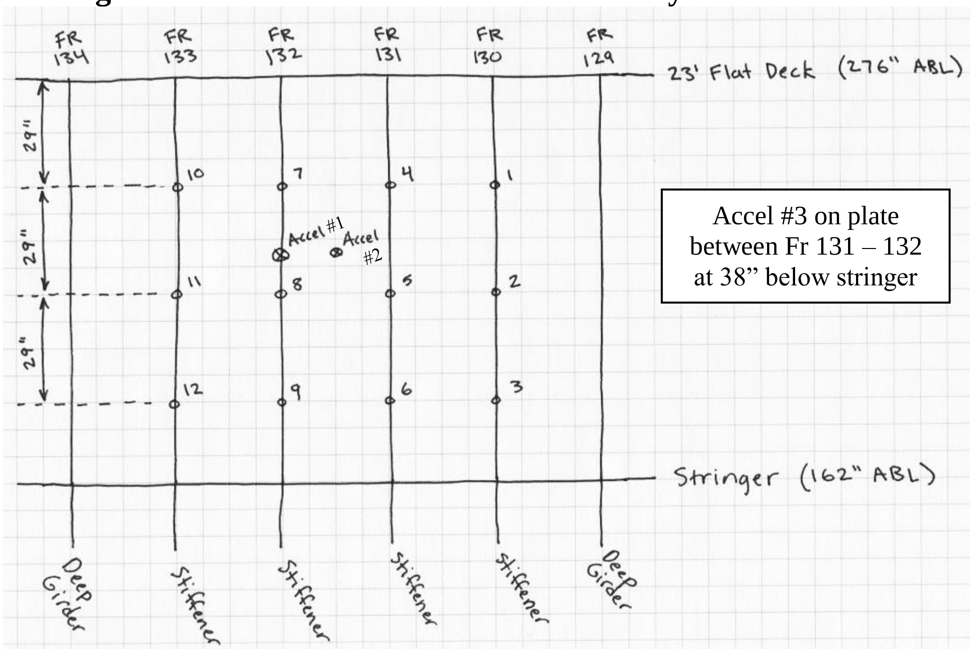

A summary of the stiffener and plating dimensions of the test bulkhead are provided in Table 29.

Table 29: Stiffener and Plating Dimensions for Machinery Room Side Shell (Below 23' Flat)

Item	Dimensions	Notes
Plate thickness	9/16"	
Small Stiffeners	9" X 4" x 5/8"	"L" Beam, cut from C-Channel 18" x 42.7#
Large Stiffeners	30" x 7/16" W/ 6" x 1/2"	"T" Beam
	36" x 1/2" W/ 12" x 1"	"T" Beam
	36" x 9/16" W/ 13" x 1"	"T" Beam
	36" x 9/16" W/ 20" x 1"	"T" Beam

6.1.5 Other Measurement Locations

Impact measurements were also performed at other test locations. In general, when measurements were performed to test vibration induced by machinery, additional impact tests were also performed. These additional measurement locations were limited to locations where accelerometers were placed, and therefore only provide point and transfer mobilities (no operational deflection shapes).

Tests were generally performed at the foundations of machinery and on structures close to machinery items that were operated for testing. These measurements were performed to help validate the finite element models created for modeling machinery induced vibration, as well as to help estimate the forces imparted to the structure by machinery.

Additional details are provided in the sections below.

6.2 Machinery Induced Vibration

Several machinery sources were operated while the vessel was on shore power. These include the starting air compressors, Genset #1, a bilge pump, and the propulsion engine. Details of the measurements performed for each source are given below.

6.2.1 Starting Air Compressor

The starting air compressor is a Hatlapa reciprocating compressor rated at 69 HP, 429 psi, 1800 RPM. It is isolation mounted on three mounts, as shown in Figure 84. The compressor was located on the 23' Flat on the starboard side of the vessel between Frames 131 and 133. Note that this was the aft compressor (total of 2 compressors on the vessel).

Figure 84: Starting Air Compressor

Vibration measurements were performed at the compressor, above and below mount in three directions, aligned with the global longitudinal, transverse, and vertical directions. Two additional vibration measurement points were located on the deck inboard and outboard of the compressor (near Frame 132) and two points were located on the stiffeners of the adjacent side shell, about 4-5 feet above the deck on the stiffeners of Frames 132 and 133. A sketch of the overall layout is provided in Figure 85. The accelerometers on the side shell can be seen in Figure 84.

Figure 85: Sketch of Starting Air Compressor Arrangement

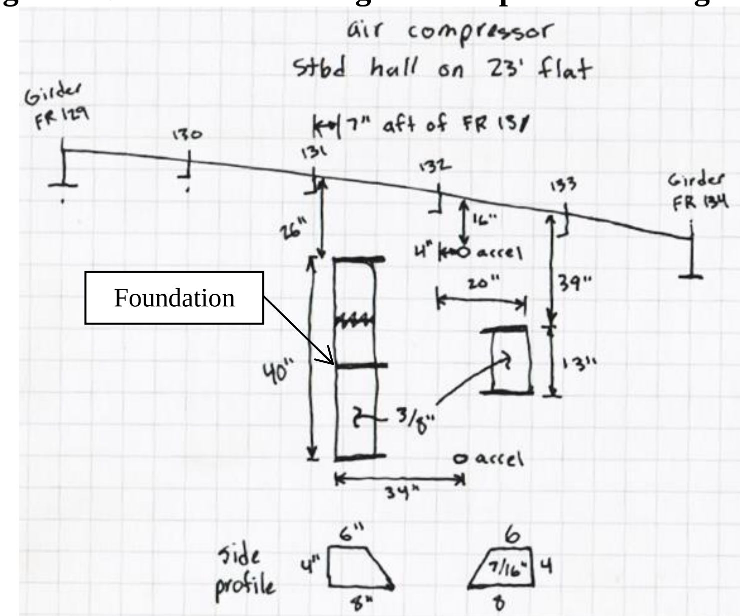

A summary of the stiffener and plating dimensions of the side shell and deck in way of the start air compressor are provided in Table 30 and Table 31.

Table 30: Stiffener and Plating Dimensions for Machinery Room Side Shell (Above 23' Flat)

Item	Dimensions	Notes
Plate thickness	9/16"	
Small Stiffeners	8" x 4" x 7/16"	"L" Beam
Large Stiffeners	22" x 1/2" W/ 7" x 1"	"T" Beam
	22" x 1/2" W/ 10" x 1"	"T" Beam
	24" x 1/2" W/ 10" x 1"	"T" Beam

Table 31: Stiffener and Plating Dimensions for Machinery Room 23' Flat Deck

Item	Dimensions	Notes
Plate thickness	9/16"	
Small Stiffeners	8" x 4" x 7/16"	"L" Beam
Large Stiffeners	22" x 1/2" W/ 7" x 1"	"T" Beam
	22" x 1/2" W/ 10" x 1"	"T" Beam
	24" x 1/2" W/ 10" x 1"	"T" Beam

It is noted that piping was located and supported beneath the deck under the test area. Details of the piping are not available, though it was visually similar to the piping located under the gensets discussed in Section 6.2.2. Damping tile was also present on the underside of the 23' Flat deck, also discussed in Section 6.2.2.

Impact data was collected at all measurement locations when the compressor was secured.

6.2.2 Genset

The vessel's gensets are MAK Model 6M332, rated at 1207 HP, 900 RPM. They are individually isolation mounted at 10 locations (5 per side) on what appear to be solid rubber blocks. A picture of the genset is provided in Figure 86. The rubber blocks are roughly 3" thick, 12" wide and 12" long. The tested genset, Genset #1, is located on the 23' Flat on the port side of the vessel between Frames 121 and 129. This is the forward genset on the port side of the vessel.

Figure 86: Genset

The foundation for the genset is a 12" wide x 1" thick solid steel billet. There is also a 4" x 3/8" flat bar coaming around the perimeter of the genset (seen in yellow in Figure 86). The dimensions of stiffeners and plating for the side shell and decks below the 2nd Deck are the same as those provided previously in Table 29 through Table 31. A summary of the stiffener and plating dimensions of 2nd Deck is provided in Table 32.

Table 32: Stiffener and Plating Dimensions for 2nd Deck

Item	Dimensions	Notes
Plate thickness	3/8"	
Small Stiffeners	5" x 3-1/2" x 3/8"	"L" Beam
Large Stiffeners	18" x 7/16" W/ 3-9/16" x 5/8"	"L" Beam
	23" x 1/2" W/ 7" x 1"	"T" Beam

The deck directly below the gensets was treated with damping material (presumed to be US Navy Standard damping tile, see Reference [19]). This area contains a significant amount of piping and pipe supports, as seen in Figure 87.

Figure 87: Deck Under Gensets

Vibration measurements were performed above and below mount in three directions, aligned with the global longitudinal, transverse, and vertical directions. Additional vibration measurements were performed on the deck near the genset, on the stiffeners of the adjacent side shell both above and below the 23' flat, and at selected locations on the 2nd Deck. An outline of the measurement locations is provided in Figure 88. Impact measurements were also performed at selected measurement locations when the genset was secured.

Figure 88: Measurement Locations for Genset

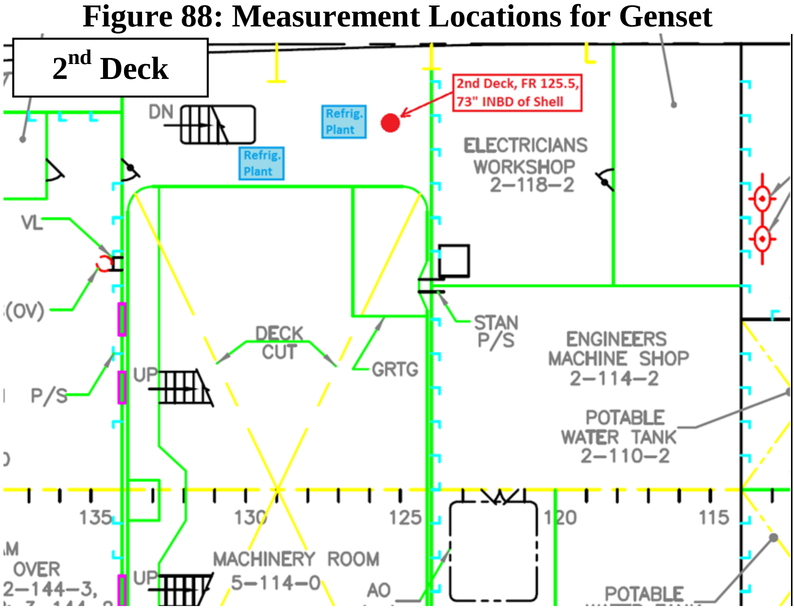

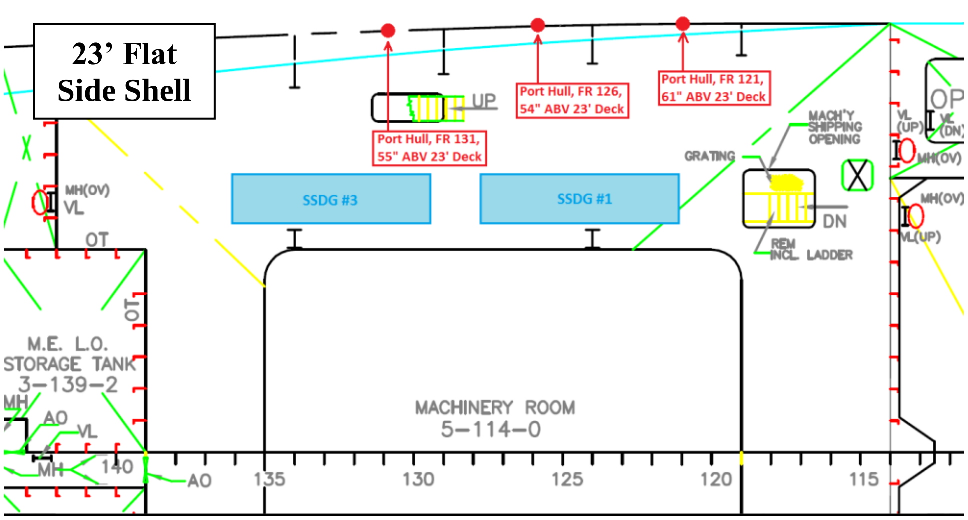

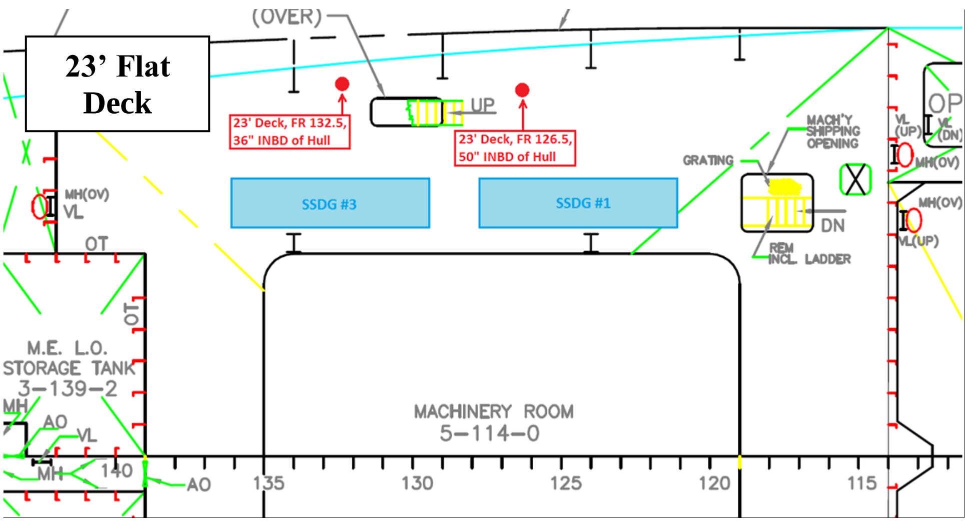

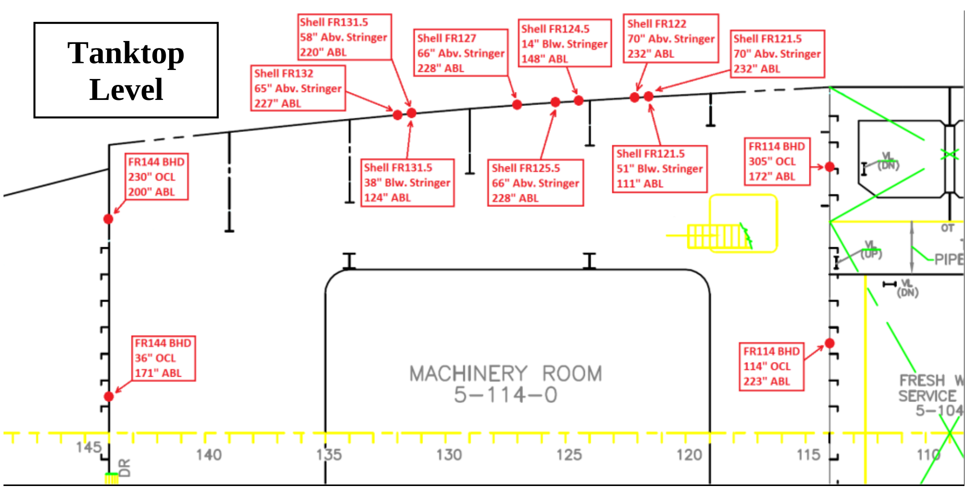

It is noted that the area surrounding the gensets and measurement locations contain many pieces of machinery such as heat exchangers, tanks, pumps, etc. Details of these items are not known, including their weight. The available machinery arrangement for the 23' Flat, shown in Figure 89, indicates the presence of other equipment items near the gensets though these items are not the same as what was seen on-site. However, this figure does provide an indication of the number and size of equipment items that are close to the gensets. It is noted that some measurement locations, such as on the 2nd Deck, were very close to these equipment items.

Figure 89: Machinery Arrangement in way of Port Gensets

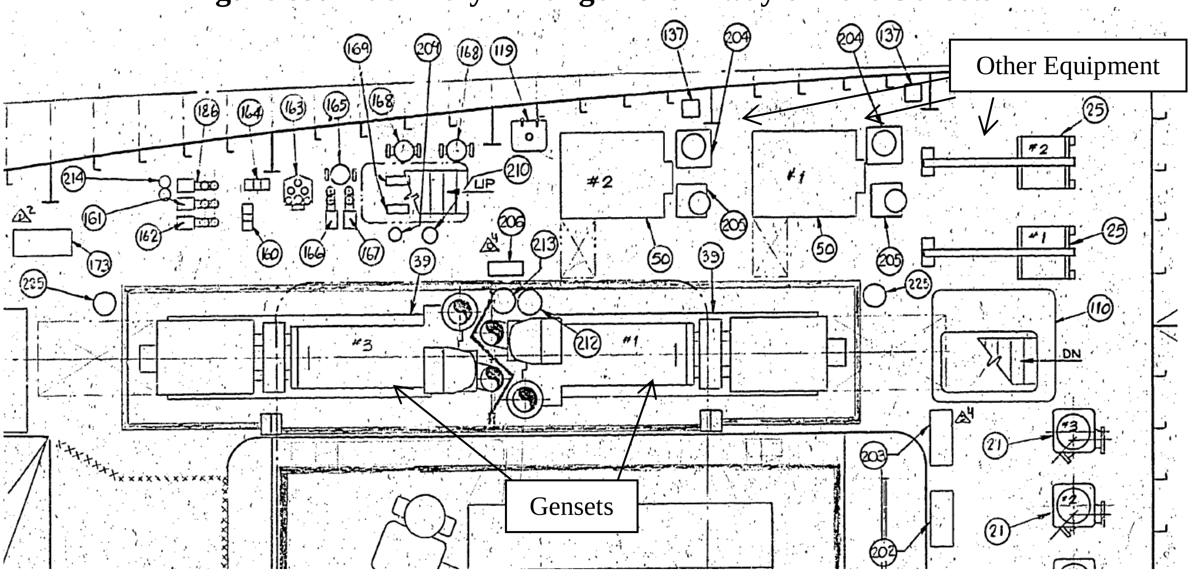

6.2.3 Bilge Pump

One of the vessel's bilge pumps was selected for testing of a hard mounted machinery item due to its proximity to previous measurements (see Section 6.1.4) and accessibility to the foundation. The pump is a LaBour Taber Model 23XW OPL, rated at 15 HP, 400 GPM, 1750 RPM. It is located between Frames 130-132 on the stringer above the Tanktop on the port side of the vessel. A picture of the pump is provided in Figure 90.

The foundation for the pump is a 'tabletop' structure, consisting of two 3-½" x ¾" vertical legs (running longitudinally) with a 15" wide x ½" thick horizontal plate directly under the pump and motor. The pump and foundation are mounted to a stringer that is 13'-6" ABL; this structure is a large cantilever, with 6" deep transverse stiffeners supporting the stringer plating directly under the pump. It is noted that the stringer has clearly been modified as there are visual differences relative to the original structural drawings shown in Appendix A. Measurements of the existing structure were made while on-site, though not all details could be captured exactly.

Figure 90: Hard Mounted Bilge Pump

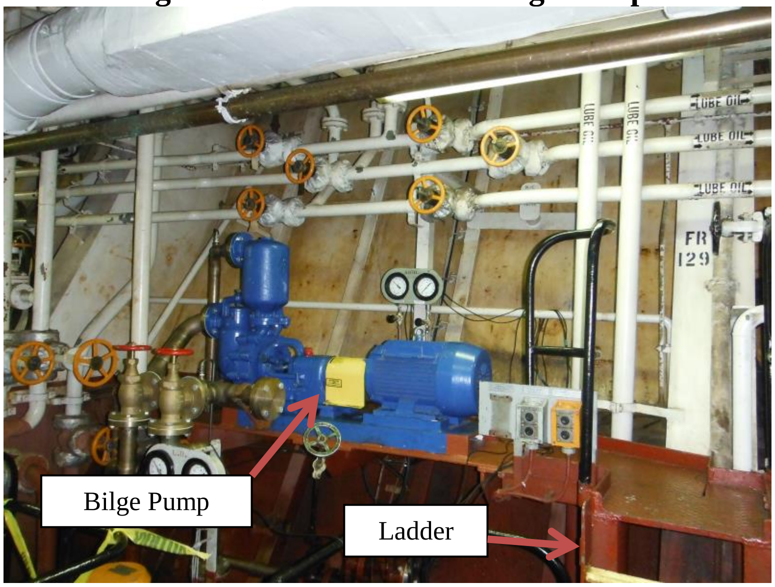

Vibration measurements were collected on the pump's foundation at 6 locations. These locations roughly correspond to the attachment locations of the pump and motor, as seen in Figure 91. There are three locations on each side; vibration data was collected in three orthogonal directions aligned with the global longitudinal, transverse, and vertical directions. Additional vibration measurements were performed at the three locations on the side shell shown previously in Section 6.1.4.

As was discussed in Section 6.1.4, this location has many items that are not represented on any structural drawing such as piping, pipe supports, and other structures. This location is below the waterline.

Figure 91: Bilge Pump Foundation Measurement Locations

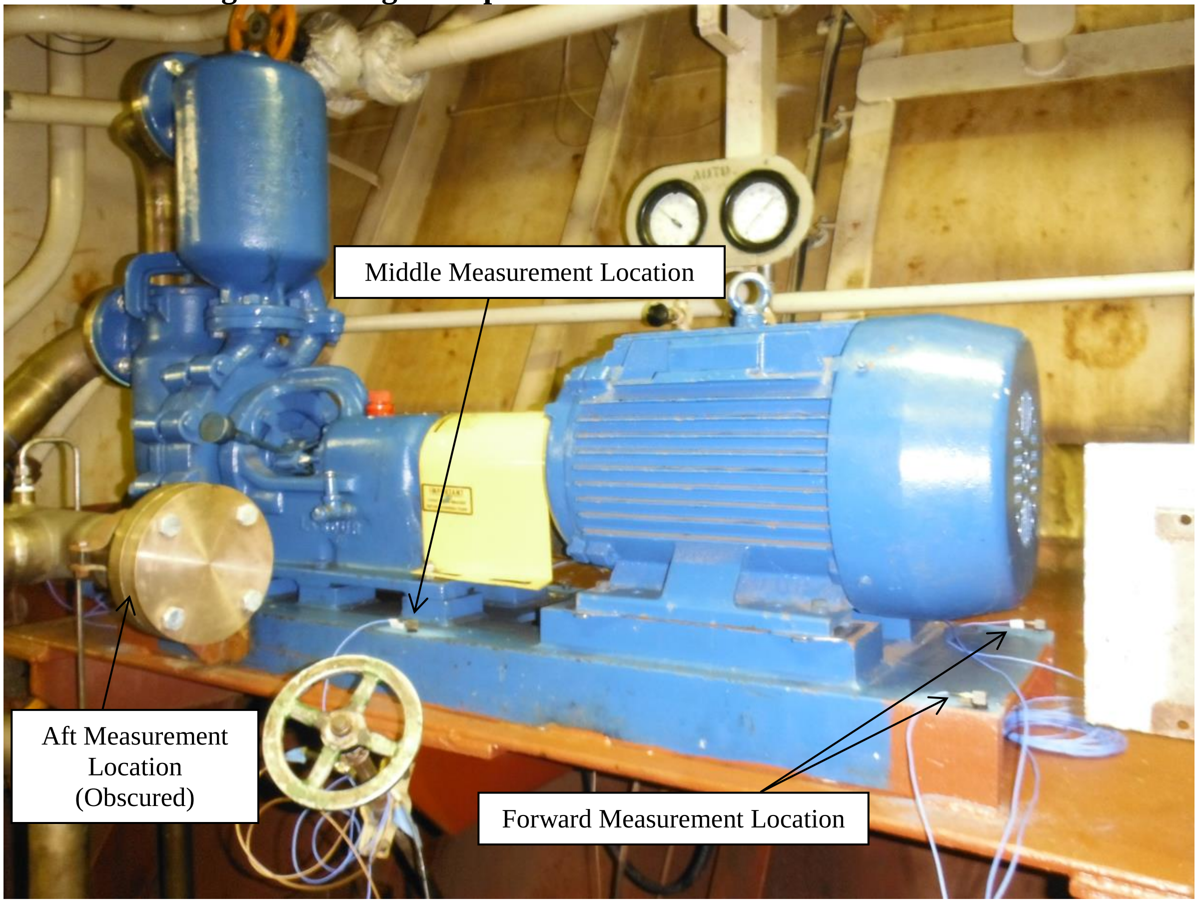

6.2.4 Propulsion Diesel

There is a single propulsion engine, MAK Model 6M01, rated at 8046 HP, 425 RPM. In the original vessel design there were two propulsion engines; the starboard engine has since been replaced by a propulsion motor. The engine is located on the Tanktop level on the port side of the vessel between Frames 121 and 129. A picture of the diesel is provided in Figure 92.

The engine is hard mounted to a large platform that is common to the engine, motor, and other auxiliary machinery. This platform was originally isolation mounted to the vessel, but is now supported by many individual steel blocks. A drawing showing the original design is provided in Figure 93. There are at least 12 steel blocks along each edge of the platform – other attachment locations are also possible but could not be seen while on-site.

Figure 92: Propulsion Engine

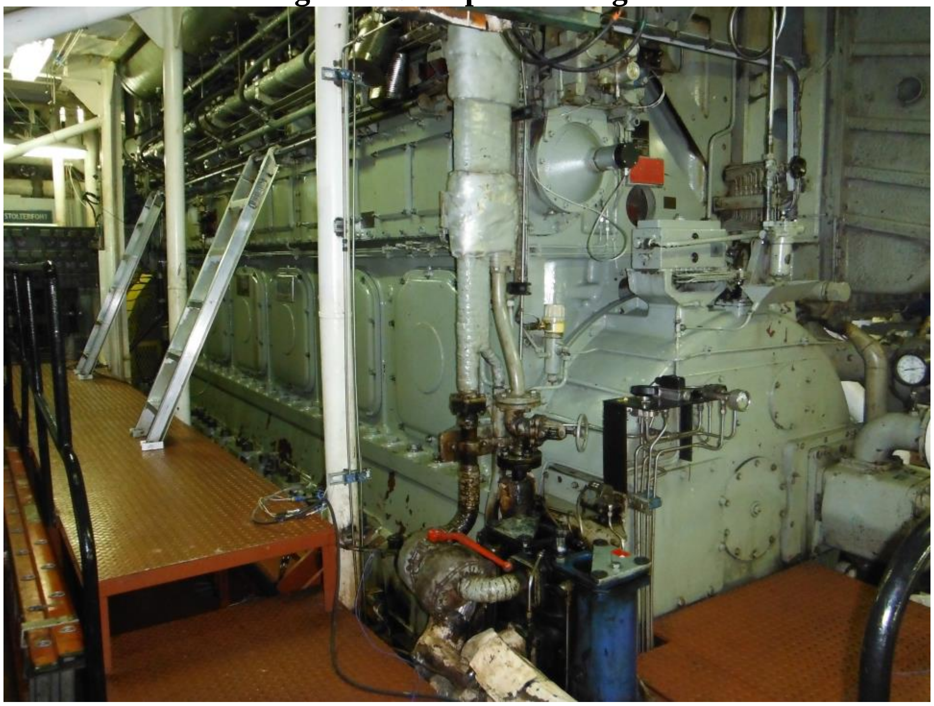

Figure 93: Drawing of Original Propulsion Diesel Installation

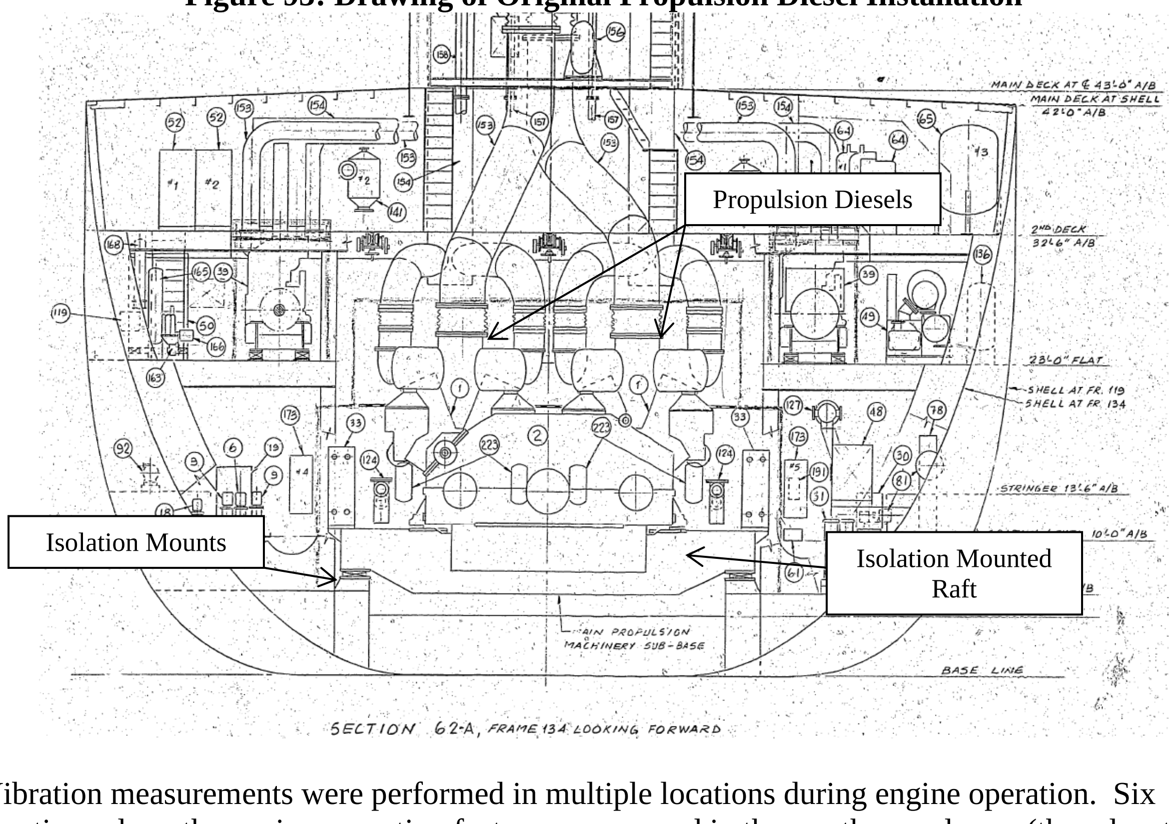

Vibration measurements were performed in multiple locations during engine operation. Six locations along the engine mounting feet were measured in three orthogonal axes (three locations on each side of the engine, spaced evenly from the forward end to the aft end). Two additional positions were set up on the raft edge, outboard of the engine. Additional measurements were performed on the side shell between the Tanktop, 23’ Flat, and 2nd Decks, as well as on the 23’ Flat and the forward and aft bulkheads of the Engine Room. These locations are the same as those shown previously in Sections 6.2.2. Vibration data was collected in a single axis, normal to the plating for these locations. Lastly, vibration data was collected in the Workshop on the 2nd Deck Level.

Measurements were performed with the propulsion engine running at multiple speeds from idle to full speed without a load.

The original intention of these measurements was to measure and model the vibration response of a large machinery item where vibration levels would be detectable at locations far from the source. Unfortunately, due to the complications discussed above with respect to the removal of the resilient mounts and unknown (and unconventional) support system for the propulsion engine, analysis of this data and comparisons to models would be highly approximate. Given the finite budget and timing of this project, it was decided to focus efforts on modeling and analyzing results from other measurements. Further discussions of measurements performed with the propulsion engine operating are not provided in this report.

6.3 Machinery Source Measurements

An investigation was performed to quantify the forces imparted to the structure by real sources, both resiliently and hard mounted. Analysis of the measurements discussed in the previous sections was performed to develop methods of estimating forces that are imparted to the ship structure during machinery operation. Three primary approaches were used, as follows:

Method 1: Above Mount Vibration

This approach is valid for resiliently mounted machinery. Forces imparted to the foundation are estimated based on measured ‘above mount’ vibration levels at each mount combined with the dynamic stiffness of the mount. The measured vibration levels are converted to displacements (assuming harmonic motion). The force on the foundation is then determined using Hooke’s Law for the force through a spring,

$$F = kd \tag{2}$$

where F is the magnitude of the force, k is the dynamic stiffness of the resilient mount, and d is the vibration displacement magnitude. The relative phase of the acceleration at the above mount measurement points is a direct indication of the relative phases of the forces on the foundation.

This approach is the simplest of the three, as it relies on measured (or estimated) above mount vibration data and the mount stiffness. These items are typically available during the design stage of a vessel. However, this approach is not applicable to hard mounted machinery.

Method 2: Generalized Inverse

In this approach, measured transfer functions (mobilities) between the foundation and other ‘response’ locations are used to determine the forces imparted to the structure at the machinery mounting feet. Multiple measurement points are used to create a force and response matrix in an attempt to improve data quality. A full description of the approach is provided in Reference [5]; a summary is given in Appendix D.

A brief summary of the test procedure is as follows:

- With the machinery operating, measure the vibration at the feet of the machine where there is a connection to the ship structure (i.e. the foundation). Also measure the vibration at one or more 'response points' away from the machinery foundation.
- Turn off the machinery and use an impact hammer to excite the structure at all locations on the foundation previously measured with the machinery operating. The vibration response resulting from the impact is collected both at the foundation and at the other 'response points'.
- The measured Frequency Response Function (FRF) from the impact point to the various measurement points can then be combined with the vibration data measured when the machinery was operating to derive the forces generated at the machine foot. The calculation procedure is outlined in Appendix D.

This approach allows for calculation of the force magnitude in all excitation directions as well as the relative phase of the forces. The quality of the resulting prediction is directly dependent on the quality of the FRF data that is collected.

This approach is a fairly rigorous method of determining forces and requires a large amount of data collection and processing. This method was selected for use here in part because it has been shown to produce accurate results for complex structures [5]. Unfortunately, it has a limitation in that, at least in its formulation, the machinery source needs to be removed from the system when collecting impact data. This is not a practical option for shipboard measurements. Resiliently mounted machinery is likely to be less susceptible to this requirement than hard mounted machinery, except at frequencies near the natural frequencies of the isolation system.

Method 3: Impact and Relative Vibration

In this approach the force imparted to the foundation is derived from measurements collected with the machinery operating combined with impact measurements made with the machinery secured. This test approach is essentially a simplified version of Method 2. The test and calculation procedure is as follows:

- With the machinery operating, the vibration levels on the foundation of the machinery are measured in three orthogonal directions.
- With the machinery secured, use an impact hammer to directly excite the foundation. This would include each below mount position for resiliently mounted machinery and each mounting foot location for hard mounted machinery. Impact in all three directions. Repeat for all mounting locations.
- The measured force from the hammer test is then directly scaled by the difference in the measured vibration levels from the two tests. Each pair of direction & location is compared directly, ignoring cross-correlation effects.

The results obtained using this method are not expected to be as accurate as Method 2. However, the processing of results is simpler and more straight-forward. Measurements must be made one foot at a time, and since cross-correlation effects between different impact/measurement locations and directions are ignored, the derived forces will be approximate. (Inspection of transfer mobilities between mounting feet and directions performed for this effort indicates that this should introduce only small errors.) Furthermore, the relative phase of the forces needs to be derived from a different method, such as direct measurement of the vibration as discussed in Method 1.

6.4 Instrumentation

Multiple data acquisition systems were used to collect vibration data during testing. The primary system was an LMS SCADAS Mobile multi-channel data acquisition system, which was used to collect all force and vibration data for tests using the impact hammer. LMS Test Lab software was used for data collection and initial processing. Additional vibration data collection during machinery operation was performed using multiple National Instruments 9234 data acquisition cards with a custom LabView program written for collecting vibration autospectra.

The acquisition setup was modified as needed in order to collect appropriate data in the frequency range of interest (1-100 Hz). For all measurements of machinery induced vibration, multiple frequency resolutions were collected ranging from approximately 0.25-1 Hz. A minimum time-bandwidth product of 30 was used for all measurements.

Impact measurements required different resolutions due to time data window requirements – data collected at each location was inspected to ensure the measured data decayed sufficiently during the time of acquisition (generally 1-4 seconds per impact). In general the frequency resolution was between 0.25-1 Hz.

Steady state measurements of machinery vibration utilized a Hanning window. No windowing was used for impact measurements – this removes deleterious effects of windowing on FRF data.

The impact hammer used during testing is a PCB model 086D50 (a large, instrumented sledgehammer). Two accelerometer models were used. One was Wilcoxon Research Model 736; these accelerometers have a nominal sensitivity of 100 mV/g and an operational frequency range of 2-10,000 Hz. The other was PCB Model 356B11; these accelerometers have a nominal sensitivity of 10 mV/g and an operational frequency range of 2-7,000 Hz (minimum).

All equipment has been calibrated to NIST standards within 1 year of testing. Calibration certificates are provided in Appendix E.

6.5 Data Analysis and Modeling Methodology Overview

A large amount of data was collected, and this data has been analyzed in many ways. This report does not present every piece of measured or analyzed data, but rather highlights pertinent examples where comparisons have been made between finite element models and measurements, as well as other calculated values such as damping loss factors and machinery forces.

The tests described in the previous sections were performed with the intention of allowing for identification of specific pieces of information regarding the accuracy of the finite element modeling process. In most cases multiple factors were analyzed for a single test or test structure, and other tests were performed to assess additional factors.

Data analysis began with the extraction of damping loss factors from the impact data at locations where a full measurement grid was used (see Section 6.1). All modal analysis processing and damping estimations were performed using LMS Polymax. This is a powerful tool which can be used to process multiple FRF data sets to derive natural frequencies and damping values. Additional information can be found in References [6, 7]. The calculated damping values were used to guide subsequent modeling efforts.

Models of the ship structure were created using the available vessel drawings, and then refined based on on-site observations. Comparisons of point and transfer mobility data were then made between the model and measurements. Changes and refinements to the models were implemented to investigate the importance of various modeling factors. The mobility (impact) results were analyzed first as these provide the most information relating to broadband vibration response of the structure. Modal results and operational deflection shapes from specific impacts were used to assist the analysis and further define model accuracy.

Comparisons between measurement and model were typically made at specific peaks in the response data to determine accuracy relating to frequency, amplitude, and overall displacement shape. In all cases where the ship structure was being analyzed (verses a machinery foundation) the out-of-plane vibration was analyzed. Attention was given to the amount of modeling detail that was required in order to obtain a certain level of accuracy. Accuracy as a function of frequency was a major focus of analysis efforts. Phase I results were used to guide modeling efforts.

The ‘simplest’ structures were analyzed first, being those in the Engine Lab and Steering Gear Room, with the thinking that these would be the most straight-forward since they have a minimum of extra piping, appendages, etc. that are connected. Other locations were then analyzed using lessons learned from previous modeling efforts.

The point mobility data (i.e. impact and response at the same location) was used initially to compare measurement and model results and to determine the quality of the model. The measured point mobility data was generally of good quality, and as expected provided the strongest response in the structure. This generally facilitated comparisons between model and measurement. Transfer mobility data (i.e. impact at one location and measurement at another) was also used to further analyze the correlation between model and measurement. The measured response data was generally weaker for transfer mobilities, though more ‘features’ (peaks and dips) were seen as a result of greater influence from more modes of the structure. A subset of the full number of measurement locations was used for transfer mobility comparisons since the quantity of data and available time does not allow for a full analysis of all transfer mobility pairs. The plots presented in this report are believed to be representative of the full data set.

Point mobility data collected on structures near machinery items discussed in Section 6.2 was also inspected and compared to model results. This was done to identify model accuracy in these areas, which were typically complex and contained additional factors such as piping, pipe supports, damping, and other complications. Machinery force estimation was performed using the methods identified in Section 6.3. These forces were then applied to the models, and the resulting modeled vibration response at accelerometer measurement locations was compared to the measurements.

The results of these efforts lead to indications of appropriate methods of modeling and analysis, as well as indications of expected accuracy using these modeling methods.

It is worth noting that the measurement data is used in this report as the 'standard' to which the model is being compared. However, the measurement data, in particular the impact data, can be flawed as well. In all cases care was taken to acquire good data, and in the majority of cases this was achieved. In some cases factors such as signal to noise issues, practical issues relating to impacting large structures, and other factors are believed to have caused some errors (small in most cases). In all cases data quality was checked using reciprocity, analysis of coherence data, and other techniques. Data with glaring errors was not used for comparison to the model (this was rare). Specific issues with data that could not be avoided and that affect the results presented here are highlighted in the sections below. However, in general it should be recognized that the measured data is not necessarily the 'ground truth', but rather the best information that is available that is generally close to reality.

Descriptions of the models generated and comparisons of model to measured results are given in the following sections. Section 7 presents the results of impact testing and modeling. Section 8 presents the results of force estimation and modeling of machinery excitation.

7.0 IMPACT TESTING – MODELS AND MEASURED RESULTS

7.1 Overview of Models

Two 'baseline' models were developed for the Phase II effort. The primary model, which encompasses the majority of the measurement locations, extends from the Frame 104 bulkhead to the Transom (roughly half the length of the vessel), and from the 01 Deck down to the hull. A screen capture of this model is shown in Figure 94. The second model, which was used to model the tested structure on the 04 Deck, includes all structures from the 03 Deck to the 05 Deck. Masts and similar items were not included in this model. A screen capture of this model is shown in Figure 95.

Both models include structural details of plating, stiffeners, and stanchions. Large stiffeners, girders, and frames were typically modeled with plate elements for the webs and beam elements for the flanges. Small stiffeners were typically modeled with beam elements. (Some additional investigations were performed to investigate stiffener modeling effects.) The baseline models typically do not account for the additional weight of machinery items, water loading from tanks, or water loading, though these items were added when deemed necessary.

Figure 94: Primary Baseline Model
Full Model (Top) & Port Side Cutaway View (Bottom)

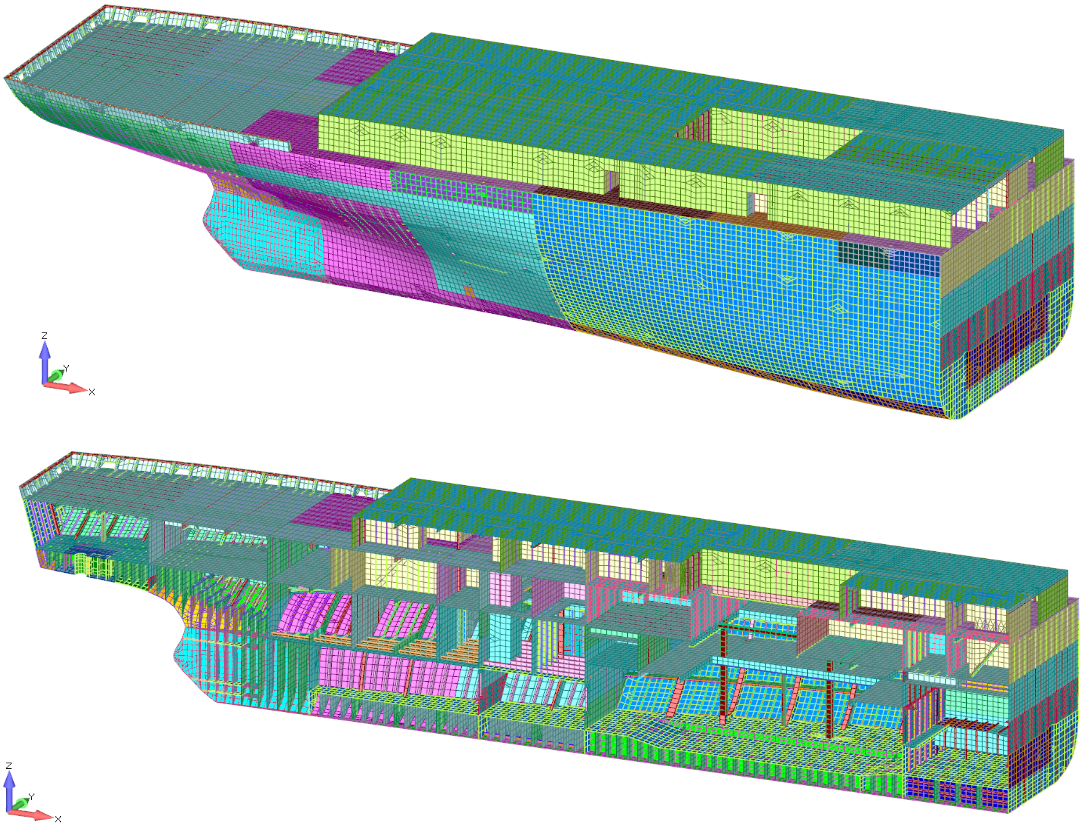

Figure 95: 04 Deck Model

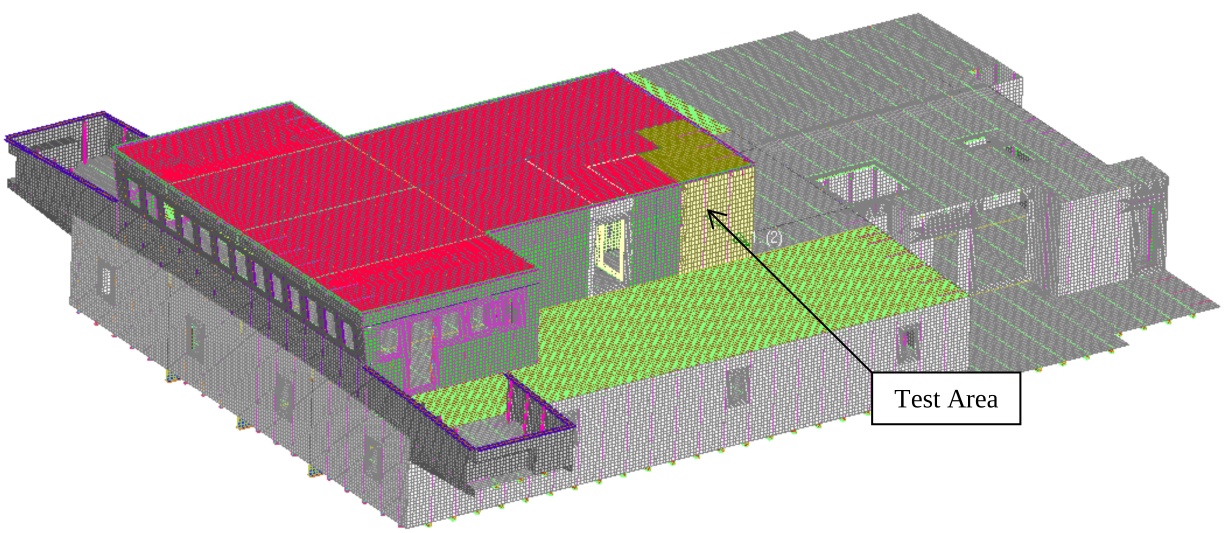

2x and 4x mesh densities were used for most models, and in a few cases the 'minimum mesh density' and an 8x mesh density was used (see Table 2).

It was not possible to develop a model of the entire vessel within the timeframe and budgetary constraints of the project. This analysis shows that this simplification does not impact the analysis, and conclusions can be drawn using the available models. The baseline model was often truncated to create a smaller model; this allowed for faster analysis of results and also provided information relating to the required model size for achieving accurate results.

In some cases other modifications were made such as the addition of mass to represent local hard mounted equipment, outfitting, or other items. Discussions of such modifications are provided in the sections below.

The effects of water loading have been investigated in some of the analyses discussed below. As discussed in Reference [1] the effective mass created by water loading is dependent in-part on the mode shape, and the added mass effect is reduced with increasing frequency. Various calculation methods exist for determining this added mass, ranging from empirical models to coupled boundary element / finite element approaches to discrete finite element modeling of the water domain. Each of these approaches has tradeoffs. It is noted that most 'general purpose' finite element codes do not have sophisticated boundary element or fluid coupling as part of their capabilities; therefore, these advanced approaches are not investigated directly here.

7.2 Analysis of Damping Loss Factor

Given the goals of this project, it is not the intention of this analysis to match specific damping values with specific modes since there is an immense variety of possible structures, and the modes of different structures are effectively guaranteed to vary. Instead, the primary goal is to determine approximate damping values that can be applied to sections of the model or to the model as a whole. This approach may induce errors in the modeled results, however the intention is to identify realistic damping values for ships that can be easily applied to models; when a given vessel is in its design stages, there is nowhere one can go to perform similar measurements to those described in this report, and approximations will be necessary.

The damping loss factors of several test structures have been analyzed using the measured impact data (See Section 6.4). Those structures where grids of impact locations were utilized were analyzed; this includes the Steering Gear Room side shell and Transom, the Engine Lab, the Battery Room bulkhead, and the side shell in the lower Machinery Room. The data from these locations were chosen primarily due to the large amount of data that is available, ideally reducing the likelihood of spurious damping estimations that may occur from a single measurement location.

Primary modes are 'selected' as part of the damping estimation process. This selection process requires some judgment, though the software used for analysis provides various indicators of modes that are likely to exist in the data – see References [6, 7] for more information. Once the modes are selected the damping loss factors are estimated using a curve fitting routine. The estimations of modes and loss factors can be checked by creating a composite response for any given pair of impact and response locations. These data were checked to determine the quality of the fit.

In general it was found that many modes were identified that have only small contributions to the actual point or transfer mobilities of the structure. When all of the identified modes were included in the estimation, the damping loss factors of all modes ranged wildly from extremely small to extremely large values. These results were deemed to be unrealistic. In an attempt to refine these estimations a subset of modes were selected; only those modes that were seen to have a strong influence on the point mobility (first) and selected transfer mobilities (second) were kept[9]. This resulted in a data set that showed much less variability in loss factor while still maintaining reasonable correlation between measured and simulated mobilities[10].

Figure 96 through Figure 100 show the estimated loss factors of major modes in the test structures.

Figure 96: Estimated Damping Loss Factors for Steering Gear Room Side Shell

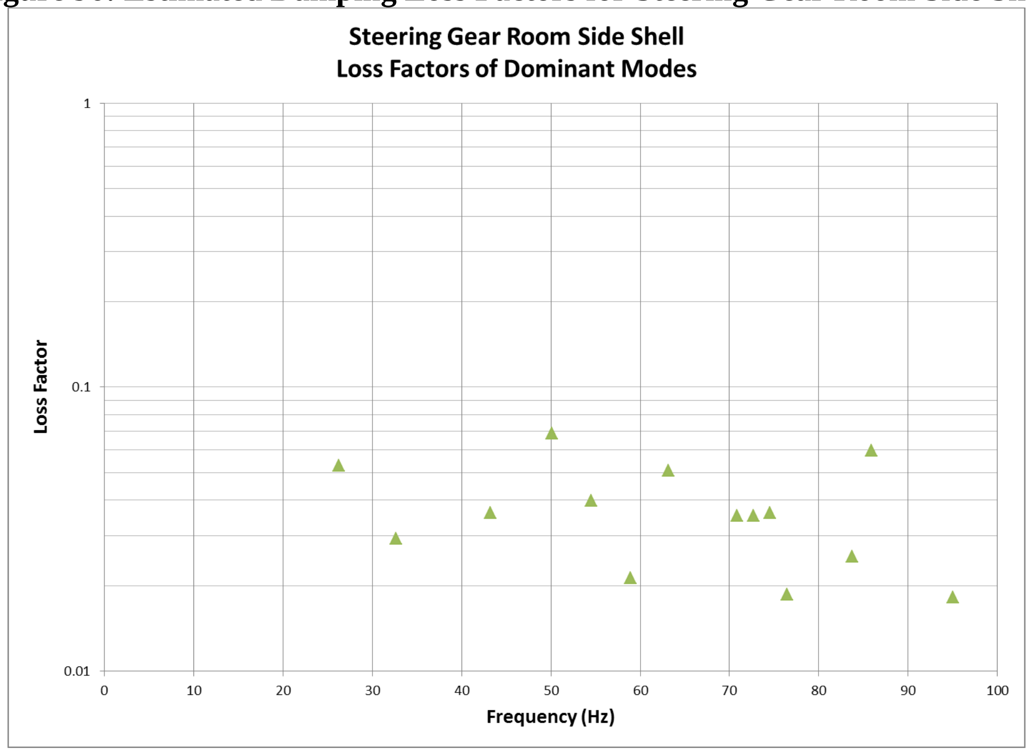

[9] This sorting was performed primarily by identifying the 'residue' of each mode and keeping only those modes where the residue was large – see Appendix B.

[10] For brevity, the simulated mobilities are not shown here.

Figure 97: Estimated Damping Loss Factors for Transom

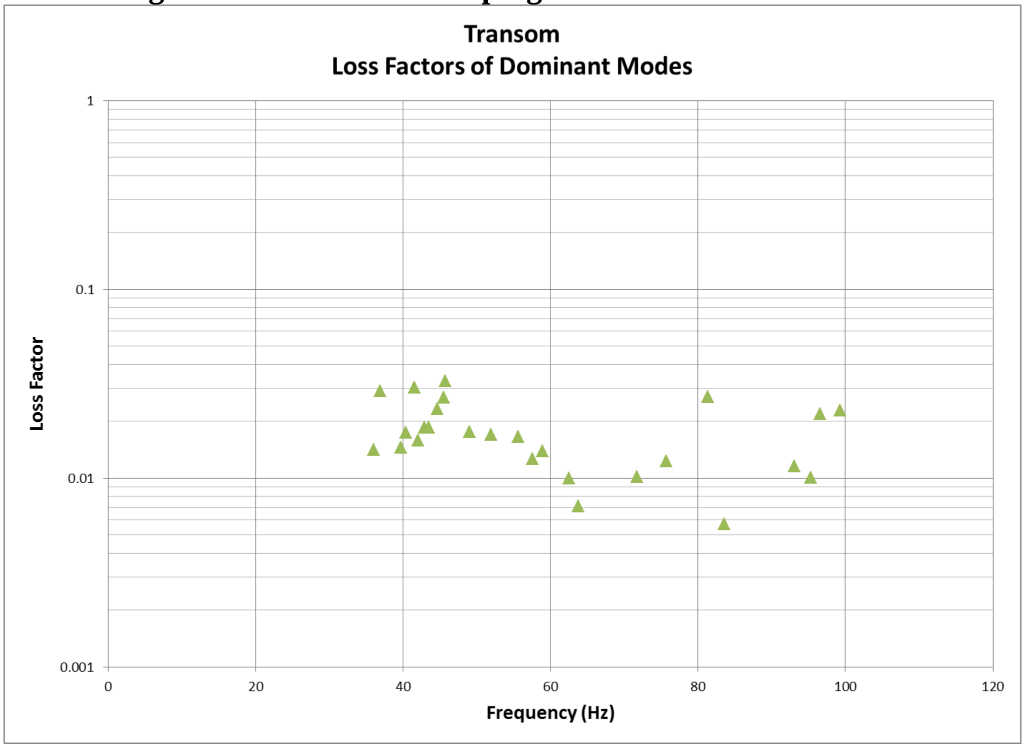

Figure 98: Estimated Damping Loss Factors for Engine Lab

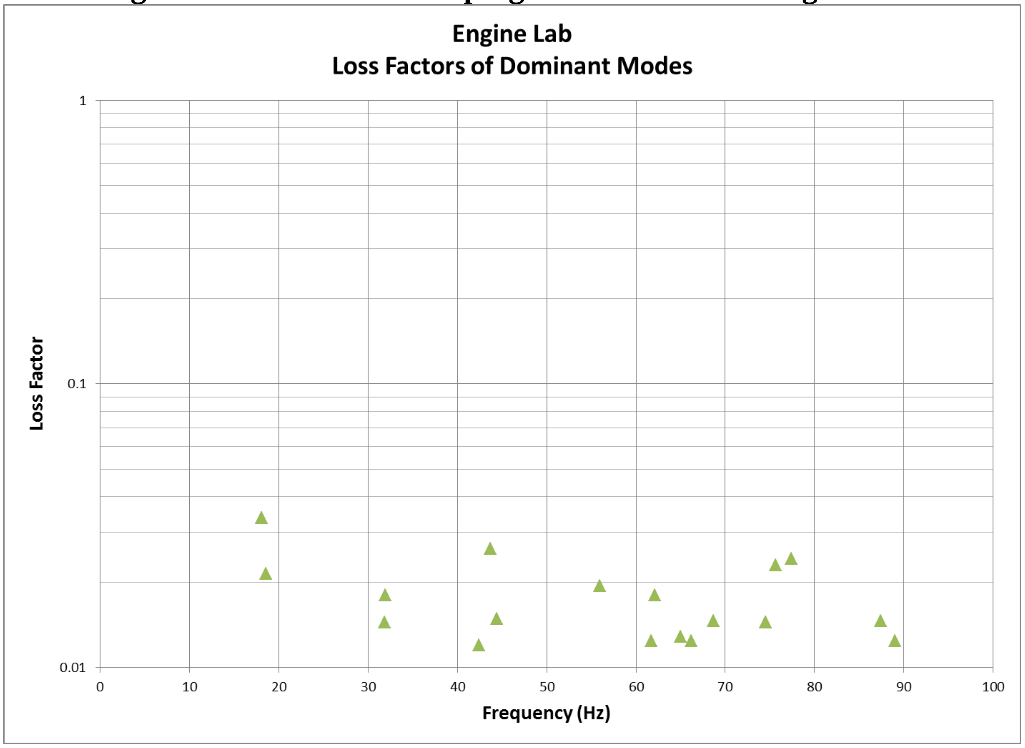

Figure 99: Estimated Damping Loss Factors for 04 Deck Bulkhead

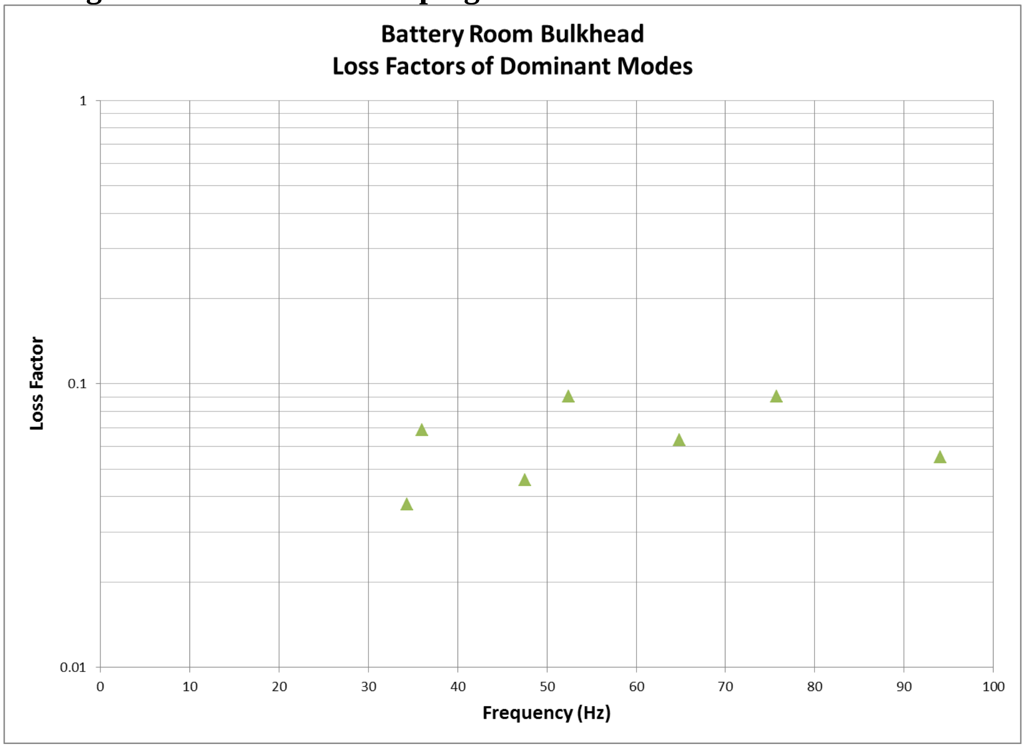

Figure 100: Estimated Damping Loss Factors for Machinery Room Side Shell

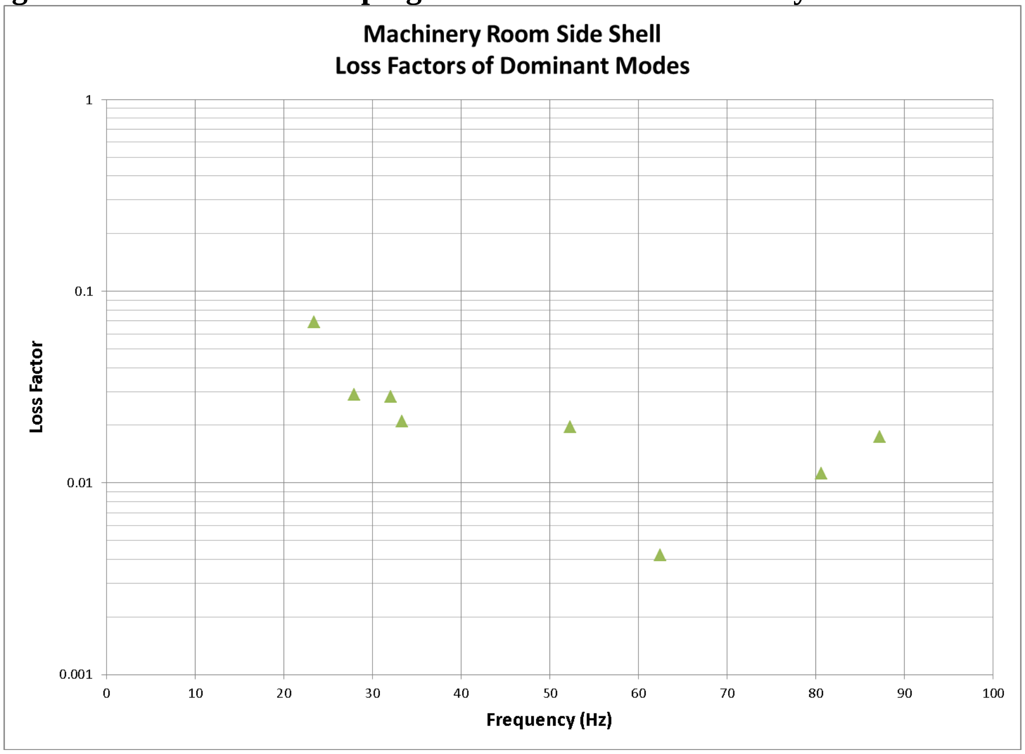

Taken as a whole, the loss factors for all structures typically range in value from 0.01 to as high as 0.09. However there is greater consistency for individual structures. For example, on the side shell in the Steering Gear Room the damping ranges from roughly 0.02 to 0.06, with much of the data falling near 0.03 to 0.04. The Engine Lab loss factors are also self-consistent, though lower, with most of the data falling between 0.01 to 0.02. Most of the loss factor data for the Transom falls between 0.015 and 0.03, though a few points fall below 0.01. This is also the case for the Machinery Room side shell. The 04 Deck appears to have higher levels of damping, with values between 0.04 and 0.09.

The data shows that different modes have different degrees of damping. This leads to some variation with frequency, but in general the 'average' loss factor is roughly constant throughout the measurement frequency range.

Given the results presented here, the loss factor value of 0.03 recommended by ABS [2] and used in Part I seems to be a reasonable first estimate for most ship structures. Loss factors for specific structures are seen to range around this value, but when applied to a ship as a whole this value provides a good mean.

It is noted that the Machinery Room side shell is in contact with the ocean, and is therefore subject to 'radiation loading' from the water. As will be discussed in Section 7.6, this 'water loading' primarily creates an added mass effect, though damping effects are also possible. The damping loss factors on the side shell are mostly between 0.01 and 0.03, as shown in Figure 100. Given the comparison of this loss factor range to other structures, it would appear that damping effects from radiation loading are small within the analysis frequency range.

A damping loss factor of 0.03 was used for all finite element analyses discussed in the following sections unless explicitly stated otherwise.

7.3 Steering Gear Room

7.3.1 Model

A screen-capture of the finite element model of the Steering Gear Room is provided in Figure 101. Note that this is a cutaway view of only the Steering Gear Room (for clarity). The model is shown at a 2x mesh density, though a 4x density model was also created. The deep frames and stringer on the side shell were modeled using plate elements for the web and beam elements for the flanges. Small stiffeners (seen in yellow) were primarily modeled using beam elements, though an investigation was performed to look at modeling with plates. Note that the Transom only contains 'small' stiffeners.

As seen in the image, the steering gear itself was not included in the model, nor were the transformers and other small items located in the space. In addition, none of the piping or additional items attached to the Transom (discussed in Section 6.1) were explicitly modeled.

Figure 101: Cutaway View of Finite Element Model of Steering Gear Room

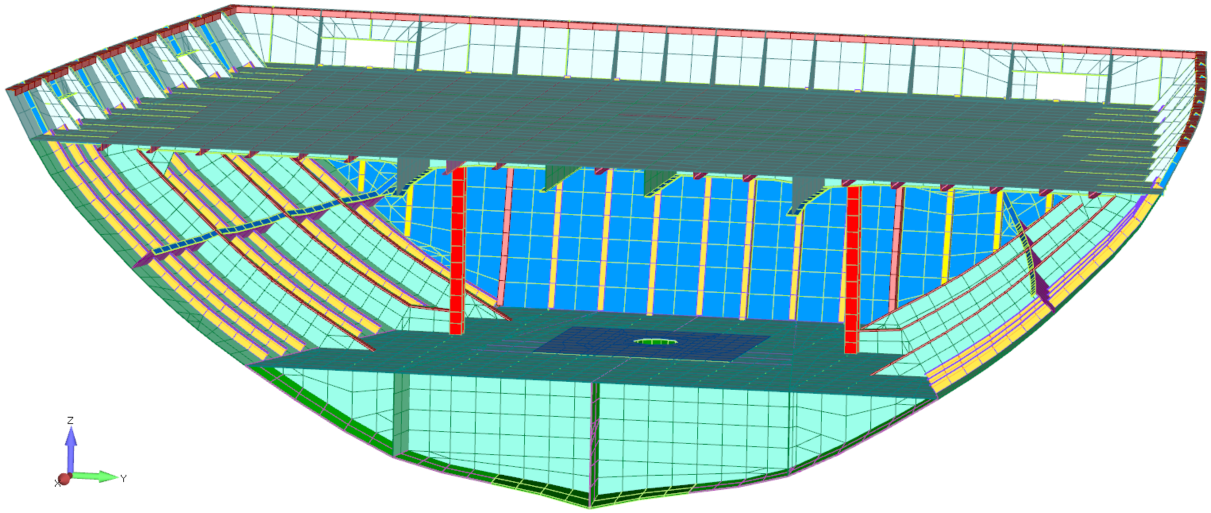

A detailed view of the model indicating the locations of measurement accelerometers is shown in Figure 102.

Two different model extents were used in this analysis: the baseline model shown in Section 7.1 and a truncated model that extends from the transom to the bulkhead at Frame 174. This is one major bulkhead forward of the Steering Gear Room. No boundary constraints were applied to the model.

Figure 102: Steering Gear Room Accelerometer Locations

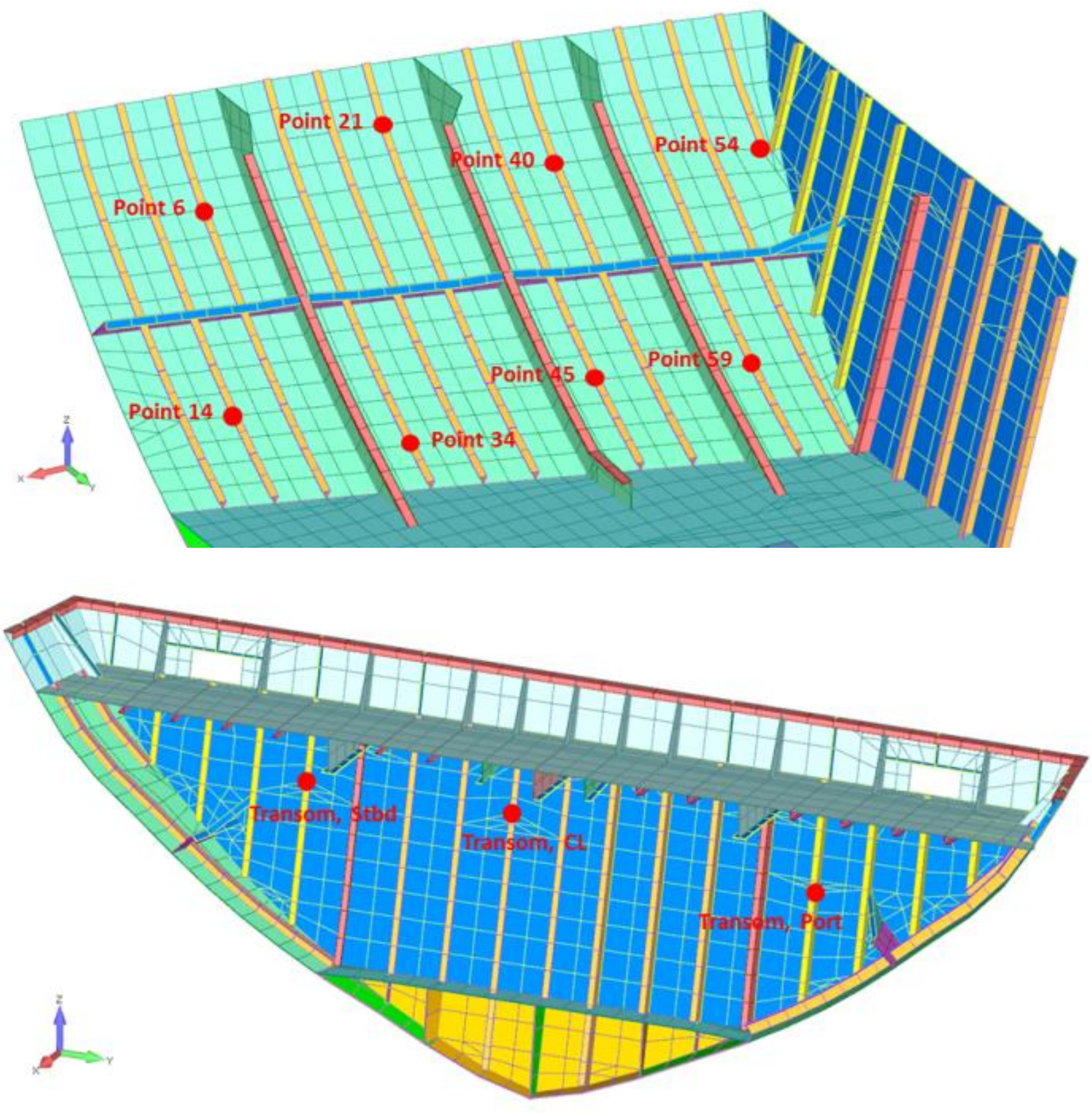

7.3.2 Notes on Measured Mobility

The side shell in the Steering Gear Room was found to be stiff relative to several of the other test structures, including the Transom. This resulted in only small peaks in the point mobility data up to frequencies over 70 Hz. Transfer mobility data generally shows more features (peaks and dips). Example measured point mobility (impact and response at the same point) and transfer mobility (impact and response at different points) spectra are shown in Figure 103 and Figure 104, respectively.

Figure 103: Steering Gear Room Side Shell, Measured Mobility, Point 40

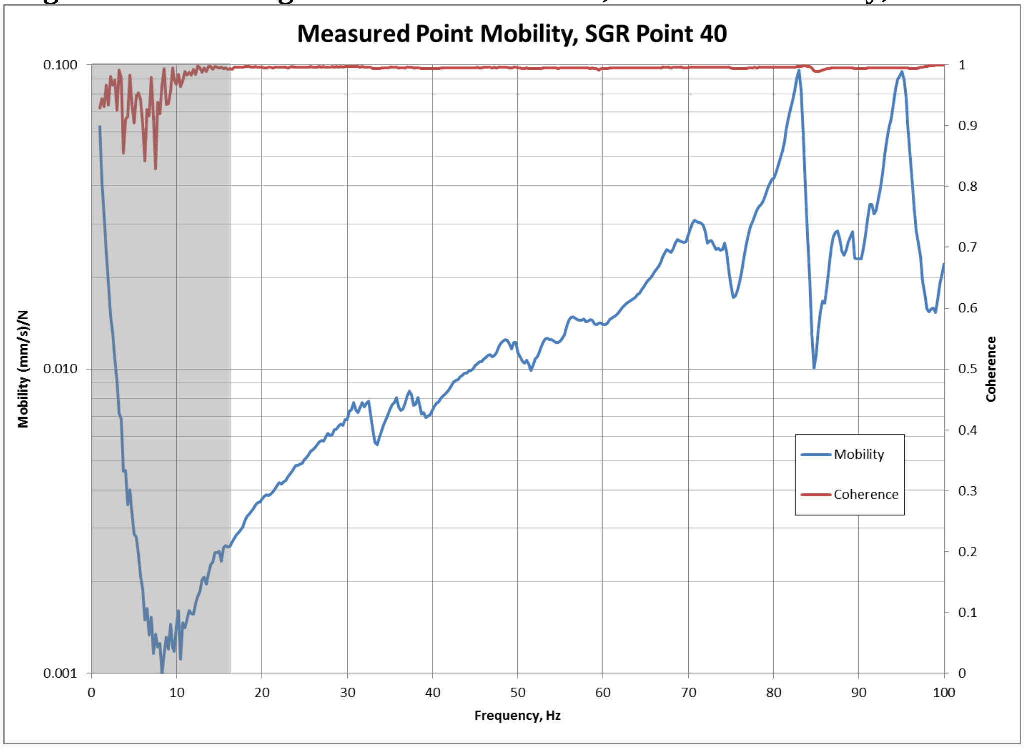

Figure 104: Steering Gear Room Side Shell, Measured Transfer Mobility, Point 40 to Point 34

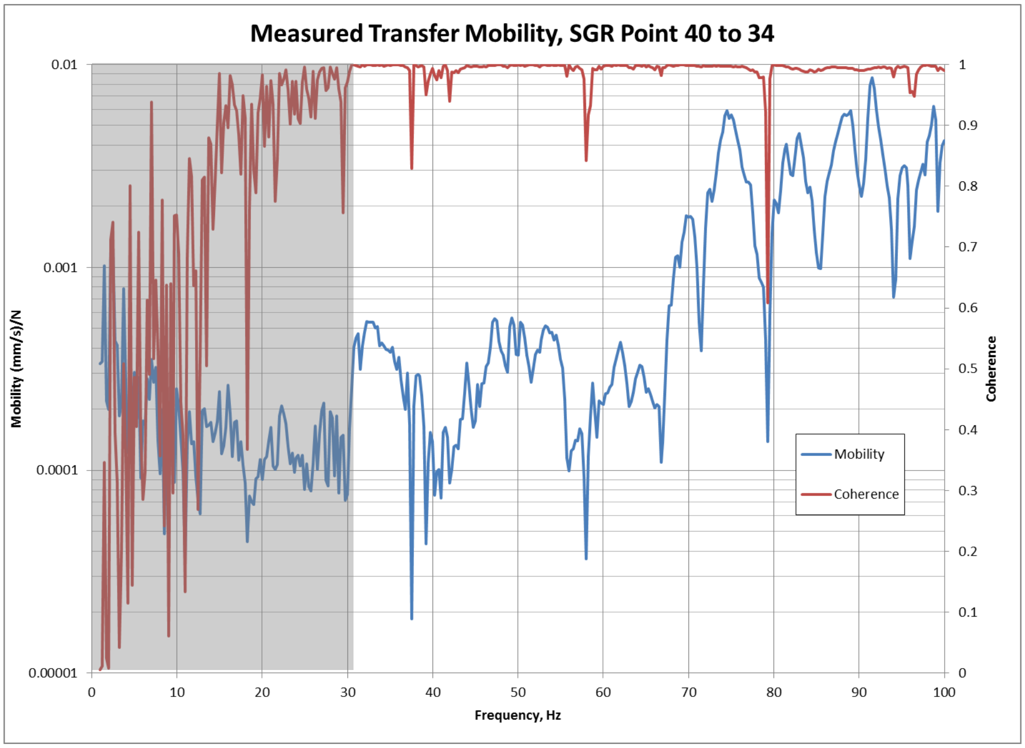

The point mobility at this location is seen to rise with increasing frequency from about 10 Hz to 70 Hz, with strong spikes in the data at higher frequencies. At first glance it may seem as though the first mode of the structure occurs at 70, or possibly even 83 Hz. However, inspection of the test results as well as the models that were created indicates that other local modes exist at frequencies down to 30 Hz. The effects of these modes can be seen in the point mobility, though they are muted.

The transfer mobility plot is far more nuanced, and reveals the presence of many modes. This can be expected as the modes of the structure at and between the impact and measurement points play a more significant role in the measured transfer mobility, whereas for the point mobility the modes in the direct vicinity of the measurement point are most significant. It is important to note the magnitude of the transfer mobility is much lower than the point mobility.

It is also important to note the quality of the data at low frequencies. In both plots the coherence is nearly equal to 1 (perfect coherence) down to 30 Hz. In the transfer mobility plot the coherence is above 0.7 down to 20 Hz, and in the point mobility plot the coherence never drops below this level. This is an indication of good data, at least at higher frequencies, though there are several additional factors to consider.

Additional inspection of the spectral data for the accelerometer used in the transfer mobility measurement (not shown here) shows that below 30 Hz the levels are the same or similar to levels recorded during a background measurement. This means that below 30 Hz (and for this specific measurement levels near 40 Hz) the transfer mobility data is unreliable.

In addition, the point mobility data shows a strong dip at about 10 Hz, with a sharp rise in level at lower frequencies. It is believed that this data is also false. First, the autopower spectrum of the impact force drops sharply at the same frequency where the point mobility is seen to rise sharply. The drop in force causes this rise in mobility since the mobility is inversely proportional to force. The sharp drop in force at low frequencies is an artifact of the measurement system and is not real.

Second, it is not likely that the impact hammer is capable of exciting the whole body modes of the structure. Inspection of the finite element models created for this effort indicate that the vessel has several whole body modes at frequencies below 10 Hz, and at least one additional mode involving gross motion of the Steering Gear Room at a frequency near 19 Hz. (This higher frequency mode is expected to shift downwards once water loading effects are considered.) Even if the specific frequencies of whole body modes are not known, the existence of such modes are guaranteed to occur, but cannot be seen in the measurement data. These factors indicate that the low frequency data in these measurements, as well as measurements elsewhere in the vessel, are suspect.

The areas of questionable data quality are shaded in grey in Figure 103 and Figure 104. Although this may seem to be a limitation of this study, it will be shown in subsequent sections that this frequency range primarily relates to non-local modes of the side shell in the Steering Gear Room. Other areas of the vessel are not affected by whole body modes in the same way, though the sharp rise in the mobility measurement (as a result of the drop-out in force) at very low frequencies is seen in nearly every measurement and should be ignored. It is noted that reciprocity of measured data[11] was verified in the frequency range of 'good data' indicated in these figures.

7.3.3 Initial Mobility Comparisons

A comparison of the modeled and measured point mobility at Point 40 on the side shell is provided in Figure 105. Data is shown for the 2x mesh density model for the 'baseline' and truncated models.

Figure 105: Steering Gear Room Side Shell, Point 40 Mobility, 2x Mesh, Baseline Model vs. Truncated Model vs. Measured

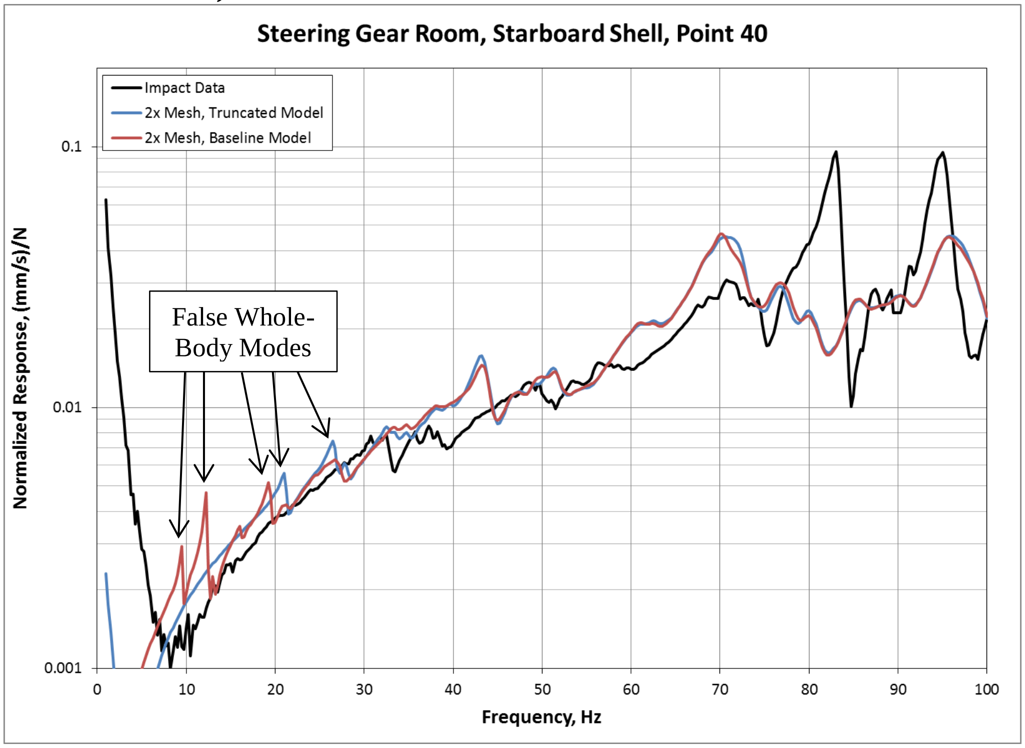

Overall, the response between 10 Hz and 70 Hz has the same character, and is generally speaking close to the measured data for both models. An important result of this comparison is the small difference between the truncated and 'baseline' models at frequencies above 30 Hz. (Strong differences do exist in the modeled vs. measured data above about 75 Hz, indicating that the model cannot capture these higher frequency modes accurately. This is investigated further in later sections.)

Several peaks are seen in the predicted response curves at frequencies between 9 and 27 Hz; these correspond to predicted 'whole body' modes, or modes that involve large motions of the Steering Gear Room as a whole[12]. As discussed in Part I, Sections 3.5 and 3.6, truncation of the

[11] Transfer mobilities between two points were seen to be nearly identical regardless of which point was used for impacting.

[12] The predicted peak at 27 Hz is something of a 'transition' mode, exhibiting both local and global behavior.

model will introduce false whole body modes. These can be seen at 9 and 12 Hz for the full model, and at 21 and 27 Hz in the truncated model.

The shift in frequency of the whole body modes between these models indicates that these are in-fact false modes (see Section 3.5).   Modeling of the full vessel would remove these peaks, though in this case their presence does not interfere with the analysis of local modes of the side shell or Transom[13].

A comparison of the measured and predicted transfer mobility between Points 40 and 34 is provided in Figure 106. Here again it is seen that the overall character of the mobility is captured particularly well between 30-60 Hz (note again that the measurement data below 30 Hz is not reliable, and the prediction data contains false modes – this area has been greyed out in this example).

Figure 106: Steering Gear Room Side Shell, Transfer Mobility Points 40 & 34, 2x Mesh, Baseline Model vs. Truncated Model vs. Measured

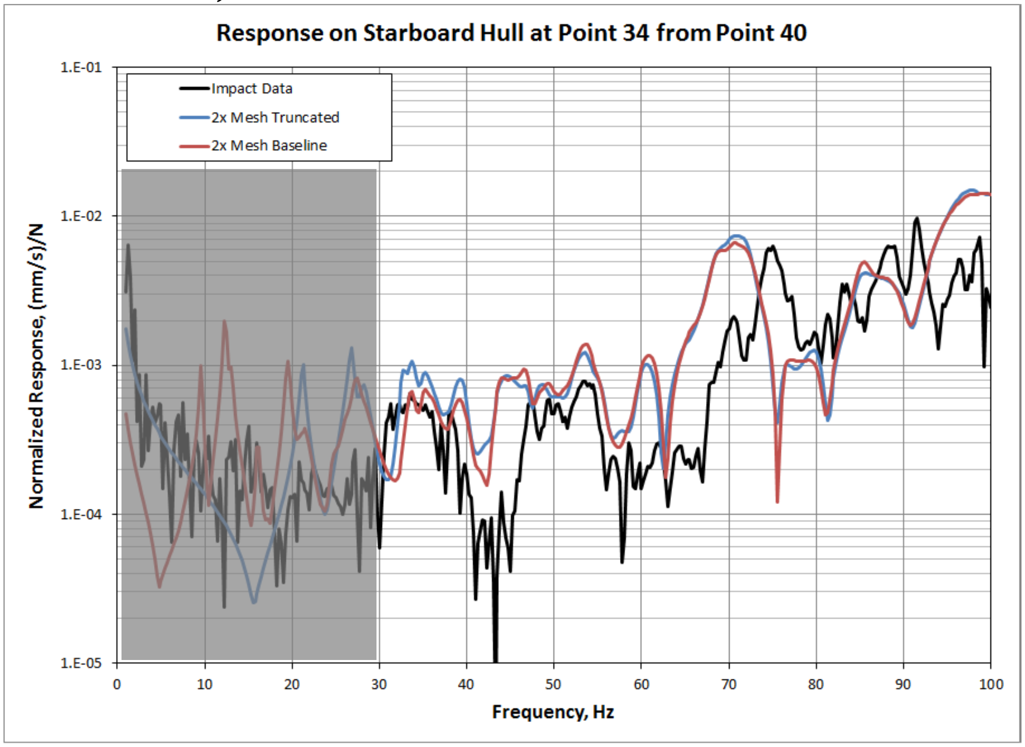

It is also seen that the differences between the baseline and truncated model are small at frequencies above 30 Hz. Given the small differences in response between the baseline and truncated models (outside of the frequency range of false modes), the truncated model was used

[13] As discussed in the previous section, the point mobility data is not reliable at frequencies below roughly 15 Hz. Although the predicted false modes in the baseline model are not real, similar modes do exist in the vessel at frequencies below 10 Hz.   If these modes were to be strongly excited they would show up in the measured data. The lack of evidence of these modes in the measured data is an indication that the measurement data at low frequencies is suspect.

for further analysis. All data used in subsequent discussions are from the truncated model. This helped to facilitate quicker run times, particularly for the 4x mesh.

7.3.4 Detailed Point Mobility Comparisons

A quantitative comparison between the measured and predicted point mobility at Point 40 is provided in Table 33. This table identifies the frequencies where major peaks occur in the FRF data for both the measured impact data and the modeled response. Also included are the percentage differences in frequency and the ratio of the response magnitudes at these peaks. This is the same approach that was used in Part I of this report. This table compares the results from both the 2x and 4x mesh models. Figure 107 presents plots of the predicted point mobility at Point 40, along with details of the operational deflection shapes that occur as a result of the impact.

Table 33: Point-Mobility Comparison for Point 40, Steering Gear Room

Impact Data		FE 2x Mesh				FE 4x Mesh			
Peak Freq., Hz	FRF Magnitude (mm/s)/N	Peak Freq., Hz	% Diff	FRF Magnitude (mm/s)/N	Magnitude Ratio	Peak Freq., Hz	% Diff	FRF Magnitude (mm/s)/N	Magnitude Ratio
30.8	8.0E-03	33.0	7%	8.3E-03	1.0	31.5	2%	8.8E-03	1.1
38.3	8.0E-03	43.3	13%	1.6E-02	2.0	41.3	8%	1.5E-02	1.9
49.5	1.2E-02	51.5	4%	1.4E-02	1.2	49.5	0%	1.7E-02	1.4
70.5	3.0E-02	70.0	1%	4.6E-02	1.5	70.3	0%	4.5E-02	1.5
83.0	9.6E-02	85.8	3%	2.6E-02	3.7	83.0	0%	2.7E-02	3.6
94.8	9.2E-02	95.5	1%	4.5E-02	2.0	88.0	7%	4.2E-02	2.2

Figure 107: Steering Gear Room Side Shell, Point 40 Mobility, Measured vs. Modeled with ODS

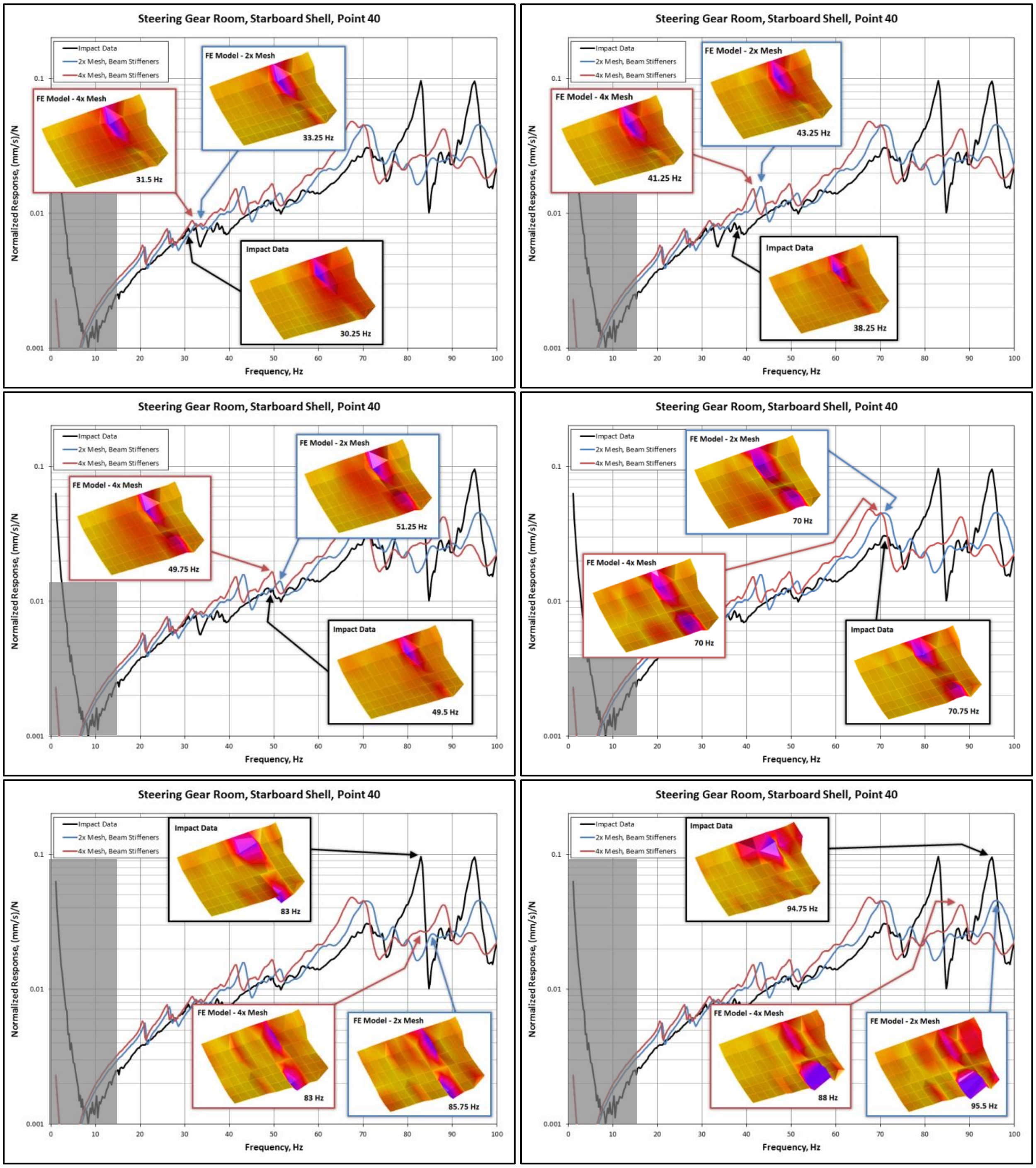

It is seen that the frequencies of predicted and measured peaks/modes are in reasonably good agreement. Some improvement in accuracy is seen with an increase in mesh density. The magnitude ratios of the peaks at 70 Hz and below are less than a factor of 2. At higher frequencies however the model clearly diverges from the measurement.

Comparisons of the operational deflection shapes indicate that both meshes provide a close match to the impact data at 70 Hz and below. At higher frequencies the deflection is not similar. It is likely that the resolution of the impact grid is not fine enough to see the actual shape of these higher order modes. Similarly, the finite element mesh may also not be fine enough for proper resolution of these modes. Higher mesh densities were not investigated in this area.

Similar point mobility data for Point 45 is shown in Table 34 and Figure 108. As was seen for Point 40, the prediction at Point 45 correlates well with the measurement at frequencies up to 70 Hz, though in this case the 4x mesh appears to provide reasonable correlation for the peak at 88 Hz. The operational deflection shapes also show good similarity, particularly at low frequencies, though arguably at the 88 Hz peak the correlation in deflection shape is a bit weaker.

Table 34: Point-Mobility Comparison for Point 45, Steering Gear Room

Impact Data		**FE 2x Mesh**				**FE 4x Mesh**			
Peak Freq., Hz	**FRF Magnitude (mm/s)/N**	**Peak Freq., Hz**	**% Diff**	**FRF Magnitude (mm/s)/N**	**Magnitude Ratio**	**Peak Freq., Hz**	**% Diff**	**FRF Magnitude (mm/s)/N**	**Magnitude Ratio**
30.8	8.0E-03	33.0	7%	8.5E-03	1.1	31.5	2%	9.4E-03	1.2
70.8	4.6E-02	70.3	1%	5.6E-02	1.2	68.0	4%	6.8E-02	1.5
76.3	3.1E-02	77.0	1%	4.0E-02	1.3	76.8	1%	4.5E-02	1.5
88.0	1.2E-01	95.3	8%	9.5E-02	1.3	88.3	0%	1.0E-01	1.2

Figure 108: Steering Gear Room Side Shell, Point 45 Mobility, Measured vs. Modeled with ODS

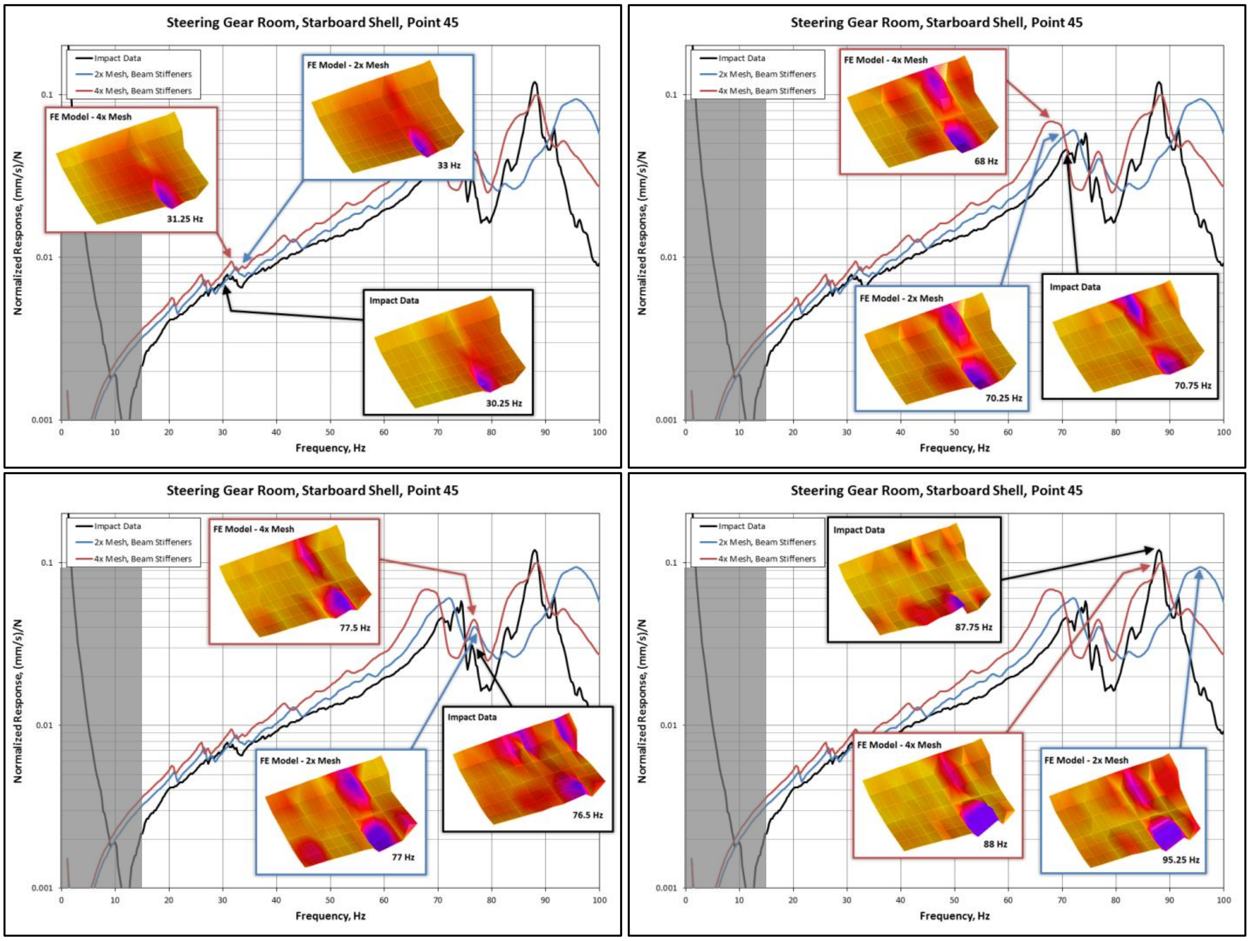

Similar results are seen for the other response locations. Figure 109 presents comparisons of measured vs. modeled point mobility for the other accelerometer locations on the side shell. It is seen that the correlation is very good up to a frequency of about 70 Hz where the results are seen to diverge. In general the point mobility at these measurement locations have fewer or less pronounced features than the other locations, which was part of the rationale for highlighting the previous measurement points for more in-depth investigations.

The locations that show the greatest discrepancy in measured vs. modeled point mobility are Points 6 and 54. The predicted level is uniformly higher than the measured level, though the error in magnitude ratio is roughly 1.2-1.5 up to frequencies near 70 Hz.

Figure 109: Steering Gear Room Side Shell, Point Mobility (Multiple Points), Measured vs. Modeled

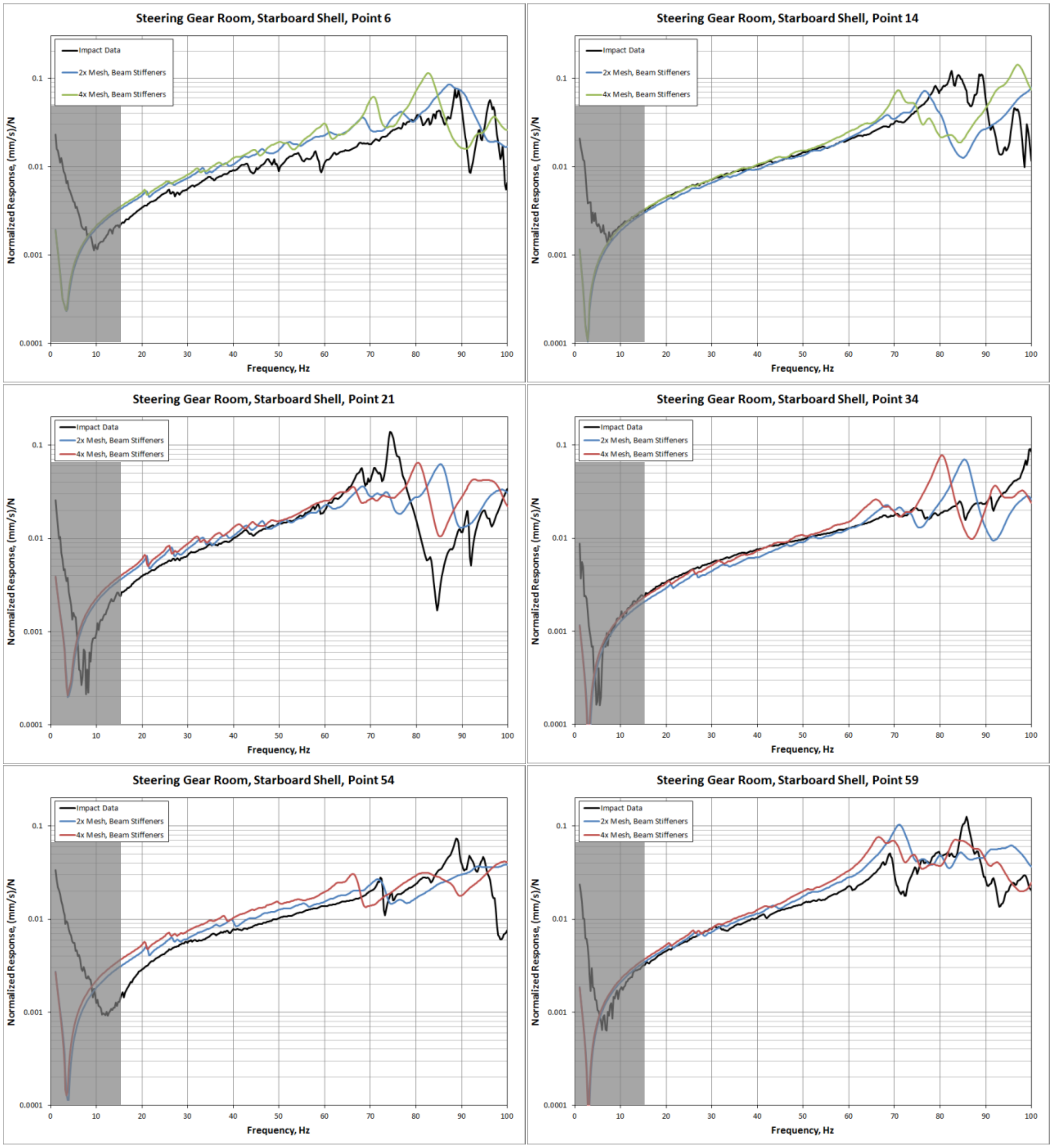

Figure 110 presents comparisons of the measured and modeled point mobility at the three measurement points on the Transom. The overall character of the mobility is clearly different than for the side shell, though the models show reasonable correlation with the measurements up to frequencies of about 60 Hz.

Figure 110: Transom Point Mobility (Multiple Points), Measured vs. Modeled

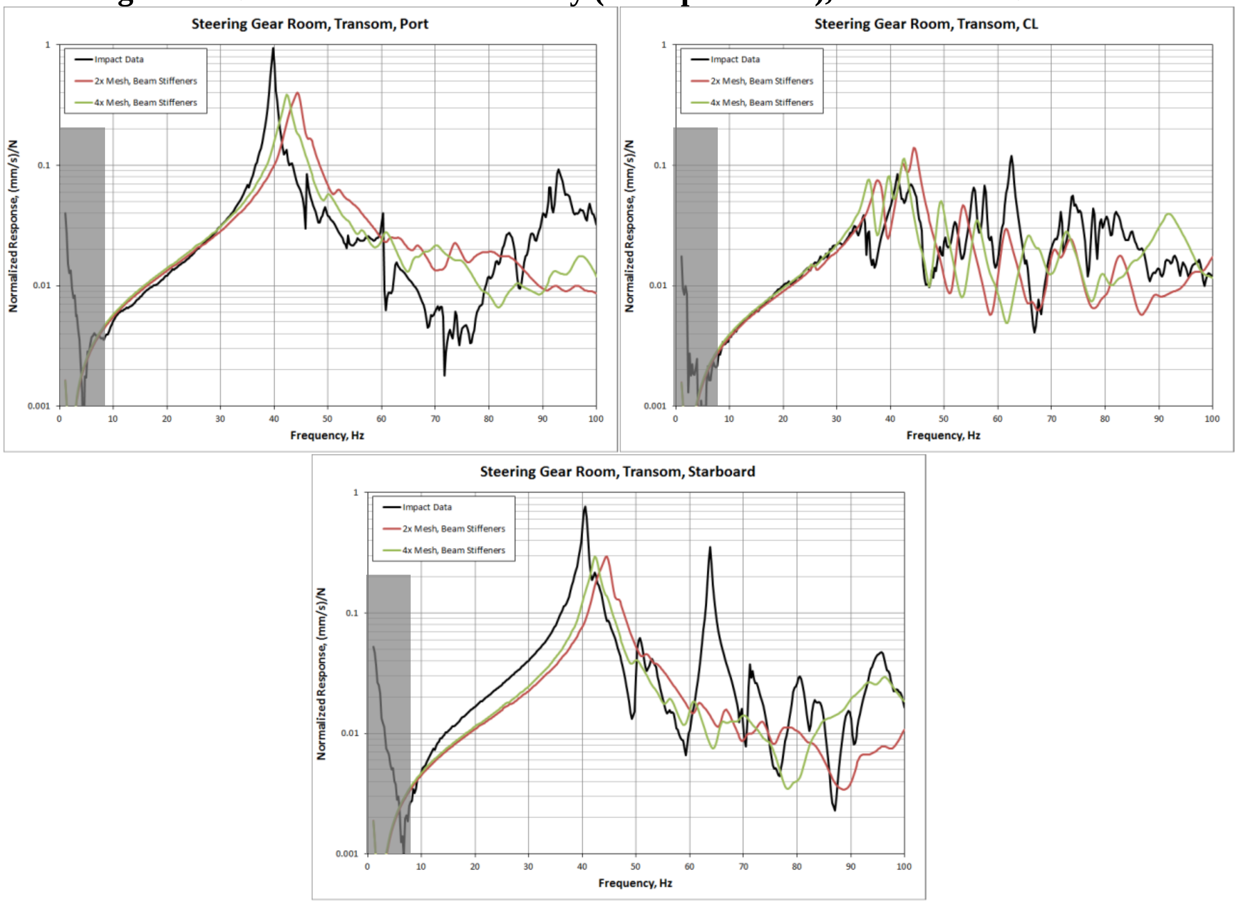

The location with the best correlation is on the port side; it is seen that the main mobility peak characteristic at 40 Hz is captured, and the correlation between model and measurement is generally reasonable at frequencies up to at least 60 Hz. The error in frequency at the 40 Hz peak is 5% for the 4x mesh and 10% for the 2x mesh. The magnitude ratio at this peak is 2.6 for both mesh densities; this may be due in part to a difference in damping between model and measurement (see below).

At the location near centerline the response character of the first several peaks is captured. The 4x mesh looks to be the better match to the measured data, and provides a reasonable approximation of the response up to 60 Hz. Greater errors are seen in the 2x mesh in general.

The predicted starboard mobility is also reasonable up to 60 Hz. The main peak at 40 Hz has similar errors to those seen on the port side. In this case there is a large peak at 64 Hz in the measured data that is not captured at all in the model.

It is believed that some of the errors seen in the point mobilities on the Transom are due to the 'extra' items mounted and welded to the Transom as well as the transformer and storage box located near the Transom. These items were not explicitly included in the model; the investigations of the Transom point mobilities were limited primarily due to the fact that good information on these structures was not readily available. The port side of the Transom is farthest from these items, and has the best point mobility correlation. The other locations are closer to these items and show response features not captured in the model.

This is an indication that auxiliary items may need to be included in order to better capture the real response of the structure at locations close to such items. However, it is arguable that for design purposes the predicted response is sufficient to capture potential problems up to 60 Hz, particularly the large peak in response at 40 Hz.

The magnitude ratio errors shown here for peak response frequencies (corresponding to local structural modes) are potentially exaggerated. This is because the 0.03 damping loss factor value used in the model is different than the values estimated from the measured data (See Section 7.2). For the side shell, the measured data indicates the actual damping is slightly greater than 0.03 at frequencies below 70 Hz, meaning the peaks will be more pronounced in the prediction than in the measured data. For the Transom the opposite appears to be the case, leading to an under-prediction of the peak response at 40 Hz. The damping value of 0.03 has been retained here to show how this estimate would affect the prediction of vibration response during a vessel's design stage.

7.3.5 Transfer Mobility Comparisons

Example transfer mobility plots comparing the predicted and measured mobility from Point 34 to other locations on the side shell and Transom are provided in Figure 111. Overall the agreement is reasonable at least up to frequencies near 70 Hz. Keep in mind that for most plots the measured data below 30 Hz is suspect as the signal at the accelerometer was low (see Section 7.3.2), and the prediction shows 'false modes' in the same frequency range.

Some discrepancies are seen at specific frequencies below 70 Hz, though in most cases it is seen that these discrepancies occur when there is a dip in the measured response. For example, in the transfer mobility from Point 34 to 14, the measured response near 50 Hz dips though the predicted response remains high. Similar features can be seen in the transfer mobilities between Points 34/21 at 50 Hz, Points 34/40 at 40 Hz, and Points 34/59 at 60 Hz.

One of the more promising plots is the transfer mobility from Point 34 to the Transom, which shows very good agreement up to 70 Hz. The peak at 40 Hz seen in the point mobility plots is also seen here both in the measured and modeled responses. Again, the 4x mesh shows significant improvement over the 2x mesh. In this case, the magnitude response has also improved, with the response ratio being closer to 2. The quality of this prediction indicates that the model is capable of predicting the transfer of vibration energy from one structure to another.

Figure 111: Transfer Mobility from Point 34 to Multiple Points, Measured vs. Modeled

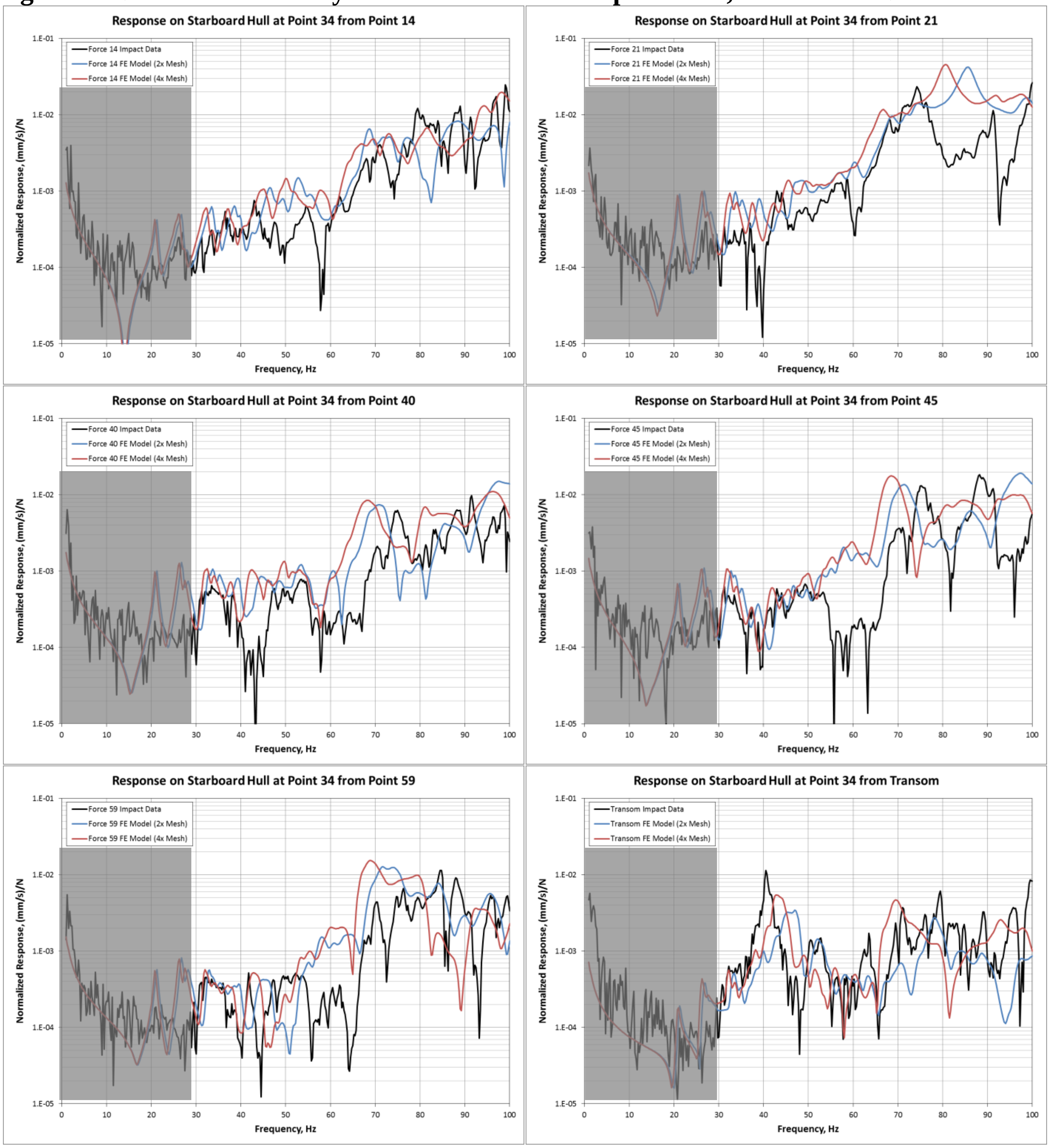

It is difficult to quantify the errors in the transfer mobility in the same manner as was done for the point mobility because, with the exception of the Transom, there are no strong peaks corresponding to a dominant single mode. Conversely, most of the data shows many sharp peaks and dips spaced very close together in frequency with some overall, broadband undulations.

If an 'average' transfer mobility is taken over a given frequency range then there is generally reasonable agreement between measurement and model. For example, if it is assumed that a fictitious machinery source creates a tone at 5 Hz intervals, it is possible to average the predicted transfer mobility data in a frequency range of +/- 5 Hz and compare this against the measured transfer mobility. This approach is in line with the ‘average response’ method discussed in Section 4.

An example plot showing this comparison is shown in Figure 112. Note that the measured data has also been averaged over the same frequency range since the choice of excitation frequencies is arbitrary. Also, only data at 30 Hz and above is shown for the reasons described above relating to measurement data quality.

Figure 112: Frequency Averaged Transfer Mobility Comparison, Point 34 to Point 21

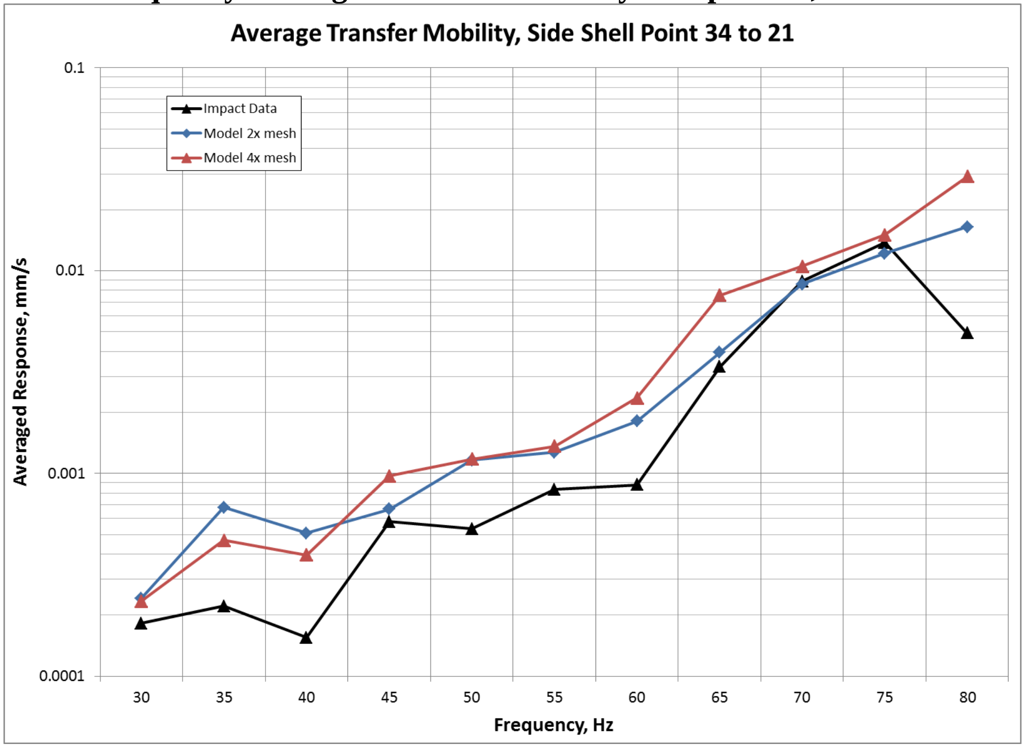

This approach provides a clearer image of the degree of accuracy that is achievable. The magnitude errors of the averaged data are typically close to a factor of 2 or less. Details of the magnitude ratios for the averaged transfer mobility between Point 34 and all response points are provided in Table 35 and Table 36 for the 2x and 4x meshes, respectively.

Table 35: Response Ratio for Averaged Transfer Mobility from Point 34, 2x Mesh

Frequency, Hz	Response Point							
	Point 6	Point 14	Point 21	Point 34*	Point 40	Point 45	Point 59	Transom
30	1.4	1.2	1.3	1.2	1.2	1.3	1.3	1.1
35	2.3	1.1	3.1	1.2	1.7	2.2	1.2	1.8
40	1.4	1.3	3.3	1.2	2.5	1.1	1.4	6.6***
45	1.2	1.7	1.2	1.1	4.1**	1.1	2.2	3.0
50	2.1	3.2**	2.2	1.1	1.4	1.0	4.1	1.5
55	2.3	2.7	1.5	1.1	1.6	3.0	1.6	1.0
60	2.0	1.4	2.1	1.0	2.9	11.4**	6.0**	1.1
65	3.7	1.6	1.2	1.1	5.6**	4.6**	4.1**	1.8
70	2.6	1.9	1.0	1.2	4.6	4.0	4.1	2.9
75	1.1	1.6	1.1	1.1	1.2	1.1	3.2	1.7
80	1.1	2.4	3.3	1.5	1.9	1.7	1.3	1.6

*This column is the point mobility for Point 34
**Discrepancy caused by large dip in measured response
***Discrepancy due to average response method vs. maximum response method

Table 36: Response Ratio for Averaged Transfer Mobility from Point 34, 4x Mesh

Frequency, Hz	Response Point							
	Point 6	Point 14	Point 21	Point 34*	Point 40	Point 45	Point 59	Transom
30	2.1	1.8	1.3	1.1	1.2	1.1	1.1	1.3
35	1.7	1.0	2.1	1.1	1.3	1.5	1.0	1.6
40	1.0	1.1	2.6	1.0	2.3	1.4	1.1	3.2***
45	1.8	2.1	1.7	1.0	4.1**	1.1	1.6	3.6
50	3.4	4.2**	2.2	1.1	2.1	1.3	1.7	1.2
55	3.1	2.5	1.6	1.1	1.6	3.4	2.2	1.9
60	1.0	2.2	2.7	1.2	3.8	12.4**	7.8**	1.4
65	2.7	2.3	2.2	1.5	14.3**	14.0**	11.9**	1.7
70	1.3	1.7	1.2	1.2	5.2	5.3	6.3	2.3
75	1.4	1.4	1.1	1.4	1.3	1.8	2.8	1.0
80	2.8	1.5	5.9	2.5	1.9	1.5	1.3	2.9

*This column is the point mobility for Point 34
**Discrepancy caused by large dip in measured response]
***Discrepancy due to average response method vs. maximum response method

For the most part, the response ratios are close to a factor of 2 or less at frequencies of 65 Hz and below. At a few frequencies and locations the response ratio reaches factors of 3 or greater, though in most of these cases this is due to a large, broadband dip in the measured response; at these frequencies the model predicts a mostly flat response, as seen in Figure 111 and noted in the tables above. This means that although the model would technically over-predict the response at these frequencies, it would be less likely to predict a strong (erroneous) peak that may exceed a given vibration limit unless the levels at other frequencies were also in excess of the limit.

At frequencies above 65 Hz the model is seen to diverge from the measurement, though some locations still appear to be acceptable using this averaging method.

The response on the Transom also looks good at nearly all frequencies except at 40 Hz; this is where there is a strong peak in response, as seen in the bottom plot of Figure 111. This error shows the limitations of the ‘average response’ method. In this case the ‘maximum response’ method provides greater correlation between the model and measurement, with response ratios of 3.2 and 2.0 for the 2x and 4x meshes, respectively.

It is worth pointing out that the point mobility data, also shown in Table 35 and Table 36, shows a nearly exact correlation at all frequencies below 80 Hz when the average response method is used.

A second example of transfer mobility comparisons is shown in Figure 113, which provides transfer mobilities from Point 6. Similar features to the previous comparisons are seen, with reasonable agreement at least up to 60 Hz (discounting the issues at frequencies below 30 Hz noted above).

Figure 113: Transfer Mobility from Point 6 to Multiple Points, Measured vs. Modeled

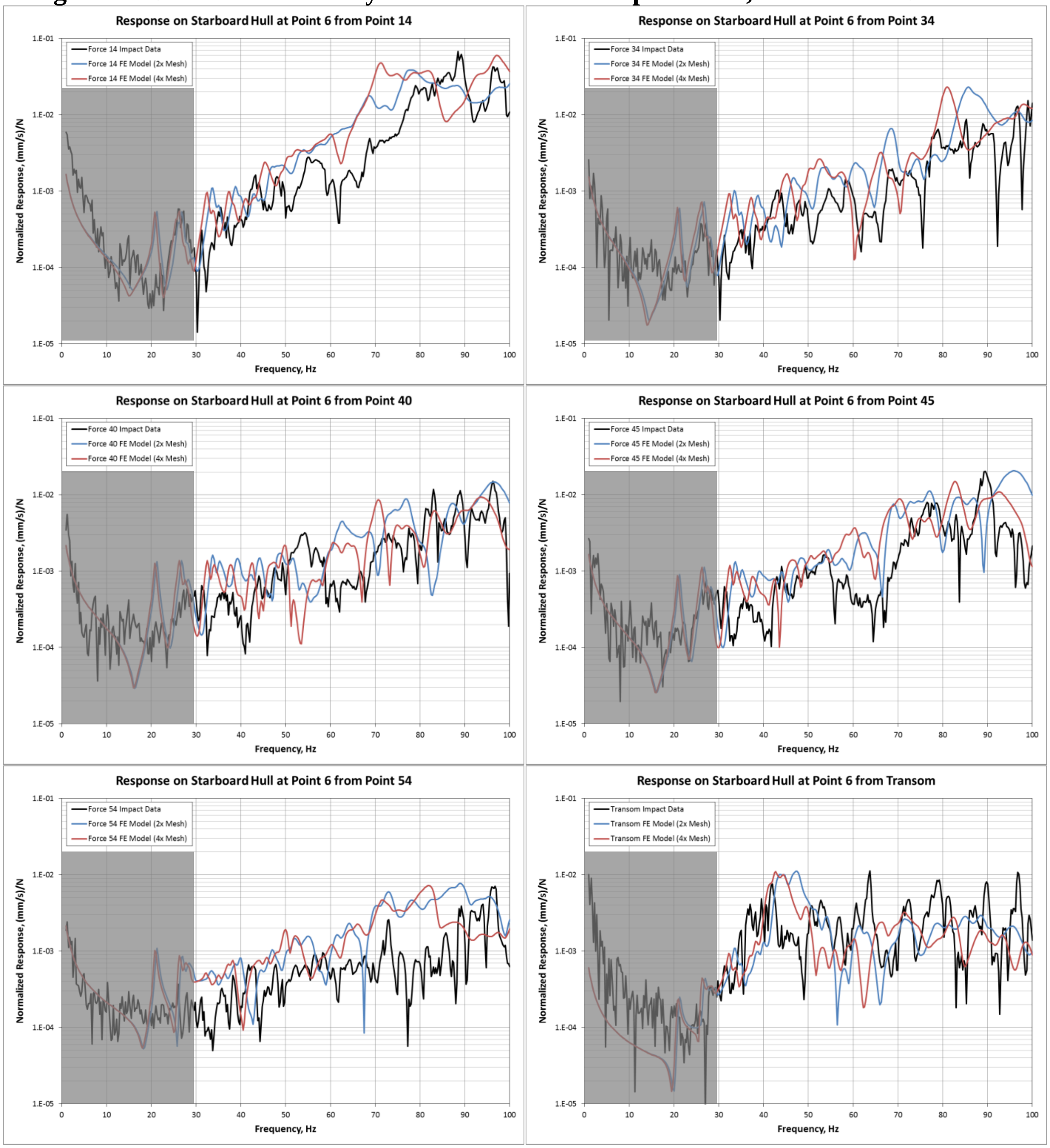

As was done for the transfer mobility data from Point 34, the 'average response' method has been applied to this data as well. The results are shown in Table 37 and Table 38 for the 2x and 4x meshes, respectively. Similar results to those seen previously are seen here as well. In general the response ratios are close to a factor of 2 or less, though some larger discrepancies exist at specific locations and frequencies. The main peak on the Transom still benefits from the 'maximum response' method and is arguably the correct approach in this case in order to predict the actual peak response (even though the average response method provides seemingly improved accuracy in this case). However, the Transom response at 45 Hz suffers from inaccuracy in both methods in this example.

Table 37: Response Ratio for Averaged Transfer Mobility from Point 6, 2x Mesh

Frequency, Hz	Response Point							
	Point 6*	Point 14	Point 21	Point 34*	Point 40	Point 45	Point 59	Transom
30	1.3	1.2	1.3	1.2	1.3	1.8	1.3	1.1
35	1.2	1.8	1.6	2.3	3.0	3.1	1.8	2.1
40	1.2	1.8	1.5	1.4	4.4**	4.1**	1.6	2.7
45	1.4	1.3	1.3	1.3	1.4	1.1	2.1	5.7
50	1.4	2.2	1.2	2.1	1.1	1.3	1.1	2.8
55	1.5	1.8	2.3	2.4	2.6	1.3	1.0	1.3
60	1.8	3.5	1.6	2.4	2.6	3.8**	2.0	2.0
65	1.7	5.8	1.7	3.8	5.0**	5.8**	3.3	2.8
70	1.5	3.9	1.2	2.5	1.8	3.4	8.5	1.2
75	1.3	2.8	2.2	1.1	2.5	1.8	5.3	1.8
80	1.3	1.7	1.2	1.2	1.1	1.4	2.6	2.0

*This column is the point mobility for Point 6
**Discrepancy caused by large dip in measured response

Table 38: Response Ratio for Averaged Transfer Mobility from Point 6, 4x Mesh

Frequency, Hz	Response Point							
	Point 6*	Point 14	Point 21	Point 34	Point 40	Point 45	Point 59	Transom
30	1.4	1.3	1.1	2.0	1.7	2.0	1.0	1.0
35	1.3	1.2	1.0	1.7	2.1	2.2	1.7	2.6
40	1.3	1.4	1.7	1.0	2.7**	2.7**	1.2	1.1
45	1.5	1.8	1.5	1.9	1.3	1.3	1.6	4.7
50	1.6	2.4	1.2	3.5	1.1	1.3	1.1	1.2
55	1.5	2.1	3.7	3.2	3.7	1.7	1.0	2.7
60	2.0	2.9	1.6	1.1	1.9	5.0**	2.7	2.8
65	1.7	4.8	1.4	2.8	2.6**	6.4**	4.3	2.1
70	2.3	7.9	1.1	1.2	2.4	3.8	9.7	1.2
75	1.4	4.5	2.1	1.6	1.5	1.1	5.0	1.5
80	2.2	1.8	2.7	3.0	1.1	1.5	2.3	2.3

*This column is the point mobility for Point 6
**Discrepancy caused by large dip in measured response

As was the case at Point 34, the Point 6 point mobility shows very good results with the average response method, particularly at frequencies below 60 Hz.

Overall, the transfer mobility comparisons indicate that the 4x mesh provides an improvement over the 2x mesh, though such improvements are small in some cases. The biggest difference is seen in the primary peak near 40 Hz in the transfer mobility to the Transom, where the 4x mesh provides the best correlation. Improvements are also seen at frequencies above 70 Hz, though the 4x mesh does not necessarily capture the measured data well.

7.3.6 Notes on Minimum Mesh Density

In some models of the Steering Gear Room the minimum mesh density was used. The ability of the minimum mesh density to capture key characteristics of the measured point and transfer mobilities was extremely limited, more so than was initially expected based on the results of Part I. An example is shown in Figure 114. It can be clearly seen that the minimum mesh density gives a very poor representation of the primary peak in response at 40 Hz. Poor results were typically seen with other models and analyses as well.

Figure 114: Point Mobility on Transom,
Illustration of Errors with Minimum Mesh Density

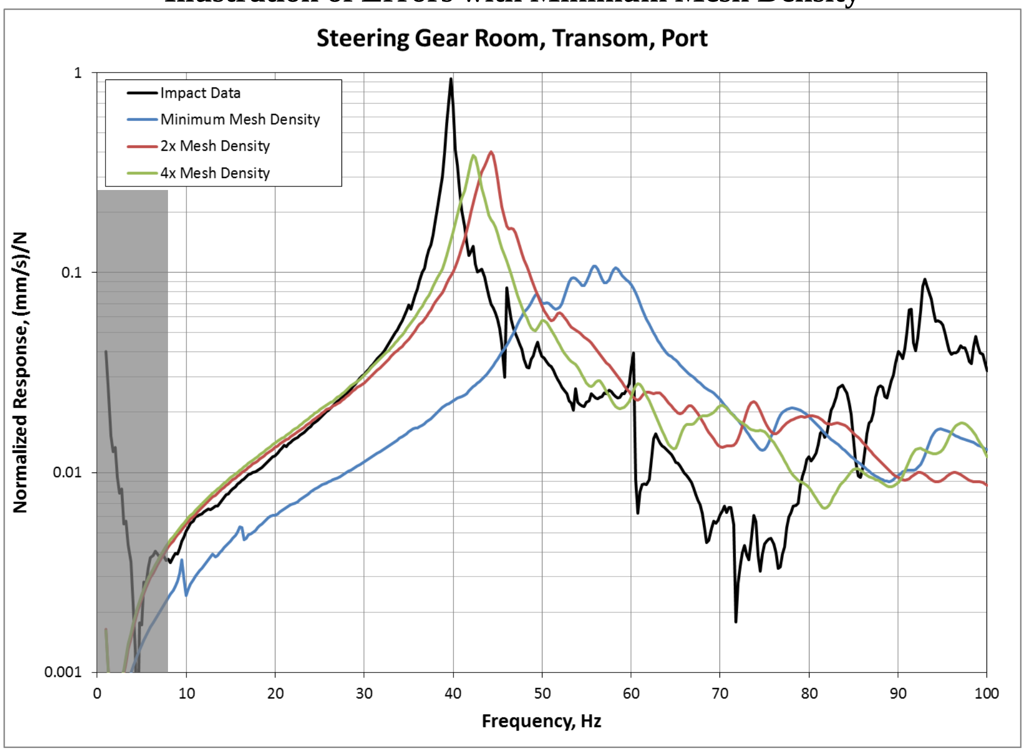

7.3.7 Notes on Beam vs. Plate Stiffeners

As discussed in Section 7.3.1, the models used in the Steering Gear Room primarily utilized beam elements for the small stiffeners. Frames, girders, and other large stiffeners were modeled using plates for the stiffener web and beams for the flanges. An investigation was performed to determine if improvements could be obtained by using plates to model the small stiffener webs as well.

Example comparisons of predicted vs. measured point mobilities for models with beam vs. plate elements for the small stiffeners are provided in Figure 115. It is seen that there are negligible differences in the mobilities for modes below 70 Hz. When changing to a plate stiffener, the predicted frequency of the first peak near 70 Hz shifts upwards slightly. A similar phenomenon can be seen at Point 6 for the predicted mode around 85 Hz.

Figure 115: Examples of the Effect of Beam vs. Plate Stiffeners on Point Mobility

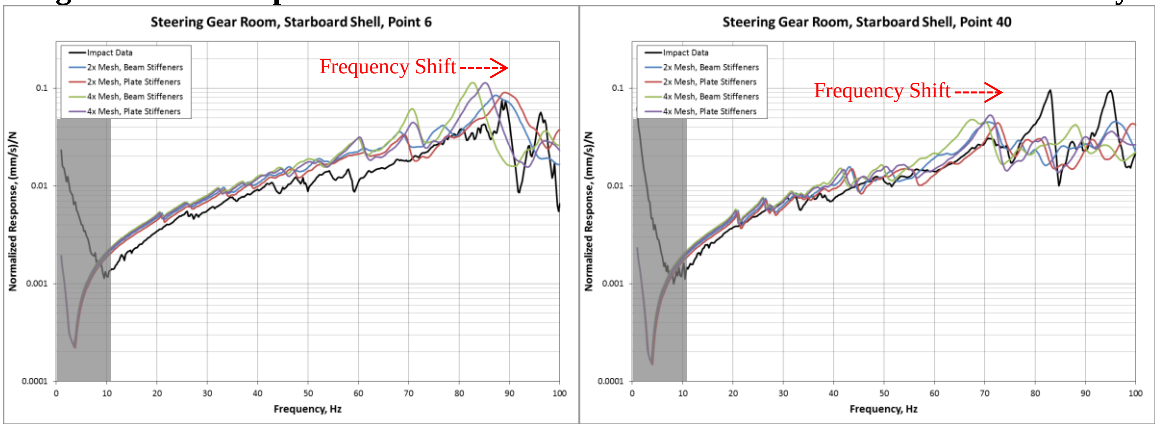

Arguably these changes are beneficial to matching the response, but they only have a significant effect on higher order modes. As seen in the Point 40 mobility, they do not necessarily 'fix' large errors in the response at high frequencies.

7.3.8 Summary of Steering Gear Room Analysis

The following points can be derived from the analyses performed in the Steering Gear Room:

- Reasonable correlation between measured and modeled point and transfer mobilities can be achieved at frequencies corresponding to the first several local modes of the structure of interest.
- At frequencies below 60-70 Hz, typical errors in the prediction of peak response frequencies is 10% or less for the 2x mesh and 5% or less for the 4x mesh.
- At frequencies below 60-70 Hz, the error in point mobility magnitude is typically less than a factor of 2. Transfer mobilities in the same frequency range also generally have magnitude errors on the order of a factor of 2, though in some cases errors can reach a factor of 3 or higher. In these cases (and for the modeled structures) this error was cause by a dip in measured response, where the predicted response remained mostly flat. This result would not typically lead to a false prediction of excessive vibration, though it is formally an error of the model.
- A 4x mesh density will generally produce better results than a 2x mesh. In some cases the improvement is slight, though in several cases, particularly the Transom, it is significant. Differences are seen in the prediction of peak frequencies, both at low order and high order modes. Improvements in magnitude ratio with the 4x mesh are seen in some cases but are not universal. Although the 4x mesh appears to perform better at frequencies above 60-70 Hz, the 4x mesh does not necessarily produce accurate results in this frequency range.
- The minimum mesh density is not recommended unless results are only required in a frequency range that is below the range of local structural responses (i.e. predicting whole body modes).

- The practical frequency limit for accurate modeling of these structures may be 70 Hz, at least when using the approaches considered here. This frequency corresponds to higher order local modes – significant motion of plating relative to stiffeners is seen here. Approximate representations of the mobilities are possible in some cases with the 4x mesh, though this is more likely to indicate the 'order of magnitude' of the response than accurately represent peaks and dips.
- Use of beam elements for small stiffeners appears to be sufficient for achieving accurate results below 60-70 Hz. Some improvements are seen for higher order modes (frequencies above 70 Hz in this case) when plate elements are used for small stiffeners, though the changes are small. Plate elements are recommended for modeling large girders, frames, and other large stiffeners.
- The results shown here were achieved without the addition of mass for the steering gear. This is likely due to the significant stiffness of the structure supporting the steering gear.
- The side shell results were achieved without the need to model the pipe that that was supported by the structure. Furthermore, the structure below the waterline (at a level below the deck of the Steering Gear Room) did not include masses for tank fluids or water loading from the ocean. Note however that comparisons of responses corresponding to whole body modes were not possible – it is expected that tank fluid mass and ocean effects would be required for such calculations.
- The results for the Transom were reasonable up to a frequency of 60 Hz, above which some local spikes in the measured mobility data were not re-created. It is believed that these spikes are the result of 'extra' items attached to the Transom, as well as the presence of a transformer and storage box which are directly adjacent to the Transom. Such items may need to be included in the model in order to capture the missing features in the prediction. (Data required to model these items was not available.)
- The model extent required to obtain accurate results in the frequency range corresponding to local structural modes was one major bulkhead away from the structures of interest. A free boundary condition was used (i.e. no constraints were applied).
- These results underscore the ideas discussed in Section 4; a prediction at any single frequency is likely to have large errors compared to the actual response at that same frequency. However, depending on the presence of strong response peaks, an average or maximum predicted response over a frequency range can be used to obtain reasonable agreement with average or maximum measured levels for the same frequency range. The maximum response approach is beneficial (if not required) when strong peaks in the response are present. Therefore, when modeling real machinery sources even if the source produces a tone at a specific frequency, a range of frequencies should be analyzed in order to capture the real response. This is explored further in Section 8.

7.4 Engine Lab

7.4.1 Model

A screen-capture of a section of the finite element model for the Engine Lab bulkhead is provided in Figure 116. The image shows the 4x mesh density version of the model. The accelerometer measurement locations discussed previously are highlighted in Figure 116. Note that some of the structure in the model has been visually removed from the screen capture to allow for an unobstructed view of the test structure.

All frames and deep girders were modeled using plate elements for the web and beam elements for the flanges. Small stiffeners were modeled using beam elements. Note that the test bulkhead itself only uses small stiffeners.

In this model, most of the vertical stiffeners do not extend all the way to the deck; this was done to simulate the actual structural condition, as discussed in Section 6.1.2. Furthermore, the two box beams that run horizontally along the bottom of the bulkhead have been added, and are seen in red in Figure 116. The model also includes a representation of the door frame, being a 2" x 1.5" x 3/16" box beam around the perimeter of the opening. This was a rough estimation, as details are not available. Additional discussion of the effects of these items is provided in Section 7.4.5.

Both the 'baseline' and a truncated model were analyzed. The truncated model includes all structure from the bulkhead at Frame 134 to the bulkhead at Frame 188. This is one major bulkhead forward and aft of the Engine Lab. Similar to what was shown in the previous section, it was found that this truncated model provided nearly identical results over the frequency range of interest (the influence of whole body modes was not significant in either the measured or modeled responses). All results shown for the Engine Lab are for the truncated model.

No constraints were applied to the model.

Figure 116: Model Section of Engine Lab Bulkhead
(Full model not shown)

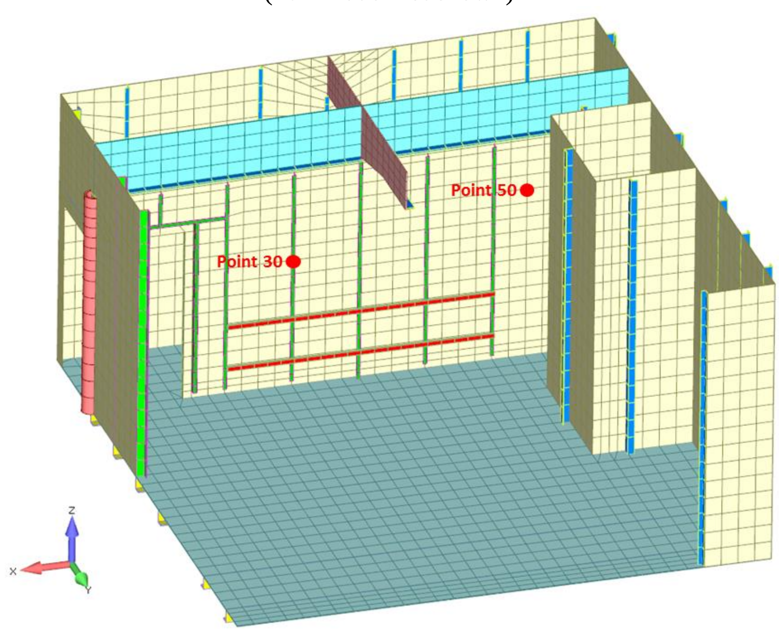

7.4.2 Notes on Measurement Mobility

Example point mobility plots for the Engine Lab are provided in Figure 117. Unlike the side shell in the Steering Gear Room, the response of the Engine Lab bulkhead was seen to contain many strong peaks. The Engine Lab bulkhead was found to be dynamically 'weak' relative to other structures that were tested, possibly due in part to the fact that most of the stiffeners were sniped at the ends. Evidence of this weakness can be seen directly from the fact that the first mode (major response peak) occurs near 15 Hz (as compared to 40 Hz for the Transom).

Figure 117: Measured Point Mobility, Engine Lab

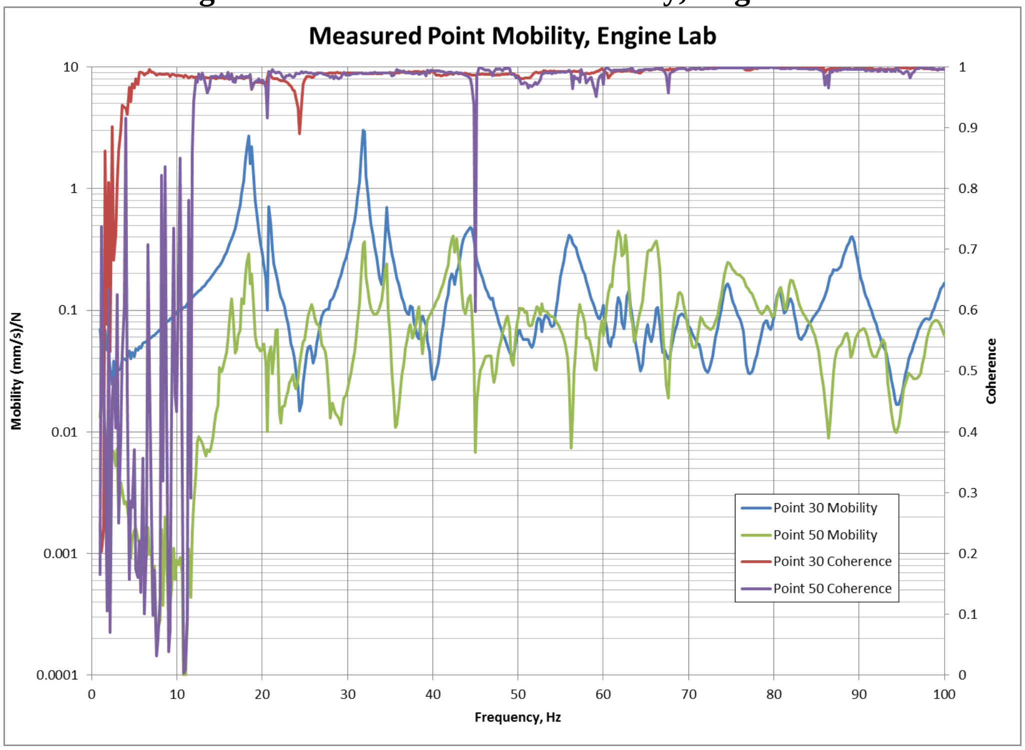

The coherence data is typically good, being nearly 1 at all frequencies above 12 Hz; there is an exception at 45 Hz in the Point 50 data, though this seems to have a negligible impact on the analysis presented here. Excellent reciprocity was seen in the data measured on this bulkhead (not shown here).

As discussed in Section 7.2, the damping of this bulkhead was found to be lower than the 0.03 value used elsewhere in this report; loss factors were generally seen to be between 0.01 and 0.02, with some exceptions. The relatively light damping of this structure was also noted during measurement, as longer acquisition times were needed for impact responses to sufficiently die out.

A value of 0.03 was used for modeling this structure, though the influence of damping is discussed further in the following sections.

7.4.3 Mobility Comparisons

A comparison of the point mobility at Point 30 between the model and measurement data is provided in Figure 118. Also shown are comparisons of the Operational Deflection Shape (ODS) at major peaks in the FRF data. Only data for the 4x mesh is shown.

Figure 118: Engine Lab Point 30 Mobility, Measured vs. Modeled with ODS

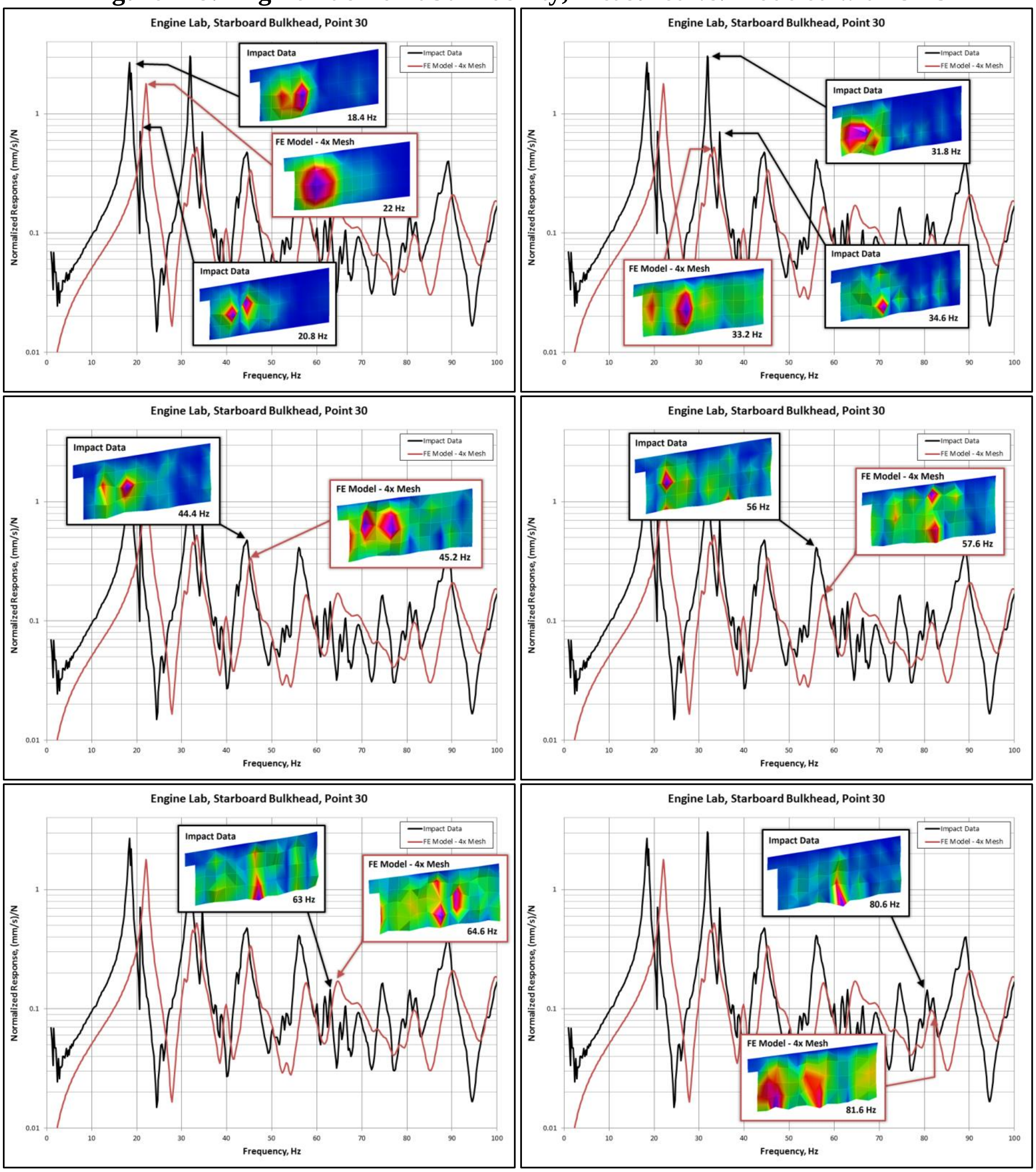

It is seen that the overall character of the predicted response is similar to the measured response. However, some discrepancies exist, particularly in the predicted frequency and magnitude at the first two major peaks.

The operational deflection shapes of the impact data provide some insight as to what is happening in this structure, though it does not provide a full explanation of why. For the first major peak near 20 Hz (upper left plot of Figure 118) the deflection shapes are very similar between the model and measurement. However, there is a second smaller peak in the measured data that is not captured at all in the model. The deflection shape corresponding to this peak shows that this is something of a second order mode localized near the door. The cause of this is not clear.

The measured and modeled deflection shapes at the next major peak near 32 Hz (top right plot of Figure 118) show some similarities in terms of the locations of peak vibration levels, though there are formally some discrepancies in the shape of the deflection. There is also a secondary peak in the measured data that is not captured in the model. Again, the measured deflection shape shows a localized higher order mode, the cause of which is uncertain.

For the peak near 45 Hz (middle left plot of Figure 118), both the deflection shapes and response peaks are similar between the model and measurement. This higher order mode arguably provides the best correlation between measurement and model for this structure.

The modeled and measured deflection shapes for the peak near 56 Hz (middle right plot of Figure 118) have similarities, particularly in their overall character. Specific differences do exist though, such as the exact location of peak response (left side in the measured data, right side in the modeled). However, the deflection shape would arguably be sufficient for identifying a practical engineering solution if a vibration excess existed.

Though similarities exist between the measured spectra and the predicted spectra for the peaks near 63 Hz (lower left plot of Figure 118) and 80 Hz (lower right plot of Figure 118), it is apparent from the deflection shapes at theses peaks that there is weak correlation between the finite element model and measured data.

A quantitative comparison between the measured data and the FE model is provided in Table 39. This table identifies the frequencies where major peaks occur in the FRF data for both the measured impact data and the modeled response, along with the percentage differences in predicted frequency and the ratio of the response magnitudes at these peaks.

It is seen that the error in frequency is greatest for the first peak, though is less than 5% for the other peaks below 60 Hz. The response magnitude shows a large error for the second peak, though the errors for the first and third peaks are good.

Table 39: Point-Mobility Comparison for Engine Lab Point 30

Impact Data		Finite Element 4x Mesh			
Peak Freq., Hz	**FRF Magnitude (mm/s)/N**	**Peak Freq., Hz**	**% Diff**	**FRF Magnitude (mm/s)/N**	**Magnitude Ratio**
18.4	2.7E+00	22.0	20%	1.8E+00	1.5
31.8	3.0E+00	33.2	4%	5.2E-01	5.9
44.4	4.8E-01	45.2	2%	3.4E-01	1.4
56.0	4.2E-01	57.6	3%	1.7E-01	2.4
63.0	1.5E-01	64.60	3%	1.7E-01	1.2
80.6	1.4E-01	81.60	1%	9.7E-02	1.5

The reasons for these discrepancies are not completely clear. Many investigations were performed to try and identify the cause of the error and determine what modeling features were missing or incorrect. Ultimately, the fact that significant portions of the modeled structure are not known to a high level of accuracy (the structural drawings were not available – see Section 6.1.2) is likely the major cause of the errors seen here.

Some factors pointing to this conclusion are as follows. First, the error in predicted peak frequency is very large for the first peak and much less for subsequent peaks. This is opposite behavior to what is seen in the results presented in the rest of this report. As seen in the operational deflection shape the first peak corresponds to a 'breathing' motion of the portion of the bulkhead near the door, and significant motion is seen at the boundaries of the bulkhead. It can be implied that the details of the structures adjacent to this bulkhead are then important in creating a proper prediction. The details of the structure above and forward of this bulkhead are not available.

An example of the significance of the surrounding structure on this bulkhead is shown in Figure 119. This figure compares the point mobility at Point 30 presented previously to the mobility at the same point for a model that only includes the bulkhead and no surrounding structures. The edges of the bulkhead-only model have been pinned in this example. Clearly, the frequency of the first peak is shifted well below the frequency of the first measured peak, indicating that the surrounding structure is providing support and stiffness to the bulkhead. This not only indicates that the details of the surrounding structure are important in creating an accurate model, but also presents additional evidence of the minimum model size required for modeling.

Figure 119: Point 30 Mobility, Truncated Model vs. Bulkhead Only Model

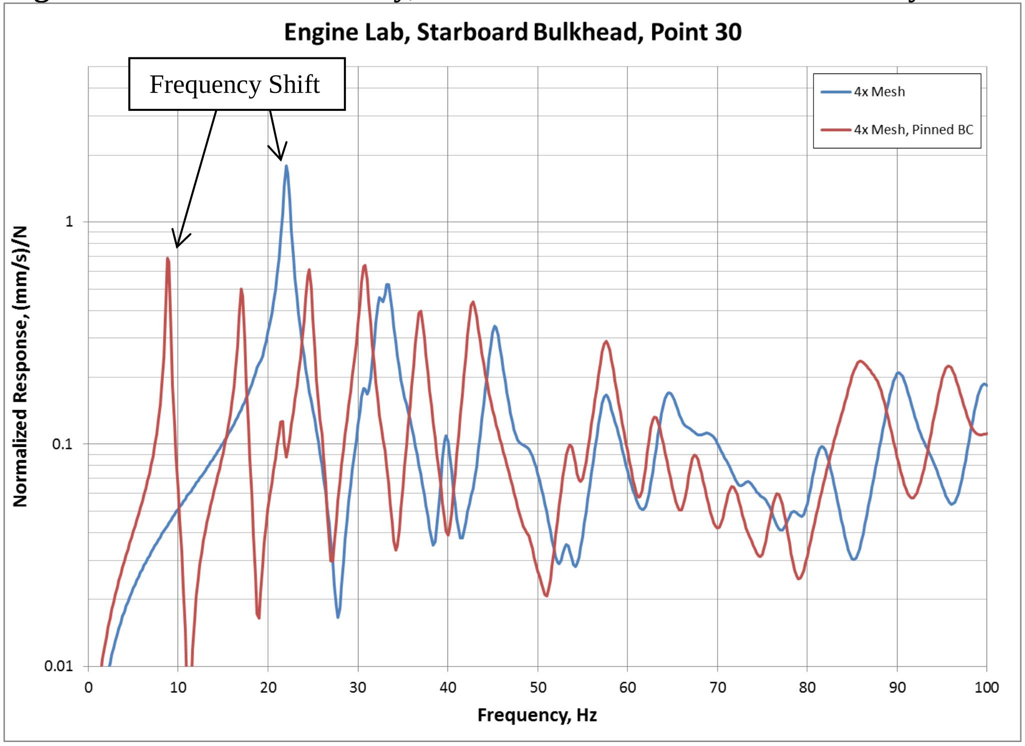

It is noted that some of the modifications that were made to the model to identify the source of the errors include changing the mass in the tank below the Engine Lab (with very minor effects), adding the details around the doorframe and lower portion of the bulkhead described previously (with some small, some significant changes), and changing the stiffener and plating dimensions on the test bulkhead and surrounding structures (with major effects). This last item was performed because of the lack of structural information, and also because, as discussed previously, the structural drawing was found to incorrectly identify the dimensions of the vertical stiffeners on the test bulkhead. The results of the changes made to the structure are not presented here as they were deemed too arbitrary. Suffice it to say, in order to avoid intense aggravation and improve model quality it is recommended that the model use the correct stiffener and plating dimensions.

The same analysis was performed for the point mobility at Point 50. Plots of the predicted and measured mobility with examples of the operational deflection shapes are provided in Figure 120. A table identifying the differences in predicted vs. measured peak frequencies and response magnitudes is provided in Table 40.

Although the overall characteristics of the point mobility are again seen to be captured, the prediction is seen to have some significant errors. The predicted frequency of the first major peak is off by 16%, and the deflection shape is also seen to differ. Comparing the operational deflection shapes, it is seen that the second predicted peak is meant to match up with the second measured peak, resulting in a frequency shift of 15%.

Figure 120: Engine Lab Point 50 Mobility, Measured vs. Modeled with ODS

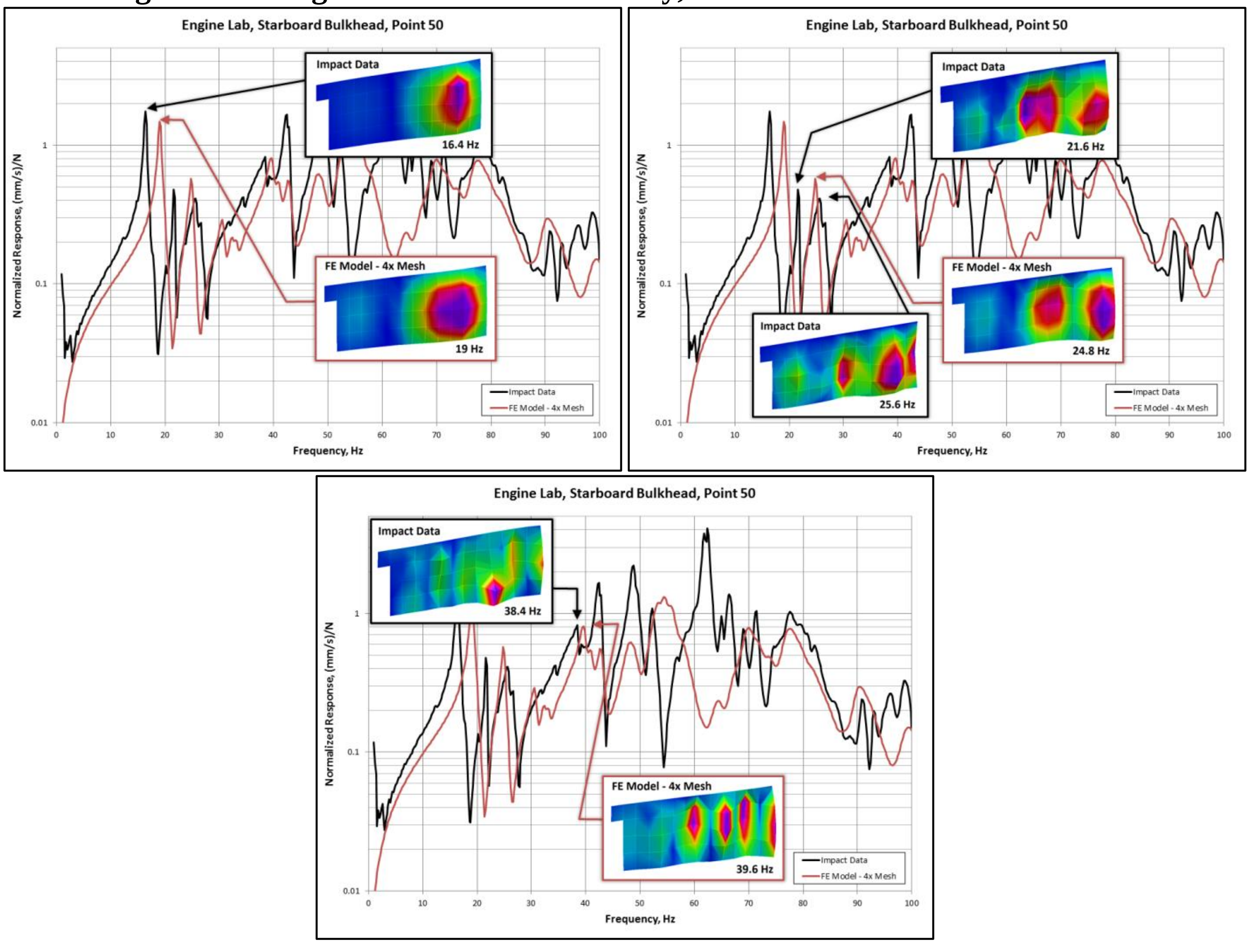

At higher order modes it is difficult to match the predicted and measured peaks, though it is believed that the peaks just below 40 Hz are similar. Again, the fact that some higher order modes are captured by the model and lower order modes are not is another indication of the need for proper modeling of the surrounding structure.

Table 40: Point-Mobility Comparison for Engine Lab Point 50

Impact Data		Finite Element 4x Mesh			
Peak Freq., Hz	FRF Magnitude (mm/s)/N	Peak Freq., Hz	% Diff	FRF Magnitude (mm/s)/N	Magnitude Ratio
16.4	1.8E+00	19.0	16%	1.5E+00	1.2
21.6	4.8E-01	24.8	15%	5.7E-01	1.2
38.4	8.3E-01	39.6	3%	8.0E-01	1.0

7.4.4 Influence of Damping

It is noted that the difference in loss factor between the model and measurement will change the error in the ratio of response peaks. At Point 30, the modeled response peaks are generally seen to be lower in magnitude than the measured response peaks, and therefore a lower level of damping would create a greater level of correlation. However, in the case of the second peak where the error in magnitude is very large the damping can only be part of the issue.

Furthermore, at Point 50 the magnitude ratios are seen to be better, and a lower level of damping would actually increase the error in some cases.

Ultimately, it is difficult to make strong conclusions from this structure due to the unknowns of the vessel construction in the area. There may be some net benefit from applying a lower loss factor to the model if the actual structure were known and could be modeled. Unfortunately the reason for the lower loss factor in this area is not known, and would be difficult to justify assigning to an area of a separate vessel where measurements of loss factor were not performed.

7.4.5 Influence of Extra Items

It is interesting to show the influence of some of the items included in the model in order to achieve better model results. As discussed above, the model results presented here reflect the inclusion of a door frame (approximation) as well as the horizontal box beams attached to the stiffeners near the bottom of the bulkhead. The predicted mobility of the structure without these items is shown here to indicate the sensitivity of the model to their inclusion.

Figure 121 presents a comparison of the measured and modeled point mobility at Point 30 with and without the horizontal box beams. It is seen that at this point the beams have the primary influence of shifting the frequency of the response peaks upwards. Similar effects are seen for Point 50. In the case of the first mode the peak actually moves farther away from the impact data, though the second two peaks are a much better match to the measured data when the beams are included. Though not shown here, the modeled deflection shapes also provide a better match to the measurements when the beams are included, which was one of the primary reasons for including them in the data presented here.

Figure 122 presents a similar comparison for a model with and without a door frame. It is seen that the door frame does not have a significant influence for the first three peaks, and changes the magnitude of the response for the fourth peak (though by less than a factor of 2). The door frame was included in the results presented above as it formally presents a closer match to the measured data, though at this point it cannot be said definitively whether or not it is needed to achieve reasonable accuracy because the magnitude error at the fourth peak may in fact be caused by other issues of unknown structural details. The influence of the door frame is reduced further for the Point 50 mobility.

Figure 121: Modeled Point 30 Mobility, Effect of Horizontal Box Beams

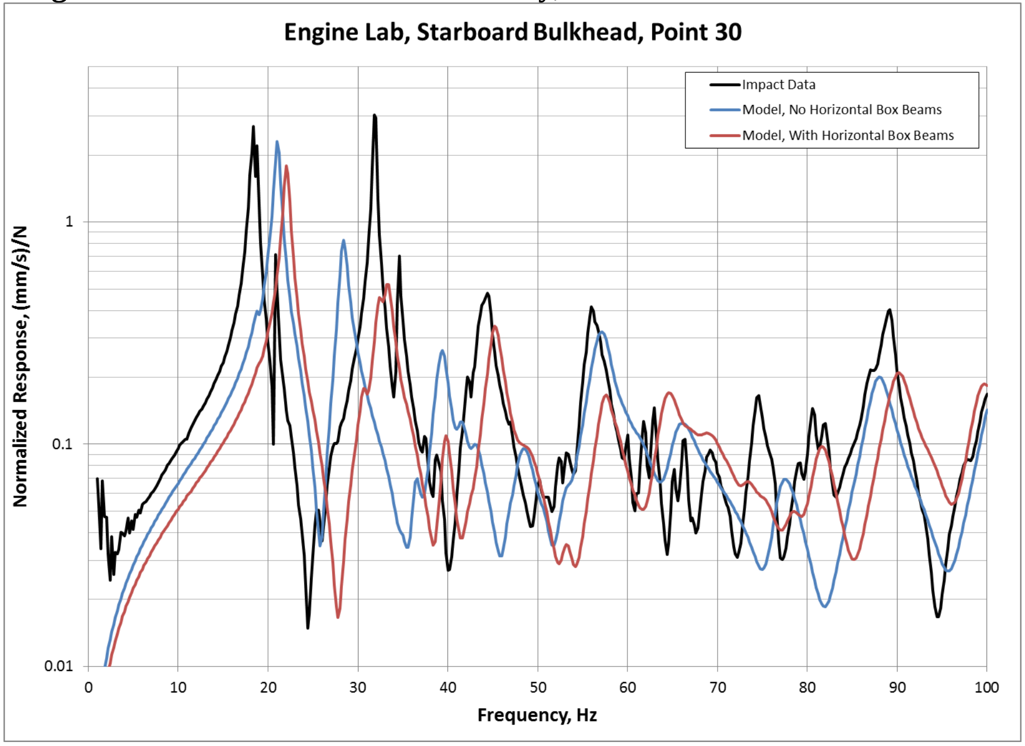

Figure 122: Modeled Point 30 Mobility, Effect of Door Frame

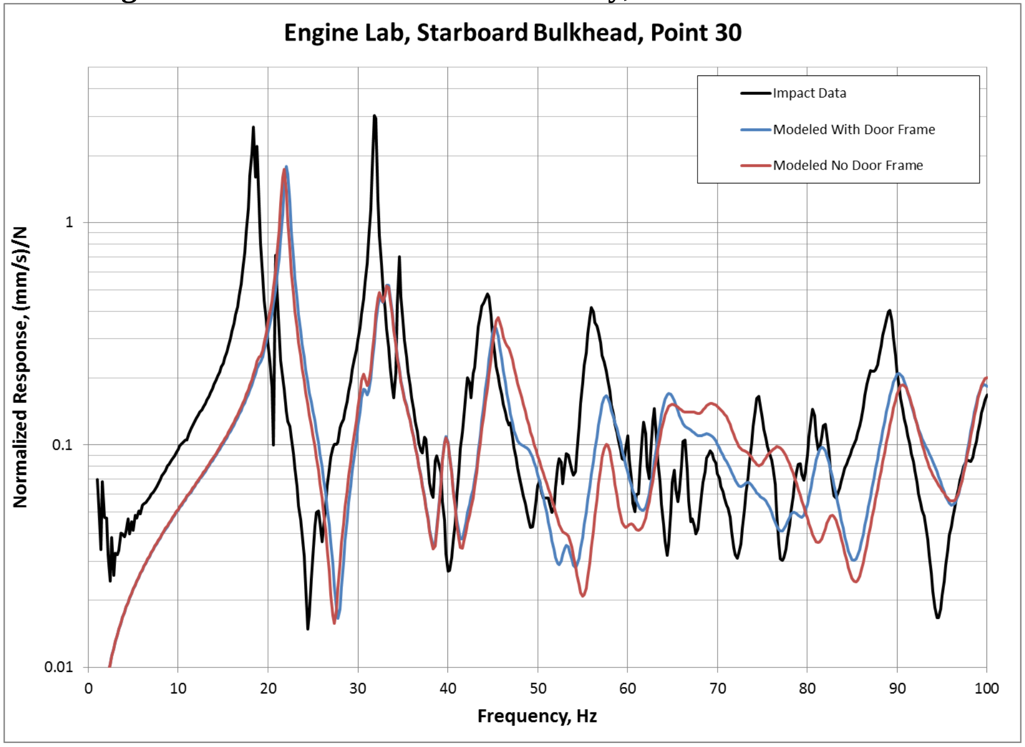

Based on these results, combined with the work that was done for Phase I of this project, it is believed that this bulkhead is subject to greater changes in vibration response as a result of the addition of the horizontal box beams as compared to what would occur for a stiffer bulkhead or deck. This underlines the importance of including such structures when modeling weaker structures, which may be more common in accommodation and living spaces than in machinery rooms. As was found for the Transom, such additions would not be negligible for other structures, but their influence is less pronounced.

Interestingly, the door frame did not appear to have a significant influence over the response except at higher order modes at locations close to the door. This is also in-line with the results discussed in Part I of this report, but for this structure indicates the relative non-importance of the door frame.

7.4.6 Summary of Engine Lab Analysis

Unfortunately the model used for the Engine Lab is flawed due to a lack of structural information for the structures surrounding the test locations. However, some information can be gained from this analysis:

- Most importantly, this analysis underscores the need for proper structural information. Incorrect stiffener and plating dimensions are guaranteed to lead to inaccurate results. This applies not only to the structure being analyzed but also to structures that are adjacent and beyond.
- Even with the issues of estimated structure, the overall characteristics of the response were captured at least for the first four (major) modes. Since this bulkhead was relatively weak, the fourth mode occurred at a frequency between 40-60 Hz, depending on the measurement location. It may be possible to infer from these results that the model accuracy is reduced at higher frequencies.
- As was found for the Steering Gear Room, the truncated model produced results that were effectively the same as for the baseline model. The truncated model only included structures one major bulkhead forward and aft of the Engine Lab.
- It is likely that ‘auxiliary’ stiffeners such as the box beams running along the bottom of the bulkhead should be included in the model. This is particularly true for weaker structures, which are subject to larger changes in response as a result of such structural modifications. Inclusion of the door frame, in this instance, provided only a modest benefit to the measured vs. predicted response and only influenced higher order modes of the structure.

7.5 Battery Room (04 Deck Bulkhead)

7.5.1 Model

One of the finite element models used for this analysis is shown in Figure 95. As discussed previously, this model includes structures from the 03 Deck to the 05 Deck, which incorporates structures at least one major deck (and bulkhead) away from the test bulkhead. Masts, railings, and other similar items were not included in the model. A pinned boundary condition was used along the lower edges of the model.

All frames and deep girders were modeled using plate elements for the web and beam elements for the flanges. Small stiffeners were modeled using beam elements. Note that the test bulkhead itself only includes small stiffeners.

The mass of insulation and sheathing located on the interior faces of the test bulkhead, as well as other bulkheads and overheads in the model, was included in the model as a non-structural mass. This mass was included using the "non-structural mass" property of the plating elements, effectively increasing the density of the plating. The available outfitting drawings indicate the insulation weight is 0.5 lb/ft^2, bulkhead sheathing is 2.2 lb/ft^2 and overhead sheathing is 1.4 lb/ft^2. For the test structure this represents an increase in mass of approximately 25%.

Note that some areas of the model include structures that are known to exist during testing but are not included in the available structural drawings. This primarily includes structures on the starboard side between the 03 and 04 Deck, from frame 70 to 80. This area is aft of the test structure on the opposite side of the vessel. These structures appear to have been added since the vessel was originally built. The modeled structures were estimated based on the construction in the surrounding area.

7.5.2 Notes on Measured Mobility and Damping

The measurements of point mobility on this structure indicate the presence of modes at frequencies above 35 Hz – further analysis shows these to be local modes of the structure. Plots of the measured point mobility spectra are shown in Figure 123. It can be seen that the coherence is good down to frequencies below 10 Hz. The large difference in the overall mobility level between the two locations is due to the fact that Point 3 is between stiffeners (larger response) and Point 12 is on a stiffener (lower response). (Note that the sharp rise in mobility at frequencies below 5 Hz is due to poor resolution of force data, discussed in Section 7.3.2.)

Figure 123: Measured Point Mobility, Battery Room Bulkhead

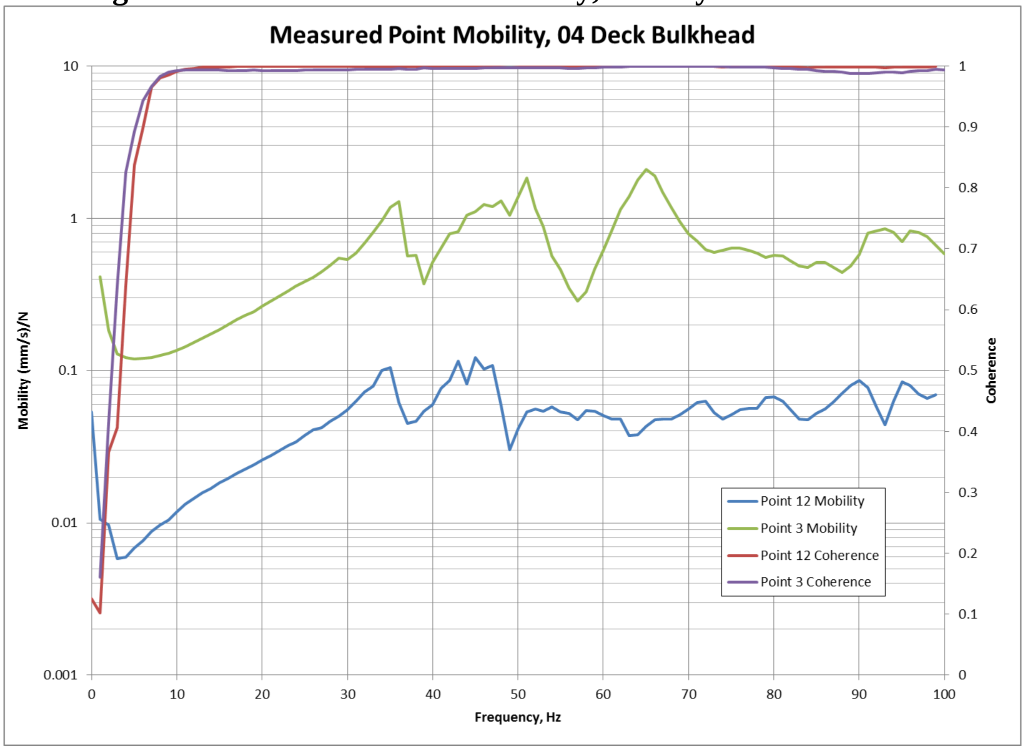

The transfer mobility data between points 3 and 12 unfortunately do not show good reciprocity, and therefore some error is seen to exist in the measurements. Good reciprocity was seen between point 12 and the deck measurement location; transfer mobility investigations focus on this pair of impact/receiver points. The measured transfer mobility and coherence for this pair are shown in Figure 124. It is seen that the coherence is good down to approximately 15 Hz. (In this case the rise in mobility due to poor force data occurs at 11 Hz and below.)

Figure 124: Measured Transfer Mobility, Battery Room Bulkhead, Point 12 to Deck

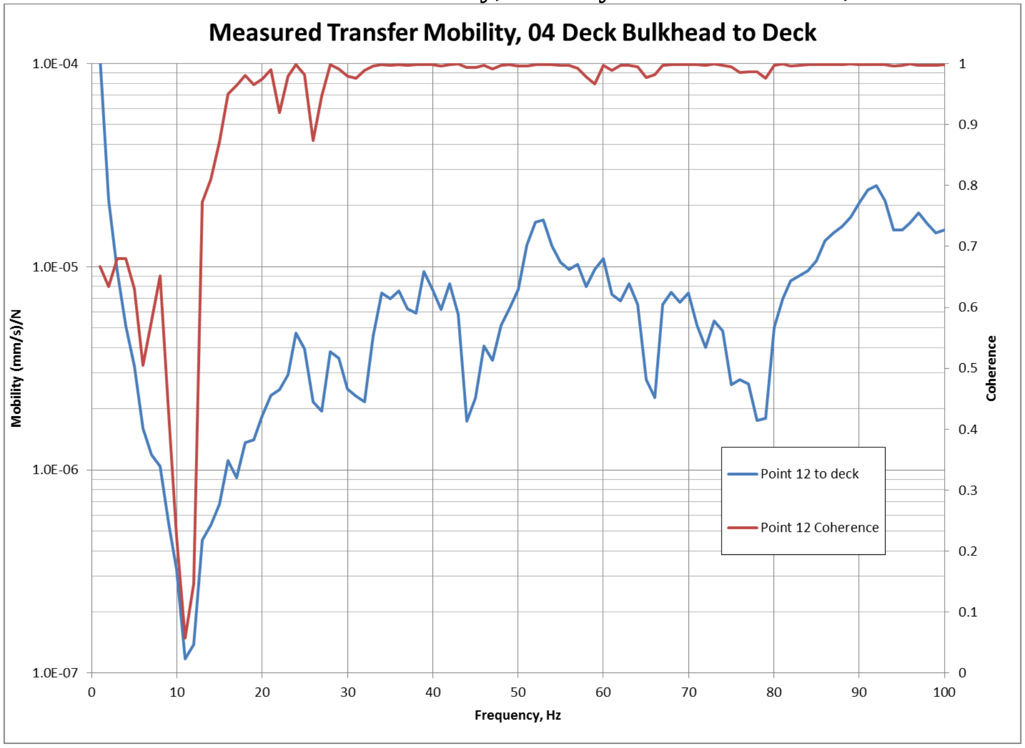

As discussed in Section 7.2, the damping loss factor for this structure is generally greater than the value of 0.03 used in the rest of this report. It is believed that this is due to the presence of insulation and sheathing on the interior side of the bulkhead. For this reason, a damping loss factor value of 0.06 was used for most of the models presented here. A comparison of responses with different damping loss factor values is also provided below.

7.5.3 Mobility Comparisons

A comparison of the measured and predicted point mobility at Point 12 is provided in Figure 125. In this case, results from both a 4x and an 8x mesh density are shown; otherwise, the models are identical. (The reasons for using an 8x mesh will be explained below.) It is seen that the overall character of the response is captured in both models at least up to a frequency of 60 Hz.

Figure 125: Battery Room Point 12 Mobility, Measured vs. Modeled

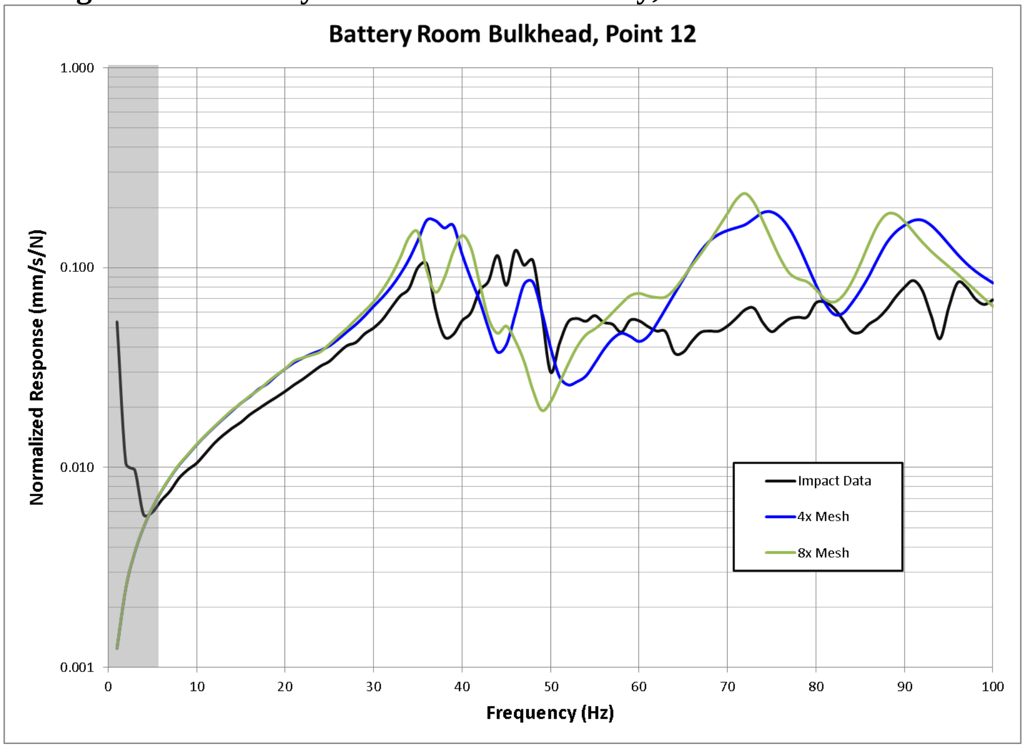

The prediction of the first main peak at 35 Hz matches the measured data nearly exactly in frequency for both models, and is higher in level by an amplitude ratio of 1.4 – 1.7 depending on the model. At frequencies below this first peak the measurement and model are in very good agreement.

The frequency range between 44 and 48 Hz shows multiple peaks in the measured response; approximations of these peaks are seen in the prediction, though the details differ depending on the mesh density. In both cases there is a peak in the predicted response which is close to these multiple peaks with very similar amplitude. Arguably, the 4x mesh provides a better match to the measurement, though this may be due to other inaccuracies in the model. The frequency and magnitude of the dip in response at 50 Hz is close in both models, and the levels between 50-60 Hz are also similar.

At frequencies above 60 Hz the response begins to diverge significantly. This is similar to the high frequency / high order mode behavior seen for other structures.

A similar comparison of the point mobility at Point 3 is provided in Figure 126. In this case the differences between the 4x mesh and the 8x mesh are clearer. Both models predict the frequency of the first peak near 37 Hz well (an error of 5% or less), though the 8x model obtains nearly exact correlation of frequency for the higher order modes at 52 and 67 Hz. Although there are benefits to the 8x mesh in this case, the 4x model does obtain a maximum error of about 10% even for these modes. Differences in the modeled and measured mobilities at frequencies above 75 Hz are clear through inspection of the data.

Figure 126: Battery Room Point 3 Mobility, Measured vs. Modeled

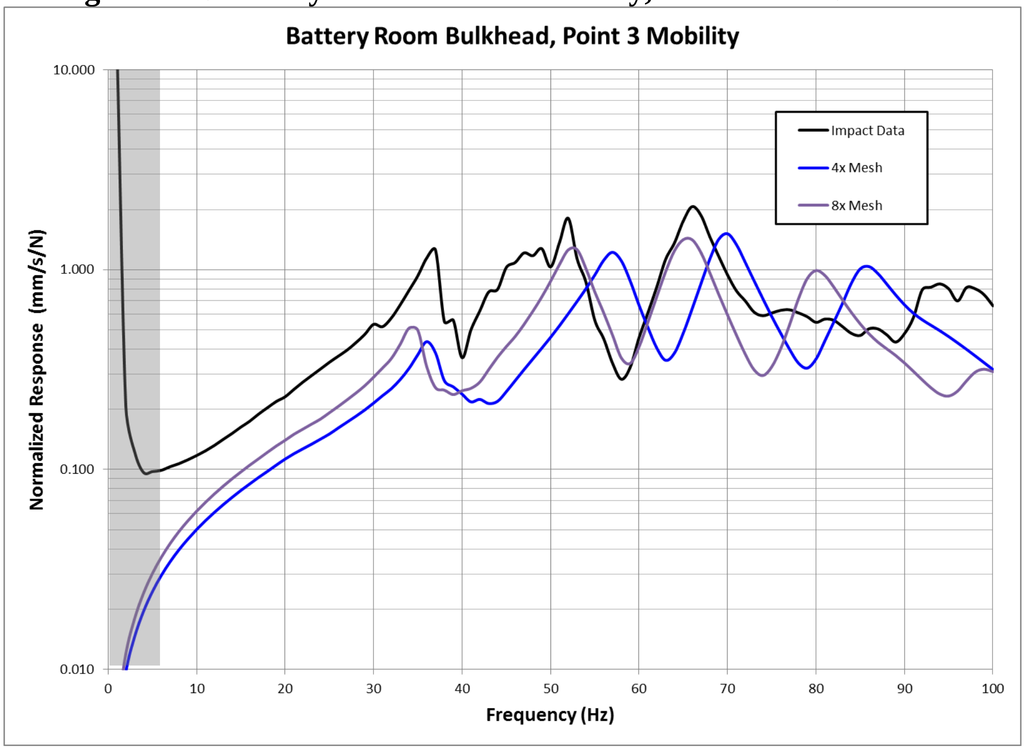

The magnitude error for the first peak at 37 Hz is roughly 2.6 for the 8x mesh. The response magnitude error for the other peaks is significantly less, with both models having errors of less than a factor of 1.5.

Unfortunately, the response between roughly 45-49 Hz is only approximated by the 8x mesh. Formally there is a maximum magnitude error of about 2.5 in this frequency range. It is not clear what causes the multiple peaks in this frequency range (seen at both Points 12 and 3) though it may be due to the specific method by which the sheathing is mounted (see Appendix A).

It is interesting to note that the deflection shape corresponding to the second peak (51 Hz) results in 6 elements per wavelength for the 4x mesh density. This is an indication as to why there is a strong shift in frequency for this and higher frequency peaks – the spatial resolution of the 4x mesh density model is limited and therefore appears to be stiffer than the actual test bulkhead. Moving to an 8x mesh density resolves this issue.

A comparison of the modeled and measured transfer mobility between points 12 and the deck measurement location is provided in Figure 127. In this case the prediction compares very well with the measurement. (Note that as discussed in the previous section, frequencies where good coherence was achieved in the impact measurements are above 15 Hz – this is the frequency range of interest for this measurement).

Figure 127: Battery Room Transfer Mobility, Point 12 to Deck, Measured vs. Modeled

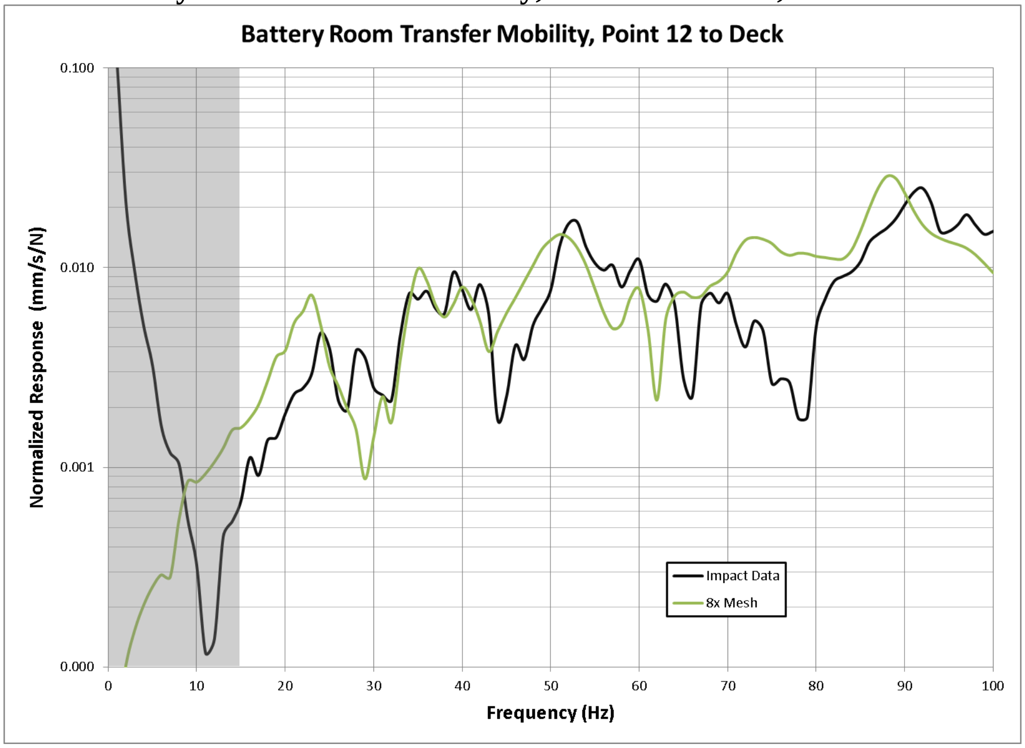

The prediction error in the frequency of the first peak near 25 Hz is 8%, and the magnitude error is a ratio of 1.5. The second measured peak at 28 Hz does not show up strongly in the prediction; it appears that the predicted peak at 31 Hz is meant to correlate with this second peak, yielding a frequency error of 11% and a magnitude error of 1.9. The rest of the spectrum from 31 to roughly 70 Hz provides a very close match to the measurement.

7.5.4 Influence of Sheathing and Insulation Mass

The influence of adding the mass of the sheathing and insulation in the manner described above (smearing the mass across the plating elements) can be seen by comparing the point mobilities at measurement points 12 and 3 with and without this mass. Comparisons are provided in Figure 128 and Figure 129.

Figure 128: Battery Room, Comparison of Point 12 Mobility, Influence of Sheathing and Insulation

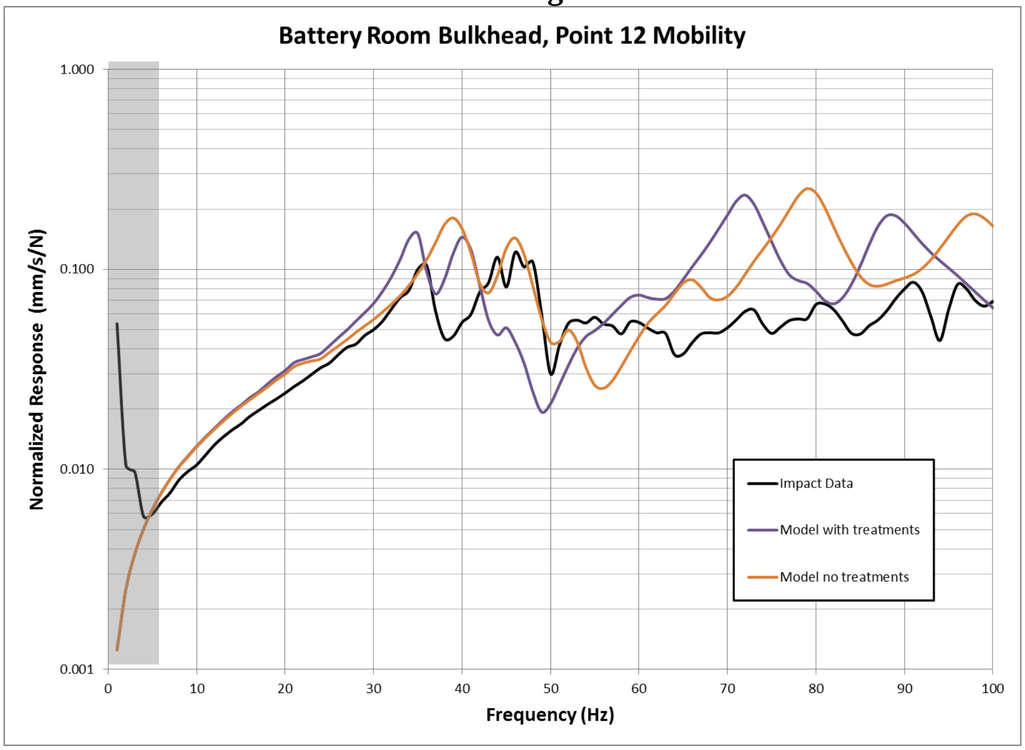

Figure 129: Battery Room, Comparison of Point 3 Mobility, Influence of Sheathing and Insulation

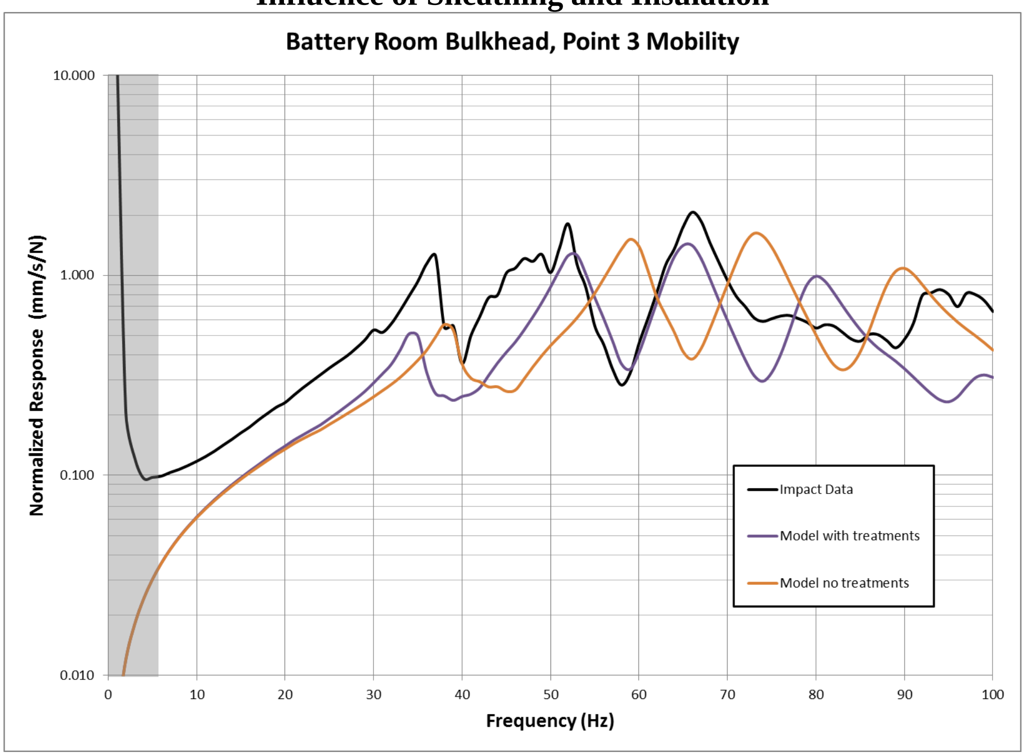

Looking at the Point 12 mobility, it would appear as though the “no treatment” result provides better correlation in the 43-50 Hz frequency range than the “with treatment” result, though this is at the expense of poorer correlation at the first peak at 35 Hz and at frequencies above 51 Hz. It is difficult to say why there is an apparent improvement in the 43-50 Hz range when the mass is removed, though it may provide an indication of the specific mechanisms at play for this particular location (being on a stiffener) and this particular sheathing arrangement; i.e. the coupling of the insulation and sheathing may not be strong for the modes in this frequency range but it is at others. However, this conclusion is weak based on the available data, and would suggest a more complex modeling approach is required than may be desirable.

Inspection of the Point 3 mobility shows a more consistent picture at all frequencies, where the frequencies of peak response uniformly shift downward. In this case the smearing of insulation and sheathing mass across the plate elements appears to be the correct approach.

The correlation of transfer mobility between Point 12 and the deck is similar though certainly poorer when the mass is removed (results not shown here for brevity). This result also points to the need for including this mass.

In summary, it appears that the mass of sheathing and insulation plays an important role in the response of the structure, particularly when that mass represents a significant increase in the total mass of the structure (25% in this case). The methodology used here of ‘smearing’ the mass across the plating elements seems to be a reasonable approximation, at least for frequencies below 70 Hz.

However, it must be noted that these results may apply to the specific sheathing used in this vessel – i.e. the sheathing is mechanically connected to the test structure. It is more common in recent builds to use a ‘composite’ joiner panel made up of compressed mineral wool and sheet metal. These composite panels are typically supported along their edges with a minimal amount of mechanical connection to the structure it is covering. In this case there may be a frequency where the joiner becomes decoupled. Testing of this joiner arrangement was not possible here.

7.5.5 Influence of Additional Structures

During the modeling process the influence of some ‘ancillary’ structures near the test bulkhead was investigated. These structures include the antenna support shown in Figure 81, the batteries inside of the Battery Room, and the handrail (see Section 6.1.3). Details of the antenna support are part of the available structural drawings. The size of the battery foundation was estimated based on available pictures and other information. Masses of the batteries were also included; the make and model of the battery was noted while on-site and mass information was collected from the vendor. The mass of the antenna was not included (this is typically small for an antenna of this type). The handrail on the exterior of the model was included using beam elements.

A direct comparison of a model with these features to the results presented above is not available as these items were investigated earlier in the modeling process. However, it can be said that at Point 12 their influence was small. For the response at Point 3, the battery foundations were seen to have the biggest effect, and tended to decrease the overall level of response. The effects of the battery foundation were disregarded as the actual structural details are not known.

The relative minimal importance of the antenna support and handrail indicate that, in general, modeling of such structures is not needed, but their inclusion should not degrade the performance of a particular model.

7.5.6 Influence of Damping Loss Factor

As discussed previously, a damping loss factor of 0.06 was used for the model results presented above. For reference, Figure 130 presents a comparison of the point mobility at Point 12 for damping loss factors of 0.06 and 0.03. (Note that these models are slightly different from those presented previously, though the overall effects of damping are clearly seen here). As expected (and seen in Part I of this report) the response with lower damping has higher peaks and lower dips in the response. It is seen that the magnitude of the first peak, in particular, increases by a factor of 1.5. This error, while higher than may be desired, is arguably still within reason, and a los factor of 0.03 could still be used to obtain reasonable results.

It may be possible to infer from these results, as well as by comparing the 'measured' damping for this structure to other structures (see Section 7.2), that the presence of insulation and sheathing acts to increase the damping on the structure. However, this is only a weak conclusion at this point as only one bulkhead with sheathing was tested.

Figure 130: Battery Room, Comparison of Point 12 Mobility, Influence of Damping

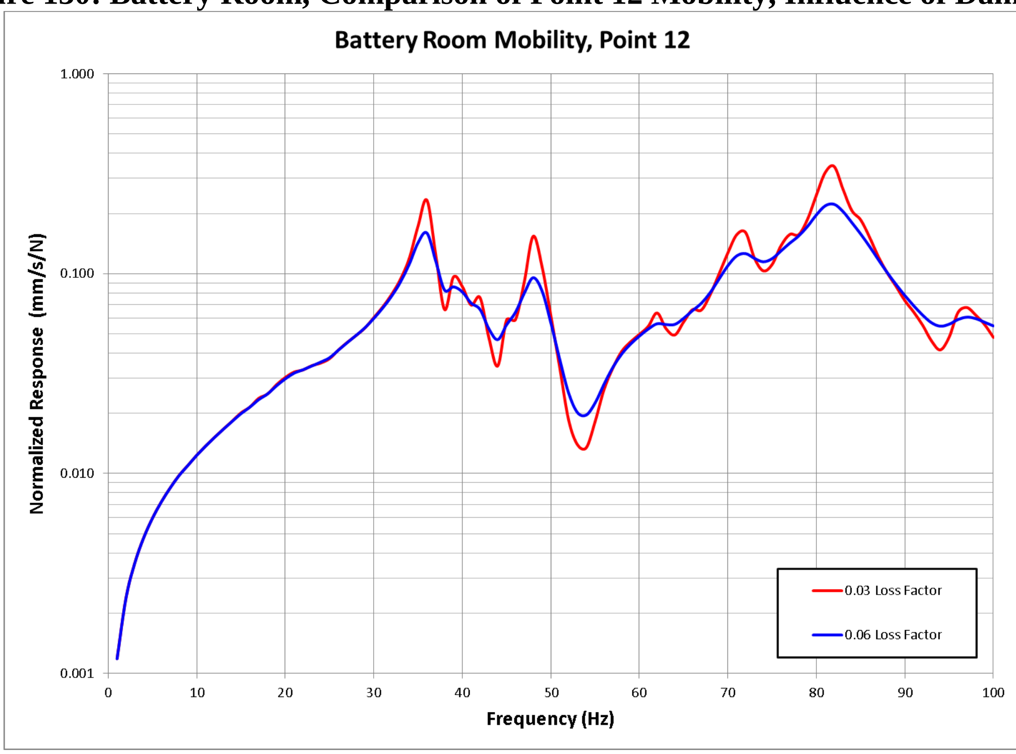

7.5.7 Summary of Battery Room Analysis

The analysis results shown here indicate again that a finite element model can be used to generate accurate results as compared to measured point and transfer mobilities on and adjacent to the test structure. The key points of this analysis are as follows:

- In this particular case, good results were obtained at frequencies up to approximately 65 Hz using an 8x mesh density. This frequency corresponds to modes where the plating between stiffeners was seen to contain significant motion relative to the stiffeners. Full wavelengths were seen in the plating between stiffeners at these frequencies.
- The 4x mesh density models showed reasonable correlation up to frequencies of approximately 65 Hz, with errors in predicted response peaks on plating of 10% or less.
- Errors in magnitude response were generally less than a factor of 2, though in some specific cases greater errors were seen. These results apply primarily to the 8x mesh density.
- The need for a finer mesh can be determined in part by inspecting the deflection shapes of the model. For locations where there are only 6 elements per wavelength or less, the model will likely benefit from refinement.
- Based on these results it is recommended that the mass of sheathing and insulation be added to the model as a non-structural or 'smeared' mass addition to the plating elements. It is possible though that this conclusion may be applicable only when sheathing and insulation are directly connected to the structure being covered. Newer joiner panel design and construction methodologies, where joiner panels are not directly connected to the structures they cover, may be more weakly coupled. Unfortunately such determinations cannot be made based on this data.
- Sheathing and insulation may have an effect of increased damping in the frequency range of interest.
- 'Auxiliary' structures such as handrails and the antenna support were not necessary to achieve these modeling results. The influence of the battery foundation and batteries themselves is less clear due to limited information about these structures.

7.6 Machinery Room Side Shell (Tanktop Level)

7.6.1 Model

As discussed in Section 6.1.4, this area was measured and modeled primarily to investigate the influence of water loading on vibration response. A truncated model was used for analysis (after checking for consistency with the baseline model, as is described in previous sections). The truncated model includes structures between Frame 104 to 154, which is one major bulkhead forward and aft of the Machinery Room. The model also extends from the baseline to the 01 Deck. An overview of the model used for the Machinery Room side shell is provided in Figure 131. Note that models of other items within the Machinery Room are based off of this same model.

Figure 131: Overview of Machinery Room Model

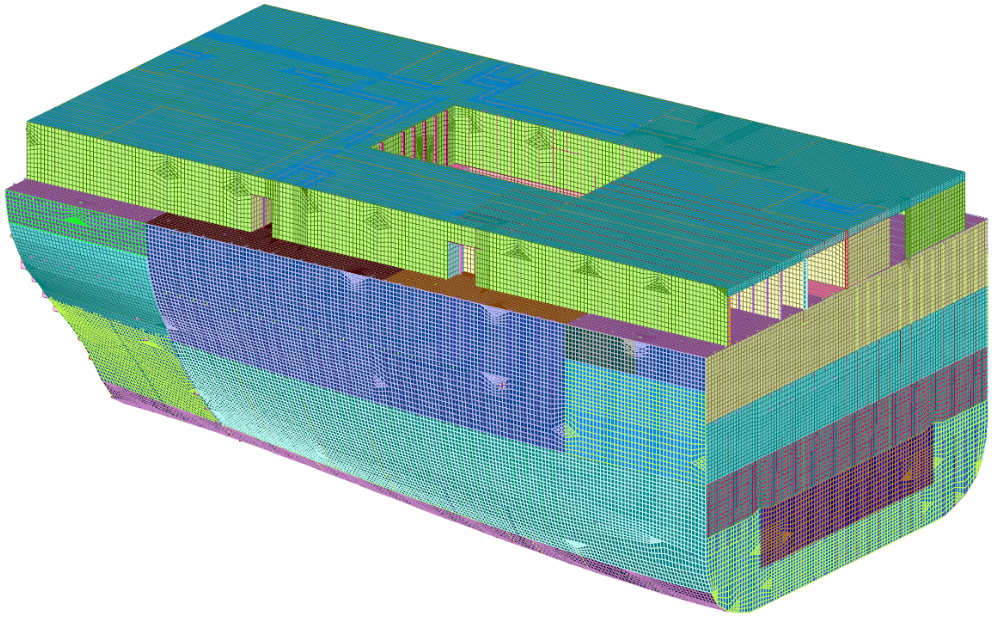

The model uses a 4x density mesh. All frames and deep girders were modeled using plate elements for the web and beam elements for the flanges. Small stiffeners were modeled using beam elements. No boundary constraints were applied to the model.

A cutaway view of the finite element model used for this analysis is shown in Figure 132. This model includes an approximation of the ladder which is forward of the bulge pump. The structural drawings do not show the details of the bilge pump foundation; the stringer has clearly been modified and extended inboard to support the bilge pump. An approximation for this structure was included in the model based on measurements taken while on-site. Note that the pipe support seen in Figure 82 has been ignored in this model.

The bilge pump itself was included in the model as a point mass connected to its foundation via rigid elements. The location of the center of gravity was estimated based on available dimensional information. Mass moments of inertia were ignored when implementing this mass.

Initially, no modeling approximations were made to account for the water loading influence on the wetted hull. Subsequent to initial modeling, a (frequency independent) smeared mass was added to the hull to approximate this effect. Additional details are provided in the following sections.

This model also includes approximations for the damping tiles that were installed under the gensets on the 23' Flat. Additional details are provided in Section 7.8.

Figure 132: Model Section of Machinery Room Side Shell

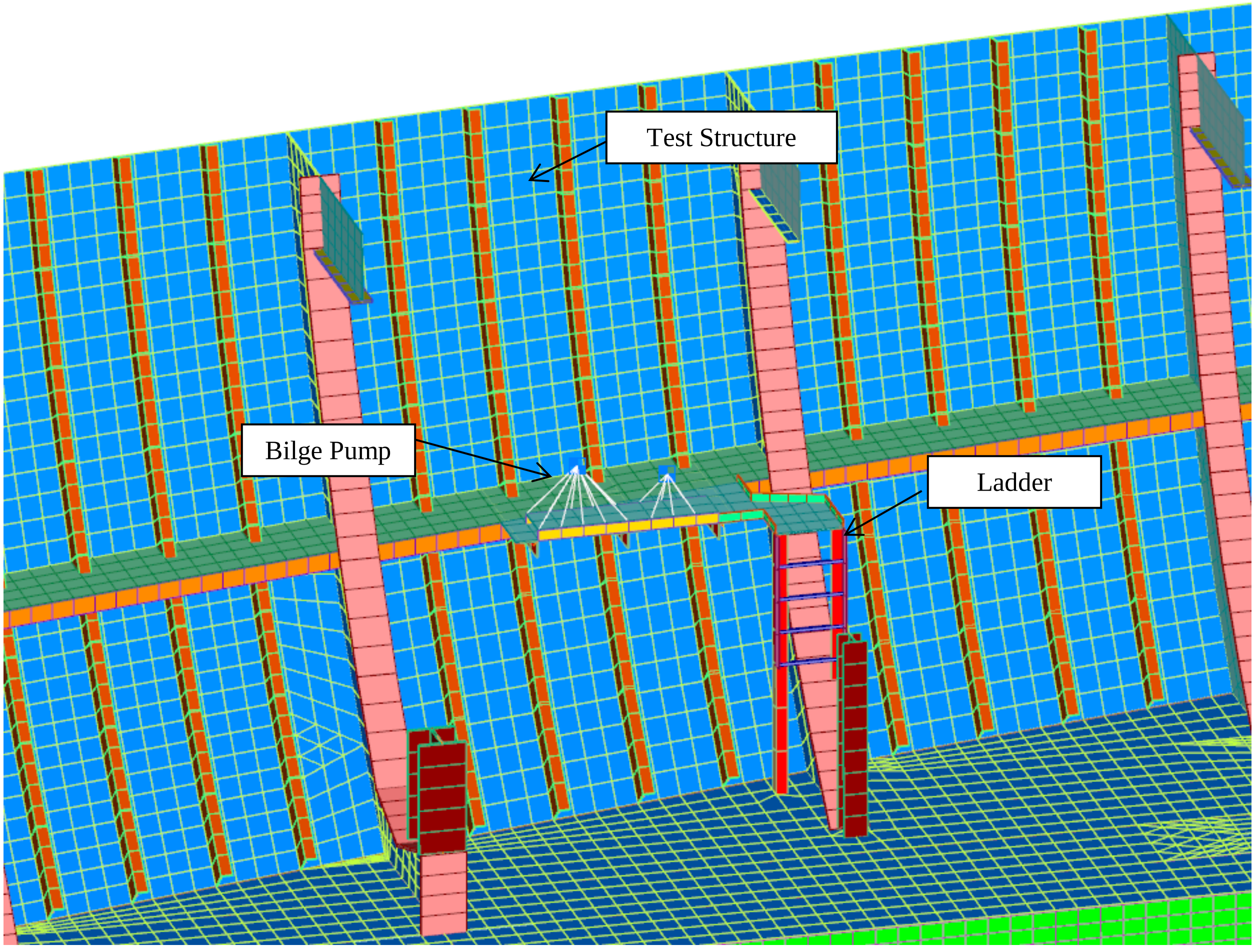

7.6.2 Notes on Measured Mobility

The measured point mobility for the two accelerometer locations inside of the test grid shown in Figure 83 (Accel #1, on Frame 132, and Accel #2, on the plate between Frames 131 and 132) is provided in Figure 133. It is seen that the coherence of these measurements is good above approximately 10 Hz. (The erroneous rise in mobility at frequencies below approximately 10 Hz discussed in Section 7.3.2 is seen in these measurements as well.)

Figure 134 presents the measured transfer mobility from impact Point 8 to Accel #3 which is located below the stringer. It is seen that the coherence is generally above 0.9 at frequencies above 17 Hz, with the exception of several sharp dips at discrete frequencies. These dips in coherence correspond to strong dips in the transfer mobility.

Figure 133: Measured Point Mobility, Lower Hull

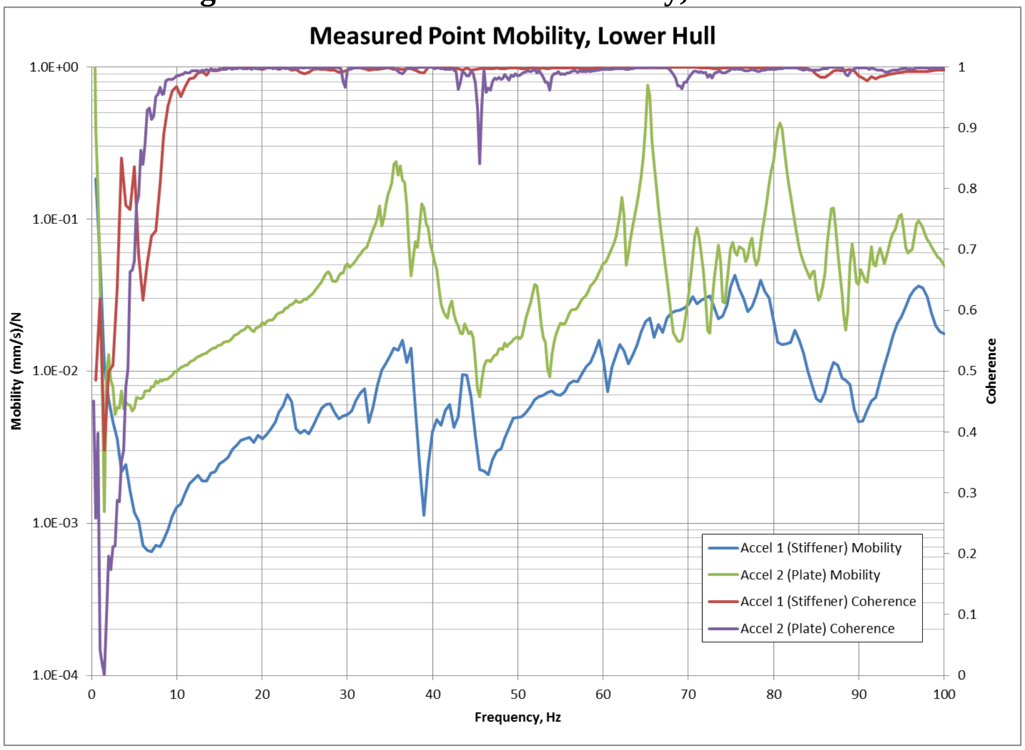

Figure 134: Measured Transfer Mobility, Point 8 to Accel #3 (Below Stringer)

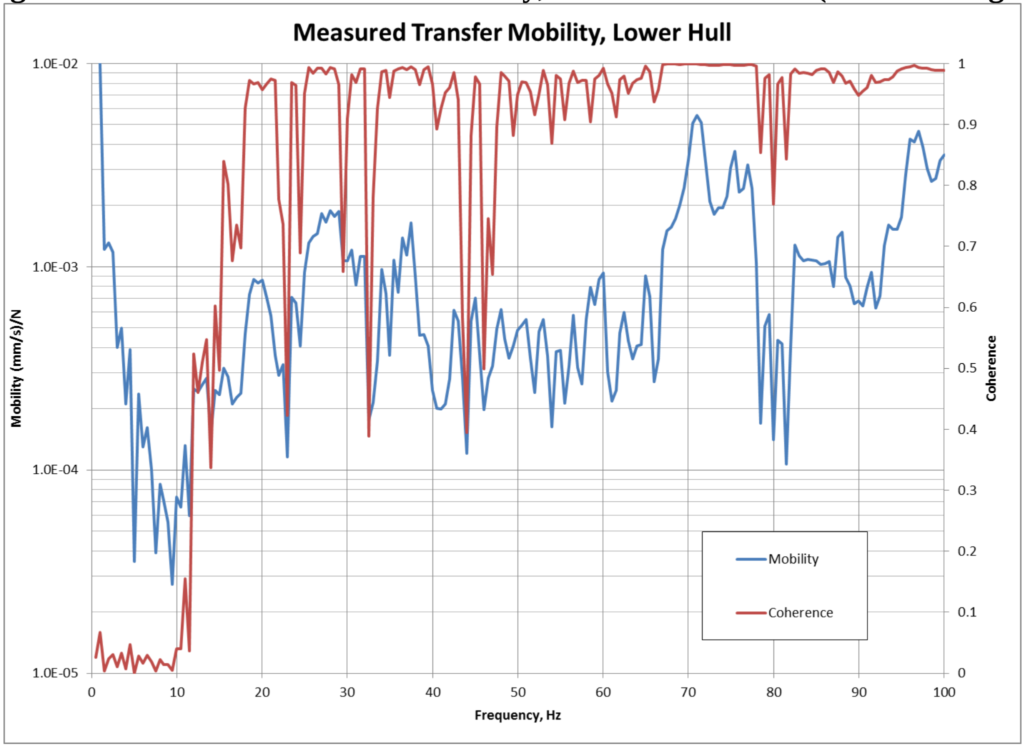

7.6.3 Mobility Comparisons

A comparison of the measured and modeled point mobility at the Accel #1 location (stiffener on Frame 132) is provided in Figure 135. Two model results are shown – one with no mass added and one with a smeared mass of 0.58 lb/in^2. (This mass is one of several that were investigated – additional comments are provided below.)

Figure 135: Lower Hull Accel #1 Point Mobility, Measured vs. Modeled

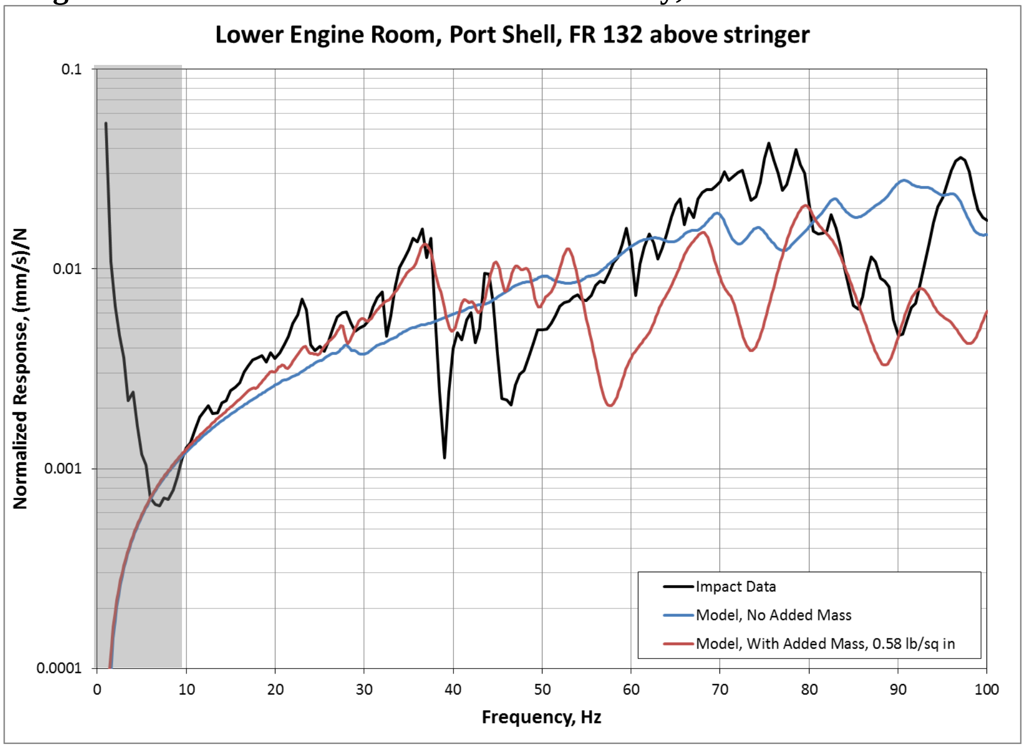

The modeled response with no added mass is a relatively flat, upward sloping line. Comparing the measured data to the model with no added mass it is seen that there are several peaks and dips that are not captured in the modeled response. However, it is interesting that the modeled response essentially cuts through the middle of the measured peaks and dips.

Mass was added to the hull plating elements in an attempt to account for water loading effects. As discussed in Reference [1], the presence of the ocean on the hull will create a mass loading effect that is frequency dependent, and therefore the approach used here is highly simplified. A 0.58 lb/in^2 mass was used to create the "with mass" response seen in Figure 135 in an attempt to optimally match the measured peak at 36 Hz to the model. (Operational deflection shapes, not shown here, were used to assist in this analysis.)

The resulting point mobility using this mass provides good agreement with the measurement up to a frequency of roughly 50 Hz, though errors are seen at the frequencies corresponding to strong dips in response in the measured data (39 and 46 Hz). Above this frequency it is interesting to note that the 'no mass' curve appears to provide better correlation to the measurement than the 'with mass' curve, at least up to 80 Hz. On the surface, this appears to be in line with the rough understanding that the effective added mass on the hull is reduced with increasing frequency and higher order deflection shapes.

Other masses were also investigated. Some examples are shown in Figure 136, including 1.9 lb/in^2 and 0.97 lb/in^2. Note that both masses are larger than the mass shown in Figure 135. The response from the 1.9 lb/in^2 mass model shows good correlation to the smaller peak seen at 23 Hz (lower in frequency to the 'main' peak noted above), and also shows a rough correlation to the dip in response at 39 Hz, but does not capture the first main peak near 36 Hz. The first peak in the 0.97 lb/in^2 response is too low to capture the response at the main 36 Hz peak, though the character between 40-50 Hz looks very close to the measurement.

Figure 136: Lower Hull Accel #1 Point Mobility, Comparison of Hull Mass Effects

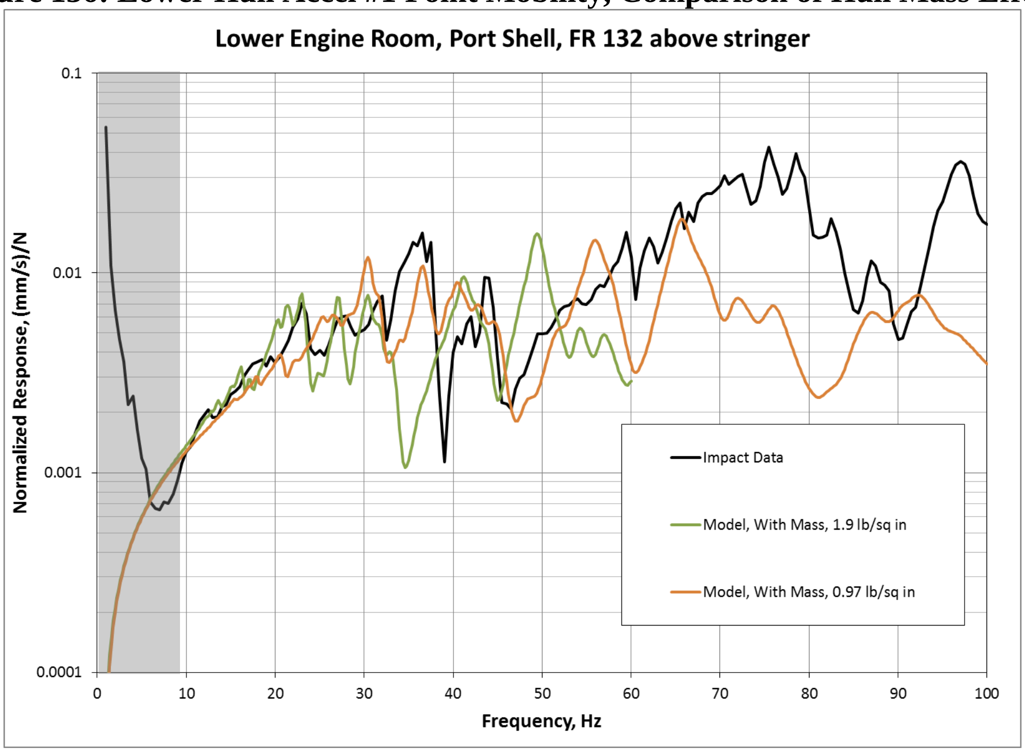

These results provide some further indication that the mass loading effect is frequency dependent, where the effective mass is a function of frequency and/or deflection shape of the hull. However, all of these models, including the 'no mass' model, provide reasonable correlation at frequencies below 30 Hz, and the 0.58 lb/in^2 could be conservatively used up to 50 Hz.

A mass of 0.58 lb/in^2 corresponds to applying a layer of water to the hull with an equivalent thickness of 1.3 feet. At 36 Hz, this also corresponds to a thickness of 1/10th of a wavelength in water. This is significantly lower than the mass that would be applied to calculate the whole body modes of the same vessel, based on the methodology presented in Reference [1].

A more rigorous analysis of appropriate water loading techniques using this data is not possible within the current scope of this project. However, given the complex nature of water loading, it is suggested that an alternative method be implemented if accuracy at higher frequencies/higher order modes is required. This could include a coupled boundary element and finite element approach or discrete finite element modeling of the water domain.

Unfortunately, the response at Accel #2 (on the plate adjacent to the stiffener) does not share the same degree of correlation with the responses shown on the stiffener. The comparison of modeled and measured point mobilities is provided in Figure 137.

Figure 137: Lower Hull Accel #2 Point Mobility, Measured vs. Modeled

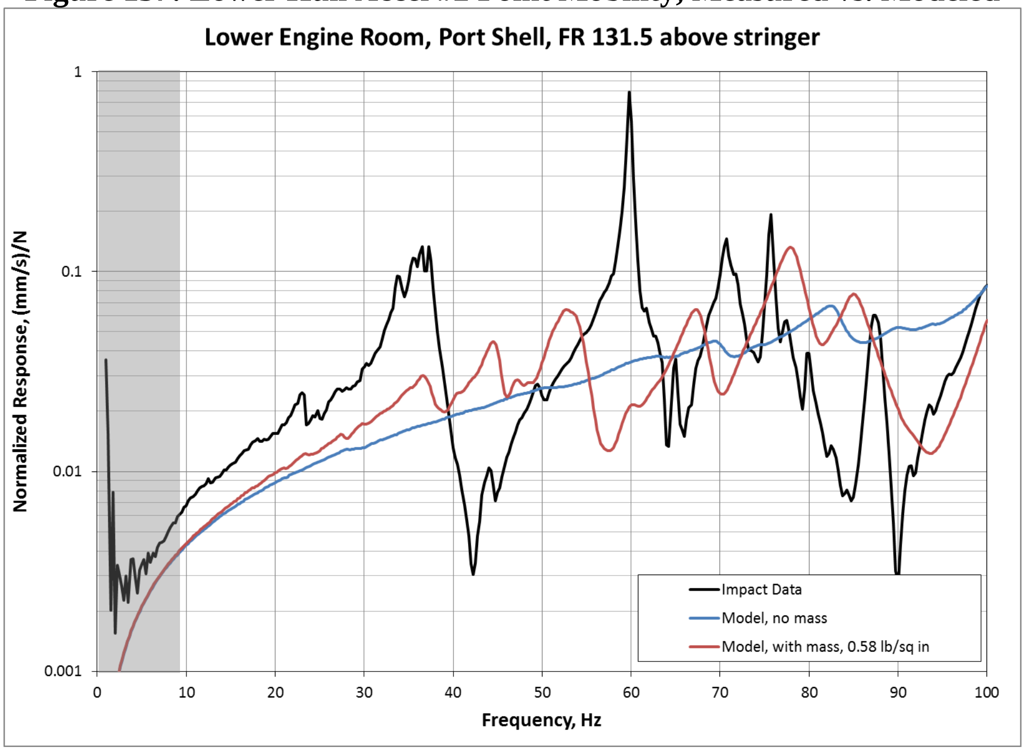

Again, the response with no mass appears to cut through the peaks and dips of the measured response. When the 0.58 lb/in^2 mass is added to the hull, the frequency of the first modeled peak does correspond to the measured data; however, the magnitude of the response is off by a factor of roughly 4. At higher frequencies the modeled response also does not match the measurement, particularly the strong spike at 60 Hz (this spike was double checked for data quality and appears to be real).

At frequencies below 30 Hz both the added mass and no mass models are within a magnitude ratio of roughly 2 with the measured data.

It is noted that the disparity between the measured and modeled response at Accel #2 may be subject not only to uncertainties in the mass loading from the hull but also to effects of the pipe support that is attached to the test bulkhead. The details of this attachment have been ignored, and no mass or stiffness of the supported piping was included.

However, comparisons of the point mobility measurements described above have been compared to additional point mobility measurements, performed at a similar location 10 frames forward of the primary test location in the Machinery Room. This forward location does not contain a similar pipe support structure. The point mobility data on stiffeners and plating is remarkably similar in both locations. This indicates that water loading likely is primarily responsible for the peaks and dips seen in the response. On a positive note, it also indicates that the pipe support and piping discussed above has a minimal effect at the measurement locations, and their omission from the model does not lead to large errors.

A comparison of the modeled and measured transfer mobility from Point 8 to Accel #3 is presented in Figure 138. (Note here that the measured data is most accurate at frequencies above 17 Hz – see the previous section.) Again, a comparison of models without mass and with a 0.58 lb/in^2 added mass are shown. In this example the model with added mass performs well up to a frequency just above 30 Hz. The measured peak at 20 Hz is approximated in the prediction with a frequency error of roughly 8% and a magnitude ratio of 1.2. The levels near 25-30 Hz are also well approximated by the "with mass" model.

Figure 138: Lower Hull Transfer Mobility from Point 8 to Accel #3, Measured vs. Modeled

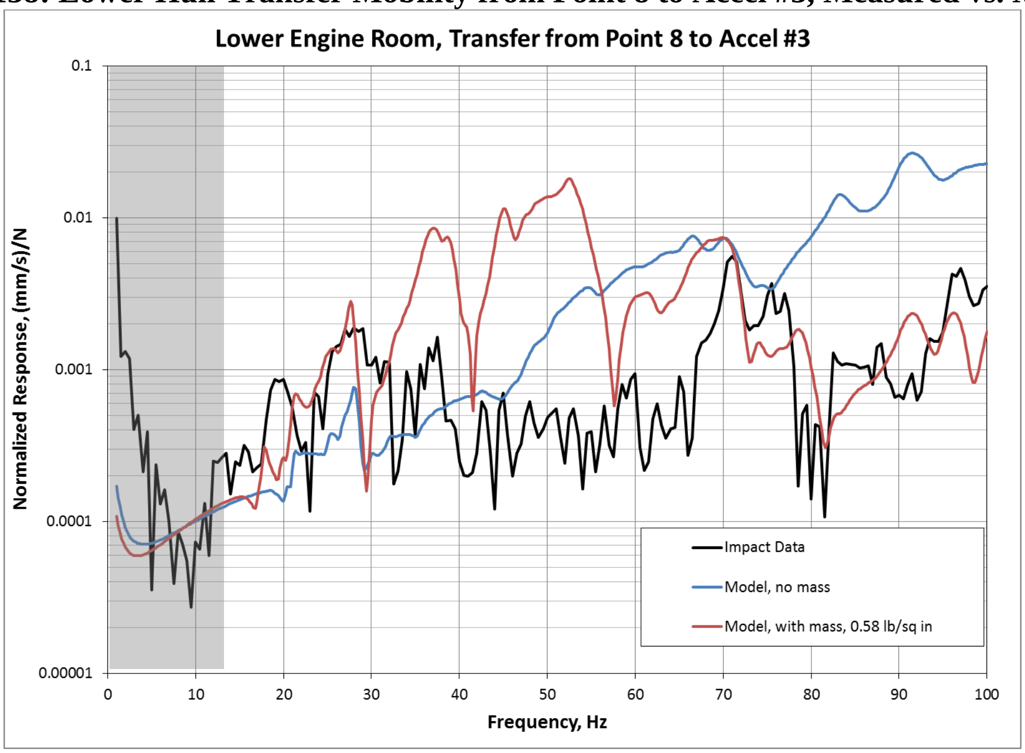

The "with mass" model over-predicts the response between 35 and 70 Hz, very significantly in most cases. Between 40-50 Hz the no mass model seems to perform better, though again at higher frequencies this model also over-predicts the response.

These results indicate that some added mass is likely needed on the side shell in order to obtain accurate results. However, the accuracy of the specific methodology implemented here may be limited to lower frequencies.

7.6.4 Summary of Machinery Room Side Shell Analysis

The results presented here indicate that water loading plays an important role in the response of the side shell, at least locally where there is wetted plating. As expected based on the discussion of water loading effects presented in Reference [1], the effects of water loading appear to be frequency and/or deflection shape dependent, with decreasing effect as frequencies are increased and the deflection shape becomes more complex.

In this analysis, a 'smeared mass' approach (applied to wetted plating) was used to simulate the effective mass of water loading. The same mass was applied to all wetted elements. This approach was seen to produce good correlation to measured data for the point mobility on a stiffener up to a frequency of roughly 45 Hz, though transfer mobility data shows reasonable correlation only up to 32 Hz.

Note that the added mass was 'tuned' so that the first primary predicted response peak matched the response peak seen in the measurement (operational deflection shapes were also used to correlate this data). For any new project such an approach would not be possible. It was seen that the additional mass that was needed to produce these results is significantly less than the mass that would be applied to the hull when performing a whole body mode analysis using the methodology outlined in Reference [1]. A more rigorous analysis is not possible within the scope of this project.

Ultimately, the calculation of appropriate water loading masses (or otherwise the effect of water loading) may be the primary limiting factor in performing finite element vibration analyses of vessels. Without the ability to apply a reasonable mass to the side shell the peaks and dips in side shell response will not be properly captured. This suggests the need for further study, at a minimum, and may require more sophisticated tools.

7.7 Machinery Room Near Start Air Compressors

7.7.1 Model

The same truncated model used for the Machinery Room side shell (Section 7.6) was used for this analysis. A cutaway view of the area near the start air compressors is shown in Figure 139. The model uses a 4x density mesh. All frames and deep girders were modeled using plate elements for the web and beam elements for the flanges. Small stiffeners were modeled using beam elements. No boundary constraints were applied to the model. No approximation was made for the piping located on the underside of the deck. No water loading was applied to the side shell[14]. Insulation on the side shell was also ignored during the modeling process.

[14] This modeling effort was performed prior to investigations on the lower hull and therefore results of added mass were not available. It important to recognize that the 23' flat is only a few feet below the waterline, and therefore most of the structures analyzed here are actually dry. Water loading effects, being related to radiation impedance, will diminish at points close to the waterline. Neglecting water loading in this case did not appear to have an adverse effect on the modeling results.

Figure 139: Model Section of Machinery Room Near Start Air Compressors
(Plan view of Deck and Side Shell – Full model not shown)

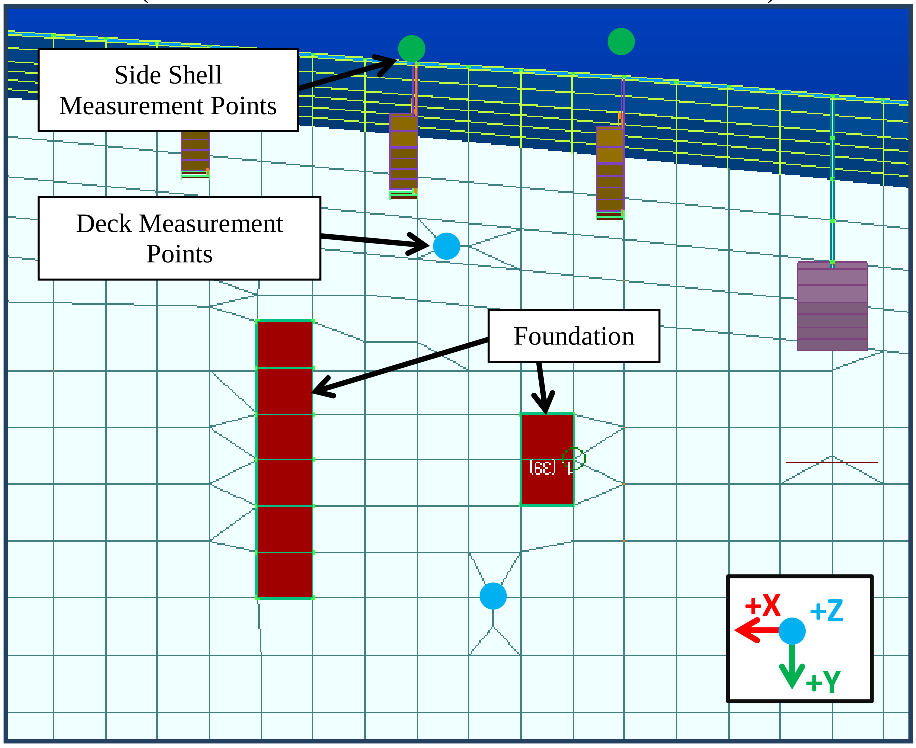

The model results presented here include an increase in the local damping on the deck to account for the damping tile that is applied to the underside of the 23' Flat. A separate material property with its own loss factor and non-structural mass was used to model the damped ship plating. It was assumed that the tile was MIL-PRF-23653C Type II Class 2 with a thickness of 0.62 inches. Reference [19] indicates that this tile has a weight of 4.5 pounds per square foot. Based on past experience with these damping tiles, it is believed that the damping loss factor that is created when the tiles are applied to steel in the thickness of 3/8 inches (the thickness of the deck) is on the order of 0.1. (The loss factor of damped plating is expected to be dependent on frequency, and will be less at low frequencies and more at high frequencies. However, a constant value was used here for simplicity.) A loss factor of 0.03 was used for the rest of the model.

The foundation of the start air compressor was modeled using plate elements. A cross section of the foundation is shown in Section 6.2.1.

7.7.2 Mobility Comparisons

The primary response locations considered for this test are the two locations on the side shell, and are the focus of the point mobility comparisons used to determine model validity. Though not highlighted here, the data quality for the point mobility measurements at these locations is good, at least at frequencies above 15 Hz. It is noted that transfer mobility measurements from the foundation to the side shell (and vice versa) had generally poor coherence; additional details and comparisons between the model and measurements are made in Section 8.1.

Figure 140 and Figure 141 present comparisons of measured and modeled point mobilities for the two measurement locations on the side shell. At 30 Hz and below the point mobility is over predicted by the model; the magnitude ratio is on the order of 2.2 at best, and over 4 at worst. The reason for this is not clear; additional investigations were not performed. However, as will be shown in Section 8.1, the predicted transfer mobility from the foundation to these locations shows good correlation, particularly at 30 Hz.

Between 35 and 65 Hz the modeled point mobility is reasonably close to the measured data for both locations, though there are several dips in the measured response that are not captured in the model. At higher frequencies the model diverges significantly from the measurements.

Figure 140: Side Shell Near Start Air Compressor, Frame 132 Point Mobility, Measured vs. Modeled

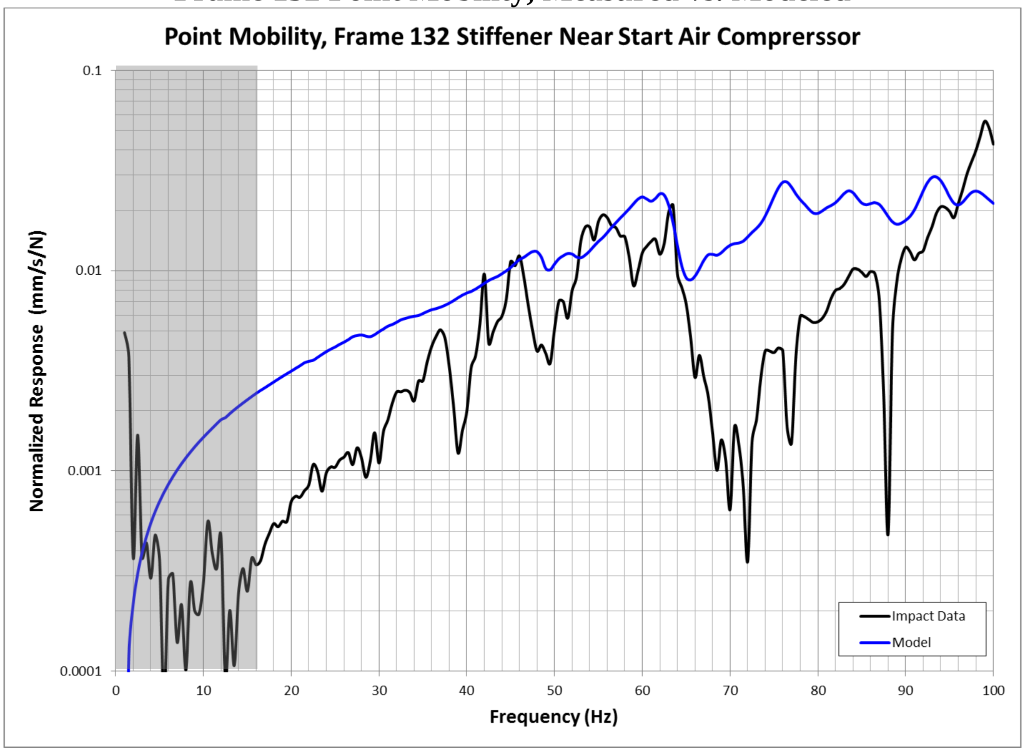

Figure 141: Side Shell Near Start Air Compressor, Frame 133 Point Mobility, Measured vs. Modeled

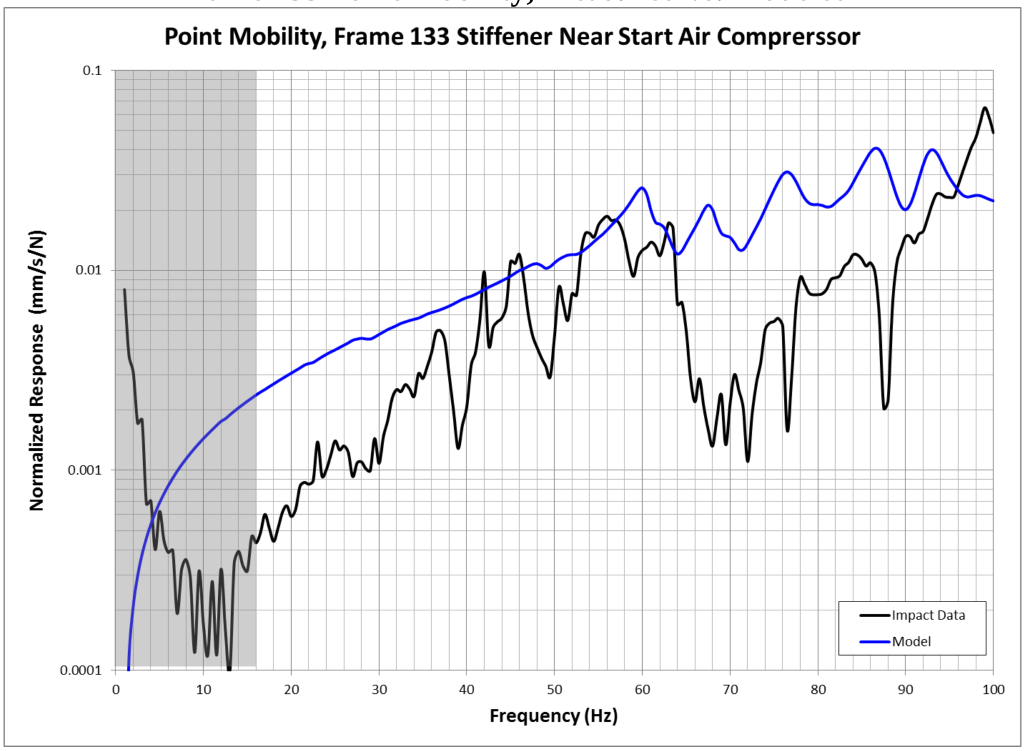

7.7.3 Summary of Analysis of Structure Near Start Air Compressor

The model is seen to have acceptable correlation at frequencies between 35-60 Hz, particularly if an averaged or maximum response approach is used. Unfortunately the nuances of various peaks and dips in the response in this frequency range do not appear in the modeled data. Furthermore, the modeled point mobility below 35 Hz shows greater error than has been seen for other areas of the vessel. Similar to other models, results above 65 Hz diverge from the measurements.

The causes of these discrepancies were not identified. It is possible that for this structure the damping values used for the main structure or on the damped deck are too high. However, this structure was assumed to be similar to the structure near the gensets (discussed in Section 7.8) where better results were obtained. It will be shown in Section 8.1 that the transfer mobilities between the start air compressor foundation and these measurement locations on the side shell show greater degrees of correlation.

7.8 Machinery Room Near Gensets

7.8.1 Model

The same truncated model used for the Machinery Room side shell (Section 7.6) was used for this analysis. A cutaway view of the area near the gensets is shown in Figure 142. The model uses a 4x density mesh. All frames and deep girders were modeled using plate elements for the web and beam elements for the flanges. Small stiffeners were modeled using beam elements. No boundary constraints were applied to the model.

Models were analyzed with a 0.58 lb/in^2 added mass on wetted hull elements below the 23' Flat to simulate a water loading effect.

Figure 142: Model Section of Machinery Room Near Gensets
(Full model not shown)

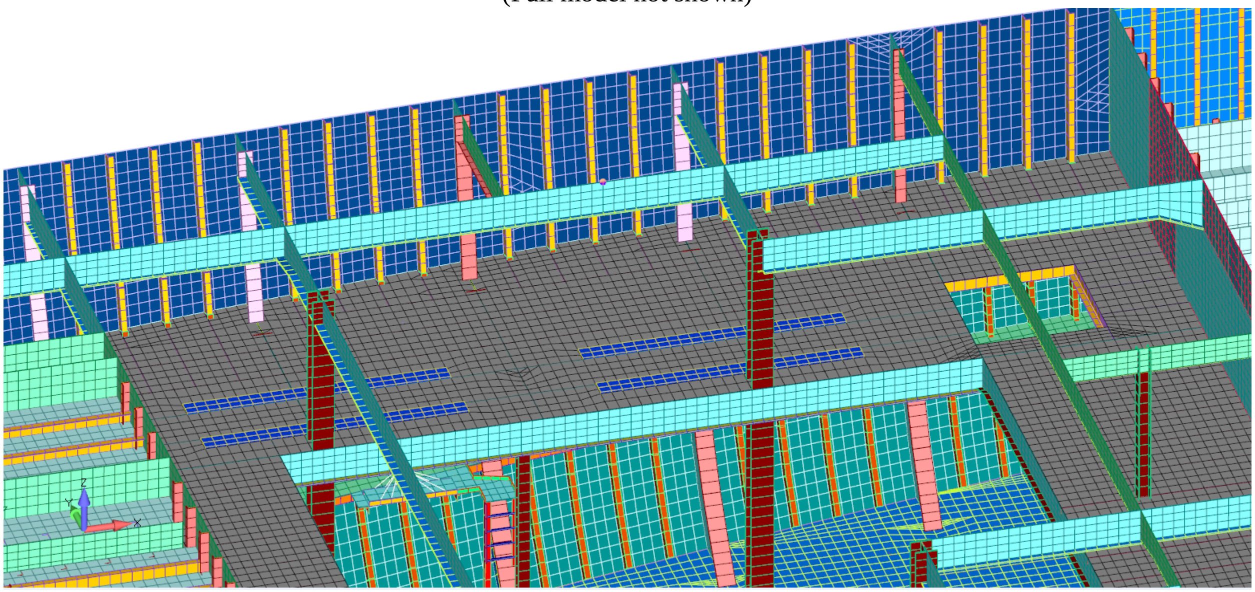

The model results presented here include an increase in the local damping on the deck to account for the damping tile that is applied to the underside of the 23' Flat. Details of this approach are the same as those used for the start air compressor, discussed in Section 7.7. A loss factor of 0.03 was used for the rest of the model.

The initial analysis that was performed of this structure did not contain weights of machinery. As noted in Section 6.2.2, there are multiple auxiliary machinery items located in close proximity to the gensets and several measurement locations. The weights and details of these items are not known. Rough approximations for these items were added to the model after the initial analysis was performed in an attempt to identify the overall effects these items will have. The masses of machinery items were added to model by applying mass elements to the nodes in the areas of machinery items. The results presented here include these mass elements.

No approximation was made for the piping located beneath the gensets, discussed in Section 6.2.2. Also, no mass was added to the side shell to account for the mass of insulation.

7.8.2 Notes on Measured Mobility

The point mobilities measured at the locations discussed in Section 6.2.2 are generally of good quality. An example is shown in Figure 143, where it is seen that the measurement is good starting at frequencies around 10 Hz. (The sharp rise in mobility is erroneous for the reasons discussed in Section 7.3.2.) Unfortunately, transfer mobilities between measurement points did not show good data in general, so no comparisons are made here.

Figure 143: Measured Point Mobility, Side Shell Between 23' Flat and 2nd Deck, Fr 126

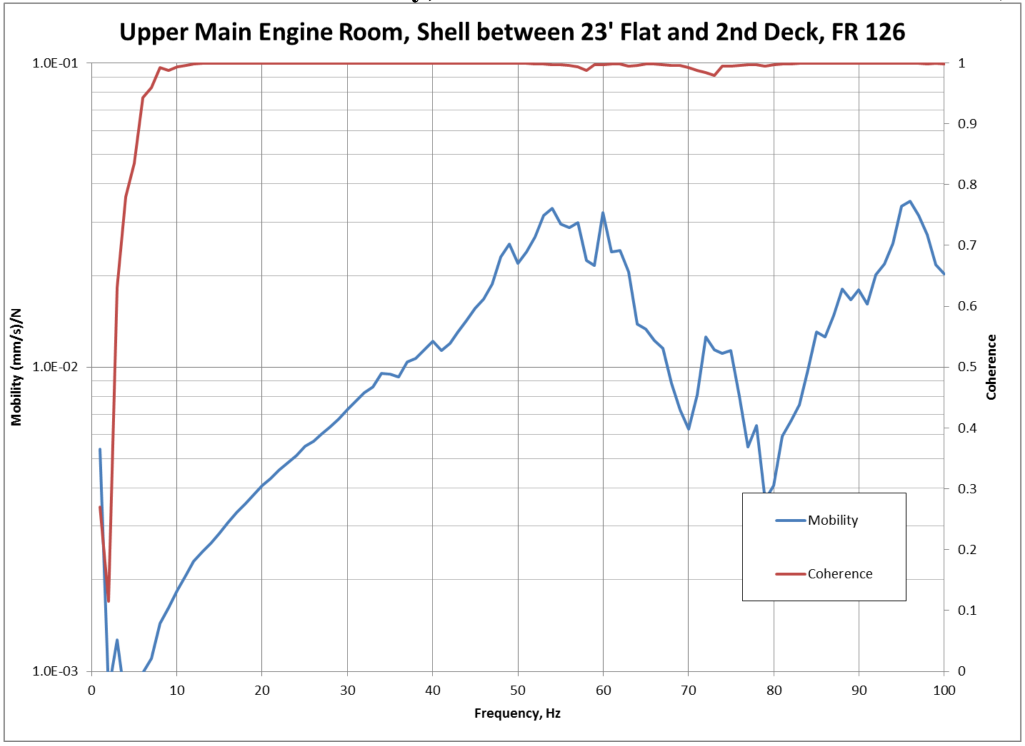

7.8.3 Mobility Comparisons

Figure 144 presents comparisons of measured and modeled point mobilities at several locations near Genset #1. Details of these locations are provided in Section 6.2.2, and include points on the side shell outboard of the genset, on the 23' Flat deck outboard and aft of the genset, and on the 2nd Deck above the genset. These plots include all added masses for machinery and water loading, and also include approximations for damping tiles, as discussed above.

The point mobility on the side shell (top two plots of Figure 144) shows reasonable correlation between model and measurement. The primary peak in the measured response which occurs near 55 Hz in both measurements is represented in the model with a worst case frequency error of 10%. The magnitude ratio between measurement and model at the peak response is between 1.4 and 1.8. The model performs well at lower frequencies as well, with magnitude ratios of 1.3 and less at frequencies below 40 Hz. At frequencies above 65 Hz the model does not correlate well with the measured data. It is noted that these locations were seen to have only small variations when masses of auxiliary machinery were added.

The point mobility on the deck (middle two plots of Figure 144) shows reasonable correlation to the model. At Frame 126.5 there is a similar characteristic of modeled and measured mobility, though the frequencies of peak response are shifted; it was not possible to identify which modeled peaks line up with the measurement as data was not collected to create operational deflection shapes. At Frame 132.5 again the overall characteristic is similar. No strong peaks and dips are present in either the model or measurement, though the magnitude error is on the order of a factor of 2 for much of the frequency range between 25 and 70 Hz; above 70 Hz the model diverges.

Figure 144: Comparisons of Point Mobility at Locations near Genset, Measured vs. Modeled

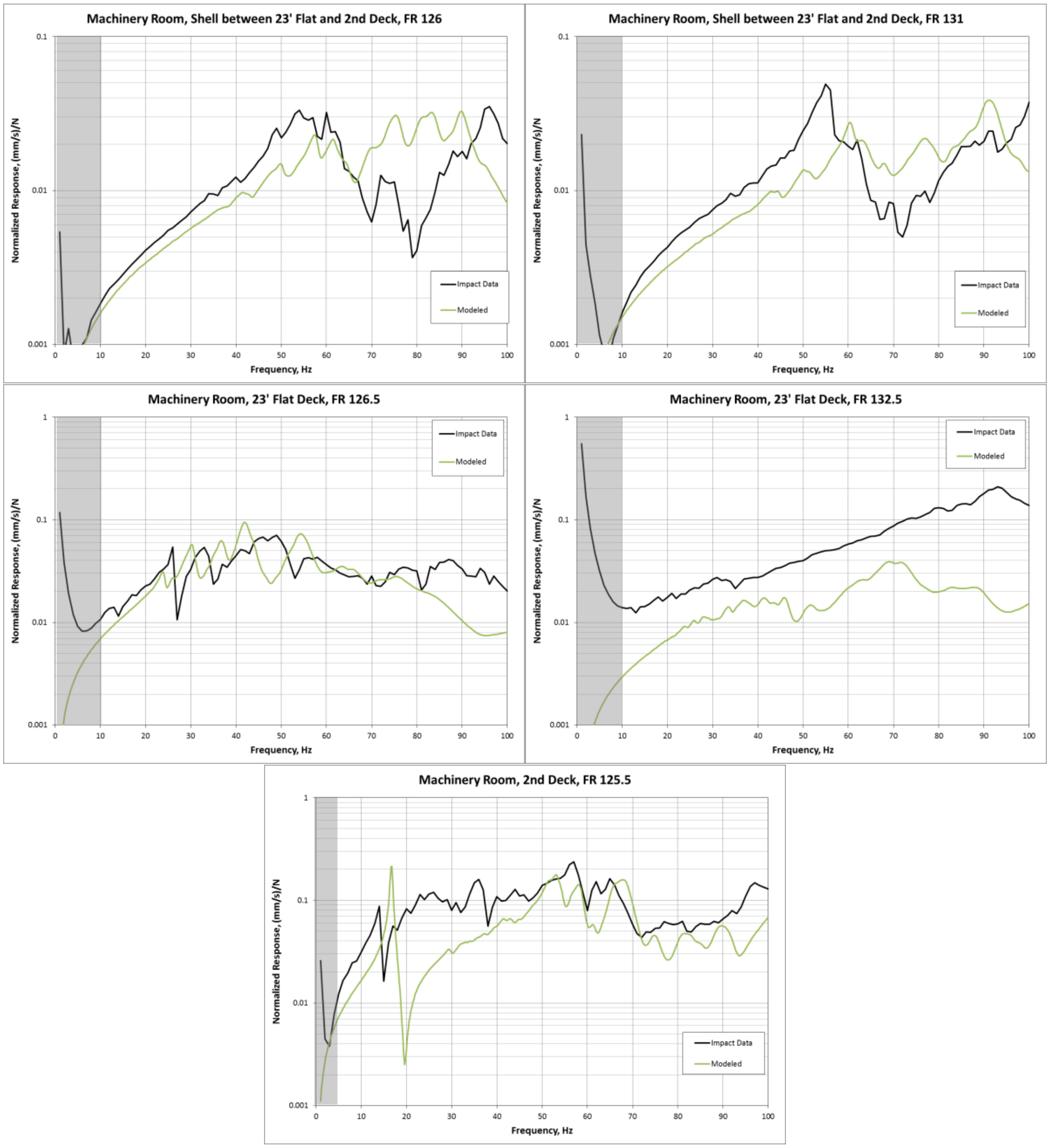

The measurement locations on the deck were more sensitive to added masses from auxiliary machinery than the side shell locations. Since the 23' Flat deck locations were not directly adjacent to any machinery item the added mass effects were small. The greatest effects were found in the predicted frequencies of the peaks between 20-50 Hz at Frame 126.5.

The point mobility on the 2nd Deck (bottom plot of Figure 144) shows a large peak and dip in the response near 15 Hz in both the measurement and model. The frequency error of the peak is on the order of 15-20%. Between 20 and 40 Hz the model significantly under-predicts the response, though at higher frequencies the model provides a reasonable estimate of the measured data.

The 2nd Deck location was highly sensitive to the effects of added auxiliary machinery mass, particularly the items on the 2nd Deck. This is because the measurement location was within several feet of one item in particular. Again, the primary effect of the added mass was to change the frequency of the peak and dip at lower frequencies (as well as the specific distribution of vibration on the deck), which in turn also affects the response between 20-40 Hz. In this model a 'best estimate' of machinery mass was used, but ultimately the choice of mass was likely erroneous. It is presumed that a more accurate model would include the correct details of these machinery items.

7.8.4 Summary of Analysis of Structure Near Gensets

The model provides a reasonable estimate of the point mobilities measured at specific locations on the decks and side shell in the area around the gensets. Some locations do show better results than others; the side shell shows the best results with good accuracy in both frequency and magnitude response up to 65 Hz. The worst case is on the 2nd Deck; although the overall characteristic is captured, some portions of the low frequency response show significant errors.

The errors shown here are believed to result from the fact that the test area contains many auxiliary machinery items, the details of which (mass, foundation arrangement, etc.) were not known. It was found that these items had to be approximated in the model (by using point or smeared masses in this case) in order to obtain reasonable results for some locations.

The side shell was seen to be least sensitive to the addition of these masses; this is also the location with the greatest accuracy, and is farthest from the masses themselves. The 2nd Deck was seen to be the most sensitive to the addition of masses (and changing their details), and was also seen to have the greatest error. This location was only a few feet from one of the auxiliary machinery items.

It is argued that better information on the size, mass, etc. of the auxiliary machinery items would lead to a better model providing more precise results.

Although not discussed explicitly above, the response at these locations was not found to be highly sensitive to the addition of mass on the lower hull simulating water loading effects.

Piping was not included in the model. It is possible that the piping had an effect on the response at the 23' Flat deck locations, though reasonable accuracy was still achievable neglecting the piping. The mass of large machinery items appears to be more important in the response of the structure.

8.0 MACHINERY FORCES AND RESPONSE

8.1 Starting Air Compressor

The following sections discuss the force estimation and prediction of vibration response from the start air compressor. The model used for these analyses is the same as the model discussed in Section 7.7.

8.1.1 Force Estimation

The starting air compressor produces tones at rotation rate and harmonics. For the frequency range of interest there are three tones, located at approximately 30, 60 and 90 Hz.

The ‘Above Mount Vibration’ and ‘Generalized Inverse’ methods (Methods 1 and 2) described in Section 6.3 were the primary approaches used to estimate the forces imparted by the start air compressor. An investigation of Method 3, ‘Impact and Relative Vibration’ was also performed.

Above mount vibration levels were recorded while the machinery was operating. Examples of above mount spectra are shown in Figure 145. The peaks at forcing frequencies can be clearly detected. It is noted that the below mount data was inspected in this case and was verified to be well below the above mount levels[15].

Figure 145: Example of Above Mount Vibration During Start Air Compressor Operation

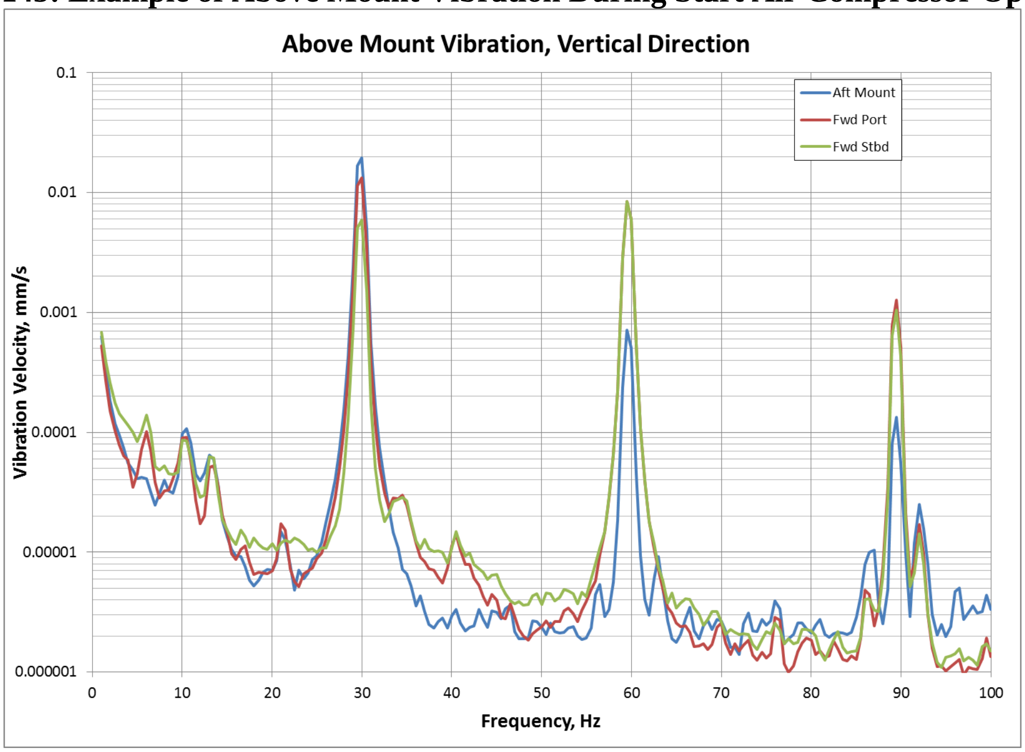

The stiffness of the isolation mounts in each direction was not provided, though they have been estimated based on additional data collected on-site. Above-mount impact data was used to determine the six whole body modes of the isolated unit. The mass of the unit (based on vendor data), estimated mass moments of inertia, and estimated center of gravity location were used to perform a six-degree of freedom analysis. By varying the mount stiffness the predicted modes and mode shapes of the resilient mounting system were aligned (approximately) with the measured data. The resulting estimates of mount stiffness are presented in Table 41. Note that

[15] Formally, the forces imparted to the structure would be the difference in displacement on both sides of the mount. However, since the below mount levels are of much lower magnitude than the above mount levels, the above mount levels can be used alone with a negligible increase in error.

the wider side of the mount (corresponding to the stiffer side) is oriented in the transverse direction.

Table 41: Estimated Dynamic Stiffness of Start Air Compressor Mounts

Direction	Mount Stiffness, kN/m
Longitudinal	500
Transverse	2000
Vertical	1700

To perform the Generalized Inverse method of force estimation, transfer and point mobilities (FRFs) were measured using impact points at the foundation of the compressor. The response points used for the calculation were the two deck measurement points and the two side shell measurement points discussed in Section 6.2.1, as well as the other foundation measurement points. Impacts were applied at each attachment location in three orthogonal directions (longitudinal, transverse, and vertical). The measured FRF's were used to define the 13 by 9 FRF matrix (13 response points and 9 force inputs), as discussed in Appendix D.

Impacting the foundation was not a simple procedure, nor was it always exactly possible, as access to the foundation was partially blocked by the compressor itself. In some cases impacts were made directly adjacent to the foundation – this is a potential source of error.

An example of the measured point mobility at one corner of the foundation is provided in Figure 146. The coherence of these measurements is not shown here for clarity (and brevity). Based on the character of these responses and further evaluation it can be said that the vertical mobility is a good measurement at least above 10 Hz while the transverse and longitudinal mobilities are noisy (vibration data near background) at least at frequencies near and below 30 Hz. Note that the transverse mobility is typically greater than the longitudinal mobility.

Figure 146: Example of Measured Point Mobility at Start Air Compressor Foundation

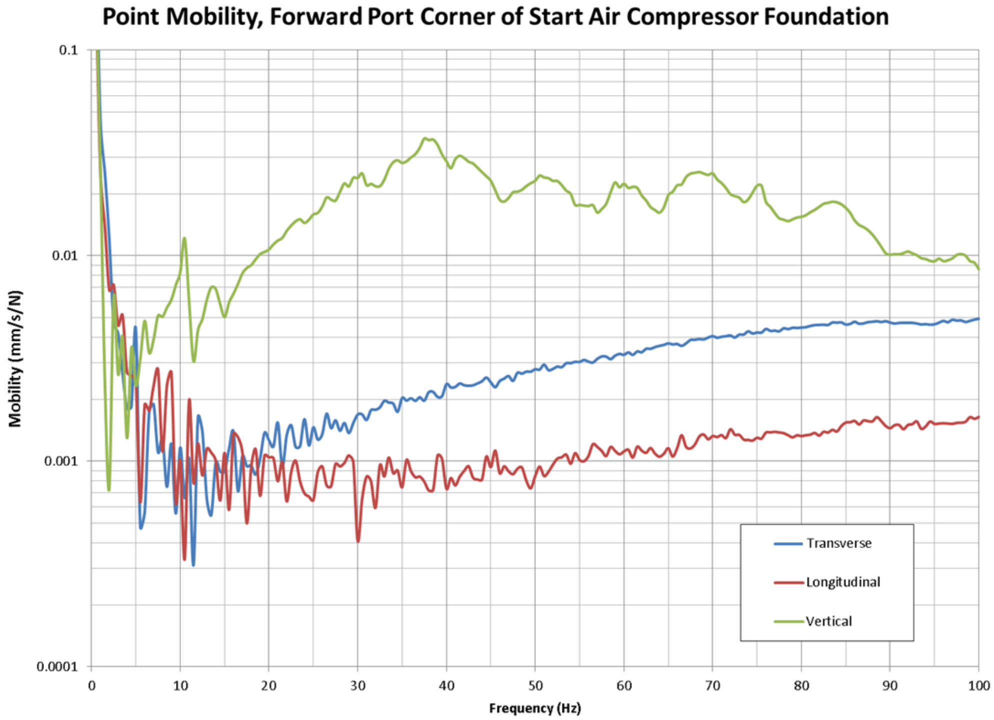

Measurement data for the other foundation locations show similar characteristics. Good quality data was seen for some measurements in the transverse and longitudinal directions. It is implied in these measurements that the foundations are much stiffer in the transverse and longitudinal directions than in the vertical direction; this is reasonable to expect given their low profile, allowing them to benefit from the in-plane stiffness of the deck.

The transfer mobilities between the foundation and the deck measurement locations are of reasonable quality at frequencies above 20 Hz, particularly for the vertical impact measurements (not shown here). The transfer mobilities from the foundation to the side shell have some good data, though there are many dips in the coherence. An example coherence plot is shown in Figure 147. It is seen that some frequencies have coherence near 1, though there are many sharp drops in coherence below 70 Hz at specific frequencies. Only the data for the vertical impact is shown here; coherence for impacts in other directions is generally lower. The poor coherence is due, in part, to the presence of other operating machinery in the area which could not be secured during measurements.

Figure 147: Example of Poor Coherence for Transfer Mobility, Start Air Compressor Foundation to Side Shell, Vertical Impact

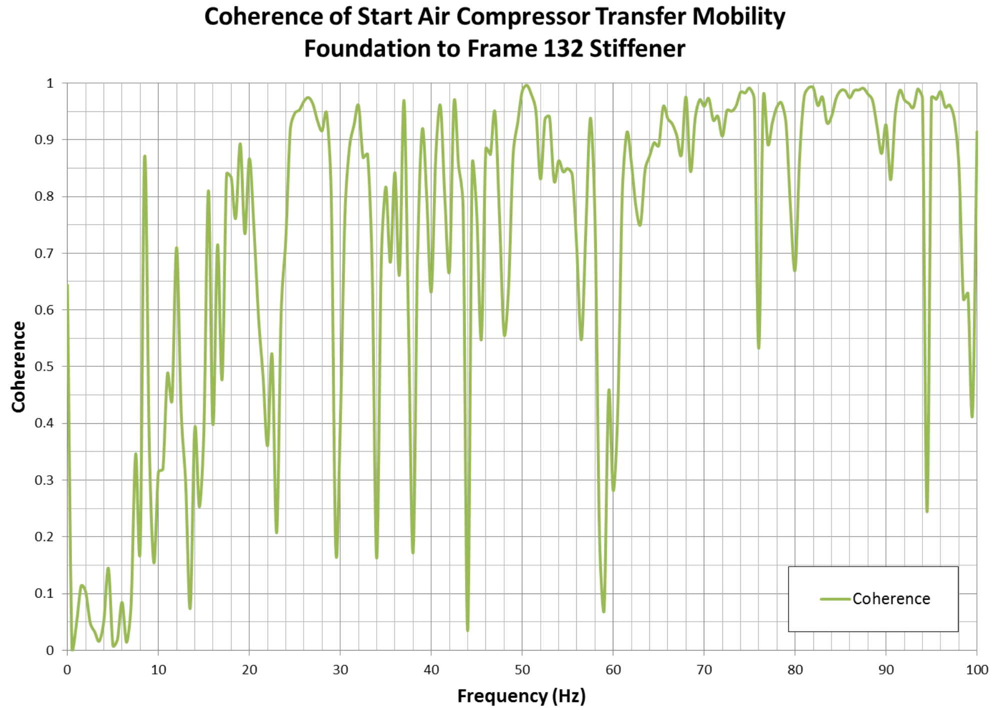

It is worth pointing out, however, that the coherence shown in Figure 147 is good at frequencies close to the forcing frequencies of the start air compressor. For example, although the coherence dips strongly at 29.5 Hz, the coherence between 25-28 Hz and at 31 Hz is good. Similar features are seen at higher frequencies.

The poor FRF quality in some directions and frequencies introduces errors into the Generalized Inverse method of force estimation. Various attempts were made to improve the quality of the force prediction that results from using this data. In the end, the data was used as-is, as there are several combinations of impact/response locations where good data was achieved at the forcing frequencies of the compressor. The Generalized Inverse approach to force estimation uses a least squares error methodology to reduce the influence of errors in the measurement data. Additional details are provided in Appendix D.

The predicted force magnitudes and phases from the two methods are presented in Table 42. The phase for the forward port mount, X direction was arbitrarily set to 0. It is seen that the force magnitudes are somewhat similar for the two methods over most frequencies, locations, and directions, though some discrepancies exist. There is also some agreement between the predicted phases, though the agreement is somewhat less than what is seen for the magnitudes.

The Above Mount Vibration method of force estimation is likely to be the preferred method as above mount data is more readily available than the data required for the Generalized Inverse method. The similarity in the force predictions is a rough validation that the Above Mount Vibration method is an appropriate approach; errors are certainly present in both methods, but the approximate correlation indicates that the predicted levels have some degree of accuracy.

Table 42: Estimated Forces of Start Air Compressor

Above Mount Vibration Technique - Magnitude									
Frequency (Hz)	**Forward Port Corner (lbf)**			**Forward Starboard Corner (lbf)**			**Aft Corner (lbf)**		
	Long	**Trans**	**Vertical**	**Long**	**Trans**	**Vertical**	**Long**	**Trans**	**Vertical**
30	8.4	50.2	40.4	8.5	50.6	16.9	7.3	77.0	52.5
60	2.6	33.0	11.9	2.1	34.2	12.7	0.5	8.7	1.3
90	0.4	1.8	1.2	0.2	1.9	1.0	0.1	1.4	0.3
Generalized Inverse Technique - Magnitude									
Frequency (Hz)	**Forward Port Corner (lbf)**			**Forward Starboard Corner (lbf)**			**Aft Corner (lbf)**		
	Long	**Trans**	**Vertical**	**Long**	**Trans**	**Vertical**	**Long**	**Trans**	**Vertical**
30	61.8	65.3	11.2	27.6	84.4	24.6	13.5	113.9	33.6
60	19.0	54.9	6.3	10.6	43.4	3.2	7.4	18.1	5.8
90	0.9	6.4	0.5	0.9	3.4	1.2	0.5	2.4	0.2
Above Mount Vibration Technique - Phase									
Frequency (Hz)	**Forward Port Corner (Degrees)**			**Forward Starboard Corner (Degrees)**			**Aft Corner (Degrees)**		
	Long	**Trans**	**Vertical**	**Long**	**Trans**	**Vertical**	**Long**	**Long**	**Vertical**
30	0	131	131	-113	132	-35	-158	128	47
60	0	14	14	7	14	-167	-169	9	17
90	0	62	62	56	61	-121	-139	52	54
Generalized Inverse Technique - Phase									
Frequency (Hz)	**Forward Port Corner (Degrees)**			**Forward Starboard Corner (Degrees)**			**Aft Corner (Degrees)**		
	Long	**Trans**	**Vertical**	**Long**	**Trans**	**Vertical**	**Long**	**Trans**	**Vertical**
30	0	7	47	-112	92	152	-25	73	153
60	0	-5	-139	-114	132	-44	-127	-6	-65
90	0	37	32	-19	-6	161	-146	55	121

8.1.2 Comparison of Force Estimation Method 3

The forces estimated using the ‘Impact and Relative Vibration’ method described in Section 6.3 have been computed based on the measured impact and operational vibration data. (Note that the point mobility data used for this calculation are of good quality.) The results are presented in Table 43. Also shown is the ratio of predicted forces using this method as compared to the Generalized Inverse method (Method 2).

Table 43: Estimated Forces of Start Air Compressor Using Method 3

Impact and Relative Vibration Technique - Magnitude									
Frequency (Hz)	**Forward Port Corner (lbf)**			**Forward Starboard Corner (lbf)**			**Aft Corner (lbf)**		
	Long	**Trans**	**Vertical**	**Long**	**Trans**	**Vertical**	**Long**	**Trans**	**Vertical**
30	29.0	100.1	7.8	17.0	122.3	10.9	26.4	81.4	34.2
60	4.8	24.9	2.2	5.8	35.2	6.0	3.8	9.2	1.4
90	0.4	1.3	0.2	0.1	1.3	0.3	0.2	0.7	0.2
Ratio of Method 3 to Method 2 Magnitude									
Frequency (Hz)	**Forward Port Corner (lbf)**			**Forward Starboard Corner (lbf)**			**Aft Corner (lbf)**		
	Long	**Trans**	**Vertical**	**Long**	**Trans**	**Vertical**	**Long**	**Trans**	**Vertical**
30	0.5	1.5	0.7	0.6	1.4	0.4	2.0	0.7	1.0
60	0.3	0.5	0.3	0.5	0.8	1.9	0.5	0.5	0.2
90	0.5	0.2	0.4	0.2	0.4	0.3	0.5	0.3	0.9

The Impact and Relative Vibration method produces similar results to the Generalized Inverse method, though clearly some error is introduced. At 30 Hz the results seem to be the closest, with ratios magnitude less than 2 (or greater than 0.5 if the Method 3 force is less than for Method 2). At 60 and 90 Hz Method 3 seems to under-predict the force in most directions. In many cases the ratio is less than a factor of 2 though in some cases it is a factor of 3 or more.

As discussed in Section 6.3, using Method 3 is a compromise to using Method 2 as less information is needed. However, Method 3 has the potential to allow for force estimation of hard mounted machinery, whereas Method 2 formally will introduce errors (See Appendix D).

8.1.3 Comparison of Transfer Mobility

The prediction of machinery vibration response within a finite element model is the combination of the predicted transfer mobilities from the machinery foundation to the response locations with the predicted force from the machinery. Therefore it is worth inspecting the transfer mobilities from the start air compressor foundation to the response locations on the side shell to help understand where errors in the prediction may originate. This comparison is made with the understanding that the measurement data quality is less than desired, though indications of accuracy can be made nonetheless.

Comparison plots of the measured and modeled transfer mobilities between the start air compressor foundation to the Frame 133 stiffener on the side shell are presented in Figure 148 to Figure 150. Each figure presents two plots, which correspond to impacts at a specific mount in the vertical and transverse directions (the longitudinal direction is not shown here due to low vibration response in the measured data).

Figure 148: Measured vs. Predicted Transfer Mobility, Start Air Compressor, Forward Starboard Mount to Side Shell

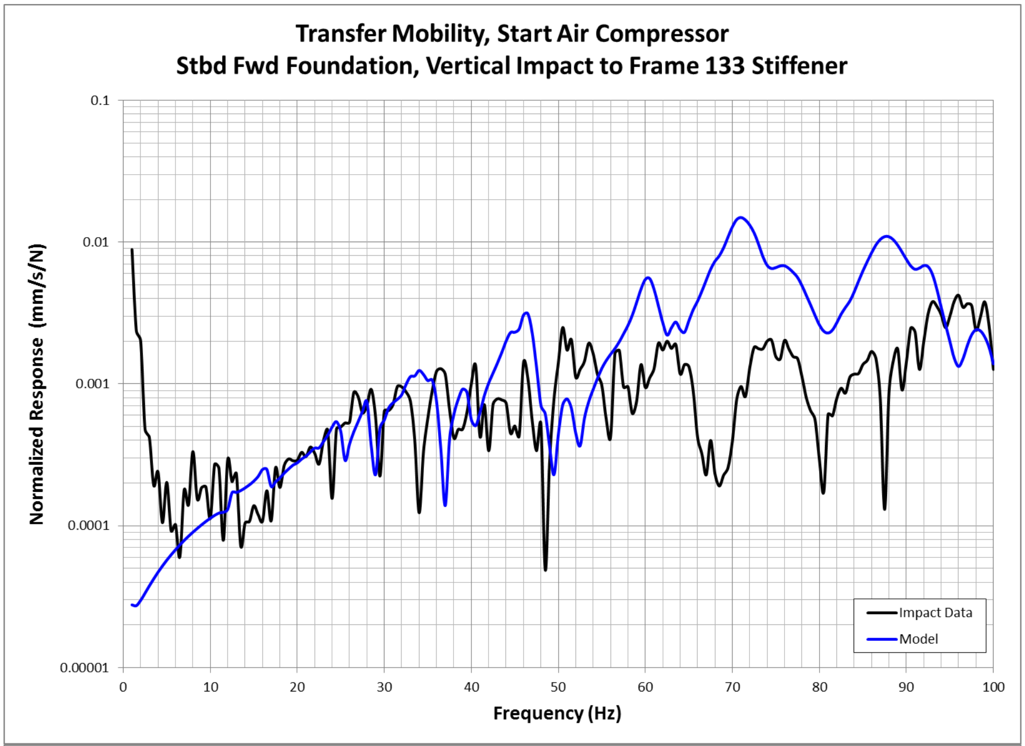

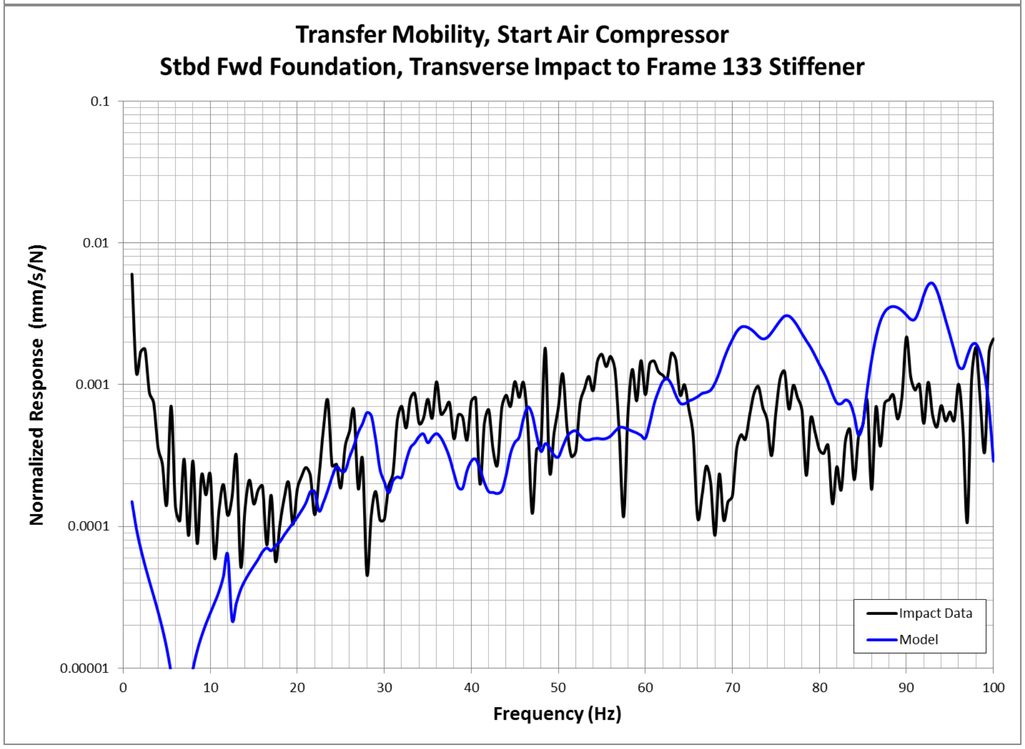

Figure 149: Measured vs. Predicted Transfer Mobility, Start Air Compressor, Forward Port Mount to Side Shell

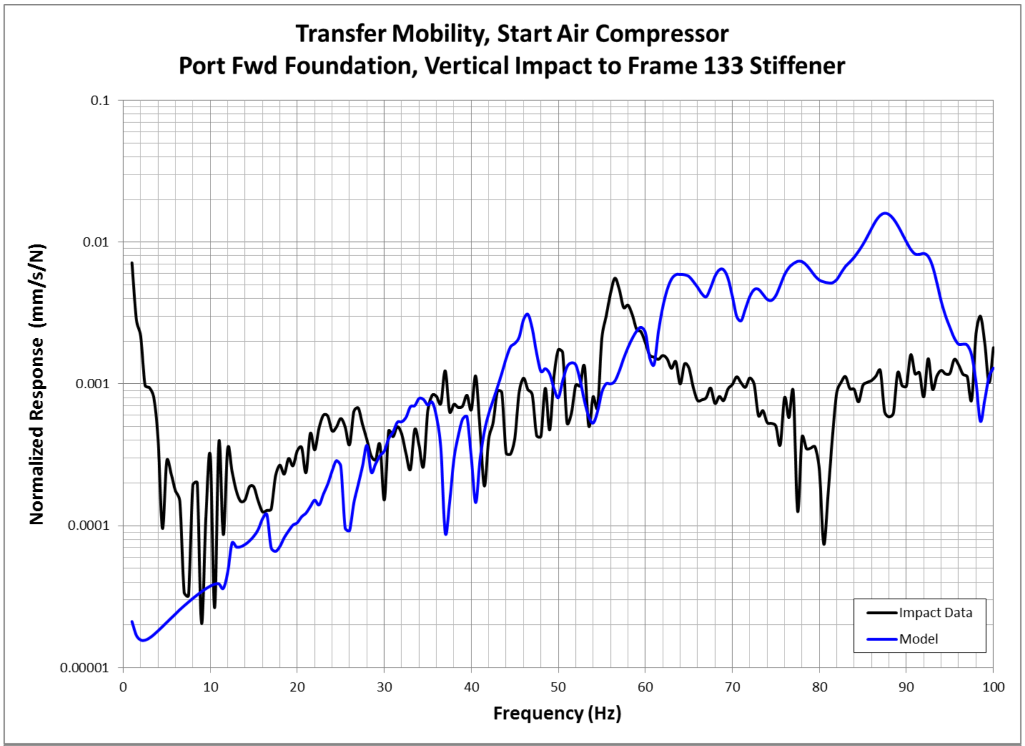

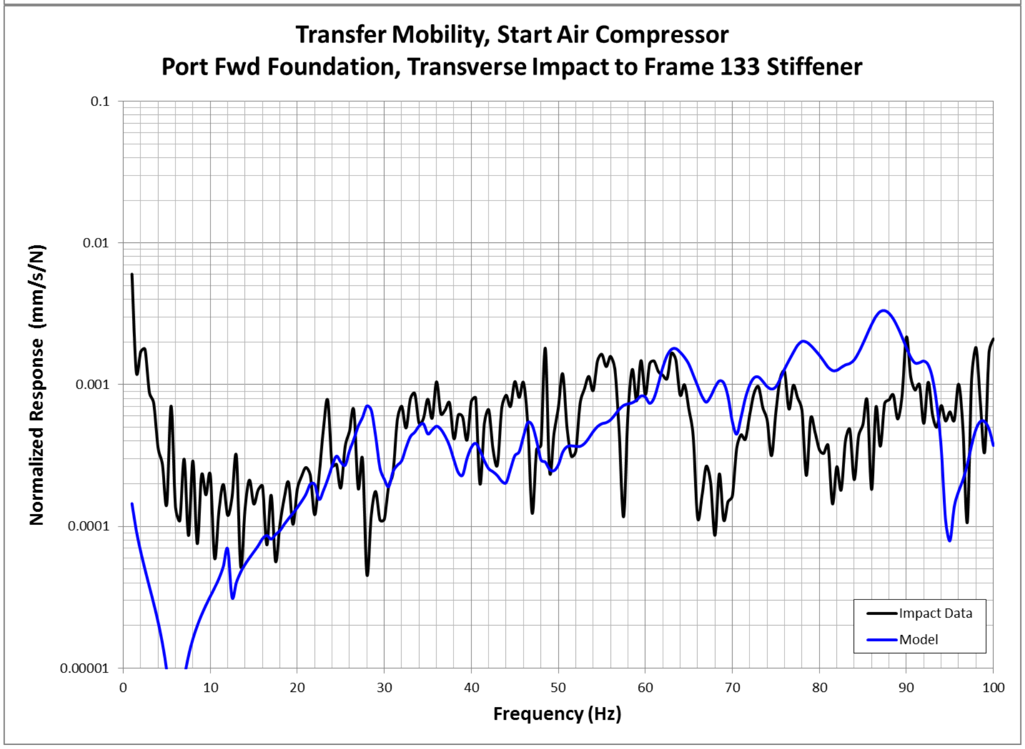

Figure 150: Measured vs. Predicted Transfer Mobility, Start Air Compressor, Aft Mount to Side Shell

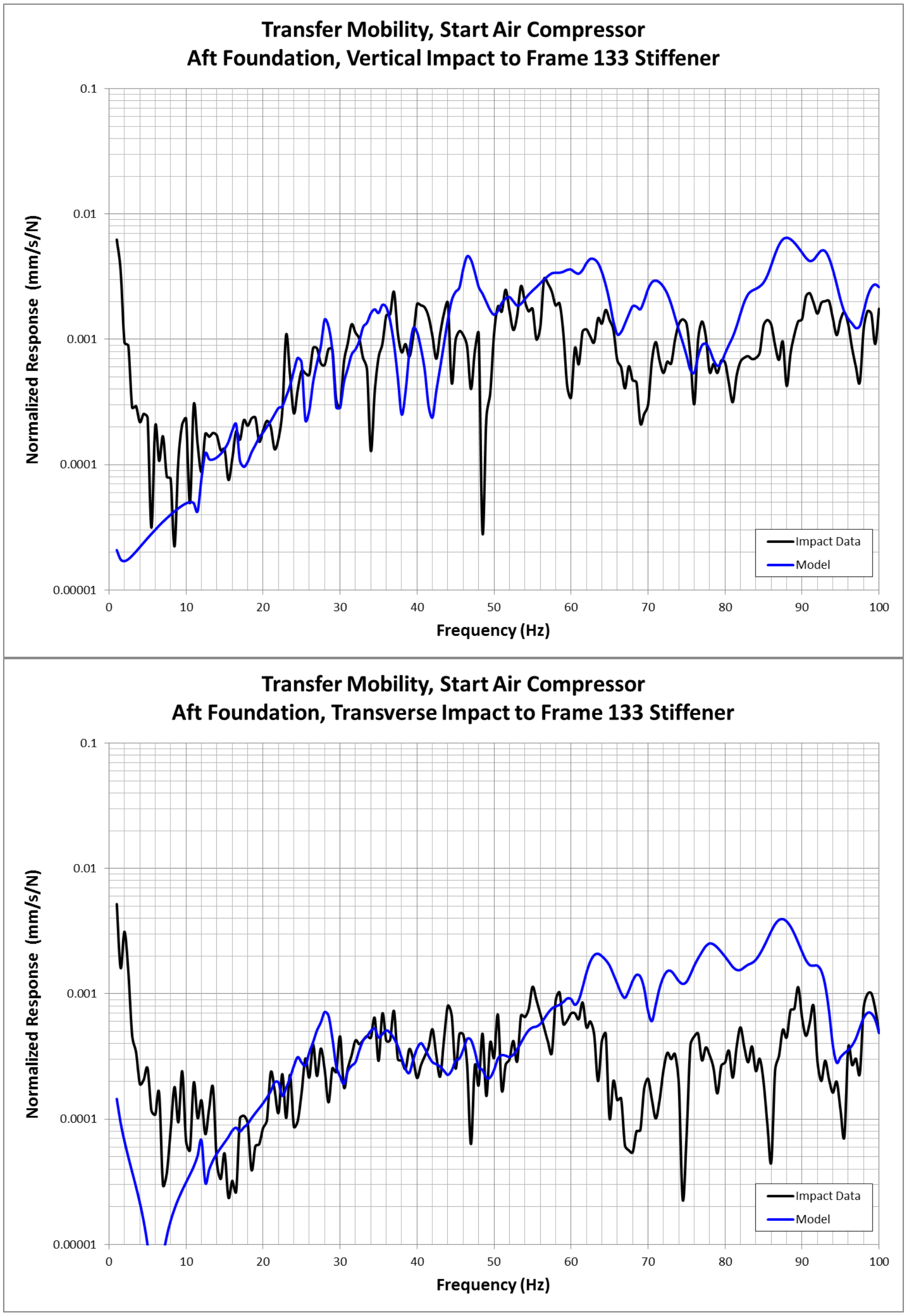

It is seen that through most of the frequency range the model is in good agreement with the measured data, in particular at frequencies near 30 and 60 Hz. Note that the over-prediction at frequencies below 30 Hz seen in the point mobility data – Section 7.7.2 – is not seen here in the transfer mobility data. Again, the cause of this is not clear. Although it is not possible in this case to correlate specific peaks, it is seen that the overall level in each frequency range is in line with the measured data. As noted previously, the measured data at 30 and 60 Hz is likely erroneous, though the data around these frequencies should be accurate. This indicates that the model is reasonably capturing the structural mobility, in spite of the seemingly erroneous results of the point impedance comparisons illustrated in Section 7.7.

At frequencies above 65 Hz (including 90 Hz) the model diverges once again from the measured data. This is in-line with findings elsewhere in the vessel.

8.1.4 Vibration Response

A plot of the measured vibration response on the side shell during operation of the start air compressor is shown in Figure 151. The forcing tones from the compressor at 30, 60, and 90 Hz can be clearly seen here.

Figure 151: Example of Measured Spectra from Start Air Compressor Operation

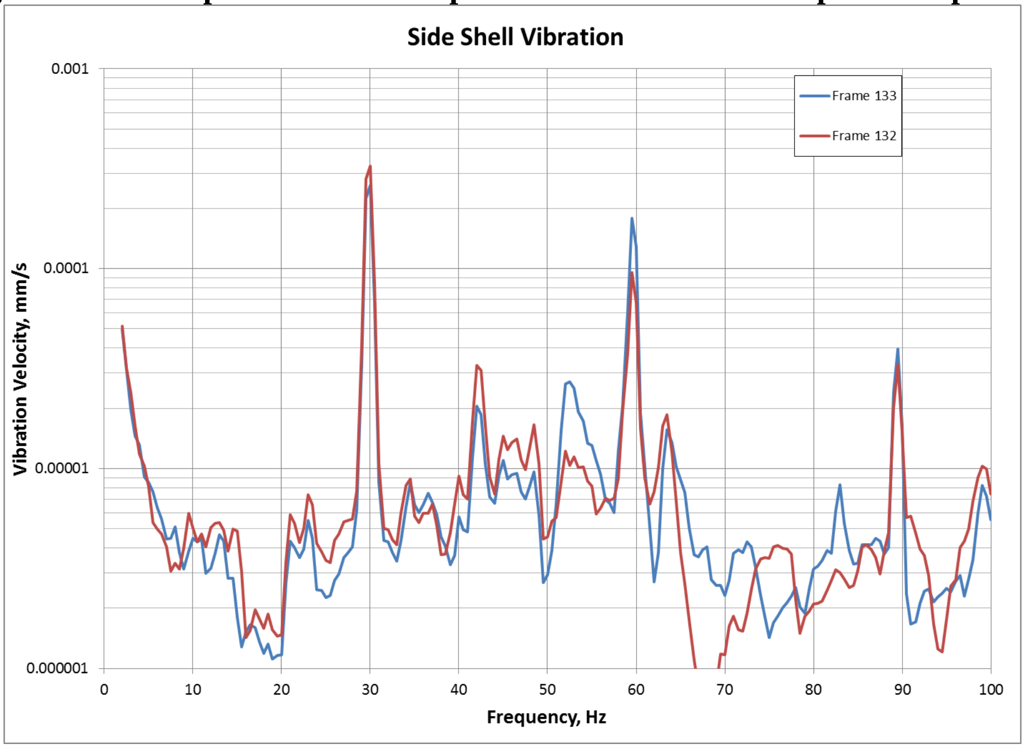

The forces discussed in Section 8.1.1 and Table 42 were entered into the model (only forces from force estimation Methods 1 and 2 were used in this analysis). The forces derived at each mount were applied to the foundation at the corresponding mount locations simultaneously, accounting for both the magnitude and phase predicted by each force estimation method (derived forces from each method were applied separately).

Two analysis approaches were used here. In both cases, the forces corresponding to each compressor tone was applied over a frequency range corresponding to the tone frequency +/-5%.

Then the average and maximum responses were calculated for each frequency range. Both of these approaches are in-line with the general modeling concepts introduced in Section 4.

Graphical results are shown in Figure 152 to Figure 155, and summary tables are provided in Table 44 and Table 45.

Figure 152: Measured vs. Predicted Vibration Response, Start Air Compressor, Frame 132, Average Response

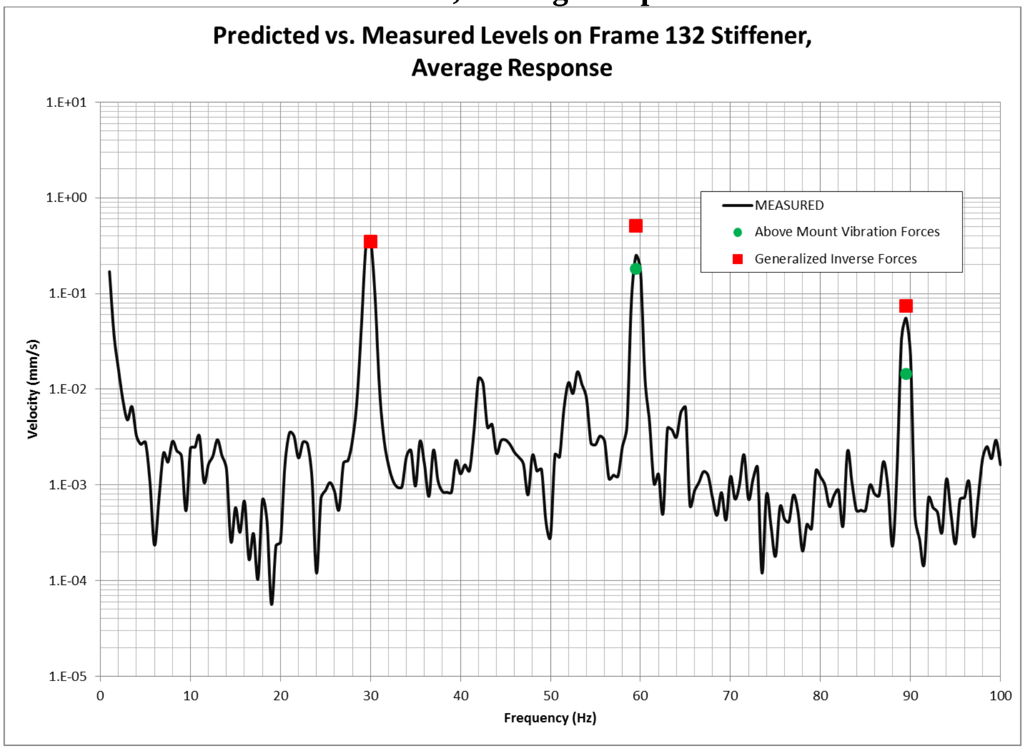

Figure 153: Measured vs. Predicted Vibration Response, Start Air Compressor, Frame 133, Average Response

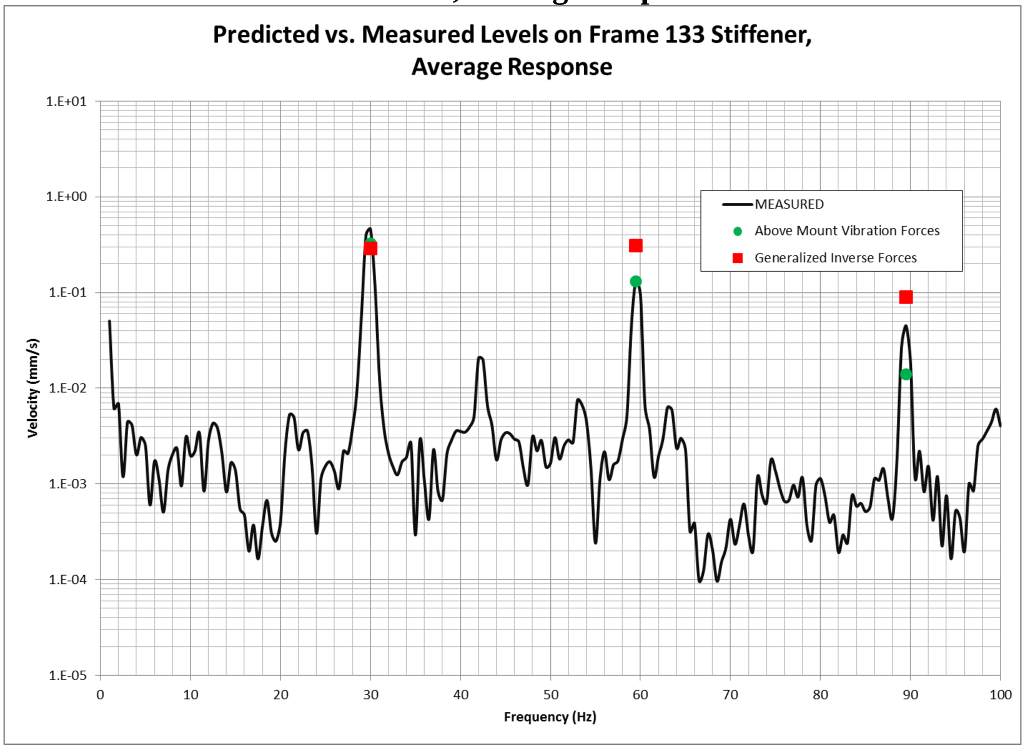

Figure 154: Measured vs. Predicted Vibration Response, Start Air Compressor, Frame 132, Maximum Response

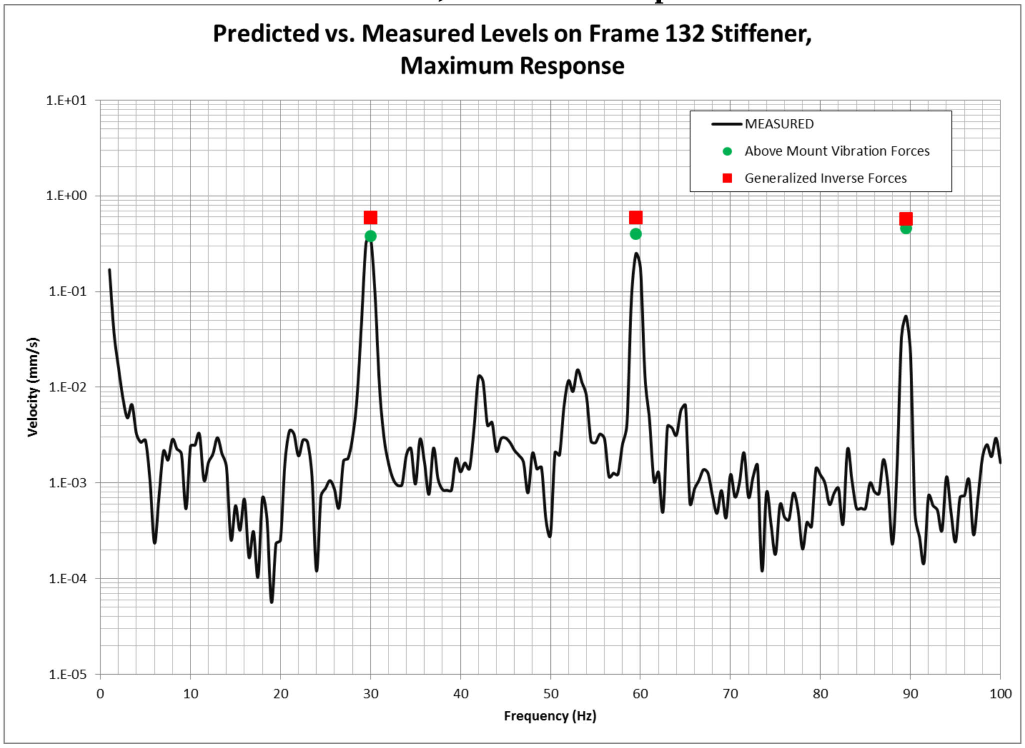

Figure 155: Measured vs. Predicted Vibration Response, Start Air Compressor, Frame 133, Maximum Response

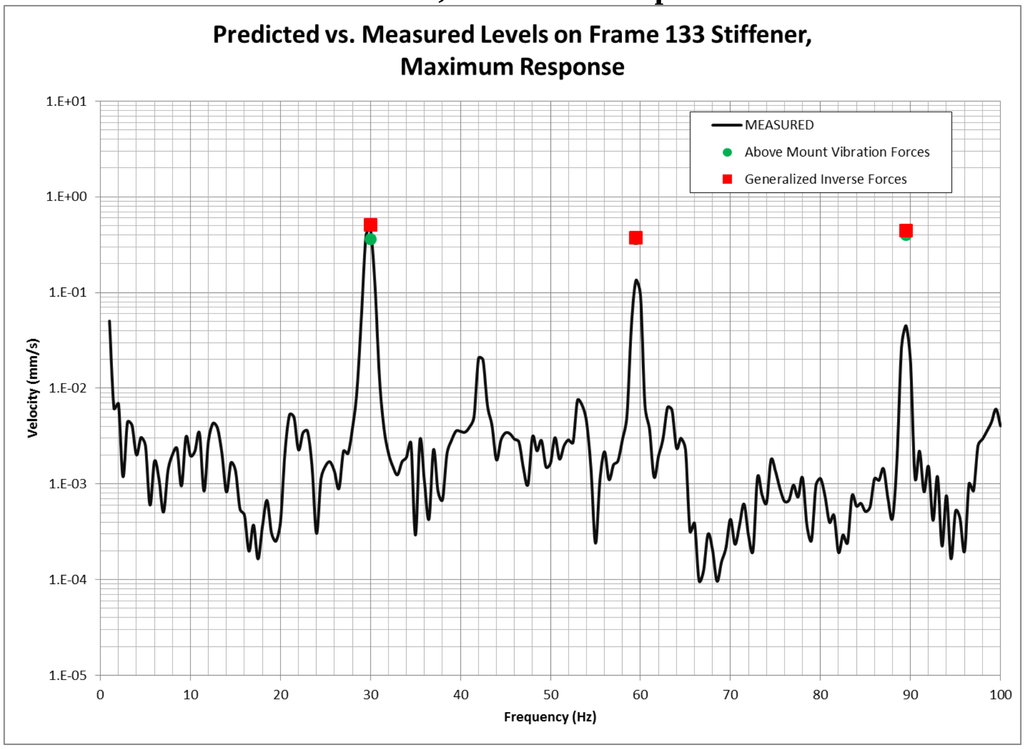

Table 44: Summary of Predicted Response to Start Air Compressor Excitation, Average Response Approach

Frequency, Hz	Measured Level, mm/s		Above Mount Vibration Prediction, mm/s		Above Mount Vibration Magnitude Ratio		Generalized Inverse Prediction, mm/s		Generalized Inverse Magnitude Ratio	
	Fr 132	Fr 133	Fr 132	Fr 133	Fr 132	Fr 133	Fr 132	Fr 133	Fr 132	Fr 133
30	3.7E-01	4.6E-01	3.5E-01	3.3E-01	1.1	1.4	3.5E-01	2.9E-01	1.1	1.6
60	2.5E-01	1.4E-01	1.8E-01	1.3E-01	1.4	1.1	5.0E-01	3.1E-01	2.0	2.2
90	5.5E-02	4.5E-02	1.4E-02	1.4E-02	3.8	3.2	7.4E-02	9.0E-02	1.3	2.0

Table 45: Summary of Predicted Response to Start Air Compressor Excitation, Maximum Response Approach

Frequency, Hz	Measured Level, mm/s		Above Mount Vibration Prediction, mm/s		Above Mount Vibration Magnitude Ratio		Generalized Inverse Prediction, mm/s		Generalized Inverse Magnitude Ratio	
	Fr 132	Fr 133	Fr 132	Fr 133	Fr 132	Fr 133	Fr 132	Fr 133	Fr 132	Fr 133
30	3.7E-01	4.6E-01	3.8E-01	3.6E-01	1.0	1.3	6.0E-01	5.1E-01	1.6	1.1
60	2.5E-01	1.4E-01	4.0E-01	3.6E-01	1.6	2.6	6.0E-01	3.7E-01	2.4	2.7
90	5.5E-02	4.5E-02	4.6E-01	4.0E-01	8.3	8.9	5.7E-01	4.3E-01	10.4	9.8

In this case the 'average response' prediction method provides the closest match to the data. The predictions at 30 Hz are within a factor of 1.6 for both locations and prediction methods, and at 60 Hz they are within a factor of 2.2. The 'Above Mount Vibration' force prediction method appears to produce more accurate results in this case, with magnitude ratios of 1.4 or less at 30 and 60 Hz, though both force estimation methods produce similar results.

Although the prediction at 90 Hz is close to the measured level for the Generalized Inverse method, it has been shown previously that the predicted mobility at this frequency is generally inaccurate. Therefore the overall accuracy of the forced response prediction in this frequency range is not expected to be highly accurate.

The maximum response analysis approach produces higher predictions of vibration response (as expected), and shows somewhat greater error than the average response at 60 and 90 Hz. This approach is meant to capture the maximum level at large peaks in the response, as discussed in Section 4. In this case, there are no distinct, large peaks in the transfer mobility (compare this to the Engine Lab or Transom) and it can be expected that taking the maximum response would lead to over-predictions.

8.1.5 Summary of Start Air Compressor Forced Response Analysis

The Above Mount Vibration method of force estimation was found to produce similar results to the more rigorous Generalized Inverse method, in terms of force magnitudes, phases, and the resulting prediction of vibration response on the hull. In this case the Above Mount Vibration method predicted vibration levels that were closer to the measured levels at 30 and 60 Hz as compared to the Generalized Inverse approach. This is further confirmation of the validity of using the Above Mount Vibration method of force estimation.

The 'Impact and Relative Vibration' method (Method 3) of force estimation also appears to produce force magnitude results that are in line with the Generalized Inverse approach though differences are clearly seen, particularly at 90 Hz. Note that this method cannot be used to derive phase information but can possibly be used to estimate forces from hard mounted machinery.

The model was seen to be capable of predicting the transfer mobilities from the compressor foundation to the side shell with reasonable accuracy. This was achieved with a truncated model which includes structures one major bulkhead forward and aft of the compartment containing the test area. No special consideration was given to the piping below the deck supporting the compressor. A damping loss factor of 0.03 was used for the entire model except in the area under the 23' Flat deck covered by damping tile where the loss factor was increased. A 4x mesh density was used.

Using the average response over a frequency range of +/-5% of each forcing frequency, the Above Mount Vibration force estimation method produces vibration levels on the side shell within a magnitude ratio of 1.4 or better. The prediction at 90 Hz is limited due to model accuracy, as discussed in previous sections.

The vibration levels predicted using the 'maximum response' method are higher than when using the 'average response' method, as can be expected. The maximum response is intended to be more conservative, and may be useful when attempting to predict the response at a frequency and location showing a strong resonance. Since the response of the side shell to forcing at the foundation did not contain strong resonance peaks, the average response method produced more accurate results (though improvements were modest in this case).

8.2 Genset

The following sections discuss the force estimation and prediction of vibration response from the genset. The model used for these analyses is the same as the model discussed in Section 7.8. Note that the side shell below the 23' Flat uses the approximation for water loading discussed in Sections 7.6 and 7.8.

8.2.1 Force Estimation

The genset produces tones at multiple frequencies. Primary tones occur at multiples of 15 Hz (being half of rotation rate), though for this genset several additional tones at quarter harmonics are seen in the spectrum. An example above mount spectrum is shown in Figure 156. Data was extracted for force estimation at all 15 Hz harmonics up to 90 Hz as well as additional tones at 37 and 52 Hz.

Figure 156: Example of Above Mount Vibration During Genset Operation

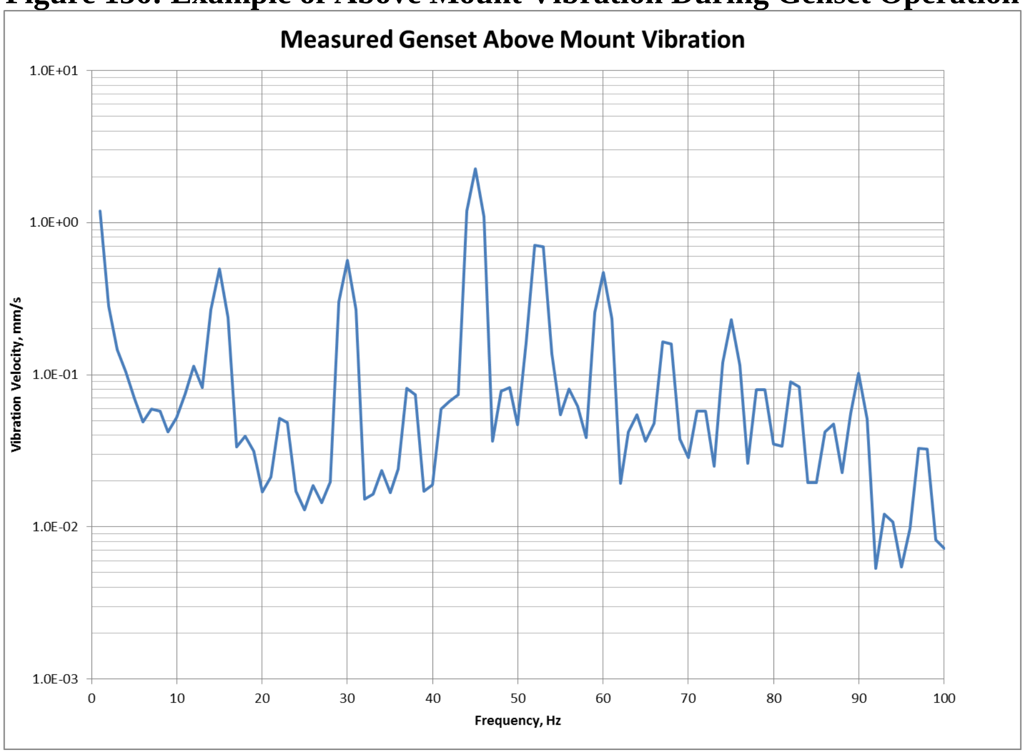

Unfortunately, impacting the genset foundation was difficult due to access restrictions and its size. Vertical impacts were performed adjacent to the foundation in an attempt to collect some data, though lateral impacts were not found to produce reasonable results or be practical. For this reason, the primary method of force estimation used is Method 1, 'Above Mount Vibration'.

As discussed in Section 6.2.2 the genset is isolation mounted on solid rubber pads. The stiffness of these pads is not known, but has been estimated based on the dimensions of the pads, an estimate of the genset weight, and comparisons to vendor data for similar existing mounts (making adjustments for differences such as pad thickness). Verification of the identified stiffness was performed based on model results. The resulting mount stiffness used for modeling is shown in Table 46. These values are believed to be reasonable for mounts of this type, given the available information.

Table 46: Estimated Dynamic Stiffness of Genset Mounts

Direction	Mount Stiffness, kN/m
Longitudinal	3650
Transverse	3650
Vertical	7300

The resulting forces are presented in Table 47. Both magnitude and phase information is presented. All phases are normalized to the forward port mount, vertical direction.

An attempt was made to calculate the vertical forces based on the 'Impact and Relative Vibration' approach (Method 3). The data quality was poor and is not presented here, though the forces generated from this method are similar the forces shown in Table 47, providing a partial confirmation of the validity of the approach.

Arguably, the derived force information provided here is more detailed than the information that would be available for a typical vessel project where the vibration response is to be estimated during the design stage. As an approximation to an approach that might be used during the design stage, "simplified" forces have been developed. These simplified forces use the same force magnitude at all locations and all forces are in phase with one another. The force magnitude in each direction was derived using the power averaged vibration level for the corresponding direction and the corresponding mount stiffness. These forces are presented in Table 48.

Table 47: Estimated Forces of Genset, Above Mount Vibration Method

Vertical Forces – Magnitude, lbf										
Frequency (Hz)	Port Fwd	Port Mid Fwd	Port Mid	Port Mid Aft	Port Aft	Stbd Fwd	Stbd Mid Fwd	Stbd Mid	Stbd Mid Aft	Stbd Aft
15	31	22	14	13	12	20	11	9	23	22
30	17	10	8	8	9	12	9	10	11	11
37	3	1	1	3	4	5	4	7	7	6
45	19	21	26	30	36	16	15	23	26	27
52	4	8	6	2	2	6	0	3	1	1
60	4	6	5	2	1	3	1	2	2	3
75	2	2	2	1	0	2	2	2	1	1
90	1	1	1	2	4	2	2	1	2	3
Transverse Forces – Magnitude, lbf										
Frequency (Hz)	Port Fwd	Port Mid Fwd	Port Mid	Port Mid Aft	Port Aft	Stbd Fwd	Stbd Mid Fwd	Stbd Mid	Stbd Mid Aft	Stbd Aft
15	6	8	10	12	13	8	10	11	13	16
30	11	8	5	3	3	11	8	5	2	2
37	3	1	1	3	5	3	1	1	3	5
45	10	8	18	30	41	9	8	18	30	41
52	3	2	3	4	5	3	2	3	3	5
60	4	2	2	4	6	4	2	2	4	6
75	1	0	0	0	0	0	1	0	0	0
90	2	2	3	4	5	2	2	3	4	5
Longitudinal Forces – Magnitude, lbf										
Frequency (Hz)	Port Fwd	Port Mid Fwd	Port Mid	Port Mid Aft	Port Aft	Stbd Fwd	Stbd Mid Fwd	Stbd Mid	Stbd Mid Aft	Stbd Aft
15	6	5	4	3	3	5	5	5	5	5
30	1	2	2	2	2	2	1	2	2	2
37	1	1	1	1	1	1	1	1	2	2
45	7	7	6	5	6	7	8	9	9	10
52	1	1	1	2	2	1	1	0	0	0
60	0	1	1	1	1	2	2	2	2	2
75	1	1	1	1	1	1	1	1	1	1
90	0	0	0	0	1	1	1	1	1	1

Table 47: Estimated Forces of Genset, Above Mount Vibration Method (Continued)

Vertical Forces – Phase, Degrees

Frequency (Hz)	Port Fwd	Port Mid Fwd	Port Mid	Port Mid Aft	Port Aft	Stbd Fwd	Stbd Mid Fwd	Stbd Mid	Stbd Mid Aft	Stbd Aft
15	0	4	61	99	116	-37	-41	-130	-153	-155
30	0	16	90	97	96	-123	-136	134	131	125
37	0	5	92	93	91	106	118	-139	-148	-149
45	0	14	61	68	74	-173	-164	-93	-104	-104
52	0	12	42	68	158	-167	165	4	-23	-44
60	0	-20	-18	-15	-64	-172	177	9	16	131
75	0	28	-13	-9	92	-115	-23	141	89	-11
90	0	-158	-144	-107	-64	-2	0	102	166	-166

Transverse Forces – Phase, Degrees

Frequency (Hz)	Port Fwd	Port Mid Fwd	Port Mid	Port Mid Aft	Port Aft	Stbd Fwd	Stbd Mid Fwd	Stbd Mid	Stbd Mid Aft	Stbd Aft
15	173	165	-68	-48	-30	-2	-19	94	-153	-168
30	166	154	-57	-63	-58	-88	-78	-81	150	153
37	-100	-66	-56	-59	-60	51	-12	-82	-130	-117
45	-144	-119	-104	-103	-101	-123	-120	-104	-102	-99
52	-172	-144	-87	-49	5	177	174	-132	-29	-51
60	-157	-164	-160	-157	-30	143	123	88	26	82
75	168	-134	155	171	-56	-126	-118	-142	-160	-64
90	-142	-51	-23	10	-53	-27	-52	-49	-158	-157

Longitudinal Forces – Phase, Degrees

Frequency (Hz)	Port Fwd	Port Mid Fwd	Port Mid	Port Mid Aft	Port Aft	Stbd Fwd	Stbd Mid Fwd	Stbd Mid	Stbd Mid Aft	Stbd Aft
15	173	-103	174	3	-50	-20	150	-165	-160	80
30	-12	169	120	55	-71	84	59	121	101	-1
37	132	143	83	75	-61	22	-94	-140	-160	57
45	-178	174	123	93	-112	175	10	-108	-117	105
52	139	168	149	165	21	102	12	-3	-54	-174
60	97	146	90	103	115	64	37	78	160	122
75	138	162	93	125	-170	68	114	150	-12	-87
90	-160	-139	-96	-73	141	-170	-157	149	-132	19

Table 48: Simplified Genset Force Magnitudes, lbf

Frequency (Hz)	Vertical	Transverse	Longitudinal
15	19	11	5
30	11	7	2
37	4	3	1
45	25	25	7
52	4	3	1
60	3	4	2
75	2	0	1
90	2	4	1

8.2.2 Vibration Response

Comparisons of predicted and measured vibration levels during genset operation are provided below. Prediction results are provided for both the “average” and “maximum” response techniques discussed in Section 8.1.4. The forces corresponding to each forcing tone was applied over a frequency range corresponding to the tone frequency +/-5%; the average and maximum responses were then calculated for each frequency range. Results for both sets of forces discussed in the previous section are also provided.

Note that the measurement data at several locations was either similar to background levels or did not contain strong peaks at one or more frequencies corresponding to genset excitation. Data at these locations/frequencies have been omitted from this report to avoid confusion.

Figure 157 to Figure 161 provide a comparison of the measured and predicted levels at genset forcing frequencies for the average and maximum response calculation methods. In these plots the "complex" force input was used for all predicted responses (different force and magnitude at each mount location, shown in Table 47). Table 49 and Table 50 provide the ratio of response magnitudes between measurement and prediction at each frequency and location.

At most locations and frequencies there is good correlation between the measurement and the prediction, though some large errors are seen at specific frequency and location parings. At locations on the side shell above the 23' Flat the response ratio is less than 3 nearly everywhere at frequencies up to and including 60 Hz, with the majority of data points having ratios less than 2. The results on the 23' Flat deck are mixed, with the location at Frame 132.5 showing much better results than the location at Frame 126.5. Similarly, the response ratios on the 2^{nd} Deck are reasonable at frequencies below 60 Hz with the exception of a large error at 15 Hz.

These results are in-line with the relative error seen in the point mobilities in similar locations, discussed in Section 7.8. Specifically, the side shell showed the greatest accuracy while the greatest errors were seen near 15 Hz on the 2^{nd} Deck. Again, these errors are believed to be associated with the presence of large masses in close proximity to the response location.

The side shell below the 23' Flat generally shows good correlation, though for any given position there appears to be a frequency where errors greater than a factor of 3 are predicted. Taking the effects of water loading into account (discussed in Section 7.6), it is believed that these frequency-specific errors are due to the approach used for water loading. At 15 and 30 Hz where the water loading produce improved model results in the point mobility (see Section 7.6) the operational results are within a factor of 2.3. Higher frequencies show high errors at some frequencies and low errors at others. A more refined approach to water loading could help to reduce these errors.

It is promising to see that the results on the aft bulkhead of the Machinery Room ('Fr 144 Outboard') show very good correlation at all frequencies below and including 60 Hz. This location is very far from the gensets (relative to measurements performed for other sources measured as part of this effort), and indicates that accurate results are possible for locations close to and far from vibration sources. (Note that measurement data at other locations on the forward and aft bulkheads was background limited.)

Some locations do show reasonable or even good correlation at frequencies above 60 Hz, though this frequency range also tends to have the largest errors. This is consistent with the findings in the rest of this report which indicate that the models loose accuracy at these higher frequencies.

Figure 157: Predicted vs. Measured Response to Genset Excitation, Side Shell Locations Above 23' Flat

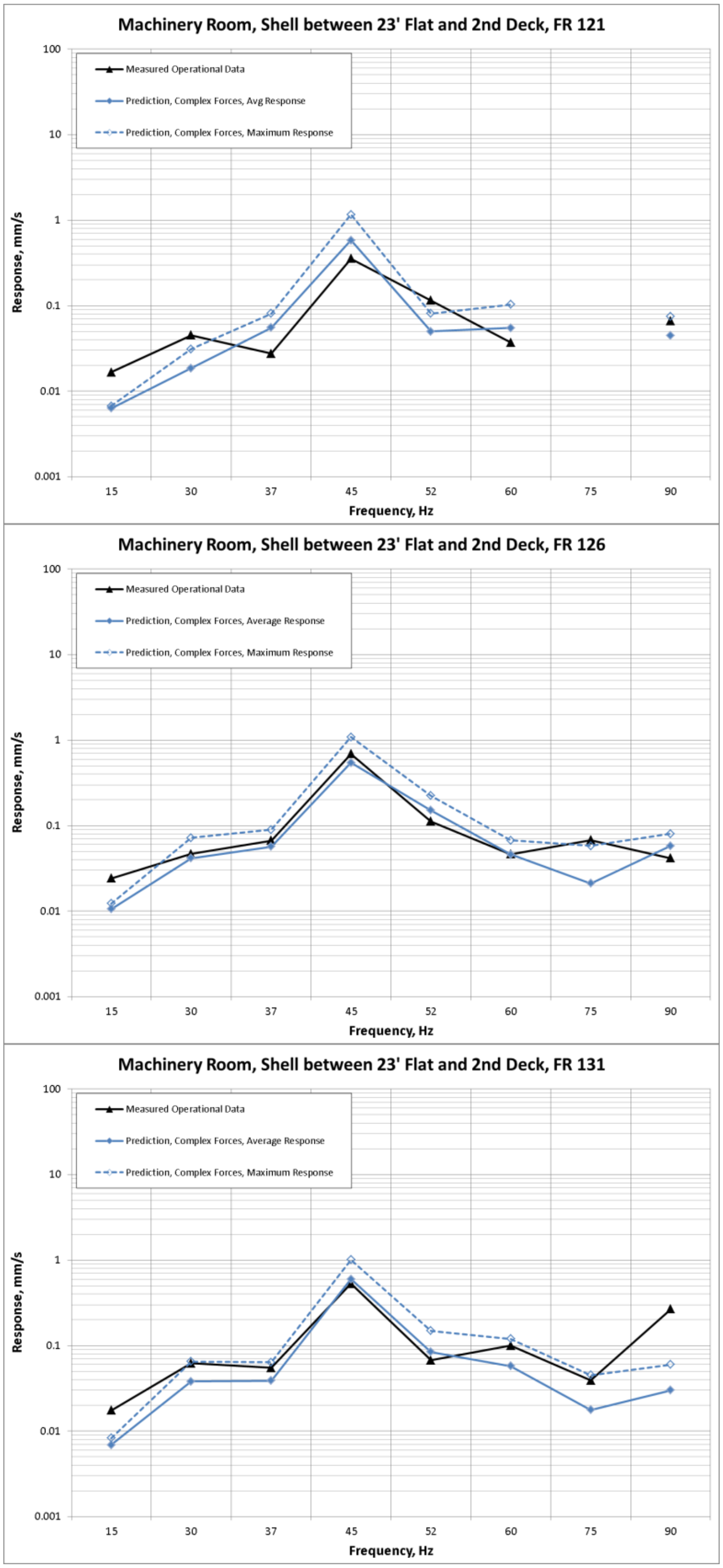

Figure 158: Predicted vs. Measured Response to Genset Excitation, 23' Flat Deck Locations

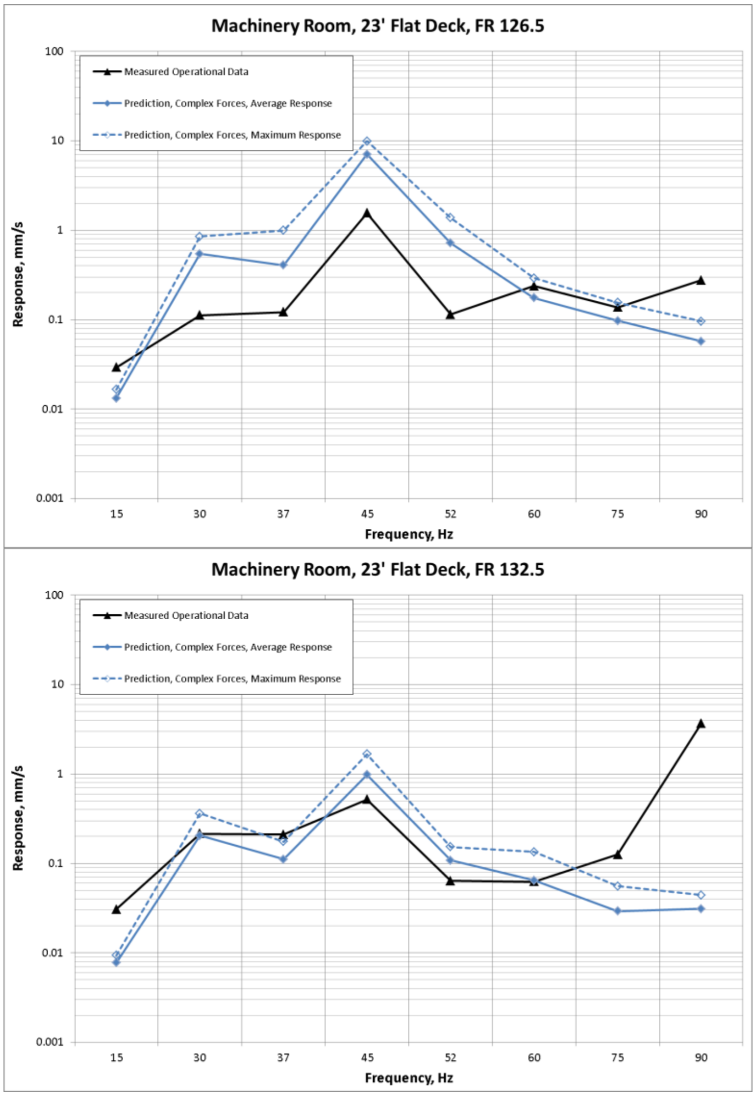

Figure 159: Predicted vs. Measured Response to Genset Excitation, 2^{nd} Deck Location

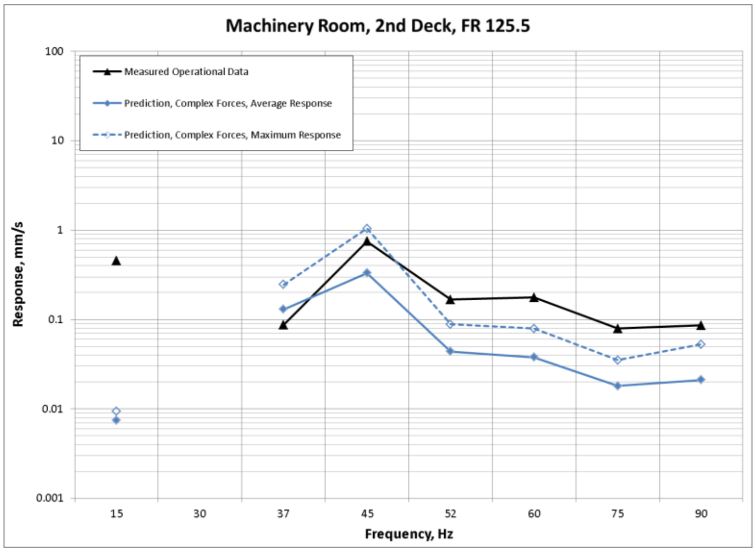

Figure 160: Predicted vs. Measured Response to Genset Excitation, Side Shell Locations Below 23' Flat

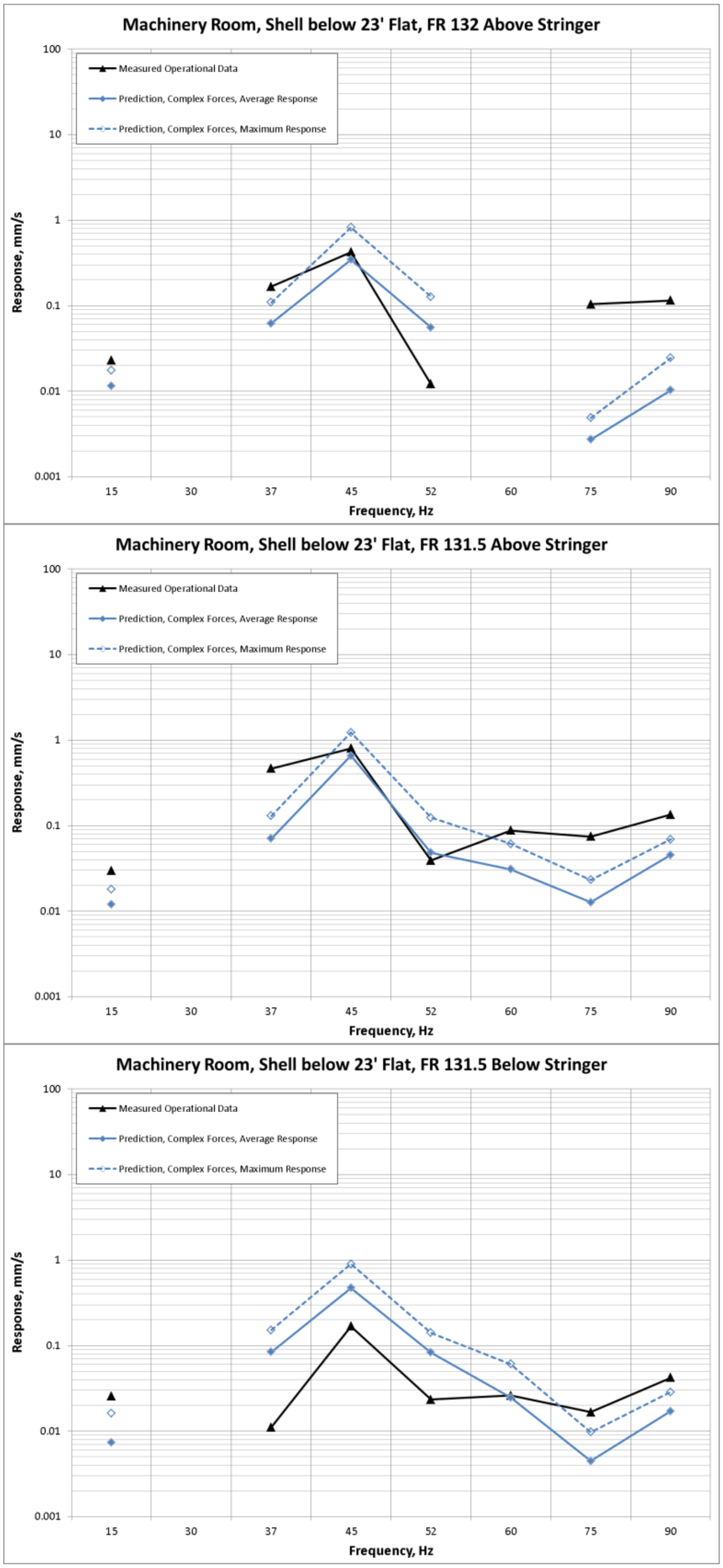

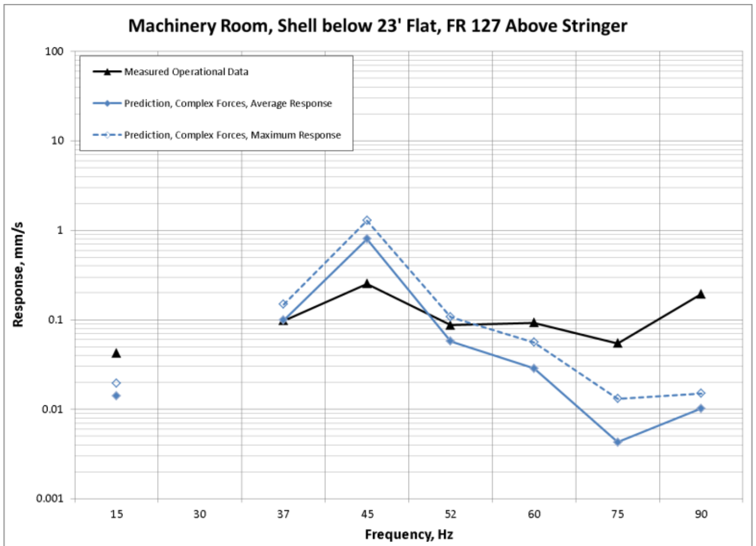
Machinery Room, Shell below 23' Flat, FR 127 Above Stringer
Measured Operational Data
Prediction, Complex Forces, Average Response
Prediction, Complex Forces, Maximum Response
Response, mm/s
100
10
1
0.1
0.01
0.001
15
30
37
45
52
60
75
90
Frequency, Hz

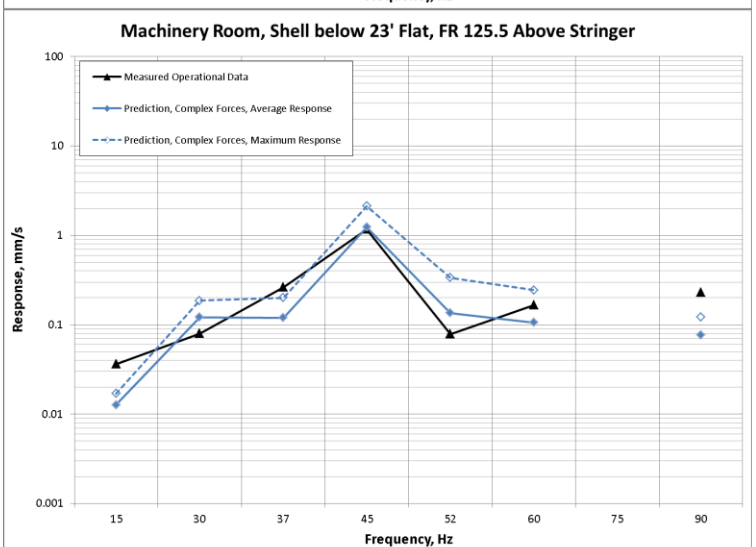
Machinery Room, Shell below 23' Flat, FR 125.5 Above Stringer
Measured Operational Data
Prediction, Complex Forces, Average Response
Prediction, Complex Forces, Maximum Response
Response, mm/s
100
10
1
0.1
0.01
0.001
15
30
37
45
52
60
75
90
Frequency, Hz

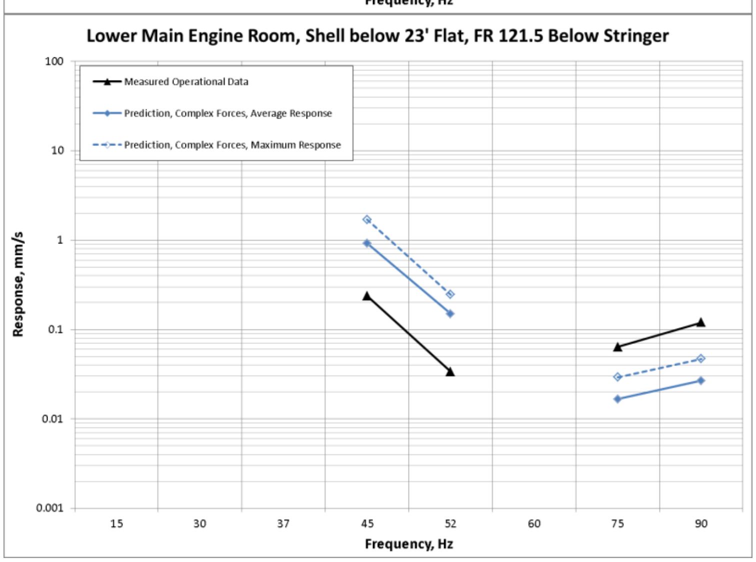
Lower Main Engine Room, Shell below 23' Flat, FR 121.5 Below Stringer
Measured Operational Data
Prediction, Complex Forces, Average Response
Prediction, Complex Forces, Maximum Response
Response, mm/s
100
10
1
0.1
0.01
0.001
15
30
37
45
52
60
75
90
Frequency, Hz

Figure 161: Predicted vs. Measured Response to Genset Excitation, Tanktop Level, Aft Bulkhead Location

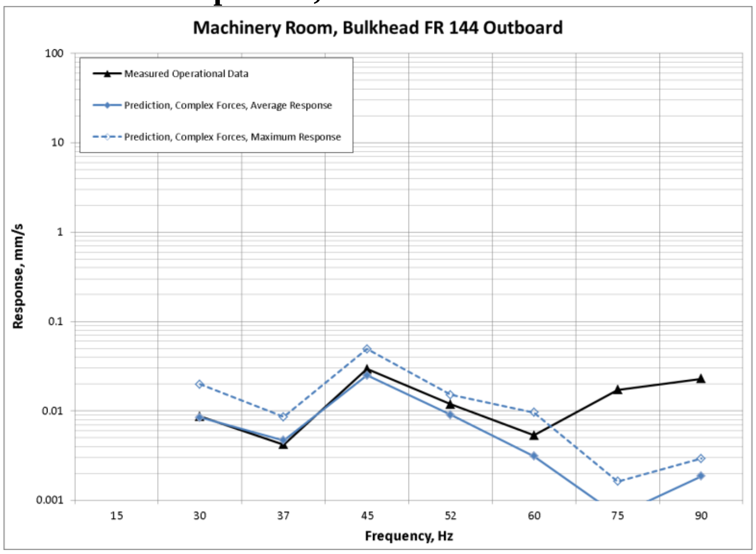

Table 49: Response Magnitude Ratio for Genset Operation, Average Response Method, Complex Forces

Location	Frequency, Hz							
	15	30	37	45	52	60	75	90
Side Shell Above 23' Flat								
FR 121	2.6	2.4	2.0	1.6	2.3	1.5	N/A	1.5
FR 126	2.3	1.1	1.2	1.3	1.4	1.0	3.2	1.4
FR 131	2.5	1.6	1.4	1.1	1.3	1.7	2.2	8.9
23' Flat Deck								
FR 126.5	2.2	4.8	3.3	4.5	6.3	1.4	1.4	4.8
FR 132.5	4.0	1.1	1.9	1.9	1.7	1.0	4.3	118
2nd Deck								
2nd Deck, FR 125.5	61	N/A	1.5	2.2	3.8	4.7	4.4	4.1
Side Shell Below 23' Flat								
FR 132 above Stringer	2.0	N/A	2.7	1.2	4.6	N/A	38.2	11.2
FR 131.5 above Stringer	2.5	N/A	6.6	1.2	1.2	2.8	5.9	2.9
FR 131.5 below Stringer	3.5	N/A	7.6	2.8	3.6	1.1	3.7	2.5
FR 127 above Stringer	3.0	N/A	1.0	3.2	1.5	3.2	12.7	19.0
FR 125.5 above Stringer	2.9	1.5	2.2	1.1	1.7	1.6	N/A	3.0
FR 121.5 below Stringer	N/A	N/A	N/A	3.9	4.5	N/A	3.8	4.5
Aft Bulkhead Below 23' Flat								
FR 144 Outboard	N/A	1.0	1.1	1.2	1.3	1.7	25.2	12.3

Table 50: Response Magnitude Ratio for Genset Operation, Maximum Response Method, Complex Forces

Location	Frequency, Hz							
	15	30	37	45	52	60	75	90
Side Shell Above 23' Flat								
FR 121	2.5	1.5	2.9	3.3	1.4	2.8	N/A	1.1
FR 126	2.0	1.5	1.3	1.6	2.0	1.4	1.2	1.9
FR 131	2.1	1.1	1.2	1.9	2.2	1.2	1.2	4.5
23' Flat Deck								
FR 126.5	1.8	7.6	8.2	6.4	12.1	1.2	1.1	2.9
FR 132.5	3.3	1.7	1.2	3.2	2.4	2.2	2.3	83
2nd Deck								
2nd Deck, FR 125.5	48	N/A	2.8	1.4	1.9	2.2	2.3	1.6
Side Shell Below 23' Flat								
FR 132 above Stringer	1.3	N/A	1.5	2.0	10.5	N/A	21.3	4.7
FR 131.5 above Stringer	1.7	N/A	3.6	1.5	3.2	1.4	3.2	1.9
FR 131.5 below Stringer	1.6	N/A	13.7	5.3	6.0	2.3	1.7	1.5
FR 127 above Stringer	2.2	N/A	1.5	5.1	1.2	1.6	4.2	12.9
FR 125.5 above Stringer	2.1	2.3	1.3	1.8	4.3	1.5	N/A	1.9
FR 121.5 below Stringer	N/A	N/A	N/A	7.2	7.3	N/A	2.2	2.6
Aft Bulkhead Below 23' Flat								
FR 144 Outboard	N/A	2.3	2.0	1.7	1.3	1.8	10.6	7.8

Overall the 'average' response method seems to produce better results than the 'maximum' response method. As was the case with the structure near the start air compressor (see Section 8.1) there are no strong peaks in the predicted transfer mobilities (not shown here) and therefore the benefit of the maximum response approach is not needed here[16].

Comparisons of the predicted responses using the 'complex' and 'simplified' genset forces (Table 47 vs. Table 48, respectively) are presented at selected locations in Figure 162. It is clear that the simplified forces increase the predicted vibration response over the 'complex' forces at all frequencies and locations. The increase in predicted vibration level changes as a function of frequency and position; the range was seen to span response ratios of 1.2 to 6, though on average the simplified approach predicts higher by a factor of 2-3. Though it is technically possible for the simplified approach to lead to a reduced level relative to the complex method (through a destructive interference effect at a given point in the structure), such results were not seen here and may not be practical for realistic sources.

[16] An exception is on the 2nd Deck near 15 Hz, where there is a large peak in response. However, as discussed previously this location and frequency is most subject to errors introduced as a result of inaccurate modeling of local machinery masses.

Figure 162: Comparison of Predictions using Complex and Simplified Genset Forces

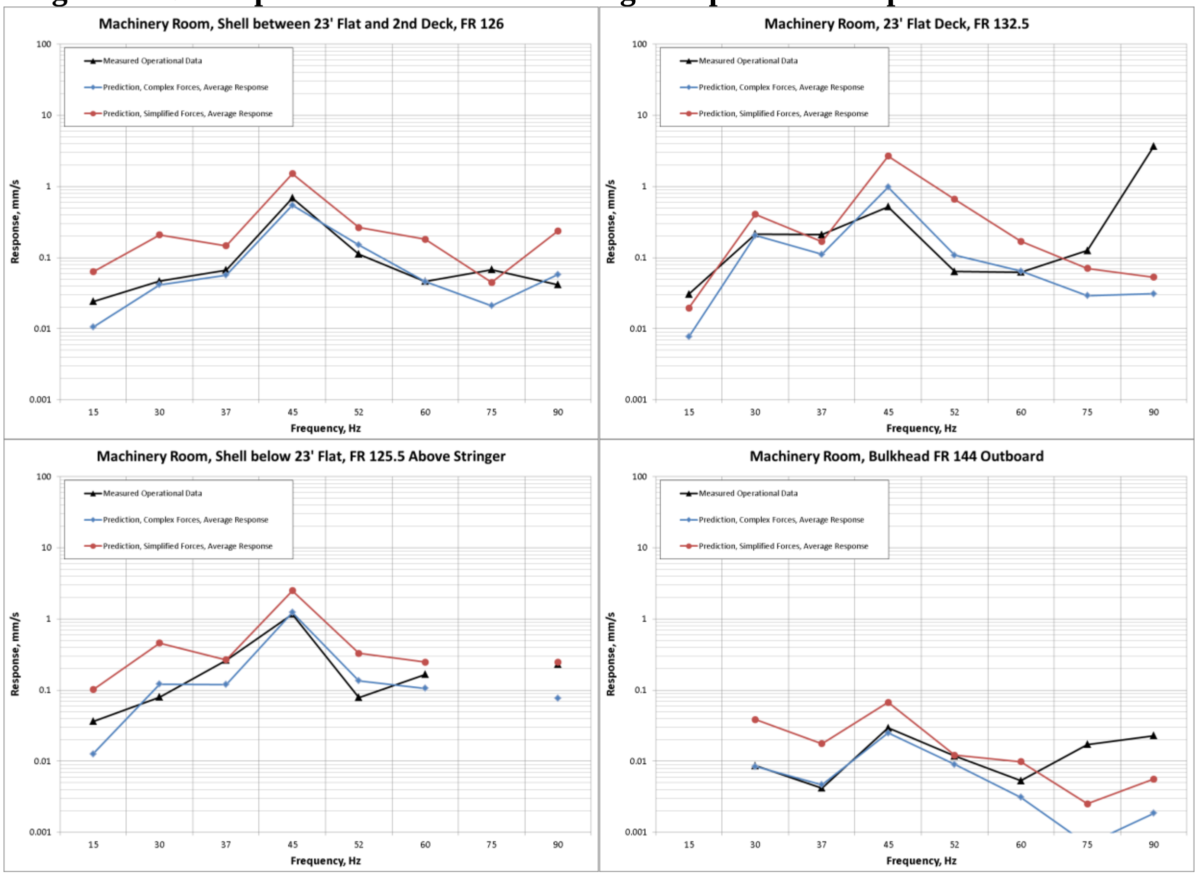

8.2.3 Summary of Genset Forced Vibration Analysis

The results shown in this section show reasonable correlation between the model and measured vibration response resulting from genset excitation at frequencies of 60 Hz and below. For locations that are not in contact with the ocean, the error in response is generally less than a factor of 3, with many location / frequency combinations having errors near or less than a factor of 2. Locations on the side shell that are in contact with the ocean also have good overall correlation (particularly at 15 and 30 Hz), though there tends to be one to a few frequencies where higher errors exist; this is likely due to errors in the method of applying water loading effects.

It is important to note that the model is a highly simplified version of the real structure. The extensive piping that exists under the 23' Flat is not included in the model at all. Many of the errors seen in these results are believed to be due either to issues with water loading or in the approximations/estimations made in modeling auxiliary machinery masses. While the modeling efforts described in this report indicate that inclusion of machinery mass is necessary, at least for nearby response locations, the actual mass of these items was only approximated based on available information for similarly sized machinery.

These results show that items such as piping only play a secondary role at best with respect to vibration response of the structure, and models that ignore piping can still be used to generate reasonably accurate results. However, increasing damping loss factor values for damped structures is recommended.

As was found for the start air compressor (Section 8.1), the method of averaging the response over a +/-5% frequency range of each machinery tone produced results that were generally better than taking a maximum level over the same range. Again, the predicted structural response in the areas of interest did not show a singularly dominant peak in the transfer mobility, meaning that the ability of the 'maximum response' method in predicting such peaks was not needed, leading to generally higher vibration predictions (with greater errors, in this case).

The 'Above Mount Vibration' method of force estimation (Method 1) was shown in Section 8.1 to lead to good approximations of force and phase for resiliently mounted machinery. The same approach was used here, and also is seen to produce reasonable results. Unfortunately a rigorous check of the force data was not possible for this source as was done for the start air compressor.

The 'simplified' set of genset forces (which uses the average force magnitude across all force locations and all points in phase with one another) was seen to predict higher vibration levels than the 'complex' genset forces (each location has its own unique force magnitude and phase). The difference in the predicted vibration magnitude ranges from a factor of 1.2 to 6, though many locations showed an increase on the order of a factor of 2-3. Clearly the phase and force distribution of sources plays an important role in the response of the structure.

While the complex forces produce better results, such detailed information will not likely be available for every project, particularly at the design stage. The simplified forces (or a similar approach) are likely to be the 'best available' information for many design projects. It should be expected that this approach will likely lead to higher predictions of vibration.

8.3 Bilge Pump

The following sections discuss the force estimation and prediction of vibration response from the bilge pump. The model used for these analyses is the same as the model discussed in Section 7.6. Note that the side shell below the 23' Flat uses the approximation for water loading discussed in Section 7.6.

8.3.1 Force Estimation

The bilge pump operates at 1750 RPM, though there are some additional tones created by the unit. Vibration levels measured on the foundation in the vertical direction are presented in Figure 163. It is seen that there is a tone at roughly 30 Hz (as expected) though there is no tone at 60 Hz. Additional tones can be seen at 26, 48, and 52 Hz.

Tones can also be seen at higher frequencies though these tones were not discernable in the vibration data collected on the side shell (which were used as the response points for this investigation).

Figure 163: Foundation Vibration During Bilge Pump Operation, Vertical Direction

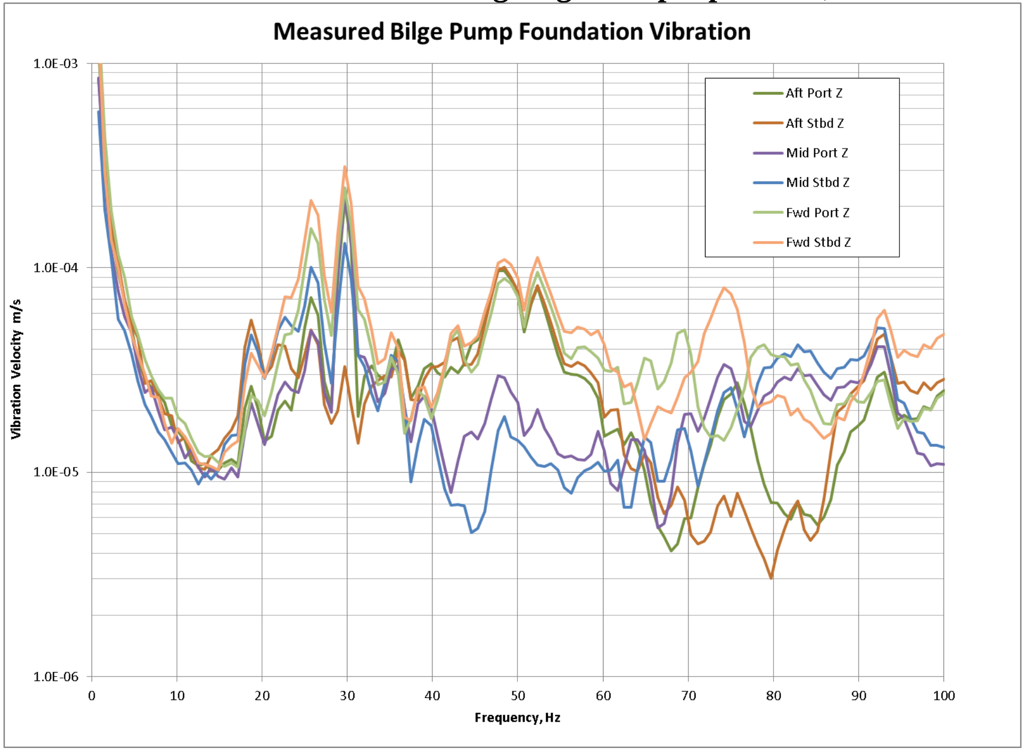

Although not shown here, levels in the transverse and longitudinal directions were lower than the levels in the vertical direction by a factor of 5-10 or more. As a result of this, combined with the difficulty in obtaining good impact data on the foundation (due to the presence of pipes and other items, as well as the size of the foundation), force excitation estimates were limited to the vertical direction.

Since this unit is hard mounted, Methods 1 and 2 cannot be used for force estimation purposes (see Section 6.3). Method 3, the 'Impact and Relative Vibration' method was the primary method of force estimation used here. Point mobility data shows good coherence at the foundation in the frequency range of interest (not shown here).

The forces obtained using Method 3 are shown in Table 51. Note that the phase relationships were obtained from the measured foundation velocity levels (cross spectra). It is believed that this is an appropriate approach in this case since the measured mobility data (impact data) shows a consistent phase relationship between force and velocity across all measurement points at each excitation frequency.

Table 51: Estimated Forces of Bilge Pump, Impact and Relative Vibration Method

Vertical Forces – Magnitude, lbf						
Frequency (Hz)	**Aft Port (Pump)**	**Aft Stbd (Pump)**	**Mid Port (Pump)**	**Mid Stbd (Pump)**	**Fwd Port (Motor)**	**Fwd Stbd (Motor)**
26	5.6	1.5	3.6	2.8	1.9	2.2
30	14.7	2.6	16.9	6.1	3.5	4.0
49	2.7	2.4	3.8	2.1	1.3	1.6
52	1.5	1.5	2.9	1.7	1.4	1.4
Vertical Forces – Phase, Degrees						
Frequency (Hz)	**Aft Port (Pump)**	**Aft Stbd (Pump)**	**Mid Port (Pump)**	**Mid Stbd (Pump)**	**Fwd Port (Motor)**	**Fwd Stbd (Motor)**
26	-174	-175	-2	0	0	0
30	-2	-23	-2	-20	0	-12
49	-176	-180	-177	164	0	1
52	-180	178	169	142	0	0

Inspection of the phase relationship between the different measurement points yields some interesting information about the nature of the vibration of this unit. At 30 Hz all points are essentially in phase, and the entire unit can be thought of as rigid. However, at 49 Hz the pump end is effectively out of phase with the motor end. Similar behavior is also seen at 52 Hz. This indicates that the pump and motor are not rigidly attached to each other. This can be inferred through inspection of the installation, where the pump and motor are only connected via the foundation and the shaft.

At 26 Hz, the aft end of the pump appears to be out of phase with the other measurement locations. This can be explained by picturing the pump as rotating about a point between its forward and aft feet, and the motor is moving in phase with the forward end.

Using this information, it can be inferred that a possible method of modeling the pump is not to treat the entire unit as rigid (as may be commonly done) but to treat the pump as one rigid mass and the motor as a second rigid mass. Clearly, this is a simplification in and of itself, and further sophistication can be added to the model such as adding a beam element for the shaft, or even explicitly modeling the pump and motor casings, etc. However, the suggested approach is simple and allows for the phase relationships shown above to be implemented in the model.

8.3.2 Vibration Response

Comparisons of the measured and predicted response on the side shell near the bilge pump during operation are shown in Figure 164. Both the 'average' and 'maximum' responses over a +/- 5% frequency window are presented. Note that the measurement data at several frequencies was not above background, and have been omitted in this report.

Figure 164: Comparison of Measured and Predicted Vibration Response to Bilge Pump Operation

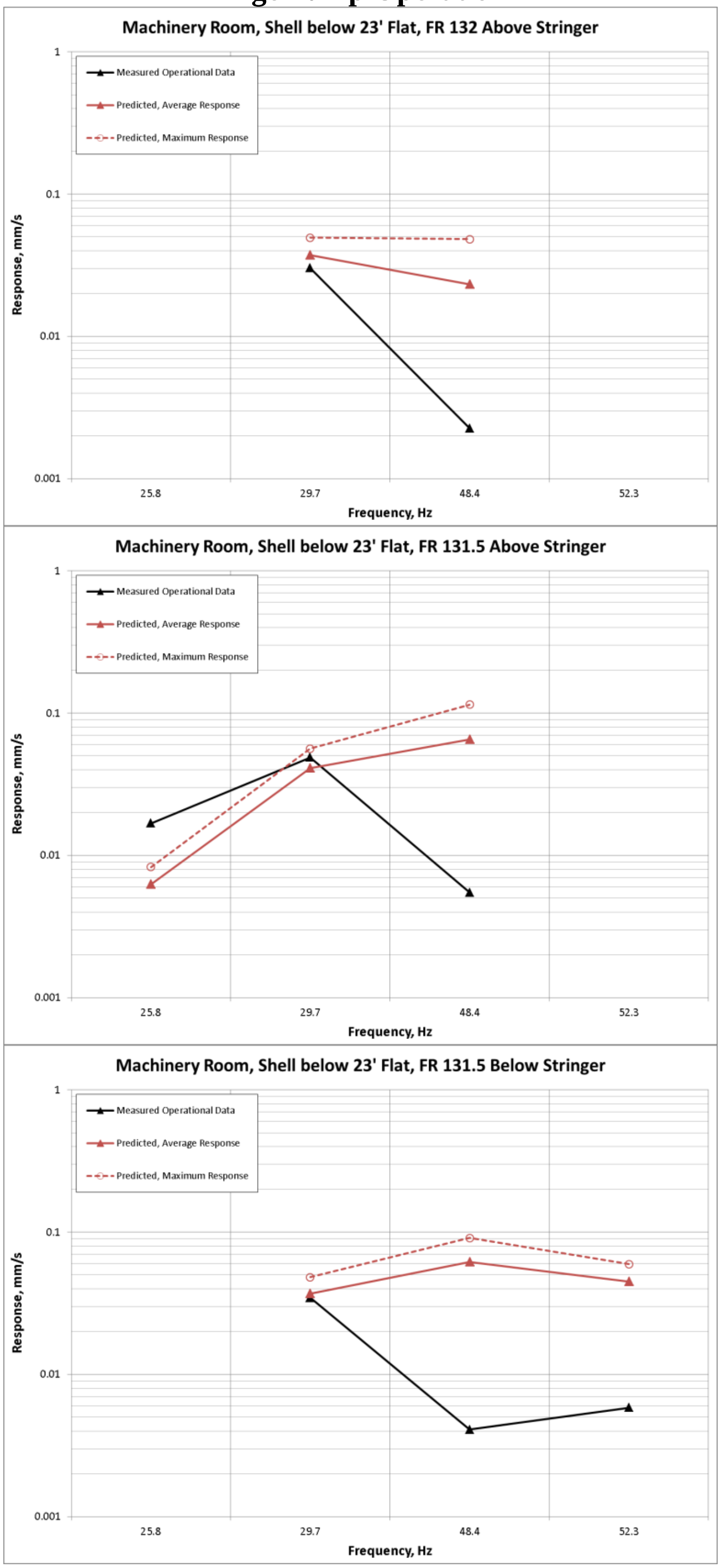

The correlation at frequencies below 30 Hz appears to be reasonable. At 29.7 Hz the 'average' method predicts the response nearly exactly at all three locations. The one available data point at 25.8 Hz shows a magnitude ratio of 2.7 for the 'average' response method.

At frequencies above 30 Hz the model diverges from the measurements significantly, with an over-prediction in all cases. Inspection of the measured transfer mobility shows a large dip in response at these frequencies. An example of the modeled and measured transfer mobility is shown in Figure 165. Note that the measurement data is of poor quality, particularly at frequencies near and below 20 Hz. However, it can be seen that the model predicts higher transfer mobility in the frequency range of 35-60 Hz, with errors on the same order as those seen in Figure 164 for the prediction of operational vibration response.

Figure 165: Comparison of Measured and Predicted Vibration Response to Bilge Pump Operation

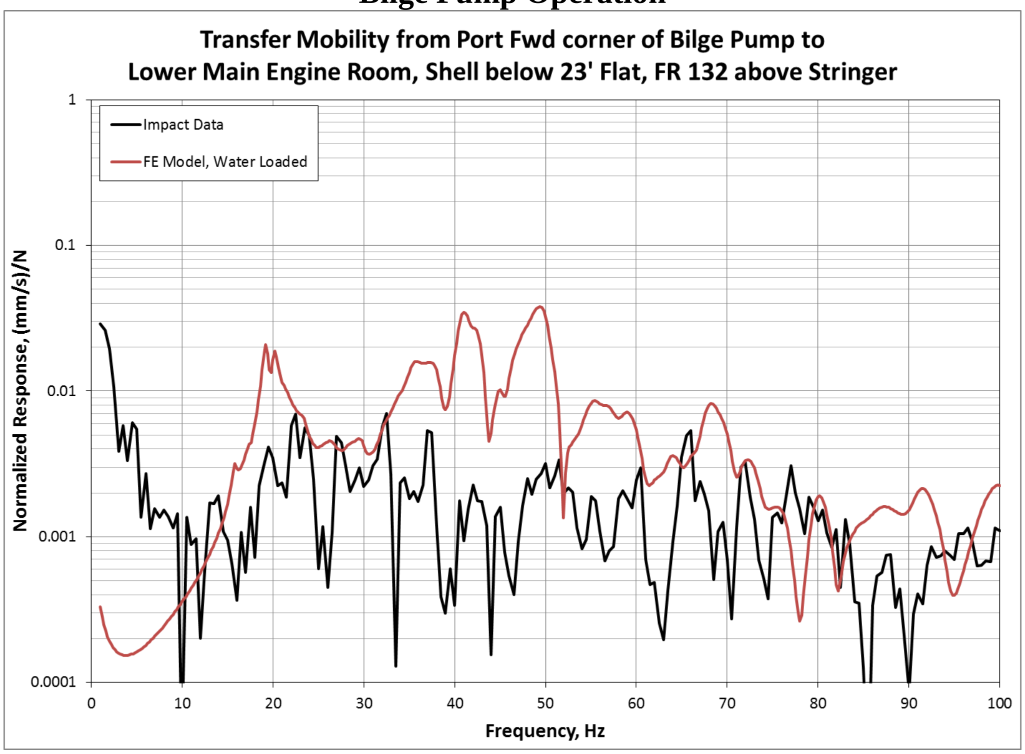

As was discussed in Section 7.6, the errors are believed to be primarily due to the uncertainty in water loading from the ocean. It is also possible that there are errors in the force estimation procedure, though based on the results of Section 8.1 these errors are believed to be lesser in magnitude than the errors in the model.

8.3.3 Summary of Bilge Pump Forced Vibration Analysis

In Section 7.6, it was found that the predicted side shell mobility was accurate at frequencies below 30 Hz, at least for the location on the stiffener, when mass is added to the side shell plating to simulate the effects of water loading. The results presented here for bilge pump vibration response predictions are consistent with these findings, and extend to plating locations as well.

Errors in the predicted response at higher frequencies are large. It has been shown that these errors are most likely related to the inaccuracies of the water loading approach used here. Again, more refined methods for applying water loading are recommended.

The similarity of the vibration response at frequencies below 30 Hz is an indication that the ‘Impact and Relative Vibration’ method of force prediction (Method 3) can be used to obtain reasonable estimates of forces imparted by hard mounted machinery, though further investigations would be needed in order to obtain strong conclusions.

The measured operational phase data suggests that for this pump/motor combination, the pump and motor should be modeled as two separate masses connected to the foundation by rigid elements. This is certainly an approximation that will break down at higher frequencies, though it appears to be reasonable at least for the analysis frequency range (up to 50 Hz in this case). These masses should be included in the model when applying forces of the operating machinery.

PART III – CONCLUSIONS

9.0 OVERVIEW

The objective of this study is to develop a set of recommendations on how to perform shipboard vibration modeling using finite element methods, with a focus on determining what factors are most important when modeling and what items can be ignored and still obtain reasonable accuracy. Modeling accuracy will always be subject to mesh resolution, stiffener and plating element selection, structural and mass approximations, damping and water loading estimations, and even accurate vessel information, among other factors. However, by using appropriate modeling and analysis techniques it is possible to perform predictions which can be used to assess of vibration levels in new builds and design appropriate mitigation approaches.

It has been shown that with reasonable modeling effort and accurate input information the following accuracy can be achieved for a majority of structures:

- Prediction of resonance frequencies for local ship structures to within 5-10% or less.
- Prediction of local response magnitudes to known input forces and machinery sources within a factor of 2-3, with results often being less than a factor of 2.

This accuracy was seen in many examples of local structural vibration from both impact testing and machinery induced vibration.

It must be recognized that prediction accuracy is subject to several limitations. For the *STATE OF MAINE* discussed in Part II of this report, it was found that this accuracy could be achieved at most locations for frequencies up to approximately 60-70 Hz, though this frequency limit depends strongly on the specific structure that is being modeled.

In order to generalize these results it is useful to identify the mode order where accuracy can be achieved instead of a specific frequency range. It has been found that accuracy can be obtained for the first several local modes of a structure, as determined through investigation of point mobilities. (Note that many modes will exist throughout the vessel for most frequency ranges of interest. The local modes of interest here are those that would be highly excited at a particular point by excitation at that point.) Accuracy typically worsens as the complexity of modes increases. At frequencies with lower accuracy, plating motion was seen to be significant relative to stiffener motion and full wavelengths occurred in the plating between stiffeners. Mesh density plays a strong role in determining accuracy, as the wavelength at a particular frequency will need to be spatially represented in the model.

Two factors have been identified as leading to the greatest uncertainty when creating and analyzing finite element models: effects of water loading and localized masses of machinery and equipment. The uncertainty due to water loading effects was seen to produce large errors at some frequencies where accurate results would otherwise be possible, and limits the frequency range where accuracy can be achieved. Water loading effects are complex and frequency dependent; they were not studied in detail as part of this effort. More advanced methods than those investigated here are recommended for calculation of appropriate masses. (Further study into appropriate methods of accounting for mass loading effects is recommended). Fortunately, the impact of water loading was seen to have more of a local effect than a global effect, at least for the structures and sources analyzed as part of this effort.

Localized masses can produce significant changes in vibration response at locations that are ‘close’ to or on the structures where such masses are applied. Analyses reported in both phases of this effort have illustrated this effect. Machinery and equipment masses were seen to affect vibration responses primarily on deck structures that were directly adjacent to these items, or at adjacent bulkhead locations. In many cases it was found that receiver locations located several frames away from large masses did not show significant sensitivity to their presence. (Note that in the Phase II study, large errors were seen in some cases due to limited information on auxiliary machinery.)

Factors such as mesh density, model extents, stiffener modeling methodology, and appropriate levels of damping were seen to be important in developing accurate models; recommendations for modeling are provided in the following section. Conversely, items such as piping, handrails, small foundations of antennas, lighting and cableways, and other similar details were not found to have a large impact on the model results. This is fortunate, because such details are often not available early in the design stages of a vessel and modeling of these details would be laborious.

The accuracy of modeling is also subject to the approach used to analyze model results. It should be expected that a model will have some level of error; the analysis approach can be selected and modified as needed to minimize the negative impacts of these errors on the resulting prediction. Additional details are provided in Section 10.10 below.

This study focuses on excitations from machinery sources; methods for identifying and modeling machinery source inputs are provided in the following section. It is important to note that propeller excitations can also be a significant source of vibration on many vessels. Propeller excitation was not investigated as part of these efforts. However, it is reasonable to expect that similar levels of accuracy as noted above can be obtained when the appropriate pressures and forces from propeller excitation are applied to a model that is created using the recommendations given in the following section.

The following sections provide a summary of the recommended modeling techniques for finite element modeling of vibration on ships. These recommendations are based on the results described in Parts I and II of this report.

10.0 RECCOMENDATIONS FOR MODELING

10.1 Mesh Density

Higher mesh densities have been shown to produce improved accuracy, particularly for weaker structures and at higher order modes of structures. Higher mesh densities will also result in larger models and increased model development and analysis time. Note that in some cases increasing mesh density does not result in a significant improvement in accuracy, such as at frequencies corresponding to the lowest order local structural modes, and therefore a balance between model size and accuracy should be determined based on the needs of the modeler.

It is generally recommended that the mesh be no coarser than the "2x density" mesh discussed in Section 2.2 and Table 2. This means that there should be at least 2 elements between adjacent stiffeners. A "4x density" mesh is preferred (4 elements between stiffeners), particularly when accurate modeling of higher order modes is required and when model sizes do not become prohibitively large. Minimum mesh density models are not recommended except when performing an analysis that is limited to whole body modes.

In one example in this report – the Battery Room Bulkhead, Section 7.5 – it was shown that an "8x density" mesh was useful in further improving the accuracy of results, particularly for the response on plating. In this case the 4x mesh resulted in a situation where there were 6 elements per wavelength or less at the higher order local modes of the structure.

However, as discussed in Section 7.5, the primary benefit of the 8x mesh was a reduction in the error of predicted peak response frequencies for higher order local modes. The error in the 8x mesh was minimal, while the 4x mesh produced errors that were 10% or less. The error in predicted magnitude did not change appreciably when moving from a 4x to 8x mesh. Therefore, it is possible that in this case the 4x mesh could be a better choice when balancing model size vs. accuracy, particularly when entire vessels or large sections of vessels are to be modeled. (For example, creating an 8x mesh of the truncated Machinery Room model would have resulted in prohibitive solution times on the computers used for this analysis.)

Ultimately, it may be beneficial to perform a sensitivity study of selected areas of the model to determine the appropriateness of the mesh density. This could be performed by selecting an appropriate section of the model and analyzing the point mobility for varying mesh densities. If the frequencies of peak responses at a given location show significant shifts as a result of a finer mesh, it may be beneficial to use the finer mesh in that area. However, this must be balanced with the solution times required to solve larger models. Selection of appropriate analysis methods can also assist with these tradeoffs (see Section 10.10).

10.2 Element Types

10.2.1 Plating Elements

It was shown in Part I (Section 3.3) that 4-noded, square or rectangular plating elements are preferred over 3-noded triangular elements. (Higher order plating element formulations were not investigated here.) However, any realistic mesh will require the use of some triangular elements, including the meshes discussed throughout this report. The occasional use of triangular elements does not appear to significantly degrade model accuracy. It is recommended that 4-noded plating elements be used whenever possible and 3-noded plating elements be used only as needed.

10.2.2 Stiffener Elements

Conventional stiffened plate ship construction makes use of both "large" and "small" stiffeners. Large stiffeners have webs that are on the order of ½ to 1x frame spacing or larger. For the *STATE OF MAINE*, the webs of large stiffeners were typically on the order of 16" deep or larger (greater than half of frame spacing), while the webs of small stiffeners ranged from 2" to 9" deep.

It is generally recommended that large stiffeners be modeled using plate elements for webs and beam elements for flanges. The modeling of large stiffeners with plates is strongly recommended on curved hull sections where the stiffeners tied to the floors. Minimal improvement is expected by modeling flanges with plate elements (for the frequency range investigated here).

Small stiffeners can be modeled using the same approach, though the accuracy noted above was obtained by modeling small stiffeners entirely as beams. The results of both the Phase I and Phase II analyses indicate that some improvement may be gained by modeling small stiffeners as plates, though this improvement is evident only for higher order local modes. Using beam elements alone is certainly easier than modeling webs with plates as the use of beams does not introduce additional nodes which need to be connected to adjacent structures. It also reduces model size and analysis run times as there are no additional degrees of freedom.

10.3 Model Extents

There are two items of concern when truncating a model. First, 'false whole body modes' of the truncated model may interfere with the analysis frequency range by producing peaks and dips in the response, confusing the interpretation of local structural vibrations.

In the case of the Steering Gear Room on the *STATE OF MAINE*, the effects of false whole body modes were present in both the modeled point mobility and transfer mobilities on the side shell. These modes were easily identifiable by changing model extents and boundary conditions. The false modes were present at frequencies below the first local mode of the structure and could be easily ignored.

However, it is possible that other models will have false modes that interfere with local modes, as seen for the small catamaran modeled in Part I of this report. In these cases the model must be extended outward from the area of interest to help move false modes down in frequency. In some cases it may be necessary to model the entire vessel.

A second concern with model truncation is model accuracy of local modes. If the model is not of sufficient extent then the results will simply be incorrect. As was seen for the Engine Lab bulkhead on the *STATE OF MAINE*, if the model includes only the immediate structure of interest without any surrounding structure the results will be vastly different from a larger model which includes structures 'far' from the area of interest.

All results discussed in Part II were taken from truncated models. In general, these models extended at least one major transverse bulkhead forward and aft (as applicable) from the area of interest, containing both the source and response locations. The models also extended at least one deck above and below the area of interest. In all cases the results for models discussed in Part II were verified to be nearly identical between truncated and non-truncated models in the frequency range of interest (local modes).

Based on these results, it is recommended that finite element models extend at least one major bulkhead/deck in each direction from the area encompassing both the source and locations where the vibration response is to be calculated. It is also recommended that the full width of the vessel be modeled to avoid complications with symmetry and anti-symmetry boundary conditions. Larger models may be necessary if false whole body modes interfere with local modes in the frequency range of interest.

10.4 Boundary Conditions

If the model extents have been properly chosen such that the model edges are 'sufficiently far' from the area of interest (per the previous section), then the choice of boundary condition should not adversely impact model results. In most cases for the models discussed in Part II, no constraints were applied to the model. This is by far the simplest boundary condition to apply, and accurate results can be obtained.

As indicated above, changing boundary conditions can be used as a tool to help identify the presence of false whole body modes.

10.5 Damping

The results of the damping investigations that were described in Part II of this report indicate that the damping loss factor for local structures (not treated with damping materials) can vary between values of 0.01 to 0.09. However, the results for a given structure, such as a bulkhead in a particular compartment, are more consistent. Several of the analyzed structures have a majority of modes with loss factors that fall within a range of 0.01 to 0.04.

The overall damping loss factor appeared to be essentially constant as a function of frequency (below 100 Hz for the analyzed structures). There were certainly variations in damping from mode to mode, but capturing these differences without the ability to test the structure would not be practical (if at all possible).

For most structures, a damping loss factor of 0.03 is recommended for all analysis frequencies, and was used for the majority of the models discussed here. This is consistent with the recommendations of ABS [2]. Use of a constant loss factor for all modeled frequencies helps to simplify the modeling process.

It is possible that structures with a joiner covering should use a higher damping loss factor (closer to 0.06). This seems to be the case for sheet metal joiner that is attached in the same manner as the joiner on the *STATE OF MAINE*. The Battery Room bulkhead, which was the only analyzed structure that contained joiner facing, had higher damping; levels varied between roughly 0.04 and 0.09. Other joiner and joiner attachment methods may yield different results. Further study is required.

Given the differences in measured loss factor for some structures vs. others, there may be other arguments to be made for increasing or decreasing the loss factor in some areas of the model. For example, the Steering Gear Room side shell had higher damping than the recommended value of 0.03, though the Transom (which was adjacent to the side shell structure) had slightly lower levels of damping. Strong conclusions as to which areas should be modified cannot be determined from this study alone.

Lastly, the values derived for damping material here were measured on a steel vessel. It is expected that values for aluminum will be similar, but some differences may exist. Further verification testing would be required.

10.6 Joiner and Insulation

The findings of this study indicate that joiner panels similar to those on the *STATE OF MAINE*, being sheet metal that is directly attached to the bulkhead (or overhead) being covered, should be modeled as a non-structural mass that is added to the structural plating being covered. The mass should be equal to the actual mass of the joiner. If insulation is present between the joiner and the bulkhead (or overhead) then this mass should also be added.

It is believed that this approach will break down and become invalid at a certain frequency. The results of the models shown here do not show such an issue, at least up to frequencies where good accuracy can generally be achieved (above roughly 60-70 Hz).

It is possible that other (newer) joiner types that have fewer and weaker connections to the covered structure would be decoupled at frequencies below 60-70 Hz. This would mean that their effective mass on the covered structure would be less than their actual mass, and different modeling approaches may be needed. Direct studies of such arrangements are recommended.

Conversely, the mass of insulation alone (without a joiner facing) was found to have a negligible influence on vibration response. This is based primarily on investigations performed on models of the *STATE OF MAINE* Machinery Room. It is believed that this mass can be neglected when modeling the local response of structures.

10.7 Auxiliary Structures and Masses

It has been shown that accurate results can be obtained without modeling some structures commonly present on vessels. This includes, for example, the extensive piping that exists on the *STATE OF MAINE* below the gensets and start air compressor as well as in areas close to the Machinery Room side shell below the 23' Flat. Similarly, small features such as handrails, small antenna supports, and structures used as piping supports, lighting, cableways, etc. were ignored in the modeling process; accurate results were still possible even with these omissions.

Conversely, inclusion of some items was seen to be beneficial to model accuracy, if not required in order to achieve reasonable results. This includes the mass of some hard mounted auxiliary machinery and equipment. Added masses are more significant when they make up a greater percentage of the local structural mass, as would be the case on aluminum vessels as compared to steel. Similarly, small structural details will have a greater effect on structures that are dynamically weak, such as the 'extra' box beams on the bottom of the Engine Lab bulkhead on the *STATE OF MAINE*.

It is generally recommended that masses of auxiliary machinery items and large equipment items be included in the model, particularly when they are hard mounted to the vessel. The general approach used here was to either smear the mass across appropriate plate elements or otherwise distribute the mass at appropriate nodes. Use of rigid elements may also be appropriate in some cases, particularly when the equipment is made of a thick steel casing.

However, it should be noted that in many cases the inclusion of masses for auxiliary equipment did not affect the response. When a significant change was noted as a result of adding these masses, the change primarily affected 1) response locations close to the mass or 2) locations somewhat removed from the mass but only at higher frequencies.

This conclusion implies that it may be possible to achieve accurate results by only including masses from large machinery items such as large pumps, compressors, etc. Refinement of this recommendation would require further study, but may result in decisions made on a case-by-case basis. It should be possible to inspect the impact of added mass for any given model by analyzing the point or transfer mobilities of a given model section.

The results of Phase I indicate that the modeling of doors, windows, and removable deck plating can have an effect on the predicted response spectrum. Again, these effects will be most significant in areas 'close' to the additional structure. The Phase II study indicates that the influence of doors is relatively small and localized to areas near the door. Based on these results, it is recommended that door frames be modeled (likely using beam elements) though the door itself can be neglected.

In Phase I it was seen that the addition of windows had a large effect on the vessel's vibration response since in that case the windows provided a significant degree of stiffening to the superstructure. In such cases modeling of windows will likely be beneficial, though the appropriate method of modeling the attachment of the window to the structure could not be studied further. For larger vessels it would likely be acceptable to neglect windows as long as the response on the bulkheads at locations adjacent to windows is of lesser concern.

Although the study of removable plates and similar structures is limited to the investigations performed in Phase I, it is recommended that these structures be included in the model. It should be reasonable to model these structures as if they were continuous structure (i.e. use the same nodes at the interface with removable plates and the primary structure). Additional investigation may be needed if the attachment method is complex.

The mass of fluids in tanks was seen to produce negligible changes in the response at all receiver points (far from tanks) during the Phase I study. Similarly, no tank loads (mass of fluid) were included in the modeling efforts of Phase II. It is expected that tank loads can influence the frequencies of whole body modes for some vessels. For this reason it is believed that the mass of fluids in tanks should be included, possibly through the use of a 'smeared mass' on plating. This approximation will likely have limitations at higher frequencies. As discussed above, the effects of these masses should have the greatest effect on local modes of the structures at locations where the masses are applied, and have less of an effect at other locations (other than for whole body modes).

It is noted that the effects of tank loads on the local response of the Engine Lab bulkhead on the *STATE OF MAINE* was investigated; tanks are located directly below this compartment. The addition of tank loads was found to have a negligible influence on the predicted point mobility of the test structure

Although cargo loads were not investigated here, similar conclusions discussed above for tanks should apply to large cargo masses. It is generally recommended that the mass of cargo be included in the model, though their impact may be more significant for the prediction of whole body modes rather than local modes.

10.8 Water Loading

Water loading presents an added mass to the structure in contact with the water [1]. The specific amount of mass that is added is a function of the vibration contour of the hull, depth of the plating below the waterline, and other factors. The effects of water loading are frequency dependent.

Water loading was seen in this analysis to be an important factor in achieving accurate results, primarily for structures that are in contact with the water. Identification of proper methods to calculate water loading effects could not be performed as part of this study. A rudimentary approach was used in this report of adding non-structural mass to the wetted hull until the first major peak in the point mobility was captured, though this is not a practical method for new builds.

It is recommended that more sophisticated approaches be used to calculate and apply water loading effects, such as through the use of coupled boundary element / finite element methods or explicit finite element modeling of the fluid domain. Further study is needed in this area.

It is important to note, however, that accurate results were obtained for structures that were not in direct contact with the wetted hull, including those structures that were immediately adjacent to wetted hull areas.

10.9 Machinery Source Definition

Machinery sources typically generate tones at their rotation rate and harmonics of rotation rate, though in some cases additional tones or broadband components are present.

In this report, all hard and resiliently mounted machinery sources were modeled by applying forces at mounting locations. This approach implies that the machinery sources are ‘force sources’ rather than ‘velocity sources’; in other words, it is assumed that the force on the foundation is largely independent of where the unit is installed, instead of the velocity being a constant regardless of installation location and details. While this aspect was not studied directly as part of this effort, experience indicates that highly stiffened foundations result in lower vibration levels for the same machinery item. A force source is consistent with this finding, where the stiffer foundation has a greater impedance (reduced mobility), and the same force applied to such a foundation will result in lower vibration levels.

In the case of resiliently mounted machinery, the machinery item itself was not included in the model. For hard mounted machinery, the mass of the machinery was included.

The hard mounted bilge pump on the *STATE OF MAINE*, which consists of both the pump itself and a motor, was found to act as two separate rigid masses. Although this is a singular result, it is consistent with the general makeup of the motor/pump system since the motor is connected to the pump only via the shaft (and the foundation). This result may be applicable to other machinery items that are made up of two or more separate components.

The most accurate modeling results are achieved when the relative phases of forces are included in the model along with the force distribution for each mounting location. A simplified approach of applying identical, averaged forces at all mounts with all forces being in phase can be used but will likely lead to increased levels of predicted vibration. If this is all that is available then the results should be understood to be conservative.

When determining appropriate forces for resiliently mounted machinery, the "Above Mount Vibration" approach (Method 1 of Section 6.3) appears to produce good results. This method is relatively easy to use, particularly when compared to other force estimation methods.

Unfortunately the same method cannot be applied to hard mounted machinery. The 'Impact and Relative Response' approach (Method 3 of Section 6.3) has been shown to produce reasonable results relative to other methods for resiliently mounted machinery, and the results of the bilge pump analysis indicates that it may also be appropriate for hard mounted machinery.

Both force estimation techniques require measurement of vibration and/or force on the unit itself. Measurements may be performed in a factory setting, or possibly on another vessel. Ideally, testing and results of these measurements would become a standard part of vendor provided information that is available to the buyer of marine machinery.

When source level information is not available it must be estimated. In such situations, it may be possible to directly transfer the forces from a similar machinery item to the current situation, or otherwise scale the forces based on differences in machinery size or other parameters. Note though that phase information may not scale or be applicable to other machinery items.

It is reasonable to expect that a database of source level information can be developed for different sources. For resiliently mounted sources, the above mount vibration levels would be needed for a given machinery item; the forces would then be scaled by the specific mount stiffness used in a particular application. For hard mounted sources, the same force determined during a particular test (performed when the unit was hard mounted) would be used in all situations as long as the mounting points are the same.

10.10 Response Assessment Methods and Frequency Analysis Range

As discussed in Section 4 and elsewhere in this report, it is recommended that analyses be performed over a range of frequencies above and below the actual vibration tone (or broadband excitation frequency range) produced by a machinery item. This is because the prediction at any single frequency is likely to be erroneous.

Two methods of results processing have been highlighted in this report: averaged response and maximum response. In both cases, the analysis is performed over a frequency range that encompasses the specific machinery tone; the same forces are applied at all analysis frequencies in this range. For the averaged vibration method, the response at a given location is averaged over the analysis frequency range. Similarly, the maximum vibration method uses the maximum predicted level over the same frequency range.

In Part II of this report an analysis frequency range of +/-5% of the machinery tone has been used. This was chosen in large part because the relatively high mesh densities used for these analyses, where errors in peak frequency were generally on the order of 5%. However, it may be beneficial to increase this range in some cases, such as when a lower density mesh is used. Furthermore, since the predicted frequencies of peak response tend to be higher than the actual peak, it may be prudent to bias the analysis frequency range to higher frequencies (such as +7/-3% of the machinery tone frequency).

The analyses presented in this report generally show the average vibration method produces results that are more consistent with measured data than the maximum vibration method. The maximum vibration method allows for the prediction of a potential worst case situation – the frequency of a tone produced by a machinery item closely matches the peak response frequency of a particular structure. This condition did not occur in this study, and arguably would not occur for a majority of cases on other vessels.

However, the condition where the frequency of excitation matches a frequency of peak response is of primary concern for all vessels, as this condition will typically lead to excessive vibration levels. For an analysis being performed during the design stage of a vessel it may be prudent to use the maximum response method first to assess the possibility of this condition. Any location that shows an excess using this method could then be further inspected to determine if there is a strong peak in the predicted transfer mobility from the machinery source to the location of interest within the analysis frequency range. If a strong peak is not predicted then the average vibration method could be used as a better prediction of the vibration response, and would reduce the likelihood of over-treating the vessel.

11.0 ACKNOWLEDGEMENTS

The authors would like to thank Mr. Andrew Girdler of Kvichak Marine Industries for his willingness to provide details of the vessel used in Phase I of this effort, and for his attempts in trying to make a measurement of the vessel take place.

The authors would also like to thank Captain Leslie Eadie, Chief Engineer Roger Lowell, Mr. Tony Margan, and the crew of the Main Maritime Academy Training Vessel *STATE OF MAINE* who facilitated and supported the measurements described in Part II of this report. The authors would also like to thank the Maine Maritime Academy and the US Department of Transportation for allowing these measurements to take place.

APPENDIX A – General Arrangement Drawings

PHASE I Vessel – KVI Catamran
(Drawings Supplied by Kvichak Marine Industries)

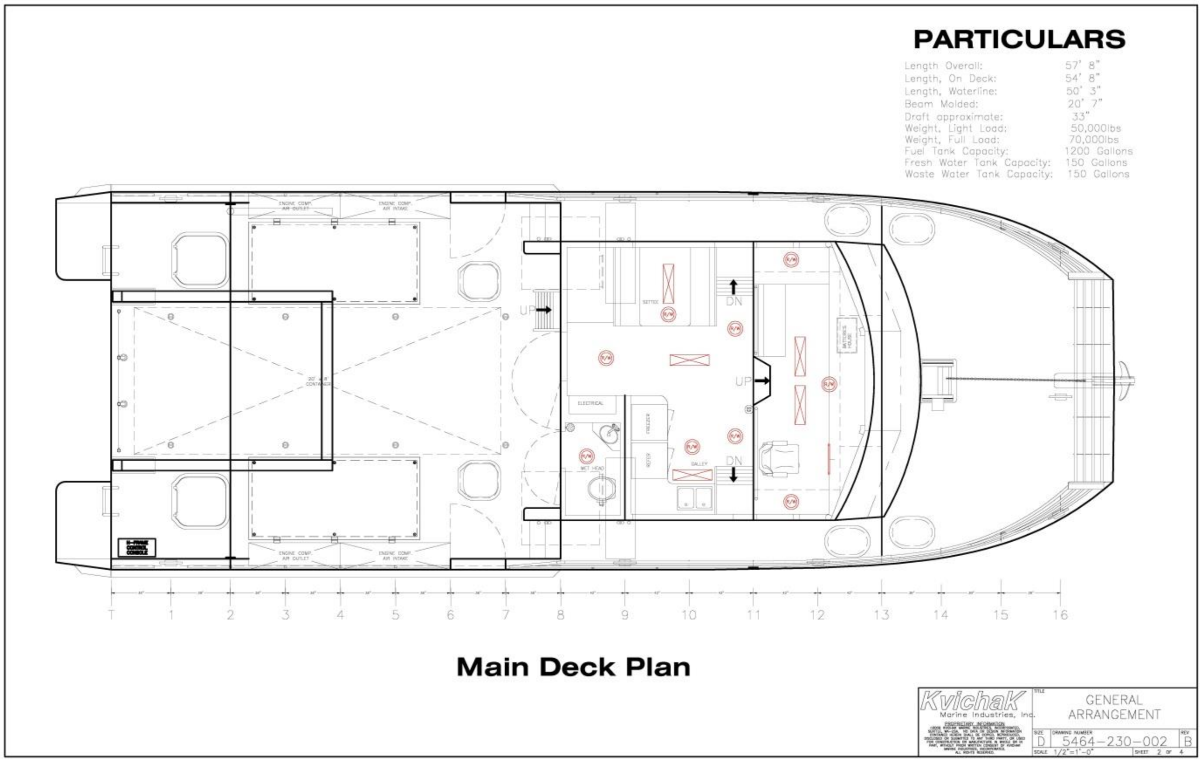

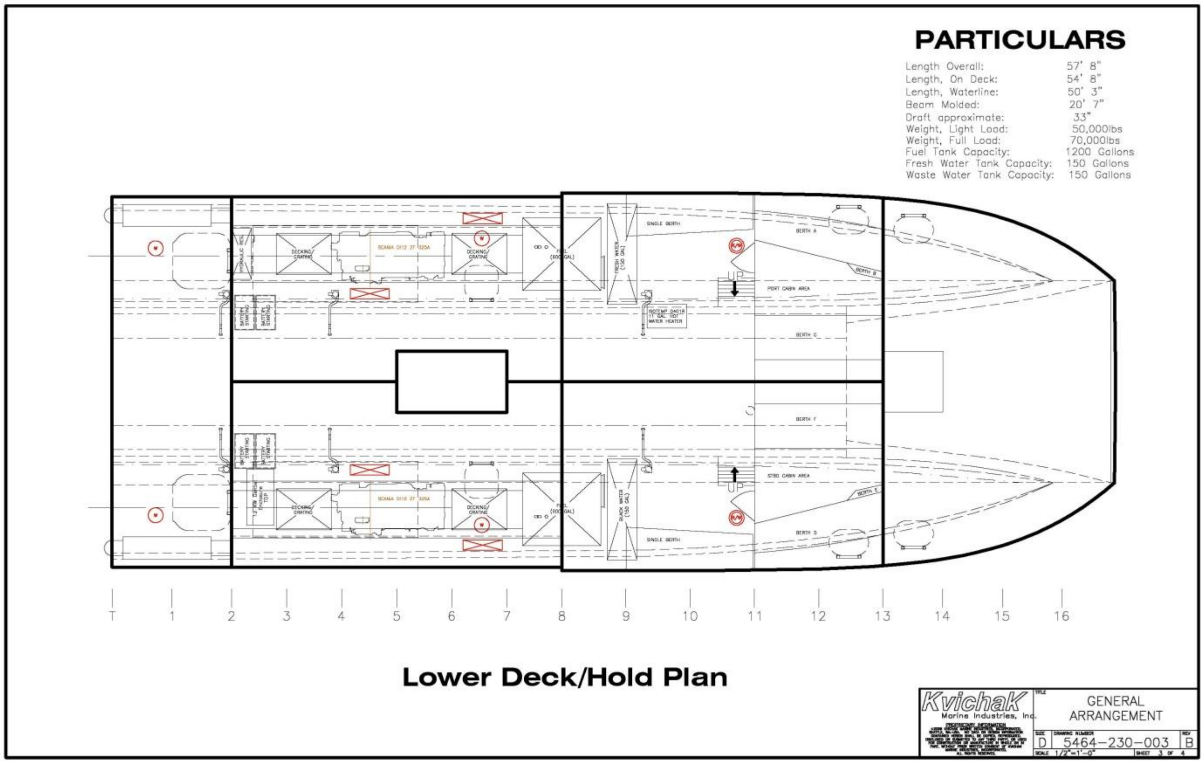
PARTICULARS
Length Overall: 57' 8"
Length, On Deck: 54' 8"
Length, Waterline: 50' 3"
Beam Molded: 20' 7"
Draft approximate: 33"
Weight, Light Load: 50,000lbs
Weight, Full Load: 70,000lbs
Fuel Tank Capacity: 1200 Gallons
Fresh Water Tank Capacity: 150 Gallons
Waste Water Tank Capacity: 150 Gallons
Lower Deck/Hold Plan
Kvichak Marine Industries, Inc.
GENERAL ARRANGEMENT
D 5464-230-003 B
1/2"=1'-0"

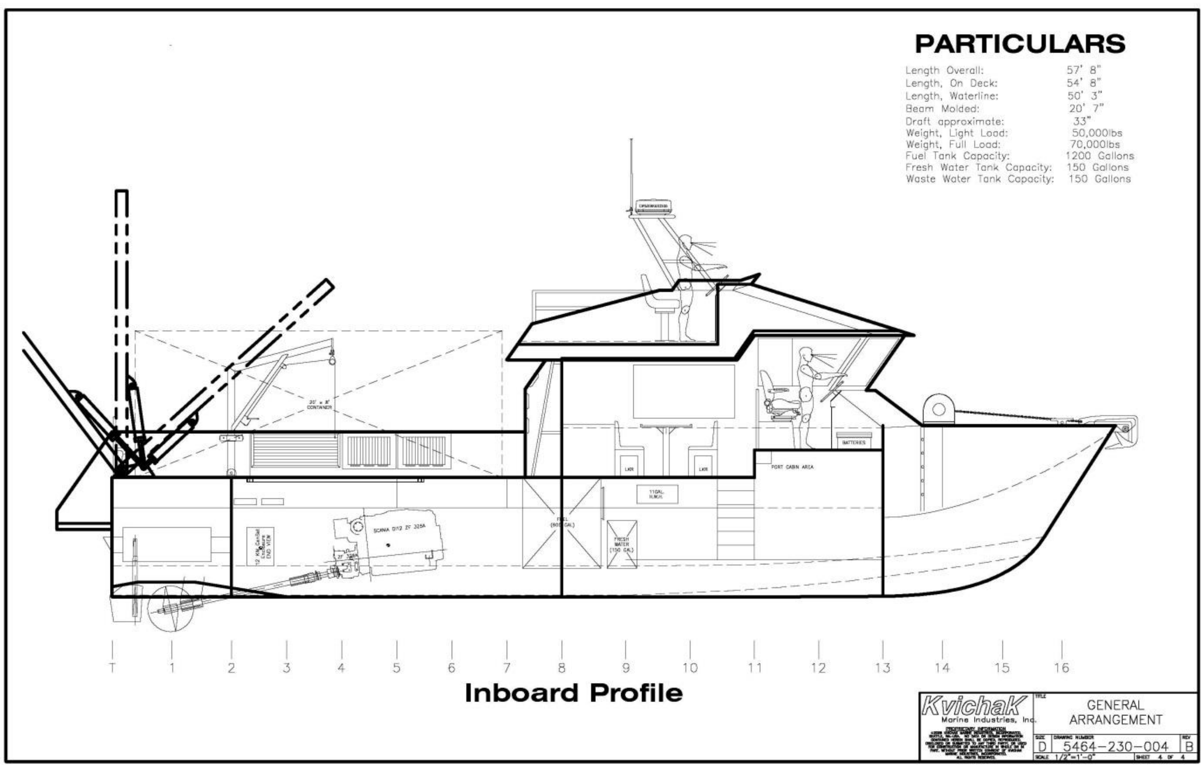
PARTICULARS
Length Overall: 57' 8"
Length, On Deck: 54' 8"
Length, Waterline: 50' 3"
Beam Molded: 20' 7"
Draft approximate: 33"
Weight, Light Load: 50,000lbs
Weight, Full Load: 70,000lbs
Fuel Tank Capacity: 1200 Gallons
Fresh Water Tank Capacity: 150 Gallons
Waste Water Tank Capacity: 150 Gallons
Inboard Profile
Kvichak Marine Industries, Inc.
GENERAL ARRANGEMENT
D 5464-230-004 B
1/2"=1'-0"

PHASE II Vessel – Maine Maritime Academy Training Vessel *STATE OF MAINE*
(Drawings Supplied by the Maine Maritime Academy)

General Arrangement

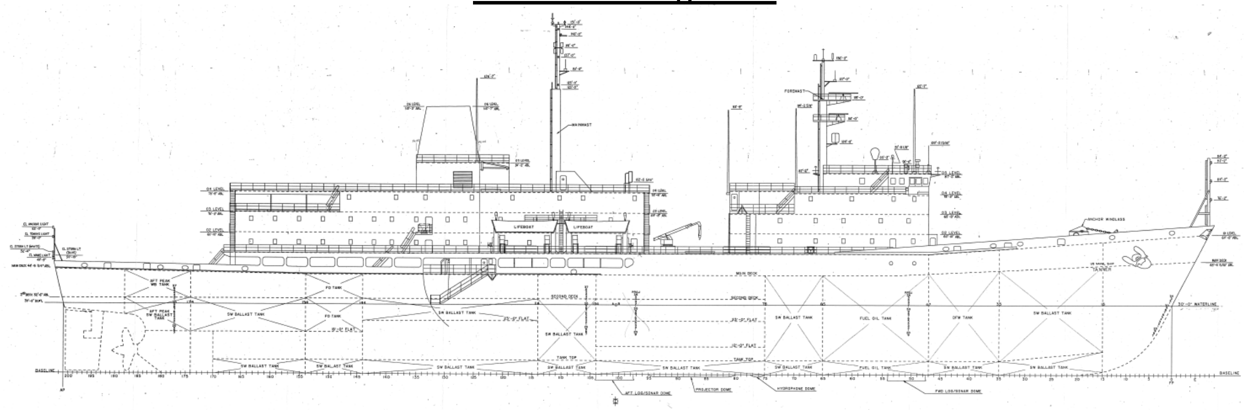

OUTBOARD PROFILE

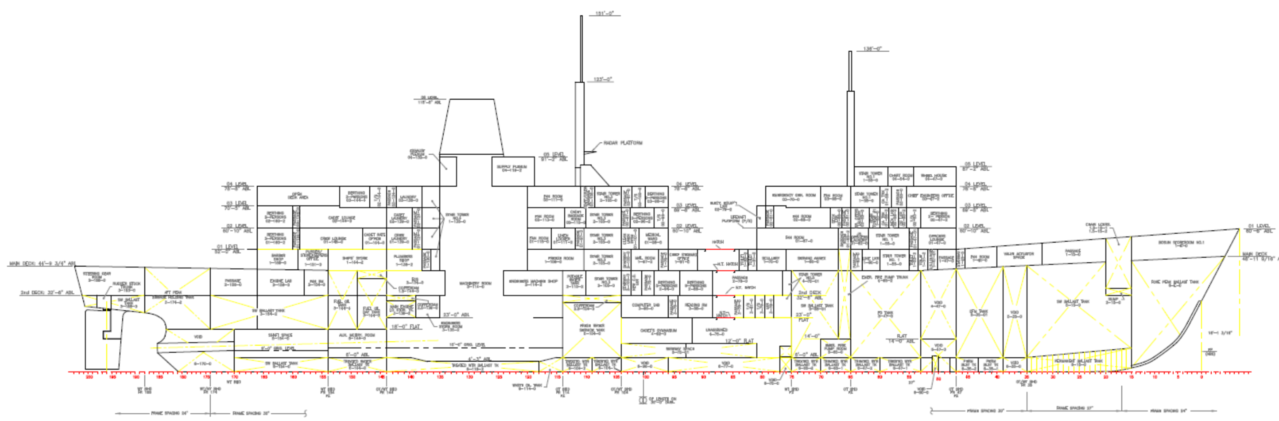

INBOARD PROFILE

05 LEVEL
91'–2" ABL AT CL

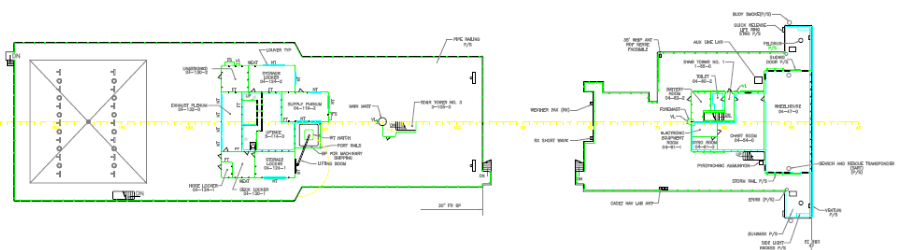

04 LEVEL
78'–8" ABL AT CL

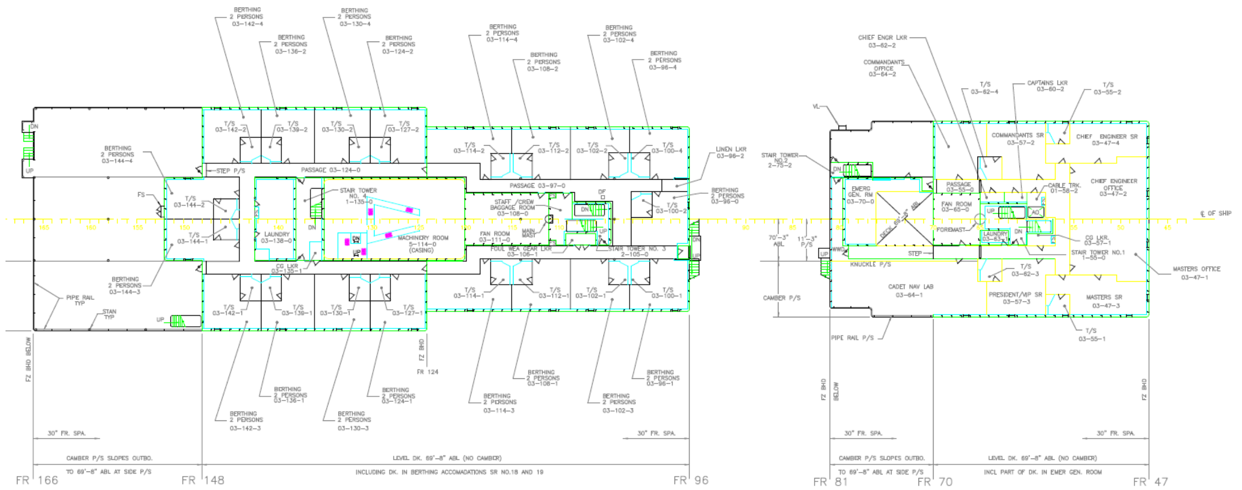

03 LEVEL

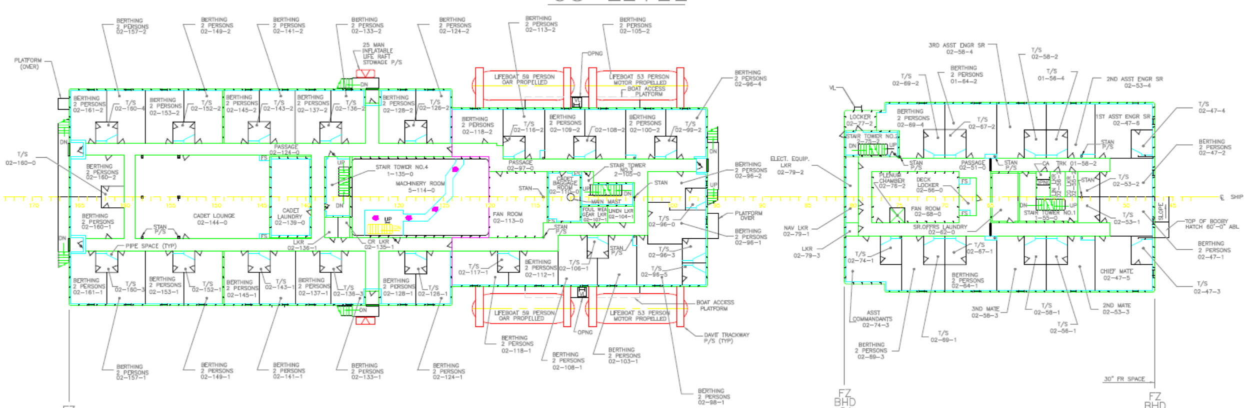

02 LEVEL

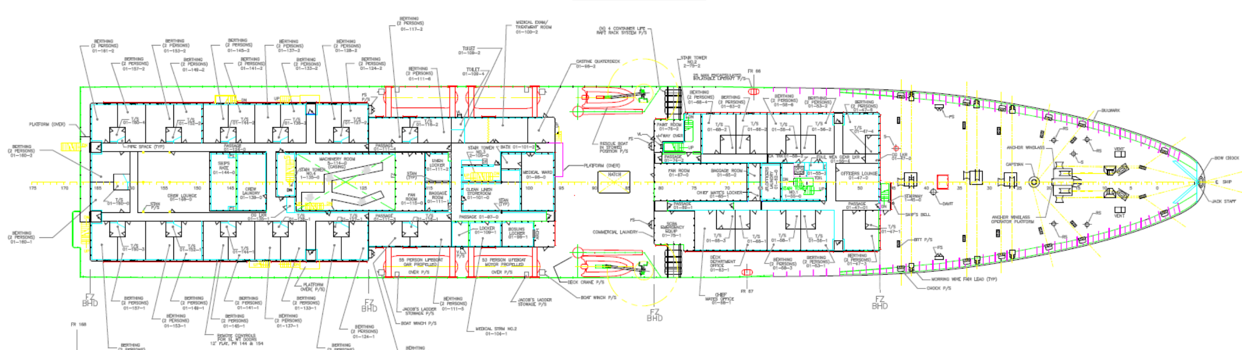

01 LEVEL

52'–0" ABL AT CL (FR 47 AFT)

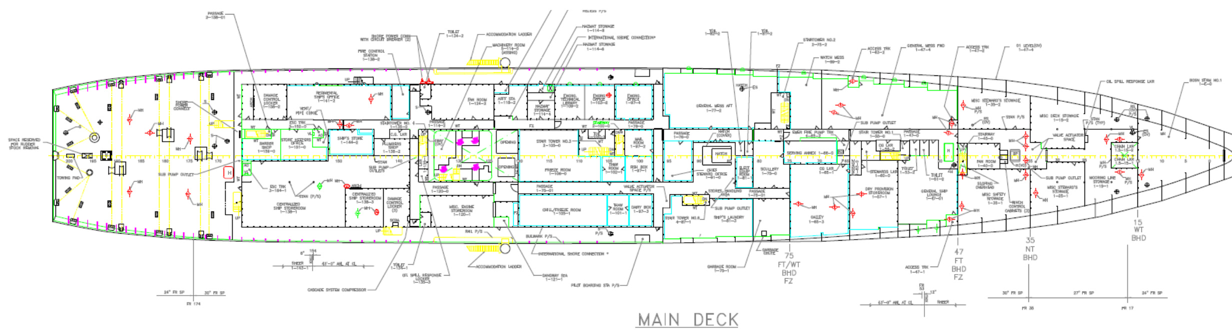

MAIN DECK

43'-0" ABL AT CL (BET FR 47 AND FR 154)

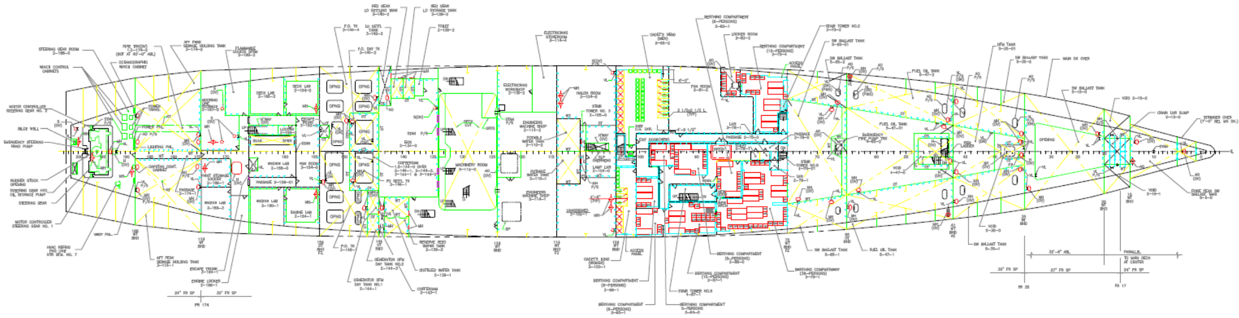

SECOND DECK

32'-6" FLAT

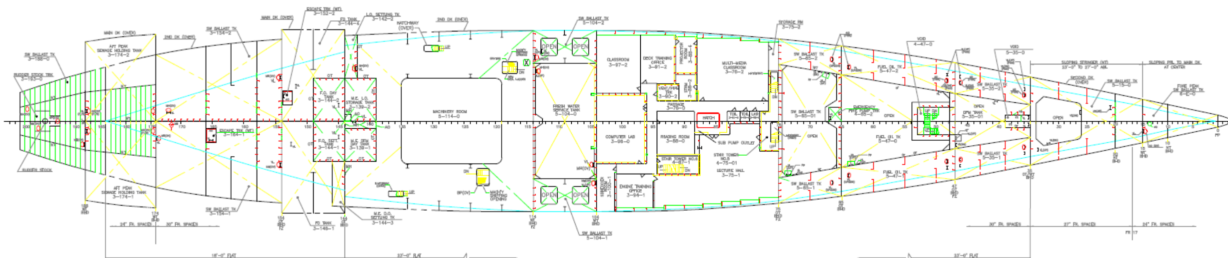

23'-0" FLAT

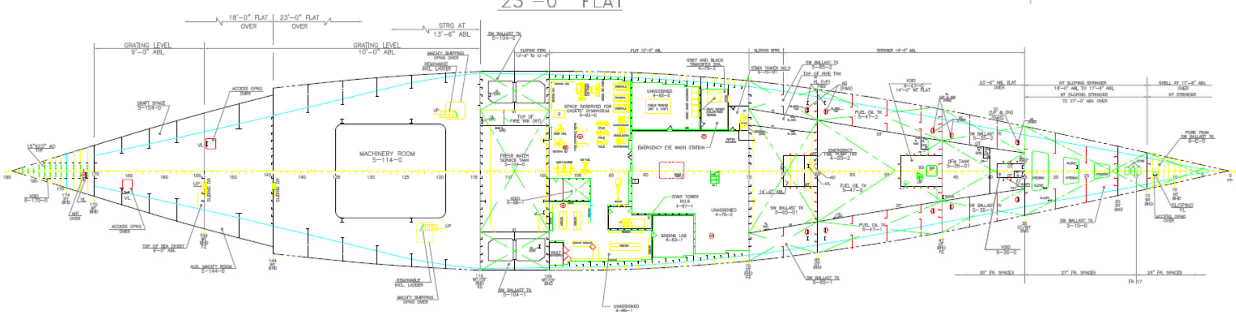

12'-0" FLAT

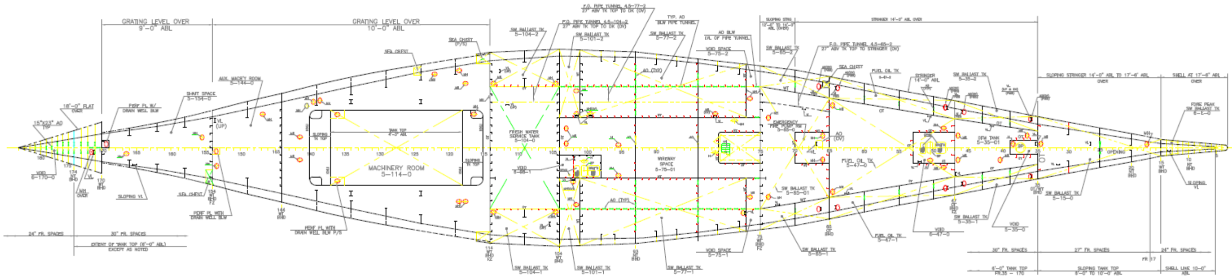

TANK TOP

Typical Outfitting - Superstructure

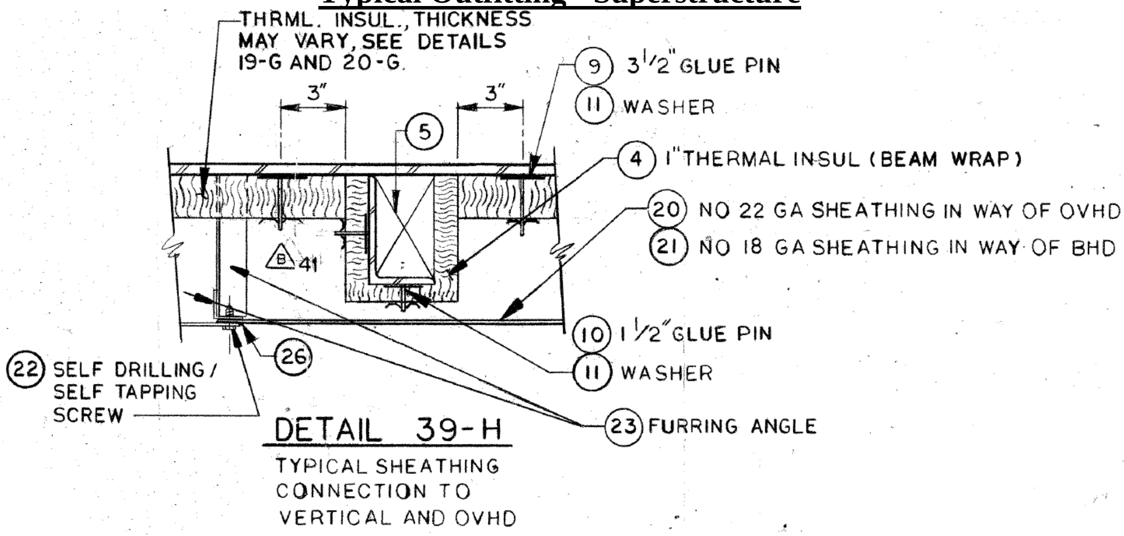

Structural Drawings
Engine Lab Bulkhead

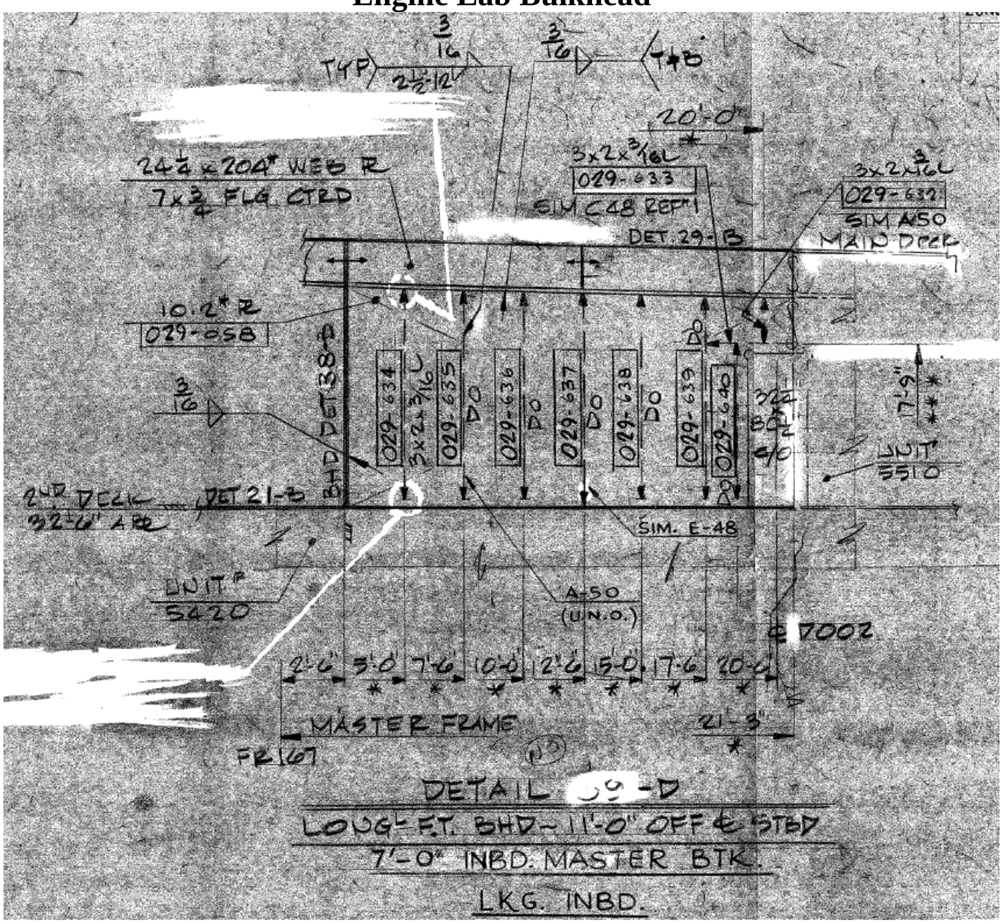

Steering Gear Room Side Shell

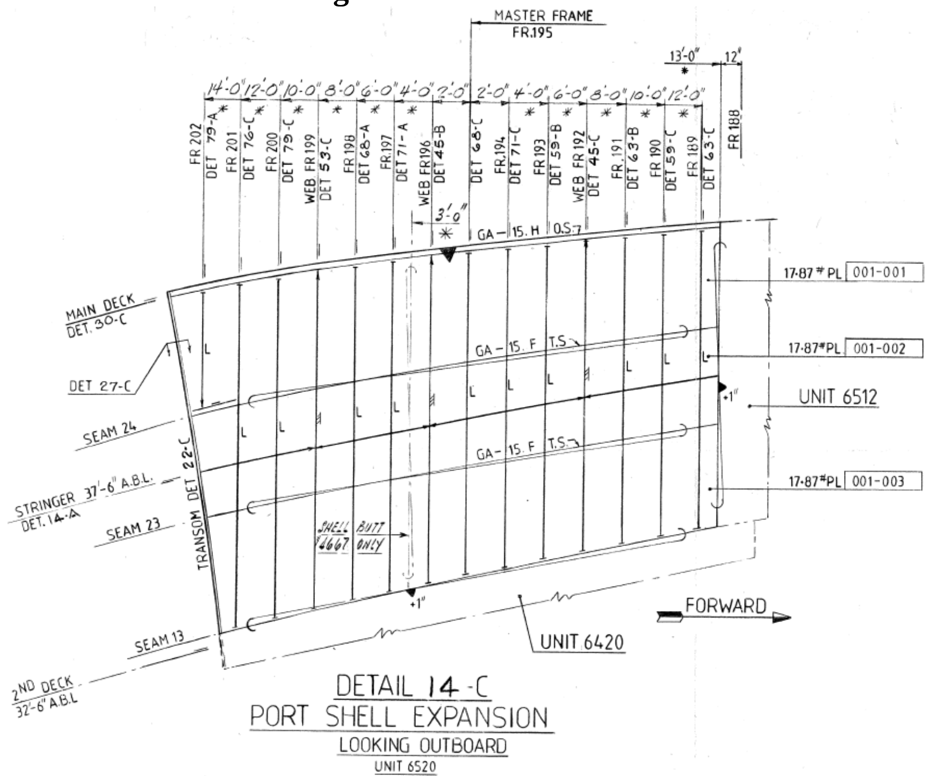

Transom

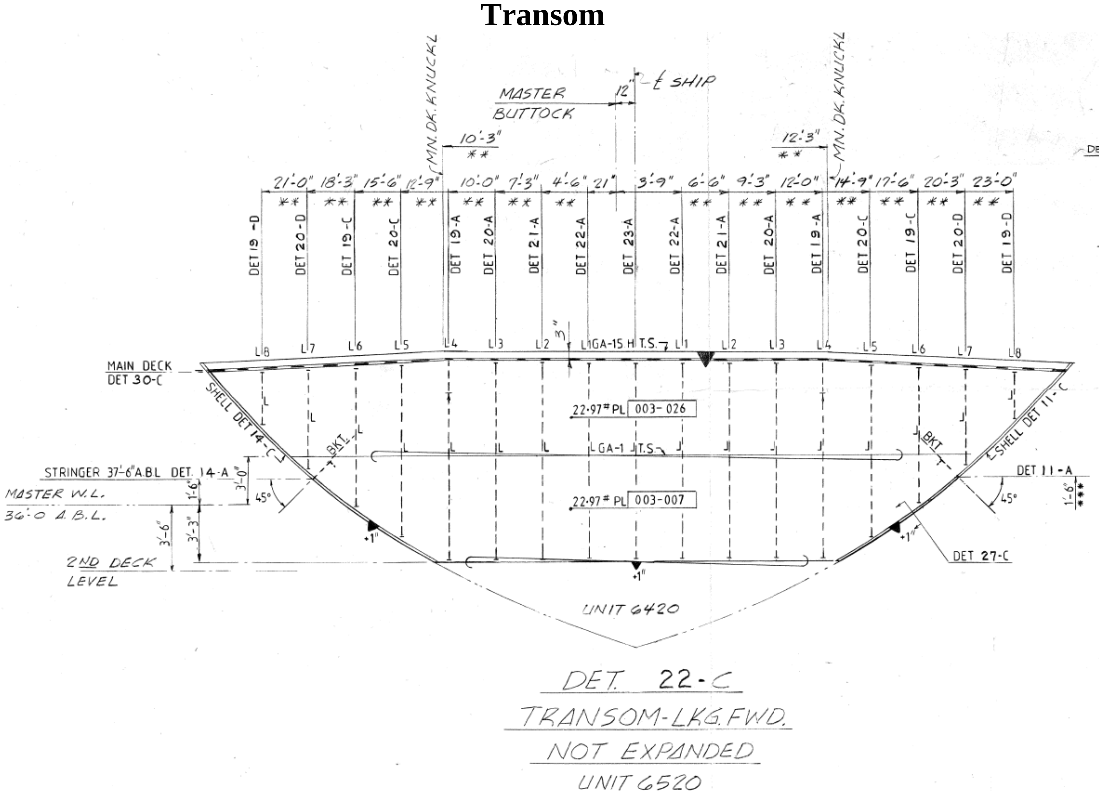

04 Deck Bulkhead

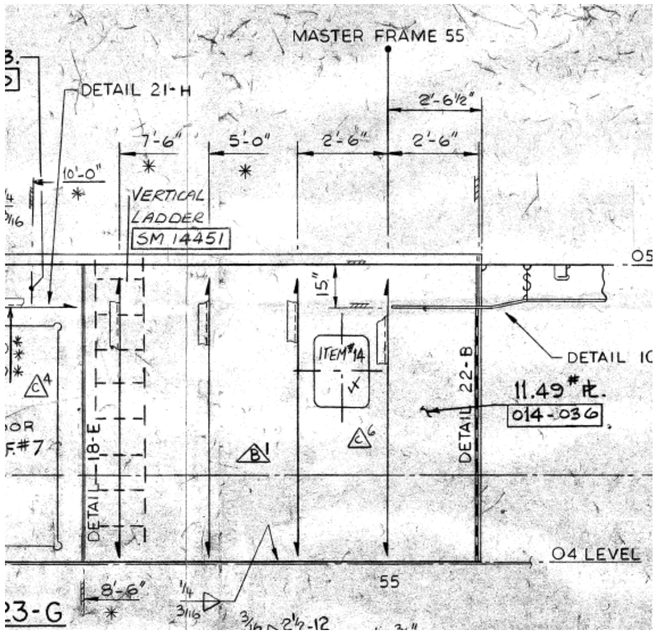

Engine Room – 23' Flat (Deck) IWO Genset #1

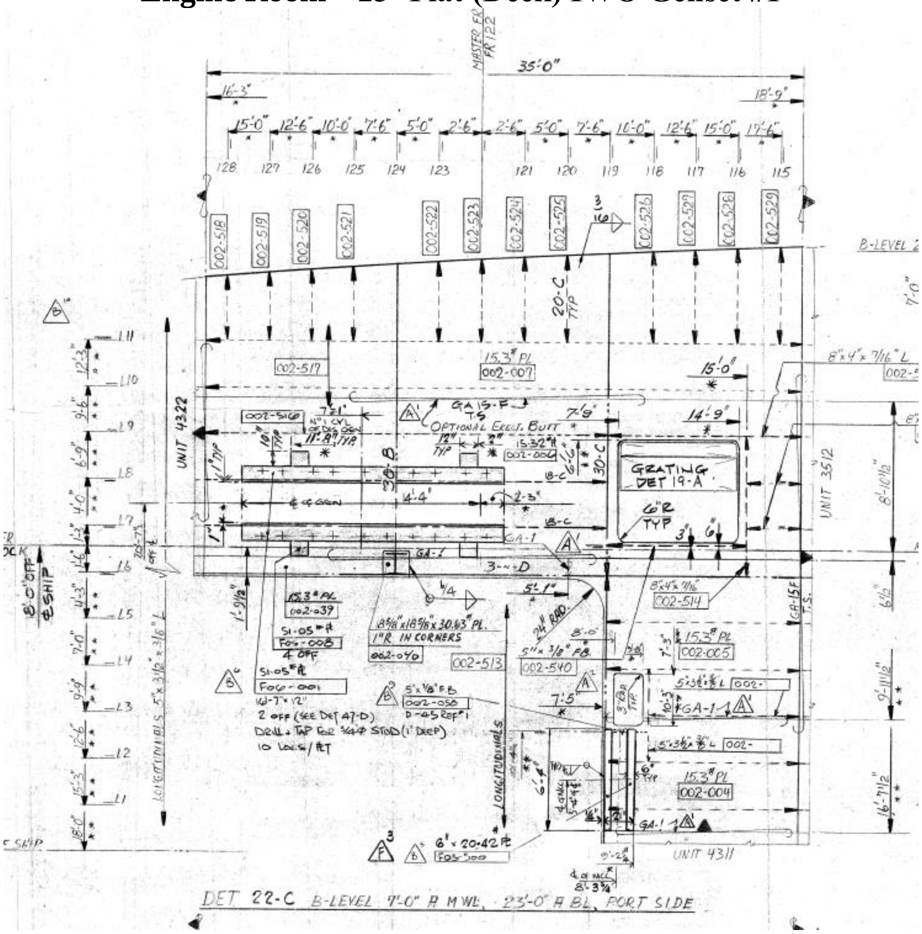

Engine Room – Side Shell IWO Genset #1

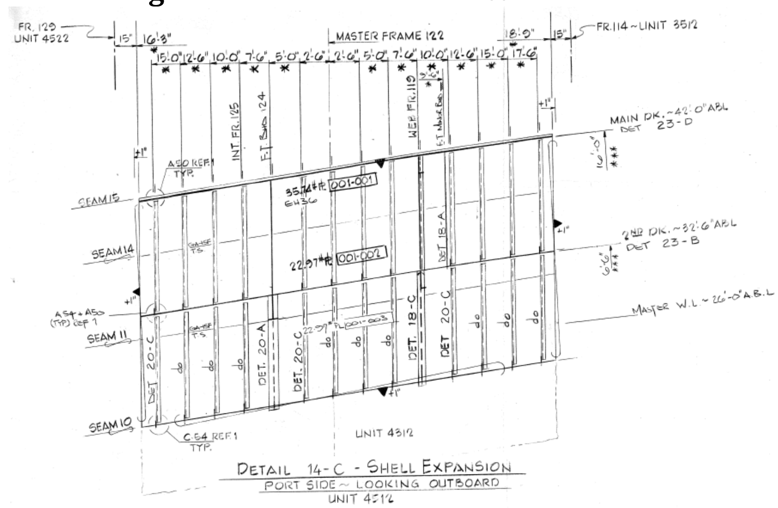

Engine Room – Lower Port Side Shell & Stringer

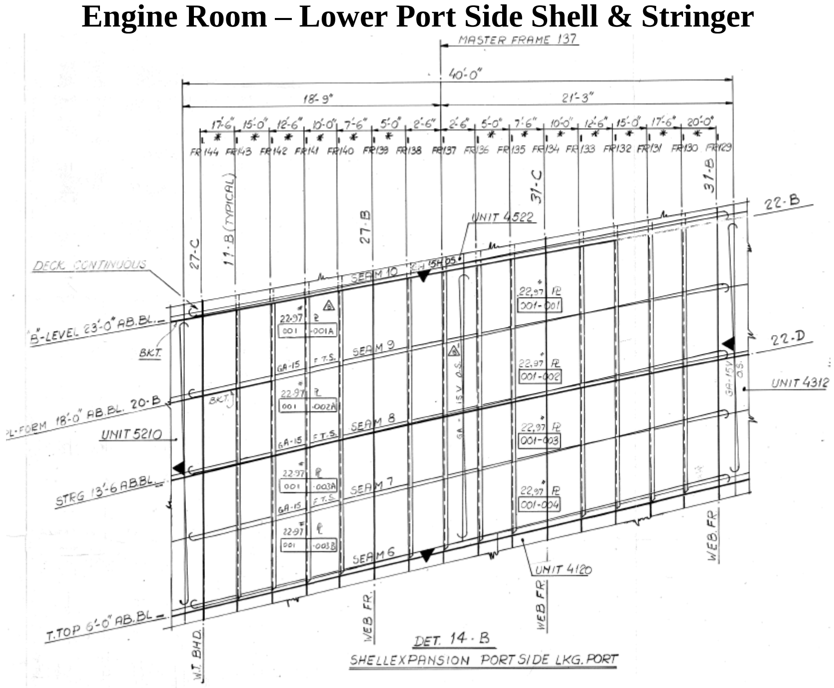

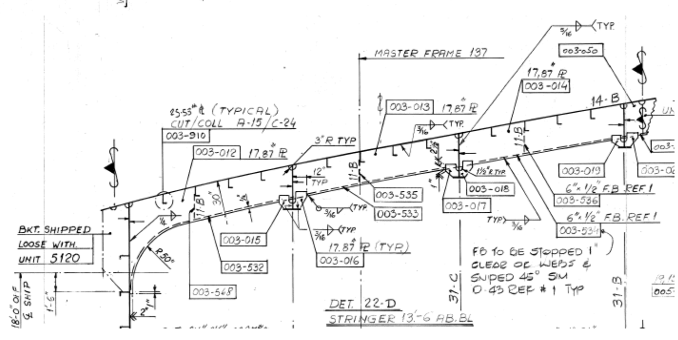

Engine Room – 23' Flat (Deck) IWO Start Air Compressor

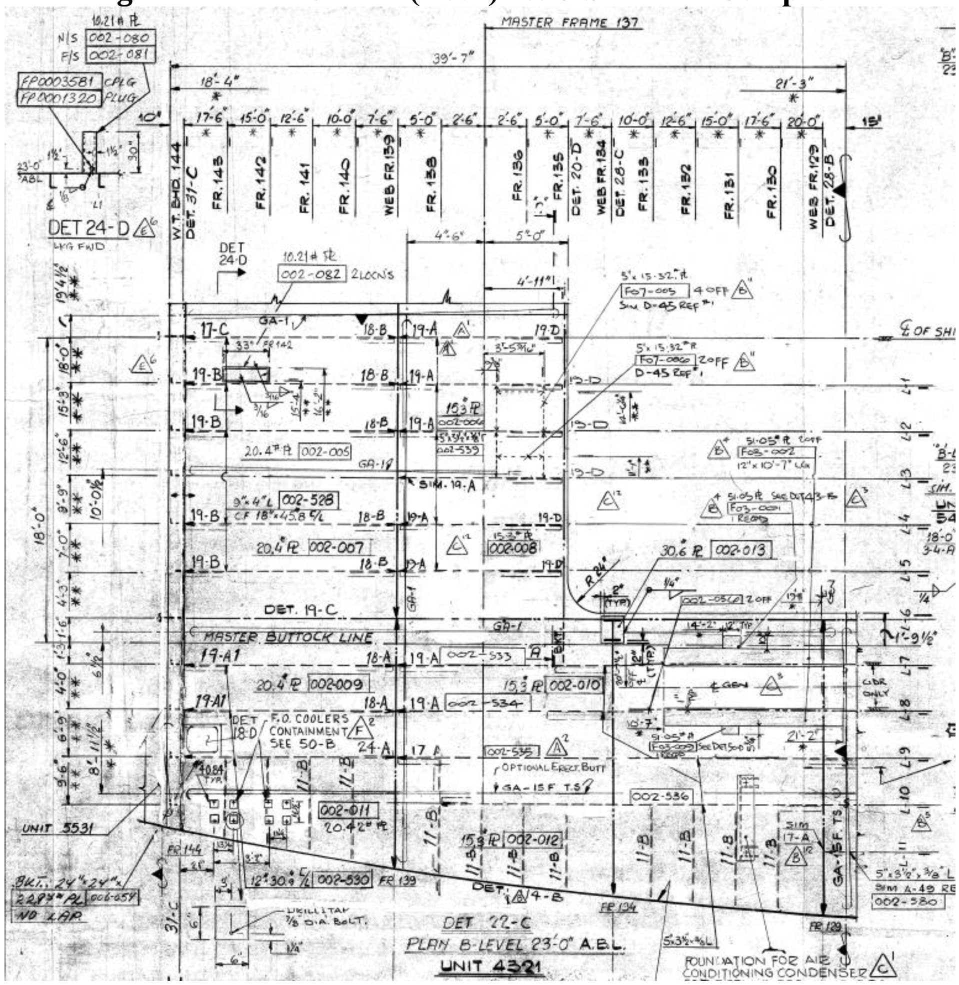

Engine Room – Side Shell IWO Start Air Compressor

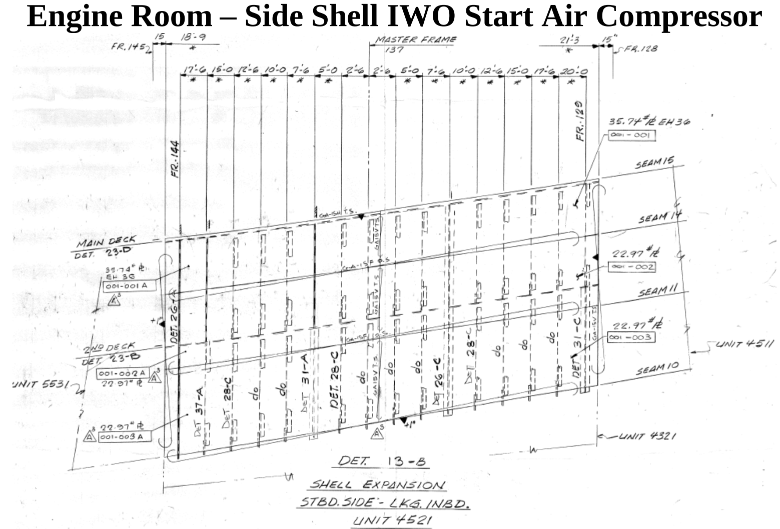

APPENDIX B – Notes on Modes and MAC

Mode Shapes and Frequency Response

The equations of motion describing the forced response of an *n-Degree-of-Freedom* (DOF) system are written as

$$[M]\{\ddot{x}\}+[C]\{\dot{x}\}+[K]\{x\}=F(t) \tag{1}$$

where [M] is the mass matrix, [C] is the viscous damping matrix, [K] is the stiffness matrix, F is the force applied to each DOF, and {x} is the displacement of each DOF. The dots over the {x} mean differentiation with respect to time. Taking the Fourier transform of Equation (1) the equations of motion in the frequency domain can be expressed as

$$[D(\omega)]\{x(\omega)\}=\{F(\omega)\} \tag{2}$$

Where [$D(\omega)$] is a $n \times n$ dynamic stiffness matrix given by

$$[D(\omega)]=-\omega^2[M]+j\omega[C]+[K] \tag{3}$$

where ω is the angular frequency (rad/s) and j is √-1. The frequency response function (FRF) matrix [$H(\omega)$] is obtained by inverting the dynamic stiffness matrix and is written as

$$[H(\omega)]=[D(\omega)]^{-1}=\frac{\mathrm{adj}[D(\omega)]}{\det[D(\omega)]} \tag{4}$$

where adj indicates the adjoint and det indicates the determinant of the dynamic stiffness matrix.

The determinant of the dynamic stiffness matrix is commonly referred to as the characteristic equation of the system and its poles or roots indicate the natural frequencies of the system. The adjoint matrix is commonly referred to as the residue matrix. It can be shown that the terms of the residue matrix are related to the mode shapes [10] and Equation (4) can be re-written in terms of the mode shapes and poles (natural frequencies and damping) of the system as

$$[H(\omega)]=\sum_{k=1}^{m}\frac{q_k\{\varphi_k\}\{\varphi_k\}^T}{(j\omega+p_k)}+\frac{q_k^*\{\varphi_k^*\}\{\varphi_k^*\}^T}{(j\omega+p_k^*)} \tag{5}$$

where q_k is a complex scaling quantity for the *k*-th mode, φ_k is the *k*-th mode shape or 'eigenvector' and p_k is the *k*-th pole. The asterisk in Equation (5) indicates complex conjugate. The *ij* entry of the transfer function matrix is the transfer function between points *i* and *j*. From Equation (5) the *ij* FRF is given by

$$h_{ij}(\omega)=\sum_{k=1}^{m}\frac{q_k\varphi_{ik}\varphi_{jk}}{(j\omega+p_k)}+\frac{q_k^*\varphi_{ik}^*\varphi_{jk}^*}{(j\omega+p_k^*)} \tag{6}$$

Equation (6) shows the relationship between the mode shapes and the FRF. The response of the full-ship model is comprised of the linear combination of multiple single DOF modal oscillators. Therefore, the full response at a given point (or in the vessel as a whole) to a given input force (or set of forces) can be calculated as the sum of the contributions from each mode as they would respond to the input force(s). This also implies that the accuracy of a given model can be determined in-part by comparing the frequencies and mode shapes of dominant modes.

Modal Assurance Criteria (MAC)

The modal assurance criterion (MAC) is a tool commonly employed to determine the similarity between eigenvectors obtained experimentally (experimental modal analysis) and to those obtained numerically with a finite element models [9]. However, the MAC is not limited to comparing experimental data and can be utilized in the comparison of two FE models. The MAC for an i,j eigenvector pair is written as

$$MAC_{i,j}=\frac{\left(\phi_i^T\phi_j\right)^2}{\left(\phi_i^T\phi_i\right)\left(\phi_j^T\phi_j\right)} \tag{7}$$

The MAC is analogous to a length normalized dot product. MAC values range between 0 and 1 with a MAC of 1 indicating a high degree of shape similarity and a MAC value of 0 indicating no shape similarity. Note that the MAC does not assess similarity in the predicted natural frequency, only mode shape.

APPENDIX C – Beam Torsion and Warping Constraints

Classic analysis of beam vibrations assumes the beam vibrates in a plane of symmetry. In beams that do not possess a plane of symmetry bending and torsional vibrations become coupled. Therefore, the torsional properties of the beam become important for the dynamic application both bending moments and torque.

When a member subjected to torque is allowed to warp freely, the member is said to be subject to St. Venant's or uniform torsion [14]. The angle of twist, ϕ, of a member subject to uniform torsion is described by

$$\frac{TL}{JG} = \phi \tag{1}$$

where T is the applied torque, L is the length of the member, J is the warping constant and G is the shear modulus.

When warping is restrained part of the applied torque generates twisting deformation in the cross-sectional plane of the beam and bending of the cross section about an axis normal to the length of the beam. The bending imparts a shear stress in the plane of the member's cross-section. With warping restrained the applied torque can be expressed as the combination of St. Venant's torque (T_{sv}) and the warping torque (T_w).

$$T = T_{sv} + T_w \tag{3}$$

The in-plane shear stress resists the applied torque, thereby reducing the torque available for twisting the member. The equation describing the angle of twist along the length (z) of a member with warping restrained is written as

$$T = GJ\frac{\partial \phi}{\partial z} - EC_w\frac{\partial^3 \phi}{\partial z^3} \tag{4}$$

Where G is the shear modulus, J is the torsion constant, E is the modulus of elasticity and C_w is the warping constant. The first term on the right hand side corresponds to the torque that generates twisting deformation (St. Venant's torque) and the second term corresponds to the torque which overcomes the shear due to warping (warping torque).

When warping is restrained the torsional stiffness of the beam is increased. When a beam cross section is allowed to warp freely (as is the case in most FE codes), the torsional stiffness of the cross-section is lower. To illustrate this point a static example is provided in Figure 166, which compares the angle of twist along the length of a cantilever beam due to a statically applied unit torque at its free end when warping is constrained vs. when the cross-section is allowed to warp freely. The ordinate of this figure is the percent increase in rotation due to the omission of constraint of warping. Table 52 lists the cross-sectional properties of each cross-section considered.

Figure 166: Illustration of Effects of Warping Restraint

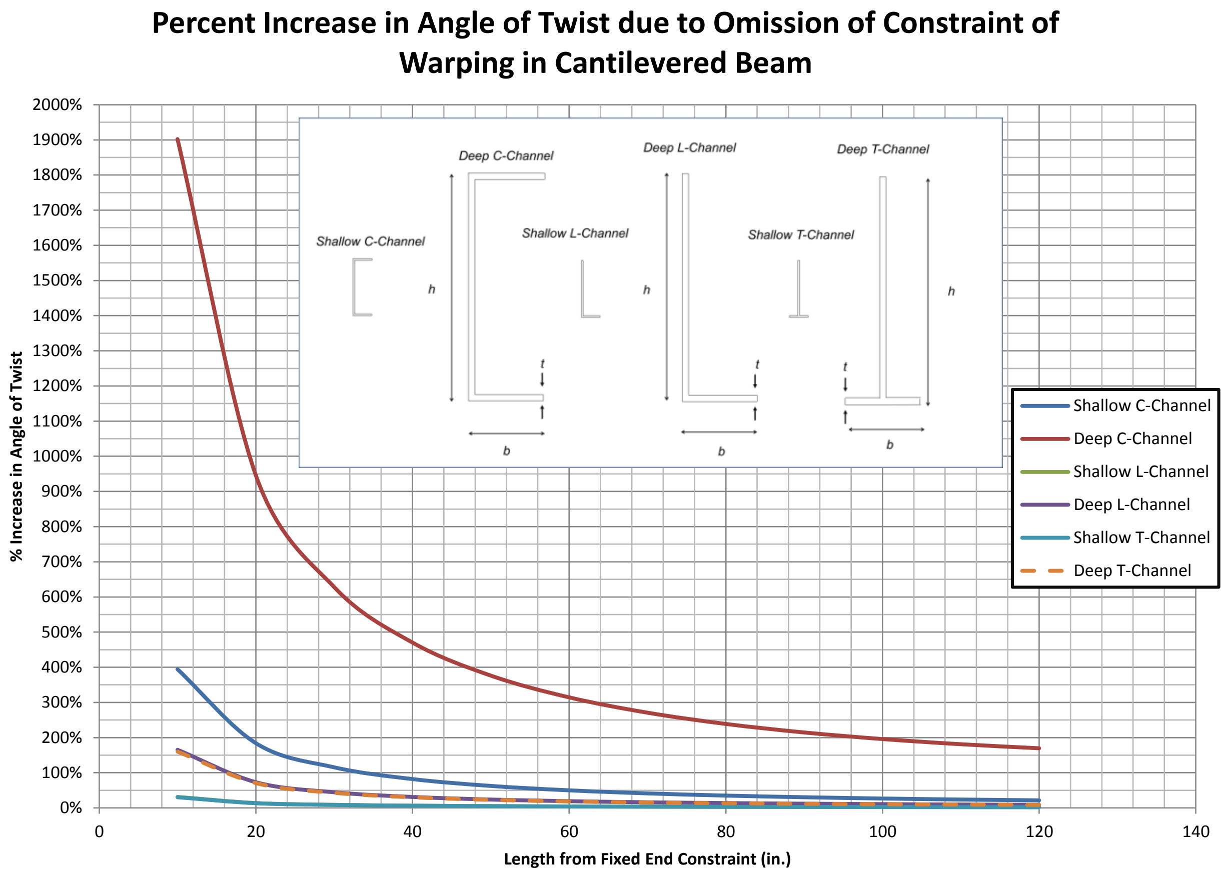

Table 52: Cross Sections of Beams Used in Warping Example

	Shallow C-Channel	**Deep C-Channel**	**Shallow L-Channel**	**Deep L-Channel**	**Shallow T-Channel**	**Deep T-Channel**
Height (h)	6	24	6	24	6	24
Width (b)	2	8	2	8	2	8
Thickness (t)	3/16	3/4	3/16	3/4	3/16	3/4
Length (L)	120	120	120	120	120	120

Figure 166 shows the effect warping constraint is greatest near the constrained end. It also indicates that the deeper the cross-section is the greater the effect of warping. The C-Channel cross-sections are shown to be the most susceptible to warping with smaller differences between the L and T-channel cross-sections.

At distances close to the constraint, angle of twist can be over-estimated by as much as 165% in deep sections and 30% in shallow sections when constraint of warping is not considered. While these results are shown for a static case conclusions can be extended to dynamic analyses. In particular, the reaction forces at junctions of stiffeners with adjacent decks and bulkheads may not be correctly modeled if warping is not considered.

Not all FE codes can account for constraint of warping. In codes which can model the constraint of beam warping, an additional degree of freedom (DOF) is introduced at each node in the beam element. This DOF captures the rate of twist of the beam. Additional information on this effect can be found in References [15-17].

APPENDIX D – Force Estimation Using Generalized Inverse Method

Overview

The following is a summary of a methodology outlined in Reference [5] for using measured vibration levels along with measured Frequency Response Functions to derive drive point mobilities from complex sources. This approach was used to estimate the forces generated by the start air compressor.

The input-out relationship for a linear time invariant system can be expressed as

$$\{S_y\} = [H]\{S_f\} \tag{1}$$

Where $\{S_y\}$ is the output response spectrum, H is the FRF matrix and S_f is the input force spectrum. Post multiplying both sides by the hermetian (complex conjugate transpose) of the output response spectrum, equation (1) can be re-written as

$$\{S_y\}\{S_y^h\} = [H]\{S_f\}\{S_f^h\}[H^h] \tag{2}$$

From the definition of the autopower/crosspower spectrum equation (2) can be simplified to

$$[G_{yy}] = [H][G_{ff}][H^h] \tag{3}$$

where $[G_{yy}]$ is a matrix with response autopower spectra on the diagonal and response cross-power spectra on the off-diagonals, $[G_{ff}]$ is a matrix with force autopower spectra on the diagonal and force cross-power spectra on the off-diagonals.

The size of $[H]$ is *n* x *r* where *n* indicates the number of measured response points and *r* is the number of reference points. Subsequently, $[G_{yy}]$ is an *n* x *n* matrix and $[G_{ff}]$ is an *r* x *r* matrix.

Using left and right sided pseudo inverses, the input force autopower spectra matrix can be written in terms of the response autopower/crosspower matrix and the FRF matrix according to

$$[G_{ff}] = \left[[H]^T[H]\right]^{-1}[H]^T[G_{yy}][H^h]^T\left[[H^h][H^h]^T\right]^{-1} \tag{4}$$

Phase information can be extracted from the off-diagonal terms of $[G_{ff}]$. For example the phase of the *(i,j)* entry of $[G_{ff}]$ provides the phase relationship between the *i-th* and *j-th* force with the *i-th* force serving as the phase reference (i.e. zero phase).

Equation (4) is a least-squares error minimization, whereby the force spectrum computed minimizes the error between the FRF matrix $\left[H\right]$ and measured spectra. As such it is possible to obtain force spectra which provide a best fit to the specified spectra given any FRF matrix. If the FRF's representing the true transfer relationships are not specified in $\left[H\right]$ the estimated forces are not physically meaningful.

Additionally, the forces estimated via (4) are extremely sensitive to the condition number of the matrix $\left[H\right]$. A large condition number is indicative of an *ill-conditioned* problem whereby small changes in the response spectra $\left[G_{yy}\right]$ can lead to large deviations in the estimated forces $\left[G_{ff}\right]$.

Therefore, it becomes imperative for the FRF matrix to be both well-conditioned and representative of the true system dynamics if meaningful results are to be obtained.

<u>Application to Start Air Compressor</u>

In this investigation the spectra in $\left[G_{yy}\right]$ were measured with the start air compressor operating and FRF's in $\left[H\right]$ were both measured onboard the ship and synthesized from FEM models.

It is important to note that the matrix $\left[G_{ff}\right]$ describes the force spectrum of externally applied forces. Therefore, to use (4) to estimate the forces imparted by the start air compressor through the resilient mounts it is essential that the FRF's in the matrix $\left[H\right]$ be those of the ship structure uncoupled from the start air compressor.

This posed a practical problem as the start air compressor could not be removed from its foundation. Additionally, space restrictions made it impossible to measure FRF's at the true force input locations.

As a result the FRF's used in (4) were not the ideal FRF's that should be used with this procedure. This introduces an inherent systematic error in the prediction. However, this is a practical limitation of this approach for ship measurements, as removal of sources is not likely to occur purely to allow a measurement of this type.

APPENDIX E – Calibration Certificates

Certificate number: **SR 1724-3740591**

Calibration report

- ‘As Left data’ -

Product type: LMS SCADAS

Calibration Suite:	**Calibration Software Production & Services**
Calibration Suite Version:	**2.07.0063**

Customer:

Company name	: Noise Control Engineering
Division / department	:
Location (city / country)	: Billerica
Contact person	: Joe Hanna

System:

System type(s)	: SCM05
Serial number(s)	: 46073310

Calibration conditions:

Location (factory, office or on-site)	: LMS Office
Date	: 02 July, 2013
Ambient temperature	: 72ºF

Calibration performed by:

Name	: Mr. T. Yocum
Calibration label	: YES

(Signature)..

Summary:

- Calibration results within specification.

LMS Instruments
Druivenstraat 47
4816 KB Breda
The Netherlands
Phone: +31 76 573 6363

LMS France
2 rue René Caudron
78960 Voisins le Bretonneux
France
Phone :+33 1 3452 1740

LMS North-America
5755 New King Street
Troy, MI 48098
USA
Phone: +1 248 952 5664

Noise Control Engineering, Inc.

799 Middlesex Turnpike
Billerica, MA 01821-3445
Phone: 978-670-5339
Fax: 978-667-7047
E-mail: nonoise@noise-control.com

Model:	736
Serial Number:	1786
Sensitivity*:	103.0 mV/G
Lab Temp:	24° C

Date:	3/7/2013
Engineer:	Joseph Hanna
Standard Deviation:	1.2 mV/G

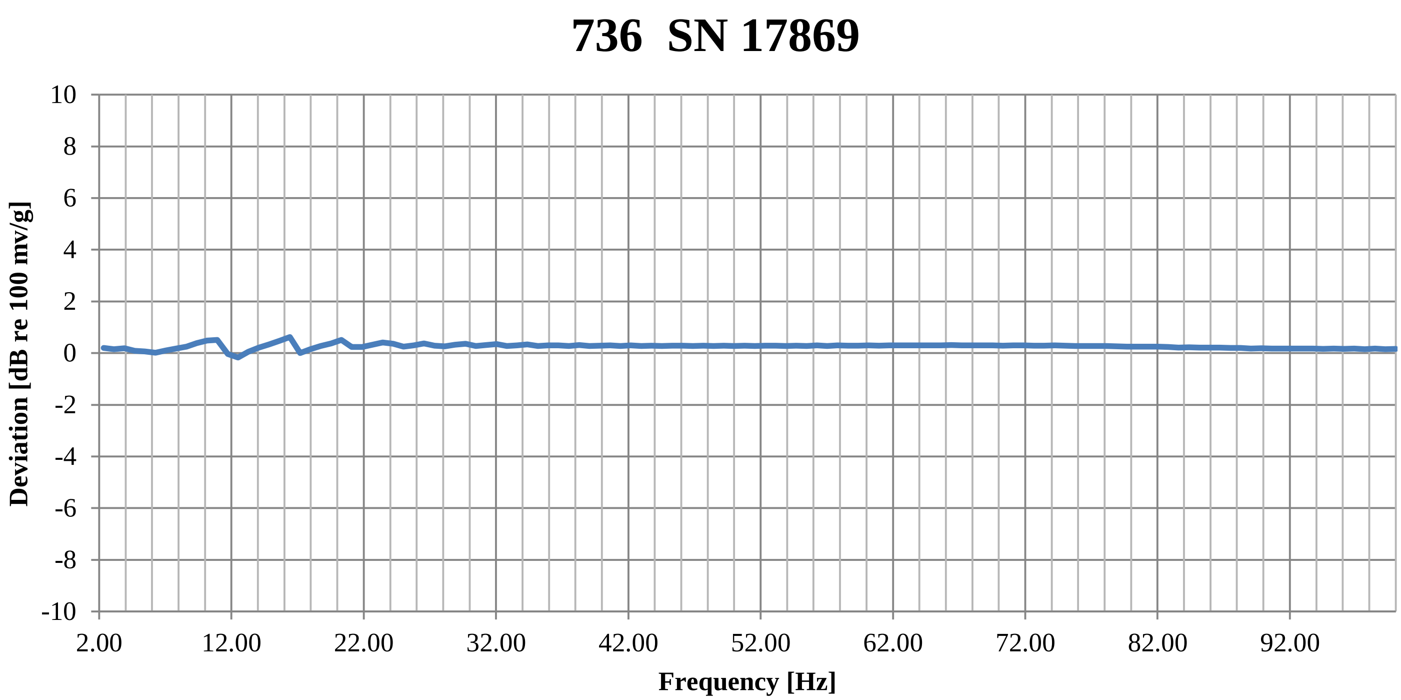

Equipment Used:

Description	Make	Model	Serial	Due Date	Nist No.
Data Acquisition	LMS	SC310	42033911	5/7/2013	-
Ref. Accel	PCB	301A11	2311	4/21/2013	10068
Electromagnetic Shaker	Wilcoxon	F4	20026	-	-
Power Amplifier	QSC	RMS	80629695	-	-

Notes:

Calibration was performed in compliance with ISO 16063-21.
Back-to-back comparison calibration method was used per ISO 16063-21 PRD-P220
Calibration traceable to NIST 10068
*Sensitivity measured from 1 - 100 Hz

Noise Control Engineering, Inc.

799 Middlesex Turnpike
Billerica, MA 01821-3445
Phone: 978-670-5339
Fax: 978-667-7047
E-mail: nonoise@noise-control.com

Model:	736
Serial Number:	1786
Sensitivity*:	98.6 mV/G
Lab Temp:	24° C

Date:	3/7/2013
Engineer:	Joseph Hanna
Standard Deviation:	0.6 mV/G

736 SN 17867

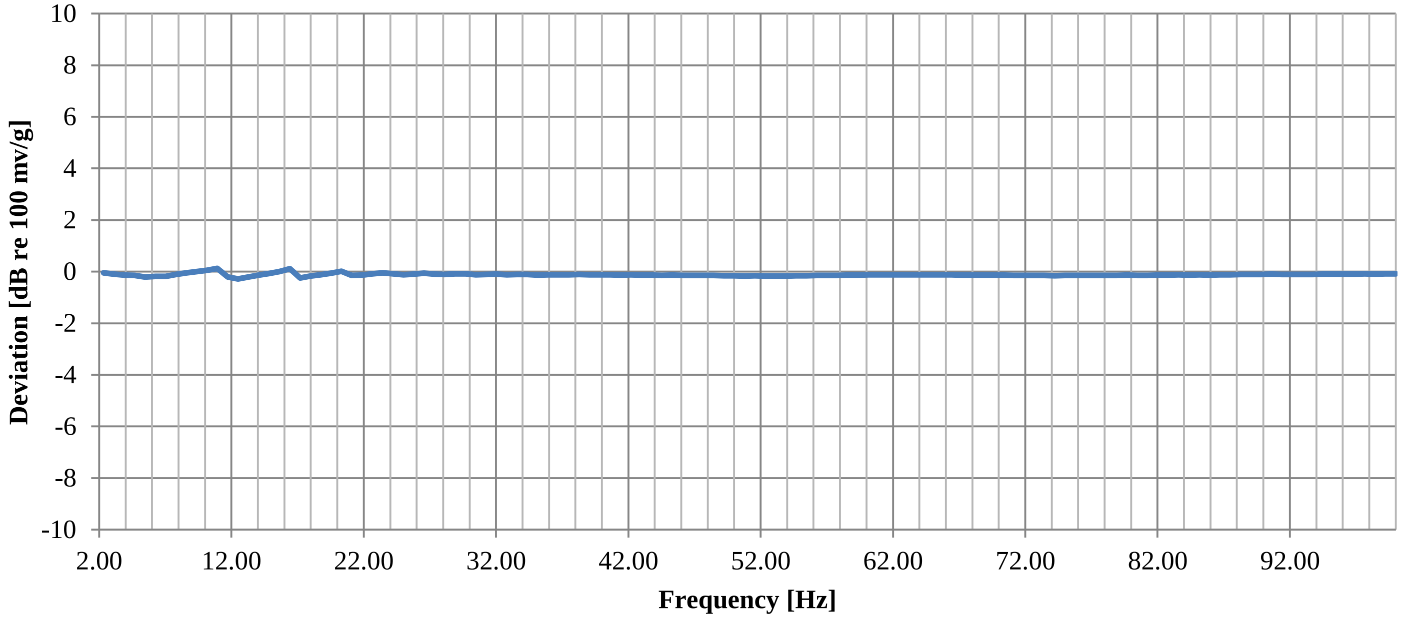

Equipment Used:

Description	Make	Model	Serial	Due Date	Nist No.
Data Acquisition	LMS	SC310	42033911	5/7/2013	-
Ref. Accel	PCB	301A11	2311	4/21/2013	10068
Electromagnetic Shaker	Wilcoxon	F4	20026	-	-
Power Amplifier	QSC	RMS	80629695	-	-

Notes:

Calibration was performed in compliance with ISO 16063-21.
Back-to-back comparison calibration method was used per ISO 16063-21 PRD-P220
Calibration traceable to NIST 10068
*Sensitivity measured from 1 - 100 Hz

Noise Control Engineering, Inc.

799 Middlesex Turnpike
Billerica, MA 01821-3445
Phone: 978-670-5339
Fax: 978-667-7047
E-mail: nonoise@noise-control.com

Model:	736
Serial Number:	1786
Sensitivity*:	98.8 mV/G
Lab Temp:	24° C

Date:	3/7/2013
Engineer:	Joseph Hanna
Standard Deviation:	1.0 mV/G

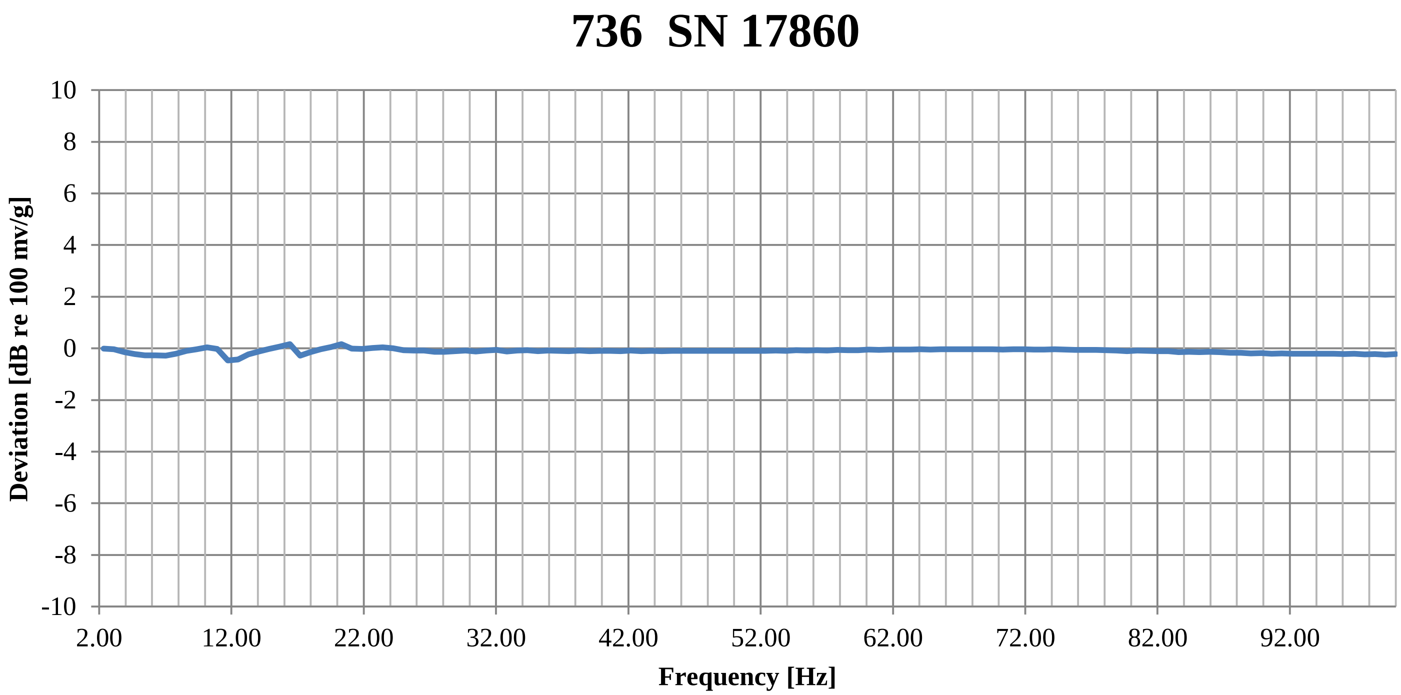

Equipment Used:

Description	Make	Model	Serial	Due Date	Nist No.
Data Acquisition	LMS	SC310	42033911	5/7/2013	-
Ref. Accel	PCB	301A11	2311	4/21/2013	10068
Electromagnetic Shaker	Wilcoxon	F4	20026	-	-
Power Amplifier	QSC	RMS	80629695	-	-

Notes:

Calibration was performed in compliance with ISO 16063-21.
Back-to-back comparison calibration method was used per ISO 16063-21 PRD-P220
Calibration traceable to NIST 10068
*Sensitivity measured from 1 - 100 Hz

Noise Control Engineering, Inc.

799 Middlesex Turnpike
Billerica, MA 01821-3445
Phone: 978-670-5339
Fax: 978-667-7047
E-mail: nonoise@noise-control.com

Model:	736
Serial Number:	1785
Sensitivity*:	101.0 mV/G
Lab Temp:	24° C

Date:	3/7/2013
Engineer:	Joseph Hanna
Standard Deviation:	1.1 mV/G

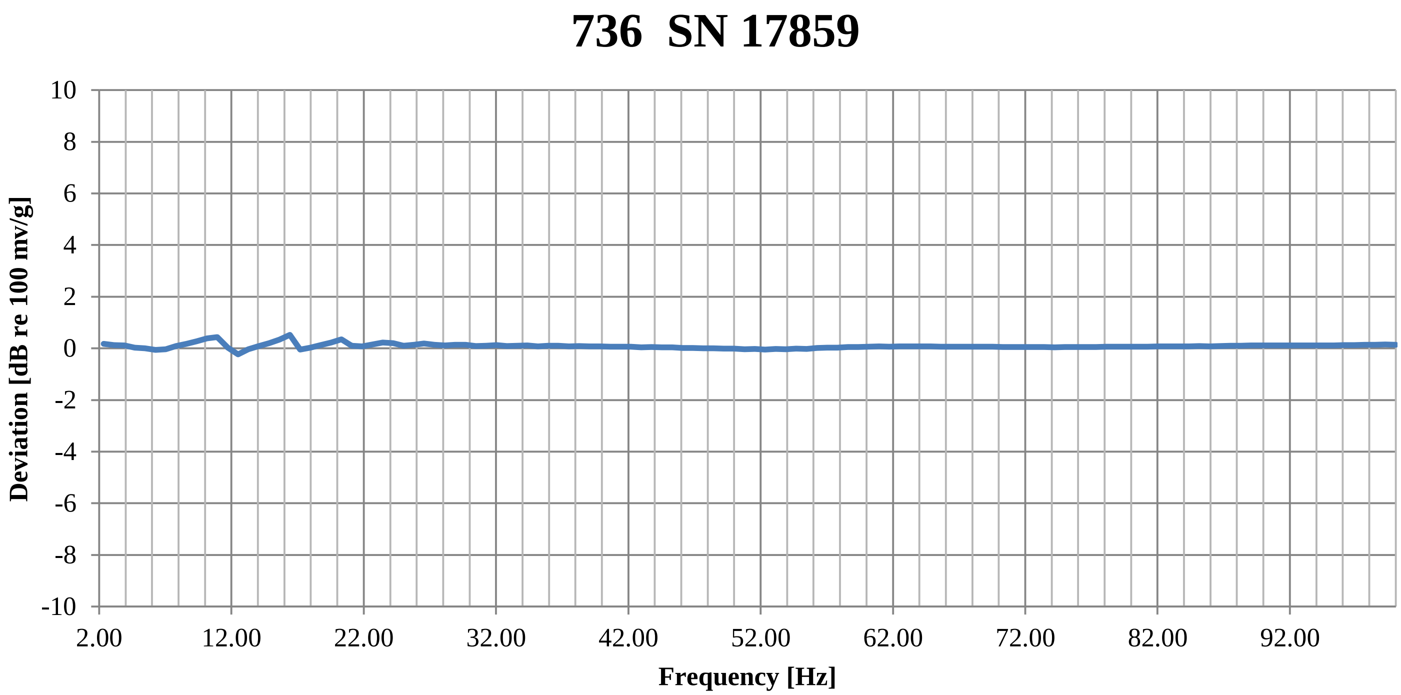

Equipment Used:

Description	Make	Model	Serial	Due Date	Nist No.
Data Acquisition	LMS	SC310	42033911	5/7/2013	-
Ref. Accel	PCB	301A11	2311	4/21/2013	10068
Electromagnetic Shaker	Wilcoxon	F4	20026	-	-
Power Amplifier	QSC	RMS	80629695	-	-

Notes:

Calibration was performed in compliance with ISO 16063-21.
Back-to-back comparison calibration method was used per ISO 16063-21 PRD-P220
Calibration traceable to NIST 10068
*Sensitivity measured from 1 - 100 Hz

Noise Control Engineering, Inc.

799 Middlesex Turnpike
Billerica, MA 01821-3445
Phone: 978-670-5339
Fax: 978-667-7047
E-mail: nonoise@noise-control.com

Model:	736
Serial Number:	1785
Sensitivity*:	98.8 mV/G
Lab Temp:	24° C

Date:	3/7/2013
Engineer:	Joseph Hanna
Standard Deviation:	0.9 mV/G

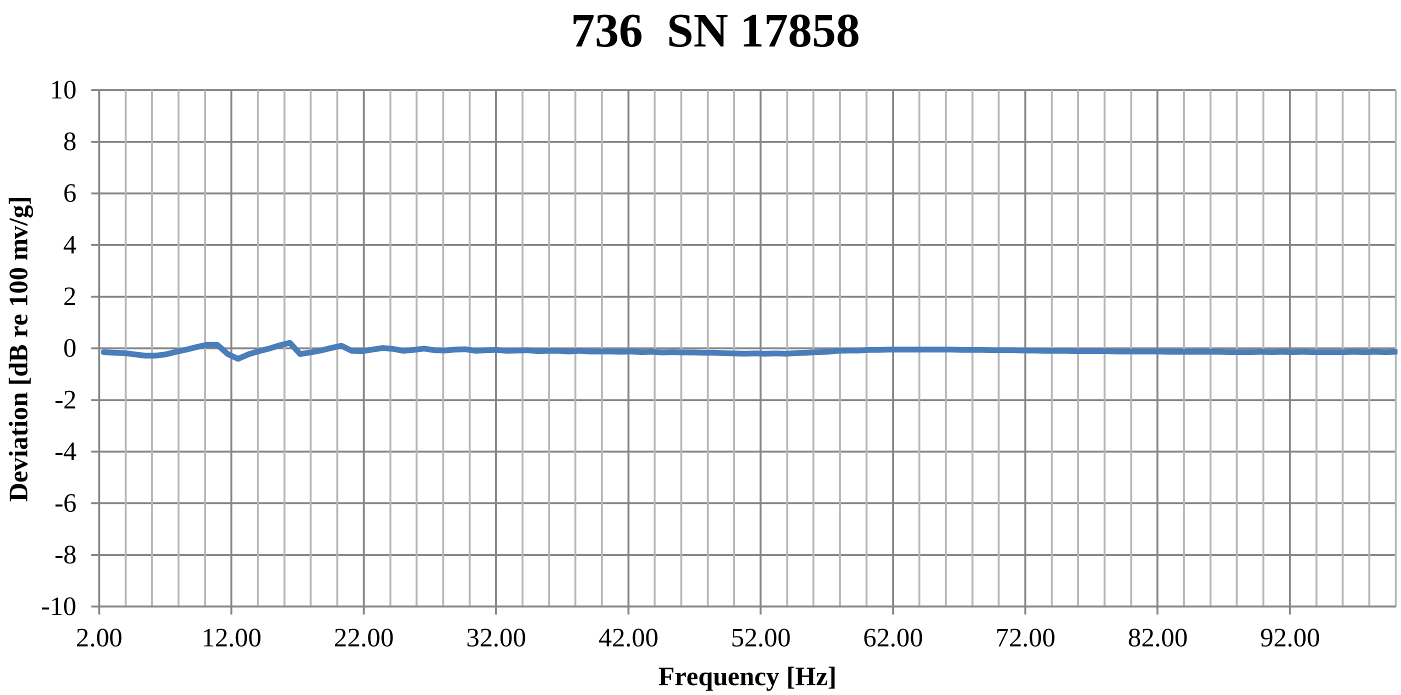

Equipment Used:

Description	Make	Model	Serial	Due Date	Nist No.
Data Acquisition	LMS	SC310	42033911	5/7/2013	-
Ref. Accel	PCB	301A11	2311	4/21/2013	10068
Electromagnetic Shaker	Wilcoxon	F4	20026	-	-
Power Amplifier	QSC	RMS	80629695	-	-

Notes:

Calibration was performed in compliance with ISO 16063-21.
Back-to-back comparison calibration method was used per ISO 16063-21 PRD-P220
Calibration traceable to NIST 10068
*Sensitivity measured from 1 - 100 Hz

Noise Control Engineering, Inc.

799 Middlesex Turnpike
Billerica, MA 01821-3445
Phone: 978-670-5339
Fax: 978-667-7047
E-mail: nonoise@noise-control.com

Model:	736
Serial Number:	1785
Sensitivity*:	102.0 mV/G
Lab Temp:	24° C

Date:	3/7/2013
Engineer:	Joseph Hanna
Standard Deviation:	1.7 mV/G

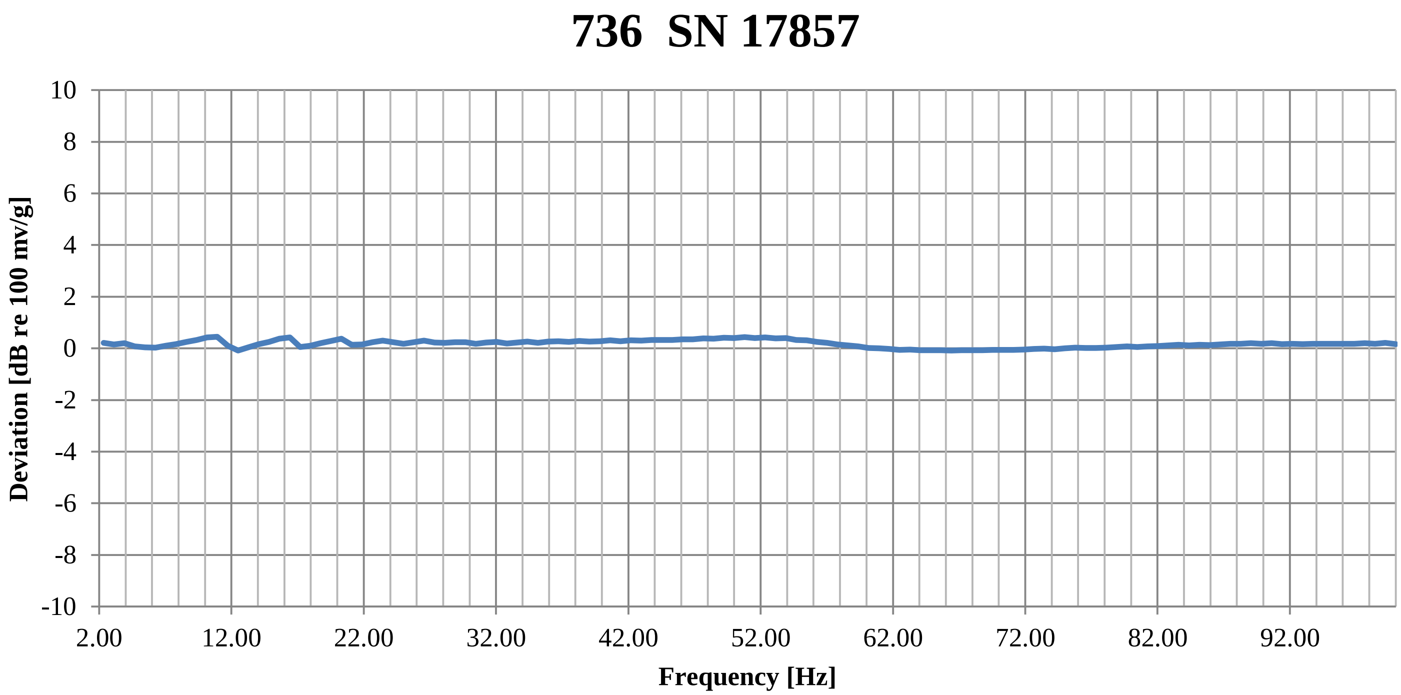

Equipment Used:

Description	Make	Model	Serial	Due Date	Nist No.
Data Acquisition	LMS	SC310	42033911	5/7/2013	-
Ref. Accel	PCB	301A11	2311	4/21/2013	10068
Electromagnetic Shaker	Wilcoxon	F4	20026	-	-
Power Amplifier	QSC	RMS	80629695	-	-

Notes:

Calibration was performed in compliance with ISO 16063-21.
Back-to-back comparison calibration method was used per ISO 16063-21 PRD-P220
Calibration traceable to NIST 10068
*Sensitivity measured from 1 - 100 Hz

Noise Control Engineering, Inc.

799 Middlesex Turnpike
Billerica, MA 01821-3445
Phone: 978-670-5339
Fax: 978-667-7047
E-mail: nonoise@noise-control.com

Model:	736
Serial Number:	1785
Sensitivity*:	100.1 mV/G
Lab Temp:	24° C

Date:	3/7/2013
Engineer:	Joseph Hanna
Standard Deviation:	1.1 mV/G

736 SN 17856

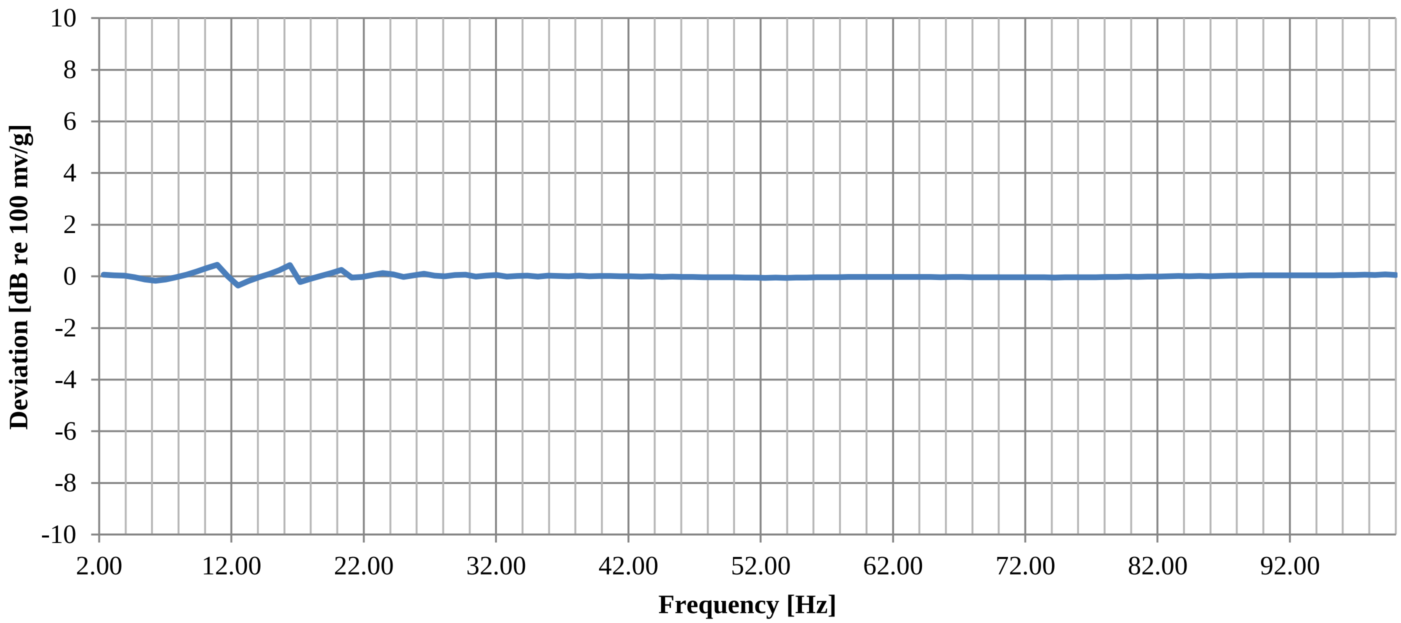

Equipment Used:

Description	Make	Model	Serial	Due Date	Nist No.
Data Acquisition	LMS	SC310	42033911	5/7/2013	-
Ref. Accel	PCB	301A11	2311	4/21/2013	10068
Electromagnetic Shaker	Wilcoxon	F4	20026	-	-
Power Amplifier	QSC	RMS	80629695	-	-

Notes:

Calibration was performed in compliance with ISO 16063-21.
Back-to-back comparison calibration method was used per ISO 16063-21 PRD-P220
Calibration traceable to NIST 10068
*Sensitivity measured from 1 - 100 Hz

Noise Control Engineering, Inc.

799 Middlesex Turnpike
Billerica, MA 01821-3445
Phone: 978-670-5339
Fax: 978-667-7047
E-mail: nonoise@noise-control.com

Model:	736
Serial Number:	1785
Sensitivity*:	98.0 mV/G
Lab Temp:	24° C

Date:	3/7/2013
Engineer:	Joseph Hanna
Standard Deviation:	0.3 mV/G

736 SN 17855

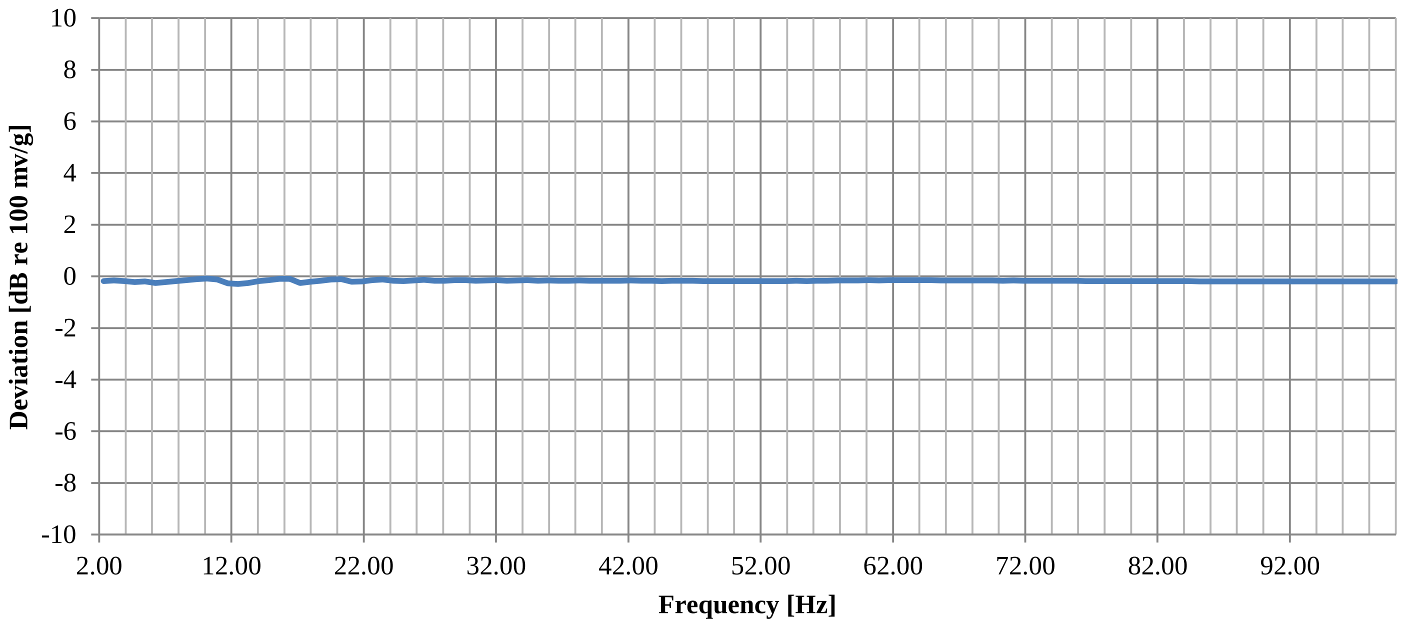

Equipment Used:

Description	Make	Model	Serial	Due Date	Nist No.
Data Acquisition	LMS	SC310	42033911	5/7/2013	-
Ref. Accel	PCB	301A11	2311	4/21/2013	10068
Electromagnetic Shaker	Wilcoxon	F4	20026	-	-
Power Amplifier	QSC	RMS	80629695	-	-

Notes:

Calibration was performed in compliance with ISO 16063-21.
Back-to-back comparison calibration method was used per ISO 16063-21 PRD-P220
Calibration traceable to NIST 10068
*Sensitivity measured from 1 - 100 Hz

Noise Control Engineering, Inc.

799 Middlesex Turnpike
Billerica, MA 01821-3445
Phone: 978-670-5339
Fax: 978-667-7047
E-mail: nonoise@noise-control.com

Model:	736
Serial Number:	1785
Sensitivity*:	98.5 mV/G
Lab Temp:	24° C

Date:	3/7/2013
Engineer:	Joseph Hanna
Standard Deviation:	0.7 mV/G

736 SN 17854

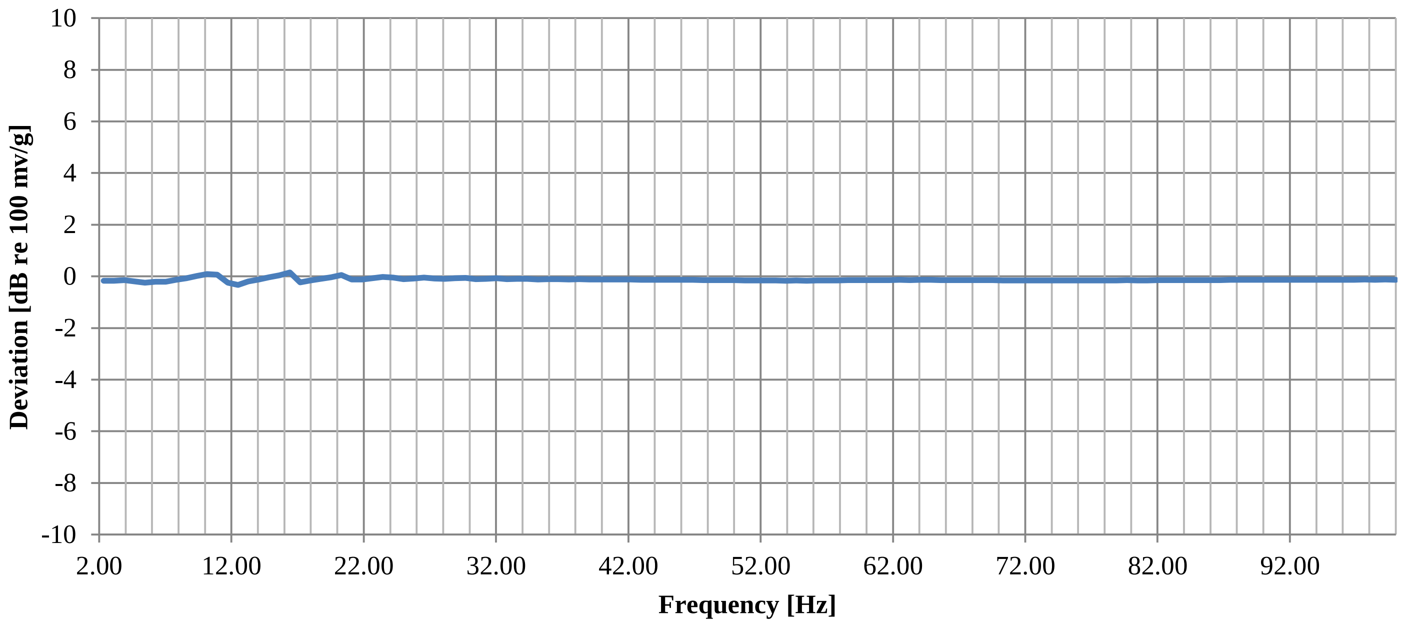

Equipment Used:

Description	Make	Model	Serial	Due Date	Nist No.
Data Acquisition	LMS	SC310	42033911	5/7/2013	-
Ref. Accel	PCB	301A11	2311	4/21/2013	10068
Electromagnetic Shaker	Wilcoxon	F4	20026	-	-
Power Amplifier	QSC	RMS	80629695	-	-

Notes:

Calibration was performed in compliance with ISO 16063-21.
Back-to-back comparison calibration method was used per ISO 16063-21 PRD-P220
Calibration traceable to NIST 10068
*Sensitivity measured from 1 - 100 Hz

Noise Control Engineering, Inc.

799 Middlesex Turnpike
Billerica, MA 01821-3445
Phone: 978-670-5339
Fax: 978-667-7047
E-mail: nonoise@noise-control.com

Model:	736
Serial Number:	1785
Sensitivity*:	98.0 mV/G
Lab Temp:	24° C

Date:	3/7/2013
Engineer:	Joseph Hanna
Standard Deviation:	1.0 mV/G

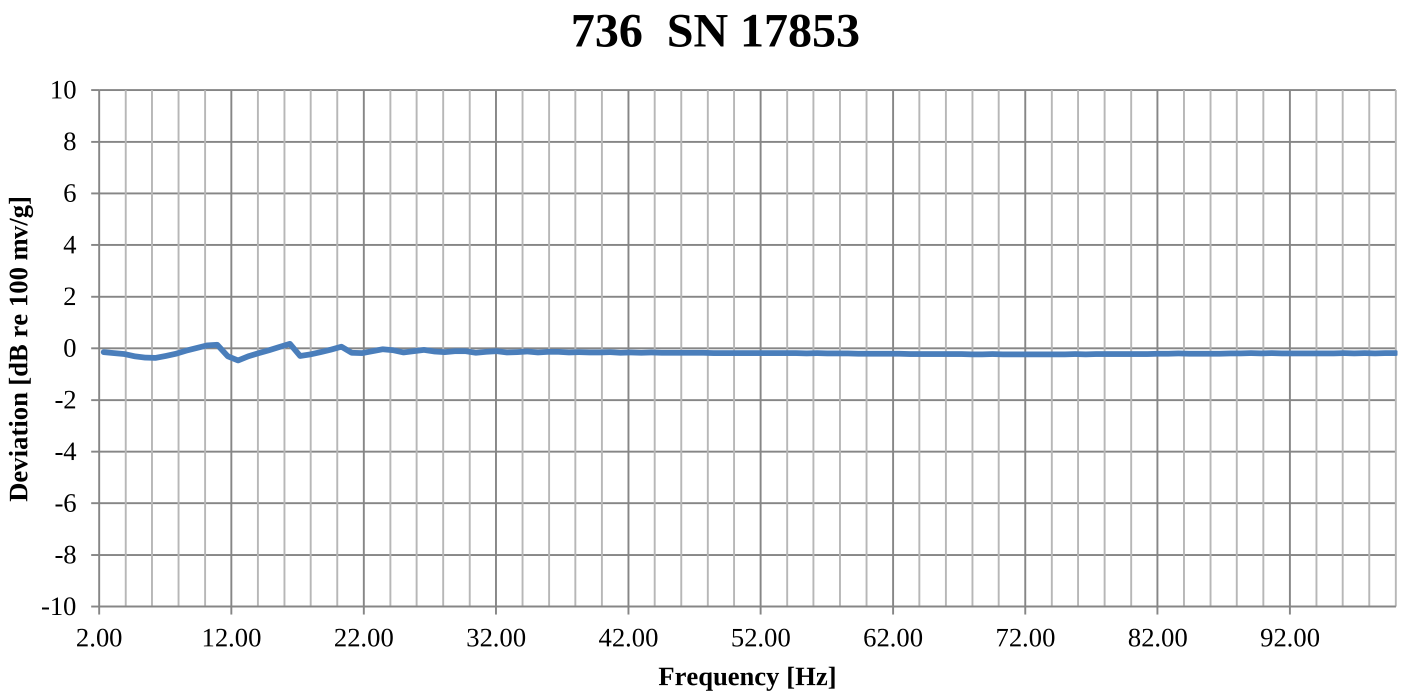

Equipment Used:

Description	Make	Model	Serial	Due Date	Nist No.
Data Acquisition	LMS	SC310	42033911	5/7/2013	-
Ref. Accel	PCB	301A11	2311	4/21/2013	10068
Electromagnetic Shaker	Wilcoxon	F4	20026	-	-
Power Amplifier	QSC	RMS	80629695	-	-

Notes:

Calibration was performed in compliance with ISO 16063-21.
Back-to-back comparison calibration method was used per ISO 16063-21 PRD-P220
Calibration traceable to NIST 10068
*Sensitivity measured from 1 - 100 Hz

Noise Control Engineering, Inc.

799 Middlesex Turnpike
Billerica, MA 01821-3445
Phone: 978-670-5339
Fax: 978-667-7047
E-mail: nonoise@noise-control.com

Model:	736
Serial Number:	1785
Sensitivity*:	97.3 mV/G
Lab Temp:	24° C

Date:	3/7/2013
Engineer:	Joseph Hanna
Standard Deviation:	1.1 mV/G

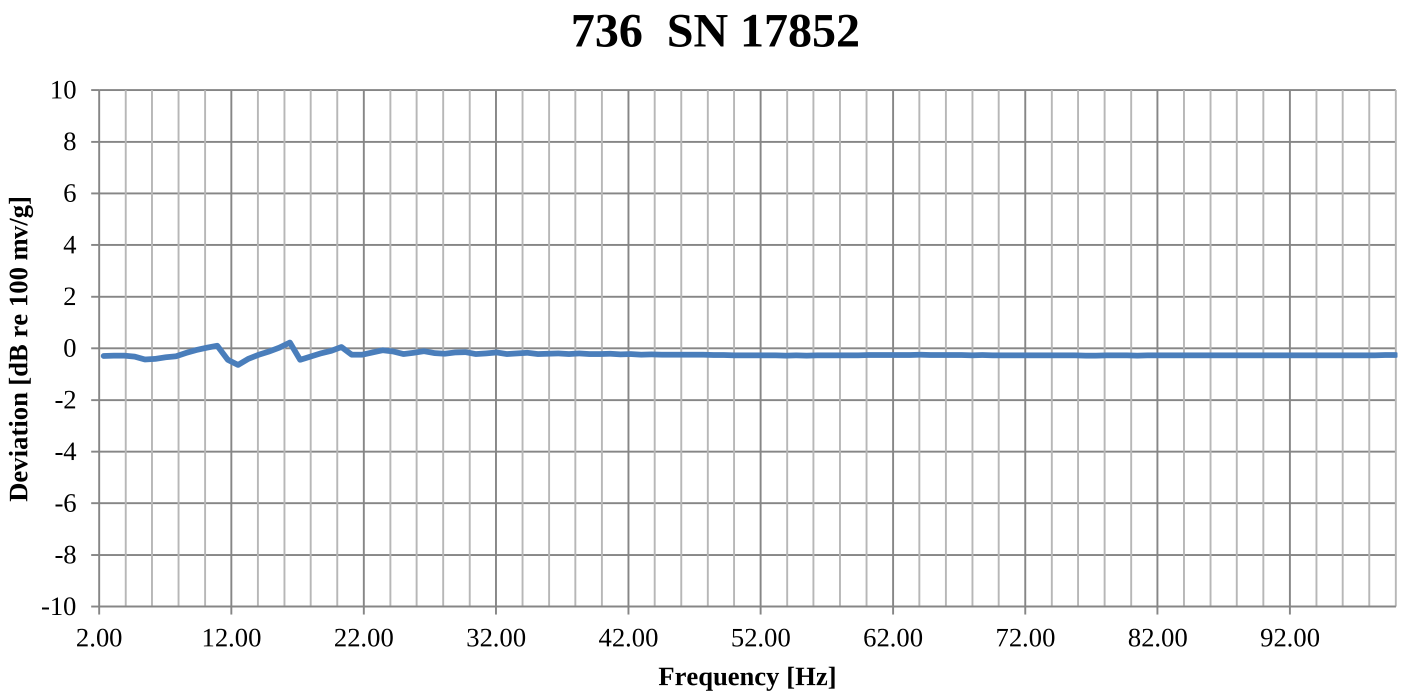

Equipment Used:

Description	Make	Model	Serial	Due Date	Nist No.
Data Acquisition	LMS	SC310	42033911	5/7/2013	-
Ref. Accel	PCB	301A11	2311	4/21/2013	10068
Electromagnetic Shaker	Wilcoxon	F4	20026	-	-
Power Amplifier	QSC	RMS	80629695	-	-

Notes:

Calibration was performed in compliance with ISO 16063-21.
Back-to-back comparison calibration method was used per ISO 16063-21 PRD-P220
Calibration traceable to NIST 10068
*Sensitivity measured from 1 - 100 Hz

Noise Control Engineering, Inc.

799 Middlesex Turnpike
Billerica, MA 01821-3445
Phone: 978-670-5339
Fax: 978-667-7047
E-mail: nonoise@noise-control.com

Model:	736
Serial Number:	1742
Sensitivity*:	99.2 mV/G
Lab Temp:	24° C

Date:	3/7/2013
Engineer:	Joseph Hanna
Standard Deviation:	1.2 mV/G

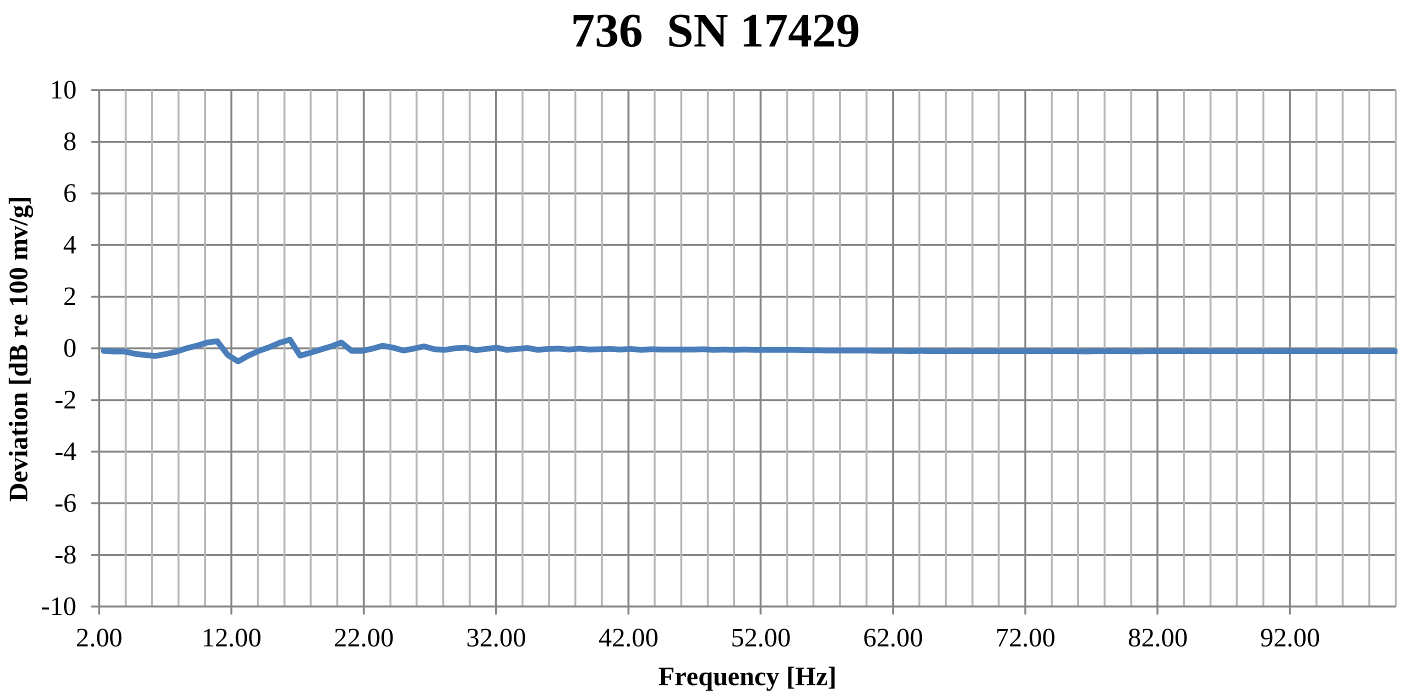

Equipment Used:

Description	Make	Model	Serial	Due Date	Nist No.
Data Acquisition	LMS	SC310	42033911	5/7/2013	-
Ref. Accel	PCB	301A11	2311	4/21/2013	10068
Electromagnetic Shaker	Wilcoxon	F4	20026	-	-
Power Amplifier	QSC	RMS	80629695	-	-

Notes:

Calibration was performed in compliance with ISO 16063-21.
Back-to-back comparison calibration method was used per ISO 16063-21 PRD-P220
Calibration traceable to NIST 10068
*Sensitivity measured from 1 - 100 Hz

Noise Control Engineering, Inc.

799 Middlesex Turnpike
Billerica, MA 01821-3445
Phone: 978-670-5339
Fax: 978-667-7047
E-mail: nonoise@noise-control.com

Model:	736
Serial Number:	1546
Sensitivity*:	99.2 mV/G
Lab Temp:	24° C

Date:	3/7/2013
Engineer:	Joseph Hanna
Standard Deviation:	1.2 mV/G

736 SN 15467

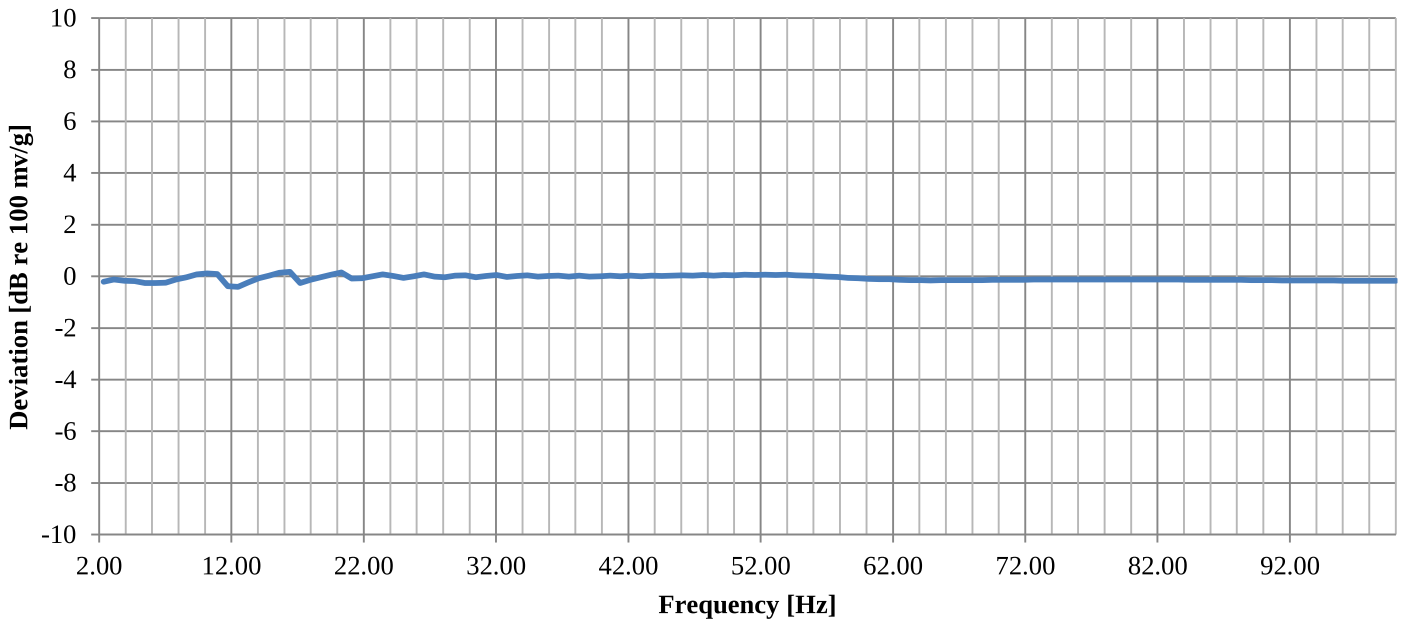

Equipment Used:

Description	Make	Model	Serial	Due Date	Nist No.
Data Acquisition	LMS	SC310	42033911	5/7/2013	-
Ref. Accel	PCB	301A11	2311	4/21/2013	10068
Electromagnetic Shaker	Wilcoxon	F4	20026	-	-
Power Amplifier	QSC	RMS	80629695	-	-

Notes:

Calibration was performed in compliance with ISO 16063-21.
Back-to-back comparison calibration method was used per ISO 16063-21 PRD-P220
Calibration traceable to NIST 10068
*Sensitivity measured from 1 - 100 Hz

Noise Control Engineering, Inc.

799 Middlesex Turnpike
Billerica, MA 01821-3445
Phone: 978-670-5339
Fax: 978-667-7047
E-mail: nonoise@noise-control.com

Model:	736
Serial Number:	1480
Sensitivity*:	95.9 mV/G
Lab Temp:	24° C

Date:	3/7/2013
Engineer:	Joseph Hanna
Standard Deviation:	1.0 mV/G

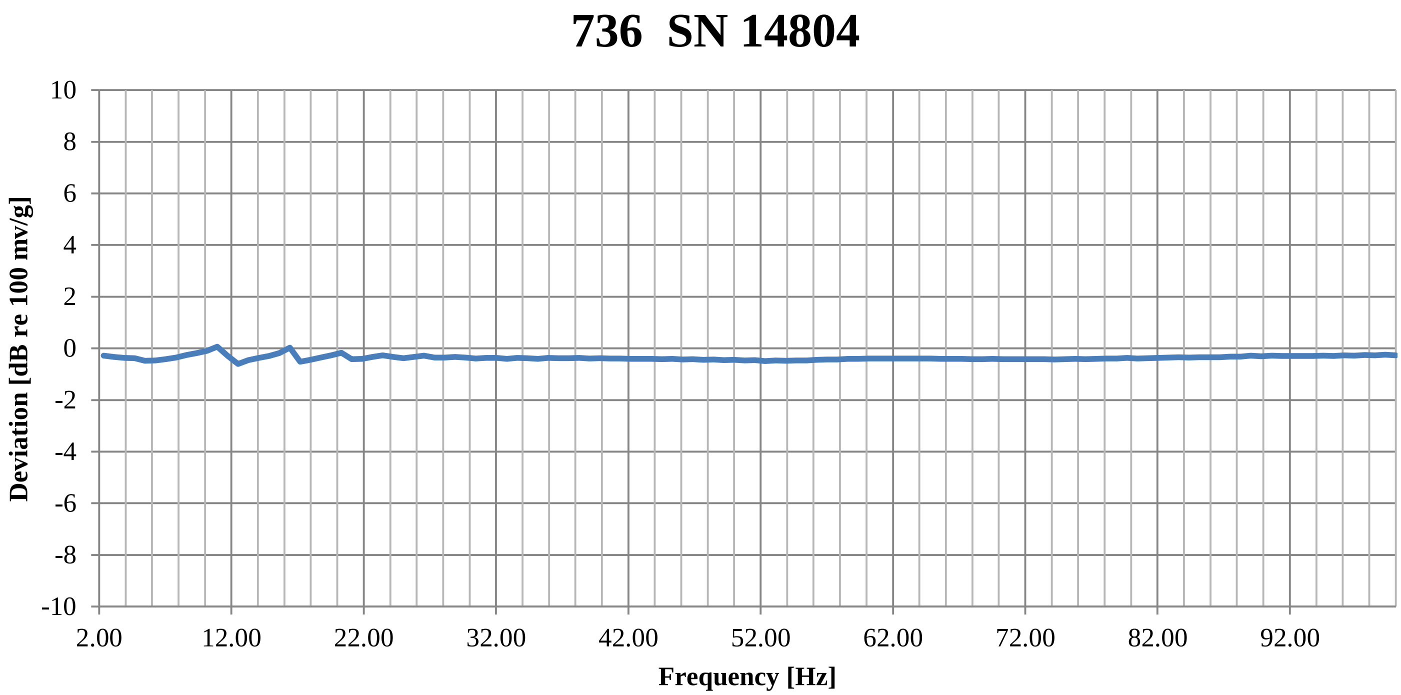

Equipment Used:

Description	Make	Model	Serial	Due Date	Nist No.
Data Acquisition	LMS	SC310	42033911	5/7/2013	-
Ref. Accel	PCB	301A11	2311	4/21/2013	10068
Electromagnetic Shaker	Wilcoxon	F4	20026	-	-
Power Amplifier	QSC	RMS	80629695	-	-

Notes:

Calibration was performed in compliance with ISO 16063-21.
Back-to-back comparison calibration method was used per ISO 16063-21 PRD-P220
Calibration traceable to NIST 10068
*Sensitivity measured from 1 - 100 Hz

Noise Control Engineering, Inc.

799 Middlesex Turnpike
Billerica, MA 01821-3445
Phone: 978-670-5339
Fax: 978-667-7047
E-mail: nonoise@noise-control.com

Model:	736
Serial Number:	1369
Sensitivity*:	102.9 mV/G
Lab Temp:	24° C

Date:	3/7/2013
Engineer:	Joseph Hanna
Standard Deviation:	1.8 mV/G

736 SN 13693

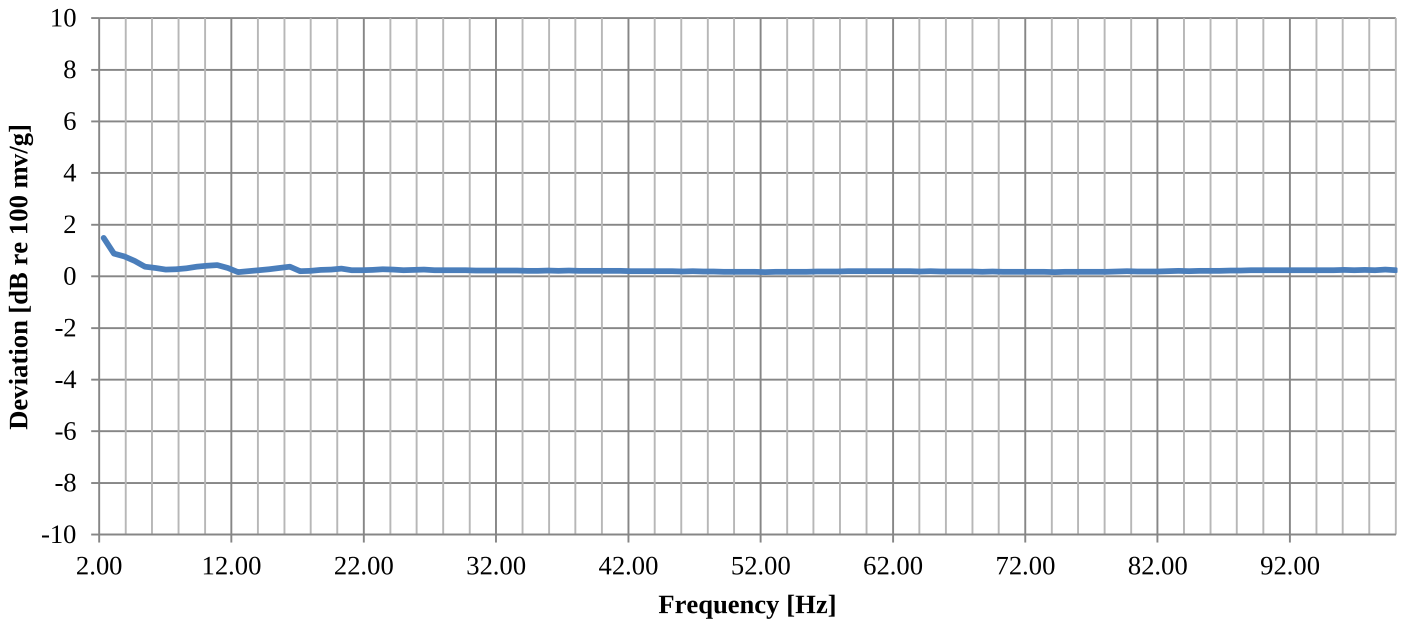

Equipment Used:

Description	Make	Model	Serial	Due Date	Nist No.
Data Acquisition	LMS	SC310	42033911	5/7/2013	-
Ref. Accel	PCB	301A11	2311	4/21/2013	10068
Electromagnetic Shaker	Wilcoxon	F4	20026	-	-
Power Amplifier	QSC	RMS	80629695	-	-

Notes:

Calibration was performed in compliance with ISO 16063-21.
Back-to-back comparison calibration method was used per ISO 16063-21 PRD-P220
Calibration traceable to NIST 10068
*Sensitivity measured from 1 - 100 Hz

Noise Control Engineering, Inc.

799 Middlesex Turnpike
Billerica, MA 01821-3445
Phone: 978-670-5339
Fax: 978-667-7047
E-mail: nonoise@noise-control.com

Model:	736
Serial Number:	1240
Sensitivity*:	96.0 mV/G
Lab Temp:	24° C

Date:	3/7/2013
Engineer:	Joseph Hanna
Standard Deviation:	1.0 mV/G

736 SN 12403

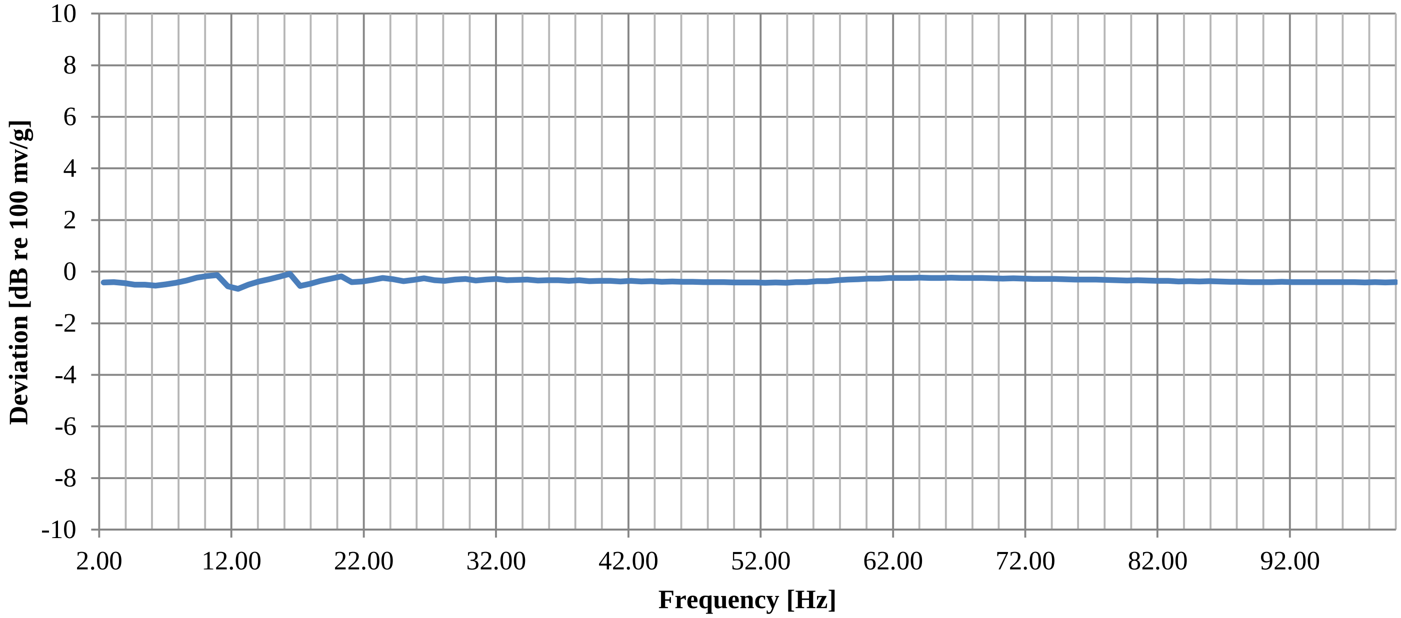

Equipment Used:

Description	Make	Model	Serial	Due Date	Nist No.
Data Acquisition	LMS	SC310	42033911	5/7/2013	-
Ref. Accel	PCB	301A11	2311	4/21/2013	10068
Electromagnetic Shaker	Wilcoxon	F4	20026	-	-
Power Amplifier	QSC	RMS	80629695	-	-

Notes:

Calibration was performed in compliance with ISO 16063-21.
Back-to-back comparison calibration method was used per ISO 16063-21 PRD-P220
Calibration traceable to NIST 10068
*Sensitivity measured from 1 - 100 Hz

Noise Control Engineering, Inc.

799 Middlesex Turnpike
Billerica, MA 01821-3445
Phone: 978-670-5339
Fax: 978-667-7047
E-mail: nonoise@noise-control.com

Model:	736
Serial Number:	1787
Sensitivity*:	99.5 mV/G
Lab Temp:	24° C

Date:	3/7/2013
Engineer:	Joseph Hanna
Standard Deviation:	1.0 mV/G

736 SN 17870

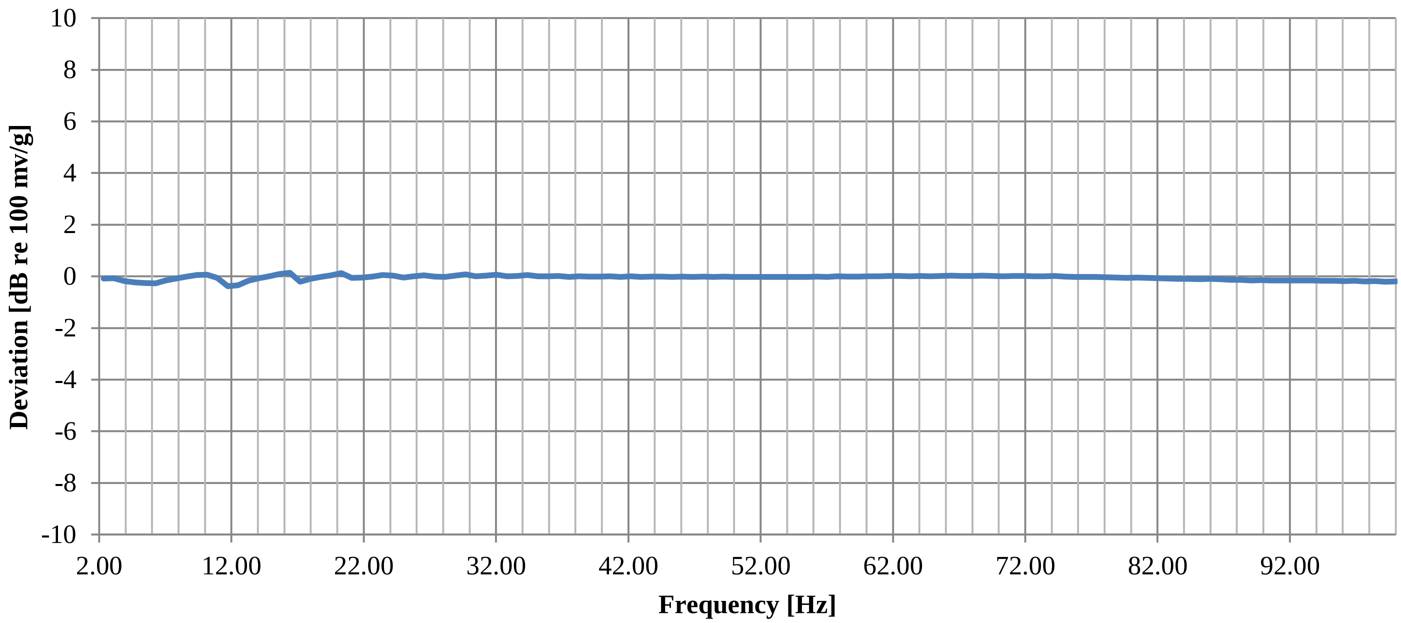

Equipment Used:

Description	Make	Model	Serial	Due Date	Nist No.
Data Acquisition	LMS	SC310	42033911	5/7/2013	-
Ref. Accel	PCB	301A11	2311	4/21/2013	10068
Electromagnetic Shaker	Wilcoxon	F4	20026	-	-
Power Amplifier	QSC	RMS	80629695	-	-

Notes:

Calibration was performed in compliance with ISO 16063-21.
Back-to-back comparison calibration method was used per ISO 16063-21 PRD-P220
Calibration traceable to NIST 10068
*Sensitivity measured from 1 - 100 Hz

Noise Control Engineering, Inc.

799 Middlesex Turnpike
Billerica, MA 01821-3445
Phone: 978-670-5339
Fax: 978-667-7047
E-mail: nonoise@noise-control.com

Model:	736
Serial Number:	1786
Sensitivity*:	101.1 mV/G
Lab Temp:	24° C

Date:	3/7/2013
Engineer:	Joseph Hanna
Standard Deviation:	1.2 mV/G

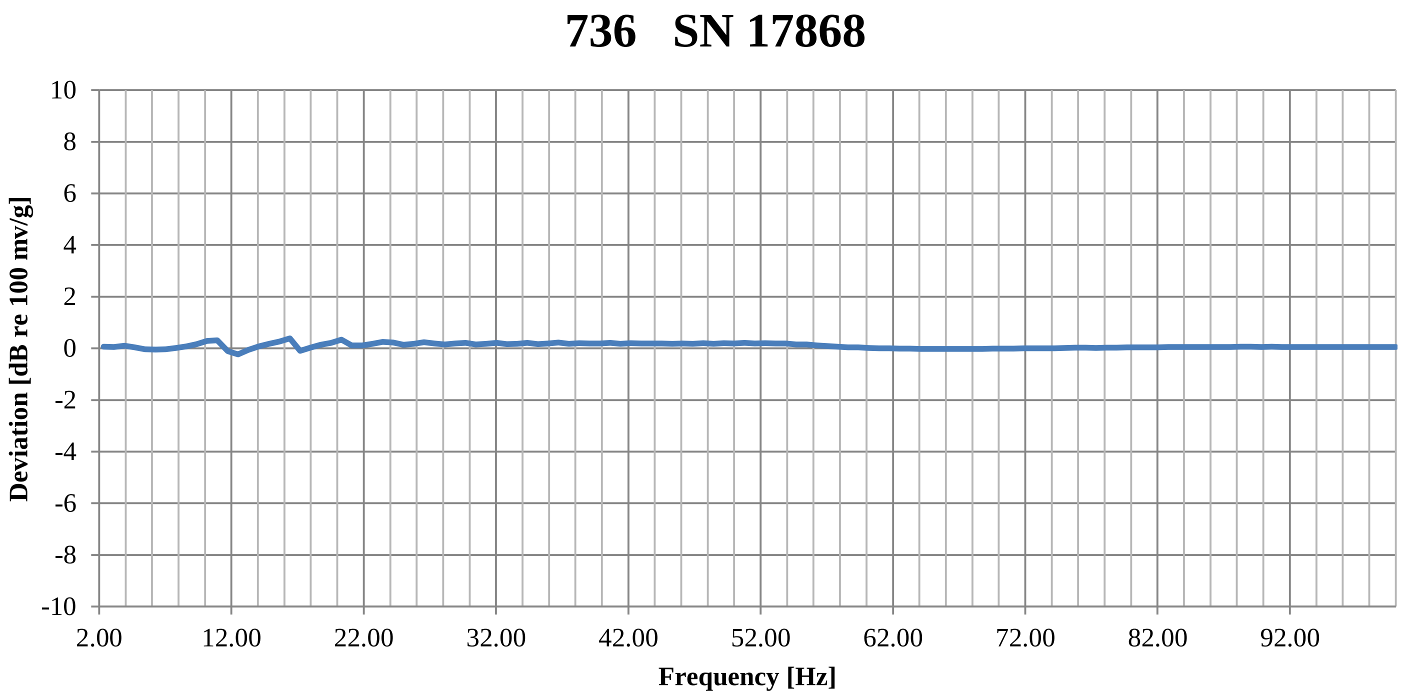

Equipment Used:

Description	Make	Model	Serial	Due Date	Nist No.
Data Acquisition	LMS	SC310	42033911	5/7/2013	-
Ref. Accel	PCB	301A11	2311	4/21/2013	10068
Electromagnetic Shaker	Wilcoxon	F4	20026	-	-
Power Amplifier	QSC	RMS	80629695	-	-

Notes:

Calibration was performed in compliance with ISO 16063-21.
Back-to-back comparison calibration method was used per ISO 16063-21 PRD-P220
Calibration traceable to NIST 10068
*Sensitivity measured from 1 - 100 Hz

Noise Control Engineering, Inc.

799 Middlesex Turnpike
Billerica, MA 01821-3445
Phone: 978-670-5339
Fax: 978-667-7047
E-mail: nonoise@noise-control.com

Model:	736
Serial Number:	1240
Sensitivity*:	95.5 mV/G
Lab Temp:	24° C

Date:	3/7/2013
Engineer:	Joseph Hanna
Standard Deviation:	1.3 mV/G

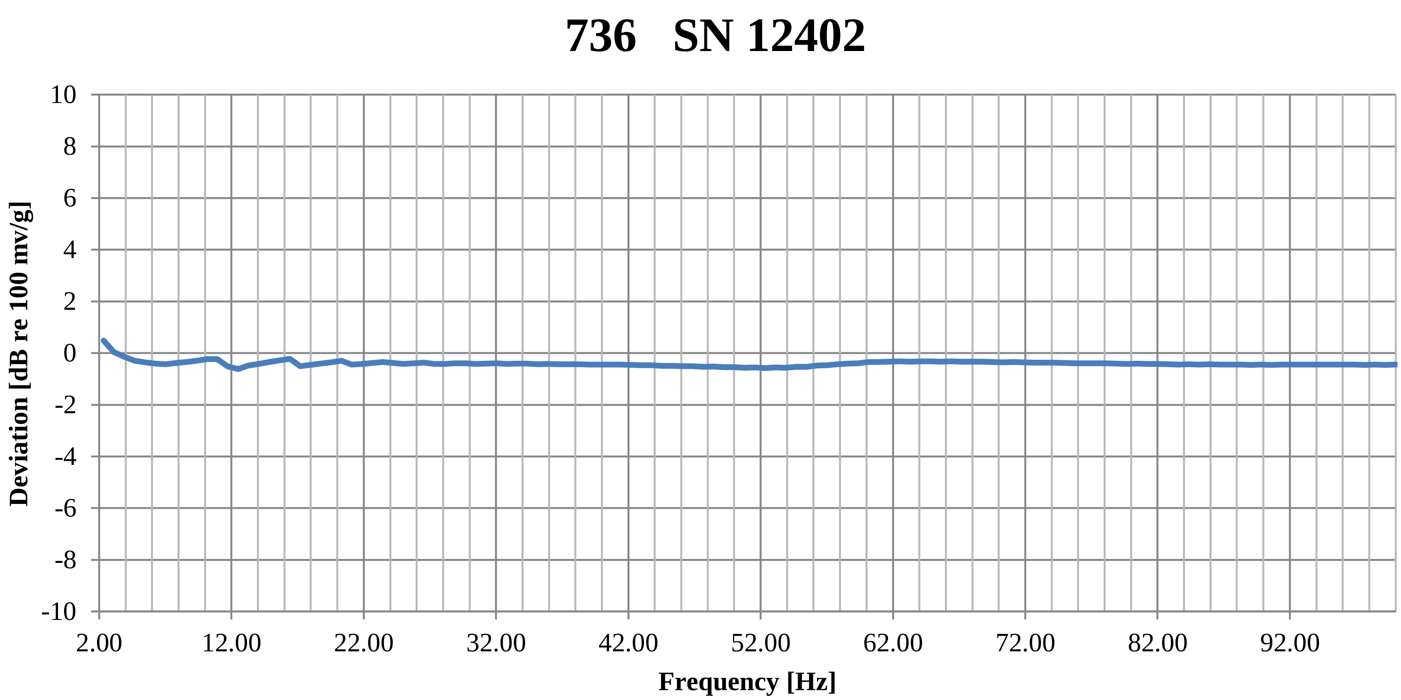

Equipment Used:

Description	Make	Model	Serial	Due Date	Nist No.
Data Acquisition	LMS	SC310	42033911	5/7/2013	-
Ref. Accel	PCB	301A11	2311	4/21/2013	10068
Electromagnetic Shaker	Wilcoxon	F4	20026	-	-
Power Amplifier	QSC	RMS	80629695	-	-

Notes:

Calibration was performed in compliance with ISO 16063-21.
Back-to-back comparison calibration method was used per ISO 16063-21 PRD-P220
Calibration traceable to NIST 10068
*Sensitivity measured from 1 - 100 Hz

THE MODAL SHOP INC. A PCB GROUP CO.

~Calibration Certificate~

3149 East Kemper Rd.
Cincinnati, OH 45241
Ph : 513-351-9919
Fax: 513-458-2172
www.modalshop.com

Sensor Information

Model Number:	HT356B21
Serial Number:	128914
Manufacturer:	PCB
ID Number:	46837
Description:	ICP® Accelerometer

Calibration Data

Sensitivity @ 100 Hz:	9.90	mV/g
Phase @ 100 Hz:	0.08	deg.
Test Level:	10.00	g
Output Bias Level:	9.8	VDC

Transducer Specifications

Amp. Range:	± 500	g
Resolution:	0.003	g
Resonant Freq:	≥ 55000	Hz
Temp. Range:	-54 to 121	°C
	-65 to 250	°F
Axis:	Z - Axis	

Data Table

Freq. (Hz)	Deviation (%)	Phase (deg)
10	-0.317	1.381
30	-0.046	0.528
50	-0.054	0.361
100	0.000	0.076
300	0.009	-0.062
500	0.112	-0.182
1000	0.316	-0.643
2000	0.173	-1.345
3000	0.443	-2.192
4000	0.774	-2.801
5000	0.903	-3.515
6000	1.698	-4.548
7000	1.195	-4.943
8000	2.052	-5.828
9000	2.472	-6.549
10000	2.938	-6.598

Phase Response

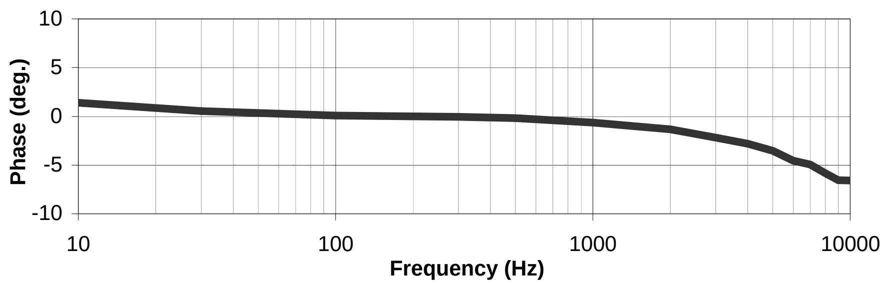

Amplitude Response

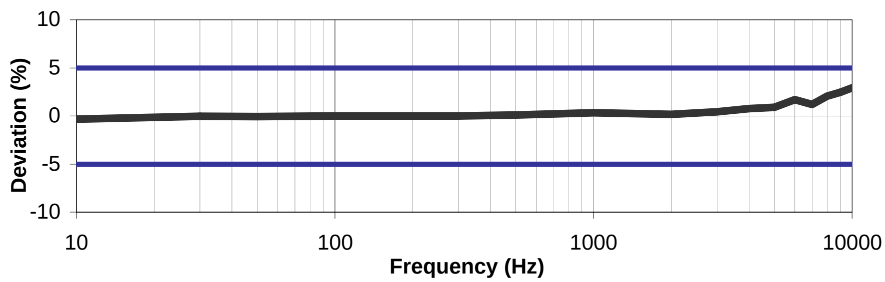

Notes

Results relate only to the items calibrated.
This certificate may not be reproduced except in full, without written permision.
Method: Calibration is performed in compliance with ISO 9001 and ISO 17025
This calibration was performed with TMS 9155 Calibration Workstation version 5.1.1
Calibration traceable to NIST (project number 822/271196).
Back-to-Back Comparison Calibration per ISO 16063-21
Procedure Used: PRD-P220
Measurement uncertainty (95% confidence level with coverage factor 2) for frequency ranges tested during calibration are as follows: 5-9 Hz; ± 1.70%, 10-99 Hz; ± 1.20%, 100 Hz; ± 0.75%, 101-920 Hz; ± 1.00%, 921-5000 Hz; ± 1.40%, 5001-10,000 Hz; ± 1.90%, 10,001-15,000 Hz; ± 2.20%, 15,001-20,000 Hz; ± 2.8%.

Customer
TMS Rental
3149 E. Kemper Rd
Cincinnati, OH 45241

User Notes

Lab Conditions

Temperature:	73 (23)	°F (°C)
Humidity:	63	%

Unit Condition

As Found: In Tolerance
As Left: In Tolerance

Cal Date: 24-Jun-13
Due Date:

Equipment Used

Description	Manufacturer	Model	Serial	Due Date
Data Aquisition Card	NI	4461	E4F2A4	11/8/2013
Std Accelerometer	PCB	080A200	110553	12/10/2013
Air Bearing Shaker	PCB	396C11	603	n/a
Std Sig Conditioner	PCB	442A102	305	12/10/2013
SUT Signal Conditioner	PCB	443B101	373	10/4/2013
Power Amplifier	TMS	2100E21-C	1001	n/a

Approval Information

Technician: Wayne Underwood
Approval:

ACCREDITED

Cal ID: 20884 2649.01

~Calibration Certificate~

THE MODAL SHOP INC.
A PCB GROUP CO.

3149 East Kemper Rd.
Cincinnati, OH 45241
Ph : 513-351-9919
Fax: 513-458-2172
www.modalshop.com

Sensor Information

Model Number: HT356B21
Serial Number: 128914
Manufacturer: PCB
ID Number: 46837
Description: ICP® Accelerometer

Calibration Data

Sensitivity @ 100 Hz:	10.23	mV/g
Phase @ 100 Hz:	0.12	deg.
Test Level:	10.00	g
Output Bias Level:	9.8	VDC

Transducer Specifications

Amp. Range:	± 500	g
Resolution:	0.003	g
Resonant Freq:	≥ 55000	Hz
Temp. Range:	-54 to 121	°C
	-65 to 250	°F
Axis:	Y - Axis	

Data Table

Freq. (Hz)	Deviation (%)	Phase (deg)
10	0.089	1.542
30	-0.180	0.581
50	0.027	0.408
100	0.000	0.116
300	0.075	-0.114
500	0.080	-0.218
1000	0.349	-0.666
2000	0.382	-1.389
3000	0.436	-2.177
4000	0.688	-2.820
5000	0.898	-3.492
6000	1.633	-4.521
7000	1.296	-5.028
8000	2.088	-5.914
9000	2.548	-6.621
10000	3.004	-6.723

Phase Response

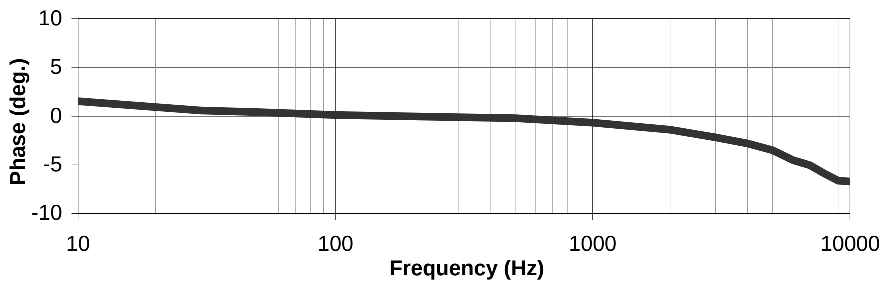

Amplitude Response

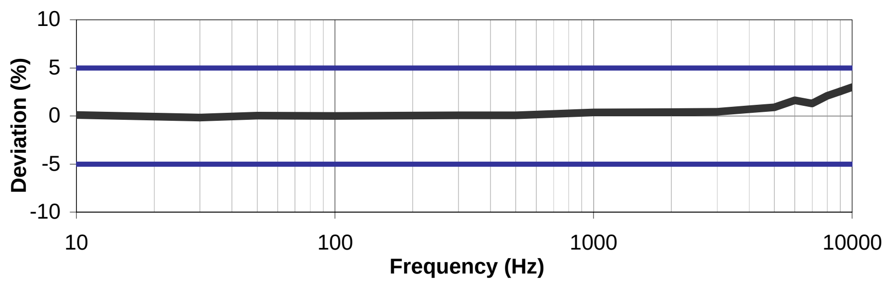

Notes

Results relate only to the items calibrated.
This certificate may not be reproduced except in full, without written permision.
Method: Calibration is performed in compliance with ISO 9001 and ISO 17025
This calibration was performed with TMS 9155 Calibration Workstation version 5.1.1
Calibration traceable to NIST (project number 822/271196).
Back-to-Back Comparison Calibration per ISO 16063-21
Procedure Used: PRD-P220
Measurement uncertainty (95% confidence level with coverage factor 2) for frequency ranges tested during calibration are as follows: 5-9 Hz; ± 1.70%, 10-99 Hz; ± 1.20%, 100 Hz; ± 0.75%, 101-920 Hz; ± 1.00%, 921-5000 Hz; ± 1.40%, 5001-10,000 Hz; ± 1.90%, 10,001-15,000 Hz; ± 2.20%, 15,001-20,000 Hz; ± 2.8%.

Customer

TMS Rental
3149 E. Kemper Rd
Cincinnati, OH 45241

User Notes

Lab Conditions

Temperature: 73 (23) °F (°C)
Humidity: 60 %

Unit Condition

As Found: In Tolerance
As Left: In Tolerance

Cal Date: 24-Jun-13
Due Date:

Equipment Used

Description	Manufacturer	Model	Serial	Due Date
Data Aquisition Card	NI	4461	E4F2A4	11/8/2013
Std Accelerometer	PCB	080A200	110553	12/10/2013
Air Bearing Shaker	PCB	396C11	603	n/a
Std Sig Conditioner	PCB	442A102	305	12/10/2013
SUT Signal Conditioner	PCB	443B101	373	10/4/2013
Power Amplifier	TMS	2100E21-C	1001	n/a

Approval Information

Technician: Wayne Underwood
Approval:

ACCREDITED

Cal ID: 20884 2649.01

THE MODAL SHOP INC.
A PCB GROUP CO.

~Calibration Certificate~

3149 East Kemper Rd.
Cincinnati, OH 45241
Ph : 513-351-9919
Fax: 513-458-2172
www.modalshop.com

Sensor Information

Model Number: HT356B21
Serial Number: 128914
Manufacturer: PCB
ID Number: 46837
Description: ICP® Accelerometer

Calibration Data

Sensitivity @ 100 Hz:	10.04	mV/g
Phase @ 100 Hz:	0.01	deg.
Test Level:	10.00	g
Output Bias Level:	10.6	VDC

Transducer Specifications

Amp. Range:	± 500	g
Resolution:	0.003	g
Resonant Freq:	≥ 55000	Hz
Temp. Range:	-54 to 121	°C
	-65 to 250	°F
Axis:	X - Axis	

Data Table

Freq. (Hz)	Deviation (%)	Phase (deg)
10	-0.534	1.411
30	-0.108	0.518
50	0.031	0.300
100	0.000	0.013
300	0.071	-0.398
500	0.087	-0.679
1000	0.384	-1.594
2000	0.411	-3.191
3000	0.908	-4.788
4000	1.772	-6.402
5000	4.650	-9.281
6000	1.242	-9.795
7000	2.527	-11.215

Phase Response

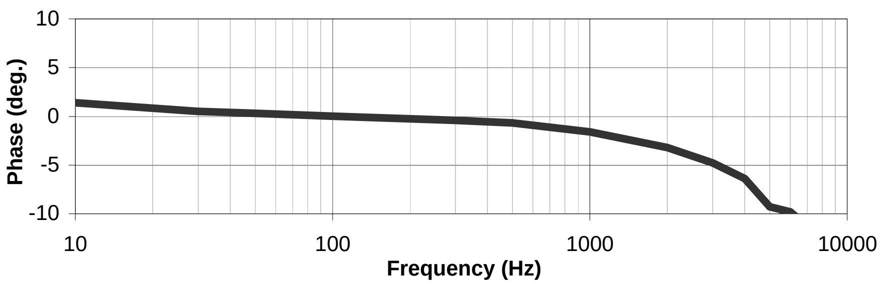

Amplitude Response

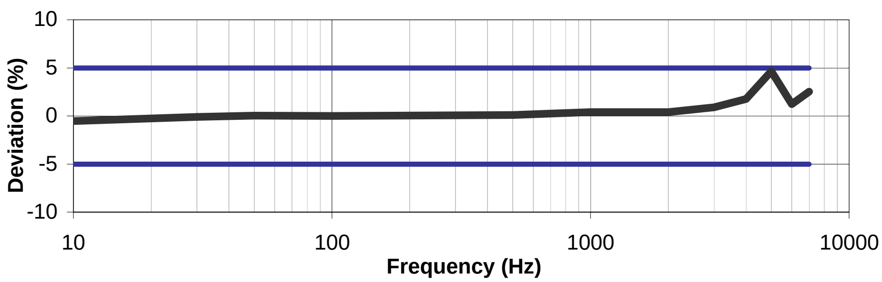

Notes

Results relate only to the items calibrated.
This certificate may not be reproduced except in full, without written permision.
Method: Calibration is performed in compliance with ISO 9001 and ISO 17025
This calibration was performed with TMS 9155 Calibration Workstation version 5.1.1
Calibration traceable to NIST (project number 822/271196).
Back-to-Back Comparison Calibration per ISO 16063-21
Procedure Used: PRD-P220
Measurement uncertainty (95% confidence level with coverage factor 2) for frequency ranges tested during calibration are as follows: 5-9 Hz; ± 1.70%, 10-99 Hz; ± 1.20%, 100 Hz; ± 0.75%, 101-920 Hz; ± 1.00%, 921-5000 Hz; ± 1.40%, 5001-10,000 Hz; ± 1.90%, 10,001-15,000 Hz; ± 2.20%, 15,001-20,000 Hz; ± 2.8%.

Customer

TMS Rental
3149 E. Kemper Rd
Cincinnati, OH 45241

User Notes

Lab Conditions

Temperature: 72 (22) °F (°C)
Humidity: 49 %

Unit Condition

As Found: In Tolerance
As Left: In Tolerance

Equipment Used

Description	Manufacturer	Model	Serial	Due Date
Data Aquisition Card	NI	4461	E4F2A4	11/8/2013
Std Accelerometer	PCB	080A200	110553	12/10/2013
Air Bearing Shaker	PCB	396C11	603	n/a
Std Sig Conditioner	PCB	442A102	305	12/10/2013
SUT Signal Conditioner	PCB	443B101	373	10/4/2013
Power Amplifier	TMS	2100E21-C	1001	n/a

Cal Date: 24-Jun-13
Due Date:

Approval Information

Technician: Wayne Underwood
Approval: Edward A. Ea...

A2LA ACCREDITED

Cal ID: 20884 2649.01

~Calibration Certificate~

THE MODAL SHOP INC.
A PCB GROUP CO.
3149 East Kemper Rd.
Cincinnati, OH 45241
Ph : 513-351-9919
Fax: 513-458-2172
www.modalshop.com

Sensor Information

Model Number:	HT356B21
Serial Number:	126679
Manufacturer:	PCB
ID Number:	46095
Description:	ICP® Accelerometer

Calibration Data

Sensitivity @ 100 Hz:	10.48	mV/g
Phase @ 100 Hz:	0.10	deg.
Test Level:	10.00	g
Output Bias Level:	10.1	VDC

Transducer Specifications

Amp. Range:	± 500	g
Resolution:	0.003	g
Resonant Freq:	≥ 55000	Hz
Temp. Range:	-54 to 121	°C
	-65 to 250	°F
Axis:	Z - Axis	

Data Table

Freq. (Hz)	Deviation (%)	Phase (deg)
10	-0.942	1.455
30	-0.253	0.569
50	0.009	0.360
100	0.000	0.104
300	0.087	-0.122
500	-0.053	-0.253
1000	0.270	-0.628
2000	0.326	-1.334
3000	0.568	-2.012
4000	0.638	-2.761
5000	0.865	-3.482
6000	0.943	-4.190
7000	1.293	-4.855
8000	1.979	-5.723
9000	2.481	-6.382
10000	2.967	-6.545

Phase Response

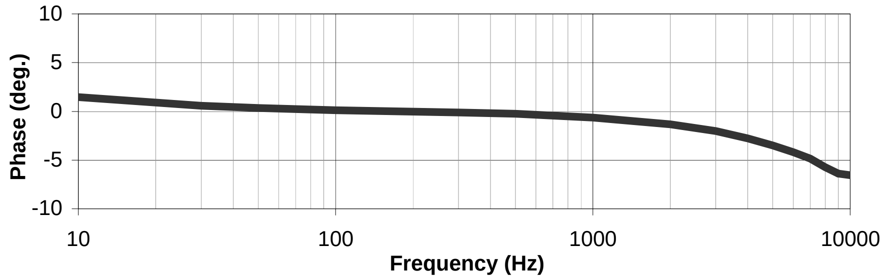

Amplitude Response

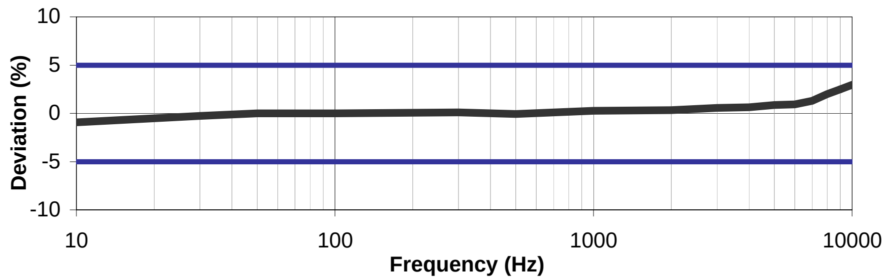

Notes

Results relate only to the items calibrated.
This certificate may not be reproduced except in full, without written permision.
Method: Calibration is performed in compliance with ISO 9001 and ISO 17025
This calibration was performed with TMS 9155 Calibration Workstation version 5.1.1
Calibration traceable to NIST (project number 822/271196).
Back-to-Back Comparison Calibration per ISO 16063-21
Procedure Used: PRD-P220
Measurement uncertainty (95% confidence level with coverage factor 2) for frequency ranges tested during calibration are as follows: 5-9 Hz; ± 1.70%, 10-99 Hz; ± 1.20%, 100 Hz; ± 0.75%, 101-920 Hz; ± 1.00%, 921-5000 Hz; ± 1.40%, 5001-10,000 Hz; ± 1.90%, 10,001-15,000 Hz; ± 2.20%, 15,001-20,000 Hz; ± 2.8%.

Customer
TMS Rental
3149 E. Kemper Rd
Cincinnati, OH 45241

User Notes

Lab Conditions

Temperature:	74 (23)	°F (°C)
Humidity:	50	%

Unit Condition

As Found:	In Tolerance
As Left:	In Tolerance

Cal Date: 24-Jun-13
Due Date:

Equipment Used

Description	Manufacturer	Model	Serial	Due Date
Data Aquisition Card	NI	4461	E4F2A4	11/8/2013
Std Accelerometer	PCB	080A200	110553	12/10/2013
Air Bearing Shaker	PCB	396C11	603	n/a
Std Sig Conditioner	PCB	442A102	305	12/10/2013
SUT Signal Conditioner	PCB	443B101	373	10/4/2013
Power Amplifier	TMS	2100E21-C	1001	n/a

Approval Information

Technician: Wayne Underwood
Approval: Edward A. Lin

ACCREDITED

Cal ID: 20885 2649.01

THE MODAL SHOP INC.
A PCB GROUP CO.

3149 East Kemper Rd.
Cincinnati, OH 45241
Ph : 513-351-9919
Fax: 513-458-2172
www.modalshop.com

~Calibration Certificate~

Sensor Information

Model Number:	HT356B21
Serial Number:	126679
Manufacturer:	PCB
ID Number:	46095
Description:	ICP® Accelerometer

Calibration Data

Sensitivity @ 100 Hz:	10.51	mV/g
Phase @ 100 Hz:	0.14	deg.
Test Level:	10.00	g
Output Bias Level:	10.2	VDC

Transducer Specifications

Amp. Range:	± 500	g
Resolution:	0.003	g
Resonant Freq:	≥ 55000	Hz
Temp. Range:	-54 to 121	°C
	-65 to 250	°F
Axis:	Y - Axis	

Data Table

Freq. (Hz)	Deviation (%)	Phase (deg)
10	-0.271	1.665
30	-0.080	0.665
50	0.158	0.403
100	0.000	0.139
300	0.209	-0.079
500	0.231	-0.173
1000	0.604	-0.623
2000	0.513	-1.410
3000	0.587	-2.220
4000	0.937	-2.895
5000	1.158	-3.609
6000	1.869	-4.599
7000	1.318	-5.053
8000	2.206	-5.773
9000	3.014	-6.559
10000	3.543	-6.751

Phase Response

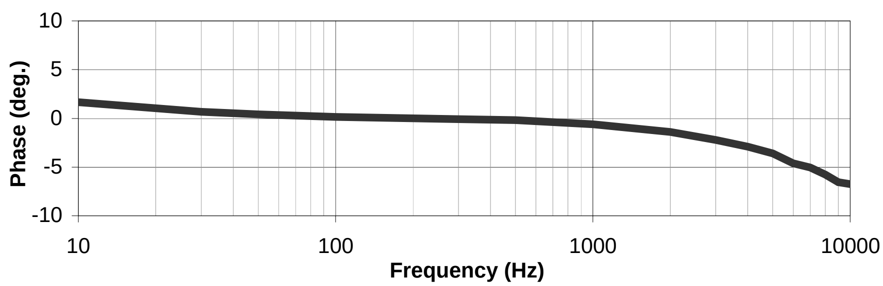

Amplitude Response

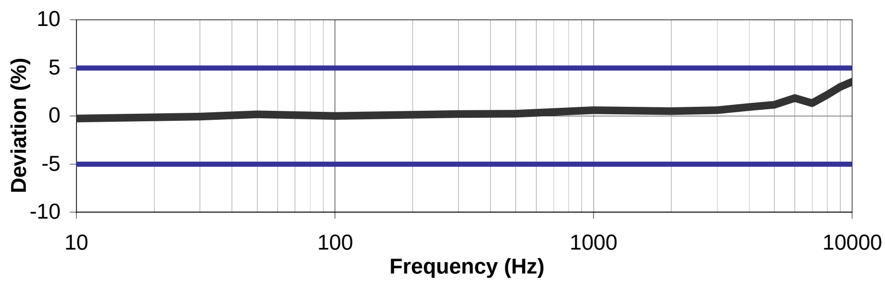

Notes

Results relate only to the items calibrated.
This certificate may not be reproduced except in full, without written permision.
Method: Calibration is performed in compliance with ISO 9001 and ISO 17025
This calibration was performed with TMS 9155 Calibration Workstation version 5.1.1
Calibration traceable to NIST (project number 822/271196).
Back-to-Back Comparison Calibration per ISO 16063-21
Procedure Used: PRD-P220
Measurement uncertainty (95% confidence level with coverage factor 2) for frequency ranges tested during calibration are as follows: 5-9 Hz; ± 1.70%, 10-99 Hz; ± 1.20%, 100 Hz; ± 0.75%, 101-920 Hz; ± 1.00%, 921-5000 Hz; ± 1.40%, 5001-10,000 Hz; ± 1.90%, 10,001-15,000 Hz; ± 2.20%, 15,001-20,000 Hz; ± 2.8%.

Customer

TMS Rental
3149 E. Kemper Rd
Cincinnati, OH 45241

User Notes

Lab Conditions

Temperature:	74 (24)	°F (°C)
Humidity:	51	%

Unit Condition

As Found: In Tolerance
As Left: In Tolerance

Equipment Used

Description	Manufacturer	Model	Serial	Due Date
Data Aquisition Card	NI	4461	E4F2A4	11/8/2013
Std Accelerometer	PCB	080A200	110553	12/10/2013
Air Bearing Shaker	PCB	396C11	603	n/a
Std Sig Conditioner	PCB	442A102	305	12/10/2013
SUT Signal Conditioner	PCB	443B101	373	10/4/2013
Power Amplifier	TMS	2100E21-C	1001	n/a

Cal Date: 24-Jun-13
Due Date:

Approval Information

Technician: Wayne Underwood
Approval:

ACCREDITED

Cal ID: 20885 2649.01

THE MODAL SHOP INC.
A PCB GROUP CO.

3149 East Kemper Rd.
Cincinnati, OH 45241
Ph : 513-351-9919
Fax: 513-458-2172
www.modalshop.com

~Calibration Certificate~

Sensor Information

Model Number:	HT356B21
Serial Number:	126679
Manufacturer:	PCB
ID Number:	46095
Description:	ICP® Accelerometer

Calibration Data

Sensitivity @ 100 Hz:	10.00	mV/g
Phase @ 100 Hz:	-0.02	deg.
Test Level:	10.00	g
Output Bias Level:	10.0	VDC

Transducer Specifications

Amp. Range:	± 500	g
Resolution:	0.003	g
Resonant Freq:	≥ 55000	Hz
Temp. Range:	-54 to 121	°C
	-65 to 250	°F
Axis:	X - Axis	

Data Table

Freq. (Hz)	Deviation (%)	Phase (deg)
10	-0.374	1.280
30	-0.101	0.458
50	0.056	0.261
100	0.000	-0.023
300	0.093	-0.391
500	0.106	-0.692
1000	0.368	-1.589
2000	0.438	-3.216
3000	0.840	-4.884
4000	0.765	-7.193
5000	1.083	-8.087
6000	2.316	-9.999
7000	2.627	-11.079

Phase Response

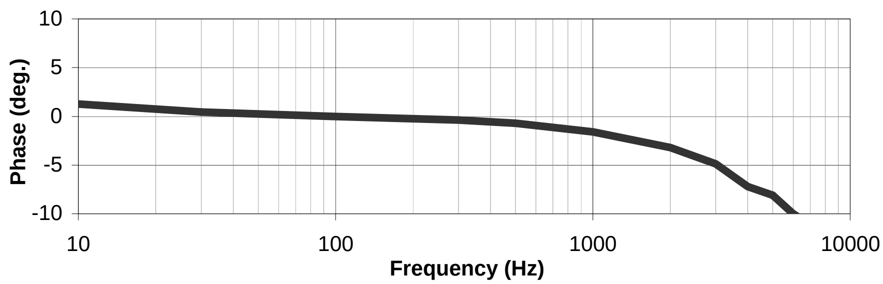

Amplitude Response

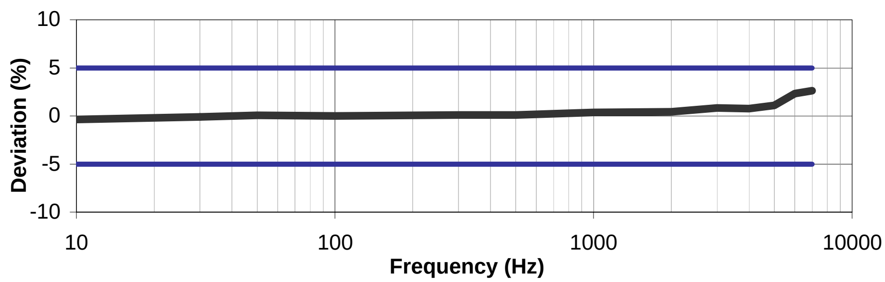

Customer

TMS Rental
3149 E. Kemper Rd
Cincinnati, OH 45241

User Notes

Notes

Results relate only to the items calibrated.
This certificate may not be reproduced except in full, without written permision.
Method: Calibration is performed in compliance with ISO 9001 and ISO 17025
This calibration was performed with TMS 9155 Calibration Workstation version 5.1.1
Calibration traceable to NIST (project number 822/271196).
Back-to-Back Comparison Calibration per ISO 16063-21
Procedure Used: PRD-P220
Measurement uncertainty (95% confidence level with coverage factor 2) for frequency ranges tested during calibration are as follows: 5-9 Hz; ± 1.70%, 10-99 Hz; ± 1.20%, 100 Hz; ± 0.75%, 101-920 Hz; ± 1.00%, 921-5000 Hz; ± 1.40%, 5001-10,000 Hz; ± 1.90%, 10,001-15,000 Hz; ± 2.20%, 15,001-20,000 Hz; ± 2.8%.

Lab Conditions

Temperature:	75 (24)	°F (°C)
Humidity:	56	%

Unit Condition

As Found: In Tolerance
As Left: In Tolerance

Cal Date: 24-Jun-13
Due Date:

Equipment Used

Description	Manufacturer	Model	Serial	Due Date
Data Aquisition Card	NI	4461	E4F2A4	11/8/2013
Std Accelerometer	PCB	080A200	110553	12/10/2013
Air Bearing Shaker	PCB	396C11	603	n/a
Std Sig Conditioner	PCB	442A102	305	12/10/2013
SUT Signal Conditioner	PCB	443B101	373	10/4/2013
Power Amplifier	TMS	2100E21-C	1001	n/a

Approval Information

Technician: Wayne Underwood
Approval:

ACCREDITED

Cal ID: 20885 2649.01

3149 East Kemper Rd.
Cincinnati, OH 45241
Ph : 513-351-9919
Fax: 513-458-2172
www.modalshop.com

~Calibration Certificate~

Sensor Information

Model Number: HT356B21
Serial Number: 126678
Manufacturer: PCB
ID Number: 46094
Description: ICP® Accelerometer

Calibration Data

Sensitivity @ 100 Hz:	10.11	mV/g
Phase @ 100 Hz:	0.12	deg.
Test Level:	10.00	g

Transducer Specifications

Amp. Range:	± 500	g
Resolution:	0.003	g
Resonant Freq:	≥ 55000	Hz
Temp. Range:	-54 to 121	°C
	-65 to 250	°F
Axis:	Z - Axis	

Data Table

Freq. (Hz)	Deviation (%)	Phase (deg)
10	-0.589	1.521
30	-0.178	0.666
50	0.063	0.411
100	0.000	0.121
300	0.162	-0.067
500	0.031	-0.116
1000	0.730	-0.572
2000	0.669	-1.415
3000	0.913	-2.179
4000	1.117	-2.996
5000	1.302	-3.813
6000	1.497	-4.705
7000	1.696	-5.301
8000	2.300	-6.260
9000	2.840	-6.934
10000	3.201	-7.119

Phase Response

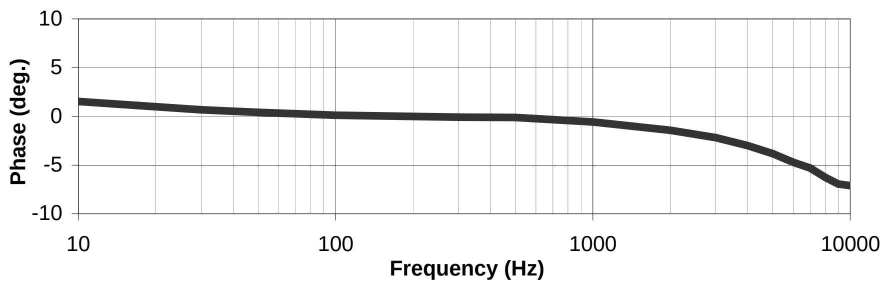

Amplitude Response

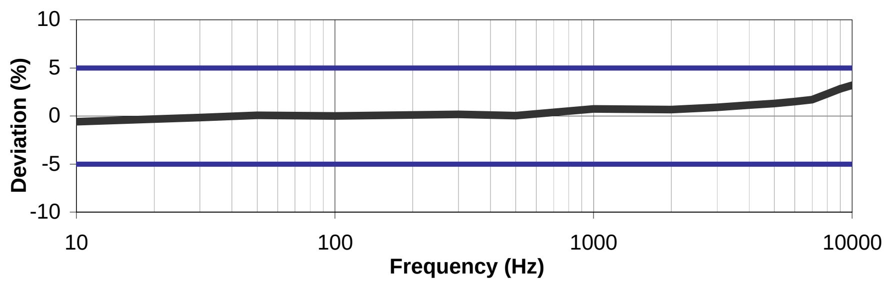

Notes

Results relate only to the items calibrated.
This certificate may not be reproduced except in full, without written permision.
Method: Calibration is performed in compliance with ISO 9001 and ISO 17025
This calibration was performed with TMS 9155 Calibration Workstation version 5.1.1
Calibration traceable to NIST (project number 822/271196).
Back-to-Back Comparison Calibration per ISO 16063-21
Procedure Used: PRD-P220
Measurement uncertainty (95% confidence level with coverage factor 2) for frequency ranges tested during calibration are as follows: 5-9 Hz; ± 1.70%, 10-99 Hz; ± 1.20%, 100 Hz; ± 0.75%, 101-920 Hz; ± 1.00%, 921-5000 Hz; ± 1.40%, 5001-10,000 Hz; ± 1.90%, 10,001-15,000 Hz; ± 2.20%, 15,001-20,000 Hz; ± 2.8%.

Customer

TMS Rental
3149 E. Kemper Rd
Cincinnati, OH 45241

User Notes

Lab Conditions

Temperature: 71 (22) °F (°C)
Humidity: 21 %

Unit Condition

As Found: In Tolerance
As Left: In Tolerance

Cal Date: 20-Mar-13
Due Date:

Equipment Used

Description	Manufacturer	Model	Serial	Due Date
Data Aquisition Card	NI	4461	E4F2A4	11/8/2013
Std Accelerometer	PCB	080A200	110553	12/10/2013
Air Bearing Shaker	PCB	396C11	603	n/a
Std Sig Conditioner	PCB	442A102	305	12/10/2013
SUT Signal Conditioner	PCB	443B101	373	10/4/2013
Power Amplifier	TMS	2100E21-C	1001	n/a

Approval Information

Technician: Ed Devlin
Approval: Edward A. Devlin

ACCREDITED

Cal ID: 20125 2649.01

THE MODAL SHOP INC.
A PCB GROUP CO.
3149 East Kemper Rd.
Cincinnati, OH 45241
Ph : 513-351-9919
Fax: 513-458-2172
www.modalshop.com

~Calibration Certificate~

Sensor Information

Model Number: HT356B21
Serial Number: 126678
Manufacturer: PCB
ID Number: 46094
Description: ICP® Accelerometer

Calibration Data

Sensitivity @ 100 Hz:	10.04	mV/g
Phase @ 100 Hz:	0.10	deg.
Test Level:	10.00	g

Transducer Specifications

Amp. Range:	± 500	g
Resolution:	0.003	g
Resonant Freq:	≥ 55000	Hz
Temp. Range:	-54 to 121	°C
	-65 to 250	°F
Axis:	Y - Axis	

Data Table

Freq. (Hz)	Deviation (%)	Phase (deg)
10	0.331	1.215
30	-0.063	0.563
50	0.056	0.288
100	0.000	0.096
300	0.162	-0.131
500	0.138	-0.221
1000	0.454	-0.670
2000	0.374	-1.469
3000	0.475	-2.241
4000	0.698	-2.955
5000	0.950	-3.658
6000	1.243	-4.410
7000	1.453	-5.149
8000	2.150	-6.026
9000	2.670	-6.723
10000	3.188	-6.841

Phase Response

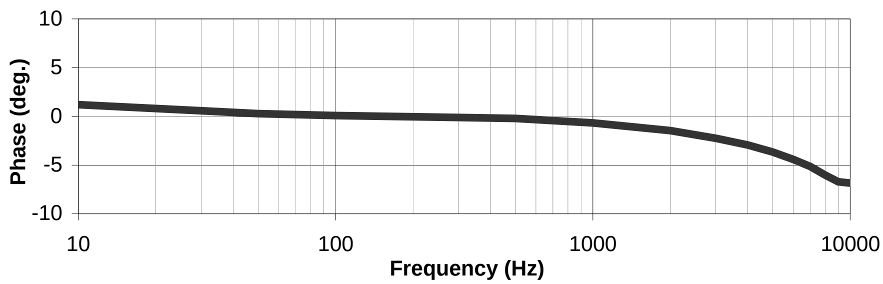

Amplitude Response

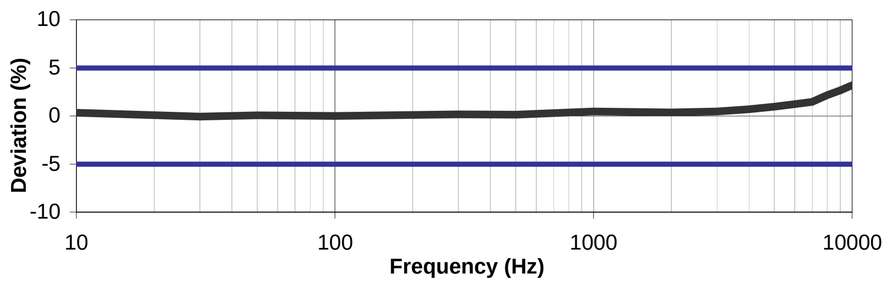

Notes

Results relate only to the items calibrated.
This certificate may not be reproduced except in full, without written permision.
Method: Calibration is performed in compliance with ISO 9001 and ISO 17025
This calibration was performed with TMS 9155 Calibration Workstation version 5.1.1
Calibration traceable to NIST (project number 822/271196).
Back-to-Back Comparison Calibration per ISO 16063-21
Procedure Used: PRD-P220
Measurement uncertainty (95% confidence level with coverage factor 2) for frequency ranges tested during calibration are as follows: 5-9 Hz; ± 1.70%, 10-99 Hz; ± 1.20%, 100 Hz; ± 0.75%, 101-920 Hz; ± 1.00%, 921-5000 Hz; ± 1.40%, 5001-10,000 Hz; ± 1.90%, 10,001-15,000 Hz; ± 2.20%, 15,001-20,000 Hz; ± 2.8%.

Customer

TMS Rental
3149 E. Kemper Rd
Cincinnati, OH 45241

User Notes

Lab Conditions

Temperature: 71 (22) °F (°C)
Humidity: 20 %

Unit Condition

As Found: In Tolerance
As Left: In Tolerance

Equipment Used

Description	Manufacturer	Model	Serial	Due Date
Data Aquisition Card	NI	4461	E4F2A4	11/8/2013
Std Accelerometer	PCB	080A200	110553	12/10/2013
Air Bearing Shaker	PCB	396C11	603	n/a
Std Sig Conditioner	PCB	442A102	305	12/10/2013
SUT Signal Conditioner	PCB	443B101	373	10/4/2013
Power Amplifier	TMS	2100E21-C	1001	n/a

Cal Date: 20-Mar-13
Due Date:

Approval Information

Technician: Ed Devlin
Approval:

ACCREDITED

Cal ID: 20125 2649.01

THE MODAL SHOP INC.
A PCB GROUP CO.

~Calibration Certificate~

3149 East Kemper Rd.
Cincinnati, OH 45241
Ph : 513-351-9919
Fax: 513-458-2172
www.modalshop.com

Sensor Information

Model Number:	HT356B21
Serial Number:	126678
Manufacturer:	PCB
ID Number:	46094
Description:	ICP® Accelerometer

Calibration Data

Sensitivity @ 100 Hz:	10.22	mV/g
Phase @ 100 Hz:	-0.01	deg.
Test Level:	10.00	g

Transducer Specifications

Amp. Range:	± 500	g
Resolution:	0.003	g
Resonant Freq:	≥ 55000	Hz
Temp. Range:	-54 to 121	°C
	-65 to 250	°F
Axis:	X - Axis	

Data Table

Freq. (Hz)	Deviation (%)	Phase (deg)
10	-0.496	1.348
30	-0.080	0.484
50	0.011	0.289
100	0.000	-0.009
300	0.081	-0.366
500	0.109	-0.666
1000	0.376	-1.565
2000	0.426	-3.140
3000	1.182	-4.756
4000	0.170	-7.086
5000	0.907	-7.864
6000	2.197	-9.540
7000	2.569	-10.958

Phase Response

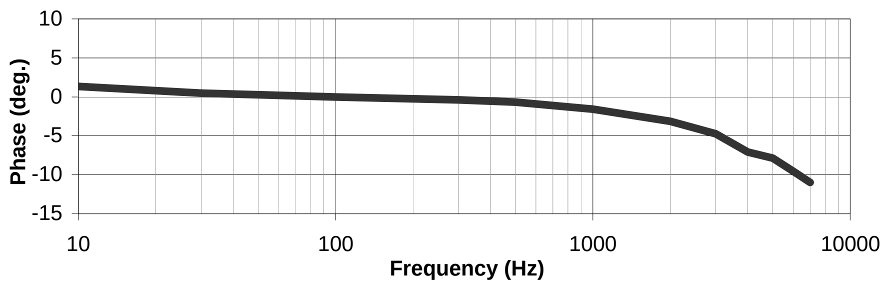

Amplitude Response

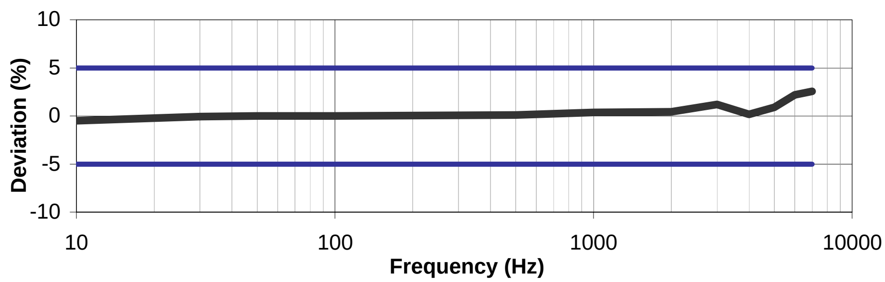

Notes

Results relate only to the items calibrated.
This certificate may not be reproduced except in full, without written permision.
Method: Calibration is performed in compliance with ISO 9001 and ISO 17025
This calibration was performed with TMS 9155 Calibration Workstation version 5.1.1
Calibration traceable to NIST (project number 822/271196).
Back-to-Back Comparison Calibration per ISO 16063-21
Procedure Used: PRD-P220
Measurement uncertainty (95% confidence level with coverage factor 2) for frequency ranges tested during calibration are as follows: 5-9 Hz; ± 1.70%, 10-99 Hz; ± 1.20%, 100 Hz; ± 0.75%, 101-920 Hz; ± 1.00%, 921-5000 Hz; ± 1.40%, 5001-10,000 Hz; ± 1.90%, 10,001-15,000 Hz; ± 2.20%, 15,001-20,000 Hz; ± 2.8%.

Customer

TMS Rental
3149 E. Kemper Rd
Cincinnati, OH 45241

User Notes

Lab Conditions

Temperature:	73 (23)	°F (°C)
Humidity:	18	%

Unit Condition

As Found: In Tolerance
As Left: In Tolerance

Cal Date: 20-Mar-13
Due Date:

Equipment Used

Description	Manufacturer	Model	Serial	Due Date
Data Aquisition Card	NI	4461	E4F2A4	11/8/2013
Std Accelerometer	PCB	080A200	110553	12/10/2013
Air Bearing Shaker	PCB	396C11	603	n/a
Std Sig Conditioner	PCB	442A102	305	12/10/2013
SUT Signal Conditioner	PCB	443B101	373	10/4/2013
Power Amplifier	TMS	2100E21-C	1001	n/a

Approval Information

Technician: Ed Devlin
Approval:

ACCREDITED

Cal ID: 20125 2649.01

3149 East Kemper Rd.
Cincinnati, OH 45241
Ph : 513-351-9919
Fax: 513-458-2172
www.modalshop.com

~Calibration Certificate~

Sensor Information

Model Number: HT356B21
Serial Number: 122922
Manufacturer: PCB
ID Number: 46092
Description: ICP® Accelerometer

Calibration Data

Sensitivity @ 100 Hz:	10.27	mV/g
Phase @ 100 Hz:	0.10	deg.
Test Level:	10.00	g

Transducer Specifications

Amp. Range:	± 500	g
Resolution:	0.003	g
Resonant Freq:	≥ 55000	Hz
Temp. Range:	-54 to 121	°C
	-65 to 250	°F
Axis:	Z - Axis	

Data Table

Freq. (Hz)	Deviation (%)	Phase (deg)
10	-0.138	1.366
30	-0.090	0.468
50	0.032	0.440
100	0.000	0.100
300	0.130	-0.099
500	0.128	-0.214
1000	0.462	-0.702
2000	0.460	-1.534
3000	0.500	-2.318
4000	0.912	-3.159
5000	1.070	-4.048
6000	1.379	-4.976
7000	1.283	-5.657
8000	1.903	-6.626
9000	2.303	-7.408
10000	2.611	-7.611

Phase Response

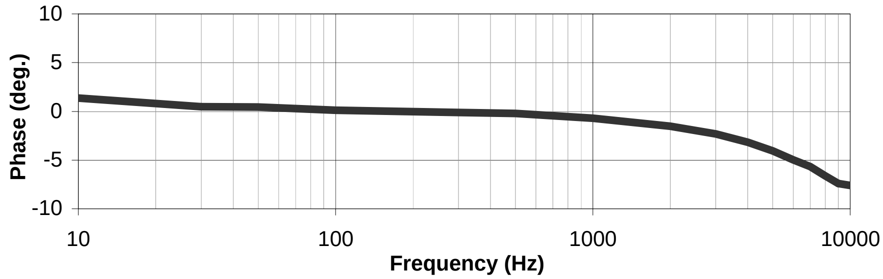

Amplitude Response

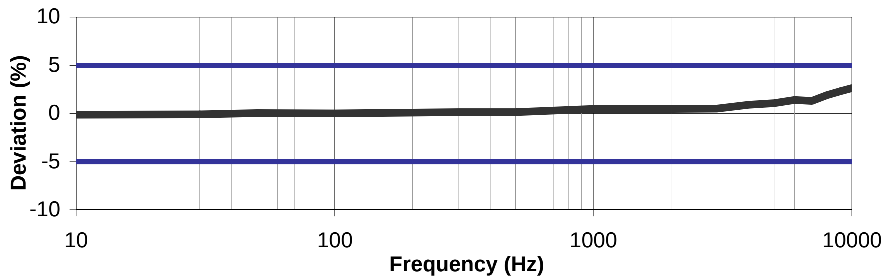

Notes

Results relate only to the items calibrated.
This certificate may not be reproduced except in full, without written permision.
Method: Calibration is performed in compliance with ISO 9001 and ISO 17025
This calibration was performed with TMS 9155 Calibration Workstation version 5.1.1
Calibration traceable to NIST (project number 822/271196).
Back-to-Back Comparison Calibration per ISO 16063-21
Procedure Used: PRD-P220
Measurement uncertainty (95% confidence level with coverage factor 2) for frequency ranges tested during calibration are as follows: 5-9 Hz; ± 1.70%, 10-99 Hz; ± 1.20%, 100 Hz; ± 0.75%, 101-920 Hz; ± 1.00%, 921-5000 Hz; ± 1.40%, 5001-10,000 Hz; ± 1.90%, 10,001-15,000 Hz; ± 2.20%, 15,001-20,000 Hz; ± 2.8%.

Customer

TMS Rental
3149 E. Kemper Rd
Cincinnati, OH 45241

User Notes

Lab Conditions

Temperature: 71 (22) °F (°C)
Humidity: 20 %

Unit Condition

As Found: In Tolerance
As Left: In Tolerance

Equipment Used

Description	Manufacturer	Model	Serial	Due Date
Data Aquisition Card	NI	4461	E4F2A4	11/8/2013
Std Accelerometer	PCB	080A200	110553	12/10/2013
Air Bearing Shaker	PCB	396C11	603	n/a
Std Sig Conditioner	PCB	442A102	305	12/10/2013
SUT Signal Conditioner	PCB	443B101	373	10/4/2013
Power Amplifier	TMS	2100E21-C	1001	n/a

Cal Date: 20-Mar-13
Due Date:

Approval Information

Technician: Ed Devlin
Approval:

ACCREDITED

Cal ID: 20128 2649.01

THE MODAL SHOP INC.
A PCB GROUP CO.

~Calibration Certificate~

3149 East Kemper Rd.
Cincinnati, OH 45241
Ph : 513-351-9919
Fax: 513-458-2172
www.modalshop.com

Sensor Information

Model Number:	HT356B21
Serial Number:	122922
Manufacturer:	PCB
ID Number:	46092
Description:	ICP® Accelerometer

Calibration Data

Sensitivity @ 100 Hz:	10.27	mV/g
Phase @ 100 Hz:	0.10	deg.
Test Level:	10.00	g

Transducer Specifications

Amp. Range:	± 500	g
Resolution:	0.003	g
Resonant Freq:	≥ 55000	Hz
Temp. Range:	-54 to 121	°C
	-65 to 250	°F
Axis:	Y - Axis	

Data Table

Freq. (Hz)	Deviation (%)	Phase (deg)
10	0.094	1.263
30	-0.099	0.520
50	0.131	0.416
100	0.000	0.096
300	0.109	-0.130
500	0.086	-0.234
1000	0.507	-0.662
2000	0.511	-1.587
3000	0.602	-2.462
4000	0.881	-3.264
5000	1.151	-4.099
6000	1.814	-5.091
7000	1.320	-5.708
8000	2.244	-6.745
9000	2.581	-7.567
10000	3.016	-7.745

Phase Response

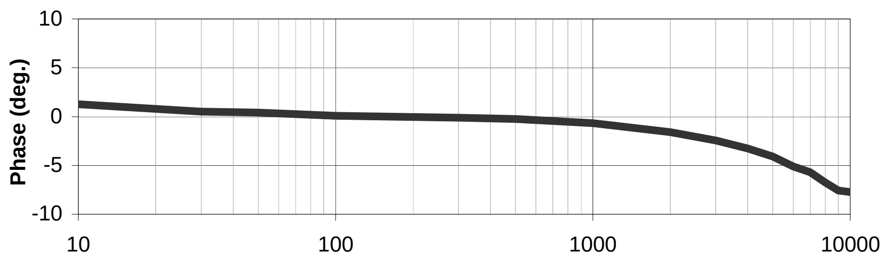

Amplitude Response

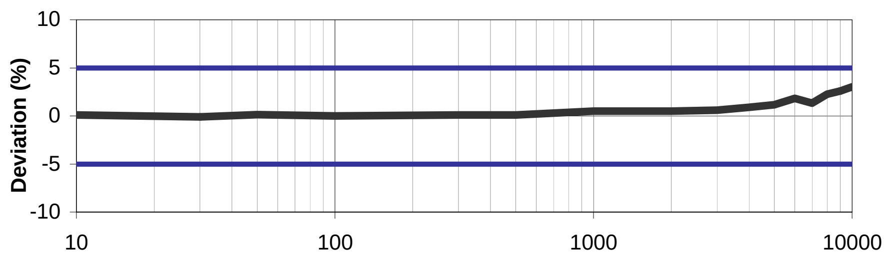

Customer

TMS Rental
3149 E. Kemper Rd
Cincinnati, OH 45241

User Notes

Notes

Results relate only to the items calibrated.
This certificate may not be reproduced except in full, without written permision.
Method: Calibration is performed in compliance with ISO 9001 and ISO 17025
This calibration was performed with TMS 9155 Calibration Workstation version 5.1.1
Calibration traceable to NIST (project number 822/271196).
Back-to-Back Comparison Calibration per ISO 16063-21
Procedure Used: PRD-P220
Measurement uncertainty (95% confidence level with coverage factor 2) for frequency ranges tested during calibration are as follows: 5-9 Hz; ± 1.70%, 10-99 Hz; ± 1.20%, 100 Hz; ± 0.75%, 101-920 Hz; ± 1.00%, 921-5000 Hz; ± 1.40%, 5001-10,000 Hz; ± 1.90%, 10,001-15,000 Hz; ± 2.20%, 15,001-20,000 Hz; ± 2.8%.

Lab Conditions

Temperature: 71 (22) °F (°C)
Humidity: 19 %

Unit Condition

As Found: In Tolerance
As Left: In Tolerance

Cal Date: 20-Mar-13
Due Date:

Equipment Used

Description	Manufacturer	Model	Serial	Due Date
Data Aquisition Card	NI	4461	E4F2A4	11/8/2013
Std Accelerometer	PCB	080A200	110553	12/10/2013
Air Bearing Shaker	PCB	396C11	603	n/a
Std Sig Conditioner	PCB	442A102	305	12/10/2013
SUT Signal Conditioner	PCB	443B101	373	10/4/2013
Power Amplifier	TMS	2100E21-C	1001	n/a

Approval Information

Technician: Ed Devlin
Approval:

ACCREDITED

Cal ID: 20128 2649.01

~Calibration Certificate~

3149 East Kemper Rd.
Cincinnati, OH 45241
Ph : 513-351-9919
Fax: 513-458-2172
www.modalshop.com

Sensor Information

Model Number:	HT356B21
Serial Number:	122922
Manufacturer:	PCB
ID Number:	46092
Description:	ICP® Accelerometer

Calibration Data

Sensitivity @ 100 Hz:	10.19	mV/g
Phase @ 100 Hz:	0.04	deg.
Test Level:	10.00	g

Transducer Specifications

Amp. Range:	± 500	g
Resolution:	0.003	g
Resonant Freq:	≥ 55000	Hz
Temp. Range:	-54 to 121	°C
	-65 to 250	°F
Axis:	X - Axis	

Data Table

Freq. (Hz)	Deviation (%)	Phase (deg)
10	-0.735	1.469
30	-0.160	0.540
50	0.093	0.336
100	0.000	0.043
300	0.197	-0.367
500	0.298	-0.674
1000	0.636	-1.674
2000	0.714	-3.485
3000	0.993	-5.363
4000	1.833	-7.189
5000	0.485	-9.552
6000	2.621	-10.686
7000	2.566	-12.080

Phase Response

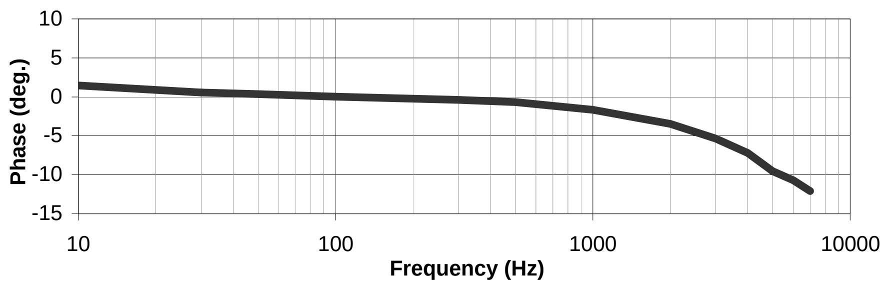

Amplitude Response

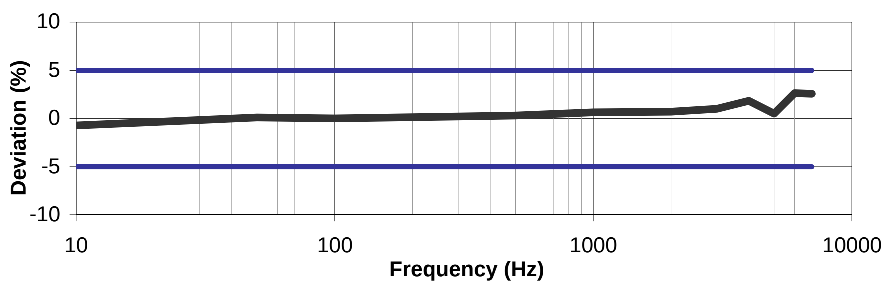

Notes

Results relate only to the items calibrated.
This certificate may not be reproduced except in full, without written permision.
Method: Calibration is performed in compliance with ISO 9001 and ISO 17025
This calibration was performed with TMS 9155 Calibration Workstation version 5.1.1
Calibration traceable to NIST (project number 822/271196).
Back-to-Back Comparison Calibration per ISO 16063-21
Procedure Used: PRD-P220
Measurement uncertainty (95% confidence level with coverage factor 2) for frequency ranges tested during calibration are as follows: 5-9 Hz; ± 1.70%, 10-99 Hz; ± 1.20%, 100 Hz; ± 0.75%, 101-920 Hz; ± 1.00%, 921-5000 Hz; ± 1.40%, 5001-10,000 Hz; ± 1.90%, 10,001-15,000 Hz; ± 2.20%, 15,001-20,000 Hz; ± 2.8%.

Customer

TMS Rental
3149 E. Kemper Rd
Cincinnati, OH 45241

User Notes

Lab Conditions

Temperature:	73 (23)	°F (°C)
Humidity:	18	%

Unit Condition

As Found: In Tolerance
As Left: In Tolerance

Cal Date: 20-Mar-13
Due Date:

Equipment Used

Description	Manufacturer	Model	Serial	Due Date
Data Aquisition Card	NI	4461	E4F2A4	11/8/2013
Std Accelerometer	PCB	080A200	110553	12/10/2013
Air Bearing Shaker	PCB	396C11	603	n/a
Std Sig Conditioner	PCB	442A102	305	12/10/2013
SUT Signal Conditioner	PCB	443B101	373	10/4/2013
Power Amplifier	TMS	2100E21-C	1001	n/a

Approval Information

Technician: Ed Devlin
Approval: Edward A. Devlin

ACCREDITED

Cal ID: 20128 2649.01

THE MODAL SHOP INC.
A PCB GROUP CO.

~Calibration Certificate~

3149 East Kemper Rd.
Cincinnati, OH 45241
Ph : 513-351-9919
Fax: 513-458-2172
www.modalshop.com

Sensor Information

Model Number:	356B21
Serial Number:	LW126834
Manufacturer:	PCB
ID Number:	46090
Description:	ICP® Accelerometer

Calibration Data

Sensitivity @ 100 Hz:	10.00	mV/g
Phase @ 100 Hz:	0.13	deg.
Test Level:	10.00	g

Transducer Specifications

Amp. Range:	± 500	g
Resolution:	0.003	g
Resonant Freq:	≥ 55000	Hz
Temp. Range:	-54 to 121	°C
	-65 to 250	°F
Axis:	Z - Axis	

Data Table

Freq. (Hz)	Deviation (%)	Phase (deg)
10	-0.237	1.401
30	-0.060	0.554
50	0.083	0.366
100	0.000	0.131
300	0.184	-0.129
500	0.201	-0.206
1000	0.461	-0.726
2000	0.440	-1.537
3000	0.570	-2.335
4000	0.865	-3.105
5000	1.068	-3.923
6000	1.586	-4.852
8000	2.245	-6.466
9000	2.757	-7.234
10000	3.303	-7.401

Phase Response

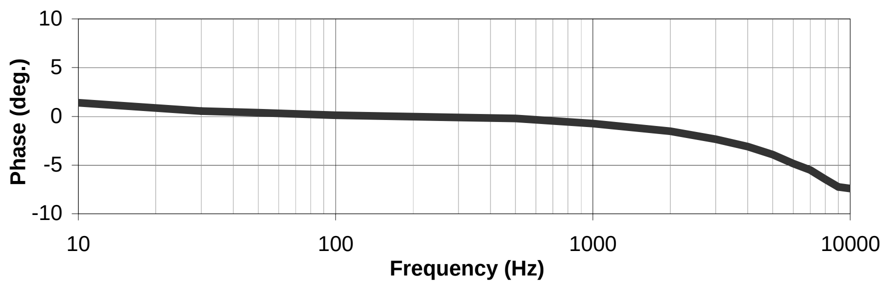

Amplitude Response

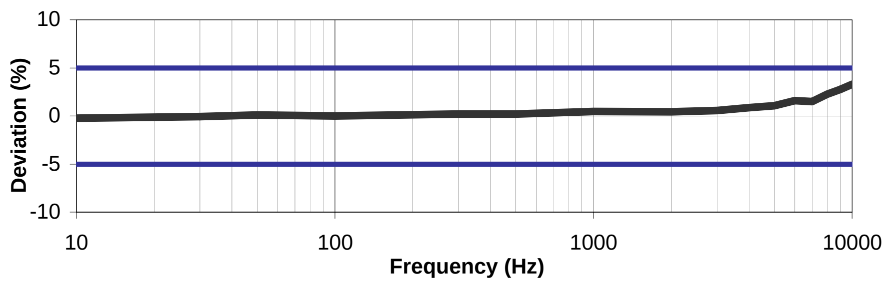

Notes

Results relate only to the items calibrated.
This certificate may not be reproduced except in full, without written permision.
Method: Calibration is performed in compliance with ISO 9001 and ISO 17025
This calibration was performed with TMS 9155 Calibration Workstation version 5.1.1
Calibration traceable to NIST (project number 822/271196).
Back-to-Back Comparison Calibration per ISO 16063-21
Procedure Used: PRD-P220
Measurement uncertainty (95% confidence level with coverage factor 2) for frequency ranges tested during calibration are as follows: 5-9 Hz; ± 1.70%, 10-99 Hz; ± 1.20%, 100 Hz; ± 0.75%, 101-920 Hz; ± 1.00%, 921-5000 Hz; ± 1.40%, 5001-10,000 Hz; ± 1.90%, 10,001-15,000 Hz; ± 2.20%, 15,001-20,000 Hz; ± 2.8%.

Customer

TMS Rental
3149 E. Kemper Rd
Cincinnati, OH 45241

User Notes

Lab Conditions

Temperature:	74 (23)	°F (°C)
Humidity:	45	%

Unit Condition

As Found: In Tolerance
As Left: In Tolerance

Equipment Used

Description	Manufacturer	Model	Serial	Due Date
Data Aquisition Card	NI	4461	E4F2A4	11/8/2013
Std Accelerometer	PCB	080A200	110553	12/10/2013
Air Bearing Shaker	PCB	396C11	603	n/a
Std Sig Conditioner	PCB	442A102	305	12/10/2013
SUT Signal Conditioner	PCB	443B101	373	10/4/2013
Power Amplifier	TMS	2100E21-C	1001	n/a

Cal Date: 9-May-13
Due Date:

Approval Information

Technician: Wayne Underwood
Approval:

A2LA ACCREDITED

Cal ID: 20422 2649.01

THE MODAL SHOP INC.
A PCB GROUP CO.

~Calibration Certificate~

3149 East Kemper Rd.
Cincinnati, OH 45241
Ph : 513-351-9919
Fax: 513-458-2172
www.modalshop.com

Sensor Information

Model Number:	356B21
Serial Number:	LW126834
Manufacturer:	PCB
ID Number:	46090
Description:	ICP® Accelerometer

Calibration Data

Sensitivity @ 100 Hz:	10.04	mV/g
Phase @ 100 Hz:	0.06	deg.
Test Level:	10.00	g

Transducer Specifications

Amp. Range:	± 500	g
Resolution:	0.003	g
Resonant Freq:	≥ 55000	Hz
Temp. Range:	-54 to 121	°C
	-65 to 250	°F
Axis:	Y - Axis	

Data Table

Freq. (Hz)	Deviation (%)	Phase (deg)
10	-0.612	1.353
30	0.004	0.539
50	0.110	0.370
100	0.000	0.062
300	0.080	-0.151
500	0.066	-0.283
1000	0.305	-0.693
2000	0.306	-1.495
3000	0.445	-2.347
4000	0.623	-3.109
5000	0.919	-3.706
6000	1.888	-4.788
8000	2.448	-6.401
9000	3.001	-7.150
10000	3.533	-7.357

Phase Response

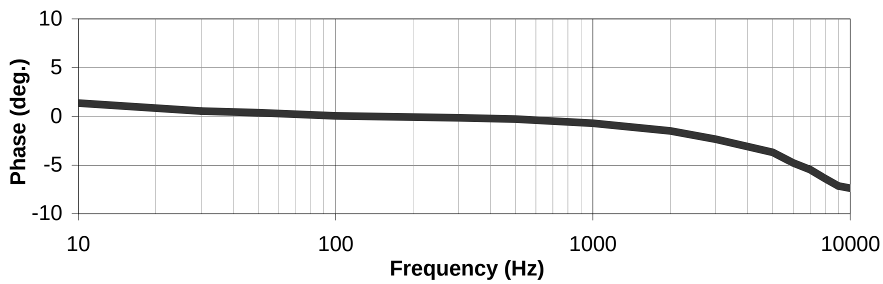

Amplitude Response

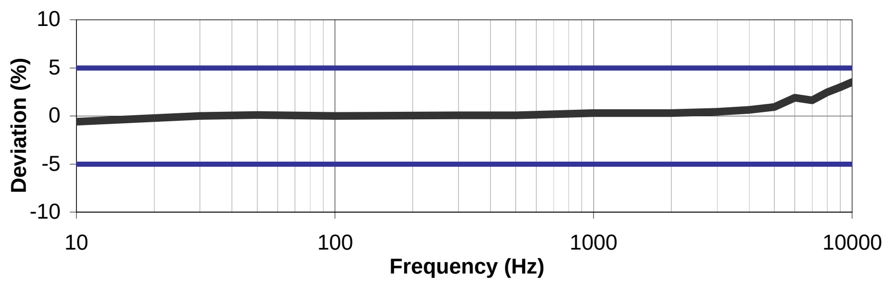

Notes

Results relate only to the items calibrated.
This certificate may not be reproduced except in full, without written permision.
Method: Calibration is performed in compliance with ISO 9001 and ISO 17025
This calibration was performed with TMS 9155 Calibration Workstation version 5.1.1
Calibration traceable to NIST (project number 822/271196).
Back-to-Back Comparison Calibration per ISO 16063-21
Procedure Used: PRD-P220
Measurement uncertainty (95% confidence level with coverage factor 2) for frequency ranges tested during calibration are as follows: 5-9 Hz; ± 1.70%, 10-99 Hz; ± 1.20%, 100 Hz; ± 0.75%, 101-920 Hz; ± 1.00%, 921-5000 Hz; ± 1.40%, 5001-10,000 Hz; ± 1.90%, 10,001-15,000 Hz; ± 2.20%, 15,001-20,000 Hz; ± 2.8%.

Customer

TMS Rental
3149 E. Kemper Rd
Cincinnati, OH 45241

User Notes

Lab Conditions

Temperature:	74 (23)	°F (°C)
Humidity:	45	%

Unit Condition

As Found:	In Tolerance
As Left:	In Tolerance

Cal Date: 9-May-13
Due Date:

Equipment Used

Description	Manufacturer	Model	Serial	Due Date
Data Aquisition Card	NI	4461	E4F2A4	11/8/2013
Std Accelerometer	PCB	080A200	110553	12/10/2013
Air Bearing Shaker	PCB	396C11	603	n/a
Std Sig Conditioner	PCB	442A102	305	12/10/2013
SUT Signal Conditioner	PCB	443B101	373	10/4/2013
Power Amplifier	TMS	2100E21-C	1001	n/a

Approval Information

Technician: Wayne Underwood
Approval:

ACCREDITED

Cal ID: 20422 2649.01

~Calibration Certificate~

3149 East Kemper Rd.
Cincinnati, OH 45241
Ph : 513-351-9919
Fax: 513-458-2172
www.modalshop.com

Sensor Information

Model Number:	356B21
Serial Number:	LW126834
Manufacturer:	PCB
ID Number:	46090
Description:	ICP® Accelerometer

Calibration Data

Sensitivity @ 100 Hz:	9.81	mV/g
Phase @ 100 Hz:	-0.02	deg.
Test Level:	10.00	g

Transducer Specifications

Amp. Range:	± 500	g
Resolution:	0.003	g
Resonant Freq:	≥ 55000	Hz
Temp. Range:	-54 to 121	°C
	-65 to 250	°F
Axis:	X - Axis	

Data Table

Freq. (Hz)	Deviation (%)	Phase (deg)
10	-0.184	1.511
30	-0.247	0.551
50	-0.040	0.318
100	0.000	-0.017
300	0.121	-0.569
500	0.060	-0.959
1000	0.375	-2.154
2000	0.449	-4.472
3000	0.642	-6.617
4000	1.000	-8.896
5000	0.181	-11.404
6000	0.723	-13.206
7000	1.912	-15.533

Phase Response

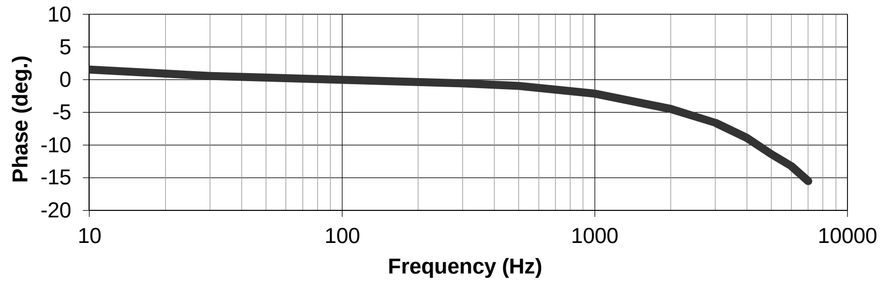

Amplitude Response

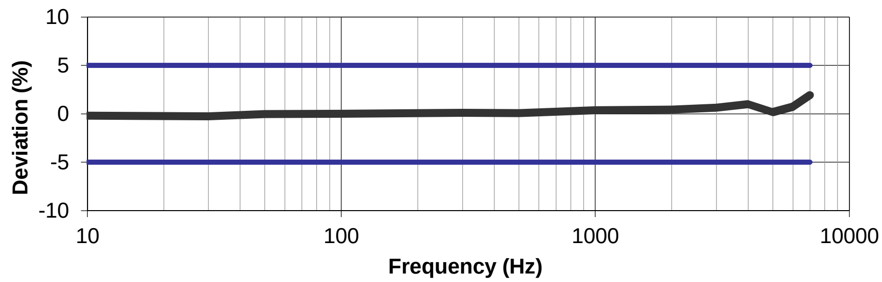

Notes

Results relate only to the items calibrated.
This certificate may not be reproduced except in full, without written permision.
Method: Calibration is performed in compliance with ISO 9001 and ISO 17025
This calibration was performed with TMS 9155 Calibration Workstation version 5.1.1
Calibration traceable to NIST (project number 822/271196).
Back-to-Back Comparison Calibration per ISO 16063-21
Procedure Used: PRD-P220
Measurement uncertainty (95% confidence level with coverage factor 2) for frequency ranges tested during calibration are as follows: 5-9 Hz; ± 1.70%, 10-99 Hz; ± 1.20%, 100 Hz; ± 0.75%, 101-920 Hz; ± 1.00%, 921-5000 Hz; ± 1.40%, 5001-10,000 Hz; ± 1.90%, 10,001-15,000 Hz; ± 2.20%, 15,001-20,000 Hz; ± 2.8%.

Customer

TMS Rental
3149 E. Kemper Rd
Cincinnati, OH 45241

User Notes

Lab Conditions

Temperature:	74 (23)	°F (°C)
Humidity:	45	%

Unit Condition

As Found: In Tolerance
As Left: In Tolerance

Cal Date: 9-May-13
Due Date:

Equipment Used

Description	Manufacturer	Model	Serial	Due Date
Data Aquisition Card	NI	4461	E4F2A4	11/8/2013
Std Accelerometer	PCB	080A200	110553	12/10/2013
Air Bearing Shaker	PCB	396C11	603	n/a
Std Sig Conditioner	PCB	442A102	305	12/10/2013
SUT Signal Conditioner	PCB	443B101	373	10/4/2013
Power Amplifier	TMS	2100E21-C	1001	n/a

Approval Information

Technician: Ed Devlin
Approval: Edward A. Devlin

ACCREDITED

Cal ID: 20422 2649.01

THE MODAL SHOP INC.
A PCB GROUP CO.

3149 East Kemper Rd.
Cincinnati, OH 45241
Ph : 513-351-9919
Fax: 513-458-2172
www.modalshop.com

~Calibration Certificate~

Sensor Information

Model Number:	356B21
Serial Number:	LW126776
Manufacturer:	PCB
ID Number:	46082
Description:	ICP® Accelerometer

Calibration Data

Sensitivity @ 100 Hz:	9.67	mV/g
Phase @ 100 Hz:	0.20	deg.
Test Level:	10.00	g

Transducer Specifications

Amp. Range:	± 500	g
Resolution:	0.003	g
Resonant Freq:	≥ 55000	Hz
Temp. Range:	-54 to 121	°C
	-65 to 250	°F
Axis:	Y - Axis	

Data Table

Freq. (Hz)	Deviation (%)	Phase (deg)
10	0.585	2.240
30	0.122	0.820
50	0.158	0.534
100	0.000	0.203
300	0.169	-0.093
500	0.071	-0.157
1000	0.348	-0.550
2000	0.528	-1.190
3000	0.641	-1.891
4000	0.876	-2.537
5000	1.132	-3.169
6000	1.718	-4.006
7000	1.555	-4.414
8000	2.518	-5.230
9000	3.041	-5.807
10000	3.746	-5.887

Phase Response

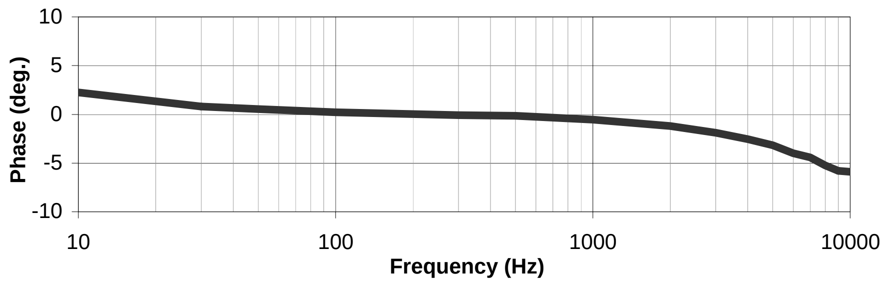

Amplitude Response

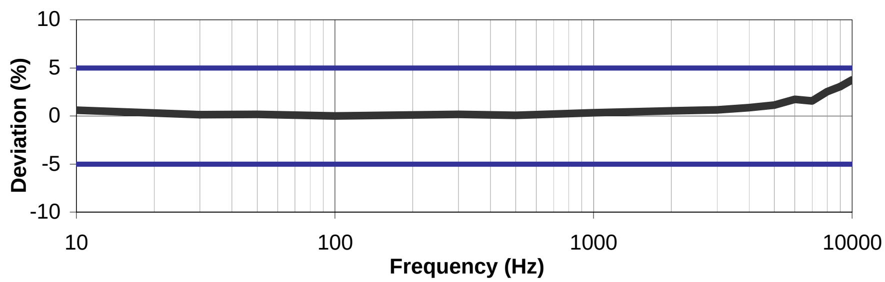

Customer
TMS Rental
3149 E. Kemper Rd
Cincinnati, OH 45241

User Notes

Notes
Results relate only to the items calibrated.
This certificate may not be reproduced except in full, without written permision.
Method: Calibration is performed in compliance with ISO 9001 and ISO 17025
This calibration was performed with TMS 9155 Calibration Workstation version 5.1.1
Calibration traceable to NIST (project number 822/271196).
Back-to-Back Comparison Calibration per ISO 16063-21
Procedure Used: PRD-P220
Measurement uncertainty (95% confidence level with coverage factor 2) for frequency ranges tested during calibration are as follows: 5-9 Hz; ± 1.70%, 10-99 Hz; ± 1.20%, 100 Hz; ± 0.75%, 101-920 Hz; ± 1.00%, 921-5000 Hz; ± 1.40%, 5001-10,000 Hz; ± 1.90%, 10,001-15,000 Hz; ± 2.20%, 15,001-20,000 Hz; ± 2.8%.

Lab Conditions

Temperature:	71 (22)	°F (°C)
Humidity:	25	%

Unit Condition

As Found:	In Tolerance
As Left:	In Tolerance

Equipment Used

Description	Manufacturer	Model	Serial	Due Date
Data Aquisition Card	NI	4461	E4F2A4	11/8/2013
Std Accelerometer	PCB	080A200	110553	12/10/2013
Air Bearing Shaker	PCB	396C11	603	n/a
Std Sig Conditioner	PCB	442A102	305	12/10/2013
SUT Signal Conditioner	PCB	443B101	373	10/4/2013
Power Amplifier	TMS	2100E21-C	1001	n/a

Cal Date: 21-Dec-12
Due Date:

Approval Information
Technician: Abby Lebowitz
Approval:

ACCREDITED

Cal ID: 19774 2649.01

THE MODAL SHOP INC.
A PCB GROUP CO.

3149 East Kemper Rd.
Cincinnati, OH 45241
Ph : 513-351-9919
Fax: 513-458-2172
www.modalshop.com

~Calibration Certificate~

Sensor Information

Model Number:	356B21
Serial Number:	LW126776
Manufacturer:	PCB
ID Number:	46082
Description:	ICP® Accelerometer

Calibration Data

Sensitivity @ 100 Hz:	9.77	mV/g
Phase @ 100 Hz:	0.01	deg.
Test Level:	10.00	g

Transducer Specifications

Amp. Range:	± 500	g
Resolution:	0.003	g
Resonant Freq:	≥ 55000	Hz
Temp. Range:	-54 to 121	°C
	-65 to 250	°F
Axis:	X - Axis	

Data Table

Freq. (Hz)	Deviation (%)	Phase (deg)
10	0.054	1.586
30	0.104	0.577
50	0.201	0.327
100	0.000	0.011
300	0.168	-0.357
500	0.117	-0.579
1000	0.336	-1.345
2000	0.361	-2.759
3000	0.567	-4.086
4000	0.836	-5.425
5000	1.379	-6.754
6000	1.889	-8.062
7000	2.857	-9.028

Phase Response

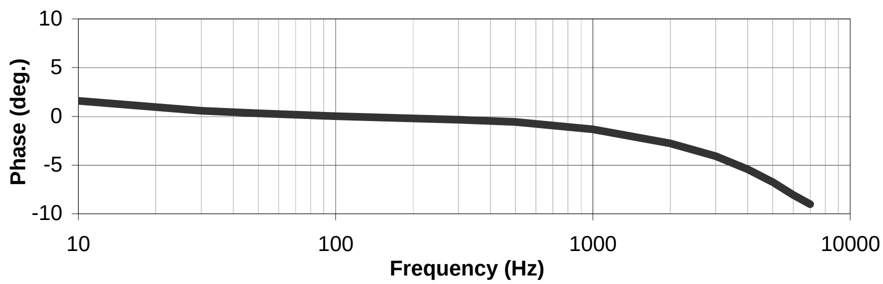

Amplitude Response

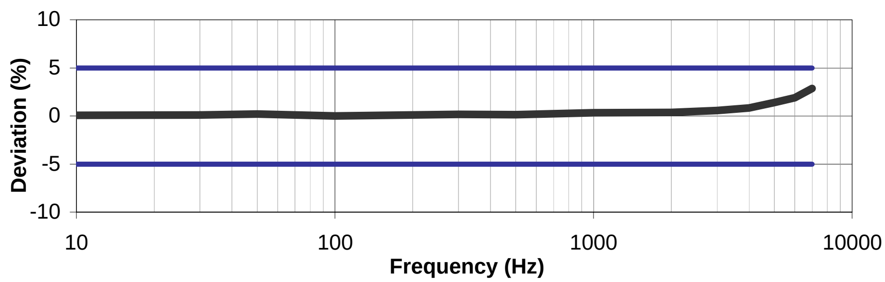

Notes

Results relate only to the items calibrated.
This certificate may not be reproduced except in full, without written permision.
Method: Calibration is performed in compliance with ISO 9001 and ISO 17025
This calibration was performed with TMS 9155 Calibration Workstation version 5.1.1
Calibration traceable to NIST (project number 822/271196).
Back-to-Back Comparison Calibration per ISO 16063-21
Procedure Used: PRD-P220
Measurement uncertainty (95% confidence level with coverage factor 2) for frequency ranges tested during calibration are as follows: 5-9 Hz; ± 1.70%, 10-99 Hz; ± 1.20%, 100 Hz; ± 0.75%, 101-920 Hz; ± 1.00%, 921-5000 Hz; ± 1.40%, 5001-10,000 Hz; ± 1.90%, 10,001-15,000 Hz; ± 2.20%, 15,001-20,000 Hz; ± 2.8%.

Customer

TMS Rental
3149 E. Kemper Rd
Cincinnati, OH 45241

User Notes

Lab Conditions

Temperature:	71 (22)	°F (°C)
Humidity:	25	%

Unit Condition

As Found: In Tolerance
As Left: In Tolerance

Cal Date: 21-Dec-12
Due Date:

Equipment Used

Description	Manufacturer	Model	Serial	Due Date
Data Aquisition Card	NI	4461	E4F2A4	11/8/2013
Std Accelerometer	PCB	080A200	110553	12/10/2013
Air Bearing Shaker	PCB	396C11	603	n/a
Std Sig Conditioner	PCB	442A102	305	12/10/2013
SUT Signal Conditioner	PCB	443B101	373	10/4/2013
Power Amplifier	TMS	2100E21-C	1001	n/a

Approval Information

Technician: Abby Lebowitz
Approval: Edward A. Lebowitz

ACCREDITED

Cal ID: 19774 2649.01

THE MODAL SHOP INC. A PCB GROUP CO.

~Calibration Certificate~

3149 East Kemper Rd.
Cincinnati, OH 45241
Ph : 513-351-9919
Fax: 513-458-2172
www.modalshop.com

Sensor Information

Model Number: HT356B21
Serial Number: 118731
Manufacturer: PCB
ID Number: 45433
Description: ICP® Accelerometer

Calibration Data

Sensitivity @ 100 Hz:	10.12	mV/g
Phase @ 100 Hz:	0.02	deg.
Test Level:	1.00	g
Output Bias Level:	10.3	VDC

Transducer Specifications

Amp. Range:	± 500	g
Resolution:	0.003	g
Resonant Freq:	≥ 55000	Hz
Temp. Range:	-54 to 121	°C
	-65 to 250	°F
Axis:	Z - Axis	

Data Table

Freq. (Hz)	Deviation (%)	Phase (deg)
10	0.032	1.360
30	-0.156	0.331
50	0.177	0.316
100	0.000	0.018
300	0.254	-0.126
500	0.184	-0.227
1000	0.447	-0.671
2000	0.461	-1.431
3000	0.770	-2.164
4000	0.678	-2.980
5000	1.085	-3.576
6000	1.438	-4.453
7000	1.477	-5.097
8000	2.309	-6.015
9000	2.911	-6.660
10000	3.391	-6.828

Phase Response

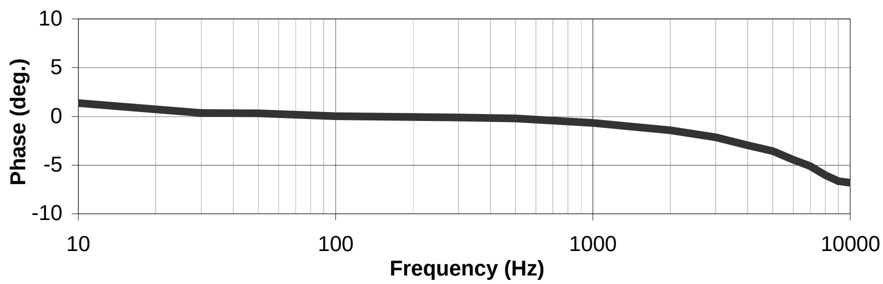

Amplitude Response

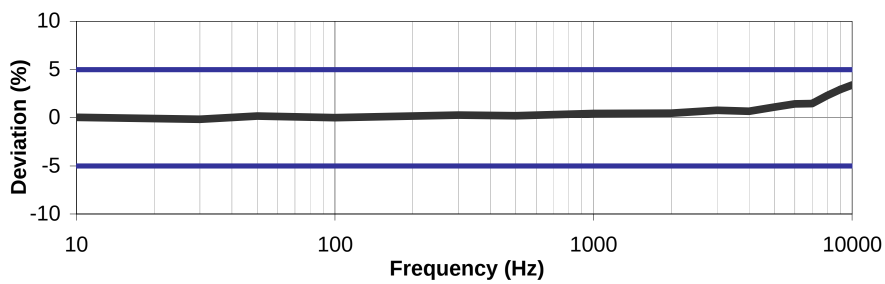

Notes

Results relate only to the items calibrated.
This certificate may not be reproduced except in full, without written permision.
Method: Calibration is performed in compliance with ISO 9001 and ISO 17025
This calibration was performed with TMS 9155 Calibration Workstation version 5.1.1
Calibration traceable to NIST (project number 822/271196).
Back-to-Back Comparison Calibration per ISO 16063-21
Procedure Used: PRD-P220
Measurement uncertainty (95% confidence level with coverage factor 2) for frequency ranges tested during calibration are as follows: 5-9 Hz; ± 1.70%, 10-99 Hz; ± 1.20%, 100 Hz; ± 0.75%, 101-920 Hz; ± 1.00%, 921-5000 Hz; ± 1.40%, 5001-10,000 Hz; ± 1.90%, 10,001-15,000 Hz; ± 2.20%, 15,001-20,000 Hz; ± 2.8%.

Customer

TMS Rental
3149 E. Kemper Rd
Cincinnati, OH 45241

User Notes

Lab Conditions

Temperature: 76 (25) °F (°C)
Humidity: 42 %

Unit Condition

As Found: In Tolerance
As Left: In Tolerance

Equipment Used

Description	Manufacturer	Model	Serial	Due Date
Data Aquisition Card	NI	4461	E4F2A4	11/8/2013
Std Accelerometer	PCB	080A200	110553	12/10/2013
Air Bearing Shaker	PCB	396C11	603	n/a
Std Sig Conditioner	PCB	442A102	305	12/10/2013
SUT Signal Conditioner	PCB	443B101	373	10/4/2013
Power Amplifier	TMS	2100E21-C	1001	n/a

Cal Date: 5-Aug-13
Due Date:

Approval Information

Technician: Wayne Underwood
Approval: Edward A. Le ...

ACCREDITED

Cal ID: 21420 2649.01

THE MODAL SHOP INC.
A PCB GROUP CO.

~Calibration Certificate~

3149 East Kemper Rd.
Cincinnati, OH 45241
Ph : 513-351-9919
Fax: 513-458-2172
www.modalshop.com

Sensor Information

Model Number: HT356B21
Serial Number: 118731
Manufacturer: PCB
ID Number: 45433
Description: ICP® Accelerometer

Calibration Data

Sensitivity @ 100 Hz: 9.93 mV/g
Phase @ 100 Hz: 0.04 deg.
Test Level: 1.00 g
Output Bias Level: 9.8 VDC

Transducer Specifications

Amp. Range: ± 500 g
Resolution: 0.003 g
Resonant Freq: ≥ 55000 Hz
Temp. Range: -54 to 121 °C
-65 to 250 °F
Axis: Y - Axis

Data Table

Freq. (Hz)	Deviation (%)	Phase (deg)
10	0.034	1.063
30	0.097	0.508
50	-0.236	0.273
100	0.000	0.044
300	-0.043	-0.193
500	0.110	-0.342
1000	0.359	-0.703
2000	0.263	-1.435
3000	0.313	-2.197
4000	0.627	-2.899
5000	0.889	-3.583
6000	1.345	-4.416
7000	1.184	-5.017
8000	2.044	-5.929
9000	2.586	-6.585
10000	3.057	-6.666

Phase Response

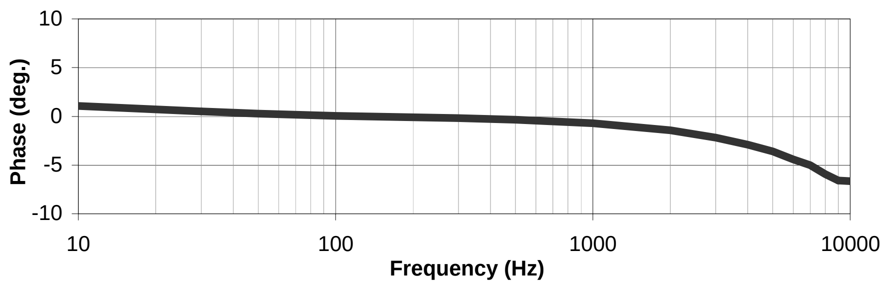

Amplitude Response

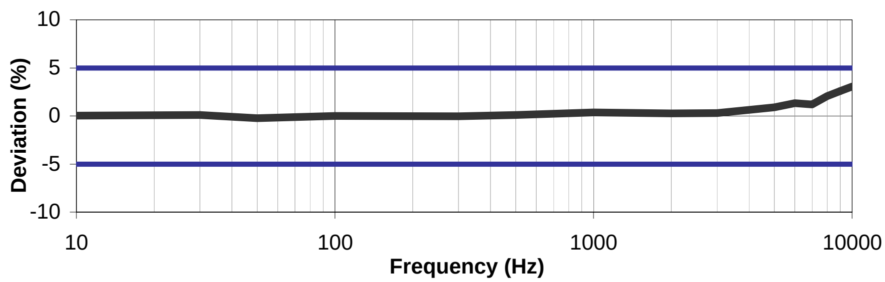

Notes

Results relate only to the items calibrated.
This certificate may not be reproduced except in full, without written permision.
Method: Calibration is performed in compliance with ISO 9001 and ISO 17025
This calibration was performed with TMS 9155 Calibration Workstation version 5.1.1
Calibration traceable to NIST (project number 822/271196).
Back-to-Back Comparison Calibration per ISO 16063-21
Procedure Used: PRD-P220
Measurement uncertainty (95% confidence level with coverage factor 2) for frequency ranges tested during calibration are as follows: 5-9 Hz; ± 1.70%, 10-99 Hz; ± 1.20%, 100 Hz; ± 0.75%, 101-920 Hz; ± 1.00%, 921-5000 Hz; ± 1.40%, 5001-10,000 Hz; ± 1.90%, 10,001-15,000 Hz; ± 2.20%, 15,001-20,000 Hz; ± 2.8%.

Customer

TMS Rental
3149 E. Kemper Rd
Cincinnati, OH 45241

User Notes

Lab Conditions

Temperature: 76 (25) °F (°C)
Humidity: 42 %

Unit Condition

As Found: In Tolerance
As Left: In Tolerance

Cal Date: 5-Aug-13
Due Date:

Equipment Used

Description	Manufacturer	Model	Serial	Due Date
Data Aquisition Card	NI	4461	E4F2A4	11/8/2013
Std Accelerometer	PCB	080A200	110553	12/10/2013
Air Bearing Shaker	PCB	396C11	603	n/a
Std Sig Conditioner	PCB	442A102	305	12/10/2013
SUT Signal Conditioner	PCB	443B101	373	10/4/2013
Power Amplifier	TMS	2100E21-C	1001	n/a

Approval Information

Technician: Wayne Underwood
Approval:

ACCREDITED

Cal ID: 21420 2649.01

3149 East Kemper Rd.
Cincinnati, OH 45241
Ph : 513-351-9919
Fax: 513-458-2172
www.modalshop.com

~Calibration Certificate~

Sensor Information

Model Number:	HT356B21
Serial Number:	118731
Manufacturer:	PCB
ID Number:	45433
Description:	ICP® Accelerometer

Calibration Data

Sensitivity @ 100 Hz:	10.03	mV/g
Phase @ 100 Hz:	0.03	deg.
Test Level:	1.00	g
Output Bias Level:	9.9	VDC

Transducer Specifications

Amp. Range:	± 500	g
Resolution:	0.003	g
Resonant Freq:	≥ 55000	Hz
Temp. Range:	-54 to 121	°C
	-65 to 250	°F
Axis:	X - Axis	

Data Table

Freq. (Hz)	Deviation (%)	Phase (deg)
10	-0.433	1.471
30	-0.172	0.554
50	-0.020	0.307
100	0.000	0.031
300	0.127	-0.359
500	0.018	-0.567
1000	0.308	-1.422
2000	0.419	-2.921
3000	0.979	-4.278
4000	2.494	-5.803
5000	0.463	-7.695
6000	2.382	-8.765
7000	3.767	-10.088

Phase Response

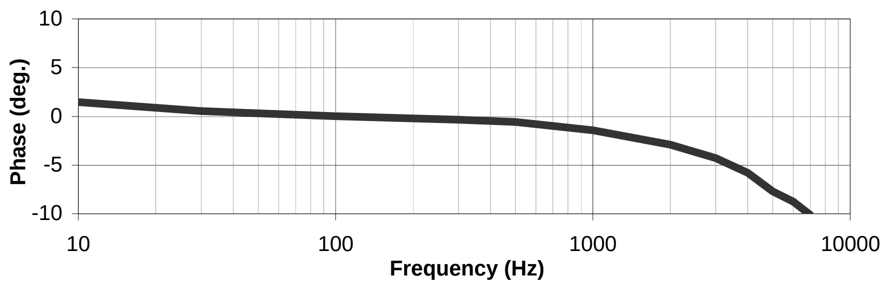

Amplitude Response

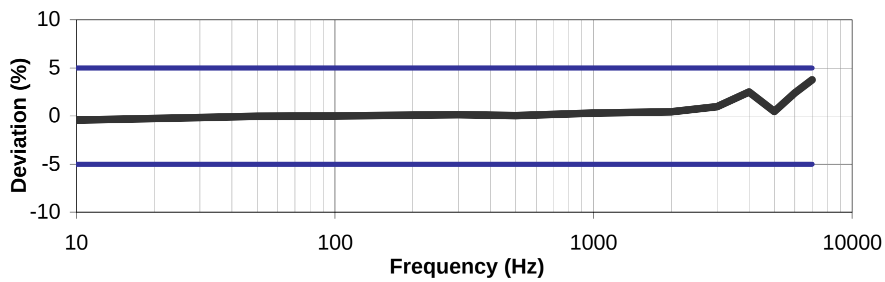

Notes

Results relate only to the items calibrated.
This certificate may not be reproduced except in full, without written permision.
Method: Calibration is performed in compliance with ISO 9001 and ISO 17025
This calibration was performed with TMS 9155 Calibration Workstation version 5.1.1
Calibration traceable to NIST (project number 822/271196).
Back-to-Back Comparison Calibration per ISO 16063-21
Procedure Used: PRD-P220
Measurement uncertainty (95% confidence level with coverage factor 2) for frequency ranges tested during calibration are as follows: 5-9 Hz; ± 1.70%, 10-99 Hz; ± 1.20%, 100 Hz; ± 0.75%, 101-920 Hz; ± 1.00%, 921-5000 Hz; ± 1.40%, 5001-10,000 Hz; ± 1.90%, 10,001-15,000 Hz; ± 2.20%, 15,001-20,000 Hz; ± 2.8%.

Customer
TMS Rental
3149 E. Kemper Rd
Cincinnati, OH 45241

User Notes

Lab Conditions

Temperature:	76 (25)	°F (°C)
Humidity:	46	%

Unit Condition

As Found: In Tolerance
As Left: In Tolerance

Equipment Used

Description	Manufacturer	Model	Serial	Due Date
Data Aquisition Card	NI	4461	E4F2A4	11/8/2013
Std Accelerometer	PCB	080A200	110553	12/10/2013
Air Bearing Shaker	PCB	396C11	603	n/a
Std Sig Conditioner	PCB	442A102	305	12/10/2013
SUT Signal Conditioner	PCB	443B101	373	10/4/2013
Power Amplifier	TMS	2100E21-C	1001	n/a

Cal Date: 5-Aug-13
Due Date:

Approval Information

Technician: Wayne Underwood
Approval: Edward A. Le...

ACCREDITED

Cal ID: 21420 2649.01

THE MODAL SHOP INC.
A PCB GROUP CO.

~Calibration Certificate~

3149 East Kemper Rd.
Cincinnati, OH 45241
Ph : 513-351-9919
Fax: 513-458-2172
www.modalshop.com

Sensor Information

Model Number: HT356B21
Serial Number: 117335
Manufacturer: PCB
ID Number: 45432
Description: ICP® Accelerometer

Calibration Data

Sensitivity @ 100 Hz:	10.40	mV/g
Phase @ 100 Hz:	0.19	deg.
Test Level:	1.00	g
Output Bias Level:	9.9	VDC

Transducer Specifications

Amp. Range:	± 500	g
Resolution:	0.003	g
Resonant Freq:	≥ 55000	Hz
Temp. Range:	-54 to 121	°C
	-65 to 250	°F
Axis:	Z - Axis	

Data Table

Freq. (Hz)	Deviation (%)	Phase (deg)
10	-0.166	1.771
30	0.271	0.886
50	-0.367	0.508
100	0.000	0.191
300	-0.048	-0.112
500	-0.008	-0.184
1000	0.233	-0.635
2000	0.084	-1.269
3000	0.993	-2.101
4000	1.059	-2.947
5000	1.429	-3.737
6000	1.743	-4.591
7000	1.741	-5.316
8000	2.529	-6.225
9000	3.057	-6.928
10000	3.529	-7.085

Phase Response

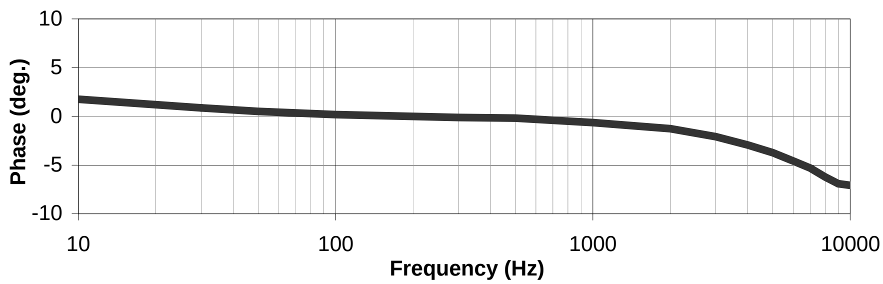

Amplitude Response

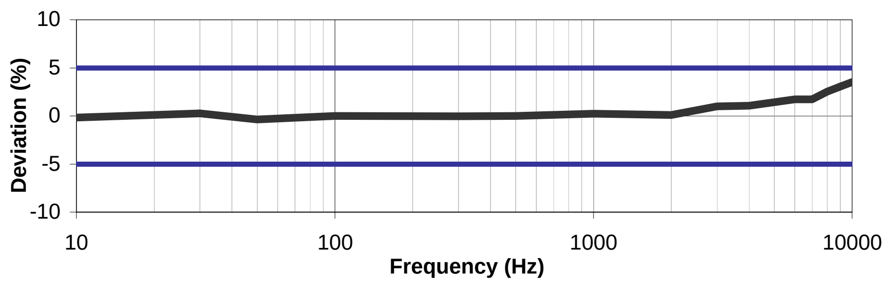

Notes

Results relate only to the items calibrated.
This certificate may not be reproduced except in full, without written permision.
Method: Calibration is performed in compliance with ISO 9001 and ISO 17025
This calibration was performed with TMS 9155 Calibration Workstation version 5.1.1
Calibration traceable to NIST (project number 822/271196).
Back-to-Back Comparison Calibration per ISO 16063-21
Procedure Used: PRD-P220
Measurement uncertainty (95% confidence level with coverage factor 2) for frequency ranges tested during calibration are as follows: 5-9 Hz; ± 1.70%, 10-99 Hz; ± 1.20%, 100 Hz; ± 0.75%, 101-920 Hz; ± 1.00%, 921-5000 Hz; ± 1.40%, 5001-10,000 Hz; ± 1.90%, 10,001-15,000 Hz; ± 2.20%, 15,001-20,000 Hz; ± 2.8%.

Customer

TMS Rental
3149 E. Kemper Rd
Cincinnati, OH 45241

User Notes

Lab Conditions

Temperature: 76 (24) °F (°C)
Humidity: 47 %

Unit Condition

As Found: In Tolerance
As Left: In Tolerance

Equipment Used

Description	Manufacturer	Model	Serial	Due Date
Data Aquisition Card	NI	4461	E4F2A4	11/8/2013
Std Accelerometer	PCB	080A200	110553	12/10/2013
Air Bearing Shaker	PCB	396C11	603	n/a
Std Sig Conditioner	PCB	442A102	305	12/10/2013
SUT Signal Conditioner	PCB	443B101	373	10/4/2013
Power Amplifier	TMS	2100E21-C	1001	n/a

Cal Date: 5-Aug-13
Due Date:

Approval Information

Technician: Wayne Underwood
Approval: Edward A. [illegible]

ACCREDITED

Cal ID: 21419 2649.01

THE MODAL SHOP INC. A PCB GROUP CO.

~Calibration Certificate~

3149 East Kemper Rd.
Cincinnati, OH 45241
Ph : 513-351-9919
Fax: 513-458-2172
www.modalshop.com

Sensor Information

Model Number:	HT356B21
Serial Number:	117335
Manufacturer:	PCB
ID Number:	45432
Description:	ICP® Accelerometer

Calibration Data

Sensitivity @ 100 Hz:	10.04	mV/g
Phase @ 100 Hz:	0.10	deg.
Test Level:	1.00	g
Output Bias Level:	9.8	VDC

Transducer Specifications

Amp. Range:	± 500	g
Resolution:	0.003	g
Resonant Freq:	≥ 55000	Hz
Temp. Range:	-54 to 121	°C
	-65 to 250	°F
Axis:	Y - Axis	

Data Table

Freq. (Hz)	Deviation (%)	Phase (deg)
10	0.124	1.638
30	-0.172	0.560
50	0.179	0.481
100	0.000	0.103
300	0.039	-0.064
500	0.082	-0.148
1000	0.352	-0.650
2000	0.555	-1.293
3000	0.559	-2.075
4000	0.878	-2.765
5000	0.997	-3.472
6000	1.261	-4.285
7000	1.648	-4.797
8000	2.284	-5.753
9000	2.802	-6.403
10000	3.382	-6.448

Phase Response

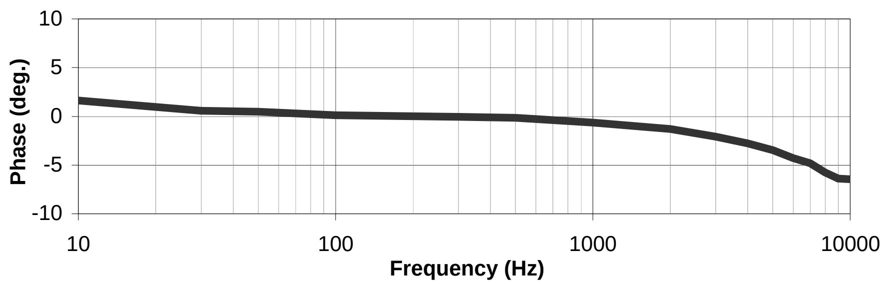

Amplitude Response

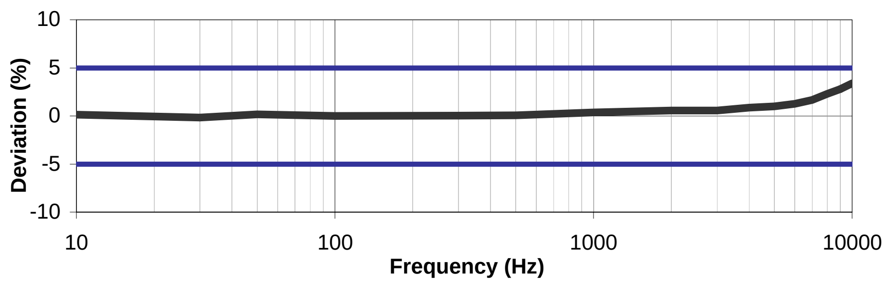

Notes

Results relate only to the items calibrated.
This certificate may not be reproduced except in full, without written permision.
Method: Calibration is performed in compliance with ISO 9001 and ISO 17025
This calibration was performed with TMS 9155 Calibration Workstation version 5.1.1
Calibration traceable to NIST (project number 822/271196).
Back-to-Back Comparison Calibration per ISO 16063-21
Procedure Used: PRD-P220
Measurement uncertainty (95% confidence level with coverage factor 2) for frequency ranges tested during calibration are as follows: 5-9 Hz; ± 1.70%, 10-99 Hz; ± 1.20%, 100 Hz; ± 0.75%, 101-920 Hz; ± 1.00%, 921-5000 Hz; ± 1.40%, 5001-10,000 Hz; ± 1.90%, 10,001-15,000 Hz; ± 2.20%, 15,001-20,000 Hz; ± 2.8%.

Customer

TMS Rental
3149 E. Kemper Rd
Cincinnati, OH 45241

User Notes

Lab Conditions

Temperature: 76 (24) °F (°C)
Humidity: 48 %

Unit Condition

As Found: In Tolerance
As Left: In Tolerance

Cal Date: 5-Aug-13
Due Date:

Equipment Used

Description	Manufacturer	Model	Serial	Due Date
Data Aquisition Card	NI	4461	E4F2A4	11/8/2013
Std Accelerometer	PCB	080A200	110553	12/10/2013
Air Bearing Shaker	PCB	396C11	603	n/a
Std Sig Conditioner	PCB	442A102	305	12/10/2013
SUT Signal Conditioner	PCB	443B101	373	10/4/2013
Power Amplifier	TMS	2100E21-C	1001	n/a

Approval Information

Technician: Wayne Underwood
Approval: Edward A. Eshi

A2LA ACCREDITED

Cal ID: 21419 2649.01

THE MODAL SHOP INC.
A PCB GROUP CO.

~Calibration Certificate~

3149 East Kemper Rd.
Cincinnati, OH 45241
Ph : 513-351-9919
Fax: 513-458-2172
www.modalshop.com

Sensor Information

Model Number:	HT356B21
Serial Number:	117335
Manufacturer:	PCB
ID Number:	45432
Description:	ICP® Accelerometer

Calibration Data

Sensitivity @ 100 Hz:	9.99	mV/g
Phase @ 100 Hz:	0.10	deg.
Test Level:	1.00	g
Output Bias Level:	9.9	VDC

Transducer Specifications

Amp. Range:	± 500	g
Resolution:	0.003	g
Resonant Freq:	≥ 55000	Hz
Temp. Range:	-54 to 121	°C
	-65 to 250	°F
Axis:	X - Axis	

Data Table

Freq. (Hz)	Deviation (%)	Phase (deg)
10	-0.641	1.366
30	-0.262	0.588
50	-0.002	0.335
100	0.000	0.100
300	0.033	-0.340
500	0.122	-0.562
1000	0.444	-1.431
2000	0.885	-2.947
3000	1.887	-4.640
4000	4.503	-6.732
5000	1.423	-8.224
6000	3.114	-9.654
7000	4.190	-11.016

Phase Response

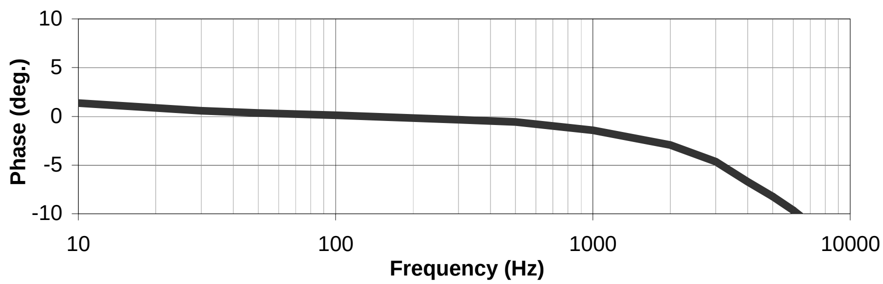

Amplitude Response

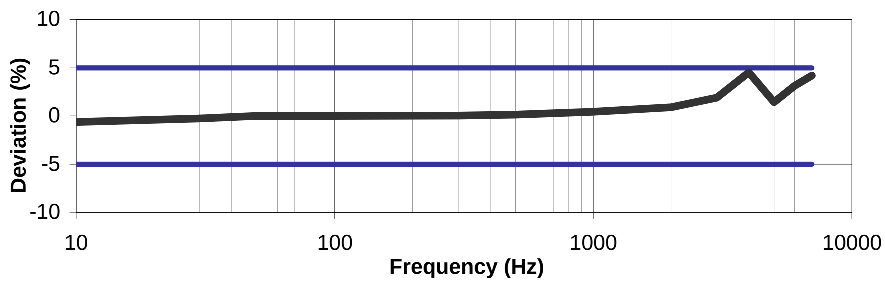

Notes

Results relate only to the items calibrated.
This certificate may not be reproduced except in full, without written permision.
Method: Calibration is performed in compliance with ISO 9001 and ISO 17025
This calibration was performed with TMS 9155 Calibration Workstation version 5.1.1
Calibration traceable to NIST (project number 822/271196).
Back-to-Back Comparison Calibration per ISO 16063-21
Procedure Used: PRD-P220
Measurement uncertainty (95% confidence level with coverage factor 2) for frequency ranges tested during calibration are as follows: 5-9 Hz; ± 1.70%, 10-99 Hz; ± 1.20%, 100 Hz; ± 0.75%, 101-920 Hz; ± 1.00%, 921-5000 Hz; ± 1.40%, 5001-10,000 Hz; ± 1.90%, 10,001-15,000 Hz; ± 2.20%, 15,001-20,000 Hz; ± 2.8%.

Customer

TMS Rental
3149 E. Kemper Rd
Cincinnati, OH 45241

User Notes

Lab Conditions

Temperature:	75 (24)	°F (°C)
Humidity:	48	%

Unit Condition

As Found: In Tolerance
As Left: In Tolerance

Cal Date: 5-Aug-13
Due Date:

Equipment Used

Description	Manufacturer	Model	Serial	Due Date
Data Aquisition Card	NI	4461	E4F2A4	11/8/2013
Std Accelerometer	PCB	080A200	110553	12/10/2013
Air Bearing Shaker	PCB	396C11	603	n/a
Std Sig Conditioner	PCB	442A102	305	12/10/2013
SUT Signal Conditioner	PCB	443B101	373	10/4/2013
Power Amplifier	TMS	2100E21-C	1001	n/a

Approval Information

Technician: Wayne Underwood
Approval: Edward A. [illegible]

ACCREDITED

Cal ID: 21419 2649.01

Traceable Calibration Certificate

Certificate Number:	1188034.1	**OE Number:**	2521652
Date:	08-MAY-2013		
Customer:	Noise Control Engineering Inc 799 Middlesex Tnpk BILLERICA, MA 01821		
Manufacturer :	National Instruments	**Model:**	NI 9234
Serial Number:	16D47C1		
Part Number:	195551B-01L	**Description:**	MODULE ASSY,NI 9234, 4 AI CONFIGURABLE
Calibration Date:	30-APR-2013	**Recommended Calibration Due:**	30-APR-2014
Procedure Name:	NI 9234	**Verification Results:**	As Found: Passed As left: Passed
Procedure Version:	3.4.1.0	**Calibration Executive Version:**	3.5.0.2
Lab Technician:	Rodolfo Maldonado	**Driver Info:**	NI-DAQmx:9.6.1
Temperature:	22.9° C	**Humidity:**	43.8% RH

The data found in this certificate must be interpreted as:

As Found The calibration data of the unit as received by National Instruments.

As Left The calibration data of the unit when returned from National Instruments

The As Found and As Left readings are identical for units not adjusted or repaired.

Results are reviewed to establish where any measurement results exceeded the manufacturer's specifications. Measured values greater than the Manufacturer's specification limits are marked as 'Failed' and reported under Calibration results. Calibration results that were evaluated as 'Passed' are not reported.

This certificate applies exclusively to the item identified above and shall not be reproduced except in full, without National Instruments written authorization. Calibration certificates without signatures are not valid.

DEKRA

ISO 9001:2008 Certificate Number: 510312.00

Victor Peña
Laboratory Manager

Calibration Notes

Type	Notes
Asset	Verification only was performed.

Standards Used

Manufacturer	Model	Type	Tracking Number	Calibration Due	Notes
FLUKE	5720A	Calibrator	8253	07-MAY-2013	

The standards used in this calibration are traceable to NIST and/or other National Measurement Institutes (NMI's) that are signatories of the International Committee of Weights and Measures (CIPM) mutual recognition agreement (MRA).

Calibration Results

As Found

Analog Input

Lower Range	Upper Range	Channel	Test Value	Low Limit	Reading	High Limit	Status
-5 V	5 V	0	4.00000, V	3.99520, V	4.00031, V	4.00480, V	Passed
-5 V	5 V	0	0.00000, V	-0.00120, V	0.00008, V	0.00120, V	Passed
-5 V	5 V	0	-4.00000, V	-4.00480, V	-4.00015, V	-3.99520, V	Passed
-5 V	5 V	1	4.00000, V	3.99520, V	4.00024, V	4.00480, V	Passed
-5 V	5 V	1	0.00000, V	-0.00120, V	0.00001, V	0.00120, V	Passed
-5 V	5 V	1	-4.00000, V	-4.00480, V	-4.00020, V	-3.99520, V	Passed
-5 V	5 V	2	4.00000, V	3.99520, V	4.00018, V	4.00480, V	Passed
-5 V	5 V	2	0.00000, V	-0.00120, V	-0.00007, V	0.00120, V	Passed
-5 V	5 V	2	-4.00000, V	-4.00480, V	-4.00029, V	-3.99520, V	Passed
-5 V	5 V	3	4.00000, V	3.99520, V	4.00024, V	4.00480, V	Passed
-5 V	5 V	3	0.00000, V	-0.00120, V	0.00003, V	0.00120, V	Passed
-5 V	5 V	3	-4.00000, V	-4.00480, V	-4.00019, V	-3.99520, V	Passed

As Left

Analog Input

Lower Range	Upper Range	Channel	Test Value	Low Limit	Reading	High Limit	Status
-5 V	5 V	0	4.00000, V	3.99520, V	4.00031, V	4.00480, V	Passed
-5 V	5 V	0	0.00000, V	-0.00120, V	0.00008, V	0.00120, V	Passed
-5 V	5 V	0	-4.00000, V	-4.00480, V	-4.00015, V	-3.99520, V	Passed
-5 V	5 V	1	4.00000, V	3.99520, V	4.00024, V	4.00480, V	Passed
-5 V	5 V	1	0.00000, V	-0.00120, V	0.00001, V	0.00120, V	Passed
-5 V	5 V	1	-4.00000, V	-4.00480, V	-4.00020, V	-3.99520, V	Passed
-5 V	5 V	2	4.00000, V	3.99520, V	4.00018, V	4.00480, V	Passed
-5 V	5 V	2	0.00000, V	-0.00120, V	-0.00007, V	0.00120, V	Passed
-5 V	5 V	2	-4.00000, V	-4.00480, V	-4.00029, V	-3.99520, V	Passed
-5 V	5 V	3	4.00000, V	3.99520, V	4.00024, V	4.00480, V	Passed
-5 V	5 V	3	0.00000, V	-0.00120, V	0.00003, V	0.00120, V	Passed
-5 V	5 V	3	-4.00000, V	-4.00480, V	-4.00019, V	-3.99520, V	Passed

National Instruments Calibration Services Austin
Building A
11500 N MoPac Expwy
AUSTIN, TX 78759-3504
USA
Tel: (800) 531-5066

NATIONAL INSTRUMENTS

Traceable Calibration Certificate

Certificate Number:	1188031.1	**OE Number:**	2521652
Date:	08-MAY-2013		
Customer:	Noise Control Engineering Inc 799 Middlesex Tnpk BILLERICA, MA 01821		
Manufacturer :	National Instruments	**Model:**	NI 9234
Serial Number:	16D47CD		
Part Number:	195551B-01L	**Description:**	MODULE ASSY,NI 9234, 4 AI CONFIGURABLE
Calibration Date:	30-APR-2013	**Recommended Calibration Due:**	30-APR-2014
Procedure Name:	NI 9234	**Verification Results:**	As Found: Passed As left: Passed
Procedure Version:	3.4.1.0	**Calibration Executive Version:**	3.5.0.2
Lab Technician:	Rodolfo Maldonado	**Driver Info:**	NI-DAQmx:9.6.1
Temperature:	23.0° C	**Humidity:**	44.1% RH

The data found in this certificate must be interpreted as:

As Found The calibration data of the unit as received by National Instruments.

As Left The calibration data of the unit when returned from National Instruments

The As Found and As Left readings are identical for units not adjusted or repaired.

Results are reviewed to establish where any measurement results exceeded the manufacturer's specifications. Measured values greater than the Manufacturer's specification limits are marked as 'Failed' and reported under Calibration results. Calibration results that were evaluated as 'Passed' are not reported.

This certificate applies exclusively to the item identified above and shall not be reproduced except in full, without National Instruments written authorization. Calibration certificates without signatures are not valid.

DEKRA

ISO 9001:2008 Certificate Number: 510312.00

Victor Peña
Laboratory Manager

Calibration Notes

Type	Notes
Asset	Verification only was performed.

Standards Used

Manufacturer	Model	Type	Tracking Number	Calibration Due	Notes
FLUKE	5720A	Calibrator	8253	07-MAY-2013	

The standards used in this calibration are traceable to NIST and/or other National Measurement Institutes (NMI's) that are signatories of the International Committee of Weights and Measures (CIPM) mutual recognition agreement (MRA).

Calibration Results

As Found

Analog Input

Lower Range	Upper Range	Channel	Test Value	Low Limit	Reading	High Limit	Status
-5 V	5 V	0	4.00000, V	3.99520, V	3.99998, V	4.00480, V	Passed
-5 V	5 V	0	0.00000, V	-0.00120, V	-0.00011, V	0.00120, V	Passed
-5 V	5 V	0	-4.00000, V	-4.00480, V	-4.00018, V	-3.99520, V	Passed
-5 V	5 V	1	4.00000, V	3.99520, V	4.00032, V	4.00480, V	Passed
-5 V	5 V	1	0.00000, V	-0.00120, V	-0.00001, V	0.00120, V	Passed
-5 V	5 V	1	-4.00000, V	-4.00480, V	-4.00032, V	-3.99520, V	Passed
-5 V	5 V	2	4.00000, V	3.99520, V	4.00024, V	4.00480, V	Passed
-5 V	5 V	2	0.00000, V	-0.00120, V	0.00010, V	0.00120, V	Passed
-5 V	5 V	2	-4.00000, V	-4.00480, V	-4.00003, V	-3.99520, V	Passed
-5 V	5 V	3	4.00000, V	3.99520, V	4.00014, V	4.00480, V	Passed
-5 V	5 V	3	0.00000, V	-0.00120, V	-0.00003, V	0.00120, V	Passed
-5 V	5 V	3	-4.00000, V	-4.00480, V	-4.00018, V	-3.99520, V	Passed

As Left

Analog Input

Lower Range	Upper Range	Channel	Test Value	Low Limit	Reading	High Limit	Status
-5 V	5 V	0	4.00000, V	3.99520, V	3.99998, V	4.00480, V	Passed
-5 V	5 V	0	0.00000, V	-0.00120, V	-0.00011, V	0.00120, V	Passed
-5 V	5 V	0	-4.00000, V	-4.00480, V	-4.00018, V	-3.99520, V	Passed
-5 V	5 V	1	4.00000, V	3.99520, V	4.00032, V	4.00480, V	Passed
-5 V	5 V	1	0.00000, V	-0.00120, V	-0.00001, V	0.00120, V	Passed
-5 V	5 V	1	-4.00000, V	-4.00480, V	-4.00032, V	-3.99520, V	Passed
-5 V	5 V	2	4.00000, V	3.99520, V	4.00024, V	4.00480, V	Passed
-5 V	5 V	2	0.00000, V	-0.00120, V	0.00010, V	0.00120, V	Passed
-5 V	5 V	2	-4.00000, V	-4.00480, V	-4.00003, V	-3.99520, V	Passed
-5 V	5 V	3	4.00000, V	3.99520, V	4.00014, V	4.00480, V	Passed
-5 V	5 V	3	0.00000, V	-0.00120, V	-0.00003, V	0.00120, V	Passed
-5 V	5 V	3	-4.00000, V	-4.00480, V	-4.00018, V	-3.99520, V	Passed

National Instruments Calibration Services Austin
Building A
11500 N MoPac Expwy
AUSTIN, TX 78759-3504
USA
Tel: (800) 531-5066

NATIONAL INSTRUMENTS

Traceable Calibration Certificate

Certificate Number:	1188028.1	**OE Number:**	2521652
Date:	08-MAY-2013		
Customer:	Noise Control Engineering Inc 799 Middlesex Tnpk BILLERICA, MA 01821		
Manufacturer :	National Instruments	**Model:**	NI 9234
Serial Number:	16D4749		
Part Number:	195551B-01L	**Description:**	MODULE ASSY,NI 9234, 4 AI CONFIGURABLE
Calibration Date:	30-APR-2013	**Recommended Calibration Due:**	30-APR-2014
Procedure Name:	NI 9234	**Verification Results:**	As Found: Passed As left: Passed
Procedure Version:	3.4.1.0	**Calibration Executive Version:**	3.5.0.2
Lab Technician:	Rodolfo Maldonado	**Driver Info:**	NI-DAQmx:9.6.1
Temperature:	22.9° C	**Humidity:**	44.2% RH

The data found in this certificate must be interpreted as:

As Found The calibration data of the unit as received by National Instruments.

As Left The calibration data of the unit when returned from National Instruments

The As Found and As Left readings are identical for units not adjusted or repaired.

Results are reviewed to establish where any measurement results exceeded the manufacturer's specifications. Measured values greater than the Manufacturer's specification limits are marked as 'Failed' and reported under Calibration results. Calibration results that were evaluated as 'Passed' are not reported.

This certificate applies exclusively to the item identified above and shall not be reproduced except in full, without National Instruments written authorization. Calibration certificates without signatures are not valid.

ISO 9001:2008 Certificate Number: 510312.00

Victor Peña
Laboratory Manager

Calibration Notes

Type	Notes
Asset	Verification only was performed.

Standards Used

Manufacturer	Model	Type	Tracking Number	Calibration Due	Notes
FLUKE	5720A	Calibrator	8253	07-MAY-2013	

The standards used in this calibration are traceable to NIST and/or other National Measurement Institutes (NMI’s) that are signatories of the International Committee of Weights and Measures (CIPM) mutual recognition agreement (MRA).

Calibration Results

As Found

Analog Input

Lower Range	Upper Range	Channel	Test Value	Low Limit	Reading	High Limit	Status
-5 V	5 V	0	4.00000, V	3.99520, V	4.00001, V	4.00480, V	Passed
-5 V	5 V	0	0.00000, V	-0.00120, V	0.00010, V	0.00120, V	Passed
-5 V	5 V	0	-4.00000, V	-4.00480, V	-3.99980, V	-3.99520, V	Passed
-5 V	5 V	1	4.00000, V	3.99520, V	3.99982, V	4.00480, V	Passed
-5 V	5 V	1	0.00000, V	-0.00120, V	-0.00006, V	0.00120, V	Passed
-5 V	5 V	1	-4.00000, V	-4.00480, V	-3.99993, V	-3.99520, V	Passed
-5 V	5 V	2	4.00000, V	3.99520, V	4.00007, V	4.00480, V	Passed
-5 V	5 V	2	0.00000, V	-0.00120, V	0.00007, V	0.00120, V	Passed
-5 V	5 V	2	-4.00000, V	-4.00480, V	-3.99991, V	-3.99520, V	Passed
-5 V	5 V	3	4.00000, V	3.99520, V	3.99998, V	4.00480, V	Passed
-5 V	5 V	3	0.00000, V	-0.00120, V	-0.00008, V	0.00120, V	Passed
-5 V	5 V	3	-4.00000, V	-4.00480, V	-4.00012, V	-3.99520, V	Passed

As Left

Analog Input

Lower Range	Upper Range	Channel	Test Value	Low Limit	Reading	High Limit	Status
-5 V	5 V	0	4.00000, V	3.99520, V	4.00001, V	4.00480, V	Passed
-5 V	5 V	0	0.00000, V	-0.00120, V	0.00010, V	0.00120, V	Passed
-5 V	5 V	0	-4.00000, V	-4.00480, V	-3.99980, V	-3.99520, V	Passed
-5 V	5 V	1	4.00000, V	3.99520, V	3.99982, V	4.00480, V	Passed
-5 V	5 V	1	0.00000, V	-0.00120, V	-0.00006, V	0.00120, V	Passed
-5 V	5 V	1	-4.00000, V	-4.00480, V	-3.99993, V	-3.99520, V	Passed
-5 V	5 V	2	4.00000, V	3.99520, V	4.00007, V	4.00480, V	Passed
-5 V	5 V	2	0.00000, V	-0.00120, V	0.00007, V	0.00120, V	Passed
-5 V	5 V	2	-4.00000, V	-4.00480, V	-3.99991, V	-3.99520, V	Passed
-5 V	5 V	3	4.00000, V	3.99520, V	3.99998, V	4.00480, V	Passed
-5 V	5 V	3	0.00000, V	-0.00120, V	-0.00008, V	0.00120, V	Passed
-5 V	5 V	3	-4.00000, V	-4.00480, V	-4.00012, V	-3.99520, V	Passed

National Instruments Calibration Services Austin
Building A
11500 N MoPac Expwy
AUSTIN, TX 78759-3504
USA
Tel: (800) 531-5066

Traceable Calibration Certificate

NATIONAL INSTRUMENTS

Certificate Number:	1188037.1	**OE Number:**	2521652
Date:	08-MAY-2013		
Customer:	Noise Control Engineering Inc 799 Middlesex Tnpk BILLERICA, MA 01821		
Manufacturer :	National Instruments	**Model:**	NI 9234
Serial Number:	16D47BE		
Part Number:	195551B-01L	**Description:**	MODULE ASSY,NI 9234, 4 AI CONFIGURABLE
Calibration Date:	30-APR-2013	**Recommended Calibration Due:**	30-APR-2014
Procedure Name:	NI 9234	**Verification Results:**	As Found: Passed As left: Passed
Procedure Version:	3.4.1.0	**Calibration Executive Version:**	3.5.0.2
Lab Technician:	Rodolfo Maldonado	**Driver Info:**	NI-DAQmx:9.6.1
Temperature:	22.9° C	**Humidity:**	44.0% RH

The data found in this certificate must be interpreted as:

As Found The calibration data of the unit as received by National Instruments.

As Left The calibration data of the unit when returned from National Instruments

The As Found and As Left readings are identical for units not adjusted or repaired.

Results are reviewed to establish where any measurement results exceeded the manufacturer's specifications. Measured values greater than the Manufacturer's specification limits are marked as 'Failed' and reported under Calibration results. Calibration results that were evaluated as 'Passed' are not reported.

This certificate applies exclusively to the item identified above and shall not be reproduced except in full, without National Instruments written authorization. Calibration certificates without signatures are not valid.

DEKRA

ISO 9001:2008 Certificate Number: 510312.00

Victor Peña
Laboratory Manager

Calibration Notes

Type	Notes
Asset	Verification only was performed.

Standards Used

Manufacturer	Model	Type	Tracking Number	Calibration Due	Notes
FLUKE	5720A	Calibrator	8253	07-MAY-2013	

The standards used in this calibration are traceable to NIST and/or other National Measurement Institutes (NMI's) that are signatories of the International Committee of Weights and Measures (CIPM) mutual recognition agreement (MRA).

Calibration Results

As Found

Analog Input

Lower Range	Upper Range	Channel	Test Value	Low Limit	Reading	High Limit	Status
-5 V	5 V	0	4.00000, V	3.99520, V	4.00014, V	4.00480, V	Passed
-5 V	5 V	0	0.00000, V	-0.00120, V	-0.00002, V	0.00120, V	Passed
-5 V	5 V	0	-4.00000, V	-4.00480, V	-4.00016, V	-3.99520, V	Passed
-5 V	5 V	1	4.00000, V	3.99520, V	4.00030, V	4.00480, V	Passed
-5 V	5 V	1	0.00000, V	-0.00120, V	0.00004, V	0.00120, V	Passed
-5 V	5 V	1	-4.00000, V	-4.00480, V	-4.00022, V	-3.99520, V	Passed
-5 V	5 V	2	4.00000, V	3.99520, V	4.00045, V	4.00480, V	Passed
-5 V	5 V	2	0.00000, V	-0.00120, V	-0.00010, V	0.00120, V	Passed
-5 V	5 V	2	-4.00000, V	-4.00480, V	-4.00064, V	-3.99520, V	Passed
-5 V	5 V	3	4.00000, V	3.99520, V	4.00016, V	4.00480, V	Passed
-5 V	5 V	3	0.00000, V	-0.00120, V	-0.00004, V	0.00120, V	Passed
-5 V	5 V	3	-4.00000, V	-4.00480, V	-4.00022, V	-3.99520, V	Passed

As Left

Analog Input

Lower Range	Upper Range	Channel	Test Value	Low Limit	Reading	High Limit	Status
-5 V	5 V	0	4.00000, V	3.99520, V	4.00014, V	4.00480, V	Passed
-5 V	5 V	0	0.00000, V	-0.00120, V	-0.00002, V	0.00120, V	Passed
-5 V	5 V	0	-4.00000, V	-4.00480, V	-4.00016, V	-3.99520, V	Passed
-5 V	5 V	1	4.00000, V	3.99520, V	4.00030, V	4.00480, V	Passed
-5 V	5 V	1	0.00000, V	-0.00120, V	0.00004, V	0.00120, V	Passed
-5 V	5 V	1	-4.00000, V	-4.00480, V	-4.00022, V	-3.99520, V	Passed
-5 V	5 V	2	4.00000, V	3.99520, V	4.00045, V	4.00480, V	Passed
-5 V	5 V	2	0.00000, V	-0.00120, V	-0.00010, V	0.00120, V	Passed
-5 V	5 V	2	-4.00000, V	-4.00480, V	-4.00064, V	-3.99520, V	Passed
-5 V	5 V	3	4.00000, V	3.99520, V	4.00016, V	4.00480, V	Passed
-5 V	5 V	3	0.00000, V	-0.00120, V	-0.00004, V	0.00120, V	Passed
-5 V	5 V	3	-4.00000, V	-4.00480, V	-4.00022, V	-3.99520, V	Passed

National Instruments Calibration Services Austin
Building A
11500 N MoPac Expwy
AUSTIN, TX 78759-3504
USA
Tel: (800) 531-5066

NATIONAL INSTRUMENTS

~Calibration Certificate~

Model No.: 086D20

Customer:

Serial No.: 32784

Description: Impulse Force Hammer

PO No.:

Manufacturer: PCB

Calibration Method: Impulse (AT-303-1)

Data

Output Bias: **10.4** Temperature: 74 °F 23 °C Relative Humidity: 43 %

HAMMER SENSITIVITY:

Hammer Configuration	Tip Extender	Medium (Red) None		
Hammer Sensitivity	mV/lb (mV/N)	1.069 0.2405		

Above data is valid for all supplied tips.

Condition of Unit:

As Found N/A.

As Left New unit in tolerance.

Notes:

1. Calibration is NIST Traceable thru Project 681/280472 and PTB Traceable thru Project 10065.
2. This certificate may not be reproduced, except in full, without written approval from PCB Piezotronics, Inc..
3. Calibration is performed in compliance with ISO 10012-1, ANSI/NCSL Z540-1-1994.
4. See Manufacturer's specification sheet for a detailed listing of performance specifications.
5. Measurement uncertainty (95% confidence level with a coverage factor of 2) is +/-3.8%.

Technician: Michael A. Dillon MAD

Date: 3/5/2013

ACCREDITED

CALIBRATION CERT # 1862.01

PCB PIEZOTRONICS INC.

3425 Walden Avenue
Depew, N.Y. 14043

TEL: 716-684-0001

FAX: 716-684-0987

www.pcb.com

Calibration Station: 13

REFERENCES

1. Veritec, *Vibration Control In Ships*, A. S. Veritec, Hovik, Norway, 1985.
2. American Bureau of Shipping, *Guidance Notes on Ship Vibration*, April 2006.
3. D. L. Logan, *A First Course in the Finite Element Method*, 4th Edition, Nelson, Toronto, Canada, 2007.
4. J. H. Ginsberg, *Mechanical and Structural Vibrations, Theory and Applications*, John Wiley & Sons, New York, 2001.
5. P.Avitabile, F.Piergentili, K.Lown, "Generation of Input Forcing Functions Through the Use of Measured Response and System Transfer Relations," Seventeenth International Modal Analysis Conference, Orlando, Florida, Feb 1999.
6. LMS, Inc., "LMS PolyMAX, A Revolution in Modal Parameter Estimation," LMS Technical Note.
7. T. Troyer, P. Guiullaume, B. Peeters, "Polyreference Frequency-Domain Least-Squares Estimation with Confidence Intervals," Proceedings of IMAC 26, Orlando FL, February 2008.
8. S.G. Stiansen, "Propeller and Wave-Induced Hull Structure Vibrations," Society of Naval Architects and Maine Engineers, Ship Vibration Symposium, Arlington, VA, October 16-17, 1978.
9. Allemang, R., "The Modal Assurance Criterion (MAC): Twenty Years of Use and Abuse", Twentieth International Modal Analysis Conference, Los Angeles, CA, February 2002.
10. Craig, R.R., Kurdila, A., *Fundamentals of Structural Dynamics*, 2nd Edition, John Wiley & Sons, Hoboken, 2006.
11. Avitabile, P., Piergentili, F., "Impedance Modeling for Machine Tool Application", Eighteenth International Modal Analysis Conference San Antonio Texas, Feb 2000.
12. Avitabile, P., "A Comparison of Some System Modeling Approaches", The Shock and Vibration Digest, Vol. 33, Number 4, July 2001
13. Nicgorski, D., Avitabile, P., "Conditioning of FRF Measurements for Use with Frequency Based Substructuring", Mechanical Systems and Signal Processing, Volume 24, Issue 2, February 2010.
14. Institute for Steel Design and Growth, "Teaching Materials – Chapter 17 Beams Subject to Bending and Torsion 1" Available From: http://www.steel-insdag.org/TeachingMaterial/Chapter17.pdf
15. Dokumaci, E. "An Exact Solution for Coupled Bending and Torsion Vibrations of Uniform Beams Having Single Cross-Sectional Symmetry", Journal of Sound and Vibration, 1987.
16. Bishop, R.E.D, Cannon, S.M., Mia, S., "On Coupled Bending and Torsional Vibration of Uniform Beams", Journal of Sound and Vibration, 1989.
17. Bercin, A.N., Tanaka, M., "Coupled Flexural-Torsional Vibrations of Timoshenko Beams", Journal of Sound and Vibration, 1997.
18. NEiNastran User's Manual, Version 10.1.
19. MIL-PRF-23653C(SHIPS), "Performance Specification, Plastic Tiles, Vibration Damping," 21 September, 1972.

SHIP STRUCTURE COMMITTEE LIAISON MEMBERS

LIAISON MEMBERS

American Society of Naval Engineers	Captain Dennis K. Kruse (USN Ret.)
Bath Iron Works	Mr. Steve Tarpy
Colorado School of Mines	Dr. Stephen Liu
Edison Welding Institute	Mr. Rich Green
International Maritime Organization	Mr. Igor Ponomarev
Int'l Ship and Offshore Structure Congress	Dr. Alaa Mansour
INTERTANKO	Mr. Dragos Rauta
Massachusetts Institute of Technology	
Memorial University of Newfoundland	Dr. M. R. Haddara
National Cargo Bureau	Captain Jim McNamara
National Transportation Safety Board - OMS	Dr. Jack Spencer
Office of Naval Research	Dr. Yapa Rajapaksie
Oil Companies International Maritime Forum	Mr. Phillip Murphy
Samsung Heavy Industries, Inc.	Dr. Satish Kumar
United States Coast Guard Academy	Commander Kurt Colella
United States Merchant Marine Academy	William Caliendo / Peter Web
United States Naval Academy	Dr. Ramswar Bhattacharyya
University of British Columbia	Dr. S. Calisal
University of California Berkeley	Dr. Robert Bea
Univ. of Houston - Composites Eng & Appl.	
University of Maryland	Dr. Bilal Ayyub
University of Michigan	Dr. Michael Bernitsas
Virginia Polytechnic and State Institute	Dr. Alan Brown
Webb Institute	Prof. Roger Compton

RECENT SHIP STRUCTURE COMMITTEE PUBLICATIONS

Ship Structure Committee Publications on the Web - All reports from SSC 1 to current are available to be downloaded from the Ship Structure Committee Web Site at URL: http://www.shipstructure.org
SSC 445 – SSC 393 are available on the SSC CD-ROM Library. Visit the National Technical Information Service (NTIS) Web Site for ordering hard copies of all SSC research reports at URL: http://www.ntis.gov

SSC Report No.	Report Bibliography
SSC 469	Strength And Fatigue Testing Of Composite Patches For Ship Plating Fracture Repair Karr, D.G.; Baloglu, C.; Cao, T.J.; Douglas, A.; Nielsen, K.; Ong, K.T.; Rohrback, B.; and Si, N. 2015
SSC 468	Development of a Structural Health Monitoring Prototype for Ship Structures Grisso, B.L 2013
SSC 467	Incorporation of Residual Stress Effects in a Plasticity and Ductile Fracture Model for Reliability Assessments of Aluminum Ship Hayden, M.J.; Gao, X,; Zhou, J.; Joyce, J.A. 2013
SSC 466	Mean Stress Assessment in Fatigue Analysis and Design Yuen, B.K.; Koko, T.S.; Polezhayeva, H.; Jiang, L 2013
SSC 465	Predictive Modeling Impact of Ice on Ship and Offshore Structures Bueno A. 2012
SSC 464	Design and Detailing for High Speed Aluminum Vessels Design Guide and Training Mish, Wh Jr., Lynch T., Hesse E., Kulis J., Wilde J., Snyder Z., Ruiz F. 2012
SSC 463	Marine Composites NDE, Inspection Techniques for Marine Composite Construction Greene, E 2012
SSC 462	Review of Current Practices of Fracture Repair Procedures for Ship Structures Wang, G, Khoo, E., ABS Corporate Technology 2012
SSC 461	Structural Challenges Faced By Arctic Ships, Kendrick A., Daley C. 2011
SSC 460	Effect of Welded Properties on Aluminum Structures, Sensharma P., Collette M., Harrington J. 2011
SSC 459	Reliability-Based Performance Assessment of Damaged Ships, Sun F., Pu Y., Chan H., Dow R.S., Shahid M., Das P.K. 2011
SSC 458	Exact Mapping of Residual Stress in Ship Hull Structures by Use of Neutron Diffraction Das S., Kenno S. 2009
SSC 457	Ship Frame Research Program – An Experimental Study of Ship Frames and Grillages Subjected to Patch Loads Daley C., Hermanski G. 2009